PHYSICAL REVIEW

VOLUME 86 NUMBER 1

AMERICAN PHYSICAL SOCIETY

THE PHYSICAL REVIEW

A journal of experimental and theoretical physics established by E. L. Nichols in 1893

Published by the American Institute of Physics
for the
AMERICAN PHYSICAL SOCIETY

Officers

President

J. H. Van Vleck
Harvard University
Cambridge, Massachusetts

Vice-President

Enrico Fermi
Institute for Nuclear Studies
University of Chicago
Chicago 37, Illinois

Secretary

K. K. Darrow
Bell Telephone Laboratories
Office:
Columbia University
New York 27, New York

Treasurer

G. B. Pegram
Columbia University
New York 27, New York

Local Secretary
for the Pacific Coast

J. Kaplan
University of California at Los Angeles
Los Angeles, California

Managing Editor

S. A. Goudsmit
Brookhaven National Laboratory
Upton, Long Island
New York

BOARD OF EDITORS

Editor

S. A. Goudsmit

Assistant Editor

S. Pasternack

Associate Editors

Harvey Brooks — M. Goldhaber — W. P. Allis
R. F. Christy — R. Hofstadter — F. G. Brickwedde
C. L. Critchfield — A. W. Lawson — W. R. Fretter
M. Deutsch — A. Pais — Corinne Hollister
T. H. Johnston — R. Serber — H. W. Lewis
Bruno Rossi — C. H. Townes — Associate Editors

Manuscripts for publication should be submitted to S. A. Goudsmit, Brookhaven National Laboratory, Upton, Long Island, New York. The author's institution is requested to pay a publication charge of $20 per page which, if honored, entitles them to 100 free reprints. Illustrations will be sent with galley proofs.

Proof and all correspondence concerning papers in the process of publication should be addressed to the Publication Manager, American Institute of Physics, 57 East 55 Street, New York 22, New York.

Subscription Price

United States and Canada $25.00
Elsewhere $27.00

Back Numbers[1]

Yearly back number rate when complete year is available:
Prior to 1949: $20.00
Thereafter: $27.00

Single copies: $2.00 each, prior to July, 1929;
$1.00 each, July, 1929–December, 1941;
$2.00 each, January, 1942–December, 1946;
$1.00 each, January, 1947–December, 1948;
$1.25 each, thereafter.

General Index, 1893–1920: $4.00.

Subscriptions, renewals, and orders for back numbers should be addressed to the American Institute of Physics, 57 East 55 Street, New York 22, New York.

Changes of address in the case of members of the American Physical Society should be addressed to the Treasurer; in the case of other subscribers to the American Institute of Physics.

[1] For Back Issues Register of Physics Departments, Cornell University, Ithaca, New York.

The Physical Review is published semi-monthly at Prince and Lemon Streets, Lancaster, Pennsylvania.

Entered as second-class matter January 6, 1948, at the Post Office at Lancaster, Pennsylvania, under the Act of March 3, 1879.

Acceptance for mailing at the special rate of postage provided for in paragraph (d-2), section 34.40, P. L. & R. of 1948, authorized January 27, [illegible]

THE
PHYSICAL REVIEW

A journal of experimental and theoretical physics established by E. L. Nichols in 1893

SECOND SERIES, VOL. 86, NO. 5 JUNE 1, 1952

Some Remarks on the *V*-Particles*

A. PAIS
Institute for Advanced Study, Princeton, New Jersey
(Received January 22, 1952)

It is qualitatively investigated whether the abundance of *V*-particle production can be reconciled with their long lifetime by using only interactions of a conventional structure. This is possible, provided a *V*-particle is produced together with another heavy unstable particle (Sec. II). Two distinct groups of interactions are needed: for one, the coupling is strong (II); for the other, it is very weak (III). Two kinds of *V*-particles are considered, Fermions of mass $\sim 2200m$ and Bosons ($\sim 800m$). The arguments are somewhat different, according to whether the latter are nonpseudoscalar (III) or pseudoscalar (V). The competition with processes involving μ-mesons is discussed (IV). Possible connections with the τ-meson are commented on in Sec. V. The preliminary nature of the present analysis is stressed (VI).

I. INTRODUCTION

IN the last few years a sizable number of events have been recorded which have been given the collective name of *V*-particle decay.[1–10] While a number of characteristics of these phenomena do require more experimental elucidation, a few qualitative features are already standing out clearly. Among these we mention first of all:

(a) In high energy events *V*-particles are produced with a probability $\gtrsim 1$ percent of the π-meson production. Thus, the production is copious.

(b) These new particles have lifetimes $\gtrsim 10^{-10}$ sec.

(c) There is a marked dissymmetry between the neutral and the charged *V*'s, the former ones being observed much more frequently. It is not quite clear yet whether this is due to the charged *V*'s being produced in lesser abundance or whether they have a shorter lifetime. Some observations tend to support the latter view.[2]

One of the most striking aspects is certainly the long lifetime of the *V*-particles. In fact, if one would consider the same mechanism which produces them to be instrumental for their decay, one would estimate lifetimes τ of the order of 10^{-21} sec. Note in this connection also that the *Q*-values involved ($\sim$30–100 Mev) are so large that a threshold argument cannot be invoked to explain the large τ.

In regard to what the nature of the decay products is, the situation is not quite clear. With certainty one has been able to identify protons as well as π-mesons among the decay products. In no single event that I know of has the identity of both observed V_0-decay products been established. Nor is it as yet a settled point whether we have to do with one (or more) three-body decays involving also neutral decay products, with a superposition of two (or more) two-body decays, or with a combination of processes of either type. Indeed, as Leighton has pointed out,[8] one must exercise caution in the use of the coplanarity argument in all cases where one of the decay products is a nucleon.

At the time of writing it is most commonly assumed that there exists at least one V_0 heavier and at least one lighter than the nucleon (masses $\sim 2200m$ and $800m$, respectively), both undergoing two-body decay.

It will be attempted in this paper to find a model for these phenomena which reconciles the copiousness of the production of the *V*'s with their longevity. Only couplings of a conventional structure will be used, not

* The principal ideas of this paper were reported at the second Rochester Conference on Meson Physics (January 11 and 12, 1952).

[1] G. D. Rochester and C. C. Butler, Nature **160**, 855 (1947).
[2] Seriff, Leighton, Hsiao, Cowan, and Anderson, Phys. Rev. **78**, 290 (1950).
[3] G. McCusker and D. Millar, Nuovo cimento **8**, 289 (1951).
[4] V. D. Hopper and S. Biswas, Phys. Rev. **80**, 1099 (1950).
[5] R. Armenteros *et al.*, Nature **167**, 501 (1951).
[6] H. S. Bridge and M. Annis, Phys. Rev. **82**, 445 (1951).
[7] Thompson, Cohn, and Flum, Phys. Rev. **83**, 175 (1951).
[8] Leighton, Wanlass, and Alford, Phys. Rev. **83**, 843 (1951).
[9] W. B. Fretter, Phys. Rev. **83**, 1053 (1951).
[10] R. Armenteros *et al.*, Phil. Mag. **42**, 1113 (1951).

so much in the conviction that our present day type of field theory constitutes the adequate framework to represent mesonic and related phenomena, but rather in an endeavor to put these structures to the test. We shall start from the following assumptions:[11]

(1) The V_0 with mass $\sim 2200m$ is a Fermion. This is not certainly so, because (a) the decay product accompanying the proton has not definitely been identified as a π- or a μ-meson; (b) it is not certain whether or not, e.g., a neutrino is also emitted.

(2) The V_0 with mass $\sim 800m$ is a Boson. This is also tentative for very similar reasons. However, one picture has been obtained by Bridge[12] in Colorado in which both charged secondaries interact strongly with matter. Thus, it would seem implausible that one can simultaneously assume proton+μ-meson for the $2200m$ particle and π-meson+μ-meson for the $800m$ case.

(3) An assumption of symmetry concerning V_0 and $V_{\rm ch}$: namely, that there are two $V_{\rm ch}$, a Fermion and a Boson with respective masses not much different from the corresponding V_0's.

(4) In the absence of interactions, the Fermion wave functions shall satisfy a Dirac equation and the Boson wave functions a Schrödinger-Gordon-Klein equation.

Thus, the heavy Fermion is here as elementary as the nucleon. In this respect, the present model differs radically from any strong coupling isobar picture for the V-particles in which the $2200m$ particle appears as an essentially composite structure. So far it has not appeared possible to stabilize isobars sufficiently against transitions to the ground state, unless such selection rules are assumed to hold as seem rather artificial. This circumstance has, in fact, led to the exploration of the present alternative.

The following analysis rests further on the idea that the Fermion-Boson interactions between all particles mentioned above can be divided in two distinct groups.[11] The first group, discussed in the next section, comprises the nucleon-π-meson interaction and certain others of comparable strength. The second group (Sec. III) comprises very weak interactions between these same particles. The order of magnitude of the couplings is indeed reminiscent of those that were introduced by Yukawa to describe β-decay as being brought about through the intermediary of Bosons (see Sec. VI). As pointed out by Oppenheimer,[13] both groups can be characterized by saying that the rule of conservation of the number of nucleons (itself an *ad hoc* assumption needed for guaranteeing sufficient stability of matter) is generalized so as to refer to nucleons and the heavier V-particles collectively.

I will now consider first the production and thereafter the decay mechanisms. The arguments will have to be qualitative in nature; the emphasis will be throughout on relative orders of magnitude and on the role of selection rules. Furthermore, certain generalizations of the Furry theorem which were discovered by the Japanese workers in their elaborate discussions of decay processes of heavy Bosons will often be used (see Sec. IIIAb). The present work also contains many elements that already appear in an extensive survey of V-particle models and that have recently been published in the *Progress of Theoretical Physics*;[14–17] especially, some of the interactions originally considered by Nambu and co-workers and by Ōneda also occur here.

II. THE PRODUCTION MECHANISMS OF THE V-PARTICLES

The schemes to be considered will all involve couplings of the "$\bar{\psi}\psi\phi$-type," i.e., bilinear in the Fermion wave function ψ and its adjoint $\bar{\psi}$ and linear in the Boson wave function ϕ. This itself is an assumption, and it cannot be asserted at this moment that we can derive very much confidence in this structure of the interaction from our experiences with the analogous π-meson-nucleon coupling. This is not the right place to discuss in any detail the problematics of the so-called unrenormalizable theories or of the complications arising from interactions involving large coupling constants. But it should be emphasized that we will operate here with these interactions in the same crude sense as is done in what we at present choose to call the theory of the π-meson-nucleon problems.

First a matter of notation: nucleons will be designated by N_0. In particular, the neutron will be denoted by N_0^0 and the proton by N_0^+. The Fermions of mass ~ 2200 will be called N_1. N_1^0 is the V_0-Fermion; $N_1^\pm$ denotes the $V_{\rm ch}$. The relation of N_1^+ to N_1^- shall be that of particle to antiparticle. π-mesons (neutral, charged) shall be denoted by π_0, (π_0^0, $\pi_0^\pm$), the Bosons of mass $\sim 800m$ by $\pi_1(\pi_1^0, \pi_0^\pm)$. This is a convenient shorthand for the following discussion.

One can now in principle admit Fermion-Boson couplings of the type mentioned above between all these various sets of particles. I denote them by $(N_i N_j \pi_k)$, $i, j, k = 0, 1$. The interaction shall, of course, have the appropriate hermiticity and covariance properties, but the detailed structure of the coupling (pseudoscalar, scalar, etc.) is left unspecified for the moment with the exception of $(N_0 N_0 \pi_0)$. This is the nucleon-π-meson interaction, which shall of course be appropriate to the experimentally known fact that π_0^0 as well as $\pi_0^\pm$ are pseudoscalar particles.

It will now be assumed: $(N_i N_j \pi_k)$ can only be strong if

$$i+j+k = \text{even}. \tag{1}$$

[11] The question of the uniqueness of these assumptions is discussed in Sec. VI.

[12] Bridge, Courant, and Rossi, Phys. Rev. **85**, 159 (1952).

[13] J. R. Oppenheimer, discussion remark at the Rochester Conference.

[14] Y. Nambu *et al.*, Prog. Theor. Phys. **6**, 615, 619 (1951).

[15] K. Aizu and T. Kinoshita, Prog. Theor. Phys. **6**, 630 (1951).

[16] H. Miyazawa, Prog. Theor. Phys. **6**, 631 (1951).

[17] S. Ōneda, Prog. Theor. Phys. **6**, 633 (1951).

Condition (1) singles out the following couplings:[18]

$$(N_0 N_0 \pi_0), \tag{2a}$$

$$(N_1 N_1 \pi_0), \tag{2b}$$

$$(N_1 N_0 \pi_1). \tag{2c}$$

However little we know about (2a), we do have a strongly coupled system here. More precisely, our assumption shall mean that (2b) and (2c) are comparable in strength with (2a). The coupling constants for all couplings (2) shall indiscriminately be denoted by the one symbol G. This does not mean a prejudice to the equality of all coupling strengths, on charge independence and the like. It shall merely indicate an order of magnitude. The scheme (2) clearly leads to matrix elements for the creation of N_1's and π_1's in high energy nucleon-nucleon collisions. According to (2) the V's are produced in pairs, pairs of either (N_1, N_1) or (N_1, π_1). In this connection we note:

(1) The couplings here considered are only between particles whose existence seems reasonably certain. Such an economy seems fair as a starting point. But it cannot at all be excluded that the $(N_i N_j \pi_k)$-scheme might prove tenable while yet the specific interactions (2) and (12) below would be of a too narrow scope. Thus the further discussion of the N_1-properties remains unaltered if the π_1 were a different Boson than the $V_{\pi 0}$, provided only that it is heavier than the $N_1 - N_0$ mass difference and has a long lifetime for decay into two or more π_0's. Conversely, retaining the present meaning of π_1, one may replace everywhere N_1 by a heavy Fermion N_1', which may be different from N_1 and must be different from N_0 without affecting the discussion of the π_1-properties. With the sole exception of the correlation between N_1- and π_1-production, mentioned in point 3 below, the entire contents of this paper can thus be taken over into a much wider framework of particles and interactions. It should be emphasized that the two points vital to the present discussion are (a) that the V's are produced together with another heavy unstable particle; it will therefore be decisive to know whether there exists production correlations between unstable particle pairs (which need not have lifetimes of the same order of magnitude), (b) that the couplings can be divided into strong ones of the type (2) and weak ones of the type (12) below.

(2) The possibility that the V's are produced in pairs is hard to rule out from the present experimental evidence.[19] Photographs showing more than one V have actually been obtained by McCusker and Millar,[3] by Thompson,[20] by Rossi's group[20] and by Leighton.[20] Such pictures may, of course, not be considered as definite evidence for the present view, as plural rather than multiple production may occur. The most conclusive argument would naturally be the determination of the threshold for the production reaction.

(3) (2c) combined with (2a) leads to such reactions as

$$N_0^0 + N_0^0 \rightarrow N_1^0 + N_0^0 + \pi_1^0. \tag{3a}$$

The lowest order matrix elements are $\sim G^3$. On the other hand, (2c) by itself gives, in order G^2,

$$N_0^0 + N_0^0 \rightarrow N_1^0 + N_1^0, \tag{3b}$$

and this reaction has a lower threshold than (3a). Hence, there must be an energy region in which N_1-production is much favored over π_1-production. Assuming that for higher energies the cross sections for the processes (3a) and (3b) become comparable and that only one of the V's produced is actually picked up by the observation, the frequency ratio of N_1^0 to π_1^0 would be $\sim 3:1$. Leighton[3] quotes a ratio $\sim 2:1$ and Armenteros[10] $\sim 1.6 \pm 0.5$, which is somewhat lower[21] but seems to bear out a preponderance of N_1^0 over π_1^0.

In higher order, the coupling (2b) can combine with the other two to contribute also to the probabilities for the events (3a, b). This coupling is not strictly necessary for the N_1 or π_1 creation. It can, however, be classed among the strong interactions without upsetting the balance between copious production and long lifetimes.

(4) In the reactions (3a, b) both emerging Fermions will be particles (meant here as a contradistinction to antiparticles), if the colliding ones are particles. Hence the presumed particle nature of the initial N_0's leads to the singling out of the particle N_1's over the antiparticle N_1's. As the difference of the number of particles and antiparticles (whether N_0 or N_1), is a constant of the motion, one can only get an anti-N_1 if enough energy is available to create a pair of heavy Fermions. Hence the anti-N_1 should be at most equally frequent as the so far spectacularly absent antiproton.

(5) The production of charged N_1's in nucleon collisions depends decisively on whether N_1^+ is a particle and N_1^- an antiparticle, or *vice versa*. This is a physically decidable distinction of the $N_1^{\pm}$-properties in relation to those of $N_0^{\pm}$. It is interesting to note that if the situation for the N_1^{ch} were the reverse of that for the N_0^{ch}, i.e., if the relation of the N_1^- to the N_0^+ is that of particle to particle, the only possible $2N_0 \rightarrow 2N_1$ reaction is the one given by (3b), always remembering the conservation law mentioned under (3). Neither a neutron-proton nor a proton-proton collision could then give rise to the production of two N_1's without violating

[18] The interaction (2b) has first been considered by Nambu (see reference 14). Interactions between the heavy V-particles, nucleons, and π-mesons that correspond closely to interaction (2c) occur in some models of Nambu and in that of Oneda (see reference 17). Also some of the interactions mentioned in (12) below occur in these papers.

[19] I am much indebted for discussions on this point with various experimentalists during the Rochester Conference.

[20] Reported at the Rochester Conference. Leighton's work was presented by W. B. Fretter.

[21] However, more recent observations reported at the Rochester Conference seem to indicate that there are relatively fewer π_1's than is stated in references 9 and 11.

either the conservation of charge or the conservation of (particles minus antiparticles). The production of N_1^- would, of course, be possible provided enough energy is available to produce mesons as well, which can carry off charge. Such processes have a threshold higher than the one for (3b), and hence there would be a dissymmetry in N_1^0 *vs* N_1^{eh} production favoring the former. Without going yet in any detail into the decay problems, it may already be remarked that in this situation the N_1^- can only decay into a neutron plus other particles, again in accordance with the generalized conservation law of the number of nucleons.

In any case, the counterpart of (3a) for the production of charged V's exists; we have

$$N_0^0+N_0^0\rightarrow N_1^-+N_0^0+\pi_1^+, \tag{3c}$$

if N_1^- is a particle, and

$$N_0^0+N_0^0\rightarrow N_1^++N_0^0+\pi_1^-, \tag{3d}$$

if N_1^+ is a particle.

The present argument is, perhaps, of somewhat more general interest, as it shows that negatively charged heavy Fermions may exist which can be produced more easily than antiprotons.

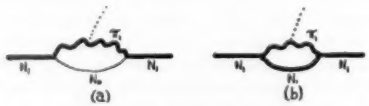

FIG. 1. Representative graphs leading to interactions of the type (5).

Too little is known to warrant at this moment a more detailed analysis of the production cross sections; such an investigation can for the rest be made along similar lines as is done for the π_0-production through (2a).[22]

It is clear that if (2) were the only couplings in the world then both the N_1 and the π_1 would be stable. Here the mass inequality

$$m(N_1)<m(N_0)+m(\pi_1)$$

is, of course, essential. But furthermore, we must immediately admit all electrically charged N_i and π_i to interact with the electromagnetic field. However, those interactions also in combination with (2) do not lead to any decay.

First of all, it is impossible that couplings of the type

$$i\epsilon\bar{\psi}_1\gamma_\mu\psi_0A_\mu+\text{h.c.} \tag{4}$$

exist. Here ϵ is the electric charge; ψ_1, ψ_0 are the wave functions of $N_1^\pm$, $N_0^\pm$, respectively; and A_μ is the electromagnetic potential. It is indeed readily seen that the presence of such "mixed" current densities occurring in (4) violates the law of conservation of charge. Thus, couplings of this type which would lead to $N_1\rightarrow N_0+\gamma$ need not concern us.

Of course, couplings with the electromagnetic field other than (4) can be envisaged, such as

$$\sim\bar{\psi}_1\gamma_\mu\gamma_\nu\psi_1F_{\mu\nu}+\text{h.c.} \tag{5}$$

$$\sim\bar{\psi}_1\gamma_\mu\gamma_\nu\psi_0F_{\mu\nu}+\text{h.c.} \tag{6}$$

Both (5) and (6) satisfy all covariance and gauge invariance requirements. Moreover, such interactions may be present for both $N_1^\pm$ and N_1^0, just as the effective anomalous magnetic moment interaction $\bar{\psi}_0\gamma_\mu\gamma_\nu\psi_0F_{\mu\nu}$ occurs for protons and neutrons. In fact, the existence of an interaction like (5) is already a consequence of the presence of either or both of (2b, c) and of the electromagnetic interaction of the charged particles of each kind which are involved. In Fig. 1 one of the typical graphs for each case is drawn. Here and in the following, these graphological conventions are used: a straight thin (heavy) line denotes an $N_0(N_1)$; a waved thin (heavy) line stands for a $\pi_0(\pi_1)$; and a dotted line for a photon.

However, interaction (5) cannot lead to radiative V-decay either. It is true that (6) could give rise to that phenomenon, but on the other hand (6) cannot be constructed from the interactions (2) combined with electromagnetic couplings. This is generally true to all orders in G and ϵ and is a consequence of the "conservation of evenness" of all the elementary couplings which we have introduced so far. Hence, if we take the general view that interactions like (5), (6) are only occurring insofar as they are derived from the elementary $\bar{\psi}\psi\phi$ couplings (and the ϕ^2A_μ couplings between Bosons and the electromagnetic field), it is a rational procedure to exclude the interaction (6), although it could always be introduced in an *ad hoc* fashion. (Actually we will introduce in Sec. III ($N_iN_j\pi_k$) couplings from which (6) can be derived in the above sense. But then the corresponding strength will be weak and the radiative decay mode will be insignificant compared to other decay schemes.)

It is also easy to see that the rule of evenness excludes the possibility of the transition

$$\pi_1^0\rightarrow 2\gamma, \tag{7}$$

which would be the analog of the ordinary neutral π-meson decay. This is again true to all orders, and the same can be said for the following interactions (insofar as they are not already forbidden for other reasons):

$$\pi_1^0\rightarrow\pi_0^0+\gamma \tag{8}$$

$$\pi_1^0\rightarrow\pi_0^++\pi_0^- \tag{9a}$$

$$\pi_1^0\rightarrow\pi_0^0+\pi_0^0. \tag{9b}$$

Indeed, any reaction is possible only if the sum of the "mass numbers" on either side is either even or odd. It is consistent with the nature of the electromagnetic

[22] See K. M. Watson and K. A. Brueckner, Phys. Rev. **83**, 1 (1951).

couplings to assign to the photon a mass number zero. The mass number rule thus also excludes decays of the types (7) to (9) with an arbitrary number of photons added on the right-hand side of the reaction. Furthermore, if

$$\pi_1^0 \to \pi_0^0 + \pi_0^0 + \pi_0^0 \tag{10a}$$

$$\pi_1^0 \to \pi_0^+ + \pi_0^- + \pi_0^0 \tag{10b}$$

were energetically and otherwise possible, it would still be a forbidden transition.

In concluding this section we note that so far no dissymmetry has explicitly been brought in between charged and neutral V's. We have seen that nevertheless it is conceivable that fewer N_1^{ch} may be produced than N_1^0 if only the N_1^- is treated on the same footing as the proton. But even apart from this possibility the production rate of V_0 and V_{ch} need not necessarily be equal. For example, a symmetrical theory of the π_0-nucleon coupling gives at least near threshold, dissimilarities in the π_0^0 and $\pi_0^\pm$-production, a.o., because of the exclusion principle, and similar effects may occur for the V's. In the subsequent sections we will, however, assume the productions to be equal and investigate whether the decay processes alone can account for the dissymmetry. It will turn out that such a dissymmetry may exist for $\pi_1^\pm$- *vs* π_1^0-decay, but not for $N_1^\pm$- *vs* N_1^0-decay.

III. THE DECAY MECHANISMS OF THE V-PARTICLES

To get sufficiently slow decay we now have to assume that the $(N_iN_j\pi_k)$ are extremely weak (and thus insignificant for the production) if

$$i+j+k = \text{odd}. \tag{11}$$

Condition (11) singles out the interactions

$$(N_1N_0\pi_0), \tag{12a}$$

$$(N_0N_0\pi_1), \tag{12b}$$

$$(N_1N_1\pi_1), \tag{12c}$$

and we will again introduce one coupling constant, g, to be representative of the whole group. As before, g indicates a general order of magnitude. The couplings (12) make possible even-odd transitions in the mass number.

The decays are generally brought about by combinations of the interactions (2) and (12). Most of the processes to be considered give divergent results for the corresponding matrix element. But even apart from that, a determination of the magnitude of g is hampered by the simultaneous dependence of the decay probabilities on the large coupling constant G. In this respect the situation is similar to that for neutrino processes where a coupling constant occurs which is very small, but the precise value of which likewise depends on G. Here we shall essentially always need the g^2-dependence to make the decay rate slow. In what follows we will confine the discussion to the lowest order matrix elements and will indicate the kinds of questions one runs into in analyzing the decay problems. With due reservations one estimates in this way

$$g^2/4\pi\hbar c \sim 10^{-11}. \tag{13}$$

(A) The Decay of the V_0's

(a) N_1^0-Decay

This is possible through (12a). This coupling comprises two possibilities:

$$N_1^0 \to N_0^+ + \pi_0^-, \tag{14a}$$

$$N_1^0 \to N_0^0 + \pi_0^0 (\to N_0^0 + 2\gamma). \tag{14b}$$

The π_0 are pseudoscalar mesons and we shall take the coupling (12a) to be of γ_5-type. The lifetime for either process (14) is then given by

$$\tau^{-1} \approx \frac{g^2}{4\pi\hbar c} \cdot \left(\frac{2\mu_0}{M_0}\right)^{\frac{1}{2}} \left(\frac{M_1 - M_0 - \mu_0}{M_0 + \mu_0}\right)^{\frac{1}{2}} \cdot \frac{\mu_0 c^2}{\hbar} \text{ sec}^{-1}. \tag{15}$$

Here p, E are the momentum and energy of the nucleon; M_1, M_0, μ_0 are the masses of N_1, N_0, and π_0, respectively. With $M_1 = 2200m$, $M_0 = 1836m$, $\mu_0 = 276m$:

$$\tau^{-1} \sim (g^2/4\pi\hbar c) \times 10^{21} \text{ sec}^{-1}, \quad \text{so} \quad g^2/4\pi\hbar c \sim 10^{-11}$$
$$\text{for} \quad \tau \sim 10^{-10} \text{ sec}.$$

FIG. 2. Graph for the $2\pi_0$-decay of the π_1.

It may be remarked that the decay (14b) is invisible in a cloud chamber. It is of course true that the γ-rays resulting from the π_0^0 decay are shower producing, but it will in general not be possible to relate such showers to (14b) as the origin of the initial photons. Assuming the g's responsible for (14a) and (14b) to be of the same order of magnitude, this means that an estimate of the production probability of the N_1^0 on the basis of the frequency of the event (14a) would be underestimated by a factor ~ 2.

Radiative decays are also $\sim g^2$ and further $\sim e^2$. They are, therefore, insignificant.

(b) *The* π_1^0-*Decay*

In discussing the decay modes of the π_1^0 it now becomes indispensable to specify in further detail the nature of the π_1^0. We will first of all investigate the possibility that the π_1^0 decays into two π_0's. Now as the latter are pseudoscalar this makes it certainly necessary to assume the π_1^0 to be nonpseudoscalar and

nonpseudovector. In the present section this assumption will be made. But in Sec. V an investigation will be made of what the consequences would be if π_1^0 were pseudoscalar all the same.

Let us now, therefore, admit the π_1^0 to be scalar or vector and analyze the decays

$$\pi_1^0 \to \pi_0^+ + \pi_0^-, \tag{16a}$$

$$\pi_1^0 \to \pi_0^0 + \pi_0^0 (\to 4\gamma). \tag{16b}$$

The simplest graph which describes the processes (16) is indicated in Fig. 2. The dot-dashed lines mean

TABLE I. Contribution of triangle graph to process (16a).

T_3	SS	SV	VV	VT
1	y	n	n	n
τ_3	n	n	y	y

that we have either an N_0 or an N_1-line. This depends on what particular combinations of interactions to be chosen from among (2) and (12) are operative in the vertices 1, 2, 3, respectively. The reader will easily verify that for any combination so chosen, the matrix element is always proportional to either gG^2 or g^3. This is, in fact, a consequence of the even-odd rules for the interactions and of the circumstance that on the left (right) of (16) we have total mass number 1(0). Only the gG^2-transitions are relevant, of course. And to any order the decay matrix element is proportional to at least the first power of g.

Provided the transition is not forbidden by any selection rule not yet mentioned, it follows from the work of Fukuda, Hayakawa, and Miyamoto[33] and of Ozaki, Ôneda, and Sasaki[34] that the lifetime is of the order of

$$\tau^{-1} \sim (10^{19} \text{ to } 10^{21}) \cdot (G^2/4\pi\hbar c)^2 \cdot (g^2/4\pi\hbar c). \tag{17}$$

The authors mentioned study decays of a Boson (with a mass comparable to that of π_1^0) into $\pi_0^+ + \pi_0^0$ (in the present notation), for all combinations of couplings of the (Boson, π_0^+, π_0^-)-system. With few exceptions the matrix elements are divergent, and regulator techniques were used to obtain a covariant cutoff.

TABLE II. Contribution of triangle graph to process (20).

T_3	SS	SV	VV	VT
1	y	n	n	n
τ_3	n	n	y	y

Quite apart from the question of trustworthiness of this procedure, the general orders of magnitude found seem to be reasonable when comparing the answers with the (finite) outcome from the $\pi_0^0 \to 2\gamma$ decay by means of simple dimensional arguments. For the decays (16) one obtains similar results.

In order to estimate g from (17) and the experimental τ, a knowledge of G is required. From the $(N_0 N_0 \pi_0)$ interaction it seems indicated that $G^2/4\pi\hbar c \gtrsim 1$, but not very much more is known owing to the aforementioned inadequacy of our methods in dealing with strongly coupled systems. However this may be, orders of magnitude of g as given by (13) seem again to be involved.

It must be added that there are further rules which in certain instances can inhibit the reactions (16a; b). Considering first (16a), if in the vertices 1, 2, 3 couplings are operative such that

$$n(v) + n(t) + n(\tau_3) = \text{odd}, \tag{18a}$$

then the contribution of the corresponding graph vanishes. Here $n(v)$ and $n(t)$ denote the total number of vector and tensor couplings, respectively, occurring in the triangle; $n(\tau_3)$ is the total number of neutral Boson couplings involving τ_3. The rule (18a) is a generalization of the Furry theorem and was first noted by Fukuda and Miyamoto.[35] It will be referred to as the first FM theorem. With the help of (18a) Table I has been constructed, which collects the allowed and forbidden transitions (16a) as calculated from the triangle graph. Notation: y=allowed, n=forbidden; SS=scalar π_1^0 with scalar coupling, etc.; T_3 indicates the isotopic spin character of π_1^0. The table holds for any choice of combinations of N_1, N_0 lines in the triangle, which need not all have the same couplings, of course; but it seems not yet worth while to make any further classification in that direction. Note that the innocuous SV case must have n throughout.[36]

As pointed out in reference 25, (18a) holds for any closed Fermion polygon in any graph, provided that the Bosons emerging from the vertices are not all neutral. In the latter case, of which (16b) is an instance, there is another rule which applies and which is[37]

$$\begin{aligned} &n(\tau_3) = \text{odd is forbidden;} \\ &\text{if } n(\tau_3) = \text{even}, \quad n(v) + n(t) = \text{odd is forbidden,} \end{aligned} \tag{18b}$$

(second FM theorem). Hence, the process (16b) is only allowed for a scalar π_1^0 with scalar coupling, irrespective of the isotopic spin characters.

The preceding brief remarks may exemplify the role of the FM theorems in analyzing the contributions of a particular kind of graph to some given process. However, the circumstance that the simple graph of Fig. 2 gives no contribution to the matrix element of the corresponding process does not necessarily mean that an absolute selection rule obtains. By using electromagnetic interactions in intermediary states it can, e.g., be shown that the process (16a) is not rigorously forbidden even if π_1^0 is a vector meson with $T_3 = 1$. A general discussion of the connection between the Furry- and the FM-theorems on the one hand and the existence of absolute selection rules on the other will be given elsewhere.

The $2\pi_0$ decay rate is obviously favored compared to the (π_0, γ) and the 2γ processes in the ratio $G^4 : : G^2 e^2 : : e^4$, independent of g. While this argument in itself has enough strength, it may yet be of interest to remember that there are additional selection rules: If π_1^0 is a vector-Boson one has the well-known forbiddenness of 2γ-decay; if it is a scalar then (π_0^0, γ) is forbidden for covariance reasons.

[33] Fukuda, Hayakawa, and Miyamoto, Prog. Theor. Phys. **5**, 283, 352 (1950).

[34] Ozaki, Ôneda, and Sasaki, Prog. Theor. Phys. **4**, 524 (1949); **5**, 25, 165 (1950).

[35] H. Fukuda and Y. Miyamoto, Prog. Theoret. Phys. **4**, 389 (1950). The relation of the theorems mentioned here and a generalized concept of charge conjugation is discussed by K. Nishijama, Prog. Theor. Phys. **6**, 614 (1951). These theorems are valid whether or not the Fermions in the closed loop have all the same mass.

[36] See F. J. Dyson, Phys. Rev. **73**, 929 (1948).

[37] In reference 25 it is incorrectly stated that the rule is $n(v) + n(t) =$ odd is forbidden if only neutral mesons are involved. The relations (18b) follow immediately, however, from the argument there presented. A third general rule could still be added: If only neutral mesons and photons are involved we have

$$n(v) + n(t) = \text{odd is forbidden.} \tag{18c}$$

The latter rule is actually the one closest to the familiar Furry theorem. See W. H. Furry, Phys. Rev. **51**, 125 (1936).

Thus, we have obtained a scheme in which there are two slow two-body decay rates, one for N_1^0 and one for π_1^0. The decay products are nucleons and π-mesons. In Sec. IV we will investigate other V_0-decay mechanisms, but we will now first discuss the V_{eh}-phenomena.

(B). The V_{eh}-Decay

The analogs of (14) and (16) for N_1^+, π_1^+ are

$$N_1^+ \rightarrow N_0^0 + \pi_0^+, \tag{19a}$$

$$N_1^+ \rightarrow N_0^+ + \pi_0^0, \tag{19b}$$

$$\pi_1^\pm \rightarrow \pi_0^\pm + \pi_0^0. \tag{20}$$

Now if it is true that all G's on the one hand and all g's on the other are of the same order of magnitude, then (19) and (20) give τ's of the same order of magnitude, if not equal, as for (14) and (16). This leads to a contradiction with the present experimental evidence: one would observe more than N_1^{eh}- than N_1^0-decays, (14b) being invisible. There are no selection rules for these processes. With regard to (20), the allowed and forbidden transitions are listed in Table II. T_0 is the isotopic spin character of π_0^0. Comparison with Table I shows some possibilities of a dissymmetry between V_0 and V_{eh} decays. But it throws no light on the observed preponderance of the former, which can in fact only be understood by assuming either less production or the existance of decay processes for the V_{eh} faster than those considered so far. In the next section it will be shown that the latter is not inconceivable.

IV. PROCESSES INVOLVING μ-MESONS

So far no decays have been considered involving μ-mesons. Now that we have discussed a model in which it is feasible, at least for V_0, to have a reasonable rate of production *vs* decay without them (and this seemed at first sight to be the greatest stumbling block), we have to ask how decays involving μ's compete with those considered so far. Such a competition has to be anticipated, as lifetimes $\sim 10^{-10}$ sec are just what one would expect for processes involving neutrinos.[9]

We first investigate π_1 decays involving neutrinos and do this in analogy with the corresponding $\pi_0^\pm$-process. It is well known that the situation here is not altogether satisfactory. In particular, it has so far not been possible to explain the $\pi_0^\pm$ decay without invoking Fermi couplings which give divergent results, on any coupling scheme, for the $\pi_0^\pm$-$\mu^\pm$ decay. On the other hand, it has been shown[28] that the $(\pi_0\mu)$ *vs* $(\pi_0 e)$ rate can be understood to be rather large ($\sim 10^4$) and this result, owing to a particular choice of interactions (*PS-PS* or *PS-PV* π_0 and *PV*-Fermi coupling), can be stated independently of the divergent integrals involved and is so far not in contradiction with experiment.[29] Anyhow, not having better suggestions, we shall follow the analogous procedure for π_1, i.e., use the $(N_i N_j \pi_k)$ couplings in conjunction with Fermi couplings between $(N_i N_j)$ and the light Dirac particles.

[28] M. Rudermann and R. Finkelstein, Phys. Rev. **76**, 1458 (1949); S. Nakamura *et al.*, Prog. Theor. Phys. **5**, 740 (1950).

[29] H. L. Friedman and J. Rainwater, Phys. Rev. **84**, 684 (1951).

The type of graph, then, which is involved in the process

$$\pi_1^\pm \rightarrow \mu^\pm + \nu \tag{21}$$

is drawn in Fig. 3, the dashed lines indicating the (μ, ν) pair. In vertex 2 the weak Fermi interaction operates. Hence, in order to get relevant decay rates we can use in vertex 1 only G- (not g-) interactions. This has an immediate consequence which we shall discuss further below. Choosing in 1 the interaction $(N_1 N_0 \pi_1)$ which is the only G-coupling involving π_1, it follows that the N_1 are unstable themselves in virtue of the same interaction in 2 which we need for the process (21).

Before continuing the discussion of (21) we remark that analogous processes can be conceived for the π_1^0, the emerging Fermions being neutral or oppositely charged. But if the isotopic spin character of the interactions in 1 and 2 is opposite, then the graph does not contribute according to the second FM theorem applied to the closed loop. Other sets of intermediate states through which the process might occur are seen to be irrelevant as they give too slow decays. Thus, choosing the isotopic spin dependences appropriately allows us to disregard this type of π_1^0-decay. This is a possible means to obtain dissymmetry between V_0- and V_{eh}-decay.

In estimating the decay rate of (21) we will attempt to free ourselves, as well as is possible, from the occurrence of the multiplicative divergent factor due to the integration over the momenta of the closed loop. This cannot be done in exactly the same way as for $(\pi_0\mu)$ *vs* $(\pi_0 e)$ decay where this factor drops out in the ratio as long as one takes the same couplings for both processes; we know the π_0^+ to be pseudoscalar whereas it has been assumed throughout that the π_1^+ is nonpseudoscalar. However, there is still one (and only one) other possibility:[30] If the π_1^+ is a VV-meson and the interaction in 2 a tensor-coupling, we get the same divergent integral[31] as for the *PS-PS* π_0^+ with *PV*-Fermi coupling.

FIG. 3. Graph for the μ-decay of the π_1.

In this way we find for the ratio of $(\pi_1^+$-$\mu)$ decay *vs* $(\pi_0^+\mu)$ decay, for equal strength of the Fermi interactions (μ is the μ-meson mass):

$$\frac{\tau^{-1}(\pi_1^+\mu)}{\tau^{-1}(\pi_0^+\mu)} = \frac{4}{3}\cdot\frac{\mu_0^3}{\mu_1^3\mu^2}\cdot\frac{(\mu_1^2-\mu^2)^2}{(\mu_0^2-\mu^2)^2}\cdot(\mu_1^2+2\mu^2) \approx 300.$$

The lifetime of π_0^+ being[32] $1.8\cdot 10^{-8}$ sec, we get a value of $\sim 10^{-10}$ sec for (21). It need hardly be added that the present argument does not pretend to show the preference of one $\pi_1^\pm$-coupling over another or to give a theoretically reliable value for the $(\pi_1\mu)$ decay lifetime; it merely illustrates the point of competition between $(\pi_1\mu)$ and $(\pi_1, 2\pi_0)$ decay. Nor does it seem profitable at this stage to discuss in any detail the occurrence of π_1-electron decay which, with the coupling used above, would be only slightly slower than (21); this process will not be taken into consideration hereafter.

It should now be observed that if $\tau(\pi_1^+, \mu) \lesssim \tau(\pi_1^+, 2\pi_0)$, the effective life time of π_1^+ decay is smaller than that for π_1^0. In fact, if the inequality holds strongly one will observe

$$\pi_1^\pm \rightarrow \mu^\pm + \nu, \quad \pi_1^0 \rightarrow \pi_0^+ + \pi_0^-,$$

as principal π_1-processes, the former being a relatively rare event compared to the latter.

[30] See J. Steinberger, Phys. Rev. **76**, 1180 (1949).

[31] This is not strictly correct. The divergent integral depends itself on the mass of the decaying particle. However, this is presumably a slow dependence if an effective cutoff would exist which, in mass units, is large compared to the π_1-mass.

[32] Jakobson, Schuls, and Steinberger, Phys. Rev. **81**, 894 (1951).

As already pointed out we are now also forced to consider the direct processes

$$N_1^0 \to N_0^+ + \mu^- + \nu, \tag{21a}$$

$$N_1^\pm \to N_0^0 + \mu^\pm + \nu, \tag{21b}$$

(two neutrino- and electron-neutrino processes are again ignored). These decays have a characteristic time given by

$$\tau^{-1} \sim (g_F/\hbar c)^2 \cdot (\mu c/\hbar)^4 \cdot (\mu c^2/\hbar) \cdot \sec^{-1},$$

where g_F is the Fermi constant involved. Giving this quantity the same value as for processes involving N_0's only, namely[33] $\approx 2\times 10^{-49}$ erg cm^3, one has $\tau \approx 0.6\times 10^{-10}$ sec. Hence, competition between these decays and the two-body decays must be expected. However, it does not seem possible to have any dissymmetry between (21a) and (21b).

Summarizing the results obtained with the present model, we have:

(a) The V_0 decays consist of three processes, one for the particle with mass $\sim 800m$:

$$\pi_1^0 \to \pi_0^+ + \pi_0^-;$$

two for the particle with mass $\sim 2200m$:

$$N_1^0 \to N_0^+ + \pi_0^-, \quad N_1^0 \to N_0^+ + \mu^- + \nu.$$

The latter might account for noncoplanar events. An estimate of the branching ratio clearly involves too much theoretical arbitrariness.

(b) If the burden of explaining the dissymmetry of V_0- with V_{ch}-decay rests with the decay mechanisms rather than with the production process, the model can account for a dissymmetry between π_1^0-decay and

$$\pi_1^\pm \to \mu^\pm + \nu.$$

It cannot[34] in any natural manner describe a dissymmetry in the behavior of N_1^0 and $N_1^\pm$ insofar as their disintegration is concerned, but it is possible that the N_1^{ch} are produced less copiously than the N_1^0 without the explicit introduction of disparities in the corresponding G's (see Sec. II). (*Added in proof:* decays like $\pi_1^0 \to \pi_0^\pm + \mu^\mp + \nu$ and $\pi_1^\pm \to \pi_0^0 + \mu^\pm + \nu$ can be discussed by similar methods.)

V. PSEUDOSCALAR HEAVY BOSONS

The assertion that π_1^0 is nonpseudoscalar is based on the presumed two-body decay of this particle into two π-mesons. The present experimental situation does not make it definitely superfluous to explore what would happen if the π_1^0 were pseudoscalar after all and the $2\pi_0$ decay therefore forbidden. Quite apart from this we know from the detailed discussion of the τ-meson decay, given by Powell,[35] that this process very probably is

$$\tau^+ \to \pi_0^+ + \pi_0^+ + \pi_0^-, \tag{22}$$

and this in turn means that the $\tau^\pm$ may be pseudoscalar; (it may also be pseudovector). We will discuss below whether or not a pseudoscalar π_1 might conceivably be related to the τ-meson. Before doing this we shall first discuss, in a general manner, the decay schemes of a heavy neutral or charged pseudoscalar Boson which we provisionally denote by B^0, $B^\pm$, respectively. The mass of these particles is taken to be $<4\mu_0$.

B^0 can of course decay according to

$$B^0 \to 2\gamma. \tag{23}$$

Apart from $B \to 2\pi_0$, also

$$B^\pm \to \pi^\pm + \gamma$$

is forbidden on gauge invariance grounds.[23,24] Hence, we are left with the following processes for B^0:

$$B^0 \to \pi_0^+ + \pi_0^- + \gamma, \tag{24}$$

$$B^0 \to \pi_0^0 + \pi_0^0 + \gamma, \tag{25}$$

$$B^0 \to \pi_0^+ + \pi_0^- + \pi_0^0, \tag{26}$$

$$B^0 \to \pi_0^0 + \pi_0^0 + \pi_0^0. \tag{27}$$

(25) is readily seen to be ruled out by the Furry theorem.[36] As to the possibility that the FM theorems can impose restrictions, the situation is this:

Process (24): In the vertex of the Fermion square in which the photon emission operates, there occurs a factor $\frac{1}{2}(1+\tau_3)\gamma_\mu$ which has, from the point of view of relation (18a), an even as well as an odd part. Hence, whatever happens in the other vertices, one can never get a selection rule from the first FM theorem.

Processes (26), (27): These are allowed if B^0 and π^0 have the same, forbidden[37] if they have different isotopic spin characters 1 or τ_3. (27) is of course "invisible."

Provided (26) and (27) are allowed, these decays are favored compared with (24) in the ratio $G^2 : e^2$. On the other hand, the phase space V_γ for reaction (24) is larger than that (V) for (26), (27). Treating the π_0's in the latter nonrelativistically, one has

$$\frac{V_\gamma}{V} = \frac{\sqrt{3}}{2\pi} \cdot \left(\frac{\mu_1}{\mu_1 - 3\mu_0}\right)^2 \cdot Z,$$

$$Z = \int_0^P p^2 dp (\mu_1 - 2E)^2 \left[\frac{3\{(\mu_1-E)^2+E^2\}}{\{(\mu_1-E)^2-p^2\}^2} - \frac{4p^2\{(\mu_1-E)^2-E^2\}}{\{(\mu_1-E)^2-p^2\}^3}\right],$$

$$E = (p^2+1)^{\frac{1}{2}}, \quad P = \left(\frac{\mu_1^2}{4\mu_0^2} - 1\right)^{\frac{1}{2}}.$$

[33] J. Tiomno and J. A. Wheeler, Revs. Modern Phys. **21**, 144 (1949).

[34] In this work further differentiations which may occur as a result of the Yang-Tiomno classification of the reflection properties of spinors have not been considered. See C. N. Yang and J. Tiomno, Phys. Rev. **79**, 495 (1950).

[35] See Powell *et al.*, Phil. Mag. **42**, 1040 (1951).

[36] See relation (18c) of footnote 27.

[37] That is to say, the graph with a Fermion square gives no contribution. Process (26) can nevertheless take place by letting an intermediary photon create the (π_0^+, π_0^-)-pair; but the probability for this process is small compared to that of (24), which is all that is needed for the argument developed hereafter.

Here μ_1 is the B^0-mass. Taking the latter to be of the order of the τ-meson mass ($\approx 960m$), $V_\gamma/V \approx 7$ which does not offset the G^2/e^2 balance in favor of (26), (27).

For the charged B's the reactions are

$$B^+ \rightarrow \pi_0^+ + \pi_0^0 - + \gamma, \tag{28}$$

$$B^+ \rightarrow \pi_0^+ + \pi_0^0 + \pi_0^0, \tag{29}$$

$$B^+ \rightarrow \pi_0^+ + \pi_0^+ + \pi_0^-. \tag{30}$$

There are no selection rules. Reaction (28) is slow compared with (29) and (30). Reactions (26), (27), (29), and (30) can be expected to have comparable lifetimes provided the former two are not forbidden. The lifetime for reaction (30) was first calculated by Sheila Power[35] and is extensively discussed in references 23 and 24.

After these preliminaries, let us now inquire whether an identification of B and π_1 is possible. Clearly the crucial point is whether (26) and (27) are allowed or not. In this connection it should first of all be noted that if a mass $\sim 800m$ is estimated on an assumed two-body decay which actually involves an invisible particle as well, this value is bound to be too low. We should thus distinguish two cases:

(a) $\mu_1 < 3\mu_0$. Reactions (26) and (27) are energetically forbidden. The π_1^0 decay is given by (24), which process is discussed in more detail below. Assuming, as we have done throughout, the mass of $\pi_1^\pm$ not to differ much from that of π_1^0, (29) and (30) are forbidden too. It would not be possible to identify $\pi_1^\pm$ with the τ-meson.

(b) $4\mu_0 > \mu_1 > 3\mu_0$. This case has further to be subdivided as follows:

(α) Reactions (26) and (27) are allowed. The radiative decays can be ignored. The identification of $\pi_1^\pm$ with the τ-meson is possible. All π_1 decays become phenomena as rare as the τ-meson decay (assuming again no disparities in the production). They would manifest themselves thus:

Process (26): a noncoplanar decay into charged π-mesons, a pair of γ-rays from the π_0^0 decay accompanying the event.

Process (29): of the $V_{\rm eh}$ decay type, noncoplanar, four γ-rays accompanying the event.

Process (30): the τ-meson decay.

The main observed V_0 decays would now be those of N_1^0, involving either π_1^0 or μ.

(β) Reactions (26) and (27) are forbidden. Now (24) becomes important. There is now also a marked dissymmetry between the π_1^0, the decay of which is accompanied by a photon, while this is not so for $\pi_1^\pm$. The latter is now faster, as we have seen, than the π_1^0 decay by a factor $\sim(1/7)G^2/e^2$.

It is thus not without interest to calculate in detail the probability of process (24). The graphs for it are given[39] in Fig. 4. The relative weight of graphs (II) and (I) is as 2:1. All Boson couplings have been taken as *PS-PS*. The contributions (apart from weight) of graphs (I) and (II) turn out to be finite and equal in absolute magnitude. They have opposite (equal) sign if the isotopic spin character of π_1^0 is $1(\tau_3)$. We can thus, e.g., assign the character 1 to π_1^0, and τ_3 to π_0^0, in order to forbid (26) and (27).

One further verifies that there are various possibilities of assigning N_1 or N_0 to the Fermion lines. Apart from terms $\sim(M_1 - M_0/M_0)$ these give the same contribution. We take one representative sample of Fermion lines. The effective energy density for the process on hand turns out to be ($\hbar = c = 1$)

$$-\frac{gG^2\epsilon}{3\pi^2 M^2}\phi_1 \frac{\partial\phi_0}{\partial x_\lambda}\frac{\partial\phi_0^*}{\partial x_\tau}\frac{\partial\phi_\sigma}{\partial x_\rho}\epsilon^{\lambda\rho\sigma\tau}. \tag{31}$$

Here ϕ_1 is the π_1-wave function, ϕ_0 that of the (charged) π_0, and ϕ_σ the electromagnetic potential. $\epsilon^{\lambda\rho\sigma\tau} = +1(-1)$ for even (odd) permutations of (1, 2, 3, 4). (31) satisfies all invariance requirements.

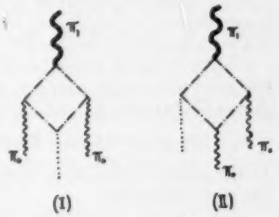

FIG. 4. Graphs for the $2\pi_0 + \gamma$-decay of the π_1.

We obtain for the absolute square of the matrix element H of the process, after summing over the polarizations of the photon,

$$|H|^2 = \frac{g^2G^4e^2\mu_1}{72\pi^4M^6}\cdot\frac{p_+^2 p_-^2\sin^2\theta}{E_+E_-k}.$$

Here $p_\pm$ is the momentum of the $\pi_0^\pm$, θ is the angle between them and k is the energy of the produced photon. The probability of the decay is found to be

$$\tau^{-1} = \frac{8}{27\pi^3}\cdot\frac{g^2}{4\pi}\cdot\left(\frac{G^2}{4\pi}\right)^2\cdot\frac{e^2}{4\pi}\cdot\left(\frac{\mu_1}{M}\right)^4\cdot\left(\frac{\mu_0}{M}\right)^2\cdot\mu_0\cdot f\ \text{sec}^{-1},$$

where

$$f = \int_0^P F(\bar{p})d\bar{p}, \quad P = \left(\frac{\bar{\mu}_1^2}{4} - 1\right)^{\frac{1}{2}}, \quad \bar{\mu}_1 = \frac{\mu_1}{\mu_0}.$$

[35] S. Power, Phys. Rev. **76**, 865 (1949).

[39] It is readily seen that graphs obtained from Fig. 2 by attaching an arbitrary number of photon lines to the π_3-lines all give zero.

Here

$$F(p)=p^4\{\bar{\mu}_1^2-2\bar{\mu}_1(p^2+1)^{\frac{1}{2}}\}^3(p^2+1)^{-\frac{1}{2}}$$
$$\cdot\{\bar{\mu}_1^2+1-2\bar{\mu}_1(p^2+1)^{\frac{1}{2}}\}^{-2}$$

is the distribution of the momenta (in units $\mu_0 c$) of one of the emerging charged particles. The distribution is much more peaked and the maximum lies at higher momenta than one would expect from the statistical factor only. It is somewhat interesting to note that if the π_1^0 mass is taken $\approx 960m$, the optimum of p lies quite near the value for the momentum of the π_0 in the process (16a), provided there the mass of π_1^0 is $\sim 800m$. For $\mu_1 \approx 960m$ one finds for the rate of decay of (24):

$$\tau^{-1}\sim\frac{g^2}{4\pi}\cdot\left(\frac{G^2}{4\pi}\right)^3\cdot 10^{17}\ \text{sec}^{-1}.$$

As was to be expected, one now gets an estimate for $g^2/4\pi$ which is much larger than the one given by (13) but still many orders of magnitude smaller than the fine structure constant, so that the qualitative features of the foregoing discussion remain essentially unaltered.

While it may be premature to decide whether the π_1 is pseudoscalar or not, it may be useful to stress these two main features of model $(b\beta)$:

(a) The π_1^0 decay should be accompanied by a γ-ray. For given momentum p of, say, π_0^+, the energy of the photon lies between K_+ and K_-, where

$$K_\pm=1/2\cdot\mu_1(\mu_1-2E)(\mu_1-E\pm p)^{-1},\quad E=(p^2+\mu_0^2)^{\frac{1}{2}}.$$

At the optimal value of p, these limits are ~ 50 and 150 Mev, respectively.

(b) If the π_1^+ is identified with the τ-meson, the lifetime for the latter should be shorter than that of the π_1^0.

It may finally be pointed out that if this identification is not possible, one may still expect V_{eh}-decays of the type (29) and, if the neutral counterpart of the τ-meson exists, rare V_0-decays of the type (26).

VI. CONCLUDING REMARKS

Whereas in the present model only interactions of a familiar form are employed, coupling constants g between heavy Fermions and Bosons occur with a novel magnitude. Such very weak couplings have so far only been considered in neutrino processes, such as β-, μ-, π-decay, etc. A consistent description of these disintegrations themselves in terms of $\bar{\psi}\psi\phi$-interactions (which, though it may be prejudice, one likes to consider as the primary structure generally) has so far not been given. The existence of the new particles and of new interactions between them may perhaps shed light on this question.

Even if one accepts the premises from which the present scheme starts, it can lay no claim to uniqueness. A main reason for this is that other particles, so far unobserved because of shorter lifetimes, for example, might very well enter the picture. As pointed out in Sec. II, one will then have to consider whether such regularities as have here been noted can still be upheld or should be replaced by others. The search for ordering principles at this moment may indeed ultimately have to be likened to a chemist's attempt to build up the periodic system if he were given only a dozen odd elements. The author would, therefore, like to stress that this work should be considered as representing a general point of view according to which one may attempt to codify the present information, rather than as an unflexible proposal for a particular set of interactions.

In the model here discussed, the heavy V cannot be considered as an isobar in the strong coupling sense; yet it seems closely related to the nucleon. A somewhat similar situation is met in comparing the μ-meson with the electron. Also these particles have markedly related properties, while their weak couplings, their large mass difference, and the long lifetime of the μ-meson render an isobar picture implausible. This is perhaps an indication of the existence of families of elementary particles (like a nucleon and an electron family) in which, not unlike the levels in a given kind of atom, the members of a given family are distinguished from each other through a quantization process, but one of a new kind.

I take great pleasure in thanking W. B. Fretter for a helpful correspondence and many physicists at the Institute, especially H. Fukuda, R. Jost, and C. N. Yang, for discussions and for their critical reading of the manuscript.

The High Frequency Resistance of Metals in the Normal and Superconducting State

C. J. GREBENKEMPER AND JOHN P. HAGEN
Naval Research Laboratory, Washington, D. C.
(Received December 17, 1951)

The high frequency resistance of lead, indium, and tin has been measured at frequencies in the vicinity of 9000 megacycles per second using resonant cavity techniques. Preliminary measurements on tin at 24,000 megacycles per second also have been made. The experimental techniques and measurement procedure are described. The effect of surface finishes is discussed for both the normal and superconducting regions. Data for the normal state are in general agreement with the Reuter-Sondheimer theory of the anomalous skin effect.

The high frequency resistance in the superconducting region was found to vary with frequency as the three-halves power rather than the predicted variation of the second power.

INTRODUCTION

THE results reported here are part of a general program of investigation of microwave condutivity of metals at low temperatures. The original objective of the investigation was to determine whether the twilight zone of superconductivity existed in the microwave region. After preliminary experiments it became evident that the bulk conductivity could easily be masked by the surface treatment given the metal. Consequently, a study of the effect of surface treatment on conductivity was undertaken.

The London[1] model of superconductivity postulates the simultaneous existence of normal and superconducting electrons. The superconducting electrons behave according to the phenomenological equations of F. London and H. London, whereas the normal conduction electrons exhibit the customary resistive behavior. If a high frequency alternating electromagnetic field is applied to a superconductor, both normal and superconducting electrons should flow in the surface of the superconductor.[2] As the temperature is reduced below the transition temperature, the fraction of normal conduction electrons remaining should decrease until at zero degrees Kelvin all normal conduction electrons should be converted into superconduction electrons. The first very high frequency resistance experiment on a superconductor was carried out by H. London[3] in 1940. A number of investigators have extended London's work both theoretically and experimentally.[4–7] Some of their results will be compared to ours.

APPARATUS AND TECHNIQUES

The present work has been carried out at two frequencies for tin and one frequency for indium and lead. The effects of surface finishes on the resistance was studied; also, the behavior of films of superconducting metals, electroplated on nonsuperconductors, were investigated. A cylindrical resonant transmission-type cavity is constructed of the metal to be investigated. The logarithmic decrement is measured by exciting the cavity in the proper mode and then observing the rate of decay of the amplitude of oscillation after the excitation is removed.

The cavities were fabricated a number of ways. Some were cast in carbon molds and then the inner surfaces turned to as good a finish as is obtainable in a lathe. Others were given various degrees of polishing with a ball mill, or polished with alumina, gamal cloth, and distilled water. Several cavities were made of a brass base on which several thousandths of an inch of the metal under study was electrodeposited. One specimen was cold-pressed from a block of tin. The die in this case was given a good surface finish and carefully cleaned before pressing. The cavities operate in the lowest mode, the TE_{111} mode, and are made in two pieces. The plane at which the two parts are joined is a section where no transverse currents flow provided symmetry is maintained. Coupling to the cavity is made through two small irises accurately located in the center of each end plate. Stainless steel wave guides are soldered to the cavity and are sealed off with mica windows. The cavity is continuously evacuated after it is assembled. A sectional view of the cavity and dewars is shown in Fig. 1.

Most of the experiments were conducted in external helium Dewar flasks surrounded by liquid nitrogen. However, the experiments with lead were conducted in the chamber of the Collins helium liquefier. The temperature measurements in the liquid helium region were determined from vapor pressure measurements using the 1937 Leiden scale. Other temperature measurements were made by a constant volume helium gas thermometer.

The rapid and accurate measurement of very high Q factors in the microwave region presents a difficult problem. Our measurement procedure uses a decay method in which the resonator is excited with a short pulse of rf energy, and the decay of energy in the cavity

[1] F. London and H. London, Physica **2**, 341 (1935).
[2] H. London, Nature **2**, 497 (1934).
[3] H. London, Proc. Roy. Soc. (London) **A176**, 522 (1940).
[4] A. B. Pippard, Nature **162**, 68 (1948); Physica **15**, 40 (1949); Proc. Roy. Soc. (London) **A203**, 98 (1950).
[5] W. M. Fairbank, Phys. Rev. **76**, 1106 (1949).
[6] G. E. H. Reuter and E. H. Sondheimer, Proc. Roy. Soc. (London) **A195**, 336 (1948).
[7] Maxwell, Marcus, and Slater, Phys. Rev. **76**, 1332 (1949).

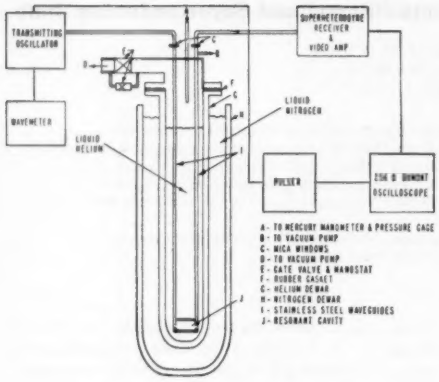

FIG. 1. Schematic diagram of apparatus.

is observed after the oscillator is shut off. The requirements of this system are:

1. The signal source should have a reasonable short time stability.
2. The response of the receiver be known.
3. An accurate system of time measurement be used.

The signal source used is a reflex klystron oscillator. The receiver is a conventional superheterodyne, and the oscilloscope is a Dumont type 256D.

The receiver may be calibrated in terms of input voltage required to give various amplitudes on the oscilloscope, or in terms of the attenuation necessary to change the amplitude at the oscilloscope from an arbitrary point A to another arbitrary point B. Care must be taken so that the receiver is linear in the usable portion of the decay trace. In most of our measurements we record about six or eight points in terms of amplitude *versus* time. Then for a decay trace, the output voltage is plotted on semi-log paper as a function of time. The best straight line is drawn through the points and Q calculated from the expression

$$Q=\frac{n\pi}{\ln(A_1/A_2)},$$

where $n=\theta f$=number of cycles in time interval θ, f=frequency, A_1=initial amplitude at θ_1, A_2=amplitude at θ_2, and $\theta=\theta_2-\theta_1$.

An alternate method may be used which involves only two points; with this system both amplitude and time must be measured more accurately. This entails measuring the time required for the signal to decay from amplitude A_1 to amplitude A_2, and the attenuation required to produce a change in amplitude from A_1 to A_2. Q is given by the expression

$$Q=27.3\theta f/\Delta \text{ db},$$

where θ=time interval, f=frequency, and Δ db=db attenuation required to produce a change in the amplitude from A_1 to A_2. Time intervals may be measured with a precision delay circuit, or by timing markers generated by a crystal-controlled oscillator. The signal source should be reasonably stable for short periods of time. This measurement procedure is rapid, and if desired the decay trace with the appropriate timing markers can be photographed.

To measure the very high Q factors encountered here by the resonance curve method would require a degree of frequency stability difficult to obtain.

Several photographs of oscilloscope patterns of the decay of oscillations in the cavity are shown in Fig. 2. Timing markers are also shown on the photographs. The decay trace labeled A was taken at 78°K for a tin cavity; trace B is for the same cavity at a temperature just above transition. This curve corresponds to a Q of approximately 40,000. The trace labeled C is for the same cavity at a temperature somewhat below the transition temperature, the Q in this case being about 2.3×10^6. The accuracy of our measurements of Q in the 10,000 megacycles per second region is about 5 percent, dependent on the values of Q, being greater for the higher values of Q.

With the preceding techniques it is possible to couple very loosely to the cavity, so corrections for energy radiated back into the wave guides can be kept small.

The radiation Q is given by the expression

$$Q_r=2\pi\frac{\text{energy stored in the cavity}}{\text{energy radiated through the irises per cycle}}.$$

Table I gives the radiation Q as a function of hole diameter. A number of hole sizes were used in the 9000 Mc/sec cavities. The highest calculated radiation Q was 62×10^6 and the lowest radiation Q was 8.2×10^6.

The Q factor of a superconducting cavity was measured at a given temperature for a number of hole

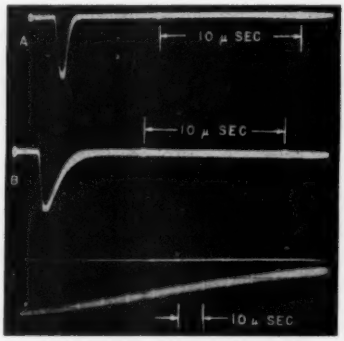

FIG. 2. Oscilloscope patterns of decay traces for a tin cavity at various temperatures: A, 78°K, sweep length 20 microseconds; B, 3.8°K, sweep length 20 microseconds; C, below transition temperature, sweep length 130 microseconds.

sizes. By this means it was possible to deduce values of Q for zero coupling, and, thus, determine experimental values of radiation Q for a given hole size. The experimental results yielded somewhat lower values of radiation Q than the calculated values. We used the calculated value of radiation Q to convert our measured loaded Q to unloaded Q. The correction amounted to but a few percent except for the extremely high Q factors. The unloaded Q or Q_0 is obtained from the measured Q corrected for the radiation Q.

$$Q_0 = 2\pi \frac{\text{energy stored in the cavity}}{\text{energy dissipated in the walls of the cavity per cycle}}.$$

The measured Q is given by

$$Q = 2\pi \frac{\text{energy stored in cavity}}{\text{energy dissipated in walls and energy radiated per cycle}}.$$

The relationship of Q_0 to Q and Q_r is given by the expression

$$1/Q_0 = 1/Q - 1/Q_r.$$

The surface resistance is obtained from the measured Q corrected for radiation loss and a knowledge of the geometry of the cavity.[8]

$$R_s = 2\pi K \mu_0 f/Q_0,$$

where R_s = surface resistance in ohms per unit square, f = resonant frequency, $\mu_0 = 4\pi \times 10^{-7}$ henry/meter, and K is a constant dependent on the geometry of the cavity. For a particular geometry this may be reduced to

$$R_s = C/Q_0,$$

where C is a constant for that geometry and mode. In the region where classical theory still prevails

$$R_s = (2\pi\omega 10^{-7}/\sigma)^{\frac{1}{2}},$$

where σ is the dc conductivity.

NORMAL STATE

The results of measurements on tin, lead, and indium indicate a pronounced anomaly in the normal region just above the transition temperature, in that the conductivity is lower than that calculated by classical theory. This is in agreement with the experiments of London, Pippard, Maxwell *et al.*, Fairbank, and others.

TABLE I. Radiation Q as a function of hole size.

Frequency Mc/sec	Hole diameter inches	Calculated radiation Q
9150	0.078	62×10^6
9150	0.088	22×10^6
9150	0.099	8.2×10^6
24000	0.060	3.6×10^6

[8] J. C. Slater, Revs. Modern Phys. **18**, 475 (1946).

TABLE II. Surface conductivity of metals in the normal state just above the transition temperature.

Frequency Mc/sec	Temperature °Kelvin	Metal	Surface conductivity ohm^{-1}	Remarks	State
9105	4.2	tin	117	cold pressed	normal
9155	4.2	tin	130	electrpolated	normal
9160	4.2	tin	133	cast and machined	normal
9145	4.2	tin	150	polished electroplated	normal
9160	4.2	tin	160	polished cast	normal
9400		tin	148–220	Pippard-single crystal	normal
9050		tin	143	Simon—cast	normal
9400		tin	115	Fairbank cold pressed	normal
24000	4.2	tin	57	Maxwell *et al.*—cold pressed	normal
24300	4.2	tin	80	preliminary NRL	normal
24000		tin	83	NRL at 9160 Mc/sec extrapolated to 24000 Mc/sec	normal
9165	8	lead	176	machined cast	normal
9100		lead	136	Simon—cast	normal
9137	3.5	indium	40	electrodeposited	normal

Reuter and Sondheimer[9] have derived an expression which replaces Ohms' law in the low temperature region and have satisfactorily explained the anomaly occurring in the normal state.

Table II gives the various surface conductivities, in the normal state, as a function of surface finish and frequency. Also included in this table are the results of Pippard, Fairbank, Simon, and Maxwell *et al.* The specimen of tin that yielded the lowest conductivity was the one formed by cold-pressing the metal into a suitable shape. The measured conductivity is in good agreement with the results obtained by Fairbank and the extrapolated results of Maxwell, Marcus, and Slater. In these cases, the cavities were formed by cold-pressing and yielded low values of conductivities. The electrodeposited surface yielded about the same conductivity as the machined cast specimen. Electrodeposition of the tin was carried out in an acid tin bath at a rather slow rate so as to obtain a dense deposit. By mechanically polishing the inner surfaces of the cast and the electroplated specimens, the conductivity was improved. Pippard's results on single crystals show that the conductivity varies with crystal orientation. The surface conductivity varies from 148–220 ohms^{-1}.

Preliminary data on tin at 24,000 Mc/sec have been obtained to date. The conductivities obtained by us were higher than those obtained by Maxwell *et al.* The surface conductivity in the normal state should vary[9] as $\omega^{-\frac{1}{2}}$. If our results at 9160 Mc/sec, for a polished surface, are extrapolated to 24,300 Mc/sec, we obtain good agreement with the measured values for a polished surface at the higher frequency.

Whether poor normal conductivity is due to surface roughness or to surface strains and dislocations, is difficult to say. For the pressed specimen, in our case, the surface appeared smooth. With any milling, machining, hobbing, or polishing process, some strains and dislocations will be set up in the surface of the material. By annealing the metal in vacuum for a sufficient length of time some of the strains in the metal should be relieved. From our measurements it would appear that

TABLE III. Experimental results in the superconducting state.

Frequency Mc/sec	R/R_n extrapolated to absolute zero	$A(\omega)$	Metal	Remarks
9145	0	0.127	tin	polished electroplated
9160	0.004	0.117	tin	cast and polished
9160	0.0075	0.118	tin	cast and machined
9105	0.028	0.110	tin	cold pressed
9200	0(?)	0.0865	tin	Pippard—cast polycrystals
9400	less than 0.001	0.105–0.20	tin	Pippard—single crystals
9400	0.019	···	tin	Fairbank—cold pressed
1200	0.007	0.0195	tin	Pippard polycrystals
24,000	0.09	···	tin	Maxwell *et al.*—cold pressed
24,300	0.006	0.265	tin	cast polished
9137	0.005	0.081	indium	electroplated
9165	0.010	0.046	lead	cast machined

cold-pressing sets up too many dislocations, thus giving rise to abnormally high resistance. It would also appear that surface roughness plays a part, since by polishing the surface the conductivity is increased. In the case of electroplated films surface strains are probably minimized while the surface tends to be less smooth. If Fairbank's results are extrapolated to 24,000 megacycles per second, a value of surface conductivity of approximately 61 ohm^{-1} is obtained; this compares with the value of 57 ohm^{-1} measured by Maxwell, Marcus, and Slater. Fairbanks and Maxwell used the same method of forming cavities. Thus, it appears that for both types of surface, the variation of conductivity with the frequency follows the law $\sigma = a\omega^{-\frac{1}{2}}$, where a is a constant.

Similar measurements were carried out with machined cast lead and electroplated indium surfaces in the 9000 megacycles per second region. The normal surface conductivity of lead just above the transition temperature was about 176 ohm^{-1}. Simon[9] obtained a value of 136 ohm^{-1} for lead at 9200 megacycles per second.

The value of normal conductivity for indium was considerably lower than that of tin. Two electroplated specimens yielded consistently low values of conductivity. Whether this is caused by a thin film, the plating process, or by some other mechanism remains to be resolved. Although the normal conductivity of indium was poor, the conductivity in the superconducting state was very high.

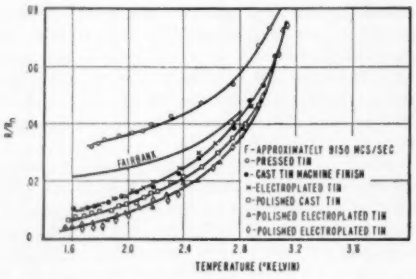

FIG. 3. Surface resistance of tin in the superconducting state for different types of surface treatment.

[9] I. Simon, Phys. Rev. **77**, 384 (1950).

SUPERCONDUCTING STATE

The experimental results obtained for the superconducting state are collected in Table III. The table includes values of normalized surface resistance extrapolated to absolute zero and values of $A(\omega)$. The normalized surface resistance is defined as equal to R/R_n, where R is the superconducting surface resistance and R_n is the surface resistance in the normal state just above the transition temperature. $A(\omega)$ is the rate of variation of R/R_n with the function of temperature $t^4(1-t^2)/(1-t^4)^2$, where t is the reduced temperature T/T_c, T = temperature, and T_c = transition temperature. The results of Pippard and others are also included in the table. The data for the individual specimens are shown in Figs. 3 to 10.

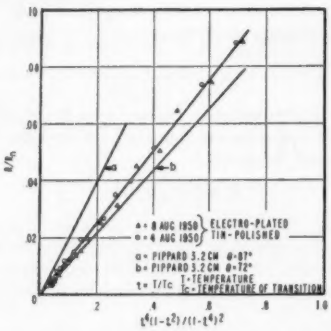

FIG. 4. Linear plot of low temperature resistance at 9145 Mc in superconducting state (polished electroplated tin specimen).

In the superconducting state the effect of surface finish is clearly evident in Fig. 3. Here the surface resistance ratio, $r = R/R_n$, of tin is plotted against temperature. Only the lower portion of the curves are shown since they are in essential agreement near the transition and start to diverge near 3.2°K. The pressed tin surface yielded the highest resistance ratio, somewhat higher than Fairbank's value; this difference may be due to differences in measurement techniques or to differences in the actual surfaces. The machined surface yielded a better value than the pressed surface and is about similar to the electrodeposited surface. The effect of mechanically polishing a cast tin specimen whose surface was turned in a lathe is also shown in this figure. The mechanical polishing was done by placing a number of clean, random sized, steel balls in the cavity and rotating it for a number of hours. A considerable improvement in the conductivity has been effected by this process. The lower curve is for an electrodeposited surface after it had been mechanically polished and then

etched with hydrochloric acid and a light tin plate deposited over the polished surface.

In Fig. 4, the surface resistance ratio is extrapolated to absolute zero in terms of a function of temperature first suggested by Pippard. The function of temperature is given by the expression[4] $t^4(1-t^2)/(1-t^4)^2$, where t is the reduced temperature T/T_c. It is apparent that the polished electrodeposited specimen does extrapolate to zero resistance at zero degrees Kelvin. Pippard's curves for single crystals of tin are also shown in the figure.

Figure 5 shows the same type extrapolation for the machined surface and the same specimen after mechanical polishing. Pippard's work on polycrystals at this frequency is also shown. When the normalized surface resistance is extrapolated to zero degrees Kelvin, it is found that the machined cast tin specimen yields a value of resistance equal to 0.0075 times its resistance just before the transition point. After polishing, this

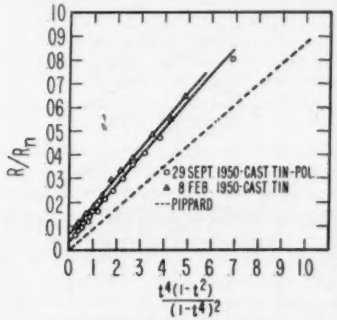

FIG. 5. Linear plot of low temperature resistance at 9160 Mc in the superconducting state (machined cast tin specimen and a polished, machined cast tin specimen).

same specimen yields at absolute zero a value of 0.004 times its initial resistance.

The experimental results on an electrodeposited indium surface are shown in Fig. 6. Indium is quite similar to tin except that the initial conductivity, for two specimens measured, was low. The normalized surface resistance extrapolated to zero degrees Kelvin yields a residual resistance of 0.005.

The results on lead are shown in Fig. 7. The curve shown is a plot of loaded Q *versus* temperature. The lead specimen was of high purity, cast in a carbon mold and then the inner surface turned in a lathe. The experiment was carried out in the Collins helium liquefier. The temperature measurements in this case are not precise since no attempt was made to stabilize the temperature. The scatter on the lead data is somewhat worse than that of the tin data. Part of the scatter is due to temperature variations. When r is extrapolated to zero degrees Kelvin, a residual resistance of 0.01 is obtained. The result is about what one would expect

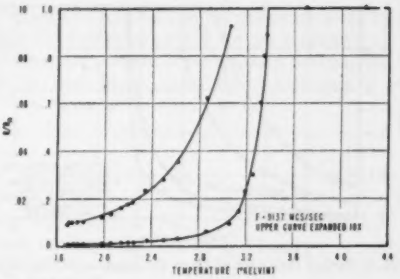

FIG. 6. Surface resistance of electrodeposited indium in the superconducting state.

from this type of surface treatment. It appears then that lead is about as good a conductor as tin in the superconducting region.

Preliminary measurements made on tin in the 24,000 megacycles per second region using a cavity cylindrical in shape and operated in its lowest mode yields results shown in Fig. 8. Also shown are the results of Maxwell *et al.*, and our results at 9160 megacycles per second for a similar surface treatment. Our results show considerably higher conductivity than those of Maxwell. On the basis of our work at 9000 megacycles and Fairbank at the same frequency it appears that the cold-pressing method of frabrication used by Maxwell and Fairbank imparts strains and dislocations, thus giving rise to abnormally high resistance in both the normal and superconducting regions.

In Table III, R/R_n is extrapolated to absolute zero to determine the residual resistance. Also included are the values of $A(\omega)$ for the different cases. Our values of $A(\omega)$ in the 9000-Mc/sec region lie between Pippard's values for single crystals and are somewhat higher than his value for polycrystals. The amount of resistance remaining at absolute zero is dependent on the surface treatment given the specimen. It appears that with appropriate surface treatment the conductivity in the superconducting state can be improved substantially.

The normalized surface resistance of tin at 24,000

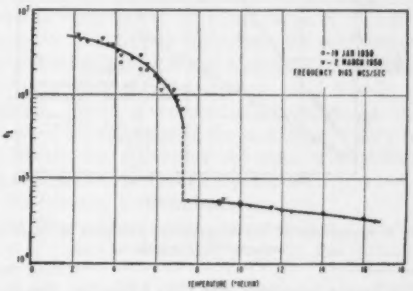

FIG. 7. Plot of loaded Q against temperature for lead.

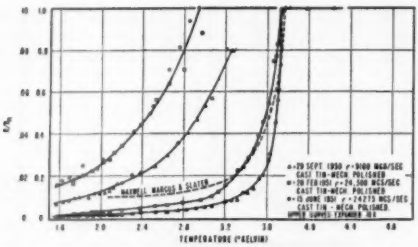

FIG. 8. Surface resistance of tin in the superconducting state.

megacycles per second is extrapolated to zero degrees Kelvin in Fig. 9. Also shown in this figure is a curve for a specimen at 9160 megacycles per second. The two specimens were given very similar surface treatment, being mechanically polished with gamal cloth, alumina, and distilled water. They extrapolate to very nearly the same values of residual resistance. It appears that the twilight region of superconductivity has not been reached at 24,000 megacycles per second. Further investigations at higher frequencies should be carried out.

The normal surface resistance R_n varies as $\omega^{\frac{1}{2}}$, which is in essential agreement with the results for these two cavities. If r is small the normal electrons are considered to have little effect on the distribution of the magnetic field in the metal. The resistive processes may be visualized as the absorption of power by the normal electrons in their collisions with the lattice as they move under the influence of the electric field induced by the varying magnetic field. If, below the transition, the magnetic field distribution is governed only by the superconducting electrons the effect of changing frequency will be to change, at some particular point within the metal, the magnitude of the electric field proportional to the frequency. Consequently,[10] the surface resistance R should vary as ω^2. Therefore, r would be proportional to $\omega^{4/3}$, since $r=R/R_n$. It is assumed that

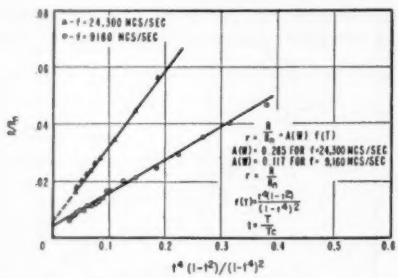

FIG. 9. Linear plot of low temperature resistance of tin in the superconducting state.

relaxation effects may be neglected in obtaining the previous expression.

At temperatures sufficiently far below the transition such that $r \ll 1$ the curves may be closely represented by the equation[4] $r=A(\omega)t^4(1-t^2)/(1-t^4)^2$, where t is the reduced temperature and A is a function of frequency only. If $A(\omega)$ is evaluated from our curves shown in Fig. 9, we obtain a value of $A(\omega)=0.117$ for $f=9160$ megacycles per second and 0.265 for $f=24{,}300$ megacycles per second. Thus the ratio of $A(\omega)$ for the two cases is 2.26.

The predicted ratio of $A(\omega)$ in the two cases is 3.67, which corresponds to $\omega^{4/3}$. The observed variation of $A(\omega)$ corresponds to $\omega^{0.886}$, or approximately $\omega^{5/6}$. Hence, R in the superconducting region is observed to vary with frequency as $\omega^{5/2}$. Pippard,[11] in his experiments at 1200 megacycles per second, obtained a value of $A(\omega)=0.0195$. If we assume r varies as $\omega^{5/6}$ and

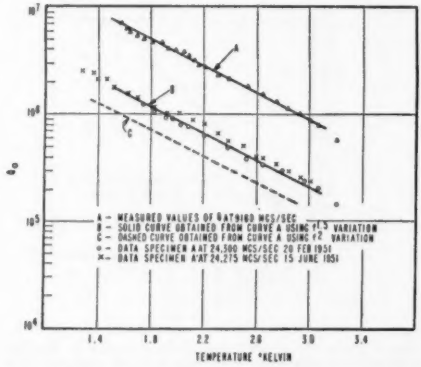

FIG. 10. Plot of the unloaded Q factor against temperature for two frequencies with curves B and C extrapolated on two assumptions from curve A.

extrapolate his results to 9160 megacycles per second and 24,300 megacycles per second, we obtain for $A(\omega)$ a value of 0.106 for the former and 0.238 for the latter. This compares with our measured values of 0.117 and 0.265 for the two cases.

A comparison of the unloaded Q factors obtained from the cavities may be used to determine the experimental variation of R with frequency. This can be done since the cavities operate in the same mode, have the same ratio of diameter/length, and were given similar surface treatment. Shown in Fig. 10 is the data obtained for a representative specimen operating at 9160 Mc/sec and for two specimens operating in the vicinity of 24,000 Mc/sec. Also shown in this figure are two curves derived from the 9160-Mc/sec data. The curve labeled C uses the predicted variation of the Q factor with

[10] F. London, *Superfluids* (John Wiley & Sons, Inc., New York, 1950) Vol. 1, p. 90.

[11] A. B. Pippard, Proc. Roy. Soc. (London) **A191**, 370 (1947).

frequency of ω^{-2}. The curve labeled B uses a variation of the Q factor with frequency of $\omega^{-3/2}$. It is apparent that the 24,000 Mc/sec data more nearly fit the curve that uses the $\omega^{-3/2}$ variation than that predicted by the London theory.

We wish to acknowledge the assistance given by Dr. Rufus G. Fellers, especially for his treatment of the radiation loss problem in the resonant cavities. We also wish to thank Mr. A. Szwed for his assistance in some of the temperature measurements.

PHYSICAL REVIEW VOLUME 86, NUMBER 5 JUNE 1, 1952

Low Energy *n-d* Scattering: Comparison of Experiment with Theory

M. M. GORDON AND W. D. BARFIELD*
University of Florida, Gainesville, Florida
(Received December 31, 1951)

D-wave effects are shown to be significant, though small, in the experimental *n-d* scattering data at 4.5 and 5.5 Mev. Consequently, since the calculations of Buckingham and Massey include only *S* and *P* wave phases, a phase shift analysis of the experimental data is carried out to determine these phases so that a suitable comparison can be effected between experiment and theory. The resulting "experimental" *P*-wave phases agree only qualitatively with those of the symmetric-interaction calculations, but they completely disagree with those of the neutral-interaction calculations. The lack of quantitative agreement in the former case could be attributed to the range, depth, and possibly shape of the inter-nucleon potential chosen by Buckingham and Massey especially since their *S*-wave phases, which they found to be insensitive to force-type, are not in satisfactory agreement with the experimental results of slow neutron scattering.

INTRODUCTION

A PAPER by Wantuch appeared recently in which experimental results were reported for the absolute values of the differential cross sections for 4.5- and 5.5-Mev neutrons scattered from deuterons.[1] A comparison was made therein of these experimental data and the theoretical calculations of Buckingham and Massey,[2] with the following conclusions. The values of the total cross section, obtained by extrapolation, definitely preferred the symmetric force theory. The actual angular distributions, however, did not agree well with either the symmetric or neutral force theory, but, on the other hand, the ratio $\sigma(\pi)/\sigma(\theta)$ definitely preferred the neutral force theory. Very much the same sort of contradictory conclusions have been drawn by others from the results of *n-d* scattering experiments at low energies.[3-5]

Rosenfeld has stated that the agreement between the variation of the experimental *n-d* total cross sections with energy and that predicted by the symmetric force theory calculations of Buckingham and Massey provides the "weightiest argument" in favor of this type of interaction.[6] Since Buckingham and Massey have considered only the *S*- and *P*-wave phase shifts in their calculations, the above mentioned discrepancies might possibly be accounted for by the presence of small *D*-wave phases which would deform the angular distributions to an appreciable extent only near $\theta=\pi$ or 0 while the total cross-section values would be effectively unchanged. The present paper is the result of an investigation into this possibility, carried out in the hope of clarifying the situation.

A more exhaustive treatment has been given to Wantuch's experimental data in order that an effective comparison could be made with the theoretical calculations of Buckingham and Massey. First, a least-square fit of the data to expansions in $\cos\theta$ revealed the presence of small *D*-wave phases and provided a reliable extrapolation of these data for calculating the corresponding total cross sections. Second, an attempt has been made to find the actual values of the experimental *S*- and *P*-phase shifts from the coefficients in these expansions in order that a more direct comparison with the theoretical calculations could thereby be effected. Finally, a more reliable method has been employed for interpolating the calculated values given by Buckingham and Massey for these phase shifts to the energies involved in the experiment.

The following notation was adopted.

$\sigma(\theta)$: differential scattering cross section as a function of θ, the neutron scattering angle in the center-of-mass system.

* Present address: Los Alamos Scientific Laboratory, Los Alamos, New Mexico.

[1] E. Wantuch, Phys. Rev. **84**, 169 (1951). The data used here were obtained from his thesis, New York University, 1950.

[2] R. A. Buckingham and H. S. W. Massey, Proc. Roy. Soc. (London) **A179**, 123 (1941). Their force-types I and III are referred to here as neutral (or "0") and symmetric (or "*X*"), respectively (see reference 3).

[3] L. Rosenfeld, *Nuclear Forces* (Interscience Publications, New York, 1948), Sec. 14.12.

[4] Martin, Burhop, Alcock, and Boyd, Proc. Phys. Soc. (London) **A63**, 884 (1940). See also discussion by R. A. Buckingham, which follows thereafter.

[5] Hamouda, Halter, and Scherrer, Phys. Rev. **79**, 539 (1950); and Helv. Phys. Acta **24**, 217 (1951); also, I. Hamouda and G. de Montmollin, Phys. Rev. **83**, 1277 (1951).

[6] See reference 3, p. 298.

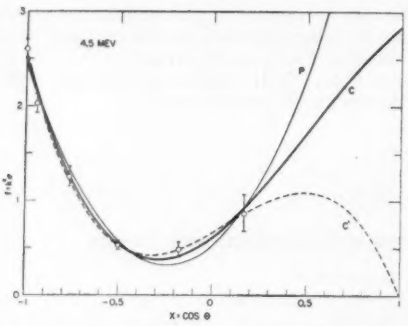

FIG. 1. Angular distribution ($f=k^2\sigma$ *versus* $x=\cos\theta$) for *n-d* scattering at 4.5 Mev. The small circles represent Wantuch's experimental points with which the associated vertical lines indicate the quoted limits of error. Curve *P* represents the best fit of a quadratic in x; curve C' represents the best fit of a cubic in x; and curve *C* represents the best fit of a cubic in x subject to the restriction that the resulting total cross section agree with an independently measured value.

E_{lab}: energy of incident neutron in laboratory system.

k: angular wave number in center-of-mass system; $k^2/E_{\text{lab}}=2.144$ Mev$^{-1}\cdot$barns^{-1}.

$f(x)=k^2\sigma(\theta)$: dimensionless form of the differential scattering cross section; $x=\cos\theta$.

$f_0=2\pi\int_{-1}^{+1}f(x)dx$: dimensionless form of corresponding total cross section.

δ_{ml}: scattering phase shift with $l=0, 1, 2, \cdots$ corresponding to *S*, *P*, *D*, $\cdots$ waves, respectively, and $m=2$ or 4 corresponding to doublet or quartet spin states, respectively.

$P_l(x)$: Legendre polynomial of degree l.

EXPANSION OF DIFFERENTIAL CROSS SECTIONS: *D*-WAVE EFFECTS

The differential cross section for *n-d* scattering in the center-of-mass system can be expressed in terms of the characteristic phases as follows:[7]

$$f(x)=\Sigma_m(m/6)\,|\,\Sigma_l(2l+1)P_l(x)(\sin\delta_{ml})\exp(i\delta_{ml})\,|^2. \quad (1)$$

Since H^3 exists in a ^2S ground state, in the central-force approximation, and has no other stable bound states, all the phases except δ_{20} (which approaches π) must approach zero as $k\to 0$. In fact, for $\delta_{ml}\neq\delta_{20}$,

$$\delta_{ml}\to C_{ml}k^{2l+1} \text{ as } k\to 0, \quad (2)$$

where C_{ml} is a constant. As k increases from zero, a particular phase shift δ_{ml} does not become significant until that value of k is reached for which

$$ka\approx l, \quad (3)$$

where a is the effective range of the *n-d* interaction.

Taking[8]

$$a\approx 5\times 10^{-13}\text{ cm}, \quad (4)$$

one then finds for $E_{\text{lab}}=5.5$ Mev,

$$ka\approx 1.72. \quad (5)$$

Hence, in accord with (3), we felt justified in taking $\delta_{ml}=0$ for $l\geqq 3$ at $E_{\text{lab}}=4.5$ and 5.5 Mev. Also, we anticipated that if *D*-wave effects are present, the δ_{m2} phases are small.

We first of all settled the question of whether *D*-wave effects are present at all in Wantuch's experimental data by investigating the consequence of assuming that they are not. Under this assumption $f(x)$, as given by Eq. (1), reduces to a second degree polynomial in x. The curves in Figs. 1 and 2 labeled *P* show, in each case, the best (least-square) fit to the given experimental points obtainable with a second degree polynomial. These curves pass reasonably close to the experimental points, but must be ruled out nevertheless, since the inordinately high values they give for $f(x>0.5)$ are completely incompatible with independently measured total cross-section values (see below). Hence, we felt assured that *D*-wave effects, though small, are indeed significantly present.

Next we considered the possibility that *D*-wave effects are present only to such an extent that all but first-order dependence on δ_{m2} can be neglected in Eq. (1). In this case, Eq. (1) reduces to a cubic in x:

$$f(x)=b_0+b_1x+b_2x^2+b_3x^3. \quad (6)$$

The curve in Fig. 1 (4.5 Mev) labeled C' and that in Fig. 2 (5.5 Mev) labeled *C* show, in each case, the best (least-square) fit of the $f(x)$ given by (6) to the experimental points. These curves pass within or close to the limits of error quoted for the experimental points—adjacent high and low values compensating for each other. In the 4.5-Mev case, however, this straight least-square fit with the cubic polynomial gives a spurious result: Although the curve C' gives an excellent fit to the experimental points, it turns over in the range ($\theta<80°$) in which no experimental readings were obtained and falls rapidly to slightly below zero at $\theta=0$.

A check on the curves determined in this manner was made by comparing the value of the total cross section, as computed from the polynomial coefficients in each case, with an independent experimental determination of this quantity. It follows from Eq. (6) that

$$f_0=4\pi(b_0+b_2/3). \quad (7)$$

Upon substituting the values of b_0 and b_2 determined by the above curve-fitting procedure, we obtained

$$f_0=10.8, \text{ for } E_{\text{lab}}=4.5 \text{ Mev}; \quad (8a)$$

$$f_0=17.9, \text{ for } E_{\text{lab}}=5.5 \text{ Mev}. \quad (8b)$$

From experimental data on total *n-d* scattering cross

[7] N. F. Mott and H. S. W. Massey, *Theory of Atomic Collisions* (Clarendon Press, Oxford, 1949), second edition, Chapter II.

[8] H. A. Bethe, Revs. Modern Phys. **9** (1937), Sec. 73A.

sections obtained by Nuckolls *et al.*,[9] we found that

$$f_0=16.3\pm0.5, \text{ for } E_{\text{lab}}=4.5 \text{ Mev}; \quad (9a)$$

$$f_0=17.9\pm0.9, \text{ for } E_{\text{lab}}=5.5 \text{ Mev}. \quad (9b)$$

Although the agreement between (8a) and (9a) is poor, the excellent agreement between (8b) and (9b) indicates that a cubic polynomial in x gives an adequate representation of the differential cross section for all θ at $E_{\text{lab}}=5.5$ Mev. Moreover, since D-wave effects should increase here with increasing energy, we concluded that Eq. (6) must also provide an adequate representation of the experimental $f(x)$ at $E_{\text{lab}}=4.5$ Mev, i.e., the assumption that higher order terms in δ_{m2} can be neglected at these energies is justified so far as the given experimental data are concerned.

In view of this conclusion and the anomalous behavior of the curve C' in Fig. 1 for $E_{\text{lab}}=4.5$ Mev, $f(x)$ given by (6) was next fitted to the data at this energy by means of a modified least-square procedure which gave the best fit subject to the restriction that the total cross section calculated from the resulting coefficients via (7) must agree exactly with the independently determined value given by (9a) above (i.e., $f_0=16.3$)—such a procedure being consistent with the results obtained above for 5.5 Mev. The resulting curve is C of Fig. 1. This curve gives a good fit to the experimental points and, accordingly, it was adopted to represent the experimental data at $E_{\text{lab}}=4.5$ Mev.

The values of the b coefficients in Eq. (6) determined, in each case, by the above procedures are

$$b_0=0.608;\ b_1=1.503;\ b_2=2.067;\ b_3=-1.337; \quad (10a)$$

$$b_0=0.746;\ b_1=1.752;\ b_2=2.024;\ b_3=-1.701; \quad (10b)$$

at $E_{\text{lab}}=4.5$ and 5.5 Mev, respectively. These coefficients have the following significance in terms of the phase shifts δ_{20}, δ_{40}, δ_{21}, δ_{41}, δ_{22}, δ_{42} as derived from Eq. (1).

$$b_0=\tfrac{1}{5}(\sin^2\delta_{20}+2\sin^2\delta_{40})-(5/3)(\delta_{22}\sin\delta_{20}\cos\delta_{20}+2\delta_{42}\sin\delta_{40}\cos\delta_{40}); \quad (11a)$$

$$b_1=2[\sin\delta_{20}\sin\delta_{21}\cos(\delta_{20}-\delta_{21})+2\sin\delta_{40}\sin\delta_{41}\cos(\delta_{40}-\delta_{41})]-5(\delta_{22}\sin\delta_{21}\cos\delta_{21}+2\delta_{42}\sin\delta_{41}\cos\delta_{41}); \quad (11b)$$

$$b_2=3(\sin^2\delta_{21}+2\sin^2\delta_{41})+5(\delta_{22}\sin\delta_{20}\cos\delta_{20}+2\delta_{42}\sin\delta_{40}\cos\delta_{40}); \quad (11c)$$

$$b_3=15(\delta_{22}\sin\delta_{21}\cos\delta_{21}+2\delta_{42}\sin\delta_{41}\cos\delta_{41}). \quad (11d)$$

Since we have found D-wave effects to be significant, though small, in the experimental data considered here, a comparison cannot be made between these data and the calculations of Buckingham and Massey, which include only S- and P-phase shifts, unless some procedure is developed which will lead to an evaluation of the distortion of the angular distributions produced by these D-wave effects. It should be noted that D-wave effects (and perhaps those of higher angular momentum) may be more significant at these energies than the foregoing results indicate, but that the experimental data, as presented, reveal no more.

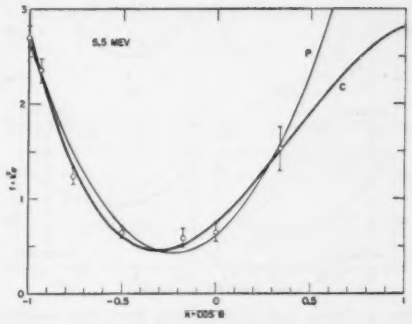

FIG. 2. Same as Fig. 1, for n-d scattering at 5.5 Mev. Curves C and C' coincide in this case.

EVALUATION OF PHASE SHIFTS

Since the results of the Buckingham and Massey calculations are expressed in terms of the phases they obtained (for the various types of interactions), the most decisive way in which a comparison could be made between their calculations and the experimental data would be to deduce a corresponding set of these phases directly from the data. It is obvious, however, that this is not possible by any straightforward procedure in our situation since, all other difficulties aside, there are six unknown phases altogether at each energy and Eqs. (10) and (11) provide for only four experimentally determined relationships between them.

We were interested at the time only in making a valid comparison of the experimental data with the theoretical work of Buckingham and Massey such that it might be possible to determine whether the data favors their calculations for a neutral or symmetric type of interaction. In the course of their calculations, Buckingham and Massey found that, independent of the force-type considered, the following equation is approximately valid:

$$\delta_{20}=\pi+\delta_{40}. \quad (12)$$

We made use of this equation to provide a fifth relationship between the six phases since it did not predispose our results in favor of either force-type. The question of a sixth relationship was left open at this point.

We chose δ_{20} as the independent variable and expressed the remaining phases in terms of it. Upon eliminating δ_{22} and δ_{42} from Eqs. (11) and making use of Eq. (12), the following simple relationships were

[9] Nuckolls, Bailey, Bennett, Bergstralh, Richards, and Williams, Phys. Rev. **70**, 805 (1946).

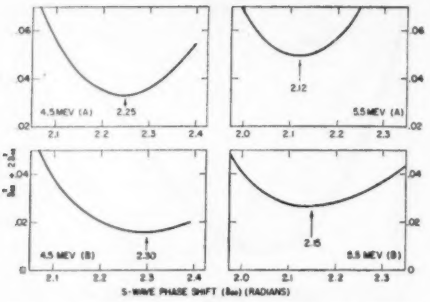

FIG. 3. Curves used in determining (from their minima) a unique value for δ_{20}. $(\delta_{22}^2+2\delta_{42}^2)$ is shown as a function of δ_{20}: the left-hand and right-hand curves correspond to 4.5 and 5.5 Mev, respectively; the upper and lower curves correspond to sets A and B of phases, respectively.

found between δ_{21}, δ_{41}, δ_{20}:

$$\sin 2\delta_{21}+2\sin 2\delta_{41}=C(\delta_{20}); \tag{13a}$$

$$\cos 2\delta_{21}+2\cos 2\delta_{41}=S(\delta_{20}); \tag{13b}$$

where

$$S(\delta_{20})=2(2-b_0-b_2/3)-\cos 2\delta_{20};$$

$$C(\delta_{20})=2(1-b_0+b_1-b_2/3-b_3/3)\csc 2\delta_{20}$$
$$-2(1-b_0-b_2/3)\cot 2\delta_{20}-\sin 2\delta_{20}.$$

The D-wave phases were expressed as functions of δ_{20} by means of the following relationships:

$$(\sin 2\delta_{20})\delta_{22}+2(\sin 2\delta_{20})\delta_{42}=(6/5)(\sin^2\delta_{20}-b_0); \tag{14a}$$

$$(\sin 2\delta_{21})\delta_{22}+2(\sin 2\delta_{41})\delta_{42}=(2/15)b_3; \tag{14b}$$

with δ_{21} and δ_{41} replaced by their values obtained from Eqs. (13). The above equations do not produce a one-to-one correspondence between a given value of δ_{20} and the resulting values of δ_{21}, δ_{41}, δ_{22}, δ_{42}. This multiple-valuedness is partially restricted, however, by the requirement that the absolute value of these latter phases must lie in the first quadrant. As a result, we obtained only two different sets of values for δ_{21}, δ_{41}, δ_{22}, δ_{42} which were consistent with a given value of δ_{20} in the range of δ_{20} values considered. These two sets of values were designated as set A and set B.

The two sets of P and D phases were calculated for values of δ_{20} between 1.8 and 2.4 radians (at intervals of 0.05 radian). Outside these limits, one or more of the resulting D-wave phases became too large to be considered possible. The values of δ_{20} were chosen to lie in the second quadrant since δ_{20} must approach π as $k\to 0$ and decrease as k increases.

Now the coefficient of the term in x^4 of Eq. (1) is

$$b_4=(75/4)(\sin^2\delta_{22}+2\sin^2\delta_{42})\to(75/4)(\delta_{22}^2+2\delta_{42}^2). \tag{15}$$

This term cannot be zero, of course, unless $\delta_{22}=\delta_{42}=0$. The results of the previous section, however, lead to the conclusion that the contribution of this term to the given differential and total cross sections must be negligible in comparison to that of the other term considered. As a result, it was decided to minimize the contribution of this term—thus providing a sixth relationship between the "experimental" phases. In Fig. 3 are shown the graphs of $(\delta_{22}^2+2\delta_{42}^2)$ as a function of δ_{20}, as deduced from the calculations described above, and the value of δ_{20} selected from the minimum in each case.

This minimization procedure can be justified in our case by a consideration of the magnitude of $(\delta_{22}^2+2\delta_{42}^2)$ over the range of δ_{20} values (Fig. 3). The contribution to the total cross section of the term in x^4 is

$$\Delta f_0=15\pi(\delta_{22}^2+2\delta_{42}^2). \tag{16}$$

At the minima of the curves in Fig. 3, this was found to have the following values:

$$4.5\text{ Mev}:\ (A),\ \Delta f_0=1.6;\ \ (B),\ \Delta f_0=0.8; \tag{17a}$$

$$5.5\text{ Mev}:\ (A)\ \Delta f_0=2.3;\ \ (B),\ \Delta f_0=1.3. \tag{17b}$$

In neither case are these values less than the experimental uncertainties in f_0 given in Eqs. (9a), (9b)—indicating, therefore, the validity of the minimization procedure. As a further check, the coefficient (15) of the term in x^4 was determined by a perturbation method in which the difference between the nominal values of the experimental points and the corresponding points of the curves C of Figs. 1 and 2 was fitted by a least-square procedure to the function b_4x^4. This gave the following values of $(\delta_{22}^2+2\delta_{42}^2)$:

$$4.5\text{ Mev}:\ 0.0002;\ \ 5.5\text{ Mev};\ \ 0.0002. \tag{18}$$

Both values are much lower than the corresponding minima of Fig. 3—hence, the minimization procedure is again indicated.

The sets A and B of phase shifts values are shown in Table I as they were determined from the foregoing analysis, in accordance with the given experimental data and the theoretical relationship (12). It should be emphasized that these results have a limited applicability, inasmuch as they depend on Eq. (12), except in a comparison of the experimental data with the calculations of Buckingham and Massey.

As indicated above, neither of the two sets A and B of phases can be ruled out on the basis of the given information, so that there is a resulting lack of uniqueness in this phase shift analysis. A possible procedure for removing this ambiguity is to rule out set B on the basis of the results of Buckingham and Massey which show that δ_{41} is positive regardless of the force-type

TABLE I. The two possible sets (A and B) of phase shift values as derived from the experimental data and Eq. (12).

Set	E_{lab}	δ_{20}	δ_{21}	δ_{22}	δ_{40}	δ_{41}	δ_{42}
A	4.5 Mev	2.25	−0.95	0.15	−0.89	0.12	−0.08
A	5.5 Mev	2.12	−0.94	0.19	−1.02	0.15	−0.08
B	4.5 Mev	2.30	0.71	−0.08	−0.84	−0.41	0.07
B	5.5 Mev	2.15	0.73	−0.11	−0.99	−0.38	0.08

considered. This procedure was used by Critchfield in his phase shift analysis of low energy p-d scattering.[10]

COMPARISON WITH THEORY AND CONCLUSIONS

Buckingham and Massey have calculated the values of the S and P phases for n-d scattering at energies corresponding to $k=2$, 4, and $5\times(10^{-12}\text{ cm})^{-1}$ for both a neutral and symmetric type of inter-nucleon interaction. In order to interpolate their results to the experimental energy values, we made use of the following expansions for these phases:[11]

$$k\cot\delta_{20}=-1/a_2+\beta_2k^2; \tag{19}$$

$$k^3\cot\delta_{21}=A_2+B_2k^2+C_2k^4; \tag{20a}$$

$$k^3\cot\delta_{41}=A_4+B_4k^2+C_4k^4. \tag{20b}$$

The best (least-square) fit of their calculated S phases

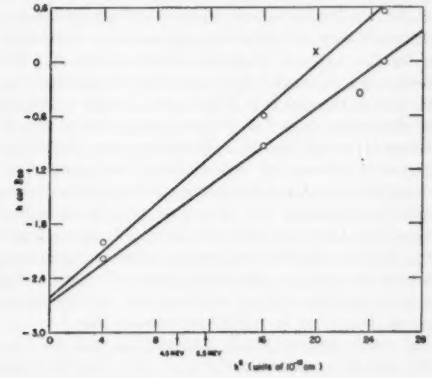

FIG. 4. Variation of (doublet) S-wave phase with energy: $k\cot\delta_{20}$ as a function of k^2 (using 10^{-12} cm as length unit). Small circles represent points calculated by Buckingham and Massey for a neutral (curve labeled O) and a symmetric (curve labeled X) type of interaction. See Eq. (19).

to Eq. (19) with $k\cot\delta_{20}$ plotted as a function of k^2 is shown in Fig. 4. The calculated points fall very close to the straight line so determined in each case. The values of the constants in Eq. (19) for each type of interaction turn out to be:

$$\text{Neutral:}\quad a_2=0.374;\quad \beta_2=0.108; \tag{21a}$$

$$\text{Symmetric:}\quad a_2=0.381;\quad \beta_2=0.129; \tag{21b}$$

using 10^{-12} cm as a unit of length.

The P-wave phases, as determined from Eq. (20)

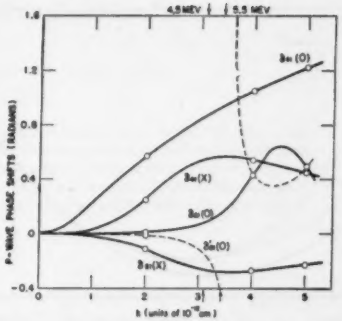

FIG. 5. Variation of P-wave phases with energy: graphs of Eqs. (20a), (20b) as fitted to points (indicated by small circles) calculated by Buckingham and Massey. Reading from top to bottom: $\delta_{41}(O)$, $\delta_{41}(X)$, $\delta_{21}(O)$, $\delta_{21}'(O)$, $\delta_{21}(X)$. The letters O and X respectively stand for the neutral and symmetric types of interaction.

and the calculated values, are graphed as functions of k in Fig. 5. Two curves are shown for δ_{21} in the neutral (O) interaction case. The broken line curve is that which was obtained by taking the Buckingham and Massey calculated values exactly as given. This curve exhibits an anomalous behavior, however—the upper, right-hand branch approaches π as $k\to0$—and was consequently ruled out here. The other curve, the one adopted for use here, was obtained by replacing their given value of -0.01 radian by $+0.01$ radian at $k=2\times(10^{-12}\text{ cm})^{-1}$. This value was rather arbitrarily chosen as being the nearest adjacent positive value proceeding in steps of 0.01 radian—a simple means of starting the curve off in the right direction.[12] The constants in Eq. (20) determined in this way for the two types of interactions are:

Neutral:

$$A_2=1220;\quad B_2=-117;\quad C_2=3.09; \tag{22a}$$

$$A_4=1.31;\quad B_4=2.98;\quad C_4=-0.05; \tag{22b}$$

TABLE II. Values of the S and P phase shifts interpolated from the theoretical calculations of Buckingham and Massey for neutral and symmetric types of interactions, together with the corresponding "experimental" values from Table I.

$E_{lab}=4.5$ Mev	δ_{20}	δ_{21}	δ_{41}
Neutral	2.07	0.08	0.86
Symmetric	1.99	−0.26	0.55
A	2.25	−0.95	0.12
B	2.30	0.71	−0.41
$E_{lab}=5.5$ Mev	δ_{20}	δ_{21}	δ_{41}
Neutral	1.96	0.15	0.94
Symmetric	1.88	−0.27	0.57
A	2.12	−0.94	0.15
B	2.15	0.73	−0.38

[10] C. L. Critchfield, Phys. Rev. **73**, 1 (1948).

[11] The derivation of these relationships, which will be omitted here, follows directly from the integro-differential equations used by Buckinham and Massey according to methods which are similar to those devised for obtaining the corresponding relationships for the n-p case by: H. A. Bethe, Phys. Rev. **76**, 38 (1949); G. F. Chew and M. L. Goldberger, Phys. Rev. **75**, 1637 (1949). The relationship (19) has also been derived by: A. Troesch and M. Verde, Helv. Phys. Acta **24**, 39 (1951).

[12] This does not imply that a negative value is necessarily incorrect—it may well be that more terms in the expansion (20a) are necessary to give a detailed description of the variation of δ_{21} with energy in this case.

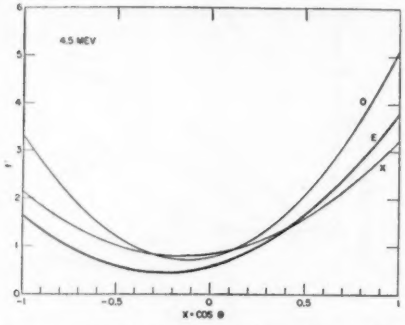

FIG. 6. Angular distribution for n-d scattering at 4.5 Mev ($f=k^2\sigma$ *versus* $x=\cos\theta$) obtained from phases in Table II alone: curve E represents experimental data minus D-wave effects; curves O and X represent calculations of Buckingham and Massey for a neutral and symmetric type of interaction, respectively.

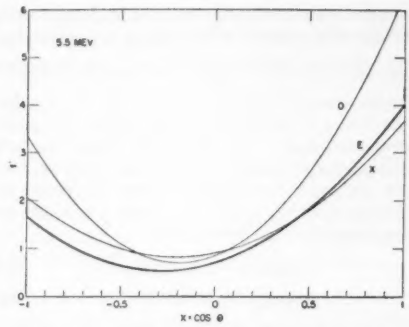

FIG. 7. Same as Fig. 6, for n-d scattering at 5.5 Mev.

Symmetric:

$$A_2=-81.6;\quad B_2=6.18;\quad C_2=-0.97; \tag{23a}$$

$$A_4=38.5;\quad B_4=-3.80;\quad C_4=0.50; \tag{23b}$$

with 10^{-12} cm as a unit of length.

The values of the Buckingham and Massey phases interpolated to 4.5 and 5.5 Mev by the use of Eqs. (19) and (20) with the constants of (21), (22), (23) are given in Table II together with the corresponding "experimental" phases from Table I. It is apparent from Table II that no possible agreement exists between either of the sets A and B of "experimental" P-wave phases and the corresponding calculated values for a neutral type of interaction. On the other hand, there is a qualitative agreement between the set A of "experimental" phases and the values calculated for a symmetric type of interaction. The lack of quantitative agreement in the latter case could be attributed to the range, depth, and possibly shape of the inter-nucleon potential chosen by Buckingham and Massey (see below).

It is instructive to compare the angular distributions which are obtained from the sets of S and P phases in Table II alone. Such a procedure, in effect, is a comparison of the theoretical calculations with the experimental angular distributions *minus* the D-wave contributions. The resulting curves are shown in Figs. 6 and 7. The sets A and B of phases in Table II produce essentially the same angular distributions for a given energy since δ_{20} is nearly the same for both—hence, only one curve representing the experimental data is shown for each energy. From these curves it is apparent that the experimental angular distributions minus D-wave effects definitely prefer the theoretical curves obtained from the symmetric type of interaction. Thus, the discrepancies which were found by Wantuch between his experimental angular distributions and those predicted by the Buckingham and Massey calculations for a symmetric type of interaction can indeed be accounted for by the presence of small D-wave effects. On the other hand, it should be noted that the general appearance of the curves in Figs. 6 and 7 tends to belittle the discrepancies in the P-wave phases found above. Moreover, these curves indicate how the qualitative agreement between the "experimental" and symmetric-interaction-calculated phases can produce a quantitative agreement between the resulting total cross-section values (i.e., the areas under the curves). It seems, therefore, that if a decisive comparison between experiment and theory is to be obtained by means of n-d scattering at low energies, a phase shift analysis of the experimental data must be carried out in each case.

In conclusion, we should like to point out that Eq. (19) and its counterpart for δ_{40}, taken together with Eq. (12), requires, in particular, that the doublet and quartet scattering lengths of the deuteron (a_2 and a_4) must be approximately equal, independent of the force-type considered. Now the experimental evidence from slow-neutron scattering reveals that:[13] $a_2=0.83\times10^{-12}$ cm and $a_4=0.24\times10^{-12}$ cm so that the validity of Eq. (12) cannot be taken too seriously. Insensitive as it is to the force-type considered, this result strongly suggests that in future calculations the form (i.e., range, depth, and shape) of the inter-nucleon potential used by Buckingham and Massey should be modified.[14] One may then find (upon analyzing the experimental phases anew) that a symmetric interaction can produce still better agreement with the experimental P-wave phases than that found above.

[13] Wollan, Shull, and Koehler, Phys. Rev. **83**, 700 (1951). In addition, compare this value of a_2 with those given in (21).

[14] In support of which, we note that A. Troesch and M. Verde (see reference 11), using a Gauss potential of 45-Mev depth and 1.9×10^{-12} cm range, found (in units of 10^{-12} cm): $(a_2, a_4)=(0.68, 0.28)$ and $(0.70, 0.32)$ for the neutral and symmetric interactions, respectively.

Particle Counting by Čerenkov Radiation*

JOHN MARSHALL
Institute for Nuclear Studies, University of Chicago, Chicago, Illinois
(Received January 25, 1952)

Čerenkov radiation particle counters of a number of types are in satisfactory use in this laboratory for the counting of high energy mesons, electrons, and protons. The problems associated with Čerenkov counting and some of the uses are discussed together with the design and performance of several types of counters. The uses include high energy electron counting with the exclusion of neutrons and protons, measurement of the velocity of mesons, and the detection of high energy neutrons in the presence of lower energy neutrons by the Čerenkov threshold counting of recoil protons.

(1) INTRODUCTION

THE Čerenkov radiation has been suggested as a means of counting fast charged particles by Getting[1] and by Dicke.[2] Recently, Jelley[3] has succeeded in showing that a photomultiplier can be made to count pulses of light coming from the Čerenkov radiation produced when cosmic-ray particles traverse water. Mather[4] has demonstrated that Čerenkov radiation is emitted when 340-Mev protons pass through suitable materials and has used it to measure accurately the energy of the deflected proton beam of the Berkeley 184-inch synchrocyclotron. The writer[5] has reported the operation of a Čerenkov counter with electrons produced by the 50-Mev bremsstrahlung beam of a betatron. The present paper is a discussion of the problems and techniques of Čerenkov counting with particular emphasis on the types of counters in use at the University of Chicago for the counting of particles produced by the 450-Mev proton synchrocyclotron. For a bibliography of the Čerenkov radiation itself the reader is referred to the papers of Getting, Dicke, and Mather.

(2) THE ČERENKOV RADIATION

The Čerenkov radiation may be considered to be an electromagnetic shock wave and is analogous to the shock wave produced when a projectile travels through air at a speed greater than that of sound. Like the pressure shock wave, the Čerenkov wave is conical with the apex of the cone coincident with the particle producing the disturbance. The radiation is produced when any charged particle traverses a dielectric medium at a speed greater than that of light in the medium. The direction of the radiation is forward at an angle θ from the direction of the particle, where θ is determined by the relation

$$\cos\theta = 1/\beta n; \qquad (1)$$

here n is the index of refraction of the dielectric medium. It is easy to derive relation (1) from Huygens' principle as illustrated in Fig. 1.

Since the Čerenkov radiation is a shock wave, it contains components of all frequencies for which the index of refraction is large enough to give a real value of θ in Eq. (1). In ordinary optical materials the radiation includes the visible spectrum with energy flux larger toward the violet end. It may be observed visually when, for example, a strong source of reasonably energetic beta-radiation is immersed in water and has a bluish white appearance to the eye. The intensity and spectral distribution are given by the relation

$$I = \frac{4\pi^2 e^2}{hc^2}\Delta\nu\left\{1-\frac{1}{\beta^2 n^2}\right\} = \frac{2\pi\Delta\nu}{137c}\sin^2\theta. \qquad (2)$$

Here I is the number of photons emitted per centimeter of path, $\Delta\nu$ is the frequency interval in cycles per second, and β is the ratio of the speed of the particle to that of light in vacuum. The index of refraction is considered to be constant over the frequency range $\Delta\nu$ of the emitted

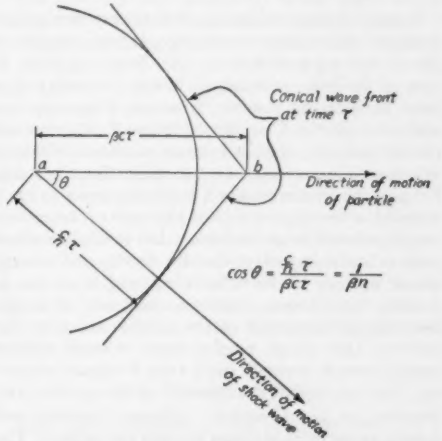

FIG. 1. Construction of Čerenkov wave front by Huygens' principle. Position of particle at time $0\cdots a$; position of particle at time $\tau\cdots b$; distance traversed by particle in time $\tau\cdots\beta c\tau$; distance traversed by light in time $\tau\cdots(c/n)\tau$.

* This work was supported by the joint program of the ONR and AEC.

[1] I. A. Getting, Phys. Rev. **71**, 123 (1947).
[2] R. H. Dicke, Phys. Rev. **71**, 737 (1947).
[3] J. V. Jelley, Proc. Phys. Soc. (London) **A64**, 82 (1951).
[4] R. L. Mather, Phys. Rev. **84**, 181 (1951).
[5] J. Marshall, Phys. Rev. **81**, 275 (1951).

light. The angle θ is the Čerenkov angle as in Eq. (1). It should be noted that the intensity is a function of the Čerenkov angle alone.

The visible spectrum covers a frequency interval of approximately 3×10^{14} cycles. If one assumes this value for $\Delta\nu$, Eq. (2) gives the intensity of the Čerenkov radiation to be $450\sin^2\theta$-photons per centimeter of particle path. As a numerical example electrons traveling essentially at the speed of light through glass with an index of refraction of 1.50 emit Čerenkov radiation with an intensity of 250 photons per centimeter in the visible spectrum.

The Čerenkov radiation is plane polarized with its electric vector in the radial direction. In other words, the electric vector lies parallel to the shock wave front and points toward or away from the particle responsible for the radiation.

In a dispersionless medium the Čerenkov radiation would remain a mathematically sharp wave front as it moved away from the path of the particle. In all actual mediums it degenerates into a wave packet, the various frequency components of which are transmitted with varying speeds and directions dependent on the values of the index of refraction for those frequencies.

(3) SCINTILLATION COUNTING WITH THE ČERENKOV RADIATION

The Čerenkov radiation can be used as a source of light for scintillation counting. As such it has certain attractive features, but in some ways its properties introduce problems. In this section some of these problems and features will be discussed.

(3a) Choice of Radiator Material

In principle one may use as a radiator any transparent material whose index of refraction is large enough to give a real value of θ in Eq. (1). From the point of view of intensity, it is helpful to use a material of as large an index as possible. However, frequently one wishes to use the Čerenkov radiation to discriminate through intensity or angle between particles of different velocities, and one may not want a high refractive index. For angular discrimination it is advantageous to use a material of low dispersion, and high index is frequently associated with large dispersion. For measurements of angle it is also important that the density and average atomic number of the radiator material be as low as possible. Low density implies a small rate of energy loss through ionization as the particle traverses the radiator. Low atomic number leads to small angular spread through multiple small angle Coulomb scattering. This means that the direction of the particle, and therefore of the Čerenkov radiation, remains well defined as the particle passes through the radiator. The material should have as wide a frequency band of essentially perfect transparency as possible. It should emit no light by phosphorescence or fluorescence, and finally, it should be easily shaped into simple optical parts.

There are liquids that satisfy quite well most of the conditions of the last paragraph, but if one includes the last one, namely that the material be easily fabricated, the best material by far is methyl methacrylate polymer, better known under the trade names of Lucite and Plexiglas. The writer has no reliable information to indicate that there is any difference between the two brands, and they have been used interchangeably in the work reported here. However, there certainly are differences in the light absorption in the violet and ultraviolet from one piece to another supplied by the same manufacturer. Through the kindness of Dr. J. R. Platt of the Physics Department, spectrophotometer transmission curves were obtained for two chance samples of Lucite. These two samples within the errors of the measurement were perfectly transparent in the visible but absorbed light by different amounts in the ultraviolet. The light absorption appears to be a result of the same substance because of the similarity of the two absorption curves, but the substance must be present in the two samples in different concentrations. Since the near ultraviolet is quite an important part of the sensitivity spectrum of most photomultipliers, one should be careful to select good pieces of plastic for radiators. Above all, one should avoid material, such as is sometimes found, which shows a yellow tint to light transmitted through large thicknesses.

Lucite and Plexiglas have been the radiator material used for most of the work reported in this paper. For simplicity of nomenclature both materials will be called Lucite from here on, although in about half the cases the material actually used was Plexiglas.

The rather meager published information and the very rough measurements made in this laboratory indicate a working value for the index of refraction of Lucite of 1.50. The dispersion seems to be slightly smaller than that of most glasses, the index increasing by 0.01, for one sample between about 5850 and 4400 angstrom units. The value of the index varies slightly from one sample to another and sometimes has significant variations inside the same piece. Inhomogeneities of this kind may be found by looking lengthwise through a rod or edgewise through a sheet of the material. Under these conditions image distortion by refraction or total reflection is a sufficiently sensitive test of the optical homogeneity of the piece for most purposes.

(3b) Intensity

Much lower intensities are available from the Čerenkov radiation than from comparable thicknesses of the usual phosphors. A quantitative evaluation of the intensity problem must include the characteristics of the photomultiplier tubes used to detect the light. For this reason there are plotted in Fig. 2 the sensitivity curves for three of the types of multipliers employed

for Čerenkov counting by the writer. The data for these curves were taken from material published by the manufacturer.[8] They are replotted in a way which is particularly adapted to the problems of Čerenkov counting. The number of electrons emitted by the cathode per photon incident thereon is plotted for each tube against the frequency of the light. It must be remembered in using these curves that there are violent variations from one tube to another of the same type, but in general shape and approximate magnitude these curves may represent some sort of average tubes.

For each of the three multiplier types there is plotted in Fig. 2 a cathode sensitivity curve for light passed through two inches of Lucite as well as the sensitivity curve for the bare tube. The transmission data used for Lucite (see Sec. 3a) apply to one chance sample, but give a rough idea of the effects involved. The sensitivity curves have been plotted with the assumption that there is no light loss from reflection as the light leaves the Lucite.

Inspection of Fig. 2 shows that, for the light frequency of maximum response, the cathode sensitivity of the 5819 is about 0.065 electron per incident photon, and that the sensitivities of the other tubes are not different from this by a great deal. A rough integration of the 5819 curve for light filtered through Lucite indicates that for the purpose of computing Čerenkov counting efficiency, one can consider the sensitivity to be constant at its maximum value over a band width of 2.9×10^{14} cycles. For the example of Sec. 2 of a highly relativistic particle traversing a medium of refractive index 1.5 (Lucite), one gets from Eq. (2) an effective intensity for this band width of 242 photons per centimeter of particle path. When multiplied by the cathode sensitivity, this figure gives the over-all sensitivity as 15.7 electrons from the cathode per centimeter of path of the particle through the radiator. The assumption is made that all of the light can be brought onto the multiplier cathode. The comparable figures for the 931A and the 1P28 are 12.0 and 12.4 electrons per centimeter.

Although the three photomultiplier types included in Fig. 2 appear to be almost equal in sensitivity, there is one important difference between the 5819 and the other two which makes the 5819 more efficient. The difference is that the 5819 has its photocathode deposited directly on the inside of the glass envelope while those of the others are internal and have only a small area of maximum sensitivity. The result is that the assumption, that all the light in the sense of the data of Fig. 2 can be made to strike the photocathode, can be realized in the 5819 and can even, in effect, be improved upon by making good optical contact between the radiator and the envelope. In the cases of the 931A and the 1P28 the condition can be realized approximately only by rather exact focusing of the light onto

[8] RCA Tube Handbook.

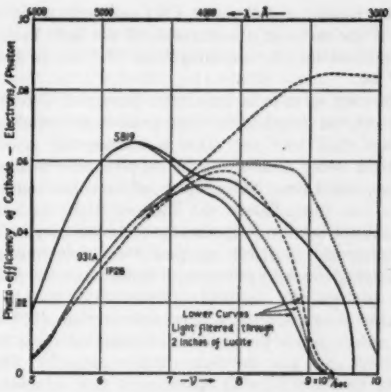

FIG. 2. Cathode efficiency curves for photomultipliers. These curves are computed from data published by the manufacturer. Upper curves represent number of electrons emitted by the photocathode of each tube type for one photon of the indicated frequency incident on its sensitive region. Lower curves are the same thing for light that has been passed through two inches of Lucite. Assumed no light loss from reflection at surface of Lucite.

the cathode through the Lucite and glass surfaces, each of which reflects some light. There is another advantage to the 5819, which is that more of its sensitive range is in the visible than is the case with the other types. This means that there is not so much effect from variations of ultraviolet absorption in the radiator, so that reasonable efficiencies should be realizable with any material which looks perfectly transparent and colorless to the eye.

The intensity and sensitivity figures given above indicate that it should be possible to achieve practically 100 percent counting efficiency with Čerenkov counters if the particles counted are penetrating and of the appropriate velocities. For counting applications it is necessary, of course, to discriminate against noise pulses generated by the photomultiplier. Amplitude discrimination is possible sometimes with large pulses of light and with good tubes, but almost always one runs the risk of losing some of the Čerenkov pulses which happen to be smaller than the ordinary. A more satisfactory method of discrimination is the use of fast coincidences, either between two tubes exposed to light from a common radiator or between a tube exposed to the Čerenkov radiation and one exposed to light from a phosphor or another radiator through which the same particle passes.

(3c) Duration of Pulse

The time of emission of the Čerenkov radiation is vanishingly small for practical purposes. This does not imply, of course, that the light pulse arriving at the photocathode of the multiplier tube in a counter will be instantaneous. Depending on what type of optical

system is used to collect the light and perhaps on the size of the radiator, the duration of the light flash at the cathode may be anything from 10^{-11} sec to about 10^{-9} sec.

For what seem to be reasonable designs of Čerenkov counters, the length of the light pulse is almost always smaller than 10^{-9} sec. This is considerably shorter than the decay time of the fastest phosphors available at the present time. This property of Čerenkov counters gives one immediately the idea of high resolution coincidence counting experiments. The difficulty is that the presently available equipment for detecting and amplifying the light pulses is all slower than the pulse. No commercially available photomultiplier tube is capable of reproducing a pulse shorter than 10^{-9} sec, and unfortunately the fastest multipliers are those with the least gain and the least efficient cathodes. There might be some hope of operating a fast coincidence circuit directly from the output of a 5819 tube responding to a Čerenkov pulse, but the 5819 is a slow tube. The 1P28 is a faster tube, but with its small cathode area it is difficult to concentrate enough light there to produce a big output pulse.

Consider the example of an infinitesimally short 15-electron pulse from the cathode of a 1P28 or 931A. A pulse of this size corresponds to the collection of all the light from a little more than a centimeter of electron path in Lucite and is probably about as large a pulse as can be generated in these tubes by Čerenkov radiation because of cathode geometry. The output pulse size, assuming a current amplification of 10^6, will be 2.4×10^{-12} coulomb. If we assume for simplicity the not unreasonable output pulse length of 2.4×10^{-9} sec, this gives an output current of one milliampere or a pulse height into 200-ohms impedance of 0.2 volt. A pulse of this size is not large enough to operate dependably any fast coincidence circuit familiar to the writer. Ordinarily, then, one must expect to use some sort of amplifier to raise the pulse voltage by about a factor ten. The best amplifiers available at the present time have band widths of about 200 megacycles. With such a band width a pulse of the length mentioned above will be broadened a little bit more. In any case one sees that the limitation on shortness of pulse is in the associated equipment and not in the light source when one is using a Čerenkov counter.

It may be possible to do very high resolution coincidence work, even with comparatively slow photomultipliers and amplifiers, by some sort of artificial pulse sharpening or by a trick in the coincidence circuit like, for instance, the one described by Bay.[7] The limitation in this direction is in the first stages of the photomultiplier where some of the pulse broadening takes place and where the number of electrons is small. Statistical variations in the electron multiplication will cause a certain amount of jitter in the time of the maximum of the output pulse. The writer has not had occasion to try for resolving times any shorter than are required for background reduction, but there seems to be no fundamental reason why resolving times of 5×10^{-10} sec or shorter should not be achieved.

(3d) Direction of Radiation

The directional properties of the Čerenkov radiation can be used to great advantage in achieving efficient collection of the light onto a photomultiplier cathode. The property that is applicable in the simplest way is that the light is all emitted in the forward direction. Thus one can use, as Jelley[2] has done, a cylindrical container with specularly reflecting walls filled with a liquid radiator material. The multiplier cathode is used as one of the ends of the container. Particles are allowed to enter the radiator from the other end, and if the walls are good reflectors, practically all of the Čerenkov light will reach the cathode.

A somewhat more convenient construction is to use as a radiator a transparent solid such as Lucite. Total internal reflection is used to contain the light and to lead it to the cathode. Total reflection is more efficient than metallic reflection, but it must be used with a certain amount of caution since the angle of incidence necessary to insure total reflection must be larger than $\sin^{-1}(1/n)$. For a particle moving at the velocity of light, the cosine of the Čerenkov angle is $1/n$, so that some of the light striking the walls of a cylinder may not be totally reflected. Consider a particle moving at the velocity of light at the axis of a dielectric cylinder but not exactly parallel to it. For this case one-half of the Čerenkov radiation emitted will be above the angle of total internal reflection at the walls and one-half will be below. The efficiency of light collection for particles moving at the velocity of light may be expected to vary somewhat with the position of the particle in the cylindrical radiator, particles near the outside yielding a higher efficiency. This is because a particle moving off the axis produces radiation which strikes the walls, for the most part in planes of incidence not parallel to the axis. This light is more likely to be totally reflected because the angle of incidence at the boundary is larger.

When considering the internal reflection of the Čerenkov radiation, one should remember that the light is radially polarized. The polarization is such that when the radiation strikes a surface normal to the direction of the particle, the electric vector is in the plane of incidence. According to the Fresnel formulas for reflection and refraction at a dielectric boundary, light with this sense of plane polarization is almost totally transmitted over a range of angles of incidence near to the Brewster angle, which for an internal ray in Lucite is about 33°. This makes more efficient the escape of Čerenkov radiation from the end of a radiator and makes particularly attractive a method suggested by Bernardini[8] for discriminating in a nonfocusing

[7] Z. Bay, Phys. Rev. **83**, 242 (1951).

[8] G. Bernardini (private communication).

Čerenkov counter against highly relativistic particles (electrons). The method of Bernardini is to exclude the radiation from electrons by providing a narrow air gap at the end of the radiator. The Čerenkov radiation from electrons being at an angle greater than the critical angle should all be totally reflected at this gap while the light from, say, 100-Mev mesons can be transmitted. In fact, because of the polarization the transmission should be practically perfect.

The polarization properties discussed above are perfect only for a radiator so short that none of the light is reflected at the walls. The difficulty is that the radial plane polarization of the light is destroyed by total internal reflection. The phase shift, with total internal reflection, of the light polarized in the plane of incidence is different from that of the light polarized in the other plane. The result is that the plane polarized Čerenkov light becomes, in general, elliptically polarized, and the considerations of the last paragraph do not apply. The radiation from a particle traveling along the axis of a cylindrical radiator strikes the walls with its electric vector in the plane of incidence. This light retains its plane polarization, but most of the light from particles traveling at other radial positions is modified somewhat, the effect being larger for those particles that are farther from the axis.

For particles of appreciably lower velocity than that of light, total internal reflection is very efficient, and the cylindrical radiator method with a photomultiplier at one end is quite effective. Such a method is being used in this laboratory for the counting of high energy protons.

The directional properties of the radiation make it possible to count particles of some narrow band of velocities in the presence of and to the exclusion of particles of other velocities. This is possible because of the fact that the radiation is all emitted at the Čerenkov angle θ as in Eq. (1). If one is able to focus all or a substantial fraction of the light emitted at a given angle onto the cathode of a photomultiplier tube and to discard light emitted at other angles, one can make a counter having the characteristics described in the first sentence of this paragraph. A focusing method of this sort has been proposed by Getting,[4] and another one has been used by the writer.[5]

(3e) Applicability

Čerenkov counting can be used with high efficiency only for quite energetic particles. First of all, the particle must be moving faster than light in the medium used as a radiator. Not only must the particle have a high velocity, however, but it must be capable of traveling for a considerable distance through the radiator so that it can emit a sufficient number of photons for efficient counting. This distance for electrons in Lucite should be at least one centimeter, and for slow particles of sufficient penetration it is desirable to use longer radiators. If one wishes to make quantitative use of the directional properties of the radiation, it is essential that the multiple small angle Coulomb scattering be small. This calls for high energy particles and, of course, for low density low z radiators.

The Čerenkov counters used so far by the writer have been designed mostly to count particles which are within a few degrees of being parallel in direction as they enter the counter. This condition is not strictly necessary for counting, but it is certainly much easier to do quantitative work if it is met.

Čerenkov counters of one sort or another show promise of being useful tools in the study of phenomena associated with high energy accelerators. For example, let us consider the various particles produced by the Chicago synchrocyclotron from the point of view of Čerenkov counting.

The primary particles accelerated by the cyclotron are protons, deuterons, or alpha-particles. The value of β for the 450-Mev protons is approximately 0.74. With this speed the protons require a radiator with a refractive index larger than 1.35. Lucite makes quite a convenient radiator, since its index is 1.50, provided that one is interested in counting only the most energetic protons. For the study of elastic scattering this is the case and plans are being made here to carry out such a study with Čerenkov counters.

Deuterons and alpha-particles from this cyclotron are of rather inconvenient energy for Čerenkov counting, since their β is about 0.49. This would make necessary a radiator with index greater than 2.04. With a radiator of index less than 2.04, one can count faster particles in the presence of and with the exclusion of the deuterons or alpha-particles. This can be convenient on occasion.

Neutrons are produced by protons striking almost any target. In turn these neutrons can be made to produce protons by allowing them to strike a hydrogenous substance. These protons can be counted with a Čerenkov counter which, if Lucite is the radiator, becomes a detector for the neutrons of only the highest energies produced. In the case of 450-Mev maximum energy protons striking a beryllium target, the effective neutron energy is about 400 Mev.

High energy gamma-rays are produced by the decay of π^0-mesons which in turn are produced by proton-nucleon reactions in the cyclotron beam. They are produced also to some extent by bremsstrahlung of protons decelerated by collisions against nucleons. These high energy gamma-rays can produce electrons which are detected easily by Čerenkov counters. In this case one can discriminate against protons produced by neutron contamination of the gamma-ray beam by using a water radiator. Water with an index of refraction of 1.31 can give Čerenkov radiation only from particles of β greater than 0.76.

Charged mesons of all varieties produced by the cyclotron can be counted with Čerenkov counters, and

for these particles the angle of emission of the light is in a convenient range for velocity discrimination. With a Lucite radiator, π-mesons down to about 70 Mev can be counted conveniently, and the counters have the distinction of being equally sensitive for positive and negative mesons which is not the case for phosphors which are sensitive to star particles.

(4) DESIGN AND PERFORMANCE OF FOCUSING CONTOURS

In this section we shall discuss in some detail the various focusing Čerenkov counters that have been proposed or used in other laboratories or in this one. For the purpose of this discussion a focusing counter is defined as one in which the light of one particular Čerenkov angle is focused to a spot where it can be directed onto a photomultiplier cathode, while light of other angles is directed elsewhere. Such a counter is capable, then, of recording particles of a narrow band of velocities and of rejecting particles of other velocities.

Before considering the various types of focusing counters, it may be well to discuss some optical properties which are common to all of them. All types used so far consist basically of a cylindrically symmetrical assembly of radiator and optical parts designed to focus light from a parallel beam of particles of one velocity onto the cathode of a photomultiplier. It is impossible, unfortunately, to focus all the light of one Čerenkov angle from a radiator of larger than infinitesimal size to a sharp point. The best possible focusing can be deduced from the following considerations.

Let us consider a particle which travels parallel to the axis of the system but removed from it by some distance d. Most of the light from such a particle follows paths which are skewed from the axis. Consequently, the photons have angular momentum around it. A very useful concept in the consideration of focusing counters is the angular momentum of the light because it is conserved as the ray moves through the system, and it can never be changed for one ray, no matter how often the light is reflected or refracted at cylindrically symmetrical boundaries. This angular momentum property of the light puts a limit on the sharpness of focus. A skew ray of light has angular momentum, and thus it can never pass through the axis of the system where by symmetry the center of the image must be. The image then has a minimum possible size which is related to the angular momentum of the most skewed light rays.

The application of the angular momentum concept is complicated by the fact that the momentum of a photon is different in a dielectric than in vacuum, the momentum of a photon like that of any other corpuscle being h/λ, which in a dielectric reduces to $h\nu n/c$ rather than $h\nu/c$, its value in vacuum. Since the momentum of a photon is smaller after it leaves the dielectric, and it does leave the dielectric in all focusing counters so far constructed. The factor by which the momentum must be multiplied to obtain the same angular momentum must be larger outside of the dielectric.

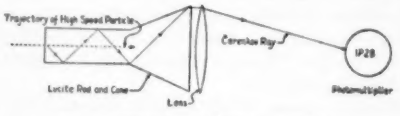

FIG. 3. Getting-Dicke Čerenkov counter.

Let us consider the case of a particle moving at a distance d from the axis of a focusing counter. The photons most highly skewed to the axis have angular momenta equal to $dp_d \sin\theta$, where p_d is the momentum of the photon in the dielectric and θ is the Čerenkov angle. Outside the dielectric the limiting angular momentum is $Dp_v \sin\theta'$, where D is the closest approach of the photon to the axis (ideally in the focal plane), p_v is the momentum of the photon in vacuum, and θ' is the angle between the ray of light outside of the dielectric and the axial direction. From equating these two angular momenta we get the relation

$$D = nd \sin\theta/\sin\theta'. \tag{3}$$

D is under ideal conditions the diameter of the image spot produced by a beam of particles of diameter d. D can never be much smaller than d, and in practical cases it is almost always larger. The effective area of a focusing counter, then, is limited to approximately the sensitive area of the photomultiplier cathode.

(4a) The Getting-Dicke Focusing Counter

In 1946, Getting[1] proposed a design of Čerenkov counter, the optical system of which is shown in Fig. 3. The counter consists of four essential parts: a cylindrical Lucite radiator; a conical Lucite section in optical contact with the radiator, designed to direct light of one Čerenkov angle into a parallel beam; a lens to focus the parallel beam to a point; and finally a diaphragm and a photomultiplier cathode.

Dicke[2] made an attempt to apply such a counter, and although he was unsuccessful in detecting cosmic radiation with it, he did find some pulses above the noise background of the tube when he exposed it to radiation from a 20-Mev betatron. Unfortunately he was unable to demonstrate that the pulses came from Čerenkov radiation rather than from some other source. At the time of Dicke's experiment the distributed type of amplifier was not yet available. The comparatively slow amplifiers he used must certainly have contributed to the failure of the counter as a practical instrument. Even with fast amplifiers and fast coincidence systems, it is difficult to get significant results with a betatron because of its usually very small duty cycle.

Application of Eq. (3) to Dicke's counter, assuming the diagram in his publication to be drawn to scale, indicates that a rather unpleasantly small fraction of the light from an off-axis electron must have been collected by the photomultiplier cathode. The difficulty is that the angle of convergence produced by the lens

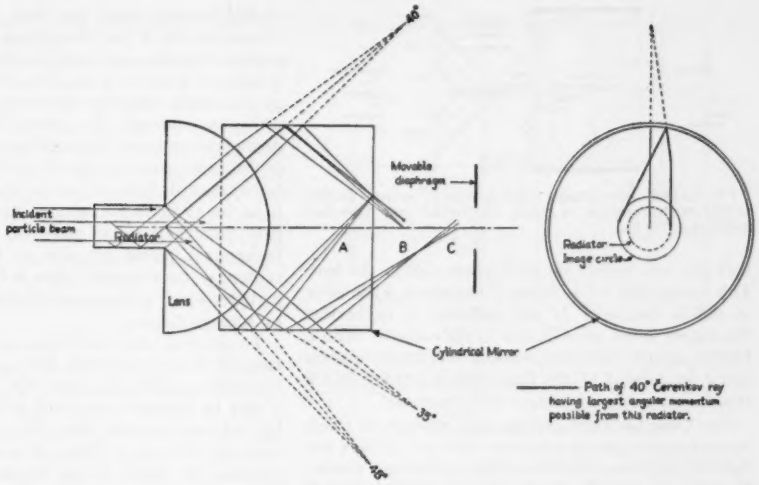

FIG. 4. Optical system of spherical lens, cylindrical mirror focusing counter. Radiator and lens are assumed to be made of Lucite with a refractive index of 1.5.

was quite small compared to the Čerenkov angle. A rough estimate indicates that approximately half of the light from a high speed electron traveling one millimeter off the axis and parallel to it was focused into a circle of 5-mm diameter at the focus. The situation must have been somewhat worse for particles farther from the axis because of imperfect radial focusing.

The considerations of the previous paragraph are based on the assumption that a particle moves through the radiator on a straight line exactly parallel to the axis. In a practical case this is not true, and in particular it was not true in Dicke's experiment, because of the low energy of the electrons available to him. The Getting-Dicke type of counter has not been used by the writer, but there appears to be no fundamental reason why it should not be usable with well-collimated beams of high energy particles.

(4b) Spherical Lens, Cylindrical Mirror Counters

A type of focusing counter that has been used by the writer is shown in Fig. 4. A beam of particles is allowed to enter the radiator from the left. Čerenkov radiation produced there is brought by total internal reflection to the center of the hemispherical lens which, like the radiator, is machined out of Lucite. The Lucite lens, since its refractive index is 1.5, has a focal length equal to twice its radius of curvature. Thus the Čerenkov light for particles of a given speed is focused into a sharp ring at a distance of three radii from the center of curvature of the lens. A cylindrical mirror (glass tubing aluminized on the inside) of half the cylindrical radius of this ring reflects the image back to the center to make a point focus for rays coplanar with the axis of the system.

Rays not coplanar with the axis, as in the case of any cylindrically symmetrical counter, retain their angular momentum and Eq. (3) applies. In this case, however, the angle of convergence is equal to the Čerenkov angle, so that the net result in the absence of spherical aberration is that the image is larger in linear dimension than the end of the radiator by the factor n (1.5 for Lucite). This effect is shown in Fig. 4 in which one skew ray is traced out and marked as a beaded line. It can be seen by reference to both views of the optical system that a skew ray returns, after focusing, to the other side of the axis, approximately 1.5 times as far away from it as its closest approach in the radiator.

A diaphragm placed at the focus will let through light only of Čerenkov angles close to that for which the system is adjusted. As can be seen in Fig. 4, the focusing is reasonably good over quite a range of angles, so that one can vary the velocity setting of such a counter simply by sliding the diaphragm and photomultiplier to different positions on the axis.

Some fraction of the light produced by any particle in the beam that enters the radiator will pass through even a small diaphragm, if it is set to the right angle, although the fraction may be quite small for a particle far from the axis and a small diaphragm. The fraction within a diaphragm circle of radius r, neglecting dispersion and small angle multiple Coulomb scattering, is

$$f=(2/\pi)\sin^{-1}(r/n\rho), \tag{4}$$

where ρ is the radius of the radiator and n is the index of refraction of the lens. The assumption is made here

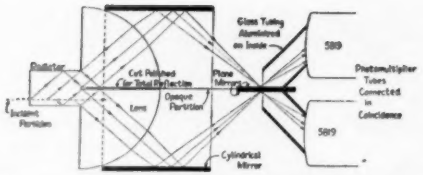

FIG. 5. Split lens focusing counter. Optical system divided beyond end of radiator to reduce background from Čerenkov radiation in the lens.

that one can neglect spherical aberration in the lens. This assumption is justifiable if the lens is made large in radius compared to the radiator. A convenient diaphragm is one equal in size to the radiator. With a Lucite radiator and lens, such a diaphragm accepts about 46 percent of the light from a particle which travels just inside the surface of the radiator.

The Čerenkov light emitted by a radiator on which monoenergetic particles impinge does not all have one definite angle measured from the axis of the system. One can expect a spread of angles of radiation which is a result of a number of causes. First of all, the radiator material always has dispersion. This gives an effective spread of Čerenkov angles which depends on what band width of light is accepted by the photomultiplier. Secondly, the particles are slowed down in passing through the radiator material. This is not serious in the case of electrons since highly relativistic particles essentially do not change their speed when they lose energy. For particles which are not completely relativistic, however, there may be a considerable change in the angle of the Čerenkov radiation as the particles traverse the radiator. Another cause of angular spread in the Čerenkov light is variation in the directions of the particles. This is due to two causes; one is the small angle multiple Coulomb scattering in the radiator, and the other is spread of angle in the incident beam of particles.

In the case of 140-Mev pions the effect of slowing down in Lucite on the Čerenkov angle is about one degree in a five-centimeter length, while in the same length the multiple scattering produces a root mean square angular deviation of about 2.5 degrees. The effect of deviation from parallelism to the axis is to produce a broadening in the radiation angle on each side of the Čerenkov angle by an amount equal to the deviation. These effects seem to account quite satisfactorily in order of magnitude for the observed widths of angular resolution curves.

To use the optical system of Fig. 4 for a counter one can simply insert a photomultiplier so that light passing through the diaphragm strikes its cathode. For the elimination of background counts, however, it is quite convenient to use some sort of coincidence arrangement. The simplest arrangement is one of coincidence between the Čerenkov counter and an external scintillation crystal through which the beam of particles passes. Experimentally it has been found that, while such a counter responds quite satisfactorily to particles of the velocity to which it is adjusted, it is subject to background pulses caused by particles of different velocities which pass through the system. One source of background pulses is the photomultiplier tube itself, which in this arrangement is directly in the beam of particles to be counted. Some of the background pulses appear to be due to Čerenkov light emitted when the particles pass through the glass envelope of the tube. Other background pulses are due to Čerenkov radiation emitted in the lens rather than in the radiator, both by particles which have passed through the radiator and by stray particles.

To obtain a large sensitive area, one likes to have a radiator of large diameter which implies a large lens. For such a counter the above effects may be large, and it may be convenient to avoid recording pulses caused by radiation emitted after the particle has left the radiator. This can be done, as is shown in Fig. 5, by splitting the whole system beyond the radiator into two separate parts, each of which has its own photomultiplier, the two multipliers being connected to a fast coincidence circuit. It should be remarked that such a split counter has not been built although there appears to be no reason why it should not be quite satisfactory.

For smaller counters, having for instance a radiator diameter of one centimeter, quite satisfactory results have been obtained using the arrangement shown in Fig. 6, which is a scale drawing of an existing counter. In this particular case there was no separate radiator, the lens itself performing the function. The lens, for this purpose, was extended $\frac{1}{4}$ inch beyond the center of the sphere. Here the light, before it is allowed to be focused on the axis, is split with a pair of plane mirrors to focus it on the cathodes of two photomultipliers which are connected to a fast coincidence circuit. This arrangement makes a self-contained counter capable of good velocity resolution but has the disadvantage of not having a definite sensitive area, and some of the

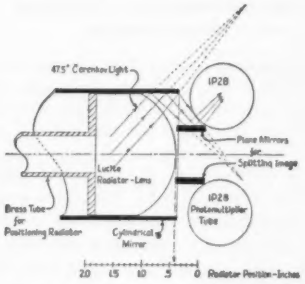

FIG. 6. Focusing counter with small sensitive area used for analysis of meson beams. Radiator in this counter is integral with the lens.

light is wasted, namely, that part which misses the surfaces of the two mirrors.

The counter of Fig. 6 was used to obtain the data shown in Fig. 7. The upper curve is the result of exposing the counter to the 145-Mev negative pion beam from the 170-inch synchrocyclotron and varying the relative position of the radiator to the rest of the optical system. The lower curve is the same thing except that a 12-grams per cm² graphite absorber was inserted in front of the counter. This amount of carbon should reduce the energy of the 145-Mev pions to about 121 Mev and should change the Čerenkov angle from 40.4° to 38.1°. The data of Fig. 7 indicate angles before and after the carbon absorber of 39.9° and 38.0°, which considering the accuracy of the measurement, are in tolerable agreement with what one would expect. The counting rate is reduced by the insertion of the absorber because of scattering which removes mesons from the beam. The data for these curves were taken with a rather high bias on the coincidence circuit to obtain better resolution. With the bias reduced to the point where single pulses were just rejected, the resolving angle of the counter was about twice what is shown in Fig. 7.

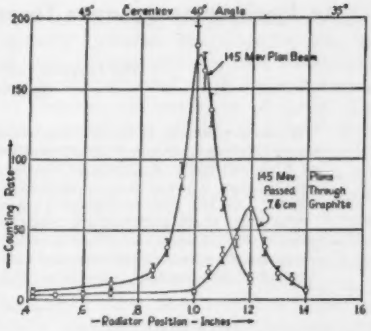

FIG. 7. Velocity resolution of counter of Fig. 6. Radiator position scale corresponds to inch scale of Fig. 6, in which counter is shown in the 0.42-inch position.

(4c) Cylindrical Mirror Counter Without Lens

This is a type of counter which has not been used by anyone so far as the writer knows. It would be constructed just as if it were a counter with a lens, but the lens would be left out and the radiator would have a plane end perpendicular to the axis. It would be applicable to particle-radiator combinations leading to small Čerenkov angles and would be considerably better for this purpose than a counter using a lens. Such a counter focuses rays with angular momentum better than does a lens counter. The reason is that the angle of convergence is larger than the Čerenkov angle. For a reasonably large mirror to radiator diameter ratio, the image has the same size as the radiator, and even for a ratio of 2.5 all the light from a one-inch radiator is focused inside a 1.2-inch image. A counter of this type is applicable best to small Čerenkov angles, electrons in Lucite giving, for instance, radiation of such an angle that it is totally reflected at the end of the radiator. Such a counter with a water radiator would be well adapted to protons with kinetic energies of about one Bev. Protons of 950-Mev kinetic energy give, for example, a convergence angle of approximately 38°.

(5) NONFOCUSING ČERENKOV COUNTERS

Counters of this type were first used by Jelley[3] who was able to count cosmic-ray particles with a water radiator in contact with an E. M. I. end-window type photomultiplier.

(5a) Nonfocusing Lucite Counter

Such a counter has been used in this laboratory[9] as a threshold detector of high energy neutrons by counting proton recoils from a paraffin converter. A 6-in. long Lucite rod, 1.5 in. in diameter, was used as a radiator. It was placed in optical contact with the cathode of a 5819 photomultiplier with the aid of a little silicone vacuum grease. The counter was operated in coincidence with a scintillation crystal placed in front of the radiator. The counting efficiency was quite high for protons of more than 400 Mev but fell off sharply for lower energies, being very little above zero for 350-Mev protons. Used as a detector for neutrons from a beryllium target in the internal 450-Mev maximum energy proton beam of the synchrocyclotron, the converter-counter assembly counted an effective neutron energy distribution having a maximum at 410 Mev and falling to zero at 450 Mev on the upper side and about 360 Mev on the lower side. This is a considerably sharper and also a higher energy spectrum than is obtained with a scintillation counter coincidence arrangement.

(5b) Nonfocusing Water Counter

A counter of this type is in use here for the counting of electrons produced by the decay gamma-rays from π^0 mesons produced by the synchrocyclotron. It operates quite satisfactorily, being superior to the ordinary scintillation pair telescope in that it is much less sensitive to stray radiation background. The water is contained in a glass tube aluminized on the inside and cemented to an aluminum fixture which makes a water tight seal to the 5819 photomultiplier with an O ring gasket. The counter is operated in coincidence either with another Čerenkov counter or with a crystal scintillator.

[9] V. A. Nedzel and J. Marshall, Bull. Am. Phys. Soc. **27**, No. 1, 29 (1952).

An Approximate Quantum Theory of the Antiferromagnetic Ground State

P. W. ANDERSON
Bell Telephone Laboratories, Murray Hill, New Jersey
(Received January 30, 1952)

A careful treatment of the zero-point energy of the spin-waves in the Kramers-Heller semiclassical theory of ferromagnetics leads to surprisingly exact results for the properties of the ground state, as shown by Klein and Smith. An analogous treatment of the antiferromagnetic ground state, whose properties were unknown, is here carried out and justified. The results are expected to be valid to order $1/S$ or better, where S is the spin quantum number of the separate atoms.

The energy of the ground state is computed and found to lie within limits found elsewhere on rigorous grounds. For the linear chain, there is no long-range order in the ground state; for the simple cubic and plane square lattices, a finite long-range order in the ground state is found. The fact that this order can be observed experimentally, somewhat puzzling since one knows the ground state to be a singlet, is explained.

I. INTRODUCTION

KRAMERS and Heller[1] were the first to give a semiclassical derivation of Bloch's spin-wave theory of ferromagnetism.[2] They started with a classical ferromagnetic lattice, with classical spins and the $-J\mathbf{S}_i\cdot\mathbf{S}_j$ Hamiltonian for exchange, found coordinates which represented classically the small vibrations of the system, and quantized these coordinates. In this way they obtained a theory which in principle should be good only to first order in $1/S$ (if the classical results are considered zero'th order) but which actually, perhaps by coincidence, is nearly exact. However, they ignored the zero-point energy of their quantized vibrations without considering its significance very deeply. Klein and Smith[3] have recently pointed out the significance of the zero-point energy, and have shown that only if it is included does one get the correct energy for the ferromagnetic ground state from the Kramers-Heller treatment. That is, the true value of the classical angular momentum S_c which should be used for atoms with spin quantum number S is

$$S_c=(S(S+1))^{\frac{1}{2}}.$$

Therefore, since classically one can expect to be able to set all spins exactly parallel, the energy available from any $-J\mathbf{S}_i\cdot\mathbf{S}_j$ interaction is $-JS_c^2=-JS(S+1)$. The total zero-point energy of the spin waves turns out to be exactly such as to increase this to $-JS^2$, the correct value.

Hulthén[4] worked out the equivalent quantization problem for small vibrations of simple antiferromagnetic lattices from their classical equilibrium state. Here one has the opposite sign, $+J\mathbf{S}_i\cdot\mathbf{S}_j$, for the nearest neighbor interaction, and the classical expectation is that successive spins will align themselves antiparallel. However, Hulthén ignored the zero-point energy.

Bethe had worked out the exact ground state for the antiferromagnetic linear chain of atoms with spin one-half.[5,6] The result was so different from what Hulthén had assumed to be true in his spin-wave theory that he considered his former result to be of questionable meaning. Aside from this simplest case, no rigorous treatment of the antiferromagnetic ground state has appeared. For this reason the very basis for the recent theoretical work which has treated antiferromagnetism similarly to ferromagnetism remains in question.[7,8] In particular, since the Bethe-Hulthén ground state is not ordered,[9] it has not been certain whether an ordered state was possible on the basis of simple $\mathbf{S}_i\cdot\mathbf{S}_j$ interactions. The best proof that it is seems so far to be the experimental results of Shull *et al.*[10] using neutron diffraction, in which they show that certain substances do have ordered antiparallel spin arrangements. In connection with these experimental results, a theory of the ground state seems also of interest for comparison with observed values of the magnetization of the various sublattices.

In this paper we apply the results of the spin-wave theory[4] to the approximate determination of the ground state energy and wave function in a fashion similar to the work of Klein and Smith,[3] by including the zero-point energy and motion. This can be done for reasonably general lattices (we do explicitly the linear, plane square, and simple cubic lattices) and for arbitrary spin quantum number S. The results obtained should be valid to order $1/S$ (or perhaps even $1/ZS$, where Z is the number of nearest neighbors) since the approximations of the so-called "semiclassical" spin-wave theory are valid quantum-mechanical approximations to this order.

We are able to get a result for the ground-state energy in all cases. This energy lies between the rigorous limits which have been derived on the variational

[1] G. Heller and H. A. Kramers, Proc. Roy. Acad. Sci. Amsterdam **37**, 378 (1934).
[2] F. Bloch, Z. Physik **61**, 206 (1930).
[3] M. J. Klein and R. S. Smith, Phys. Rev. **80**, 1111 (1951).
[4] L. Hulthén, Proc. Roy. Acad. Sci. Amsterdam **39**, 190 (1936).
[5] L. Hulthén, Arkiv. Mat., Astron. Fysik **26A**, No. 1 (1938).
[6] H. A. Bethe, Z. Physik **21**, 205 (1931).
[7] J. H. van Vleck, J. Chem. Phys. **9**, 85 (1941).
[8] P. W. Anderson, Phys. Rev. **79**, 350, 705 (1950); C. Kittel, Phys. Rev. **82**, 565 (1951).
[9] This fact has been checked by Kramers and Kasteleijn (Kramers, private communication).
[10] C. G. Shull and J. S. Smart, Phys. Rev. **76**, 1256 (1949); also Shull, Wollan, and Strauser, Phys. Rev. **83**, 333 (1951).

principle,[11] $-\frac{1}{2}NJZ(S^2)$ and $-\frac{1}{2}NJZ(S^2)(1+1/ZS)$. In fact, it is roughly equal to but slightly lower than $-\frac{1}{2}NJZS^2(1+1/2ZS)$. For the linear chain with $S=\frac{1}{2}$, there is good agreement with the rigorous result of Bethe in spite of the fact that this is the worst possible case for the approximation method, which in fact should break down here, as we shall see.

More interesting results are obtained for the long-range order. The quantity related to long-range order which the theory furnishes directly is $(\bar{S}_z)^1$, the average z-component of the spin in one of the two sublattices into which all the lattices we treat can be subdivided. z is the direction in which we assume the spins of our original unperturbed (i.e., classical) system were pointing. In turns out that the average spin on a given atom is reduced by a small correction factor of order of magnitude $1/2Z$ in the case of 2- and 3-dimensional lattices. This result may be susceptible of experimental verification by accurate neutron diffraction measurements.

In the case of the one-dimensional lattice $(\bar{S}_z)^1$ vanishes: The separate sublattices are on the average in singlet states. A little consideration of the situation for this lattice, in which it requires at most an energy of the order J to break up the long-range order, while N perturbation terms of order J are available to destroy the ordered state, convinces one that this is a reasonable result, and in fact it can be shown to agree with the result for the rigorous ground state derived by Hulthén and Bethe.[5,6,9] Physically, the situation is this: It is known that in the one- and two-dimensional lattices in ferromagnetism only an infinitesimal amount of thermal energy in the spin-waves is necessary to break up long-range order. In ferromagnetism, however, the zero-point energy of the spin waves is not adequate to break up long-range order because the quantized amplitudes of the long-wavelength spin-waves, which are those important in the thermal destruction of order, are small. In the antiferromagnetic case it seems reasonable to expect that the total amount of energy necessary to break up long-range order is again infinitesimal in these two cases; this is certainly true in the classical limit of large S. However, here the zero-point energy can do the job, because the large amplitudes of the longest wavelength spin-waves permit a larger proportion of the zero-point energy to go into them as compared to the unimportant short-wavelength waves. This is only true for the one-dimensional case; the two-dimensional case is probably similar to the one- and two-dimensional ferromagnets, having long-range order in the ground state but losing it immediately under thermal excitation.

Another result which has bearing on experiments, while helping to give internal consistency to the theory, can be derived by looking at the properties of the spin-waves of longest wavelength, which actually represent motion of the transverse components of the total spin of the entire sublattice. The sublattice spin, in the ground state at least, certainly does not maintain a constant, definite direction, since the ground state is a singlet. Therefore, the amplitudes of motion of these transverse components of the total spin show an apparent divergence, indicating that the coupled total spins of the sublattices are indeed compelled to rotate around at will in space. One might think that since the approximate quantization of the spin-waves requires that we assume a constant, large spin for the sublattice, the fact that our theory then tells us that this is not true represents an inconsistency in our reasoning. This objection can be shown to be invalid in several ways, particularly by assuming that a small anisotropy energy is present which holds the spins constant in the z-direction. It then appears that the required anisotropy is actually infinitesimal, so that one can easily go to the limit of zero anisotropy, using the anisotropy merely as a convergence factor. Another way to answer this objection is to assume that our theory really starts out from "wave packets" of states, chosen in such a way that the z-component of the total spin is roughly constant. Inquiry into the properties of the longest wavelength spin-waves shows that the energy required to form such a packet is infinitesimal of order $1/N$, where N is the number of atoms in the lattice. This energy is very small. An equivalent result, of experimental interest, is that the time required for the total spin to drift around from one orientation to another essentially different one, in case we prepared the system originally in a state of definite spin orientation, is of order N, and thus extremely large. It is clear that the fact that the neutron diffraction experiments do indicate definite sublattice arrangements, in spite of having been averaged over some finite time, is perfectly reasonable.

This argument, justifying the assumption of a large, constant z-component of spin on the sublattice, is admittedly somewhat circular: We have used the spin-waves, derived on the basis of this assumption, to verify it. However, it is difficult to find any reason why the equation of motion of $(S_z)_{\text{total}}$ should change very much if the correction terms of the theory were included. In any case, the argument shows internal consistency. Every other result furnished by the theory is at least not in disagreement with expectations arrived at by other reasoning. For instance, the fact that the sublattice spins are indeterminate in direction agrees with our knowledge of singlet states; the energy values lie between close limits set by a rigorous argument[11]; order does not exist in one dimension, agreeing with the rigorous result,[5,6,9] while it does exist in three dimensions, agreeing with experiment.[10] Further calculations which will be reported later on models for a ferrimagnet, and for an antiferromagnet with next nearest neighbor interaction, again give results whose

[11] P. W. Anderson, Phys. Rev. **83**, 1260 (1951).

consistency with one's expectations furnishes further strong confirmation of the theory. Thus, while we cannot claim to have proved rigorously that this picture of the ground state is the correct one, it can be said that the probability is high that it is.

II. SPIN WAVES IN AN ANTIFERROMAGNET

Hulthén[4] has carried through the quantization of the spin waves in an antiferromagnet, but we shall repeat the derivation here, both for ready reference and because his way of doing it is not easily adapted to our purpose.

The Hamiltonian for an antiferromagnet is taken to be, assuming that the Heisenberg exchange coupling is responsible for the phenomena,

$$H=J\sum_{\langle j,\,k\rangle}\mathbf{S}_j\cdot\mathbf{S}_k, \tag{1}$$

with J positive. The notation $\sum_{\langle j,\,k\rangle}$ will be used repeatedly to mean a sum over all pairs j and k of neighboring atoms. j and k, of course, represent each a set of D numbers, where D is the dimensionality; they may be thought of as D-dimensional vectors. We are assuming nearest neighbor interaction, and also we shall work only with lattices which can be divided into two sublattices with the neighbors of one all on the other and vice versa; the linear, plane square, and simple cubic lattices only will be used as examples. None of these restrictions is essential to carrying out a theory of this general type.

The basic assumption we make in deriving the semiclassical spin waves is that the state of the antiferromagnet is not greatly different from the classical ground state in which the spins of one sublattice all point in one direction (say $+z$), the spins of the other all in the other direction. This is an assumption which must be justified, and which cannot, unfortunately, be justified by external reasoning, as is possible in the ferromagnetic case. We must use for this justification results of the theory itself (as well as its internal consistency and its agreement with other ideas).

Mathematically, we assume

$$S_{zj}\cong+S,\quad S_{zk}\cong-S. \tag{2}$$

Here and later, atoms labeled j are always on sublattice (1), while those labeled k are on sublattice (2). For the linear chain, for example, this would mean that j is odd and k is even. Where there is some possibility of confusion, we shall also use a superscript (1) or (2) to denote the sublattice. Now

$$S_z^2=S_c^2-(S_x^2+S_y^2), \tag{3}$$

where S_c is the "classical" total spin of an atom with spin quantum number S,

$$S_c=[S(S+1)]^{\frac{1}{2}}. \tag{4}$$

If our fundamental assumption, Eq. (2), is correct, we can use the following binomial theorem expansion for the z components,

$$\begin{aligned}S_{zj}&\cong S_c-(S_{xj}^2+S_{yj}^2)/2S_c,\\ S_{zk}&\cong-S_c+(S_{xk}^2+S_{yk}^2)/2S_c.\end{aligned} \tag{5}$$

Then the Hamiltonian is, by substitution,

$$\begin{aligned}H=-\tfrac{1}{2}ZNJS_c^2+\tfrac{1}{2}ZJ\{&\textstyle\sum_j(S_{xj}^2+S_{yj}^2)+\sum_k(S_{xk}^2+S_{yk}^2)\}\\ &+J\sum_{\langle j,\,k\rangle}S_{xj}S_{xk}+S_{yj}S_{yk}.\end{aligned} \tag{6}$$

This is valid to first order in the small quantities S_x^2 and S_y^2. We introduce two sets of spin waves, one pair for each sublattice:

$$\begin{aligned}S_{xj}&=(2S/N)^{\frac{1}{2}}\textstyle\sum_\lambda\exp(i\boldsymbol{\lambda}\cdot\mathbf{j})Q_\lambda\\ S_{yj}&=(2S/N)^{\frac{1}{2}}\textstyle\sum_\lambda\exp(-i\boldsymbol{\lambda}\cdot\mathbf{j})P_\lambda\\ S_{xk}&=(2S/N)^{\frac{1}{2}}\textstyle\sum_\lambda\exp(-i\boldsymbol{\lambda}\cdot\mathbf{k})R_\lambda\\ S_{yk}&=-(2S/N)^{\frac{1}{2}}\textstyle\sum_\lambda\exp(i\boldsymbol{\lambda}\cdot\mathbf{k})S_\lambda.\end{aligned} \tag{7}$$

Here the wave number λ runs only over $N/2$ values from $-\pi$ to π, giving $2N$ coordinates in all[12]; for example, for the linear chain of length N,

$$\lambda=2\pi n/N,\quad n=-\tfrac{1}{2}N+2,\cdots-2,0,2\cdots\tfrac{1}{2}N. \tag{8}$$

Thus, we have the correct number of degrees of freedom. To show the commutation relations, let us write down the inverse of (7):

$$\begin{aligned}Q_\lambda&=(2/NS)^{\frac{1}{2}}\textstyle\sum_j\exp(-i\boldsymbol{\lambda}\cdot\mathbf{j})S_{jx}\\ P_\lambda&=(2/NS)^{\frac{1}{2}}\textstyle\sum_j\exp(i\boldsymbol{\lambda}\cdot\mathbf{j})S_{jy}\\ R_\lambda&=(2/NS)^{\frac{1}{2}}\textstyle\sum_k\exp(i\boldsymbol{\lambda}\cdot\mathbf{k})S_{zk}\\ S_\lambda&=-(2/NS)^{\frac{1}{2}}\textstyle\sum_k\exp(-i\boldsymbol{\lambda}\cdot\mathbf{k})S_{yk}.\end{aligned} \tag{7'}$$

That Q_λ commutes with $Q_{\lambda'}$, $R_{\lambda'}$, and $S_{\lambda'}$, etc., is obvious. We need to verify only the following commutation rules:

$$\begin{aligned}[Q_\lambda,P_{\lambda'}]&=\frac{2}{NS}\sum_j\sum_{j'}\exp[-i(\boldsymbol{\lambda}\cdot\mathbf{j}-\boldsymbol{\lambda}'\cdot\mathbf{j}')][S_{xj},S_{yj'}]\\ &=\frac{2}{NS}\sum_j\exp[i\mathbf{j}\cdot(\boldsymbol{\lambda}-\boldsymbol{\lambda}')]iS_{zj}.\end{aligned}$$

Under our assumption (2) as to the sublattice spins, this gives

$$[Q_\lambda,P_{\lambda'}]=\delta_{\lambda\lambda'}i\textstyle\sum_j S_{zj}/\frac{1}{2}NS\simeq i\delta_{\lambda\lambda'} \tag{9}$$

$$\begin{aligned}[R_\lambda,S_{\lambda'}]&=-(2i/NS)\textstyle\sum_k\exp[i\mathbf{k}\cdot(\boldsymbol{\lambda}-\boldsymbol{\lambda}')]S_{zk}\\ &\simeq i\delta_{\lambda\lambda'}.\end{aligned} \tag{10}$$

We use the well-known equation

$$\textstyle\sum\exp[i(\boldsymbol{\lambda}-\boldsymbol{\lambda}')\cdot\mathbf{j}]=\frac{1}{2}N\delta_{\lambda\lambda'}. \tag{11}$$

[12] The use of λ as a wave number, or inverse wavelength, for the spin waves, is perhaps unfortunate; it is hoped that no confusion will be caused.

Note that the sign change in S_λ comes from the requirement that the two commutators (9) and (10) be equal.

Now we must substitute (7) into the Hamiltonian (6). First we replace S_{xj}^2 by $|S_{xj}|^2$, etc., which simplifies the presentation somewhat but does not change the results. Then, of course [using (11)],

$$\sum_j S_{xj}^2 = (2S/N)\sum_\lambda \sum_{\lambda'} \sum_j \exp[i(\lambda-\lambda')\cdot \mathbf{j}] Q_\lambda Q_{\lambda'} = S\sum_\lambda Q_\lambda^2,$$

and so forth for the squared terms. The cross-terms are

$$\sum_{\langle j,k\rangle} (S_{xj}S_{xk}+S_{yj}S_{yk}) = \frac{2S}{N}\sum_{\lambda,\lambda'}\sum_{\langle j,k\rangle} \exp[i(\lambda\cdot\mathbf{j}-\lambda'\cdot\mathbf{k})](Q_\lambda R_{\lambda'} - P_\lambda S_{\lambda'})$$

$$= \frac{2S}{N}\sum_{\lambda,\lambda'}\sum_{\langle k-j\rangle} \exp[i\lambda\cdot(\mathbf{k}-\mathbf{j})](Q_\lambda R_{\lambda'} - P_\lambda S_{\lambda'}) \times \sum_j \exp[i(\lambda-\lambda')\cdot\mathbf{j}]$$

$$= S\sum_\lambda (Q_\lambda R_\lambda - P_\lambda S_\lambda) \sum_{\langle k-j\rangle} \exp[i\lambda\cdot(\mathbf{k}-\mathbf{j})],$$

again using (11). The sum over $\langle k-j\rangle$, of course, is meant to run only over neighbors. We define

$$2D\gamma_\lambda = \sum_{\langle k-j\rangle} \exp[i\lambda\cdot(\mathbf{k}-\mathbf{j})], \tag{12}$$

where D is the dimensionality of the lattice. For the three lattices we consider, the linear, plane square, and simple cubic, γ_λ is

$$\gamma_\lambda = \sum_{i=1}^{D} \frac{\cos\lambda_i}{D}. \tag{13}$$

(The λ_i are the D components of the vector $\boldsymbol{\lambda}$.) Then the total Hamiltonian (6) is, in terms of the spin-wave coordinates (again only for our three lattices):

$$H = -NDJS_c^2 + DJS\sum_\lambda [(P_\lambda^2+Q_\lambda^2+R_\lambda^2+S_\lambda^2 + 2\gamma_\lambda(Q_\lambda R_\lambda - P_\lambda S_\lambda)]. \tag{14}$$

For our three lattices, of course, $Z=2D$. Similar expressions may obviously be found for other simple lattice types.

H is not quite in normal coordinate form, but a canonical transformation may easily be found to make it so. This transformation is

$$\begin{aligned} P_\lambda &= (p_{1\lambda}+p_{2\lambda})/\sqrt{2}, \quad Q_\lambda = (q_{1\lambda}+q_{2\lambda})/\sqrt{2}, \\ S_\lambda &= (p_{1\lambda}-p_{2\lambda})/\sqrt{2}, \quad R_\lambda = (q_{1\lambda}-q_{2\lambda})/\sqrt{2}. \end{aligned} \tag{15}$$

It leaves the commutation relations unchanged. The Hamiltonian then becomes

$$H = -DJNS_c^2 + DJS\sum_\lambda [q_{1\lambda}^2(1+\gamma_\lambda)+p_{1\lambda}^2(1-\gamma_\lambda) + q_{2\lambda}^2(1-\gamma_\lambda)+p_{2\lambda}^2(1+\gamma_\lambda)]. \tag{16}$$

The eigenvalues of the harmonic oscillator terms in (16) are easily found. The eigenvalues of

$$H = (p^2/m)+m\omega^2 q^2, \tag{17}$$

if

$$[q, p] = i,$$

are

$$H = (2n+1)\omega, \tag{17'}$$

so that

$$H = -DJNS_c^2 + DJS\sum_\lambda [(2n_{1\lambda}+1)(1-\gamma_\lambda^2)^{\frac{1}{2}} + (2n_{2\lambda}+1)(1-\gamma_\lambda^2)^{\frac{1}{2}}]. \tag{18}$$

For the ground state all $n_\lambda = 0$, so that

$$E_g = -DJNS_c^2 + 2DJS\sum_\lambda (1-\gamma_\lambda^2)^{\frac{1}{2}}. \tag{19}$$

The frequencies of the spin waves fall into two identical branches, as we see by (18); using (17), these frequencies are

$$\omega = DJS(1-\gamma_\lambda^2)^{\frac{1}{2}}. \tag{20}$$

Notice that $\gamma_\lambda \sim 1-\frac{1}{2}\lambda^2$, $\lambda \to 0$, so that

$$\omega_\lambda \sim DSJ\lambda, \quad \lambda \to 0. \tag{21}$$

This dispersion law is quite different from the ferromagnetic case, where $\omega \sim \lambda^2$. The resulting decrease in magnetization of a sublattice, and specific heat, will vary as T^3 at low temperatures if this dispersion law is correct. Thus, they will differ from the ferromagnetic case in which these quantities vary as $T^{\frac{3}{2}}$. It is questionable whether this could be observed.

The difference in dispersion laws is not the most important difference between the two types of spin waves; it is the difference in amplitude per quantum of excitation which leads to the more striking effects. Since the potential and kinetic energies of a harmonic oscillator are on the average the same,

$$\langle q_{1\lambda}^2\rangle_{n_\lambda}(1+\gamma_\lambda) = \langle p_{1\lambda}^2\rangle_{n_\lambda}(1-\gamma_\lambda) = \tfrac{1}{2}(1-\gamma_\lambda^2)^{\frac{1}{2}},$$

or

$$\begin{aligned} \langle q_{1\lambda}^2\rangle_{n_\lambda} &= \tfrac{1}{2}[(1-\gamma_\lambda)/(1+\gamma_\lambda)]^{\frac{1}{2}}, \\ \langle p_{1\lambda}^2\rangle_{n_\lambda} &= \tfrac{1}{2}[(1+\gamma_\lambda)/(1-\gamma_\lambda)]^{\frac{1}{2}}, \end{aligned} \tag{22}$$

in the ground state. These quantities are also proportional to the extra amplitude per quantum of excitation. Note that, for small λ,

$$\langle p_{1\lambda}^2\rangle_{n_\lambda} \to 1/(\sqrt{2}\lambda); \tag{23}$$

the mean amplitude of $p_{1\lambda}^2$ per quantum diverges as $1/\lambda$ (i.e., as the wavelength) for very long wavelengths. This could be predicted from the dispersion law (21), because one expects from analogy with ferromagnetism that it requires only an energy proportional to λ^2 to create a periodic disturbance in the spins of a certain amplitude and of wavelength $1/\lambda$; since here we require an energy proportional to λ per quantum, the amplitude of disturbance per quantum must be as $1/\lambda$.

III. THE ZERO-POINT ENERGY

We will compute first the energy of the ground state as it is given by (19), assuming for the moment that the basic premise (2) is right. In (19) the sum over λ may be replaced by an integral, since the values (8) of λ are quite dense. Since there are $\frac{1}{2}N$ values of λ,

$$\sum_\lambda[(1-\gamma_\lambda^2)]^{\frac{1}{2}} \simeq N/2\langle(1-\gamma_\lambda^2)^{\frac{1}{2}}\rangle_{Av}$$

$$= (2\pi)^{-D}\frac{N}{2}\int_{-\pi}^{\pi}\int\cdots\int d_{\lambda 1}\cdots d_{\lambda D}$$

$$\times\left[1-\left(D^{-1}\sum_{i=1}^{D}\cos\lambda_i\right)^2\right]^{\frac{1}{2}}, \quad (24)$$

$$\sum_\lambda[(1-\gamma_\lambda^2)]^{\frac{1}{2}} = (\tfrac{1}{2}N)I_D.$$

This equation defines I_D. A rough value of I_D may be obtained by expanding the square root in (36) by the binomial theorem and keeping only the first term,

$$I_D \simeq 1-\left\langle\left(\sum_{i=1}^{D}\cos\lambda_i\right)^2\right\rangle_{Av}\Big/\,2D^2 = 1-\langle\cos^2\lambda\rangle_{Av}/2D,$$

$$I_D \simeq 1-1/4D;$$

since $D=Z/2$, this is equivalent to

$$I_D \simeq 1-1/2Z. \quad (25)$$

This value leads to a rough ground-state energy-value, from (19):

$$E_g \simeq -NDJ[S_e^2-S(1-1/2Z)]$$
$$E_g \simeq -\tfrac{1}{2}NZJS^2(1+1/2ZS). \quad (26)$$

In this approximation, the correction factor for the energy is $1+1/2ZS$, which certainly lies between the rigorous limits 1 and $1+1/ZS$.[11] For most known antiferromagnets this correction is fairly small, as discussed in reference 11.

The approximation (25) for I_D is not very good because of the slow convergence of the series of which (25) is the first two terms. More accurate values of I_D have been computed for $D=1$, 2 and 3.[13] For $D=1$, I_D is,

$$I_1 = \frac{1}{2\pi}\int_{-\pi}^{\pi}|\sin\lambda|\,d\lambda = \frac{2}{\pi}. \quad (27)$$

Thus, the energy for the linear chain is

$$E_g|_{D=1} = -NJ[S(S+1)-(2/\pi)S]$$
$$= -NJS^2(1+0.363/S). \quad (28)$$

This is to be compared with the rigorous ground-state energy in the case $S=\frac{1}{2}$ for the linear chain, computed by Bethe,[6]

$$(E_g)_{\text{Bethe}} = -1.77NJS^2,$$
$$(E_g)_{\text{Eq. (28)}} = -1.73NJS^2. \quad (29)$$

This agreement is good, which is unexpected, both because $S=\frac{1}{2}$ is a bad case for our assumption that S is large,[14] and because, as we shall see, in this case the basic premise that the sublattice spin is large and nearly equal to S, on the average, is incorrect. One can only suppose that the basic premise is fulfilled temporarily over large enough regions of the lattice that the energy parameter is not badly approximated. An interesting comment which might be appended here is that for the antiferromagnet, as for the ferromagnet, the theory gives entirely correct results for the case $N=2$: Two atoms coupled by one exchange interaction. For the antiferromagnetic case, (8) gives $\lambda=\pi$ only, and thus $\gamma_\lambda=-1$, and the zero-point energy vanishes entirely. This is correct: for two spins, the singlet state has energy $-JS(S+1)$. The zero-point motion, however, does not vanish in this case, and as discussed in Sec. V shows us that no directional preferences exist. For the ferromagnetic case one also obtains the correct ground-state energy, $-JS^2$.

The integrals I_2 and I_3 were evaluated numerically, essentially by computing or approximating higher terms in the binomial series for the square root.[13] The results were

$$I_2 = 1-0.158, \quad I_3 = 1-0.097, \quad (30)$$

so that the energies are

$$(E_g)_{D=2} = -2NJS^2(1+0.158/S), \quad (31)$$

$$(E_g)_{D=3} = -3NJS^2(1+0.097/S). \quad (32)$$

The energies (28), (31), and (32) are all somewhat lower than the rough approximation (26) but lie between the rigorous limits derived on the variational principle.[11]

IV. THE TOTAL SPIN OF THE SUBLATTICE

A parameter which represents the state of long-range order of the lattice is the total spin of one of the two sublattices. It can easily be shown that the square of this total spin divided by the square of the number of atoms in the sublattice is, except for quantities infinitesimal to order $1/N$, the more usual order parameter

$$\lim_{j-j'\to\infty}\mathbf{S}_j\cdot\mathbf{S}_{j'}.$$

[13] I am indebted to Dr. R. W. Hamming for helpful suggestions in connection with the evaluation of these integrals. Dr. J. M. Luttinger has kindly pointed out that one of them, J_2, has been shown to be an elliptic integral by G. N. Watson [Quart. J. Math. 10, 266 (1939)]. His more exact value agrees well with our numerical integration.

[14] The direct use of the expansion (5) is rather dubious in case $S=\frac{1}{2}$. One can justify at least the long-wavelength spin-wave approximation on another basis, however: For the long wavelengths one can think that there are relatively large regions of parallel spin, leading to large S's in total so that something like (5) holds. In other words, one sums $S_{ij}S_{ik}$ over fairly large regions first, and then expands into an expression like (5). Since the contribution to the energy is most critical for the long wavelengths, this procedure might well lead to good energy eigenvalues. In other words, for long wavelengths we think more nearly in terms of the phenomenological type of spin-wave theory of C. Herring and C. Kittel [Phys. Rev. **81**, 869 (1951)].

The total spin, however, is the more direct physical parameter, since it is what is measured in a neutron diffraction experiment: What is measured is the average spin per atom parallel to the total sublattice spin, which comes directly from the total spin.

The total z-component of the spin of a sublattice, which we shall call $(S_z)_{\text{tot}}^{(1)}$ (or (2), for the second sublattice) is easily computed, simply by adding up the expressions (5) for the whole sublattice. We shall see later that the x and y components may be neglected; for the time being we shall assume this to be true.

Let us, then, start from (5) and compute

$$(S_z)_{\text{tot}}^{(1)}=\sum_j S_{zj}=(\tfrac{1}{2}N)S_c-\sum_j(S_{xj}^2+S_{yj}^2)/2S_c. \quad (33)$$

By (7),

$$\sum_j S_{xj}^2+S_{yj}^2=S\sum_\lambda(Q_\lambda^2+P_\lambda^2),$$

and by (15)

$$\sum_\lambda(Q_\lambda^2+P_\lambda^2)=\sum_\lambda \tfrac{1}{2}(q_{1\lambda}^2+p_{1\lambda}^2+q_{2\lambda}^2+p_{2\lambda}^2+q_{1\lambda}q_{2\lambda}+p_{1\lambda}p_{2\lambda}),$$

so that

$$(S_z)_{\text{tot}}^{(1)}=(\tfrac{1}{2}N)S_c-(S/2S_c)\sum_\lambda \tfrac{1}{2}(q_{1\lambda}^2+p_{1\lambda}^2+q_{2\lambda}^2+p_{2\lambda}^2+q_{1\lambda}q_{2\lambda}+p_{1\lambda}p_{2\lambda}).$$

In the ferromagnetic case, $(S_z)_{\text{tot}}$ is a constant of the motion. This is not true for the sublattices here, as could in fact be shown from the original Hamiltonian (1). The sum of $(S_z)^{(1)}$ and $(S_z)^{(2)}$ is, however, a constant of the motion, since this is the z-component of total spin. Because of this lack of constancy we must content ourselves with average values,

$$\langle(S_z)_{\text{tot}}^{(1)}\rangle_{Av}=\tfrac{1}{2}NS_c-(S/4S_c)\sum_\lambda\langle q_{1\lambda}^2+p_{1\lambda}^2+q_{2\lambda}^2+p_{2\lambda}^2\rangle_{Av}, \quad (34)$$

since q_1q_2 and p_1p_2 vanish on the average. The average values of the q's and p's are given in (22), so that

$$\langle(S_z)_{\text{tot}}^{(1)}\rangle_{Av}=\frac{N}{2}S_c-\frac{S}{4S_c}\sum_\lambda\left\{\left(\frac{1-\gamma_\lambda}{1+\gamma_\lambda}\right)^{\frac{1}{2}}+\left(\frac{1+\gamma_\lambda}{1-\gamma_\lambda}\right)^{\frac{1}{2}}\right\}$$
$$=\frac{N}{2}S_c-\frac{S}{2S_c}\sum_\lambda\frac{1}{(1-\gamma_\lambda^2)^{\frac{1}{2}}}. \quad (35)$$

Again we can replace the λ-sum by an integral,

$$\sum_\lambda\frac{1}{(1-\gamma_\lambda^2)^{\frac{1}{2}}}=\frac{N}{2}\frac{1}{(2\pi)^D}\int_{-\pi}^{\pi}\int\cdots\int d\lambda_1\cdots d\lambda_D \times\left[1-\left(D^{-1}\sum_{i=1}^{D}\cos\lambda_i\right)^2\right]^{-\frac{1}{2}}, \quad (36)$$

$$\sum_\lambda\frac{1}{(1-\gamma_\lambda^2)^{\frac{1}{2}}}=\frac{N}{2}J_D.$$

This equation defines J_D.

It is obvious that the integral J_1 diverges logarithmically. This means that the original assumption that long-range order exists in the one-dimensional case is wrong; no component of the sublattice spin is finite, and the method breaks down. This, as we pointed out in the introduction, is in agreement with the rigorous result of Bethe and Hulthén.[5,6,9]

For the other two cases, the integral does not diverge. Because of the slow convergence, however, a rough approximation such as (25) is quite useless, so that it is necessary to use values computed in much the same way as the exact values (30) for I_2 and I_3.[13] These are

$$J_2=1.393, \quad J_3=1.156. \quad (37)$$

This leads to the following values for the total z-component of spin (in all cases we neglect terms of order $1/S$, so that we set $S_c=S+\frac{1}{2}$, etc.):

$$(S_{z\text{ tot}})_{Av}\big|_{D=2}=\tfrac{1}{2}N(S-0.197). \quad (38)$$

$$(S_{z\text{ tot}})_{Av}\big|_{D=3}=\tfrac{1}{2}N(S-0.078). \quad (39)$$

These corrections to S are small, and one expects them to become smaller as the number of neighbors increases beyond $Z=6$. Nonetheless, it is entirely possible that this correction term (or the similar term that would be present in more complicated lattices) can eventually be observed by neutron diffraction methods.

The results (38) and (39) cannot immediately be taken at their face values. To see why this is so, let us compute the x- and y-components of $(S_{\text{tot}})^{(1)\text{ or }(2)}$. These are given by the particular spin wave coordinates for $\lambda=0$:

$$\begin{aligned}&\textstyle\sum_j S_{xj}=(\tfrac{1}{2}NS)^{\frac{1}{2}}Q_0, \quad \sum_k S_{xk}=(\tfrac{1}{2}NS)^{\frac{1}{2}}R_0,\\ &\textstyle\sum_j S_{yj}=(\tfrac{1}{2}NS)^{\frac{1}{2}}P_0, \quad \sum_k S_{yk}=-(\tfrac{1}{2}NS)^{\frac{1}{2}}S_0.\end{aligned} \quad (40)$$

The two quantities

$$\sum_j S_{xj}+\sum_k S_{xk}=S_{x\text{ tot}}=(NS)^{\frac{1}{2}}q_{10} \quad (41)$$

and

$$\sum_j S_{yj}+\sum_k S_{yk}=S_{y\text{ tot}}=(NS)^{\frac{1}{2}}p_{20}$$

[by (15)] have finite mean squares, as we see by (22); the squares are somewhat smaller than or of order N, so that the actual quantities are always very small. This was to be expected from the fact that S_{tot} is a constant of the motion for the Hamiltonian (1). We see that we have, by our basic assumption (2), accidentally limited ourselves exclusively to singlet states or at least states of very low total spin quantum number. This is acceptable; the ground state is certainly a singlet,[5] while actually the majority of all states have very small total spins.

On the other hand, the differences between the two x- and y-components,

$$\begin{aligned}&\textstyle\sum_j S_{xj}-\sum_k S_{xk}=(NS)^{\frac{1}{2}}q_{20},\\ &\textstyle\sum_j S_{yj}-\sum_k S_{yk}=(NS)^{\frac{1}{2}}p_{10},\end{aligned} \quad (42)$$

have divergent mean square amplitudes, as we saw in

(23). The meaning of this fact is perfectly clear from our basic knowledge of the problem. The ground state of the antiferromagnet is certainly a singlet state, and a singlet state cannot, by general reasoning, show in any way a preference for one direction over another. Therefore, while the spins of the two sublattices can certainly be said to be opposite in direction, in the ground state of the lattice, on an average basis, we cannot define the direction in space of the spin of either one. One may think of the system as similar to the singlet state of two spins, $(\alpha\beta-\beta\alpha)$, in which the spins are certainly opposite but each is directed with equal probability in all directions.

The quantities (42) are the degrees of freedom which represent the rotation of the two oppositely directed sublattices in space. We know that in the ground state, at least, we cannot "pin down" these degrees of freedom in any way; the lattices will rotate around at will in the course of time. The apparently infinite zero-point amplitude of motion is the mathematical result in this theory of this fact, and is therefore not to be thought of as a fault of the theory.

The tendency of the pair of lattices to rotate around is, however, a weak one, as we can show in two ways. One way is more physical: Since every real lattice will certainly have some kind of anisotropy, we introduce in the Hamiltonian (6) an anisotropy of axial symmetry which makes the z-axis the preferred direction. It is easily verified that such an anisotropy energy can be expressed by

$$H_{\text{anis}}=K[\textstyle\sum_j(S_{xj}^2+S_{yj}^2)+\sum_k(S_{zk}^2+S_{yk}^2)], \quad (43)$$

where K is the anisotropy energy constant per atom. (43) can be re-expressed in terms of the spin-waves (7) and is

$$H_{\text{anis}}=KS\textstyle\sum_\lambda(Q_\lambda^2+R_\lambda^2+P_\lambda^2+S_\lambda^2). \quad (44)$$

Then the total Hamiltonian becomes, instead of (14),

$$\begin{aligned}H&=-NDJS_c^2+DJS\textstyle\sum_\lambda[(P_\lambda^2+Q_\lambda^2+R_\lambda^2+S_\lambda^2)\\&\qquad\times(1+K/DJ)+2\gamma_\lambda(Q_\lambda R_\lambda-P_\lambda S_\lambda)]\\&=-NDJS_c^2+DJS\textstyle\sum_\lambda[q_{1\lambda}^2(1+K/DJ+\gamma_\lambda)\\&\qquad+p_{1\lambda}^2(1+K/DJ-\gamma_\lambda)+q_{2\lambda}^2(1+K/DJ-\gamma_\lambda)\\&\qquad+p_{2\lambda}^2(1+K/DJ+\gamma_\lambda)]. \quad (45)\end{aligned}$$

The amplitudes (22) become

$$\begin{aligned}\langle q_{1\lambda}^2\rangle_{\text{Av}}=\langle p_{2\lambda}^2\rangle_{\text{Av}}&=\tfrac{1}{2}\left[\frac{1+(K/DJ)-\gamma_\lambda}{1+(K/DJ)+\gamma_\lambda}\right]^{\frac{1}{2}}\\\langle p_{1\lambda}^2\rangle_{\text{Av}}=\langle q_{2\lambda}^2\rangle_{\text{Av}}&=\tfrac{1}{2}\left[\frac{1+(K/DJ)+\gamma_\lambda}{1+(K/DJ)-\gamma_\lambda}\right]^{\frac{1}{2}},\end{aligned} \quad (46)$$

and, in particular,

$$\langle(\textstyle\sum_j S_{xj}-\sum_k S_{zk})^2\rangle_{\text{Av}}\cong NS-\frac{1}{(2K/DJ)^{\frac{1}{2}}} \quad (47)$$

for very small K. This shows us that, unless K is small in the order $1/N$, the root mean square values of $\sum S_{xj}$ or $\sum S_{yj}$ to be expected is reduced from infinity to something of the order $\sqrt{N}$, completely negligible in comparison with the value of $\sum_j S_{zj}$, which is of order N. Thus, we may consider an infinitesimal K to be present as a convergence factor, and then the truly interesting physical parameter,

$$[(S_{\text{tot}}{}^{(1)})^2]^{\frac{1}{2}}=[(S_{x\text{ tot}}{}^{(1)})^2+(S_{y\text{ tot}}{}^{(1)})^2+(S_{z\text{ tot}}{}^{(1)})^2]^{\frac{1}{2}},$$

is simply given by

$$\langle S_{z\text{ tot}}{}^{(1)}\rangle_{\text{Av}},$$

which is the value computed in (38) or (39).

A second way of clarifying the meaning of the divergence of the amplitudes (42) is the following. Let us return to the consideration of the original Hamiltonian (16):

$$\begin{aligned}H=-DNJS_c^2+DJS\textstyle\sum_\lambda[&q_{1\lambda}^2(1+\gamma_\lambda)+p_{1\lambda}^2(1-\gamma_\lambda)\\&+q_{2\lambda}^2(1-\gamma_\lambda)+p_{2\lambda}^2(1+\gamma_\lambda)].\end{aligned}$$

For spin waves $\lambda=0$, the energy terms are

$$H_{\lambda=0}=2DJS(q_{10}^2+p_{20}^2). \quad (48)$$

Now besides the ground state of the $\lambda=0$ oscillators, there will be a number of higher states, which happen, since $\omega=0$, to form a continuum. As the first question let us ask: how much energy will it cost to form a wave packet of higher states which, instead of having a large amplitude of p_{10} or q_{20}, has a reasonably small one? This is easily answered by means of (48). From the commutation relations it can be derived that

$$p_\lambda=i\partial/\partial q_\lambda, \quad q_\lambda=-i\partial/\partial p_\lambda. \quad (49)$$

Thus, if we limit q_λ to some definite range, say Δq_λ, we must contribute a certain amount of p_λ, given in order of magnitude by

$$\Delta p_\lambda\cong 1/\Delta q_\lambda, \quad (50)$$

or vice versa. Thus, to limit q_{20} to a value Δq_{20} we require

$$E_{1\text{lim}}=2DJS/(\Delta q_{20})^2. \quad (51)$$

Thus

$$\begin{aligned}E_{1\text{lim}}&=\frac{2DJS}{[\Delta(\sum S_{xj}-\sum S_{zk})]^2/NS}\\&=\frac{2DJ}{N}\left\{\frac{NS}{\Delta(\sum S_{xj}-\sum S_{zk})}\right\}^2.\end{aligned} \quad (52)$$

From this relation it becomes clear that to limit the rotation of the sublattice spins to a finite angle (this means limiting $\sum S_{xj}$, etc., to a value of order of magnitude NS) the excess energy required is only of order of magnitude $1/N$, and thus is extremely small. It is clear that we can even limit $\sum S_{xj}$ to a quantity of order of magnitude $(N)^{\frac{1}{2}+\alpha}$, $\alpha>0$, without requiring any perceptible energy.

An equivalent way of looking at Eq. (52) is this: Suppose the lattice had been looked at at one time (say with neutron diffraction) and it had been determined that the sublattices were pointing in the $+z$ and $-z$ directions, respectively. How long would it then take for them to turn to the x-directions under the effects of the Hamiltonian (1)? The answer to this is given by

$$\begin{aligned}(h\times\text{frequency of rotation})&\simeq E_{\text{lim}};\\ \text{Frequency of rotation}&\simeq J/hN;\\ \text{Time to rotate}&\sim hN/J.\end{aligned}\tag{53}$$

This time is of the order of magnitude 10^8 sec$=3$ years.

These two arguments based on Eq. (52), I think, show that our original assumption that S_z total$\simeq NS$ is justified, at least according to its own consequences. It seems very difficult indeed to find a reason why, at least in order of magnitude, (52) should not hold even for the rigorous problem. If we assume initially that $(S_x^{(1)})$ is large, the S_x, S_y commutation relation tells us that S_z can then be localized easily, and this in turn justifies the entire theory, which tells us then that S_z is large.

This argument also has the consequence that we can definitely predict the result of observing the spins on the two sublattices. The direction of the spins will no doubt in any real case be determined primarily by anisotropy energies. Their magnitude is given to a fair approximation by (39) or the equivalent formula for the lattice under consideration.

V. SOME CONCLUSIONS

The apparent success of the spin wave theory in elucidating the complications of the ground state of the antiferromagnet leads one to have some confidence in its validity as a description of the higher lying states; thus such things as Bloch wall theory may be capable of being carried over practically unchanged from ferromagnet theory. This is of some practical interest in connection with ferrimagnetism, which will also be discussed in a way similar to the present theory in a later paper. It seems, too, that the "sublattice" picture of antiferromagnetism which has been used in some theoretical papers[6,7] is at least not qualitatively affected by the present picture of the complications of the ground state. This is of importance because these theories have had considerable success in explaining experimental results in a semiquantitative way, and because they do lean rather heavily on the assumption that the ground state has order and is not greatly different from what one would naively expect.

The only approximate energies which seem to have been given in the literature for two- and three-dimensional antiferromagnets are the energies of very small aggregates (6 and 8 spins) with periodic boundary conditions, which were computed by Harrison.[16] However, these energies lie even below the rigorous limits computed previously,[11] because of the fact that the aggregates are so small that certain paired electrons can have an over-riding effect (just as in the linear case the binding energy of the two-spin case is far too great). Thus, it does not seem fruitful to make a comparison with Harrison's results.

The conclusions of this paper about long-range order have implications in the theory of metallic binding. If one describes a substance by the Heitler-London model, (1) is at least a fair approximation for the effective spin coupling, unless one has a case such as diamond in which the interatomic exchange integrals may be thought of as over-riding the internal spin-coupling which leads to a total S for the atom. (Of course, such substances as ionic crystals have $S=0$, and we do not treat them.) In most metals, however, and particularly in the single-electron metals such as the alkalis, the description by the Heitler-London model certainly leads to (1). Then, as we have shown, (1) requires a long-range spin order to be present, which is probably not the case in most metals. Thus, we conclude that the Heitler-London model is not even a good qualitative description of metallic binding, in agreement with Schubin and Wonsowski[18] and Mott;[17] the band theory must be used in metals, the Heitler-London theory may be used in insulators.

I have profited greatly in doing this work from stimulating discussions with a number of my colleagues, particularly Dr. Wannier, Dr. Herring, Dr. Holden, and Dr. Kittel. Dr. Hamming's valuable help has been mentioned in the text.

---

[16] R. J. Harrison, M.I.T. Research Laboratory of Electronics Technical Report, No. 172 (1950).

[18] S. Schubin and S. Wonsowski, Proc. Roy. Soc. (London) **145**, 159 (1934); also Physik. Z. Sowjetunion **7**, 292 (1935) and **10**, 348 (1936).

[17] N. F. Mott, Proc. Phys. Soc. (London) **A62**, 416 (1949).

On a Theorem of Irreversible Thermodynamics*

HERBERT B. CALLEN AND RICHARD F. GREENE†
Department of Physics, University of Pennsylvania, Philadelphia, Pennsylvania
(Received January 24, 1952)

A relation is obtained between the parameter describing the irreversible response of a driven dissipative system and the spontaneous fluctuations of the thermodynamic extensive parameters of the system in equilibrium. The development given in this paper extends the theorem, previously proven in the statistical mechanical domain, to the macroscopic thermodynamic domain.

1. INTRODUCTION

THIS paper is one of a series of contributions to the development of a theory of "irreversible thermodynamics"—that is, to the extension of the methods of thermodynamics to the treatment of real irreversible processes. We shall show that the mean square deviation of the spontaneously fluctuating extensive parameters of a thermodynamic system in equilibrium is related to the dissipative part of the admittance function which characterizes the irreversible response of the system to applied forces. If $\langle \xi^2 \rangle$ denotes the mean square fluctuation in the frequency interval determined by the range of integration, we shall show that

$$\langle \xi^2 \rangle = \frac{-2k}{\pi} \int d\omega \sigma_s(\omega) \omega^{-2} \tag{1.1}$$

or

$$\langle \xi^2 \rangle = \frac{2kT}{\pi} \int d\omega \sigma_U(\omega) \omega^{-2}. \tag{1.2}$$

The first of these equations applies to a system in which all extensive parameters other than that which fluctuates are held constant, whereas the second equation applies to a system with similar constraints except that the constraint on the energy is replaced by the condition of adiabatic insulation. The quantities $\sigma_s(\omega)$ and $\sigma_U(\omega)$ are conductances defined appropriately to these respective constraints. These equations may be re-expressed, although somewhat less directly, in terms of equivalent fluctuating forces and then appear as generalizations of the Nyquist electrical noise formula.[1]

The modern theory of irreversible thermodynamics was first projected in 1931 by Onsager[2] with the formulation of a general relation of reciprocity in the mutual interference of two simultaneous irreversible processes. Applications of this one basic theorem constitute the totality of the existing theory of irreversible thermodynamics.[3]

There are two possible methods of approach to the theory of irreversible thermodynamics, which might be characterized as the statistical approach and the thermodynamic approach. The statistical approach consists of generalizing the methods of statistical mechanics, and a theorem proved in this framework must then, of course, be projected into the macroscopic thermodynamic domain by a reasoning similar to that which projects the statistical mechanical H theorem into the macroscopic second law of thermodynamics. The alternative, or thermodynamic, approach consists in generalizing the methods of thermodynamics itself, which is already on a macroscopic level. Whereas the results of the thermodynamic approach are thus in more immediate contact with macroscopic irreversibility than are the results of the statistical approach, the postulates of the latter are closer to fundamental theory. Each approach clearly has its advantages and each may be independently prosecuted. The Onsager reciprocity theorem, originally obtained by a thermodynamic approach, has also been derived by the statistical approach.[4]

The touchstone of the thermodynamic approach to irreversibility theory lies in the intimate connection between irreversible processes and the regression of spontaneous fluctuations in equilibrium systems. This connection has occasionally been criticized because conventional thermodynamic fluctuation theory is an approximate theory valid only for small fluctuations, whereas real irreversible processes may involve appreciable deviations from equilibrium.[5] However, in a previous paper[6] of this series we have reformulated thermodynamic fluctuation theory on an exact basis which is valid for fluctuations of arbitrary size. The thermodynamic approach, based on the analysis of the regression of spontaneous fluctuations, will be employed in this paper.

In addition to Onsager's reciprocity theorem a new theorem has recently been established.[7] This relates the dissipation parameter (the "resistance") to the spectral density of the equilibrium fluctuations and is the

* This work was supported in part by the ONR.
† Now at the Department of Physics, University of Illinois, Urbana, Illinois.
[1] H. Nyquist, Phys. Rev. **32**, 110 (1928).
[2] L. Onsager, Phys. Rev. **37**, 405 (1931); **38**, 2265 (1931); see also H. B. G. Casimir, Revs. Modern Phys. **17**, 343 (1945).
[3] See S. R. DeGroot, *Thermodynamics of Irreversible Processes* (North-Holland Publishing Company, Amsterdam, 1951).
[4] H. B. Callen, thesis, Department of Physics, Massachusetts Institute of Technology, 1948.
[5] The extent of the deviation from equilibrium which is compatible with the validity of the Onsager reciprocity theorem is established by the statistical approach (reference 4) and has also been considered by I. Priogogine (see bibliography in reference 3).
[6] R. F. Greene and H. B. Callen, Phys. Rev. **83**, 1231 (1951).
[7] H. B. Callen and T. A. Welton, Phys. Rev. **83**, 34 (1951).

generalized analog of the Nyquist electrical noise formula. The statistical approach was employed in the derivation of this theorem, and the final projection of the theorem into the macroscopic domain was omitted. Thus, although a number of significant implications can be drawn from the theorem, nevertheless it remains a statistical mechanical rather than a thermodynamic theorem. It is, in fact, difficult to see from the statistical derivation what the macroscopic operational meaning of certain quantities appearing in the formulas would be. It is, therefore, necessary either to close the hiatus between the statistical theorem and the macroscopic domain or to re-establish the theorem entirely within the thermodynamic domain. In this paper we shall establish the theorem by a totally thermodynamic approach.

An extension of these results to systems having more than one fluctuating parameter will be shown in a subsequent paper to yield a generalization of Onsager's reciprocal relations.[8]

2. THE METHOD OF APPROACH

The theorem which we wish to establish is a relation between the generalized admittance (or impedance) of a dissipative system and the spectral density of the spontaneous fluctuations exhibited by the system in equilibrium. The proof employs certain theorems relating to random variables, as summarized in Appendix A. In particular the Wiener-Khinchin formula (A.18) relates the spectral density $G(\omega)$ to the autocorrelation function $\langle \xi(t)\xi(t+\tau)\rangle$,

$$G(\omega)=\frac{1}{(2\pi)^{\frac{1}{2}}}\int_{-\infty}^{\infty} d\tau\langle \xi(t)\xi(t+\tau)\rangle e^{-i\omega\tau}. \qquad (2.1)$$

The autocorrelation function, in turn, is given by (see Eq. (A.6))

$$\langle \xi(t)\xi(t+\tau)\rangle=\int d\xi' W_1(\xi')\xi'\langle \tau, \xi' | \xi\rangle, \qquad (2.2)$$

where $W_1(\xi')d\xi'$ is the probability of finding ξ in the range $\xi'<\xi<\xi'+d\xi'$ and where $\langle \tau, \xi' | \xi\rangle$ is the expectation value of ξ at a given time if it is known that ξ had the value ξ' at τ seconds earlier. Thus the theory of random variables permits us to compute the spectral density of the equilibrium fluctuations if we know the two quantities $W_1(\xi)$ and $\langle \tau, \xi' | \xi\rangle$. The function $W_1(\xi)$ is, however, simply the distribution function of conventional thermodynamic fluctuation theory. The method of computing the conditional average $\langle \tau, \xi' | \xi\rangle$ is the essential element of the proof. The average shape of a spontaneous fluctuation pulse is identical with the observed shape of a macroscopic irreversible decay toward equilibrium and is, therefore, describable in terms of the macroscopic admittance function. The conditional average $\langle \tau, \xi' | \xi\rangle$ can, therefore, be computed in terms of the admittance function, and Eqs. (2.1) and (2.2) then yield the desired relation between the spectral density $G(\omega)$ and the admittance function.

Spontaneous fluctuations under various types of constraint are of interest. A system may be placed under constraints microcanonical with respect to all but that particular extensive parameter in the fluctuation of which we are interested. Alternatively, the microcanonical constraint on the energy may be replaced by thermal isolation (all extensive parameters other than the energy and the parameter whose fluctuation we are interested in remain microcanonically constrained). Finally, the constraints may be such that more than one parameter is permitted to fluctuate. We shall confine ourselves in this paper to consideration of the first two of the above mentioned types of constraints, postponing treatment of several simultaneously fluctuating parameters to a later paper. The microcanonical constraints will be considered first, and only minor alterations in this development (considered in Sec. VI) will be required to adapt the results to the fluctuations under thermal isolation.

3. THE ADMITTANCE OF THERMODYNAMIC SYSTEMS

In this section we shall formulate a thermodynamic definition of the admittance which characterizes the response of thermodynamic systems to applied "forces." Certain analytic characteristics of the admittance will be dictated by thermodynamic considerations.

It is intuitively clear that a thermodynamic system can be subjected to periodic generalized forces, evoking periodic changes in the thermodynamic parameters. Thus, a gas enclosed in a cylinder with a movable piston can be subjected to a periodic external pressure evoking periodic changes in the volume. Similarly, a periodic ambient temperature will evoke periodic changes in the internal energy. For very low frequencies the system will respond quasi-statically to the applied force, but at higher frequencies the system responds in an essentially irreversible way. The fact that the conventional intensitive parameters (temperature, pressure, etc.) have no strict meaning in a nonequilibrium system constitutes the chief difficulty in the formulation of a quantitative thermodynamic definition of the forces and hence also of the admittance.

We shall find it convenient to frame our thermodynamic analysis in the "entropy language," in which the entropy S is taken as a function of the internal energy X_0 and of the equilibrium values of the various other extensive parameters of the system $X_1, X_2 \cdots$ (volume, mole numbers, etc.),

$$S=S(X_0, X_1, X_2, \cdots). \qquad (3.1)$$

The intensive parameters in this formulation are

$$F_K \equiv \partial S/\partial X_K, \qquad (3.2)$$

[8] A preliminary expression of these results appears in R. F. Greene, thesis (University of Pennsylvania, September, 1951) (unpublished).

so that $F_0 = 1/T$, and various other intensive parameters are P/T, $-\mu/T$, etc. Except for F_0, the intensive parameters in the entropy language are simply $-1/T$ times the intensive parameters in the more common "energy language." The instantaneous values of the extensive parameters will be denoted by x_j, as distinguished from the equilibrium values denoted by X_j. The deviation of x_j from its equilibrium value will be denoted by ξ_j,

$$\xi_j \equiv x_j - X_j. \tag{3.3}$$

The boundary conditions on an equilibrium system are generally idealized as being of either of two limiting types. That is, the extensive parameters may be rigidly constrained (as is the volume of a system enclosed in a rigid box) or they may be completely unconstrained (as is the volume of a system enclosed within a cylinder fitted with a freely movable piston). In order that the latter type of system may be in equilibrium it must be in interaction with another system, and the condition of equilibrium is the equality of the appropriate intensive parameters. Thus, a system enclosed in a cylinder with a movable diathermal piston will be in equilibrium if the outside of the piston is in contact with another system and if the two systems have equal values of the intensive parameters $1/T$ and P/T. A system may be said to be "microcanonical" with respect to those of its extensive parameters which are rigidly constrained and to be "canonical" with respect to those of its extensive parameters which are not constrained. The external system, with which the system of interest is in contact, will here be referred to as the "driving reservoir"; the rationale of this nomenclature will become evident immediately.

Let us suppose that the various extensive parameters of the driving reservoir are now varied in such a way that the intensive parameters of the driving reservoir vary sinusoidally with angular frequency ω. The system of interest is, in turn, acted upon by these *generalized forces* and will respond with a suitable time variation of its extensive parameters. *The generalized force is defined as the intensive parameter of the driving reservoir.* For the purpose of this definition we require two distinct characteristics of the driving reservoir. Firstly, the driving reservoir must have characteristic relaxation times small compared with $1/\omega$, so that it is always in quasi-static equilibrium and hence may be assigned instantaneous intensive thermodynamic parameters. Secondly, the size of the driving reservoir must be large in comparison with that of the system of interest, so that the induced changes in extensive parameters of the system do not react to change the instantaneous values of the intensive parameters of the driving reservoir.

Consider a system canonical with respect to a particular extensive parameter x (where for convenience we omit the subscript j) and microcanonical with respect to all other extensive parameters. Let the corresponding intensive parameter of the driving reservoir be $f(t)$ and write

$$f(t) = F + \frac{1}{(2\pi)^{\frac{1}{2}}} \int_{-\infty}^{\infty} d\omega \beta(\omega) e^{i\omega t}. \tag{3.4}$$

This time-dependent applied force will induce a time-dependent response $x(t)$, which may be written in the form

$$x(t) = X + \frac{1}{(2\pi)^{\frac{1}{2}}} \int_{-\infty}^{\infty} d\omega \alpha(\omega) e^{i\omega t}, \tag{3.5}$$

where X is the equilibrium value of x associated with the value F of f. The amplitude of the response $\alpha(\omega)$ will be proportional to the amplitude of the applied force $\beta(\omega)$ for sufficiently small amplitudes. This linearity-in-the-small may be characterized by an impedance or an admittance function.

$$Y(\omega) = i\omega\alpha(\omega)/\beta(\omega). \tag{3.6}$$

An important analytic requirement on the admittance function follows from the fact that a constant impressed force induces a finite and definite value of the extensive parameter x. To formulate this requirement in terms of the properties of the admittance function, consider an impressed force of the constant magnitude

$$f(t) = F + \Delta F, \quad \text{or} \quad \delta f(t) = \Delta F, \tag{3.7}$$

which may be written in the form

$$\delta f(t) = \Delta F \int_{-\infty}^{\infty} d\omega \delta(\omega) e^{i\omega t}, \tag{3.8}$$

where $\delta(\omega)$ is the Dirac delta-function. The response follows from the definition (3.6) of the admittance function

$$\xi(t) = \Delta F \int_{-\infty}^{\infty} d\omega \delta(\omega) Y(\omega) e^{i\omega t}/i\omega, \tag{3.9}$$

and we now inquire as to what properties $Y(\omega)$ must have in order that $\xi(t)$ shall be a finite constant ΔX. Expanding $Y(\omega)$ in a Laurent series in the vicinity of $\omega = 0$

$$Y(\omega) = \sum_{-\infty}^{\infty} y_n \omega^n, \tag{3.10}$$

and inserting this expansion into (3.9) we immediately see that all y_n with $n \leqslant 0$ must vanish if $\delta x(t)$ is to be bounded. Thus, we find

$$Y(\omega) = \omega y_1 + O(\omega^2), \tag{3.11}$$

where $0(\omega^2)$ denotes a function of the order of ω^2. This gives, in turn, from (3.11) and (3.9)

$$\Delta X = \Delta F y_1 / i, \tag{3.12}$$

or

$$y_1 = i\partial X/\partial F, \tag{3.13}$$

where the partial derivative is a thermodynamic

derivative implying constant values of all other extensive parameters. We thus finally conclude that the admittance function is of the form

$$Y(\omega)=i\omega\partial X/\partial F+O(\omega^2). \tag{3.14}$$

The causal relationship between the applied force and the induced response has its analytic statement in the further requirement that the impedance function $Y(\omega)$ may have poles only in the upper half of the complex ω-plane. For then Jordan's Lemma[9] indicates that

$$\int_{-\infty}^{\infty} d\omega Y(\omega)e^{i\omega(t-\theta)}/i\omega=0 \text{ for } t<\theta, \tag{3.15}$$

so that

$$\xi(t)=x(t)-X$$

$$=\frac{1}{2\pi}\int_{-\infty}^{\infty}d\omega\int_{-\infty}^{\infty}d\theta\delta f(\theta)Y(\omega)e^{i\omega(t-\theta)}/i\omega \tag{3.16}$$

receives no contribution from $\delta f(\theta)\equiv f(\theta)-F$ except for times θ which precede t; that is, the response of the system is independent of the future behavior of the force.

It should be kept in mind that the admittance function describes the response to small changes in the force in the vicinity of some equilibrium value F. The admittance function is, therefore, a function of the equilibrium value F and is consequently a state function of the system. This is reflected in the relation between $Y(\omega)$ and $\partial X/\partial F$, the latter derivative being a conventional state function of the system.

4. THE CONDITIONAL EXPECTATION VALUE $\langle\tau, \xi'|\xi\rangle$

Having now formulated a thermodynamically acceptable definition of the admittance function, we proceed with the analysis as outlined in Sec. 2. In particular we are interested in computing the conditional expectation value $\langle\tau, \xi'|\xi\rangle$. That is, we seek the expectation value of ξ at time $t+\tau$ conditional on ξ having had the value ξ' at time t. This problem may be indicated schematically as follows: Let Fig. 1 represent a record of the spontaneous fluctuations of ξ as a function of time in an equilibrium system. On such a record we may locate all of the times at which ξ assumes the value ξ'. From each such value we then translate a distance τ to the right and read a new value of ξ. The average of all of these displaced values of ξ is $\langle\tau, \xi'|\xi\rangle$.

Consider now the collection of all the states represented in Fig. 1 by the condition $\xi=\xi'$. In this collection of macroscopic states every microstate consistent with the condition $\xi=\xi'$ is equally represented. This fact follows directly from the theory of thermodynamic fluctuations.[6] *Thus, the ensemble of microstates associated with the fluctuations to the value ξ' is precisely the conventional microcanonical ensemble associated with the extensive parameter $X+\xi'$.*

To illustrate the above statement we may consider that the parameter x denotes the energy. The probability of an energy eigenstate with energy $X_0+\xi_0'$ is proportional to $\exp[-(X_0+\xi_0')/kT]$ and is, therefore, the same for every microstate of energy $X_0+\xi_0'$. Thus the collection of microstates associated with spontaneous fluctuations to the energy $X_0+\xi_0'$ is composed of all energy eigenstates with eigenvalues $X_0+\xi_0'$, each with equal probability. This is just the microcanonical ensemble associated with a system with total internal energy equal to $X_0+\xi_0'$.

The problem of obtaining $\langle\tau, \xi'|\xi\rangle$ may now be reformulated. If a microcanonical ensemble corresponding to $X+\xi'$ is established at time t, the ensemble average of ξ at time $t+\tau$ will be $\langle\tau, \xi'|\xi\rangle$. This suggests a direct macroscopic method of observing $\langle\tau, \xi'|\xi\rangle$. One merely imposes microcanonical constraints on the system, forcing it to have $x=X+\xi'$, and allows the system to come to equilibrium. The macroscopic system then represents the microcanonical ensemble of interest.

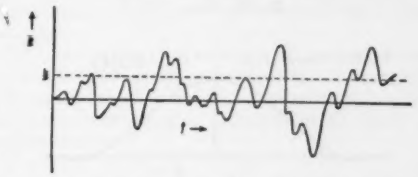

FIG. 1. The spontaneous fluctuations in an equilibrium system.

At time $t=0$ the microcanonical constraint is lifted, and the external force F is applied. The system then decays toward the value $x=X$. The macroscopically observed value of ξ at time $t=\tau$ is $\langle\tau, \xi'|\xi\rangle$. *Thus, by a consideration of the associated statistical ensembles we are led to a connection between spontaneous fluctuations and macroscopic irreversible processes.*

We can now identify the average regression of a spontaneous fluctuation with the decay function which describes the macroscopic behavior of a system after a microcanonical constraint has been lifted. Now there is a simple way to get this macroscopic decay function. Rather than impose a constraint which is to be lifted at $t=0$, we may impose an appropriately chosen force which is again to be lifted at $t=0$. This force, of course, is chosen so as to induce the same initial macroscopic state of the system as would the constraint which it replaces.[10] That is, we shall consider that until $t=0$ the system is in equilibrium with an applied force $F+\delta F$ of such a magnitude as to produce a value $X+\xi'$

[9] E. Whittaker and G. Watson, *A Course of Modern Analysis* (Cambridge University Press, London, England, 1927).

[10] From the microscopic point of view we have merely replaced the initial microcanonical ensemble by a canonical ensemble—a change which, as we know, does not influence the macroscopic thermodynamics of the system.

of x. At time $t=0$ the applied force is suddenly changed to F, and the macroscopically observed value of ξ at $t=\tau$ is again $\langle \tau, \xi' | \xi \rangle$. The problem is now in a form suitable for analysis in terms of the impedance function. The applied force is

$$\delta f = \begin{cases} \delta F = (\partial F/\partial X)\xi', & t<0 \\ 0, & t>0 \end{cases} \tag{4.1}$$

or

$$\delta f = \frac{1}{(2\pi)^{\frac{1}{2}}} \frac{\partial F}{\partial X} \xi' \int_{-\infty}^{\infty} d\omega \left[\left(\frac{\pi}{2}\right)^{\frac{1}{2}} \delta(\omega) + \frac{i}{(2\pi)^{\frac{1}{2}}\omega} \right] e^{i\omega t}, \tag{4.2}$$

where the improper integral is to be interpreted in terms of a Cauchy principal value. The response to this applied force is

$$\xi(t) = \frac{1}{(2\pi)^{\frac{1}{2}}} \frac{\partial F}{\partial X} \xi' \int_{-\infty}^{\infty} d\omega \frac{Y(\omega)}{i\omega} \left[\left(\frac{\pi}{2}\right)^{\frac{1}{2}} \delta(\omega) + \frac{i}{(2\pi)^{\frac{1}{2}}\omega} \right] e^{i\omega t}, \tag{4.3}$$

or using Eq. (3.14),

$$\xi(t) = \tfrac{1}{2}\xi' + \frac{1}{2\pi} \frac{\partial F}{\partial X} \xi' \int_{-\infty}^{\infty} d\omega Y(\omega) \omega^{-2} e^{i\omega t}. \tag{4.4}$$

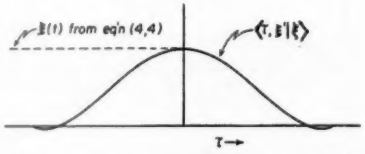

FIG. 2. The conditional expectation value $\langle \tau, \xi' | \xi \rangle$.

This equation gives a response such as is indicated schematically in Fig. 2. A moment's reflection makes it clear that $\xi(\tau)$ will be equal to $\langle \tau, \xi' | \xi \rangle$ only if τ is positive. The value of $\langle \tau, \xi' | \xi \rangle$ for negative values of τ may be immediately obtained, however, by invoking the principle of microscopic reversibility.[2] That is, we need merely realize that $\langle \tau, \xi' | \xi \rangle$ must be an even function of τ, because the spontaneous fluctuations of Fig. 1 are, on the average, symmetric.[11] Thus $\langle \tau, \xi' | \xi \rangle$ is given by the solid curve in Fig. 2, or

$$\langle \tau, \xi' | \xi \rangle = \tfrac{1}{2}\xi' + \frac{1}{2\pi} \frac{\partial F}{\partial X} \xi' \int_{-\infty}^{\infty} d\omega Y(\omega) \omega^{-2} e^{i\omega\tau}, \quad \tau > 0$$

and (4.5)

$$\langle \tau, \xi' | \xi \rangle = \tfrac{1}{2}\xi' + \frac{1}{2\pi} \frac{\partial F}{\partial X} \xi' \int_{-\infty}^{\infty} d\omega Y(\omega) \omega^{-2} e^{-i\omega\tau}, \quad \tau < 0.$$

Now Fig. 2 shows that $\langle \tau, \xi' | \xi \rangle$ can be written as

$$\langle \tau, \xi' | \xi \rangle = \xi(\tau) + \xi(-\tau) - \xi', \tag{4.6}$$

so that, for all τ we obtain

$$\langle \tau, \xi' | \xi \rangle = \frac{1}{2\pi} \frac{\partial F}{\partial X} \xi' \int_{-\infty}^{\infty} d\omega Y(\omega) \omega^{-2} (e^{i\omega t} + e^{-i\omega\tau}), \tag{4.7}$$

or

$$\langle \tau, \xi' | \xi \rangle = \frac{1}{2\pi} \frac{\partial F}{\partial X} \xi' \int_{-\infty}^{\infty} d\omega [Y(\omega) + Y^*(\omega)] \omega^{-2} e^{i\omega\tau}. \tag{4.8}$$

5. THE SPECTRAL DENSITY

The essential part of our analysis has been carried out with the calculation in the previous section of the conditional average $\langle \tau, \xi' | \xi \rangle$. It now remains merely to substitute this quantity into Eqs. (2.2) and (2.1) to obtain the spectral density of the spontaneous fluctuations of ξ. From (2.2) and (4.8) we compute the autocorrelation function

$$\langle \xi(t)\xi(t+\tau) \rangle = \int d\xi' W_1(\xi') \xi' \times \left[\frac{1}{2\pi} \frac{\partial F}{\partial X} \xi' \int_{-\infty}^{\infty} d\omega [Y(\omega) + Y^*(\omega)] \omega^{-2} e^{i\omega\tau} \right], \tag{5.1}$$

or

$$\langle \xi(t)\xi(t+\tau) \rangle = \frac{1}{2\pi} \frac{\partial F}{\partial X} \langle \xi^2 \rangle \int_{-\infty}^{\infty} d\omega [Y(\omega) + Y^*(\omega)] \omega^{-2} e^{i\omega\tau}. \tag{5.2}$$

Now, from Eq. (2.1) or more directly from Eq. (A.15), we find

$$G(\omega) = \frac{1}{(2\pi)^{\frac{1}{2}}} \frac{\partial F}{\partial X} \langle \xi^2 \rangle [Y(\omega) + Y^*(\omega)] \omega^{-2}. \tag{5.3}$$

The theory of thermodynamic fluctuations predicts precisely the mean square fluctuation $\langle \xi^2 \rangle$. For a system canonical only with respect to a single extensive parameter x, the mean square fluctuation is simply[6]

$$\langle \xi^2 \rangle = -k \partial X / \partial F, \tag{5.4}$$

where the partial differentiation connotes constant values of all the other extensive parameters.

The spectral density of the spontaneous fluctuations now becomes

$$G(\omega) = -(2/\pi)^{\frac{1}{2}} k \sigma_s(\omega)/\omega^2, \tag{5.5}$$

where the conductance,

$$\sigma_s(\omega) \equiv \tfrac{1}{2}[Y(\omega) + Y^*(\omega)], \tag{5.6}$$

is the real, or dissipative, part of the admittance. The mean square fluctuations may be written in terms of the spectral density by (A.17);

$$\langle \xi^2 \rangle = -\frac{2k}{\pi} \int_{-\infty}^{\infty} d\omega \sigma_s(\omega)/\omega^2 \tag{5.7}$$

[11] We here implicitly ignore magnetic or Coriolis fields. If these are present $\langle \tau, \xi' | \xi \rangle$ is symmetric only with respect to a simultaneous inversion of the time and the magnetic (or Coriolis) field.

which is our essential result for a system with microcanonical constraints.

It is sometimes convenient to describe the spontaneous fluctuations in the extensive parameters in terms of a hypothetical generalized force $\mathfrak{F}$. This equivalent force is taken as that which, if it were to act on the system, would induce the observed spontaneous behavior of the extensive parameter. This hypothetical force and the fluctuating extensive parameter are thus related by the admittance function as in Eqs. (3.4) to (3.6), and the spectral density of the force is, therefore, given by [see Eq. (A.16)]

(Spectral density of "force")

$$= \frac{\omega^2}{Y(\omega)Y^*(\omega)} G(\omega) \tag{5.8}$$

$$= -\frac{k}{(2\pi)^{\frac{1}{2}}} [Y^{-1}(\omega) + Y^{*-1}(\omega)] \tag{5.9}$$

$$= -(2/\pi)^{\frac{1}{2}} k R_s(\omega), \tag{5.10}$$

where $R_s(\omega)$, the resistance, is the real part of the impedance $\mathfrak{Z}^{-1}(\omega)$. The mean square of the effective force is

$$\langle \delta \mathfrak{F}^2 \rangle = -(2/\pi) k \int R_s(\omega) d\omega. \tag{5.11}$$

6. FLUCTUATIONS UNDER AN ADIABATIC CONSTRAINT

We have now obtained a theorem relating admittance function and spontaneous fluctuations, each measured under conditions in which all but a single extensive parameter of the system is held constant. Our theorem would apply to energy fluctuations if volume and mole number were to be held constant or to volume fluctuations if energy and mole number were to be kept constant. Unfortunately these are not always operationally convenient requirements. In particular, in studying spontaneous volume fluctuations we may easily keep the mole number constant, but we would find it extremely impractical to attempt to keep the internal energy constant. A more practical arrangement would be to study the spontaneous volume fluctuations of an adiabatically insulated system, of constant mole number. We thus seek to adapt our theorem to the replacement of the condition $X_0 = \text{constant}$ by the condition of adiabatic insulation when treating the spontaneous fluctuations of any parameter x_K, $K \neq 0$.

Consider an adiabatically insulated system—that is, a system enclosed by a wall which is impervious to the flow of heat. For such a system the energy x_0 and the other extensive parameters $x_1, x_2, \cdots$ are not independent. In fact, if x_K is the fluctuating parameter (all x_j, $j \neq 0$ or K, being held constant), then the work done by the reservoir on the system is simply

$$\delta x_0 = P_K \delta x_K, \tag{6.1}$$

where

$$P_K \equiv \frac{\partial X_0}{\partial X_K}\Big)_{S,X_j \cdots}$$

is the intensive parameter in the energy language of the driving reservoir. Then we can see that the first-order differential change in the entropy of the system vanishes

$$\delta s = (1/T)\delta x_0 - (P_K/T)\delta x_K = (P_K/T)\delta x_K - (P_K/T)\delta x_K = 0. \tag{6.2}$$

Thus, we see that the adiabatic constraint is equivalent, although only to first order in differentials, to the condition of constant entropy. Therefore, the appropriate set of independent variables for the analysis of fluctuations under an adiabatic constraint is S, X_1, $X_2, \cdots$. This is just the set of independent parameters which defines the energy language in which the fundamental relation is

$$X_0 = X_0(S, X_1, X_2, \cdots). \tag{6.3}$$

This is to be contrasted with the use of the set of independent parameters $X_0, X_1, X_2, \cdots$ which was appropriate for the analysis of fluctuations under microcanonical constraints, and which defines the entropy language.

In adapting the analysis of the microcanonical case to fluctuations under an adiabatic constraint, the generalized force F is to now be replaced by P (where for convenience we omit the subscript K). Thus we replace (3.4) by

$$p(t) = P + \frac{1}{(2\pi)^{\frac{1}{2}}} \int_{-\infty}^{\infty} d\omega \beta(\omega) e^{i\omega t}, \tag{6.4}$$

and $Y(\omega)$, as defined in (3.6), now has the dimensions of X/P rather than of X/F. The Laurent expansion of the energy language admittance function in analogy with (3.14) is

$$Y(\omega) = i\omega \partial X/\partial P)_S + O(\omega^2). \tag{6.5}$$

Similarly, appropriately replacing (4.1) and succeeding equations we find in analogy with (5.3)

$$G(\omega) = (2\pi)^{-1} \partial P/\partial X)_S \langle \xi^2 \rangle [Y(\omega) + Y^*(\omega)] \omega^{-2}, \tag{6.6}$$

or

$$G(\omega) = (2/\pi)^{\frac{1}{2}} \partial P/\partial X)_S \langle \xi^2 \rangle \sigma_U(\omega) \omega^{-2}, \tag{6.7}$$

where

$$\sigma_U(\omega) = \tfrac{1}{2}[Y(\omega) + Y^*(\omega)]. \tag{6.8}$$

The conductance $\sigma_U(\omega)$ carries the subscript U to explicitly indicate the fact that it is the real part of an energy language admittance.

In order to complete the analysis it remains only to evaluate the mean square fluctuation $\langle \xi^2 \rangle$ under an adiabatic constraint. This result is shown in Appendix B to be

$$\langle \xi^2 \rangle = +kT \partial X/\partial P)_S. \tag{6.9}$$

Then we obtain the final result

$$\langle \xi^2 \rangle = \frac{2kT}{\pi} \int_0^\infty d\omega \sigma_U(\omega) \omega^{-2}. \tag{6.10}$$

This result may also be expressed in terms of the mean square fluctuation of an equivalent generalized force, [see Eq. (5.11)],

$$\langle \delta \mathcal{F}^2 \rangle = \frac{2kT}{\pi} \int_0^\infty d\omega R_U(\omega), \tag{6.11}$$

where $R_U(\omega)$ is the real part of the energy language impedance function.

7. CONCLUSION

We have now obtained the explicit relation between the spontaneous fluctuations in an equilibrium system and the function characterizing the irreversible response of the system to applied forces. The results have been obtained for two types of constraints which allow the independent fluctuation of but a single extensive parameter. The theorems are the generalization of the Nyquist electrical noise formula and are the thermodynamic statement of an analogous statistical theorem previously proven.[7] Applications of the relations have been indicated in the paper on the statistical theorem.

In a succeeding paper the analysis will be extended to systems in which more than one extensive parameter is capable of independent fluctuation. It will then be shown that the extended theorem includes[8] a generalized form of the Onsager reciprocy theorem.

APPENDIX A: RANDOM VARIABLES AND THE WIENER-KHINCHIN FORMULA

We here review certain pertinent aspects of the theory of stationary random variables.[12] At a given time we can consider the past behavior of a random variable ξ to be described by a definite mathematical function $\xi(t)$. The future behavior of a stationary random variable is, however, only defined by a set of probability functions

$$W_1(\xi'), W_2(\xi'; \xi'', \tau), W_3(\xi'; \xi'', \tau; \xi''', \tau''') \cdots$$

such that $W_1(\xi')d\xi'$ is the probability of ξ being in the range $\xi' < \xi < \xi' + d\xi'$ at any given future time; and $w_2(\xi'; \xi'', \tau)d\xi' d\xi''$ is the joint probability of ξ being in the range $\xi' < \xi < \xi' + d\xi'$ at any given future time, and of also being in the range $\xi'' < \xi < \xi'' + d\xi''$ at τ seconds later.

A conditional probability function may be conveniently defined by the relation

$$P_2(\xi' | \xi'', \tau) = W_2(\xi'; \xi'', \tau)/W_1(\xi'), \tag{A.1}$$

and $P_2(\xi' | \xi'', \tau)d\xi''$ gives the probability that a measurement, made τ seconds after a previous measurement which gave $\xi = \xi'$, will give a value of ξ in the range $\xi'' < \xi < \xi'' + d\xi''$.

In terms of these probability functions we may compute any desired average values. Thus, the expectation value of ξ is

$$\langle \xi \rangle = \int \xi' W_1(\xi') d\xi', \tag{A.2}$$

and

$$\langle \xi^2 \rangle = \int (\xi')^2 W_1(\xi') d\xi'. \tag{A.3}$$

The autocorrelation function is defined as the expectation value of the product $\xi(t)\xi(t+\tau)$ (which, for a stationary variable, is independent of t). Then

$$\langle \xi(t)\xi(t+\tau) \rangle = \int d\xi' \int d\xi'' \xi' \xi'' W_2(\xi'; \xi'', \tau), \tag{A.4}$$

or

$$\langle \xi(t)\xi(t+\tau) \rangle = \int d\xi' \xi' W_1(\xi') \int d\xi'' \xi'' P_2(\xi' | \xi'', \tau). \tag{A.5}$$

This equation can be written in the useful form

$$\langle \xi(t)\xi(t+\tau) \rangle = \int d\xi' W_1(\xi') \xi' \langle \tau, \xi' | \xi \rangle, \tag{A.6}$$

where

$$\langle \tau, \xi' | \xi \rangle \equiv \int d\xi'' P_2(\xi' | \xi'', \tau) \xi''. \tag{A.7}$$

This latter quantity $\langle \tau, \xi' | \xi \rangle$ has the significance of the expectation value of ξ at a given time if it is known that ξ had the value ξ' at τ seconds previous.

For a stationary random variable the probability functions defining its future behavior may be determined by observations on its past behavior. Similarly various average values may be computed by direct reference to the known function $\xi(t)(t<0)$. In particular the autocorrelation function is given by

$$\langle \xi(t)\xi(t+\tau) \rangle = \lim_{T \to \infty} \frac{1}{T} \int_{-T}^{0} dt \xi(t)\xi(t+\tau). \tag{A.8}$$

It is convenient to analyze the past behavior of the variable in terms of the Fourier transform of $\xi(t)$ rather than in terms of $\xi(t)$ itself. A minor complication arises, however, because $\xi(t)$ is not integrable square in the infinite range of t. This difficulty may be overcome by defining a "cut-off function" $\xi_T(t)$ such that

$$\xi_T(t) \equiv \begin{cases} \xi(t), & -T < t < 0 \\ 0 & \text{otherwise.} \end{cases} \tag{A.9}$$

Then

$$\xi_T(t) = \frac{1}{(2\pi)^{\frac{1}{2}}} \int_{-\infty}^{\infty} d\omega \beta_T(\omega) e^{i\omega t}, \tag{A.10}$$

[12] See M. C. Wang and G. E. Uhlenbeck, Revs. Modern Phys. 17, 323 (1945); and N. Wiener, Acta Math. 55, 117 (1930).

and inversely

$$\beta_T(\omega)=\frac{1}{(2\pi)^{\frac{1}{2}}}\int_{-\infty}^{\infty}dt\xi_T(t)e^{-i\omega t}=\beta_T^*(-\omega). \quad (A.11)$$

The autocorrelation function becomes

$$\langle\xi_T(t)\xi_T(t+\tau)\rangle=\frac{1}{2\pi T}\int_{-\infty}^{\infty}dt\int_{-\infty}^{\infty}d\omega\int_{-\infty}^{\infty}d\omega' \times\beta_T(\omega)\beta_T(\omega')e^{i(\omega+\omega')t}e^{i\omega\tau}. \quad (A.12)$$

But

$$\int_{-\infty}^{\infty}dte^{i(\omega+\omega')t}=2\pi\delta(\omega+\omega'), \quad (A.13)$$

whence

$$\langle\xi_T(t)\xi_T(t+\tau)\rangle=\frac{1}{T}\int_{-\infty}^{\infty}d\omega|\beta_T(\omega)|^2e^{i\omega\tau}, \quad (A.14)$$

or

$$\langle\xi(t)\xi(t+\tau)\rangle=\frac{1}{(2\pi)^{\frac{1}{2}}}\int_{-\infty}^{\infty}d\omega G(\omega)e^{i\omega\tau}, \quad (A.15)$$

where

$$G(\omega)=(2\pi)^{\frac{1}{2}}\lim_{T\to\infty}\frac{1}{T}|\beta_T(\omega)|^2. \quad (A.16)$$

If we take the particular value $t=0$, Eq. (A.15) becomes

$$\langle\xi^2(t)\rangle=\frac{1}{(2\pi)^{\frac{1}{2}}}\int_{-\infty}^{\infty}d\omega G(\omega)=\left(\frac{2}{\pi}\right)^{\frac{1}{2}}\int_0^{\infty}d\omega G(\omega), \quad (A.17)$$

so that $G(\omega)$ is identified as the spectral density. Equation (A.15) is the statement of the Wiener-Khinchin relation, to the effect that the autocorrelation function and the spectral density are mutual Fourier transforms. We use this theorem in its inverted form

$$G(\omega)=\frac{1}{(2\pi)^{\frac{1}{2}}}\int_{-\infty}^{\infty}dt\langle\xi(t)\xi(t+\tau)\rangle e^{-i\omega\tau}. \quad (A.18)$$

APPENDIX B: FLUCTUATIONS UNDER AN ADIABATIC CONSTRAINT

The theory of thermodynamic fluctuations has not been extended to the treatment of fluctuations under an adiabatic constraint. We recall that for a system canonical with respect to both the energy X_0 and some other particular extensive parameter X the probability of a fluctuation to instantaneous values x_0, x is[5]

$$W=\Omega_0\exp\left\{-\frac{1}{k}\left[S-s-\frac{1}{T}(X_0-x_0)-\frac{P}{T}(X-x)\right]\right\}. \quad (B.1)$$

From this ensemble, however, only that subset of states consistent with the condition

$$P(x-X)=x_0-X_0 \quad (B.2)$$

is accessible to a system under an adiabatic constraint. Thus, for such a system the probability of fluctuation to the state x is [inserting (B.2) in (B.1)]

$$W=\Omega_0e^{-[S-s]/k}, \quad (B.3)$$

where by virtue of (B.2) s is now to be considered a function of x only. Then we can write

$$\langle\xi^2\rangle=\int dx(x-X)^2W \quad (B.4)$$

$$=\Omega_0\int dxe^{-(S-s)/k}(x-X)^2. \quad (B.5)$$

This integral may be evaluated by making a series expansion in the exponential and discarding higher order terms

$$s=S+\frac{\partial S}{\partial X_0}\delta x_0+\frac{\partial S}{\partial X}\delta x +\frac{1}{2}\left[\frac{\partial^2S}{\partial X^2}\delta x^2+2\frac{\partial^2S}{\partial X\partial X_0}\delta x\delta x_0+\frac{\partial^2S}{\partial X_0^2}\delta x_0^2\right], \quad (B.6)$$

whence using (B.2) to eliminate the first-order terms

$$(s-S)=\frac{1}{2}\left[\frac{\partial^2S}{\partial X^2}\delta x^2+2\frac{\partial^2S}{\partial X\partial X_0}\delta x\delta x_0+\frac{\partial^2S}{\partial X_0^2}\delta x_0^2\right],$$

$$(s-S)=\frac{1}{2}\left[-\frac{\partial}{\partial X}\left(\frac{P}{T}\right)+2P\frac{\partial}{\partial X_0}\left(\frac{P}{T}\right) +P^2\frac{\partial}{\partial X_0}\left(\frac{1}{T}\right)\right](\delta x)^2,$$

$$(s-S)=\frac{1}{2}\left[-\frac{\partial}{\partial X}\left(\frac{P}{T}\right)_s-P\frac{\partial}{\partial X_0}\left(\frac{P}{T}\right) +\frac{\partial}{\partial X_0}\left(\frac{1}{T}\right)P^2\right](\delta x)^2, \quad (B.7)$$

where the subscript s indicates that s is held constant in the differentiation rather than X_0 as would be implied by the derivative with no explicit subscript. Then by the identity

$$\frac{\partial}{\partial X_0}\left(\frac{P}{T}\right)=-\frac{\partial}{\partial X_0}\frac{\partial S}{\partial X}=\frac{-\partial}{\partial X}\frac{\partial S}{\partial X_0}=-\frac{\partial}{\partial X}\left(\frac{1}{T}\right), \quad (B.8)$$

we find

$$(s-S)=\frac{1}{2}\left[-\frac{\partial}{\partial X}\left(\frac{P}{T}\right)_s+P\frac{\partial}{\partial X}\left(\frac{1}{T}\right)\right.$$
$$\left.+P^2\frac{\partial}{\partial X_0}\left(\frac{1}{T}\right)\right](\delta x)^2$$
$$=\frac{1}{2}\left[-\frac{\partial}{\partial X}\left(\frac{P}{T}\right)_s+P\frac{\partial}{\partial X}\left(\frac{1}{T}\right)_s\right](\delta x)^2$$
$$=-\frac{1}{T}\frac{\partial P}{\partial X_0}\Big)_s(\delta x)^2. \tag{B.9}$$

Thus

$$W=\Omega_0\exp\left\{\frac{1}{2k}\left[-\frac{1}{T}\frac{\partial P}{\partial X}\right)_s\right](\delta x)^2\right\}, \tag{B.10}$$

whence

$$\langle\xi^2\rangle=\frac{\int dx(\delta x)^2\exp\left\{\frac{1}{2k}\left[-\frac{1}{T}\frac{\partial P}{\partial X}\right)_s\right](\delta x)^2\right\}}{\int dx\exp\left\{\frac{1}{2k}\left[-\frac{1}{T}\frac{\partial P}{\partial X}\right)_s\right](\delta x)^2\right\}}. \tag{B.11}$$
$$=2kT\frac{\partial X}{\partial P}\Big)_s\int d\theta\theta^2e^{-\theta^2}\Big/\int d\theta e^{-\theta^2}.$$
$$\langle\xi^2\rangle=kT\partial X/\partial P)_s. \tag{B.12}$$

PHYSICAL REVIEW VOLUME 86, NUMBER 5 JUNE 1, 1952

Second-Order Acoustic Fields: Relations Between Density and Pressure*

JORDAN J. MARKHAM
Applied Physics Laboratory, Johns Hopkins University, Silver Spring, Maryland
(Received June 11, 1951)

In acoustics the relations between the excess pressure and the excess density neglect effects of the fluid flow. The object of this paper is to derive a general relation between the pressure and density which includes streaming. This is done for a nonabsorbing ideal fluid from general thermodynamic arguments. The results justified the static derivations (neglecting flow terms) which are used for more complex media.

I. INTRODUCTION

IN acoustics, one assumes (for a nonabsorbing medium) that the relation between the excess pressure p_e and the excess density ρ_e is of the form

$$p_e=F(\rho_e), \tag{1}$$

where F is some function. For second-order fields the pressure and density are expanded into first- and second-order terms, i.e., $p_e=p_1+p_2$ and $\rho_e=\rho_1+\rho_2$ (p_1 and ρ_1 are solutions of the wave equation[1]). Equation (1) can be expanded in the form

$$p_1+p_2=c_0^2(\rho_1+\rho_2)+\tfrac{1}{2}(c_p^2+c_0^2c_p^2)\rho_1^2, \tag{2}$$

where

$c_0^2=(\partial F/\partial\rho)_s$, evaluated at equilibrium values of the pressure, p_0, and density, ρ_0;

$c_p^2=(\partial c_0^2/\partial p)_s$, evaluated at p_0 and ρ_0;

$c_s^2=(\partial c_0^2/\partial\rho)_p$, evaluated at p_0 and ρ_0;

and s is the entropy. Using directional derivatives we can see that the term in (2) which multiplies ρ_1^2 is $(\partial^2F/\partial\rho^2)_s$.

The above argument takes no account of the fluid flow. In this paper a relation is derived between p_e and ρ_e which takes the flow into account. The derivation is based on Eckart's irreversible thermodynamics.[2] From this new equation a relation corresponding to (2) will be obtained.

II. EXACT PRESSURE DENSITY RELATION

We shall be interested only in a simple fluid where ϵ is a function of p and ρ alone. Since the time does not enter explicitly into ϵ, thermal or structural relaxation is thus eliminated.[3] Because of the simplicity of the case considered, standard equilibrium thermodynamic equations can be used.

Eckart has considered the energy relations in a moving medium composed of a simple fluid. An equation relating the energy, pressure, density, and particle velocity[4] is

$$\rho D\epsilon/Dt+p\nabla\cdot\mathbf{u}=0, \tag{3}$$

* Supported by the Bureau of Ordnance, U. S. Navy.

[1] C. Eckart, Phys. Rev. **73**, 68 (1948).

[2] C. Eckart, Phys. Rev. **58**, 267 (1940).

[3] L. I. Mandelstam and M. A. Leontovich, J. Exp. Theoret. Phys. **7**, 438 (1937), have treated relaxation of fluids by considering the Helmholtz free energy to be given by the usual thermodynamic variables and an additional one which can be associated with time. It would seem that the assumption $\epsilon(\rho, p)$ elimates thermal and structural relaxation.

[4] Equation (3) follows from the first equation after Eq. (9) of Eckart's paper (see reference 2). The entropy change is set equal to zero.

where ρ= total density $\rho_0+\rho_s$; p= total pressure p_0+p_s; ϵ= energy per unit mass; $\mathbf{u}$= particle velocity, and $D/Dt=\partial/\partial t+\mathbf{u}\cdot\nabla$. Equation (3) applies to an isentropic system. By using the equation of continuity,

$$\partial\rho/\partial t+\nabla\cdot(\rho\mathbf{u})=0,$$

a useful variation of (3) is obtained,

$$\frac{D\epsilon}{Dt}+p\frac{D}{Dt}\left(\frac{1}{\rho}\right)=0. \tag{4}$$

ϵ may be eliminated from (4) by means of a transformation, using well-known thermodynamic equations. (A convenient summary of these is found in Slater.[5]) One may obtain the following equalities

$$(\partial\epsilon/\partial v)_p=(\rho/\beta)c_p-p, \tag{5}$$

and

$$(\partial\epsilon/\partial p)_v=(1/\beta\kappa)c_v. \tag{6}$$

Here c_p and c_v are the specific heats per unit mass, β is the coefficient of volume expansion, and κ is the isothermal bulk modulus.

Returning to (4) we find that it can be written in the form

$$\left(\frac{\partial\epsilon}{\partial p}\right)_v\frac{Dp}{Dt}-\frac{1}{\rho^2}\left[\left(\frac{\partial\epsilon}{\partial v}\right)_p+p\right]\frac{D\rho}{Dt}=0.$$

Using (5) and (6), this transforms to

$$Dp/Dt=(\kappa_s/\rho)D\rho/Dt, \tag{7}$$

where κ_s is the adiabatic bulk modulus.

Equation (7) is a new relation between the pressure and the density which includes flow terms. It, with the equations of motion and continuity, is the exact equation for a nonabsorbing medium. Using (7) we can show exactly how $c^2=\kappa_s/\rho$ enters into the acoustic field equations. This will be done in the next section.

III. METHOD OF APPROXIMATION

At present we are unable to solve the acoustic field problem exactly. One is, therefore, interested in applying a method of successive approximations.[1] Equation (7) can be written as

$$(c^2\partial\rho/\partial t)-(\partial p/\partial t)+\mathbf{u}\cdot(c^2\nabla\rho-\nabla p)=0. \tag{8}$$

Expanding c^2 into a series,

$$c^2(p,\rho)=c_0^2(p_0,\rho_0)+(\rho_1+\rho_2)c_\rho^2(p_0,\rho_0)+(p_1+p_2)c_p^2(p_0,\rho_0).$$

c_ρ^2 and c_p^2 have already been defined, and substituting into (8) we have

$$c_0^2\partial\rho_1/\partial t-\partial p_1/\partial t+\mathbf{u}_1\cdot(c_0^2\nabla\rho_1-\nabla p_1)=0, \tag{9.1}$$

for the first-order term, and

$$c_0^2\partial\rho_2/\partial t+(c_\rho^2+c_p^2c_0^2)\rho_1\partial\rho_1/\partial t-\partial p_2/\partial t+c_0\mathbf{u}_1\cdot\nabla\rho_2+(c_\rho^2+c_p^2c_0^2)\rho_1\mathbf{u}_1\cdot\nabla\rho_1-\mathbf{u}_1\cdot\nabla p_2+c_0^2\mathbf{u}_2\cdot\nabla\rho_1-\mathbf{u}_2\cdot\nabla p_1=0, \tag{9.2}$$

for the second-order term. Whether one should include terms such as $\mathbf{u}_1\cdot\nabla p_1$ in the first-order equation is debatable. For high intensity waves in liquids $\mathbf{u}_1$ can be of the order of unity and would dictate the inclusion. On the other hand, $\partial\rho_1/\partial t$ is much larger than $\nabla\rho_1$. The results we are after are not affected by this step so that we include additional terms in (9.1) and (9.2) for generality.

Equation (9.1) can be written in the operational form

$$[(\partial/\partial t)+\mathbf{u}_1\cdot\nabla](c_0^2\rho_1-p_1)=0.$$

The solution of interest is

$$c_0^2\rho_1=p_1. \tag{10.1}$$

The constant of integration has been evaluated by assuming that $\rho_1=0$ when $p_1=0$. This equation is consistent with the usual development of first-order acoustics which of course starts with (10.1) as a basic assumption. Using (10.1) we may write (9.2) in the operational form:

$$(\partial/\partial t+\mathbf{u}_1\cdot\nabla)[c_0^2\rho_2+\tfrac{1}{2}(c_\rho^2+c_p^2c_0^2)\rho_1^2-p_2]=0$$

or again

$$p_2=c_0^2\rho_2+\tfrac{1}{2}(c_\rho^2+c_p^2c_0^2)\rho_1^2, \tag{10.2}$$

where it has been assumed that $\rho_1=\rho_2=0$ when $p_1=p_2=0$.

Although this method gives results equivalent to those obtained by the method discussed in the introduction, it seems to the author that this paper gives a more basic approach. A great deal of work on absorption is based on an acoustical equation of state (the relation between p and ρ) which is obtained by neglecting fluid streaming.[6] The argument presented here seems to justify this omission at least in a simple case. This is the importance of the above result.

ACKNOWLEDGMENTS

The author would like to thank Dr. C. Eckart for suggesting this problem, Dr. F. T. McClure for help in writing the manuscript, and Miss A. Fogelgren for typing. Finally, the author would like to thank his wife for her encouragement.

[5] J. C. Slater, *Introduction to Chemical Physics* (McGraw-Hill Book Company, Inc., New York, 1939), pp. 23–31.

[6] See, for example Markham, Beyer, and Lindsay, Revs. Modern Phys. 23, 353 (1951).

Second-Order Acoustic Fields: Energy Relations*

JORDAN J. MARKHAM
Applied Physics Laboratory, Johns Hopkins University, Silver Spring, Maryland
(Received June 11, 1951)

The expression for the potential energy stored in an acoustic field is examined. Two corrections to the accepted results are found. These corrections are small for a liquid but of major importance for a gas. Indeed, to obtain the average stored acoustic energy for a gas, it is necessary to have more exact solutions than are usually used. Thermodynamic arguments are made to show the meaning of the corrections introduced into the expression for the stored energy.

I. INTRODUCTION

CERTAIN energy relations for an acoustic field are generally assumed to be well known. One such expression is

$$E_A=\tfrac{1}{2}\rho_0 u^2+\tfrac{1}{2}(c^2/\rho_0)\rho_e^2, \tag{1}$$

where E_A=the acoustic energy per unit volume, ρ_0=the equilibrium density, $\mathbf{u}$=the particle velocity, c=the phase velocity, and ρ_e=the excess density.

The first term represents the kinetic energy and will prove to have little interest for the discussion given here. The second term is the contribution of the stored potential energy. Although it is not the potential energy at a given instant of time, it appears to be generally assumed that its time average would equal the time average of the potential energy.

The object of this paper is to obtain a correct expression for the stored energy. The time-average value of the correct expression does not equal the time-average of the expression given in Eq. (1). For gases the difference is important. Since the average energy is a second-order term (term proportional to ρ_e^2), we must consistently carry all second-order terms in the energy. We shall derive the correct expression in general and then evaluate it for a plane wave.

II. ENERGY RELATION

We shall now calculate the stored energy when a fluid is compressed.[1] The energy per unit mass is given by

$$\epsilon=-\int p\,dv, \tag{2}$$

where p=total pressure and v=specific volume. Absorption phenomena are not going to be considered here, so that the integration path is taken to be adiabatic, and we may assume that p may be considered a function of the density, ρ. It is convenient to expand p and v in terms of ρ_e, namely,

$$p=p_0+c^2\rho_e \text{ (to first order in } \rho_e), \tag{3}$$

$$dv=-\frac{1}{\rho^2}d\rho=-\frac{1}{\rho_0^2}\left(1-2\frac{\rho_e}{\rho_0}\right)d\rho \text{ (to first order in } \rho_e). \tag{4}$$

In the above equations: p_0=the equilibrium pressure, and $c^2=(\partial p/\partial\rho)_s$=the square of the phase velocity evaluated at p_0 and ρ_0. Substituting into Eq. (2) and integrating between $\rho_0+\rho_e$ and ρ_0, we obtain

$$\epsilon=\frac{1}{\rho_0^2}\Big[\underset{(a)}{p_0\rho_e}+\underset{(b)}{\left(\frac{c^2}{2}-\frac{p_0}{\rho_0}\right)}\underset{(c)}{\rho_e^2}\Big] \text{ (to second order in } \rho_e). \tag{5}$$

The energy we have defined is related to a fixed quantity of matter. Other definitions are possible. One is the energy for the mass contained in unit volume at equilibrium (ϵ_{v0}). This definition still considers a fixed quantity of matter. Another type of energy, ϵ_v, is obtained by multiplying ϵ by ρ. It is the stored energy per unit volume. Carrying out the multiplication gives for ϵ_v,

$$\epsilon_v=(1/\rho_0)[p_0\rho_e+\tfrac{1}{2}c^2\rho_e^2] \text{ (to second order in } \rho_e). \tag{6}$$

Now we shall compare our ϵ's with the terms found in the literature. As far as the author knows the distinction between ϵ_{v0} and ϵ_v is not made in the standard treatments of the subject. They consider a fixed quantity of matter and, therefore, set out to calculate ϵ_{v0}. One should therefore compare their results with (5).

The termwise comparison of Eq. (5) with the usual expression for the energy shows that:

Term (*a*) does not appear. The first order ρ_e (the solution of the wave equation) is harmonic with time and does not contribute to the time average. To second order ρ_e is not harmonic with time and term (*a*) contributes to ϵ. We shall shortly calculate its contribution for a plane wave and show that this term cannot be neglected in gases.

Term (*b*) always appears, and we shall call it the Rayleigh term since its origin dates back to his time.

Term (*c*) appears, in Eq. (5) but not in Eq. (6). It is because of the fact we are considering ϵ, not ϵ_v. The usual treatments either omit terms (*c*) or fail to make the distinction between ϵ_v and ϵ_{v0}.

To obtain the average energy within a volume V we may proceed by first finding the time average of the

* This paper was supported by the Bureau of Ordnance, U. S. Navy.

[1] We neglect the flowing of the medium. This can be justified for the case considered here where absorption is neglected. This point is discussed in the preceding paper. There c_0 is equivalent to c of this paper.

potential energy associated with unit mass. This can be done by using Lagrangian coordinates which move with the particles. For a plane wave, Fubini-Ghiron has been able to evaluate the particle displacement to second order. His treatment has been reproduced by Westervelt.[2]

A solution for the particle velocity, ζ, to second order is[3]

$$\zeta=\frac{1}{\rho_0 k}R\sin(\omega t-kx)+\frac{1}{2\rho_0{}^2}\left[1+\frac{\rho_0}{c}\left(\frac{\partial c}{\partial \rho}\right)\right]\times\cos^2(\omega t-kx)R^2x, \quad (7)$$

where x=the rest position of the particle, ω=the angular frequency, $k=\omega/c$, and R=a constant which equals the density amplitude of the harmonic term.

For simplicity in algebra we introduce the excess specific volume, v_e. The excess density ρ_e is related as follows to v_e,

$$\rho_e=\frac{1}{v}-\frac{1}{v_0}=-\frac{1}{v_0{}^2}\left(v_e-\frac{v_e{}^2}{v_0}\right) \text{ (to second order).} \quad (8)$$

Equation (5) now reads,

$$\epsilon=-p_0v_e+\tfrac{1}{2}c^2v_e{}^2/v_0{}^2. \quad (9)$$

The time average of v_e and $v_e{}^2$ can be calculated from Eq. (7) and the Lagrangian equation of continuity which states,

$$(v_0+v_e)/v_0=1+\partial\zeta/\partial x. \quad (10)$$

This results in the following time averages,

$$\langle v_e\rangle_{Av}=\frac{1}{4}\frac{1}{\rho_0{}^2}\left(1+\frac{\rho_0}{c}\frac{\partial\rho}{\partial c}\right)R^2 \quad (11a)$$

and

$$\langle v_e{}^2\rangle_{Av}=R_1{}^2/2\rho_0{}^4. \quad (11b)$$

Finally, the time average of stored energy is

$$\langle\epsilon\rangle_{Av}=\frac{1}{4\rho_0{}^2}\left\{c^2-\frac{p_0}{\rho_0}\left[1+\frac{\rho_0}{c}\frac{\partial c}{\partial\rho}\right]\right\}R^2. \quad (12)$$

As one would expect, one may show that $\langle\epsilon_v\rangle_{Av}=\rho_0\langle\epsilon\rangle_{Av}$ with the use of Eqs. (6), (7), and (12).

Let us now examine Eq. (12) for two special cases. Consider first the ideal gas here

$$c^2=\gamma p_0/\rho_0,$$

and

$$dc/d\rho=\tfrac{1}{2}(\gamma-1)c/\rho_0,$$

where γ is the ratio of the specific heats. Substituting into (12) we obtain

$$\langle\epsilon\rangle_{Av}=\tfrac{1}{8}(p_0/\rho_0{}^2)(\gamma-1)R^2. \quad (13)$$

The time average of the total energy per unit mass is obtained by adding $(1/4\rho_0{}^2)c_0{}^2R_1{}^2$ to (13). This follows because for a plane wave the kinetic energy equals the Rayleigh energy. (See for example Stuart and Lindsay.[4]) Finally, the time average of the energy per unit mass

$$\langle\epsilon\rangle_{Av}=\tfrac{1}{8}(p_0/\rho_0{}^2)(3\gamma-1)R_1{}^2, \quad (14)$$

which is greater than zero for $\gamma>\frac{1}{3}$.

This should be contrasted with $(1/2\rho_0{}^2)\gamma p_0R_1{}^2$ obtained by a direct application of Eq. (1).

Let us turn now to a liquid, and as an example, let us consider the ocean where the velocity of sound as a function of depth is well known. It is given in cm/sec by 141,000+0.175 d where d is the depth in cm.[5] Now

$$(1/c)(\partial c/\partial\rho)_s=c\partial c/\partial p,$$

and the partial derivative should be taken along an adiabatic path. For water γ nearly equals one, and we shall not distinguish between the adiabatic or the isothermal path. Using the equations given above, we find that $c_0\partial c/\partial p$ is of the order of unity. Equations (2a) and (7) show that the average of the potential energy will be given to a very good approximation by the average of the first term of (7) (Rayleigh's term) and that no correction need be made. One may hope that Rayleigh's potential energy term is a good approximation for liquids, although it gives incorrect results for gases.

In general, we can say that the standard expression for the acoustic energy is incorrect. The correct expression for a gas requires a detailed knowledge of the sonic field, and its evaluation requires the inclusion of all the second-order terms. The correction for a liquid seems to be small.

III. THERMODYNAMICS OF THE ENERGY RELATION

In the previous section the energy was expanded in terms of the density. The energy can be expressed equally well in terms of the specific volume, v, and the entropy per unit mass, s. This will be done in this section. For clarity we shall denote the energy by ϵ' in this case. The alternate expansion will show us precisely to what thermodynamic quantity the Rayleigh energy term corresponds. It will also give an alternate derivation of the basic energy equation, i.e., Eq. (5). (Further, the restriction that $\Delta s=0$ will be removed.)

It is convenient to use the expansion used by Eckart.[6] The excess volume and the excess entropy are given by v_1+v_2 and s_1+s_2. v_1 is the solution of the usual acoustic equation and is harmonic in time. For a non-

[2] P. J. Westervelt, J. Acoust. Soc. Am. **22**, 319 (1950).

[3] This corresponds to Eq. (17) of reference 2 where $f(t-x/c)$ has been replaced by $(R/\rho_0k)\sin\omega(t-x/c)$. The constant R/ρ_0k is selected so that the final expression for the average energy appears in terms of the density amplitude R. That R is the density amplitude for the first-order solution follows from the equation of continuity.

[4] G. E. Stuart and R. B. Lindsay, *Acoustics* (D. Van Nostrand Company, Inc., New York, 1930).

[5] G. P. Harnwell, Am. J. Phys. **16**, 127 (1948).

[6] C. Eckart, Phys. Rev. **73**, 68 (1948).

absorbing medium, s_1 equals zero except at very high and very low frequencies.[7] In our general energy expressions we shall not assume $s_1=0$. Use of this condition will be made later. The second-order terms appear because in deriving the wave equation, higher order terms have been omitted. We assume that the second-order terms are much smaller than the first-order terms, i.e., $v_1 \gg v_2$, etc. This approach suggests the following definitions of first- and second-order energy terms,

$$\epsilon_1' = \epsilon_s' s_1 + \epsilon_v' v_1 \tag{15}$$

and

$$\epsilon_2' = \epsilon_s' s_2 + \epsilon_v' v_2 + \tfrac{1}{2}(\epsilon_{ss}' s_1^2 + 2\epsilon_{sv}' s_1 v_1 + \epsilon_{vv}' v_1^2), \tag{16}$$

where the following abbreviations have been used,

$$(\partial\epsilon'/\partial v)_s = \epsilon_v'; \quad (\partial\epsilon'/\partial s)_v = \epsilon_s', \text{ etc.}$$

We shall now show that $\frac{1}{2}\epsilon_{vv}' v_1^2$ is the Rayleigh term. From thermodynamics we know that $\epsilon_v' = -p$ and that[8]

$$\epsilon_{vv}' = -(\partial p/\partial v)_s = c^2\rho_0^2,$$

where c^2 has been defined in (3). We relate ρ_1 to v_1 by

$$v_1 = -(1/\rho_0^2)\rho_1$$

and

$$\tfrac{1}{2}\epsilon_{vv}' v_1^2 = \tfrac{1}{2}(c^2/\rho_0^2)\rho_1^2. \tag{17}$$

In Eq. (5) we can replace ρ_s^2 by ρ_ϵ^2. This shows that $\frac{1}{2}\epsilon_{vv}' v_1^2$ is the Rayleigh term.

If we relate v_2 to the ρ's as follows

$$v_2 = (1/\rho_0)[(\rho_1^2/\rho_0^2) - (\rho_2/\rho_0)], \tag{18}$$

one may readily show that $\epsilon_1' + \epsilon_2'$ equals ϵ of Eq. (5) for an adiabatic process, namely $s_1 = s_2 = 0$.

We may thus conclude that $\epsilon_v' v_2$ has been omitted previously from the energy relations and that $\frac{1}{2}\epsilon_{vv}' v_1^2$ is the term which has usually been included.

IV. DISCUSSION

Curiously enough, term (c) of (5) is commonly neglected. For example, Morse[9] states that "the average value of the term $P_0(V_0 - V)$ will be zero." His $P_0(V_0 - V)$ equals our $p_0(v_1 + v_2)$. Equation (18) shows that this is not true even if $\rho_2 = 0$ and accounts for the missing term. Other texts use equivalent approximations.

We would like to discuss briefly a relation which has been given by Eckart[6] and Bergmann.[10] They have interpreted it as an equation for the conservation of acoustic energy. The relation can be obtained by multiplying the first-order equation of continuity by $c^2\rho_1/\rho_0$ and adding to it the first-order equation of motion multiplied by $\mathbf{u}_1$. We get

$$(c^2/\rho_0)\rho_1 \partial\rho_1/\partial t + \rho_0 \mathbf{u}_1 \cdot \partial\mathbf{u}_1/\partial t = -c^2\rho_1 \nabla\cdot\mathbf{u}_1 - \mathbf{u}_1\cdot\nabla p_1 = -\nabla\cdot p_1\mathbf{u}_1, \tag{19}$$

where $\mathbf{u}_1$ is the first-order particle velocity. Integrating over an arbitrary volume and using the divergence theorem, one obtains

$$\frac{\partial}{\partial t}\int_v \left(\frac{1}{2}\frac{c^2}{\rho_0}\rho_1^2 + \frac{1}{2}\rho_0 u_1^2\right) d\tau = -\int_s p_1 \mathbf{u}_1 \cdot d\boldsymbol{\sigma}. \tag{20}$$

At first sight this relation certainly looks like an acoustic conservation of energy equation. There are, however, several points that make this interpretation seem questionable. For one thing, the first term on the left is not the instantaneous potential energy. Even if the Rayleigh results were correct as they seem to be for a liquid, it still is not the energy at instant t. It is true that the average of the first term equals the average value of the Rayleigh energy, but Eq. (20) holds at every instant t. The same can be said about the right-hand side. Equation (20) is certainly a correct and a useful relation, but it is not an expression for the energy flow.

V. ACKNOWLEDGMENT

In conclusion, the author would like to thank Professor C. Eckart for many valuable suggestions. The author would like to express his indebtedness to Dr. R. C. Morse, Dr. F. T. McClure, Mrs. M. E. Gordon, and Miss Agnes Fogelgren for help with the manuscript. Finally, the author would like to thank his wife for her encouragement.

Note added in proof:—Recently the writer has seen another paper on this subject by N. Andrejew, J. Physics (U.S.S.R.) **2**, 305 (1940). The first reading indicates interesting and useful results. The author would like to thank Dr. P. J. Westervelt for this reference.

[7] See for example Markham, Beyer, and Lindsay, Revs. Modern Phys. **23**, 353 (1951).

[8] J. C. Slater, *Introduction to Chemical Physics* (McGraw-Hill Book Company, Inc., New York, 1939), pp. 23–31.

[9] P. M. Morse, *Vibration and Sound* (McGraw-Hill Book Company, Inc., New York, 1936), p. 188.

[10] P. G. Bergmann, J. Acoust. Soc. Am. **17**, 329 (1946).

The Intermediate Coupling Theory of the Pseudoscalar Meson-Nucleon Interaction

P. T. MATTHEWS* AND ABDUS SALAM†
Institute for Advanced Study, Princeton, New Jersey
(Received December 19, 1951)

Tomonaga's intermediate coupling theory for scalar mesons is extended to pseudoscalar mesons with pseudoscalar coupling. The single free nucleon is discussed. Recoil is included nonrelativistically and the divergences are removed arbitrarily by a cutoff at the nucleon rest mass. Effects involving one virtual pair are allowed for, on the assumption that two or more virtual pairs may be neglected. The calculations are of a preliminary nature and certain possibilities for refining them are discussed. As they stand, they indicate that even for $f^2/4\pi \simeq 10$, a renormalized weak coupling expansion should give a very slowly converging, but not entirely distorted picture of the meson cloud surrounding a nucleon for pseudoscalar coupling.

INTRODUCTION

THE interpretation of recent meson experiments, based on general considerations such as parity conservation and detailed balancing, shows that the π-meson is pseudoscalar.[1] On the other hand, purely theoretical arguments have shown that only the theories of scalar and pseudoscalar mesons with scalar coupling can be made finite to any order in the coupling constant by renormalization, and of these the pseudoscalar is preferable since it contains one less arbitrary constant.[2] This much agreement between pure theory and the experimental facts is encouraging. But it is still not possible to make a detailed comparison of renormalized pseudoscalar meson theory with experiment because renormalization has been carried out in the general framework of an expansion in the coupling constant. Calculations made on the assumption that this constant, f, is small lead to values of f, to give the required orders of magnitude, ($f^2/4\pi \simeq 10$), which invalidate this assumption.[3] This paper attempts to develop methods of calculation which do not depend on the smallness of the coupling constant and thereby to check how much can safely be deduced from the first one or two terms in the small coupling expansion. Preliminary calculations are presented, and the work is mainly of methodological interest.

The simplest system which one can consider is that of a single free nucleon. By "free" we mean a real physical particle capable of interaction with the meson field. For the purpose of calculation it is usual to analyze this state in a representation based on the bare mesons and bare nucleons. By "bare" we mean fictitious mathematical particles which are eigenstates of the bare Hamiltonians with no interaction term. The free nucleon state has nonzero representatives, besides that corresponding to a single bare nucleon, and for this reason the free nucleon is sometimes pictured as a bare nucleon surrounded by a cloud of bare mesons and bare nucleon antinucleon pairs. Our purpose is to examine the probability distribution of this cloud.

More explicitly if ψ is the state vector of the interacting meson and nucleon fields, which represents a single free nucleon, then we wish to calculate the representatives $(\psi|\mathbf{p}, \cdots; \mathbf{q}, \cdots; \mathbf{k}, \cdots)$ where $\mathbf{p}, \cdots; \mathbf{q}, \cdots; \mathbf{k}\cdots$ is a state vector in Fock space, $\mathbf{p}$, $\mathbf{q}$, and $\mathbf{k}$ being the momenta of the bare nucleons, antinucleons, and mesons, respectively.

These representatives are the solutions to a set of Schrödinger equations which are derived in Sec. 2. For comparison with the later work these equations are then solved by successive approximation in f, according to ordinary weak coupling theory. To first order, this allows for, at most, one meson or one meson and one pair in the cloud, and assumes that by far the largest representative is that for which there are no particles in the cloud at all, $(\psi|\mathbf{p})$.

An alternative approach is Tomonaga's theory of intermediate coupling,[4] which was applied by him to the free nucleon in scalar meson theory with complete neglect of recoil. In this approximation no pairs can occur, but one allows for any number of mesons in the cloud, with the simplifying assumption that they all lie in the same state. An exact solution can be obtained in this form for neutral scalar mesons, and indeed Glauber and Luttinger[5] have developed a neat method for deriving a complete set of exact solutions. These show that if the coupling constants of the order here considered are inserted in scalar theory the largest representative corresponds to a state in which at least one meson is present, and the small coupling approximation breaks down completely.[4]

In Sec. 3, this method is extended to the positive energy subspace of pseudoscalar theory with recoil included nonrelativistically. (That is to say pairs are

* Now at Cavendish Laboratory, Cambridge, England.
† Now of Government College, Lahore, Pakistan, and St. John's College, Cambridge, England.
[1] R. E. Marshak, Revs. Modern Phys. **23**, 137 (1951).
[2] P. T. Matthews and Abdus Salam, Revs. Modern Phys. **23**, 311 (1951).
[3] For nuclear forces $f^2/4\pi \simeq 4$; H. Bethe, Phys. Rev. **76**, 191 (1949). For photomeson production $f^2/4\pi \simeq 40$; K. A. Brueckner, Phys. Rev. **79**, 645 (1950). While to give the right orders of magnitude for the anomalous nucleon magnetic moments $f^2/4\pi \simeq 10$; K. M. Case, Phys. Rev. **76**, 14 (1949).
[4] S. Tomonaga, Prog. Theoret. Phys. **2**, 6 (1947). Applications with the same approximations have been made by K. M. Watson and E. W. Hart, Phys. Rev. **79**, 918 (1950).
[5] R. J. Glauber and J. M. Luttinger, unpublished. We are deeply indebted to Dr. Glauber for showing us his work on this subject.

arbitrarily excluded, and it is assumed that the momenta of the particles in the cloud are small compared with the nucleon rest mass.) It is shown in subsections 3 (a), (b), and (c) that for this model the Hamiltonian can be split into two parts, the largest of which can be treated exactly by the Glauber-Luttinger method. The remainder is then considered in subsection (d) as a perturbation, using the complete set of exact solutions as a basis.

In Sec. 4 the method is extended to the case in which it is assumed that one pair, but not more, may appear in the cloud. Unlike the model of Sec. 3, this may be regarded as an approximation to the real problem. In treating the pair, only large components of the interaction are considered. A solution similar to that obtained above proves to be still possible, and is compared with that given by weak coupling theory.

The energy, corresponding to the eigenstate considered, includes the self energy of the free nucleon and is divergent. In this paper all divergent integrals are cut off at the nucleon rest mass. This is a questionable assumption in pseudoscalar theory which affects the numerical conclusions. This is discussed in the last section.

We deal so far with a single stationary nucleon in interaction with neutral mesons. This is a purely academic problem. In the appendix a method for extending these considerations to charged mesons is indicated. If the results were further generalized to describe a nucleon of given momentum, the matrix elements of an electromagnetic potential between two such states would lead directly to an estimate of the nucleon magnetic moments. It was felt that the method must be considerably refined before it would be worthwhile carrying out such a calculation, but we have this possibility in mind in the final discussion.

1. STATE VECTORS IN FOCK SPACE

We wish to find the representatives in Fock[5a] space of the state vector which represents a single free nucleon. As a preliminary we consider an assembly of bare bosons which may lie in any of an infinite set of states determined by the momenta $\mathbf{k}_1, \mathbf{k}_2, \cdots, \mathbf{k}_a \cdots$. If the assembly consists of particles in a particular set of states represented by the upper suffices $1, \cdots, r, \cdots, n$, this can be represented by the ket

$$\mathbf{k}^1, \cdots, \mathbf{k}^r, \cdots, \mathbf{k}^n) \quad r=1, 2, \cdots, n \tag{1.1}$$

or alternatively by the normalized ket

$$n_1, \cdots, n_a, \cdots), \tag{1.2}$$

where[6]

$$n_a=\sum_r \delta_{ra} \tag{1.3}$$

is the number of particles in the state a.[7] If we distinguish between the orderings of the factors in the ket (1.1), the number of such kets which corresponds to a single ket (1.2) is

$$n!\prod_a (n_a!)^{-1}. \tag{1.4}$$

Define the normalization of (1.1) by

$$\cdots n_a \cdots)=(n!)^{\frac{1}{2}}\prod_a (n_a!)^{-\frac{1}{2}}|\mathbf{k}^1, \cdots, \mathbf{k}^r, \cdots, \mathbf{k}^n), \tag{1.5}$$

where $\mathbf{k}^1, \cdots, \mathbf{k}^n)$ is any particular ket satisfying (1.3). Now since (1.2) is normalized we have the unit matrix

$$\begin{aligned} 1&=\sum_{\cdots n_a \cdots} \cdots n_a \cdots)(\cdots n_a \cdots \\ &=\sum_{\cdots n_a \cdots} |\mathbf{k}^1, \cdots, \mathbf{k}^r, \cdots, \mathbf{k}^n)n! \\ &\qquad \times\prod_a (n_a!)^{-1}(\mathbf{k}^1, \cdots, \mathbf{k}^r, \cdots \mathbf{k}^n| \\ &=\sum_n \int\cdots\int |\mathbf{k}^1, \cdots, \mathbf{k}^r, \cdots, \mathbf{k}^n) \\ &\qquad \times(\mathbf{k}^1, \cdots, \mathbf{k}^r, \cdots, \mathbf{k}^n| \; d\mathbf{k}^1 \cdots d\mathbf{k}^n \end{aligned} \tag{1.6}$$

by (1.5) and (1.4). We will have frequent occasion to use the unit matrix in its latter form.

Now we have the relations

$$q_a^*|\cdots, n_a, \cdots)=(n_a+1)^{\frac{1}{2}}|\cdots, n_a+1, \cdots), \tag{1.7}$$

and

$$q_a|\cdots, n_a, \cdots)=n_a^{\frac{1}{2}}|\cdots, n_a-1, \cdots). \tag{1.8}$$

Combining (1.5) and (1.7)

$$q^*(\mathbf{k})|\mathbf{k}^1, \cdots, \mathbf{k}^n)=(n+1)^{\frac{1}{2}}|\mathbf{k}^1, \cdots, \mathbf{k}^n, \mathbf{k}). \tag{1.9}$$

Combining (1.5), (1.8), and (1.3),

$$\begin{aligned} &q(\mathbf{k}_a)|\mathbf{k}^1, \cdots, \mathbf{k}^r, \cdots, \mathbf{k}^n) \\ &\qquad =n^{-\frac{1}{2}}\textstyle\sum_r \delta_{ra}|\mathbf{k}^1, \cdots, \mathbf{k}^r, \cdots \mathbf{k}^n, \mathbf{k}_a^{-1}), \end{aligned}$$

where the notation on the right-hand side means that $\mathbf{k}^r$ is dropped from the ket $\mathbf{k}^1, \cdots, \mathbf{k}^r, \cdots \mathbf{k}^n)$ if $\mathbf{k}^r=\mathbf{k}_a$. It follows immediately that

$$\begin{aligned} &\textstyle\sum_a f(\mathbf{k}_a)q(\mathbf{k}_a)|\mathbf{k}^1, \cdots, \mathbf{k}^n) \\ &\qquad =n^{-\frac{1}{2}}\textstyle\sum_r f(\mathbf{k}^r)|\mathbf{k}^1, \cdots, \mathbf{k}^{r-1}, \mathbf{k}^{r+1}, \cdots, \mathbf{k}^n) \end{aligned} \tag{1.10}$$

For a field of bare fermions[8] we can define a ket by the relation

$$\cdots, n_a, \cdots)=(-1)^P(n!)^{\frac{1}{2}}|\mathbf{p}^1, \cdots, \mathbf{p}^r, \cdots \mathbf{p}^n), \tag{1.11}$$

where $\cdots, n_a, \cdots)$ is again normalized. From this it follows that

$$\mathbf{p}^1, \cdots, \mathbf{p}^r, \cdots, \mathbf{p}^n)=(n!)^{-\frac{1}{2}}a^{*1}a^{*2}\cdots a^{*r}\cdots a^{*n})_0. \tag{1.12}$$

[5a] V. Fock, Z. Physik **75**, 622 (1932).

[6] By δ_{ra} we mean zero except when $k^r=k_a$.

[7] The ket $k^1, \cdots, k^n)$ defined above is equal to $(n!)^{-\frac{1}{2}}\Sigma_P$ times the ket $k^1, \cdots, k^n)$ defined by Dirac. P. A. M. Dirac, *Quantum Mechanics* (Oxford University Press, London, 1947), Chapter X, Eq. (3).

[8] The notation is that of Dirac (see reference 7, Sec. 65) except that $a^*=\eta$, $a=\eta$ ond our $p^1, \cdots, p^n)$ is equal to $(n!)^{-\frac{1}{2}}\Sigma_{\pm P}$ times $p^1, \cdots, p^n)$ defined by Dirac.

It can then be deduced that

$$\sum_s \int \cdots \int \mathbf{p}^1, \cdots, \mathbf{p}^n)(\mathbf{p}^1, \cdots, \mathbf{p}^n \quad d\mathbf{p}^1 \cdots d\mathbf{p}^1 = 1. \tag{1.13}$$

(Here the upper suffixes also specify spin and the integrals include sums over spins.) and

$$a^*(\mathbf{p})|\mathbf{p}^1, \cdots, \mathbf{p}^n) = (n+1)^{\frac{1}{2}}|\mathbf{p}, \mathbf{p}^1, \cdots, \mathbf{p}^n),$$

$$\sum_s f(\mathbf{p}_s)a(\mathbf{p}_s)|\mathbf{p}^1, \cdots, \mathbf{p}^r, \cdots, \mathbf{p}^n)$$

$$= n^{-\frac{1}{2}} \sum_r (-1)^{r-1} f(\mathbf{p}^r)|\mathbf{p}^1, \cdots, \mathbf{p}^{r-1}, \mathbf{p}^{r+1}, \cdots \mathbf{p}^n). \tag{1.14}$$

With these relations it is a simple matter to derive the equations for the representatives, $(\psi|\mathbf{p}, \cdots; \mathbf{q}, \cdots; \mathbf{k}, \cdots)$.

2. WEAK COUPLING THEORY

The stationary Schrödinger equation for the interaction of nucleons with pseudoscalar mesons, with pseudoscalar coupling is, in the bra form,

$$(\psi|H_0+H_1-E| = 0, \tag{2.1}$$

where E is an eigenvalue and $(\psi$ an eigenstate;

$$H_0 = \int d\mathbf{p} \sum_r \{a_r^*(\mathbf{p})a_r(\mathbf{p}) + b_r^*(\mathbf{p})b_r(\mathbf{p})\}p_0 + \int d\mathbf{k} q^*(\mathbf{k})q(\mathbf{k})k_0,$$

$$p_0 = (|\mathbf{p}|^2+\kappa^2)^{\frac{1}{2}}, \quad k_0 = (|\mathbf{k}|^2+\mu^2)^{\frac{1}{2}}; \tag{2.2}$$

and

$$H_1 = f' \int d\mathbf{p} d\mathbf{p}' d\mathbf{k} \sum_{rs} \delta(\text{momentum})(a_r^*(\mathbf{p}') + b_r(\mathbf{p}'))(a_s(\mathbf{p}) + b_s^*(\mathbf{p}))(q^*(\mathbf{k}) + q(\mathbf{k})) \times iu_r^*(\mathbf{p}')\beta\gamma_5 u_s(\mathbf{p})k_0^{-\frac{1}{2}}, \tag{2.3}$$

$$f' = 2^{-\frac{1}{2}}(2\pi)^{-\frac{1}{2}}f. \tag{2.4}$$

a^*, a; b^*, b; and q^*, q are the creation and annihilation operators for bare nucleons, antinucleons, and mesons, respectively. β and γ_5 are the usual Dirac matrices.[9] δ (momentum) is a δ-function of the momentum transfer produced by the operators. The bare Hamiltonian defines a complete set of kets for the bare particles,

$$H_0 - E'|\mathbf{p}_r^1, \cdots, \mathbf{p}_{r'}^L; \mathbf{q}_s^1, \cdots \mathbf{q}_{s'}^M; \mathbf{k}^1, \cdots, \mathbf{k}^n) = 0, \tag{2.5}$$

where the suffixes r and s denote spin. These can be normalized as in Sec. 1 and form the basis of a representation in which (2.1) becomes

$$(\psi|H_0+H_1-E|\mathbf{p}_r^1, \cdots \mathbf{p}_{r'}^{L+1}; \times \mathbf{q}_s^1, \cdots, \mathbf{q}_{s'}^L; \mathbf{k}^1, \cdots, \mathbf{k}^n) = 0. \tag{2.6}$$

[9] We take $\hbar = c = 1$, Heaviside units and δ-function normalization. r, s, t $(=1, 2)$ denote spin states.

The state $(\psi$, which represents a single free nucleon, reduces to a single bare nucleon as f tends to zero, and the only nonzero representative would then be $(\psi|\mathbf{p})$. We have inserted in (2.6) the typical ket which is related to $\mathbf{p}$) through the interaction (2.3). Our object is to solve this equation as generally as possible by Tomonaga's method of intermediate coupling.[4]

For comparison with later results we first solve this equation by successive approximation in f to obtain the familiar results of weak coupling theory. To first order in f (2.6) is

$$(p_0 - E)(\psi|\mathbf{p}_s) = -f'\Big[\sum_t \int d\mathbf{k} i u_+^*(\mathbf{p}-\mathbf{k}_t)\beta\gamma_5 u_+(\mathbf{p}_s)k_0^{-\frac{1}{2}}(\psi|\mathbf{p}-\mathbf{k}_t; \mathbf{k}) + \sum_{a,b} \int\int d\mathbf{p}' d\mathbf{k} 2^{\frac{1}{2}} u_+^*(\mathbf{p}_a')\beta\gamma_5 u_-(-\mathbf{p}'-\mathbf{k}_b) \times k_0^{-\frac{1}{2}}(\psi|\mathbf{p}_a', \mathbf{p}_s; -\mathbf{p}'-\mathbf{k}_b; \mathbf{k})\Big], \tag{2.7}$$

$$(p_0^1 + k_0 - E)(\psi|\mathbf{p}_s^1, \mathbf{k}) = -f' \sum_u i u_+^*(\mathbf{p}^1+\mathbf{k}_u)\beta\gamma_5 u_+(\mathbf{p}_t)k_0^{-\frac{1}{2}}(\psi|\mathbf{p}^1+\mathbf{k}_u), \tag{2.8}$$

$$(p_0' + p_0'' + q_0 + k_0 - E)(\psi|\mathbf{p}_a', \mathbf{p}_s''; q_b; \mathbf{k}) = -f' 2^{-\frac{1}{2}}[i u_-^*(-\mathbf{p}'-\mathbf{k}_b)\beta\gamma_5 u_+(\mathbf{p}_a')k_0^{-\frac{1}{2}} \times \delta(\mathbf{p}''-\mathbf{p})(\psi|\mathbf{p}_s'') - i u_-^*(-\mathbf{p}''-\mathbf{k}_b) \times \beta\gamma_5 u_+(\mathbf{p}_s'')k_0^{-\frac{1}{2}}\delta(\mathbf{p}'-\mathbf{p})(\psi|\mathbf{p}_a')]. \tag{2.9}$$

These equations are obtained by (1.7), (1.8), (1.13), and (1.14), the bra $(\psi$, being brought through to the left after the operation of the operators. The δ-functions appear because all representatives have the same momentum. To zero order in f'

$$E = p_0, \quad (\psi|\mathbf{p}_s) = 2^{-\frac{1}{2}}. \tag{2.10}$$

(The factor $2^{-\frac{1}{2}}$ is a normalization to allow for the two possible spin states.) Substituting (2.10) into (2.8) and (2.9), determines $(\psi|\mathbf{p}, \mathbf{k})$ and $(\psi|\mathbf{p}', \mathbf{p}''; \mathbf{q}; \mathbf{k})$ to this order. Substituting these expressions back into (2.8) gives the usual expression for the self-energy,

$$\Delta E = E - p_0.$$

The terms arising from $(\psi|\mathbf{p}', \mathbf{p}''; \mathbf{q}; \mathbf{k})$ are

$$(f')^2 \sum_{a,b} \int d\mathbf{p}' d\mathbf{k} u_+^*(\mathbf{p}_a')\beta\gamma_5 u_-(-\mathbf{p}'-\mathbf{k}_b) \times k_0^{-1}(p_0' + q_0 + k_0)^{-1}[u_-^*(-\mathbf{p}'-\mathbf{k}_b)\beta\gamma_5 u_+(\mathbf{p}_a')\delta(0) - u_-^*(-\mathbf{p}-\mathbf{k}_b)\beta\gamma_5 u_+(\mathbf{p}_a)\delta(\mathbf{p}'-\mathbf{p})]. \tag{2.11}$$

The first term is a vacuum effect due to unrestricted creation of the pair $(\mathbf{p}', \mathbf{q}, \mathbf{k})$ for any values of $\mathbf{p}'$. The second term is the restriction on this because of the presence of the electron $\mathbf{p}$. The state $(\psi$ represents a free nucleon plus the vacuum. Only the second term

contributes to the nucleon energy. One thus obtains the usual expression for the self-energy of the nucleon itself.

A similar separation of vacuum terms is required when considering the probability of finding a pair in the nucleon cloud. Thus the squaring of (2.9) gives the probability of a pair and a meson in the vacuum and in the nucleon cloud. The probability for the nucleon cloud alone is given by the cross terms only, namely,

$$R\left[\frac{-(f')^2}{2}\sum_{a,b,c}\frac{u_+^*(\mathbf{p}_a)\beta\gamma_5 u_-(\mathbf{q}_b)u_-(\mathbf{q}_b)\beta\gamma_\xi u_+^*(\mathbf{p}_c)}{k_0(p_0+q_0+k_0)^2}\right],$$

where

$$\mathbf{q}=-\mathbf{p}-\mathbf{k}.$$

Note that this separation of vacuum effects is exact in weak coupling theory because the analogous calculations for the vacuum state alone lead to precisely the expressions which have been dropped. (The separation of vacuum effects is dealt with particularly neatly in Feynman's formulation.[10])

3. INTERMEDIATE COUPLING—NO PAIRS

(a) The Energy

We now develop Tomonaga's solution which is independent of the size of f, but with the quite arbitrary restriction that all representatives involving pairs are neglected, (projection on the positive energy subspace). For pseudoscalar theory this cannot be regarded as an approximation to the complete system since we are actually neglecting the large components of the interaction. The typical equation is

$$(\psi|H_0+H_1-E|\mathbf{p}_t{}^n;\mathbf{k}^1,\cdots,\mathbf{k}^n)=0, \quad (3.1)$$

where

$$\mathbf{p}^n=\mathbf{P}-\textstyle\sum^n\mathbf{k}^r. \quad (3.2)$$

$\mathbf{P}$ is the total momentum of the cloud, which will be taken to be zero in the rest of this work. It is legitimate to put in the restriction on the form of the representatives, since, as will be seen immediately below, the Eqs. (3.3) only relate representatives of the same momentum. [Alternatively, one could insert a δ-function in the form for $(\psi|\mathbf{p}_t{}^n;\mathbf{k}^1,\cdots,\mathbf{k}^n)$.] Substituting for H and H_1 from (2.2) and (2.3) and using (1.7) and (1.8), one obtains an equation in which all operators have been replaced by c-numbers. The bra $(\psi$ can then be brought through to give directly the (stationary Schrödinger) equation for the representatives (wave function);

$$\begin{aligned}(E-p_0{}^n+\textstyle\sum^n k_0{}^r)&(\psi|\mathbf{p}_t{}^n;\mathbf{k}^1,\cdots,\mathbf{k}^n)\\ =f'[&(n+1)^{\frac{1}{2}}\textstyle\sum_s\int U^*(\mathbf{p}_t{}^n,\mathbf{p}_s{}^{n+1})\\ &\times(\psi|\mathbf{p}_s{}^{n+1};\mathbf{k}^1,\cdots,\mathbf{k}^{n+1})d\mathbf{k}^{n+1}\\ &+n^{-\frac{1}{2}}\sum_r^n\sum_s U(\mathbf{p}^n+\mathbf{k}_s{}^r,\mathbf{p}_t{}^n)\\ &\times(\psi|\mathbf{p}^n+\mathbf{k}_s{}^r;\mathbf{k}^1,\cdots,\mathbf{k}^{r-1},\mathbf{k}^{r+1},\cdots,\mathbf{k}^n)], \quad (3.3)\end{aligned}$$

[10] R. P. Feynman, Phys. Rev. **76**, 649, 669 (1949).

where

$$U(\mathbf{p}+\mathbf{k}_s,\mathbf{p}_t)=iu_s^*(\mathbf{p}+\mathbf{k})\beta\gamma_5 u_t(\mathbf{p})(k_0)^{-\frac{1}{2}}. \quad (3.4)$$

The energy for the state $(\psi$ is

$$\begin{aligned}W&=(\psi|H_0+H_1|\psi)\\ &=\sum_n^\infty\int(d\mathbf{k})^n\textstyle\sum_t(\psi|H_0+H_1|\mathbf{p}_t{}^n;\mathbf{k}^1,\cdots,\mathbf{k}^n)\\ &\qquad\times(\mathbf{p}_t{}^n;\mathbf{k}^1,\cdots,\mathbf{k}^n|\psi), \quad (3.5)\end{aligned}$$

where

$$\int(d\mathbf{k})^n=\int\cdots\int d\mathbf{k}^1\cdots d\mathbf{k}^n.$$

This can be derived immediately from (3.3), giving

$$\begin{aligned}W=\sum_n^\infty\int(d\mathbf{k})^n\sum_t\Big\{&(p_0{}^n+nk_0{}^n)(\psi|\mathbf{p}_t{}^n,\mathbf{k}^1,\cdots,\mathbf{k}^n)^2\\ &+f'\Big[(n+1)^{\frac{1}{2}}\int\sum_s U^*(\mathbf{p}_t{}^n,\mathbf{p}_s{}^{n+1})\\ &\times(\psi|\mathbf{p}_s{}^{n+1};\mathbf{k}^1,\cdots,\mathbf{k}^{n+1})\\ &\times(\mathbf{p}_t{}^n;\mathbf{k}^1,\cdots,\mathbf{k}^n)|\psi)d\mathbf{k}^{n+1}\\ &+n^{\frac{1}{2}}\textstyle\sum_s U(\mathbf{p}_s{}^{n-1},\mathbf{p}_t{}^n)(\psi|\mathbf{p}_s{}^{n-1};\mathbf{k}^1,\cdots,\mathbf{k}^{n-1})\\ &\times(\mathbf{p}_t{}^n;\mathbf{k}^1,\cdots,\mathbf{k}^n|\psi)\Big]\Big\}. \quad (3.6)\end{aligned}$$

Here we have also replaced

$$\sum_r^n f(\mathbf{k}^r)$$

by $nf(\mathbf{k}^n)$ in the integrands (where f is any function). If we now change the variable of summation in the second term from n to $n+1$, the last two terms are the complex conjugates of each other. Thus

$$\begin{aligned}W=\sum_n^\infty\int(d\mathbf{k})^n\textstyle\sum_t\{&(p_0{}^n+nk_0{}^n)(\psi|\mathbf{p}_t{}^n;\mathbf{k}^1,\cdots,\mathbf{k}^n)^2\\ &+2n^{\frac{1}{2}}R[f'\textstyle\sum_s U(\mathbf{p}_s{}^{n-1},\mathbf{p}_t{}^n)\\ &\times(\psi|\mathbf{p}_s{}^{n-1};\mathbf{k}^1,\cdots,\mathbf{k}^{n-1})\\ &\times(\mathbf{p}_t{}^n;\mathbf{k}^1,\cdots,\mathbf{k}^n|\psi)]\}. \quad (3.7)\end{aligned}$$

We now introduce the Tomonaga approximation which is that

$$(\mathbf{p}_t{}^n;\mathbf{k}^1,\cdots,\mathbf{k}^n|\psi)=2^{-\frac{1}{2}}c_n\prod_r^n f(k^r), \quad (3.8)$$

where $\int f^2(k)d\mathbf{k}=1$, and thus

$$\sum_n^\infty c_n{}^2=1. \quad (3.9)$$

$f(k)$ is the wave function in momentum space for a

single meson, giving its momentum distribution. $f(k)$ is interpreted as the lowest state for a meson bound to the nucleon and the assumption is that all the mesons in the cloud go independently into this single state. [Note that the wave function is assumed to be independent of the spin direction of the nucleon. However, for a given set of k^r the nucleon momentum is fixed by (3.2). The factor $2^{-\frac{1}{2}}$ is a normalization caused by the two possible spin states of the nucleon for a given set k^r.] Substituting (3.8) into (3.7), we have

$$W=\sum_n^\infty\{n\alpha_n c_n^2+2n^{\frac{1}{2}}\beta_n c_{n-1}c_n\}, \tag{3.10}$$

where

$$\alpha_n=\int(d\mathbf{k})^n(n^{-1}p_0+k_0^n)\prod_r^n f^2(k^r), \tag{3.11}$$

and

$$\beta_n=f'\int(d\mathbf{k})^n\sum_{s,t}2^{-1}U(\mathbf{p}_s^{n-1},\mathbf{p}_t^n)f(k^n)\prod_r^{n-1}f^2(k^r). \tag{3.12}$$

It is now our main purpose to find $f(k)$ and c_n which make W a minimum, subject to the condition (3.9). The momentum distribution of each meson is given by $f(k)$ and c_n^2 gives directly the probability distribution of the numbers of mesons in the cloud. The first step is to reduce the expressions α_n and β_n to integrals over a single variable.

We have (introducing the cutoff at κ)

$$\alpha_n=n^{-1}\int^\kappa(|\mathbf{k}^1+\cdots+\mathbf{k}^n|^2+\kappa^2)^{\frac{1}{2}}\prod_r^n f^2(k^r)(d\mathbf{k})^n$$
$$+\int^\kappa(k^2+\mu^2)^{\frac{1}{2}}f^2(k)d\mathbf{k} \tag{3.13}$$

where κ and μ are the nucleon and meson masses, respectively. Make the assumption that

$$|\mathbf{k}^1+\cdots+\mathbf{k}^n|<\kappa, \tag{3.14}$$

and expand in terms of the ratio. Then the first term of α_n is approximately

$$n^{-1}\int^\kappa\{\kappa+[(\mathbf{k}^1)^2+\cdots+(\mathbf{k}^n)^2]/(2\kappa)\}\prod_r^n f^2(k^r)(d\mathbf{k})^n;$$

and we thus have

$$\alpha_n=n^{-1}\kappa+\alpha, \tag{3.15}$$

$$\alpha=\int^\kappa k_0' f^2(k)d\mathbf{k}, \tag{3.16}$$

where

$$k_0'=k_0+(k^2/2\kappa). \tag{3.17}$$

By inserting the explicit values[11] for $u(p)$ we find

$$\sum_{s,t}\tfrac{1}{2}U(\mathbf{p}_s^{n-1},\mathbf{p}_t^n)$$
$$=i\left[\frac{p_s^{n-1}}{\kappa+p_0^{n-1}}-\frac{p_s^n}{\kappa+p_n^0}\right]\mathcal{G}(p^n)\mathcal{G}(p^{n-1})(k_0^n)^{-\frac{1}{2}}, \tag{3.18}$$

where

$$\mathcal{G}(p)=[1+p^2/(\kappa+p_0)^2]^{-\frac{1}{2}}. \tag{3.19}$$

By expanding the integrand of β_n in the same way as was done for α_n and dropping odd terms which will not contribute,

$$\beta_n=f'\int^\kappa(d\mathbf{k})^n ik_s(\kappa+p_0^n)^{-1}(k_0^n)^{-\frac{1}{2}}\mathcal{G}(p^n)$$
$$\times\mathcal{G}(p^{n-1})f(k^n)\sum_r^{n-1}f^2(k^r). \tag{3.20}$$

Putting $n=1$ (and dropping the suffix on β_1),

$$\beta=f'\int^\kappa\sum_{s,t}U(\mathbf{p}_s^0,\mathbf{p}_t^1)f(k)d\mathbf{k}, \tag{3.21a}$$
$$=f'\int^\kappa ik_s(\kappa+p_0^1)^{-1}k_0^{-\frac{1}{2}}\mathcal{G}(p^1)f(k)d\mathbf{k},$$
$$=f'\int^\kappa g(k)f(k)d\mathbf{k}, \tag{3.21}$$

where $g(k)$ is defined by the final equality. Returning to β_n we replace $(p^n)^2$ by $n\bar{k}^2$ (not $n^2\bar{k}^2$), where $\bar{k}$ is defined as the average value of k,

$$\bar{k}^2=\int^\kappa f^2(k)k^2d\mathbf{k}. \tag{3.22}$$

This is reasonable since the directions of the vectors $\mathbf{k}^r$ are assumed to be at random. The k^n dependence of the integrand is made to be the same as in β by the insertion of the required factors. In the compensating factors k^n is replaced by $\bar{k}$. Then,

$$\beta_n=\beta[\kappa+(\bar{k}^2+\kappa^2)^{\frac{1}{2}}][\kappa+(n\bar{k}^2+\kappa^2)^{\frac{1}{2}}]^{-1}$$
$$\times\mathcal{G}(\bar{k})\mathcal{G}(n^{\frac{1}{2}}\bar{k})\mathcal{G}[(n-1)^{\frac{1}{2}}\bar{k}]$$
$$=\beta[1-(n-1)(\bar{k}^2/2\kappa^2)];\quad n=2,3,\cdots, \tag{3.23}$$

the last equation following from an expansion in $(\bar{k}^2/\kappa^2)$.

(b) Evaluation of C_n

Let

$$W_0=\sum_n^\infty\{n\alpha c_n^2+2n^{\frac{1}{2}}\beta c_{n-1}c_n\}, \tag{3.24}$$

and

$$W'=\sum_n^\infty 2n^{\frac{1}{2}}\beta_n' c_{n-1}c_n, \tag{3.25}$$

[11] W. Heitler, *Quantum Theory of Radiation* (Oxford University Press, London, 1944), Chapter III, Sec. 9.

where

$$\beta_n' = \beta_n - \beta, \tag{3.26}$$

so that

$$W - \kappa = W_0 + W'. \tag{3.27}$$

The significance of this splitting of W is that α and β are independent of n. This allows us to employ methods previously applied to the no recoil approximation to derive a complete set of exact solutions for the minimizing of W_0. W' will then be treated as a perturbation using this set of solutions as a basis for the expansion.

The minimal equations for W_0 subject to the condition (3.9) are

$$(n\alpha - E)c_n + \beta(n^{\frac{1}{2}}c_{n-1} + (n+1)^{\frac{1}{2}}c_{n+1}) = 0, \tag{3.28}$$

where E is the eigenvalue of the energy. This can be written

$$(n-\epsilon)c_n + b(n^{\frac{1}{2}}c_{n-1} + (n+1)^{\frac{1}{2}}c_{n+1}) = 0, \tag{3.29}$$

where

$$\epsilon = E/\alpha \quad \text{and} \quad b = \beta/\alpha. \tag{3.30}$$

We now introduce the notation

$$c_n = (n|c), \tag{3.31}$$

where the bras $(n$ can be interpreted as the eigenbras of a family of bosons with only one available energy level (or, equivalently, to the eigenbras of a single harmonic oscillator). Now,

$$c) = \textstyle\sum_n n)(n|c). \tag{3.32}$$

so that, if q and q^* are the annihilation and creation operators associated with n), the Eq. (3.29) can be written

$$|q^*q + b(q+q^*)|c) = \epsilon c). \tag{3.33}$$

A complete set of solutions to this equation has been given[12] by Glauber and Luttinger, namely,

$$\epsilon^m = m - b^2, \tag{3.34}$$

$$(n|c^m) = \exp[-\tfrac{1}{2}b^2]\sum_{l=0}^{m} \frac{(m!)^{\frac{1}{2}}(n!)^{\frac{1}{2}}(-1)^{n-m+l}}{l!(m-l)!(n-m+l)!}b^{n-m+l}. \tag{3.35}$$

The solution belonging to the lowest level is thus

$$(n|c^0) = \exp[-\tfrac{1}{2}b^2](-b)^n(n!)^{-\frac{1}{2}}, \tag{3.36}$$

with corresponding energy

$$E^0 = -\beta^2/\alpha. \tag{3.37}$$

Both $(n|c^0)$ and E^0 are here given as functions of $f(k)$ which has now to be chosen to make E^0 a minimum. This can also be done exactly using Schwarz' inequality[13] and gives

$$f(k) = L^{-1}g(k)(k_0')^{-1}, \tag{3.38}$$

where $g(k)$ and k_0' are defined in (3.21) and (3.17) and L is a normalizing factor.

$$L = 4\pi\int^{\kappa} f^2(k)k^2dk = 4\pi A. \tag{3.39}$$

Substituting for $f(k)$ into (3.17) and (3.21), we obtain from (3.30)

$$b = f''(A/\pi)^{\frac{1}{2}}, \tag{3.40}$$

where

$$f'' = (f/2\pi^{\frac{1}{2}}). \tag{3.41}$$

A has been evaluated graphically (with cutoff at κ) and leads to

$$b = f''(2/25). \tag{3.42}$$

The plot of $f(k)$ is given in Fig. 1. $(n|c^0) = c_n{}^0$ can readily be evaluated for particular values of f''. For $f^2/4\pi = 10$ we have

$$c_0{}^2 = 0.95, \quad c_1{}^2 = 0.05, \quad c_2{}^2 = 0.00. \tag{3.43}$$

For $f^2/4\pi = 40$ we have

$$c_0{}^2 = 0.79, \quad c_1{}^2 = 0.18, \quad c_2{}^2 = 0.02. \tag{3.44}$$

By substituting (3.40), (3.38), (3.36), [with $g(k)$ defined by (3.21a)] into (3.8), it will be found that, apart from the normalizing factor $\exp[-\frac{1}{2}b^2]$, the intermediate coupling gives exactly the same expression for $\sum_i(\psi|p_i, k)$ as small coupling theory. Thus one goes into the other as the coupling becomes small.

---

[12] On (3.33) make the unitary transformation

$$c) = \exp[-b(q^*-q)]c').$$

The equation reduces to $|q^*q - b^2 - \epsilon|c') = 0$. But this is the standard oscillator equation so that we have a set of solutions

$$c') = m), \quad m = 1, 2, \cdots$$

giving the spectrum for ϵ, $\epsilon^m = m - b^2$. From (5.14) and (5.16)

$$c^m) = \exp[-b(q^*-q)]m).$$

Since $[q^*, q](=1)$ is a c-number, [see R. J. Glauber, Phys. Rev. 84, 395 (1951)]

$$\exp[-b(q^*-q)] = \exp[-\tfrac{1}{2}b^2]\exp[-bq^*]\exp[bq].$$

After substitution in (5.18) we have the equation for the ket

$$c^m) = \exp[-\tfrac{1}{2}b^2]\sum_{j=0}^{\infty}\sum_{l=0}^{m}(-1)^j b^{j+l}\frac{q^{*j}q^l}{j!\,l!}\Big|m\Big)$$

$$= \exp[-\tfrac{1}{2}b^2]\sum_{j=0}^{\infty}\sum_{l=0}^{m}(-1)^j b^{j+l}\frac{(m!)^{\frac{1}{2}}(m-l+j!)^{\frac{1}{2}}}{j!\,l!\,m-l!}|m-l+j),$$

which follows from repeated use of (1.7) and (1.8). Equation (3.35) is direct consequence of this relation.

[13] This is also due to Dr. Glauber and Dr. Luttinger. The lowest energy $E^0 = -\beta^2/\alpha$. By (5.1) and (5.2)

$$E^0 \sim -\left(\int f(k)g(k)d\mathbf{k}\right)^2\left(\int f^2(k)k_0'd\mathbf{k}\right)^{-1}.$$

Let

$$\bar{f}(k) = k(k_0')^{\frac{1}{2}}f(k), \quad \bar{g}(k) = k(k_0')^{-\frac{1}{2}}g(k).$$

Then

$$E^0 \sim -\left(\int \bar{f}(k)\bar{g}(k)dk\right)^2\left(\int \bar{f}^2(k)dk\right)^{-1},$$

which, by Schwarz' inequality, is a minimum if $\bar{f}(k) \sim \bar{g}(k)$. We thus have (3.38).

(c) The Perturbation

With the notation introduced in (3.31), (3.24) can be written as

$$W_0=(c|w|c)=\sum_{n,n'}(c|n)(n|w|n')(n'|c), \quad (3.45)$$

where

$$(n|w|n)=n\alpha, \quad (3.46)$$

$$(n-1|w|n)=(n|w|n-1)=n^{\frac{1}{2}}\beta. \quad (3.47)$$

The operator w has the eigenkets and eigenvalues $c^m)$ and E^m derived in the last section;

$$w|c^m)=E^m c^m). \quad (3.48)$$

Similarly,

$$W'=\sum_{n,n'}(c|n)(n|w'|n')(n'|c), \quad (3.49)$$

where

$$(n-1|w'|n)=(n|w'|n-1)=n^{\frac{1}{2}}\beta_n' \ (n=2,3,\cdots). \quad (3.50)$$

Suppose that the eigenkets for $w+w'$ are $c^m)+d^m)$ where $d^m)$ is of the same order as w'. Then by general perturbation theory

$$(c^m|d^0)=(c^m|w'|c^0)/(E^m-E^0). \quad (3.51)$$

The modification of $(n|c^0)$ due to w' is thus

$$\begin{aligned}(n|d^0)&=\sum_{m=1}^{\infty}(n|c^m)(c^m|d^0),\\ &=\sum_{m=1}^{\infty}\sum_{l,j}(n|c^m)(c^m|l)(l|w'|j)(j|c^0)(\alpha m)^{-1},\\ &=\sum_{m=1}^{m}\sum_{j=2}^{\infty}-(n|c^m)(c^m|j)(j-1|c^0)j^{\frac{1}{2}}\\ &\qquad\times(j-1)(\bar{k}^2/2\kappa^2)(\beta/\alpha m). \quad (3.52)\end{aligned}$$

The final equality follows from (3.23). The only term which is nonzero is $j=2$, since $(j-1|c^0)$ is negligible for $j\geqslant 3$. Thus

$$(n|d^0)=\sum_{m=1}^{\infty}-(n|c^m)(c^m|2)(1|c^0)(\bar{k}^2/2\kappa^2)(\beta/\alpha m). \quad (3.53)$$

Now, by (5.21),

$$(n|c^m)=(-1)^{n-m}(m|c^n), \quad (3.54)$$

so that the largest component of $d^0)$ is

$$(0|d^0)=-(0|c^1)(c^1|2)(1|c^0)(\bar{k}^2/2\kappa^2)(\beta/\alpha). \quad (3.55)$$

This is readily evaluated and leads to a negligible reduction (less than 0.01 for $f^2/4\pi=10$) in the probability for the single bare nucleon state.

4. ONE PAIR APPROXIMATION

We now attempt to solve the problem under the less restrictive assumption that one nucleon pair may be present in the cloud, but that the representatives which involve more than one pair are negligible. (The energy contained in the rest mass alone of these neglected components is so large that it is unlikely that they are appreciable, unless the average energy of the mesons in the cloud is comparable with that of a pair.) The typical representatives are

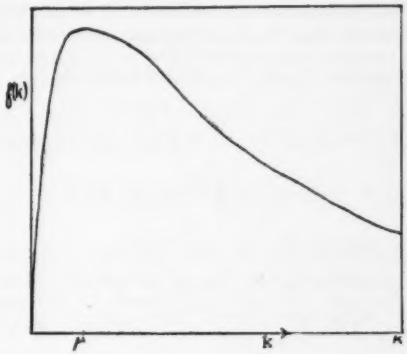

FIG. 1. Plot of $f(k)$.

$$(\psi|\mathbf{p}_i{}^n,\mathbf{k}^1\cdots\mathbf{k}^n)=(\psi|1,n), \quad (4.1)$$

and

$$(\psi|\mathbf{p}_s',\mathbf{p}_t'';\mathbf{q}_r{}^n;\mathbf{k}^1\cdots\mathbf{k}^n)=(\psi|3,n), \quad (4.2)$$

where

$$\mathbf{q}^n=-(\mathbf{p}'+\mathbf{p}''+\textstyle\sum^n\mathbf{k}^n). \quad (4.3)$$

The representatives satisfy the equations

$$(\psi|H-E|3,n)=0, \quad (4.4)$$

and the energy is given by[14]

$$\begin{aligned}(\psi|H|\psi)&=(\psi|H|1,n)(1,n|\psi)+(\psi|H|3,n)(3,n|\psi)\\ &=(\psi|H|1,n)(1,n|\psi)+E(\psi|3,n)^2, \quad (4.5)\end{aligned}$$

where

$$H=H_0+H_1.$$

Also

$$1=(\psi|\psi)=(\psi|1,n)^2+(\psi|3,n)^2. \quad (4.6)$$

Now

$$\delta((\psi|H|\psi)-E(\psi|\psi))=0. \quad (4.7)$$

Substituting from (4.5) and (4.6),

$$\delta X=\delta(Y-E(\psi|1,n)^2)=0, \quad (4.8)$$

where (4.8) defines X and

$$Y=(\psi|H|1,n)(1,n|\psi). \quad (4.9)$$

We will minimize X, subject to the Tomonaga approximation for $(\psi|1,n)$. Note that Y depends on $(\psi|3,n)$ through the operation of H_1 on $|1,n)$. This can be determined in terms of $(\psi|1,n)$ through the Schrödinger

[14] $1,n)$ $(1,n$ implies summation over all such states. $1,n)$ $(1,n+3,n)$ $(3,n$ is the unit operator, if representatives with more than one pair can be neglected.

Eq. (4.4) provided we approximate by taking only large components (that is, for pseudoscalar interaction, the pair creation or annihilation parts) of the interaction. This equation, derived just like (3.3) with the help of (1.11–13) is

$$(p_0'+p_0''+q_0^n+\textstyle\sum^n k_0^n-E)(\psi|\,\mathbf{p}_s',\mathbf{p}_t'';\mathbf{q}_v^n;\mathbf{k}^1\cdots\mathbf{k}^n)$$
$$=-f'\Big[(n+1)^{\frac{1}{2}}2^{-\frac{1}{2}}\int\{V^*(\mathbf{p}_s',\mathbf{q}_v^n,\mathbf{k}^{n+1})$$
$$\times(\psi|\,\mathbf{p}_t'',\mathbf{k}^1\cdots\mathbf{k}^{n+1})\delta(\mathbf{p}''-\mathbf{p}^{n+1})$$
$$-V^*(\mathbf{p}_t'',\mathbf{q}_v^n,\mathbf{k}^{n+1})(\psi|\,\mathbf{p}_s',\mathbf{k}^1\cdots\mathbf{k}^{n+1})$$
$$\times\delta(\mathbf{p}'-\mathbf{p}^{n+1})\}d\mathbf{k}^{n+1}+(2n)^{-\frac{1}{2}}$$
$$\times\sum_r^n\{V^*(\mathbf{p}_s',\mathbf{q}_v^n,\mathbf{k}^r)(\psi|\,\mathbf{p}_t'',\mathbf{k}^1\cdots\mathbf{k}^{r-1},\mathbf{k}^{r+1}\cdots k^n)$$
$$\times\delta(\mathbf{p}''+\sum_{r'\neq r}^n\mathbf{k}^{r'})-V^*(\mathbf{p}_t'',\mathbf{q}_v^n,\mathbf{k}^r)$$
$$\times(\psi|\,\mathbf{p}_s',\mathbf{k}^1\cdots\mathbf{k}^{r-1},\mathbf{k}^{r+1}\cdots\mathbf{k}^n)$$
$$\times\delta\Big(\mathbf{p}'+\sum_{r'\neq r}^n\mathbf{k}^{r'}\Big)\Big\}\Big], \quad (4.10)$$

where

$$V(\mathbf{p}_s,\mathbf{q}_r,\mathbf{k})=iu_t^*(p)\beta\gamma_5u_v(\mathbf{q})k_0^{-\frac{1}{2}}. \quad (4.11)$$

[$u(q)$ is a negative energy state]. This expression for the representative (wave function) $(\psi|\,\mathbf{p}',\mathbf{p}'';\mathbf{q}^n;\mathbf{k}'\cdots\mathbf{k}^n)$ is antisymmetrical in $\mathbf{p}'$, $\mathbf{p}''$, as it should be for Fermi statistics.

V can also be evaluated with the use of the equations of Sec. 1. We have

$$V=\sum_n\int(d\mathbf{k})^n\sum_t\Big\{(p_0^n+nk_0^n)(\psi|\,\mathbf{p}_t^n,\mathbf{k}^1\cdots\mathbf{k}^n)^2$$
$$+f'\Big[\sum_s n^{\frac{1}{2}}U(\mathbf{p}_s^{n-1},\mathbf{p}_t^n)(\psi|\,\mathbf{p}_s^{n-1},\mathbf{k}^1\cdots\mathbf{k}^{n-1})$$
$$\times(\mathbf{p}_t^n,\mathbf{k}^1\cdots\mathbf{k}^n|\psi)+\text{c.c.}+2^{\frac{1}{2}}(n+1)^{\frac{1}{2}}$$
$$+\int d\mathbf{p}'d\mathbf{k}^{n+1}\sum_{s,v}V(\mathbf{p}_s',\mathbf{q}_v''^{n+1},\mathbf{k}^{n+1})$$
$$\times(\psi|\,\mathbf{p}_s',\mathbf{p}_t^n;\mathbf{q}_v''^{n+1};\mathbf{k}'\cdots\mathbf{k}^{n+1})(\mathbf{p}_t^n,\mathbf{k}^1\cdots\mathbf{k}^n|\psi)$$
$$+2^{\frac{1}{2}}n^{\frac{1}{2}}\int d\mathbf{p}'\sum_{s,v}V(\mathbf{p}_s',\mathbf{q}_v'^{n-1},\mathbf{k}^n)$$
$$\times(\psi|\,\mathbf{p}_s',\mathbf{p}_t^n;\mathbf{q}'^{n-1};\mathbf{k}^1\cdots\mathbf{k}^{n-1})(\mathbf{p}_t^n,\mathbf{k}^1\cdots\mathbf{k}^n|\psi)\Big]\Big\}, \quad (4.12)$$

where

$$\mathbf{q}''^n=\mathbf{q}^n(\mathbf{p}''=\mathbf{p}^{n-1})=-(\mathbf{p}'+\mathbf{k}^n), \quad (4.13)$$
$$\mathbf{q}'^n=\mathbf{q}^n(\mathbf{p}''=\mathbf{p}^{n-1})=-(\mathbf{p}'-\mathbf{k}^{n+1}). \quad (4.14)$$

The four terms of (4.10) are referred to as (*a*), (*b*), (*c*), and (*d*). These are substituted into the fourth term of (4.12) to give A, B, C, and D, and into the third term to give A^1, B^1, C^1, and D^1.

When these substitutions are made the terms appear consistently in a certain pattern. Some terms (D, A, C^1, and A^1) come from unrestricted pair creation, as though no other Fermi particles were present. The other terms D, B, D^1, and B^1 represent the restrictions on these terms, because of the presence of a Fermi particle, through the operation of the Pauli principle. As is done in perturbation theory (see (2.12) and following discussion), we treat the first type of term as a vacuum effect and consider only the second (or restricting) terms as genuine contributions to the energy of the free particle under consideration. In this way one obtains an expression for Y, similar to that for W, with the addition of an extra term coming from D and B^1, which represent either the annihilation or creation of two mesons in the cloud. These two terms are the complex conjugates of each other. There are also the terms D^1 and B, which modify α, the coefficient of c_n^2. Of these, D^1 corresponds to the positron part of the nucleon self energy in which a meson is created and annihilated again with virtual pair creation; B is the absorption of one meson and the creation of another, with, again, pair creation in the intermediate state. These two terms are small compared with α and will not be considered further. We thus have, finally, the expression,

$$Y=\sum_n[n\alpha_nc_n^2+2n^{\frac{1}{2}}\beta_nc_{n-1}c_n+2n^{\frac{1}{2}}(n-1)^{\frac{1}{2}}\gamma_nc_{n-2}c_n], \quad (4.15)$$

where α_n and β_n are the same as in the no-pair expression, (3.11 and 3.12), and γ_n, after putting in the Tomonaga assumption for $(\psi|\,p^n,k^1\cdots k^n)$, (3.8), is

$$\gamma_n=-(f')^2\,2^{-1}\int^\kappa(\mathbf{dk})^n\sum_{v,s,t}V(\mathbf{p}_s^{n-2},\mathbf{q}_r,\mathbf{k}^n)$$
$$\times V^*(\mathbf{p}_t^n,\mathbf{q}_v,\mathbf{k}^{n-1})(p_0^{n-2}+p_0^n+q_0$$
$$+\sum^{n-1}k_0^r-E)f(k^{n-1})f(k^n)\prod_r^{n-2}f^2(k^r), \quad (4.16)$$

where

$$\mathbf{q}=\mathbf{p}^n+\mathbf{k}^n=\mathbf{p}^{n-2}-\mathbf{k}^{n-1}.$$

γ_n can be reduced by the methods applied to β_n to the approximate expression

$$\gamma_n=(f')^2\,4^{-1}\kappa^{-3}\Big[\int^\kappa k_sk_0^{-1}f(k)d\mathbf{k}\Big]^2. \quad (4.17)$$

To this approximation γ_n is independent of n and the suffix will be dropped.

We can proceed by the same method as before.

$$Y-\kappa=Y_0+Y', \quad (4.18)$$

where

$$Y_0=\sum_n\{n\alpha c_n^2+2n^{\frac{1}{2}}\beta c_{n-1}c_n+2n^{\frac{1}{2}}(n-1)^{\frac{1}{2}}c_nc_{n-2}\}, \quad (4.19)$$

and

$$Y'=\sum_n 2\beta_n' n^{\frac{1}{2}}c_{n-1}c_n. \quad (4.20)$$

The minimal Eq. (4.8) for Y_0 can again be solved exactly, giving a complete spectrum for E^m and the corresponding solutions c_n^m), which again form the basis for treating Y' as a perturbation. We proceed to the exact solution.

The minimal Eq. (4.8) for Y_0 is

$$(n-\epsilon)c_n+b(n^{\frac{1}{2}}c_{n-1}+(n+1)^{\frac{1}{2}}c_{n+1})+g(n^{\frac{1}{2}}(n-1)^{\frac{1}{2}}c_{n-2}+(n+2)^{\frac{1}{2}}(n+1)^{\frac{1}{2}}c_{n+2})=0, \quad (4.21)$$

where

$$\epsilon=E/\alpha, \quad b=\beta/\alpha, \quad g=\gamma/\alpha. \quad (4.22)$$

Introducing the notation of (3.31) this can be written

$$|q^*q-\epsilon+b(q+q^*)+g(qq+q^*q^*)|c)=0. \quad (4.23)$$

Instead of solving this equation in operator form, we use the more general method of transforming to the Schrödinger representation of the q-operators.[15]

Multiplying (4.23) by $(x$, we have

$$q^*=-i2^{-\frac{1}{2}}(d/dx-x), \quad q=-i2^{-\frac{1}{2}}(d/dx+x), \quad (4.24)$$

and the equation becomes

$$\{\tfrac{1}{2}[(1+2g)d^2/dx^2-x^2(1-2g)+1]+i2^{\frac{1}{2}}bd/dx+\epsilon\}(x|c)=0. \quad (4.25)$$

To eliminate the term in d/dx, make the transformation

$$(x|c)=\exp[-i2^{\frac{1}{2}}\delta](x|c'), \quad (4.26)$$

where

$$\delta=b(1+2g)^{-1}, \quad (4.27)$$

then

$$\{(1+2g)(d^2/dx^2-2\epsilon)+r^2(1-2g)+1+2\delta^2\}(x|c')=0. \quad (4.28)$$

Define r, y, and ϕ) by the equations,

$$r^2=(1-2g)(1+2g)^{-1}, \quad (4.29)$$

and

$$r^{\frac{1}{2}}x=y, \quad (4.30)$$

$$(x|c')=(y|\phi). \quad (4.31)$$

Then,

$$\{d^2/dy^2+\lambda-y^2\}(y|\phi)=0, \quad (4.32)$$

where

$$\lambda=(2m+1)=(1-4g^2)^{-\frac{1}{2}}[1+2\delta^2(1+2g)+2\epsilon]. \quad (4.33)$$

But (4.32) is the representative form of the standard oscillator equation.[16] This has solutions of the form

$$(y|\phi^m)=H_m^*(y)\exp[-\tfrac{1}{2}y^2], \quad (4.34)$$

where H_m^* is the Hermite polynomials, satisfying

$$H_m^{*\prime\prime}-2yH_m^{*\prime}+2mH_m^*=0. \quad (4.35)$$

Thus, by (4.26) and (4.30)

$$(x|c^m)=H_m^*(r^{\frac{1}{2}}x)\exp[-\tfrac{1}{2}rx^2-i2^{\frac{1}{2}}\delta x]. \quad (4.36)$$

The components

$$(n|c^m)=\int_{-\infty}^{\infty}(n|x)(x|c^m)dx, \quad (4.37)$$

where $(n|x)$ are the solutions of the standard oscillator equation, (4.32), with m replaced by n. (We are here repeating in representative form the argument of reference 12.) Thus

$$(n|c^m)=K^m\int_{-\infty}^{\infty}H_n^*(x)H_m^*(r^{\frac{1}{2}}x)\times\exp[-\tfrac{1}{2}(1+r)x^2-i\delta 2^{\frac{1}{2}}x]dx, \quad (4.38)$$

where K^m is a normalizing factor. This is a complete set of exact solutions to the Eq. (4.32).

The corresponding spectrum E^m is given by (4.33). We are primarily interested in the lowest level

$$E^0=-\beta^2/[\alpha(1+2g)]-\tfrac{1}{2}\alpha[1-(1-4g^2)^{\frac{1}{2}}]. \quad (4.39)$$

This is a function of $f(k)$ and $f(k)$ must be chosen to make a minimum. Expanding (4.39) in powers of g,

$$E^0=-(\beta^2/\alpha)(1-2g)+O(g^2). \quad (4.40)$$

If g is small we can take $f(k)$ to be the same as in the no-pair approximation, (3.38).

The values of $(n|c^0)$ or $c_n{}^0$ are determined by

$$c_n{}^0=K\int_{-\infty}^{\infty}H_n^*(x)\exp[-\tfrac{1}{2}(1+r)x^2-i\delta 2^{\frac{1}{2}}x]dx, \quad (4.41)$$

which can be evaluated exactly by substituting the explicit expressions for $H_n^*(x)$,

$$H_0^*(x)=1, \qquad H_1^*(x)=2x,$$
$$H_2^*(x)=4x^2-2, \qquad H_3^*(x)=8x^3-12x. \quad (4.42)$$

One thus finds after some elementary integration

$$c_0{}^0=K,$$

$$c_1{}^0=-K\left(\frac{2\delta}{1+r}\right),$$

$$c_2{}^0=K\left(\frac{1}{2}\right)^{\frac{1}{2}}\left[\left(\frac{2\delta}{1+r}\right)^2+\frac{r-1}{r+1}\right]$$

$$c_3{}^0=K\left(\frac{1}{3}\right)^{\frac{1}{2}}\left[\left(\frac{2\delta}{1+r}\right)^3+\frac{3\delta(r-1)}{(r+1)^2}\right] \quad (4.43)$$

where K is determined by the normalization of the state function.

[15] P. A. M. Dirac, (see reference 7) Sec. 34 and 60. Our q is Dirac's $\bar{\eta}$.

[16] L. I. Schiff, *Quantum Mechanics* (McGraw-Hill Book Company, Inc., New York, 1949), Chapter IV.

Since we are using the same form for $f(k)$, α and β are the same functions as before. The values of α and γ are obtained by substituting for $f(k)$ in (3.16) and (8.1) and by graphical integration. Then

$$g=(f^2/4\pi)(1/350). \tag{4.44}$$

c_n^0 can now be evaluated for different values of f. To determine K we must satisfy the equation

$$(\psi|1,n)^2+(\psi|3,n)^2=1,$$

or

$$\sum_n^\infty\Big[(c_n^0)^2+\sum_{a,b,c}\int d\mathbf{p}'d\mathbf{p}''(d\mathbf{k})^n \times(\psi|\mathbf{p}_a',\mathbf{p}_b'';\mathbf{q}_c^n;\mathbf{k}^1,\cdots,\mathbf{k}^n)\Big]=1. \tag{4.45}$$

The second term of the left-hand side has to be evaluated using (4.10) with the Tomonaga assumption for $(\psi|1,n)$ and $f(k)$ given by (3.38). In general this is a calculation very similar to that for Y which involves the separation of vacuum terms. For the values of f we are considering only $(\psi|3,1)^2$ is significant, which reduces to just the small coupling expression (2.13) multiplied by $(c_0^0)^2=K^2$. Expanding in (k/κ)

$$(\psi|3,1)^2=d_1^2\text{ (say)}=K^2(f')^2\int^\kappa(1-k^3/4\kappa^3)k_0^{-1} \times(2\kappa+k^2/2\kappa+k_0)^{-2}d\mathbf{k}. \tag{4.46}$$

This has been evaluated graphically, giving

$$d_1^2=K^2(f^2/4\pi)(1/60). \tag{4.47}$$

Combining this with the values for c_n^0 for particular values of f, K can be chosen to satisfy (4.45). The results are, for $f^2/4\pi=10$,

$$c_0^2=0.83,\quad c_1^2=0.04,\quad d_1^2=0.13. \tag{4.48}$$

For $f^2/4\pi=40$,

$$c_0^2=0.57,\quad c_1^2=0.05,\quad d_1^2=0.38. \tag{4.49}$$

These are exact solutions for the expression Y_0 for the lowest energy level. The expression (4.38) for the complete set of solutions for Y_0 could now be used to treat Y' as a perturbation, as was done in Sec. 3(c). These are negligible to the degree of accuracy to which we are working and will not be treated here.

Using (4.40) one can also evaluate E^0. The result is

$$E^0=-(f^2/4\pi)(1/500). \tag{4.50}$$

Thus for $f^2/4\pi=10$,

$$E^0=-(\kappa/50). \tag{4.51}$$

5. DISCUSSION

The approximations made in the above calculations are certainly crude. (To the order of magnitude considered electromagnetic effects are entirely negligible.) However, if the reasonableness of the cutoff at κ is accepted provisionally, they are at least self consistent. The technique would have to be considerably refined before it could be made the basis for a reliable calculation (of the nuclear magnetic moments for instance), but even in its present form there are certain interesting indications.

One striking feature is the way in which the representatives get smaller with increasing numbers of mesons, and the fact that for a coupling constant $(f^2/4\pi)$ as large as ten, the representative $(\psi|\mathbf{p})^2$ is still the largest by a factor of six. Even for a coupling constant of forty, the representatives fall off in the same order, but not nearly as rapidly as is assumed in small coupling theory. A quite different result is obtained for scalar mesons, where already for a coupling constant of two the free nucleon is just as likely to be in the bare nucleon plus bare meson state as in the single bare nucleon state, and the small coupling approximation breaks down altogether.[4] This is because the significant parameter in intermediate coupling theory (and to a rough approximation in weak coupling theory also) is not f^2 but f^2A [see (3.40)], and A is particularly small for pseudoscalar mesons. (It is this which leads one to consider large values of the coupling constant in the first place!) In fact the only difference between the values (4.49) quoted for $f^2/4\pi=10$ and those given by weak coupling theory lies in the wave function renormalization, which is treated as negligible to lowest order in a genuine expansion in f. This is certainly not correct and is particularly important in magnetic moment calculations, where a large part of the effect comes from the $(\psi|p)$ term. (The concept of *anomalous* magnetic moments ceases to have much meaning as soon as the normalization factor is appreciably different from one.)

The rate at which successive terms in the weak coupling expansion will fall off is very roughly indicated by b. For $f^2/4\pi=10$ we have $b=\frac{1}{4}$. Judging by particular calculations which have been made,[17] this is a very optimistic estimate and it is more probable that successive terms in the S-matrix will diminish in the ratio of about one-half. The great advantage of a renormalized weak coupling theory is that it deals exactly with the fundamental problems of divergences, virtual pair creation, and the separation of vacuum effects. The calculations presented here indicate that, although the weak coupling method yields a very slow convergence for the size of coupling which is required, the implicit assumption of the relative importance of the different

[17] E. Corinaldesi and G. Field, Phil. Mag. **40**, 1159 (1949); K. A. Brueckner, Phys. Rev. **79**, 641 (1950); K. Nakabayasi and I. Sato, Prog. Theoret. Phys. **6**, 252 (1951). These general remarks, based as they are on the consideration of the self-energy problem only, should not be taken too seriously. It may well be that the weak coupling expansion for a particular S-matrix element starts to diverge at about the third term. If this is so, the only line of progress seems to lie in a refinement of some intermediate coupling theory.

representatives is correct, and that the first two terms of the expansion should give correctly the general features of the theory. More reliance could be placed on an equation such as that of Bethe and Salpeter[18] for the deuteron in which the important terms are iterated to all orders in the coupling constant.

All the quantitative conclusions given above depend on the cutoff at κ. This was inserted because it was felt that the problem of the divergences was solved in principal for pseudoscalar coupling by renormalization, which would, in general, cut down the integrals at about this value. The qualitative conclusions just reached are much less sensitive to the cutoff, since to alter them the estimate of $(\psi|3,1)^2$ would have to be wrong by a factor of three, which we consider unlikely.

A mathematically rigorous method for incorporating renormalization into such a calculation has been given by Dyson.[19] In his theory a modified Schrödinger equation is obtained in the Schrödinger representation [IV, Eq. (99)] in which the Hamiltonian itself is an expansion in the charge. Each term in this expansion is finite after renormalization and also contains a convergence factor [IV, Eq. (102)] which may be made powerful enough to render finite any integral in which it occurs (for example the expressions for α, β, and γ above). The idea is (III) that only the first few terms in the Hamiltonian are important. The point at which the convergence factors cut down the integrands depends on certain arbitrary constants, Γ. The great advantage of Dyson's theory over a simple cutoff is that the convergence factors are introduced by a unitary transformation. Thus, if one approximates by considering only a certain number of terms in the Hamiltonian, it is always possible to write down an expression for what has been neglected, and, in principle at least, the validity of the approximation for particular values of Γ can be tested.

The other main source of error in the above calculations is in the reduction of the multiple integrals for α_n, β_n, and γ_n, [Sec. 3(*a*) and (4.15)]. These were complicated by the fact that any number of mesons was allowed for. On the basis of the above conclusion, that only representatives with a limited number of mesons are significant, a more accurate evaluation should be possible. If only two representatives were considered the method would reduce to that suggested by Tamm and Dancoff for the deuteron.[20] Refinements along these and other lines are being considered.

The greater part of this work was done when both authors were enjoying the hospitality of the Institute for Advanced Study, Princeton, for which they would like to express their gratitude to Dr. J. R. Oppenheimer. They are further indebted to Dr. Oppenheimer and the other members of the Institute for numerous helpful discussions. They also gratefully acknowledge discussions with Dr. F. J. Dyson and with Professor R. E. Peierls and other members of the Birmingham group. The work was completed while one of us (P. T. M.) was holding an Imperial Chemicals Industry Fellowship at Cambridge University, England.

Note added in proof:—The calculations of Koba, Kotani, and Nakai [Prog. Theoret. Phys. **6**, 849 (1951)], which have appeared recently, of the higher order e corrections to photomeson production, indicate that the optimistic view of renormalized perturbation theory for nuclear phenomena taken above is not justified, but the assumption in reference 17 is much more likely to be correct.

APPENDIX

The Charged No-Pair Model

If we consider a charged meson field, then the Hamiltonian of the Schrödinger equation is the same as (2.3) except that the factor $(q^*(\mathbf{k})+q(\mathbf{k}))$ is replaced by

$$(q_+(\mathbf{k})+q_-{}^*(\mathbf{k}))\tau+(q_+{}^*(\mathbf{k})+q_-(\mathbf{k}))\tau^*, \quad \text{(A.1)}$$

where the suffixes $+$ and $-$ denote operators associated with positive and negative mesons, respectively. If P and N denote protons and neutrons and P_A and N_A antiprotons and antineutrons, then

$$\begin{aligned} &\tau N=P, \quad \tau P=0; \quad \tau^* N=0 \quad \tau^* P=N; \\ &\tau P_A=N_A, \quad \tau N_A=0; \quad \tau^* P_A=0 \quad \tau^* N_A=P_A; \end{aligned} \quad \text{(A.2)}$$

which simply states that τ creates charge and τ^* annihilates.

If we consider a state which represents a single free stationary proton in the no-pair approximation, the various representatives all have zero momentum and unit positive charge, and are thus of the typical forms, (i),

$$(\psi|\mathbf{p}_i{}^{2n};\mathbf{l}^1,\cdots,\mathbf{l}^n;\mathbf{m}^1,\cdots,\mathbf{m}^n)=(\psi|1,n,n), \quad \text{(A.3)}$$

where l and m refer to positive and negative mesons, respectively, and

$$\mathbf{p}^{2n}=-(\sum_r^n \mathbf{l}^r+\sum_s^n \mathbf{m}^s) \quad \text{(A.4)}$$

represents a bare proton; or (ii),

$$(\psi|\mathbf{p}_i{}^{2n+1};\mathbf{l}^1,\cdots,\mathbf{l}^{n+1};\mathbf{m}^1,\cdots,\mathbf{m}^n) =(\psi|1,n+1,n), \quad \text{(A.5)}$$

where $\mathbf{p}_i{}^{2n+1}$ is a neutron.

[18] H. A. Bethe and E. E. Salpeter, Phys. Rev. **82**, 309 (1951); F. Low and M. Gell-Mann, Phys. Rev. **84**, 350 (1951).

[19] F. J. Dyson, Phys. Rev. **82**, 428 (1951); **83**, 608 (1951); Proc. Roy. Soc. (London) **A207**, 395 (1951); Phys. Rev. **83**, 1207 (1951); to be referred to as I, II, III, and IV, respectively. See in particular the first and last sections of IV for the modified Schrödinger equation. In I methods are developed for obtaining the terms of the Hamiltonian from generalized Feynman graphs. In II the machinery for renormalizing such a term is set up.

[20] I. G. Tamm, J. Phys. (U.S.S.R.) **9**, 449 (1945); S. M. Dancoff, Phys. Rev. **78**, 382 (1950).

The energy of the state ψ is

$$W=\sum_n^\infty \int (d\mathbf{l})^n (d\mathbf{m})^n \sum_s \Big\{ (\psi|H|1,n,n)(1,n,n|\psi) + \int d\mathbf{l}^{n+1} (\psi|H|1,n+1,n)(1,n+1,n|\psi) \Big\}. \quad (A.6)$$

This can be evaluated just as in Sec. 3, and we make the Tomonaga approximation,

$$(\psi|1,n,n)=2^{-\frac{1}{2}} c_{2n} \prod_r^n f_+(l^r) \prod_s^n f_-(m^s). \quad (A.7)$$

We thus obtain

$$W=\sum_n^\infty \int (d\mathbf{l})^n (d\mathbf{m})^n \Big\{ (p_0^{2n}+n\mathbf{l}_0^n+n\mathbf{m}_0^n) c_{2n}^2 \times \prod_r^n f_+^2(l^r) \prod_s^n f_-^2(m^s) + \int (p_0^{2n+1} + (n+1)\mathbf{l}_0^n + n\mathbf{m}_0^n) c_{2n+1}^2 \prod_r^{n+1} f_+^2(l^r) \prod_s^n f_-^2(m^s) d\mathbf{l}^{n+1} + f' 2^{-1} \sum_{s,t} \Big[n^{\frac{1}{2}} U(p_s^{2n+1}, p_t^{2n}) c_{2n-1}^* c_{2n} \times \prod_r^n f_+^2(l^r) \prod_s^{n-1} f_-^2(m^s) f_-(m^n) + \text{c.c.} + (n+1)^{\frac{1}{2}} \int \Big(U(p_s^{2n}, p_t^{2n+1}) c_{2n} c_{2n+1}^* f_+(l^{n+1}) \times \prod_r^n f_+^2(l^r) \prod_s^n f_-^2(m^s) + \text{c.c.} \Big) d\mathbf{l}^{n+1} \Big] \Big\}. \quad (A.8)$$

This expression can be considerably simplified if we introduce the notation

$$\mathbf{l}^n=\mathbf{k}^{2n-1}, \quad \mathbf{m}^n=\mathbf{k}^{2n}, \quad (A.9)$$

in which case

$$W=\sum_n \big[n\alpha_n c_n^2 + 2n^{\frac{1}{2}} (\beta_{2n-1} c_{2n-2} c_{2n-1} + \beta_{2n} c_{2n-1} c_{2n}) \big], \quad (A.10)$$

where

$$\alpha_n = n^{-1} p_0^n + k_0^n, \quad (A.11)$$

$$\beta_n = f' 2^{-1} \sum_{s,t} \int (d\mathbf{k})^n U(\mathbf{p}_s^{n-1}, \mathbf{p}_t^n) f(k^n) \prod_r^{n-1} f^2(k^r), \quad (A.12)$$

where $f(k^r)$ is $f_+(k)$ or $f_-(k)$ according to whether r is odd or even. If we make the further assumption that

$$f_+(k)=f_-(k)=f(k), \quad (A.13)$$

thus neglecting the correlation due to charge,[21] we can write

$$\begin{aligned} W &= \sum_n \big[n c_n^2 \alpha_n + 2\{ (n-\tfrac{1}{2})^{\frac{1}{2}} c_{2n-2} c_{2n-1} \beta_{2n-1} \\ &\quad + n^{\frac{1}{2}} c_{2n-1} c_{2n} \beta_{2n} \} + 2(n^{\frac{1}{2}} - (n-\tfrac{1}{2})^{\frac{1}{2}}) \\ &\quad \times c_{2n-2} c_{2n-1} \beta_{2n-1} \big] \\ &= \sum_n \big[n\alpha_n c_n^2 + 2n^{\frac{1}{2}} c_{n-1} c_n (\beta_n 2^{-\frac{1}{2}}) \\ &\quad + 2(n^{\frac{1}{2}} - (n-\tfrac{1}{2})^{\frac{1}{2}}) c_{2n-2} c_{2n-1} \beta_{2n-1} \big]. \end{aligned} \quad (A.14)$$

The final expression is obtained by summing over $2n=n'$ in the bracket $\{\cdots\}$, in which case the two terms can be combined into a single sum over all values of n'. We can obtain an exact solution for the n independent parts of the first two terms and treat the remainder as a perturbation.

[21] Investigations of R. H. Dalitz and D. G. Ravenhall show that this is not a bad approximation. Phil. Mag. **42**, 1378 (1951).

A Phase Shift Analysis of Neutron-Deuteron Scattering*

A. L. LATTER†
Department of Physics, University of California, Los Angeles, California
AND
R. LATTER
Nuclear Energy Division, The RAND Corporation, Santa Monica, California
(Received January 7, 1952)

A simultaneous phase shift analysis of n-d and p-d angular cross sections is shown to be consistent with the charge-independence hypothesis. Disagreement is found with the theoretical phase shifts of Buckingham and Massey.

1. INTRODUCTION

EXPERIMENTAL angular cross sections for n-d scattering at 4.5 and 5.5 Mev have been determined by Wantuch[1] at Brookhaven. The d-p cross section at 10.4 Mev has been determined by Allred and Rosen[2] at Los Alamos. Breit has considered these data for consistency with charge-independence of nuclear forces.[3] He assumed the p-d cross section to be the square of the Coulomb plus nuclear scattering amplitudes and the nuclear scattering amplitude to be the square root of the n-d cross section. The difference between p-d and n-d cross sections, so calculated, he found to be of the same order of magnitude as the observed difference in the experimental curves.

We shall also treat the Wantuch and Allred-Rosen data, but more quantitatively by means of a thorough phase shift analysis. Our purpose is twofold, however; not only to test the charge-independence hypothesis, but also to make a direct comparison with the theoretical n-d phase shifts of Buckingham and Massey.[4] Noncentral and velocity dependent forces are presumed to be negligible throughout the present analysis.

A previous attempt has been made to check phase shifts with the Buckingham and Massey theory by Critchfield,[5] using the p-d angular cross sections at 1.5 to 3.5 Mev of Sherr, Blair, *et al.*[6] In that analysis it is supposed that p-d and n-d phase shifts should be comparable on the basis of charge-independence. Unfortunately, in order to reduce the cross sections to unique phase shifts, Critchfield was forced to make auxiliary assumptions using the Buckingham and Massey theory itself. In particular, he assumed that the quartet and doublet S-wave phase shifts are equal and negative.[7] His convention (which we shall also adopt) is that phase shifts lie in the first and fourth quadrants only.

In our analysis we want to avoid such auxiliary assumptions. In fact, it is just this result of the Buckingham and Massey theory, that the S-wave phase shifts are equal and negative, that seems most interesting to check against experiment. It is impossible, however, to analyze n-d or p-d cross sections individually in terms of phase shifts without some auxiliary assumptions. In the p-d case large uncertainties in small angle measurements allow a fit of the data with a whole spectrum of sets of nuclear phase shifts. In the n-d case the matter is even worse because if, say, $2L$ phase shifts are involved (including quartet and doublet), the highest harmonic that can occur in the cross section is a $P_{L-1}{}^2$, which contains a P_{2L-2}. One derives one equation on the phase shifts for each harmonic from P_0 to P_{2L-2}, a total of $2L-1$, one less than the number of phase shifts. Hence, the n-d phase shifts are not even in principle determinable from the cross section.

In our procedure we shall try to avoid the indeterminacy of the individual phase shift analyses by considering the n-d and p-d cross sections conjointly. First we shall analyze the n-d cross section into the whole spectrum of sets of phase shifts consistent with it, and then see what portion, if any, of this spectrum is also consistent with the p-d cross section (actually d-p) under the assumption of charge-independence. In this way we hope to avoid the need for auxiliary information.

The problem arises of inferring from charge-independence a precise relationship between the p-d and n-d phase shifts themselves. The usual statement is, of course, that the p-d and n-d phase shifts ought to be approximately equal. A theoretical study of this problem has been carried out by one of us,[8] with the result that the phase shifts may be taken as equal (at the energies being considered) provided a suitable compensation is made for Coulomb effects. In particular, it is shown that the usual device of comparing the cross

* Part of a thesis submitted by A. L. Latter to the Physics Department at the University of California, Los Angeles, in partial fulfillment of the requirements for the degree of Doctor of Philosophy.
† Now at The RAND Corporation, Santa Monica, California.
[1] E. Wantuch, Phys. Rev. **84**, 169 (1951).
[2] L. Rosen and J. C. Allred, Phys. Rev. **82**, 777 (1951).
[3] G. Breit, Phys. Rev. **80**, 1110 (1950).
[4] R. A. Buckingham and H. S. W. Massey, Proc. Roy. Soc. (London) **A179**, 123 (1942).
[5] C. L. Critchfield, Phys. Rev. **73**, 1 (1948).
[6] Sherr, Blair, Kratz, Bailey, and Taschek, Phys. Rev. **72**, 662 (1947).
[7] Buckingham and Massey found this to be true irrespective of energy and the nature of exchange forces.
[8] A. L. Latter, Ph.D. thesis, University of California, Los Angeles, California, 1951.

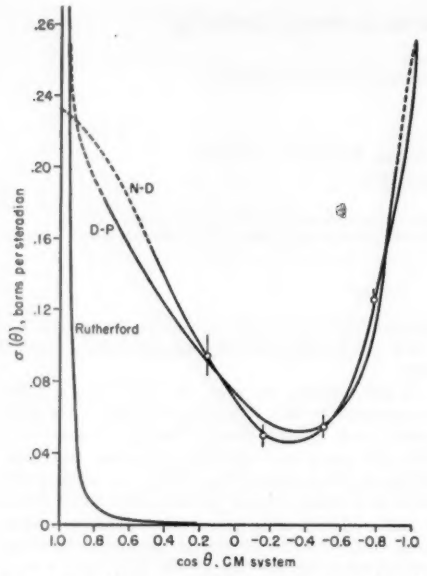

FIG. 1. Differential cross sections: 4.7-Mev *n-d*, 10.4-Mev *d-p*, and 5.2-Mev Rutherford.

sections at different energies is a good approximation. More precisely, the *p-d* energy should be about 0.5 Mev (lab) higher than the *n-d*, corresponding roughly to the *p-d* Coulomb barrier.

Since the *d-p* cross section is at 10.4 Mev, which is equivalent to *p-d* at 5.2 Mev, the *n-d* cross section should be taken at 4.7 Mev. The *n-d* at 4.7 Mev can be found by interpolation from the 4.5- and 5.5-Mev curves. Figure 1 shows the version of the data to be used in the calculations below. Experimental uncertainties in the *n-d* curve are indicated as usual by cross-lines. The dashed portion of the curve is an extrapolation made to fit the total cross section, 1.56 barns, known independently from the work of Nuckolls *et al.*[9] (No angular data were obtained in the Wantuch experiment below about 60°.)

Also shown in Fig. 1 is the 10.4-Mev *d-p* cross section. No errors are indicated because, for the most part, the data are good to 3 percent, which for our purposes is presumed to be exact. Dashed portions of the curve represent regions of insufficient data filled in by guesswork.

2. *n-d* PHASE SHIFTS

Six partial waves are expected to contribute to the cross section: *S*, *P* and *D*, quartet and doublet. This number may be estimated on the basis of the *kR* value for the interaction. For a neutron or proton scattered by a deuteron at 5 Mev, with a radius *R* of, say, 4×10^{-13} cm for the deuteron, the *kR* value is 1.3. As usual,

$$k^2=(2\mu/\hbar^2)E,$$

where μ is the reduced mass ($\frac{2}{3}$ the mass of a nucleon)

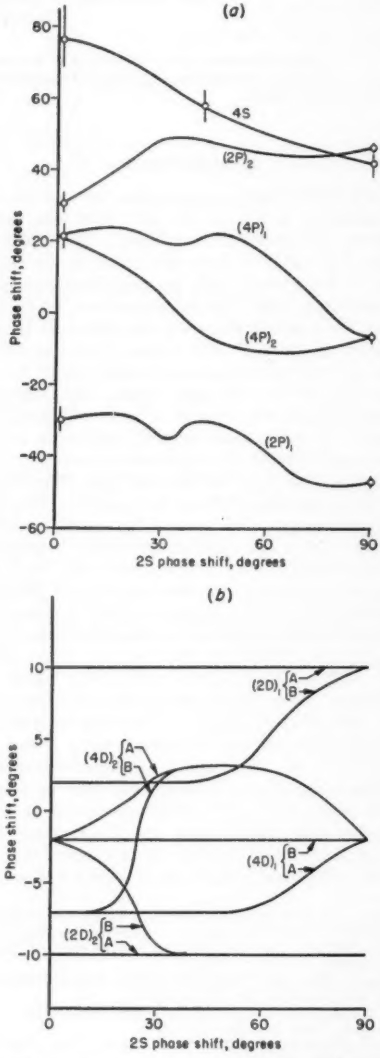

FIG. 2(a). Quartet *S* and *P*, and doublet *P*, phase shifts corresponding to assumed values of doublet *S*, for the 4.7-Mev *n-d* cross section; (b). Quartet and doublet *D*-wave phase shifts.

[9] Nuckolls, Bailey, Bennett, Bergstralh, Richards, and Williams, Phys. Rev. **70**, 805 (1946).

TABLE I. Right side of Eq. (8) for $\theta=54.7°$, to be compared with left side which equals -0.026 ± 0.012 (empirical value).

u	1++	2++	1+−	2+−	1−+	2−+	1−−	2−−
0	−0.014*	−0.029*	−0.029*	−0.013	+0.022	+0.007	+0.007	+0.022
0.2	−0.017*	−0.030*	−0.028*	−0.008	+0.021	+0.002	+0.010	+0.023
0.4	−0.019*	−0.031*	−0.027*	−0.004	+0.021	−0.002	+0.013	+0.024
0.6	−0.021*	−0.027*	−0.027*	+0.001	+0.021	−0.008	+0.015	+0.021
0.7	−0.023*	−0.023*	−0.028*	+0.006	+0.022	−0.013	+0.017	+0.017
0.8	−0.022*	−0.022*	−0.029*	+0.007	+0.022	−0.013	+0.015	+0.015
0.9	−0.017*	−0.020*	−0.027*	+0.006	+0.021	−0.013	+0.011	+0.014
0.95	−0.012	−0.020*	−0.024*	+0.005	+0.017	−0.011	+0.005	+0.013
1.00	−0.001	−0.020*	−0.020*	−0.001	+0.013	−0.005	−0.005	+0.013

and E is the relative energy in the center-of-mass system.

A Fourier analysis of the n-d cross section confirms the estimate that the D wave is the highest to enter. The result is

$$\sigma(\theta)=a_0+a_1P_1(\theta)+a_2P_2(\theta)+a_3P_3(\theta)+a_4P_4(\theta), \quad (1)$$

where $a_0=0.124\pm0.004$, $a_1=0.051\pm0.008$, $a_2=0.118\pm0.006$, $a_3=-0.057\pm0.004$, and $a_4=0.013\pm0.001$. Errors were estimated from the error lines on the n-d curve in Fig. 1, except for a_0, which was derived from the total cross section of Nuckolls *et al.*

Let $\delta_L{}^Q$ and $\delta_L{}^D$ denote the Lth quartet and doublet phase shifts, respectively. In terms of these,

$$\sigma(\theta)=(2/3k^2)\,|g_n{}^Q|^2+(1/3k^2)\,|g_n{}^D|^2, \quad (2)$$

where

$$\begin{aligned} g_n{}^Q&=\exp(i\delta_0{}^Q)\sin\delta_0{}^Q+3\exp(i\delta_1{}^Q)\sin\delta_1{}^Q P_1(\theta)\\ &\quad+5\exp(i\delta_2{}^Q)\sin\delta_2{}^Q P_2(\theta),\\ g_n{}^D&=\exp(i\delta_0{}^D)\sin\delta_0{}^D+3\exp(i\delta_1{}^D)\sin\delta_1{}^D P_1(\theta)\\ &\quad+5\exp(i\delta_2{}^D)\sin\delta_2{}^D P_2(\theta). \end{aligned} \quad (3)$$

It is convenient to introduce the following notation:

$$\begin{aligned} x&=\sin\delta_0{}^Q, \quad u=\sin\delta_0{}^D,\\ y&=\sin\delta_1{}^Q, \quad v=\sin\delta_1{}^D,\\ z&=\sin\delta_2{}^Q, \quad w=\sin\delta_2{}^D. \end{aligned} \quad (4)$$

If we compare the expressions (1) and (2) for $\sigma(\theta)$ and equate coefficients of P_0, P_1, $\cdots P_4$, we obtain the five equations which the six quantities in (4) must satisfy.

$$\text{(a)}\quad 2x^2+u^2+3(2y^2+v^2)=3.54\pm0.12$$

$$\text{(b)}\quad 2[xy(1-x^2)^{\frac{1}{2}}(1-y^2)^{\frac{1}{2}}+x^2y^2]+[uv(1-u^2)^{\frac{1}{2}}(1-v^2)^{\frac{1}{2}}+u^2v^2]=0.44\pm0.04$$

$$\text{(c)}\quad 2[xy(1-x^2)^{\frac{1}{2}}(1-z^2)^{\frac{1}{2}}+x^2z^2]+[uw(1-u^2)^{\frac{1}{2}}(1-w^2)^{\frac{1}{2}}+u^2w^2]+\tfrac{3}{5}(2y^2+v^2)=0.33\pm0.02 \quad (5)$$

$$\text{(d)}\quad 2[yz(1-y^2)^{\frac{1}{2}}(1-z^2)^{\frac{1}{2}}+y^2z^2]+[vw(1-v^2)^{\frac{1}{2}}(1-w^2)^{\frac{1}{2}}+v^2w^2]=-0.094\pm0.007$$

$$\text{(e)}\quad 2z^2+w^2=0.030\pm0.005.$$

We have set $k=3.17\times10^{12}$ cm^{-1} corresponding to 4.7-Mev n-d.

To solve Eq. (5) we ignore the uncertainties in the constants and treat the equations as exact. The effect of the uncertainties will be discussed later. Since there are six unknowns but only five equations, we shall have a one-parameter family of solutions; and because the totality of solutions encompasses the entire permissible range of u from -1 to $+1$, it is convenient to choose u as the parameter. The equations can then be solved by a simple perturbation technique. The quantities z and w are expected to be small and are set equal to zero in (c). Then (a), (b), and (c) become a set of three equations in three unknowns, with u regarded as a parameter. These equations can be easily solved and the solution introduced into (d), and then (d) and (e) solved for z and w. The values of z and w so obtained are then applied to improving (c) and the whole process iterated.

The solutions of Eq. (5) are plotted in Fig. 2. As shown, both S-waves have positive phase shifts, but this is not the only possibility since Eq. (5) is invariant under a complete change of signs of the set x, y, z or u, v, w, or both concomitantly. Hence, there are really four sets of solutions implied by Fig. 2. Note that for a given value of the $2S$ phase shift, there is only one value for the quartet S-wave phase shift ($4S$) but two possible P-wave phase shifts denoted by subscripts 1 and 2. For each set of P-wave phase shifts, there are two possible D-wave phase shifts, denoted by A and B. Error lines are not indicated for the D-wave phase shifts because this part of the analysis was rather crude. For the S and P waves, errors were estimated by solving Eq. (5) with the constants varied over the limits of the experimental certainty.

3. COMPARISON WITH d-p CROSS SECTION

Let $\bar{\sigma}(\theta)$ be the 10.4-Mev d-p angular cross section (center-of-mass system). The wave number $\bar{k}$ is given by

$$\bar{k}^2=(2\mu/\hbar^2)\bar{E},$$

where $\bar{E}=\frac{2}{3}(5.2)$ Mev. Setting n-d and p-d nuclear phase shifts equal, we have approximately

$$\bar{k}^2\bar{\sigma}(\theta)=\tfrac{2}{3}\,|g_c+g_n{}^Q|^2+\tfrac{1}{3}\,|g_c+g_n{}^D|^2, \quad (6)$$

with $g_n{}^Q$ and $g_n{}^D$ as defined by Eq. (3), and

$$g_c=-(\eta/1-\cos\theta)\exp[i\eta\ln(2/1-\cos\theta)],$$
$$\eta=e^2\mu/\hbar^2\bar{k}. \quad (7)$$

TABLE II. Right side of Eq. (8) for $\theta=125.3°$, to be compared with left side which equals -0.003 ± 0.005 (empirical value).

u	$1++$	$2++$	$1+-$	$2+-$	$1-+$	$2-+$	$1--$	$2--$
0	+0.001**	+0.004	+0.004	0	−0.004	0	0	−0.004
0.2	0**	+0.003	+0.005	−0.001	−0.005	+0.001	0	−0.003
0.4	−0.002**	+0.001**	+0.005	−0.001	−0.005	+0.001	+0.002	−0.001
0.6	−0.003**	−0.001**	+0.004	−0.003	−0.004	+0.003	+0.003	+0.001
0.7	−0.003**	−0.003**	+0.004	−0.005	−0.004	+0.005	+0.003	+0.003
0.8	−0.003**	−0.003**	+0.004	−0.005	−0.004	+0.005	+0.003	+0.003
0.9	−0.004**	−0.003**	+0.003	−0.006	−0.003	+0.006	+0.004	+0.003
0.95	−0.004	−0.003**	+0.003	−0.006	−0.003	+0.006	+0.004	+0.003
1.00	−0.006	−0.001**	+0.001**	−0.006	+0.001	+0.006	+0.006	+0.001

The approximation in Eq. (6) is in setting $\arg\Gamma(L+1+i\eta)$ equal to zero, which makes little difference in our results because η is small ($=0.069$).

Subtracting Eq. (2) from (6), we find

$$\bar{\sigma}(\theta)-(\bar{k}^2/k^2)\sigma(\theta)-\sigma_c(\theta) = (2/3k^2)\,\mathrm{Re}[g_c^*(2g_n^Q+g_n^D)], \quad (8)$$

where $k^2\sigma_c(\theta)=|g_c(\theta)|^2$. The left side of (8) is known directly from experiment. The right side assumes different values depending upon the choice of phase shifts. Our procedure is to sample all the phase shifts of Fig. 2 and see what sets give agreement with the left side. In principle, this might be done at several angles leading eventually to a unique determination of the phase shifts. However, since the D-wave analysis of Fig. 2(b) is very unreliable, and the $(2L+1)$-weighting favors the importance of the D-wave in the cross section, our procedure would lead to indefinite results at angles where the D-wave makes a large contribution.

There are two angles where the D-wave does not enter at all, 54.7° and 125.3° (the roots of P_2). For the reasons given above, we shall confine our attention to these two angles. Table I shows the results for $\theta=54.7°$. The tabulated values represent the right-hand side of Eq. (8) for various possible choices of the phase shifts given in Fig. 2(a). The phase shifts used were those corresponding to the most probable experimental values of the cross section, but the error incurred this way is negligible for our purposes. Note that any value of $|u|$ from 0 to 1 is permitted. The P-wave solutions are bifurcated, the forks being 1 and 2. Other solutions are generated by sign changes of x, y, z and u, v, w, independently. Thus for each $|u|$ we have eight cases to consider, of which $(2+-)$ is typical.[9] The symbols mean: the second fork of the P-wave, the positive solution for x, and the negative solution for u. The values in the table are to be compared with the left-hand side, which is -0.026. Actually the uncertainty in the n-d data makes this comparison value -0.026 ± 0.012. Those entries that are in agreement with these limits have been marked by an asterisk.

The same procedure is followed for $\theta=125.3°$. The right side of Eq. (8) is shown in Table II and is to be compared this time with -0.003 ± 0.005. Those values that are allowed at this angle as well as at 54.7° are distinguished now by a double asterisk.

The most significant fact about Table II is that there are any double asterisks at all. Their occurrence may be construed as evidence in favor of the charge-independence hypothesis, since our comparison of p-d and n-d cross sections has depended primarily on this feature of nuclear forces. On the other hand, it is gratifying that the possibilities can be so well delimited by using data at two angles only.[10]

With improved n-d data the phase shifts could probably be determined uniquely. But from Table II alone we can already point out a sharp disagreement with the theory of Buckingham and Massey. For ordinary forces their values of $2S$ and $4S$ is about $-64°$ at 4.7 Mev, and $-71°$ for "mixed exchange," whereas according to Table II the S-wave phase shifts are almost certainly positive. To be sure, Buckingham and Massey have considered only a few particular types of exchange, and it is possible that a different choice of nuclear parameters would lead to better agreement.

We wish to thank Dr. R. J. Finkelstein and Dr. D. S. Saxon for helpful discussion.

[10] Other angles were considered but no further elimination occurred.

Renormalized S-Matrix for Scalar Electrodynamics

ABDUS SALAM*
Institute for Advanced Study, Princeton, New Jersey
(Received February 16, 1951)

By a consistent use of the concepts of mass and charge renormalization Dyson has demonstrated the possibility of constructing a divergence-free S-matrix for scattering problems in spinor-electrodynamics, valid to all orders in the fine-structure constant. In this paper a proof is given of the possibility of renormalizing theories of charged scalar (or pseudoscalar) particles in the presence of the electromagnetic field. It is found that in addition to the renormalization of mass and charge, an infinite constant of direct interaction $\delta\lambda$ has to be introduced in a term $\delta\lambda\phi^{*2}\phi^2$ added to the Hamiltonian, in order to cancel consistently all divergences arising from the Møller scattering of one spinless particle by another. This, combined with the fact that theories of charged scalar and pseudoscalar mesons in scalar interaction with the nucleons can be renormalized with the same additional term in the Hamiltonian, seems to be of some significance.

1. INTRODUCTION

BY establishing the equivalence of Tomonaga-Schwinger formalism for spinor electrodynamics with that of Feynman, Dyson[1] has formulated an S-matrix theory for scattering problems in spinor electrodynamics. In this theory any real process taking place with specific virtual processes can be represented by a graph, the contribution to the matrix element for this process being an integral in the writing of which each line and each vertex of the aforementioned graph contributes a single factor. By analyzing the divergences in these integrals and giving precise rules for separating divergent parts from the (physically significant) convergent parts of these integrals, Dyson has further demonstrated that all divergences in the theory can be absorbed in the unobservable mass and charge renormalization of the theory.

For scalar electrodynamics it has been possible[2] to develop corresponding graphical methods and thus to analyze the possible divergences of the theory. It is the purpose of this paper to consider the adequacy of the concepts of renormalization for dealing with these divergences.

If $\phi(x)$ and $A_\mu(x)$ represent the meson and electromagnetic fields, respectively, the interaction Hamiltonian for mesons interacting with the electromagnetic field is

$$H_0(x)=\frac{ie}{\hbar c}A_\mu(x)\left[\phi^*(x)\frac{\partial\phi}{\partial x_\mu}-\frac{\partial\phi^*(x)}{\partial x_\mu}\phi(x)\right]-\left(\frac{ie}{\hbar c}\right)^2\phi^*(x)\phi(x)\delta_{\mu\nu}A_\mu(x)A_\nu(x)-\left(\frac{ie}{\hbar c}\right)^2\phi^*(x)\phi(x)[A_\mu(x)n_\mu]^2. \quad (1)$$

$A_\mu(x)$ creates and annihilates photons, while $\phi^*(x)$ and $\phi(x)$ are interpreted as creation and annihilation charge operators, so that ignoring the surface-dependent terms in the Hamiltonian, we have effectively[3]

$$\left\langle P\frac{\partial\phi(x)}{\partial x_\mu}\frac{\partial\phi^*(y)}{\partial y_\nu}\right\rangle_0=\tfrac{1}{2}\hbar c\frac{\partial^2}{\partial x_\mu\partial y_\nu}\Delta_F(x-y).$$

In Feynman graphs, the terms in the Hamiltonian linear in $A_\mu(x)$ lead to 3-vertices, with 2 meson lines and 1 photon line incident, while the term bilinear in $A_\mu(x)$ leads to 4-vertices, with 2 meson and 2 photon lines incident.

The contribution of this graph to the matrix[2] element appears as an integral in momentum space; in the integrand there appear[4]

(i) constant factors $\phi^*(p)$, $\phi(p)$, or $A_\mu(p)$, corresponding to each external line of the graph.

(ii) a factor $\delta_{\mu\nu}(2\pi)^{-3}D_F(p)$ for each internal photon line.

(iii) a factor $\hbar c(2\pi)^{-3}\Delta_F(p)$ for each internal meson line.

(iv) a factor $ie(\hbar c)^{-2}(2\pi)^4(p+p')_\mu\delta(p-p'+q)$ for each 3-vertex. The suffix μ gives the polarization of the photon line.

(v) a factor $-ie(\hbar c)^3(2\pi)^4\delta_{\mu\nu}\delta(p-p'+q-q')$ for each 4-vertex, where p is the momentum vector of the incoming meson, p' that of the meson leaving the 4-vertex, and q, q' refer to the photon lines incident at the 4-vertex.

(vi) the whole integral is multiplied by the number of different ways the operators can be paired off by interchanging the roles of photon operators $A_\mu(x)$ and $A_\nu(x)$ at the 4-vertices.

Thus, in general, it is possible to make a formal distinction between the factors $\delta_{\mu\nu}$ and $\delta_{\nu\mu}$ for a 4-vertex. If this distinction is not made, the integral obtained by following rules (i) to (v) must be multiplied by a "weight factor" 2 for each 4-vertex. Some exceptions

* Now at Government College, Lahore, Pakistan.

[1] F. J. Dyson, Phys. Rev. **75**, 1736 (1949), hereafter referred to as D II.

[2] P. T. Matthews, Phys. Rev. **80**, 282 (1950); F. Rohrlich, Phys. Rev. **80**, 666 (1950). The author is indebted to P. T. Matthews for sending him a copy of F. Rohrlich's work prior to publication.

[3] P. T. Matthews, Phys. Rev. **76**, 1657 (1949).

[4] These rules were already implicit in Feynman's work [R. P. Feynman, Phys. Rev. **76**, 769 (1949)].

occur, however, when the weight factor is not 2, and these have been discussed in detail by Rohrlich.[2] For theoretical considerations, however, we shall always distinguish (if possible) between factors $\delta_{\mu\nu}$ and $\delta_{\nu\mu}$ for 4-vertices and no weight factor will be used.

The genuine primitive divergents[2] are of the same type as in spinor electrodynamics, namely, meson and photon self-energies and vertex parts (parts with 2 external meson lines and 1 external photon line), with the addition of logarithmically divergent graphs with two external photon and meson lines (C parts), and four external meson lines (M parts). The self-energy (S) and vertex (V) parts modify the factors from single lines or single 3-vertices, while the divergent C parts can be regarded as modifications of 4-vertices. Define $\sum_M{}^*(p)$ as the function arising from adding together all integrals corresponding to proper[3] meson self-energy parts, $\Pi^*(p)$ the corresponding sum for photon self-energy parts, $\Lambda_\mu(p, p')$ the function arising from adding the integrals corresponding to proper V parts, $\theta_{\mu\nu}(p, p', q)$ as the sum arising from adding integrals corresponding to proper C parts, and

$$D_F' = D_F + D_F\Pi^* D_F'$$
$$\Delta_F' = \Delta_F + \Delta_F \sum_M{}^* \Delta_F'$$
$$\Gamma_\mu(p, p') = (p+p')_\mu + \Lambda_\mu(p, p')$$
$$C_{\mu\nu}(p, p', q) = \delta_{\mu\nu} + \theta_{\mu\nu}(p, p', q).^6$$

Every graph G, other than a primitive divergent graph, has a uniquely defined "skeleton" which is the graph obtained by omitting all self-energy parts from the lines, vertex parts from the 3-vertices, and C parts from the 4-vertices. A graph which is its own skeleton will be called "irreducible," and a graph not containing M parts inside it "simple." With the foregoing definition of irreducibility, an irreducible graph may still contain divergent M parts.

For simple irreducible primitive divergent graphs, the forms of the functions $\sum_M{}^*$, Π^*, Λ_μ, and $\theta_{\mu\nu}$ are given as follows by invariance consideration:

$$\sum_M{}^*(p) = A + B(p^2+\kappa^2) + \Delta_c(p)(p^2+\kappa^2),$$
$$\Pi^*(p) = Cp^2 + D_c(p)p^2,$$
$$\Lambda_\mu(p, p') = L(p+p')_\mu + \Lambda_{\mu c}(p, p'),$$
$$\theta_{\mu\nu}(p, p', q) = R\delta_{\mu\nu} + \theta_{\mu\nu c}(p, p', q),$$

where the suffix c stands for the convergent parts of the functions on the left-hand side of the equations.

A, B, C, L, and R are divergent constants, while the definitions of the convergent parts are such that

$$\Delta_c(p_0) = 0$$

when

$$p_0{}^2 + \kappa^2 = 0$$

and

$$D_c(0) = 0$$

$\Lambda_{\mu c}(p, p')$ can be written in the form[7]

$$\Lambda_{\mu c}(p, p') = M(p+p')_\mu(p^2+\kappa^2+p'^2+\kappa^2) + F_\mu(p, p') \quad (2a)$$

where

$$F_\mu = \partial F_\mu/\partial p_\nu = \partial F_\mu/\partial p_\nu' = 0 \quad \text{for} \quad p = p' = p_0$$

and in general we can write $\theta_{\mu\nu c}$ as

$$\theta_{\mu\nu c}(p, p', q) = N(p+p')_\mu(p+p')_\nu + F_{\mu\nu}(p, p', q) \quad (2b)$$

with

$$F_{\mu\nu}(p_0, p_0, 0) = 0.$$

We notice that M is finite and, furthermore, that with the foregoing (unique) definition, $\Lambda_{\mu c}(p_0, p_0) \equiv 0$. Similarly, N in (2b) is a finite constant. The precise significance of these particular separations will become clear in Sec. III when we establish relations between $\sum_M{}^*$, Λ_μ, and $\theta_{\mu\nu}$.

It is possible to obtain a divergence free S-matrix if we can show:

(a) That all infinities associated with self-energy of a free-field meson can be canceled by bringing into the interaction Hamiltonian by means of a unitary transformation,[8] the mass renormalization term $-\delta\kappa^2\phi^*\phi$. The free meson field now propagates with the term $\kappa^2\phi^*\phi$ in the "free" Hamiltonian ($\kappa = mc/h$ where m is the observed meson mass).

(b) That all M divergences occurring anywhere in the theory can be consistently compensated by suitably choosing a constant $\delta\lambda$ in a term $\delta\lambda\phi^{*2}\phi^2$ which is added to the interaction Hamiltonian.[9] After the additions (a) and (b) the Hamiltonian is

$$H_1(x) = H_0(x) - \delta\kappa^2\phi^*\phi + \delta\lambda\phi^{*2}\phi^2. \quad (3)$$

The additional terms give rise to new graphs containing 2- and 4-vertices, with 2 and 4 meson lines incident, respectively. Graphs containing no such 2- or 4-vertices will be called "original."

Unlike spinor electrodynamics $H_0(x)$ contains two constants, e and e'^2, with $e = e'$. The graphs arising entirely from e-vertices (3-vertices) contain S divergences and V divergences; those from e^2 vertices (4-vertices) contain S divergences and C divergences. It would be possible to absorb these divergences in the renormalization of charge if we could show (c).

(c) That by a suitable choice of constants Z,

$$\left.\begin{aligned} D_F' &= Z_3 D_{F1}'(e_1) \\ \Delta_F' &= Z_2 \Delta_{F1}'(e_1) \\ \Gamma_\mu &= Z_1^{-1}\Gamma_{\mu 1}(e_1) \quad \text{and} \quad C_{\mu\nu} = Z_4^{-1} C_{\mu\nu 1}(e_1) \end{aligned}\right\} \quad (4)$$

where the renormalized (and the observed) charge of the meson

$$e_1 = Z_1^{-1} Z_2 Z_3^{\frac{1}{2}} e = Z_4^{-\frac{1}{2}} Z_2^{\frac{1}{2}} Z_3^{\frac{1}{2}} e'.$$

[6] The external lines of any proper part contain no self-energy insertions. In general a proper part is one which cannot be divided into two pieces joined by a single line.

[6] The factor for a 4-vertex is $-e^2\delta_{\mu\nu}$. For $\theta_{\mu\nu}$ as defined here we obtain the e-factor $(-1)^r e^{2r} e^{2s}$ where r is the number of 4-vertices and $2s$ that of 3-vertices, and then divide by $-e^2$. This gives $C_{\mu\nu}$ (to replace $\delta_{\mu\nu}$) as $= \delta_{\mu\nu} + \theta_{\mu\nu}$.

[7] This separation into convergent and divergent parts was given by Dyson (private communication).

[8] F. J. Dyson, Phys. Rev. **75**, 486 (1949); P. T. Matthews, Phil. Mag. **185**, XLI (1950).

[9] The necessity of this condition was pointed out by P. T. Matthews (reference 2).

(d) If $H_0(x)$ is gauge-invariant, so that $e=e'$, it has to be shown that the Z's defined satisfy a further condition,

$$Z_4^{-1}=Z_2Z_1^{-2}.$$

D_F', Δ_F', Γ_μ, $C_{\mu\nu}$ are the functions already defined, except that they now include the graphs with the new 2- and 4-vertices, as well as the original graphs. $C_{\mu\nu 1}=\delta_{\mu\nu}+\theta_{\mu\nu c}$ where $\theta_{\mu\nu c}$ is the function arising by adding together the (absolutely) convergent parts of each integral corresponding to each "original" C part. $\Gamma_{\mu 1}$, Δ_{F1}', D_{F1}' are defined in a similar manner from sums of convergent parts of the original integrals concerned. The procedure for obtaining the (absolutely) convergent part of an integral will be presently explained. It is to be noticed that the "convergent functions," on the right-hand side of the relations (4) appear to be expressed as functions of the renormalized charge e_1.

The general procedure for isolating divergences[10] from an n-fold integral was given in reference 2 in Sec. III. In this procedure the concept of true divergence plays an important part. In general if we subtract from any divergent integral over the variables $l_1\cdots l_n$, the true divergence over l_1 subintegration $D(l_1)\times$ the reduced integral (R) over $l_2l_3\cdots l_n+$ the true divergence over $l_2\times$ the reduced integral over $l_1l_3\cdots l_n+\cdots+$ the true divergence over $l_1l_2\times$ the reduced integral over $l_3\cdots l_n+\cdots+\cdots+\cdots+$ finally the true divergence over $l_1l_2\cdots l_n$, the remainder is an integral which is absolutely convergent and is the convergent part of the n-fold divergent integral we started with. Each reduced integral corresponds to a graph obtained from the graph under consideration by omitting that part of the graph whose true divergence multiplies this particular reduced integral. If a subintegration is "superficially convergent," its true divergence is zero; while the true divergence over a subintegration $l_a\cdots l_b\cdots l_i\cdots l_jl_p\cdots l_q\cdots l_y\cdots l_z$ where $(l_a\cdots l_b)$, $(l_i\cdots l_j)$, $(l_p\cdots l_q)\cdots$ are k groups of variables belonging to nonoverlapping parts of the graph, equals $(-i)^{k-1}$ times the product of the true divergences over each of the k groups, $(l_a\cdots l_b)$, $(l_i\cdots l_j)$, $\cdots$ (Remark b, I, Sec. III[11]). It is in terms of the convergent parts of the integrals defined as above that the functions $C_{\mu\nu 1}$, $\Gamma_{\mu 1}$, etc. are defined. The true divergence of a subintegration corresponding to a meson self-energy graph is characterized by two divergent constants A, B; while all other true divergences are characterized by one divergent constant. The factors multiplying these constants $[(p^2+\kappa^2)$, for example, which occur multiplying B in the meson self-energy case] are absorbed in the reduced integral.

Considering the "original" graphs, the finite and physically significant expressions $C_{\mu\nu 1}$, $\Gamma_{\mu 1}\cdots$ are defined, as already stated, in the first place by an apparently arbitrary dropping (subtracting off) of the infinite terms (true divergences $\times$ the reduced integrals) from the infinite expressions $C_{\mu\nu}$, Γ_μ, etc. Some of the divergent terms thus subtracted can be interpreted under (a) and (b) as direct cancellations with terms from $\delta\kappa^2$ and $\delta\lambda$ arising in graphs which are not original so that, as we shall show, both these divergences as well as the "non-original" graphs need never be considered. The establishment of (c) and (d) shows that the remaining divergent terms isolated can equally well be interpreted as the extraction of infinite constant multiplicative factors Z, from $C_{\mu\nu}$, Γ_μ, $\cdots$, so that each of these functions, instead of appearing as a sum of infinite $(D\times R)+$finite terms, now appears, as in Eq. (4), as a product of a (divergent) constant (Z) multiplying finite and physically significant terms. After this is accomplished, these Z factors can be completely absorbed in renormalizing the charge, so that all infinities occurring in the theory can be eliminated.

The main difficulty of the proof lies in establishing (e). In each of Eqs. (4) the functions appearing on the left-hand side are completely known, while so are the finite parts of these functions $C_{\mu\nu 1}$, $\Gamma_{\mu 1}$, $\cdots$. Let us assume that the relations (4) hold, with the factors Z for the present unknown. Consider an irreducible C graph, T_{IRR}, for example, such that in its lines and vertices, self-energy, vertex, and C parts can be inserted without any one of these insertions overlapping with any other insertion. Each insertion is thus completely localizable and does not simultaneously modify more than one vertex or line. The result of these insertions analytically is that we replace in the integral for the irreducible graph Δ_F by Δ_F', D_F by D_F', $(p+p')_\mu$ by Γ_μ and $\delta_{\mu\nu}$ by $C_{\mu\nu}$. It was shown (Remark c, I, Sec. III), that if, for example, a meson line p has a self-energy insertion with associated momenta $l_al_b\cdots l_k$, and if this self-energy insertion defines no overlap with any other part of the graph, then we can arrange our general subtraction procedure so that we isolate divergences corresponding to the subintegrations l_a, $l_al_b\cdots$, etc., first. After the true divergence corresponding to $l_al_b\cdots l_k$, itself is removed, the integration over this set is left absolutely convergent and it can be performed unambiguously so that the variables l_a, l_b, $\cdots l_k$ no longer need be considered explicitly from this stage onward. Since this procedure of removing divergent terms corresponding to this self-energy insertion is precisely the one we would adopt for obtaining Δ_{F1}' from Δ_F', and, since we have assumed that, in the latter case (Eq. (4)), the divergent terms separated are

[10] The proof given by Rohrlich for the possibility of renormalization (reference 2) for scalar electrodynamics is invalidated because the general procedure for isolating divergences was not available. A "hierarchy" of divergences was somewhat arbitrarily defined and a prescription given according to which a divergence higher in the hierachy should be removed first. This procedure is not equivalent to the one given above and when overlaps occur, does not leave behind an absolutely convergent integral after the proposed subtractions. In a note added in proof (reference 2) Rohrlich has observed that the problem of "b-divergences" (overlaps) has not received proper treatment in his paper. The present paper deals with these difficulties.

[11] Abdus Salam, Phys. Rev. **82**, 217 (1951), hereafter referred to as I.

completely interpreted as the extraction of the divergent factor Z_2 in $\Delta_F' = Z_2\Delta_{F1}'(e_1)$, we can make this same replacement for Δ_F' for this internal line p in the C graph under consideration. It is emphasized again that this is true if and only if no overlap occurs.

Going back to consider T_{IRR}, by inserting all S, V, and C parts in its lines and vertices we obtain an entire class of C parts $T_{\mu\nu}$ "derived" from T_{IRR}. Analytically we replace in the integral for T_{IRR}, Δ_F by $Z_2\Delta_{F1}'(e_1)$, D_F by $Z_3D_{F1}'(e_1)$, $(p+p')_\mu$ by $Z_1^{-1}\Gamma_{\mu 1}$, and $\delta_{\mu\nu}$ by $Z_4^{-1}C_{\mu\nu 1}$.

A C part of order $e^{2r+2s-2}$ with s 4-vertices and $2r$ 3-vertices contains $2r+s-1$ meson and $r+s-1$ photon lines. The foregoing replacements give an e factor

$$e^{2r+2s-2}Z_4^{-s}Z_1^{-2r}Z_2^{2r+s-1}Z_3^{r+s-1} = Z_4^{-1}e_1^{2s+2r-2}.$$

Δ_{F1}', D_{F1}', $\cdots$ are themselves power series in e_1, and their behavior for large p is precisely the same as that of Δ_F, D_F, etc. (D II Sec. VII), so that the new integral for $T_{\mu\nu}$ is again logarithmically divergent. Making a separation of the finite and the infinite part,

$$T_{\mu\nu} = Z_4^{-1}(T_d(e_1)\delta_{\mu\nu} + T_{\mu\nu c}(e_1)). \tag{5}$$

Equation (5) gives in a compact form the sum of integrals from the entire class of graphs $T_{\mu\nu}$, "derived" (uniquely) from the one graph T_{IRR} by insertions. This form for $T_{\mu\nu}$ will be referred to as the fundamental form. It is to be emphasized that the content of $T_{\mu\nu}$ is not altered in the fundamental form by expressing it thus in terms of the renormalized charge; and that the equality of both sides is exact considered up to any order in e_1 and e (expressed in terms of e_1).

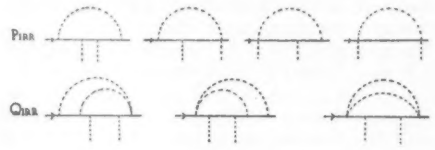

FIG. 1.

If it were possible to make unambiguous nonoverlapping insertions in all the irreducible C parts, this procedure would have given us all the reducible and irreducible C parts. Analytically from each T_{IRR} we would have obtained $T_{\mu\nu}$ in the form (5) so that summing over all C parts and adding $\delta_{\mu\nu}$ for the 4-vertex itself we would obtain

$$C_{\mu\nu} = \delta_{\mu\nu} + Z_4^{-1}(R_d\delta_{\mu\nu} + \theta_{\mu\nu c}(e_1)).$$

But if Eqs. (4) hold, $C_{\mu\nu}$ ought to equal $Z_4^{-1}C_{\mu\nu 1}$. Thus

$$Z_4^{-1}C_{\mu\nu 1} = Z_4^{-1}(\delta_{\mu\nu} + \theta_{\mu\nu c}(e_1)).$$

This gives us an equation with just one unknown, Z_4, which could then be determined (and so the consistency of the relations (4) established.

However, as soon as overlaps occur the whole idea of an unambiguous insertion in a line or a vertex loses validity. The reduction of a reducible graph cannot be defined unambiguously and, conversely, the replacement of all vertex and line factors of irreducible parts by $C_{\mu\nu}$, Γ_μ, etc., leads to the counting of certain graphs more than once. [This is a definite redundance, quite apart from the "weight factors" occurring under rule (vi).] Thus, a proof on the aforementioned lines can no longer be given.

For C parts it is always possible to make unambiguous insertions in all the lines and 3-vertices. However there are certain classes of C parts in which a C part inserted in one 4-vertex appears simultaneously as a C part inserted at some other vertex.

For vertex parts the complexity of overlaps increases greatly and $C-V$ overlaps can occur. For self-energies, besides these overlaps, vertex parts overlap with vertex parts. Also, if any meson (or photon) line is opened in a self-energy graph, this leads to parts with four external lines which (except for photon-photon scattering graphs) always diverge. M parts, which have not been considered so far, can complicate the picture still further by producing simultaneously $M-M$, $M-C$, or $M-S$ overlaps.

A great simplification can be effected by applying a powerful technique first introduced by Ward[12] in spinor electrodynamics. Ward's technique can be extended to reduce the complexity of the overlaps to be considered. However, if a primitive divergent is logarithmically divergent and still suffers from overlaps, this technique in general fails. The general procedure to be followed then for obtaining a proof of (4) and for the construction of the relevant functions is that of categorization, as developed in I, Sec. IV. By analyzing the overlaps, such categories of reducible graphs are defined in which certain insertions of S, V, and C parts cause no overlap, so that the substitutions $C_{\mu\nu}$, Γ_μ, etc., can be made in a defined way. By considering the implications of the subtraction rules, I, Sec. III, it is then possible to derive recurrence relations for such graphs in terms of graphs of lower order in the same category and their true divergences. The required values for the Z's are obtained by substituting Eqs. (4) into these recurrence relations and demanding that they lead back to the fundamental form for the type of part under consideration. These various techniques are illustrated in Secs. 2, 3, and 4 and in Appendix I where it is assumed that condition (b) can be satisfied. A proof of this is given in Sec. 5.

2. C PARTS

The most general C part consists of an open polygon formed by the meson line entering (and leaving) the graph, this line (the base line of the graph) being joined by photon lines to one or more (possibly interconnected)

[12] J. C. Ward, Proc. Phys. Soc. (London) **64**, 54 (1951). The author is deeply indebted to J. C. Ward for sending him a copy of his work prior to publication.

closed loops of meson lines with a structure inside them. If the external photon lines (with polarization vectors μ and ν) belong to the base line, the graph will be called a base-line graph. For base-line C parts it is possible to distinguish between $\theta_{\mu\nu}$ and $\theta_{\nu\mu}$. For such graphs $\theta_{\mu\nu}(p, p', q)$ is defined such that μ occurs topologically "before" ν and carries momentum q.

In order to construct the function $C_{\mu\nu}$ (and the corresponding convergent function $C_{\mu\nu 1}$) it is possible as explained in Sec. I, to take irreducible C parts and to make unambiguous insertions in their lines and 3-vertices, replacing in the corresponding integrals Δ_F by Δ_F', D_F by D_F', and $(p+p')_\mu$ by Γ_μ. Furthermore, it is possible to replace the factor $\delta_{\mu\nu}$ by $C_{\mu\nu}$ for the 4-vertices of all irreducible C parts except for the 4-vertices in the graphs P_{IRR} and Q_{IRR} shown in Fig. 1. (There is another class of graphs R which are defined in Appendix II and in the 4-vertices of which the foregoing insertion is also not valid.) Taking all other irreducible C parts and making the foregoing insertions gives all reducible C parts "derived" from them. If $T_{\mu\nu}$ denotes the sum of corresponding integrals, by counting the number of lines and vertices in the irreducible C parts in which insertions are being made, we have

$$T_{\mu\nu}=Z_4^{-1}[T_d(e_1)\delta_{\mu\nu}+T_{\mu\nu c}(e_1)], \tag{6}$$

where $T_d(e_1)$ is the sum of the true divergences from all such graphs.

In this section the graphs P_{IRR} and a linear chain of graphs "derived" from them (the whole class being called P) will be treated in detail. For Q and R we assume the result in Appendix II, namely, that with a proper choice of Z_4 the corresponding functions $Q_{\mu\nu}$ and $R_{\mu\nu}$ can also be expressed in the fundamental form of Eq. (6). In fact, at this stage $T_{\mu\nu}$ will be understood to contain $Q_{\mu\nu}$ and $R_{\mu\nu}$.

Consider the graph in Fig. 2, of order e^7. We can obtain (2^5-1) other topologically distinct graphs from it by shrinking $1\to1$, $2\to2$, $3\to3$, $4\to4$, $5\to5$ in all possible ways. If $4\to4$, for example, the resulting 4-vertex will be (uniquely) numbered 4. In Fig. 2 the letters $a, b, \cdots$ give the polarization of the photon. The order of the numbers 1, 2, 3$\cdots$ and the letters $a, b, c, \cdots$ are important. If 2 is a 4-vertex, it could be denoted equally well by δ_{ab} or by δ_{ba} so that the number of formally different graphs obtained from the graph in Fig. 2 by joining $1\to1$, $2\to2$, $\cdots$ is 3^5-1, when the graphs with factors δ_{ab} and δ_{ba} are treated as different.

Let $P_{\mu\nu}$ stand for the graphs obtained by drawing chain graphs of the type illustrated in Fig. 2 in all orders in the powers of e, and also the graphs obtained by joining $1\to1$, $2\to2$, $\cdots$, in all possible ways.

Let $[n]$ stand for such graphs (3^n in number) of order e^{2n}, $[n|1]$ stand for all graphs $[n]$ such that the first vertex is necessarily a 4-vertex. These are 3^n in number. Similarly, let $[n|i, j]$ stand for all graphs(3^{n-1} in number) which have their ith and jth vertices necessarily δ_{pq} and δ_{rs} 4-vertices (the order of photon polarization-vectors p, q and r, s is to be noted), irrespective of the character of the other vertices, and so on for $[n|i, j, \cdots]$. Let $X_{\mu\nu}$ stand for all those graphs of all orders (and the sum of corresponding integrals) from among the P graphs which have their last end vertex a $\delta_{\mu\nu}$ 4-vertex, irrespective of the character of other vertices, $Y_{\mu\nu}$ stand for all graphs with the first and the last end-vertices, $\delta_{\mu a}$ and $\delta_{\mu a}$ vertices, and $Z_{\mu\nu}$ for those with the first end-vertex a 4-vertex $\delta_{\mu a}$, again irrespective of the character of the other vertices. Thus, Y, for example, equals

$$[1|1, 2]+[2|1, 3]+\cdots+\cdots+[n|1, n+1]+\cdots.$$

With the foregoing definitions we prove Lemma 1.

Lemma 1

$$P_{\mu\nu}=P_d(\delta_{\mu\nu}+X_{\mu\nu})(\delta_{\tau\rho}-P_dY_{\tau\rho}+P_d^2Y_{\tau\rho}{}^2-\cdots)(\delta_{\rho\nu}+Z_{\rho\nu})+P_{\mu\nu c}. \tag{7}$$

Here P_d is the sum of the true divergences from the graphs P. In particular if P_n stands for the sum of the true divergences from $[n]$, then $P_d=P_1+P_2+P_3+\cdots$.

For the proof we make use of the property of a 4-vertex occurring in this type of linear chain of graphs P to split the chain into two parts.

FIG. 2.

Consider, for example, the graphs in Fig. 3. It is obvious that the double integral over t_1t_2 corresponding to Fig. 3(a) is the product of two single integrals over t_1 and t_2, so that symbolically $(a)=(b)\times(c)$. In the sequel we shall further specialize this splitting off of graphs. A split will be made for a δ_{ab} vertex but it will never be made for a δ_{ba} 4-vertex.

$[n]$ is an n-fold integral over variables $t_1t_2\cdots t_n$, each one of the subintegrations being logarithmically divergent. If $ij\cdots q$ is a group of indices from the set $123\cdots n$ (where $ij\cdots$ run consecutively) then isolating the divergence over the subintegration $t_it_j\cdots t_q$ gives $P_{(q-i+1)}\times$the corresponding reduced integral. This reduced integral contains a 4-vertex of the type with a factor δ_{ab} (and not δ_{ba}) corresponding to the divergence which has been separated and this immediately splits the chain (if, of course, this 4-vertex is not one of the two possible end 4-vertices).

To obtain the coefficient of $(P_d)^f$ in (7), consider all subsets of indices $123\cdots n$, such that each subset divides naturally into f groups, the indices in each group running consecutively, the different groups being such that if k is the first and i the last index of two consecutive groups, then $k-i\geqslant1$. The true divergence for a subintegration corresponding to these subsets consists of $(-1)^{f-1}P_aP_\beta\cdots(f$ factors), (I, Remark b, Sec. III) corresponding to the number (f) of nonoverlapping graphs, the true divergences of which are in fact thus being simultaneously removed. The reduced integral itself necessarily contains f 4-vertices (again of the type δ_{ab} and not δ_{ba}), which may split the graph according to the scheme XY^{f-1}, Y^{f-1}, $Y^{f-1}Z$, or $XY^{f-1}Z$. By considering all possible subsets and the groups in them of the type mentioned we readily establish the lemma.

We can show this by considering, as an example, the coefficient of P_d^2 in (7) in detail. Only graphs up to $[n]$ are considered. In our symbolic notation $[1|1,2]\times[n-1|1]$ would be equal to $[n|1,2]$. We consider all subsets of indices which fall into two nonoverlapping groups. If the first of these two groups starts with index 1, we have the following terms to separate:[13]

$$
\begin{aligned}
&-P_1[1|1,2]\times \\
&\quad\Big[P_1[n-3|1]+P_2[n-4|1]+P_3[n-5|1]+\cdots+P_{n-2} \\
&\qquad +P_1[n-4|1]+P_2[n-5|1]+\cdots+P_{n-3} \\
&\qquad\quad +P_1[n-5|1]+\cdots+P_{n-4} \\
&\qquad\qquad +\cdots+\cdots \\
&\qquad\qquad\quad +P_1\Big] \\
&-P_2[1|1,2]\times \\
&\quad\Big[P_1[n-4|1]+P_2[n-5|1]+\cdots+P_{n-3} \\
&\qquad +P_1[n-5|1]+\cdots+P_{n-4} \\
&\qquad\quad +\cdots+\cdots \\
&\qquad\qquad +P_1\Big] \\
&\quad\cdots\cdots\cdots\cdots\cdots\cdots\cdots\cdots \\
&-P_{n-2}[1|1,2]P_1\Big]
\end{aligned}
\qquad (8)
$$

The terms (8) sum up to

$$
\begin{aligned}
&=-P_d[1|1,2]P_d(1+[1|1]+[2|1]+[3|1]+\cdots+[n-3|1]) \\
&=-P_d^2[1|1,2](\delta_{\mu\nu}+Z_{\mu\nu})
\end{aligned}
$$

if the equality of both sides is supposed to hold to the order e^{2n}. Also, there are terms such as

$$
\begin{aligned}
&-P_1[2|1,3]\Big[P_1[n-4|1]+P_2[n-5|1]+\cdots+P_{n-3} \\
&\qquad +P_1[n-5|1]+\cdots+P_{n-4} \\
&\qquad\quad +\cdots+\cdots \\
&\qquad\qquad +P_1\Big] \\
&-P_2[2|1,3][\qquad P_1[n-5|1]+\cdots\cdots\cdots] \\
&\quad\cdots\cdots\cdots\cdots\cdots\cdots\cdots\cdots
\end{aligned}
$$

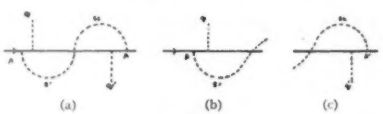

(a) (b) (c)

FIG. 3.

which sum up to $-P_d^2[2|1,3](\delta_{\mu\nu}+Z_{\mu\nu})$. We similarly obtain $-P_d^2[3|1,4](\delta_{\mu\nu}+Z_{\mu\nu})$ and so on, concluding with $-P_1^2[n-2|1,n-1]$. The sum of all these terms is $-P_d^2Y_{\mu\rho}(\delta_{\rho\nu}+Z_{\rho\nu})$.

If we consider the two groups of indices such that the first group does not contain the index 1, it may be easily verified that the sum of corresponding contributions is $-P_d^2X_{\mu\tau}Y_{\tau\rho}(\delta_{\rho\nu}+Z_{\rho\nu})$ so that the entire sum is $-P_d^2(\delta_{\mu\tau}+X_{\mu\tau})Y_{\tau\rho}(\delta_{\rho\nu}+Z_{\rho\nu})$ precisely as in (7).

We now notice an important property of these graphs P. Whereas the insertion of any graph P_{ab} for δ_{ab} leads only to a graph already belonging to P, an insertion of P_{ba} for δ_{ba} gives a new graph unambiguously.

In order to obtain all reducible graphs "derived" from the graphs in Fig. 1. We proceed as follows:

(i) Draw all graphs P of all orders in e^2.

(ii) Insert at all 4-vertices δ_{ji}, all reducible and irreducible C parts including $P^*{}_{ji}$; analytically, replace δ_{ji} in the integrals by C_{ji}.

(iii) Insert at all 4-vertices δ_{ij}, the graphs T_{ij}; i.e., replace δ_{ij} by $\delta_{ij}+T_{ij}$. In the lines and the 3-vertices, all self-energy and vertex parts are inserted. The result after these insertions is $P_{\mu\nu}{}^*$.

It is easy to verify that no graph occurs more than once provided we adhere to the convention of distinguishing between δ_{ij} and δ_{ji} and further that all graphs "derived" from the graphs P_{IRR} do appear in the foregoing scheme of categorization, so that

$$C_{\mu\nu}=\delta_{\mu\nu}+T_{\mu\nu}+P_{\mu\nu}{}^*. \qquad (9)$$

Since all the insertions (i) to (iii) are unambiguous and localizable, we can replace Δ_F by $\Delta_F'=Z_2\Delta_{F1}'$, D_F by $D_F'=Z_3D_{F1}'(e_1)$, $(p+p')_\mu$ by $Z_1^{-1}\Gamma_{\mu1}(e_1)$, δ_{ji} by $C_{ij}=Z_4^{-1}C_{ji1}(e_1)$ while δ_{ij} is replaced by

$$
\begin{aligned}
\delta_{ij}+T_{ij}&=\delta_{ij}+Z_4^{-1}(T_d\delta_{ij}+T_{ijc}(e_1)) \\
&=Z_4^{-1}[(T_d+Z_4-1)\delta_{ij}+\delta_{ij}+T_{ijc}(e_1)] \\
&=Z_4^{-1}[S\delta_{ij}+S_{ij1}(e_1)].
\end{aligned}
$$

(definition of S)

The effect of these substitutions is to give Z_4^{-1} times the correct number of Z factors to renormalize the charge while all integrals now appear explicitly as functions of e_1. While at each δ_{ji} vertex, δ_{ji} has been replaced by C_{ji1}, each δ_{ij} vertex gives rise to two terms; one in which the integral corresponding to the graph is merely multiplied by S, the other in which δ_{ij} is replaced by $S_{ij1}(e_1)$.

Denote by $P_{\mu\nu}{}^\times$ the sum of integrals corresponding to all graphs thus formed, for whose 4-vertices appear the factors S_{ij1} or C_{ji1} while for the lines and 3-vertices Δ_{F1}, D_{F1}, $\Gamma_{\mu1}$ appear. $X_{\mu\nu}{}^\times$ denotes the corresponding sum for all graphs in which only the last end-vertex is an unchanged 4-vertex $\delta_{s\nu}$ while all other 4-vertices are replaced by factors S_{ij1} or C_{ji1}. $Y_{\mu\nu}{}^\times$ similarly denotes the sum of integrals for all graphs with only the first and the last end-vertices unchanged 4-vertices, and $Z_{\mu\nu}{}^\times$ the sum for graphs with only the first end-vertex an unchanged 4-vertex.

With these definitions we prove the following lemma.

Lemma 2

$$
\begin{aligned}
P_{\mu\nu}{}^*=Z_4^{-1}[&S(\delta_{\mu\tau}+X_{\mu\tau}{}^\times)(\delta_{\tau\rho}+SY_{\tau\rho}{}^\times \\
&+S^2Y_{\tau\rho}{}^{\times2}+\cdots)(\delta_{\rho\nu}+Z_{\rho\nu}{}^\times)-S\delta_{\mu\nu}+P_{\mu\nu}{}^\times].
\end{aligned}
\qquad (10)
$$

Defining $[n|l,m]^\times$, etc., to represent all graphs $[n|l,m]$ for the lines and vertices of which replacements Δ_{F1}', D_{F1}', $\Gamma_{\mu1}$, C_{ji1} or S_{ij1} have been made, except at the lth and mth 4-vertices where the factors δ_{pq} and δ_{rs} remain unchanged, the proof of the lemma follows by noticing that

$$
\begin{aligned}
[n]^*=&[n]^\times+S([n|1]^\times+[n|2]^\times+\cdots) \\
&+S^2([n|1,2]^\times+[n|1,3]^\times+\cdots \\
&+[n|i,l]^\times+\cdots)+S^3([n|1,2,3]^\times+\cdots \\
&+[n|i,l,k]^\times+\cdots)+\cdots+\cdots \\
&+S^{n+1}[n|1,2,3,\cdots,n+1]^\times.
\end{aligned}
\qquad (11)
$$

[13] To verify that a term like $-P_1[1|1,2]P_3[n-5|1]$, for example, takes account of all the 3^{n+1} graphs in $[n]$, one can make a check as follows: $[n-5|1]$ contains 3^{n-5} graphs, P_3 is the true divergence of 3^{3+1} graphs in $[3]$, $[1|1,2]$ accounts for 3^0 and P_1 for 3^2 graphs. Thus, the foregoing term expresses the sum of relevant contributions from all the 3^{n+1} graphs in $[n]$.

By splitting the graphs and arranging the sumations as in Lemma 1, the result (10) is established.

Since Δ_{F1}', D_{F1}', etc., have the same behavior for large values of p, as the corresponding functions Δ_F, D_F (DII, Sec. VII), an immediate consequence of Lemma 1 is Lemma 3.

Lemma 3

$$P_{\mu\nu}{}^{\times}=P_d{}^{\times}(\delta_{\mu\tau}+X_{\mu\tau}{}^{\times})(\delta_{\tau\rho}-P_d{}^{\times}Y_{\tau\rho}{}^{\times}+P_d{}^{\times 2}Y_{\tau\rho}{}^{\times 2}-\cdots)(\delta_{\rho\nu}+Z_{\rho\nu}{}^{\times})+P_{\mu\nu c}{}^{\times}. \quad (12)$$

We have now reached the stage in our inductive argument, when we can establish the consistency of our procedure by an explicit choice of the unknown constant Z_4. We desire to choose Z_4 such that

$$C_{\mu\nu}=\delta_{\mu\nu}+T_{\mu\nu}+P_{\mu\nu}{}^{*}=Z_4{}^{-1}C_{\mu\nu 1}=Z_4{}^{-1}(\delta_{\mu\nu}+T_{\mu\nu c}+P_{\mu\nu c}{}^{\times}). \quad (13)$$

From (6), (11), and (12), however,

$$\delta_{\mu\nu}+T_{\mu\nu}+P_{\mu\nu}{}^{*}=\delta_{\mu\nu}+Z_4{}^{-1}[(S-T_d)\delta_{\mu\nu}+P_{\mu\nu c}{}^{\times}+T_{\mu\nu c}]+Z_4{}^{-1}(\delta_{\mu\tau}+X_{\mu\tau}{}^{\times})[S/(1-SY^{\times})+P_d{}^{\times}/(1+P_d{}^{\times}Y^{\times})](\delta_{\rho\nu}+Z_{\rho\nu}{}^{\times}). \quad (14)$$

Let $S+P_d{}^{\times}=Z_4+T_d+P_d{}^{\times}-1=0$, then $[S/(1-SY^{\times})+P_d{}^{\times}/(1-P_d{}^{\times}Y^{\times})]\equiv 0$ and simultaneously Eq. (13) is satisfied.

Thus, with the choice $Z_4=1-T_d-P_d{}^{\times}$ we finally establish that we can express $C_{\mu\nu}=Z_4{}^{-1}C_{\mu\nu 1}(e_1)$. Furthermore, by thus expressing Z_4 in terms of the true divergences of all original C parts, we have also expressed $P_{\mu\nu}{}^{*}$ in Lemma 2 in the fundamental form

$$P_{\mu\nu}{}^{*}=Z_4{}^{-1}[P_d{}^{\times}(e_1)\delta_{\mu\nu}+P_{\mu\nu c}{}^{\times}(e_1)]. \quad (15)$$

3. VERTEX PARTS AND MESON SELF-ENERGY GRAPHS

We now desire to show that it is possible to choose the constants Z_1 and Z_2 such that $\Delta_F'=Z_2\Delta_{F1}'$ and $\Gamma_\mu=Z_1{}^{-1}\Gamma_{\mu 1}$ and furthermore that $Z_4{}^{-1}=Z_2Z_1{}^{-2}$. The proof can be made to depend on that in Sec. II for C parts, by employing a technique due to Ward. It will be found that at least for Δ_{F1}', it is not even necessary to obtain its value by evaluating the absolutely convergent parts of all self-energy integrals. For this purpose we utilize the following differential identities,[14]

$$\Lambda_\mu(p,\,p)=-(1/2\pi i)(\partial/\partial p_\mu)\Sigma^{*} \quad (16)$$

$$(\partial/\partial p+\partial/\partial p')_\nu\Lambda_\mu(p,\,p')=\theta_{\mu\nu}(p,\,p',\,p'-p)+\theta_{\nu\mu}(p,\,p',\,0). \quad (17)$$

To prove these identities, we notice the differential relation,

$$-(1/2\pi i)(\partial/\partial p_\mu)\Delta_F(p)=\Delta_F(p)2p_\mu\Delta_F(p),$$

which correctly describes the insertion of an external photon line (with its energy-momentum set equal to zero) in a meson line with momentum p. A second differentiation with respect to ν describes not only the insertion of another photon 3-vertex on the same meson line, but also the complication of the first 3-vertex into a 4-vertex, with the proper weight factor.

To prove (16) we notice first that the sum of the contributions to $\Lambda_\mu(p,\,p)$ from all (reducible or irreducible) non-base-line vertex parts vanishes identically. Let the momentum p be always associated with the base line. If l_i represent the momentum variables associated with closed meson loops (connected to the base line and to each other), then the sum of the contributions to $\Lambda_\mu(p,\,p)$ from non-base-line vertex parts is

$$\sum_i\int(\partial/\partial l_i)[F_\mu(p,\,l_a)]dl_a$$

which vanishes identically because F_μ is uniformly small for large values of momenta l_a.

Similarly, for a C part, if the photon ν has its energy-momentum zero, and does not belong to the base line, the sum of the contributions for such graphs to $\theta_{\mu\nu}(p,\,p',\,p'-p)$ and $\theta_{\nu\mu}(p,\,p',\,0)$ identically vanishes.

Thus, (a) the only vertex parts giving a contribution to $\Lambda_\mu(p,\,p)$ are the base-line vertex parts,

(b) The only C parts contributing to $\theta_{\mu\nu}(p,\,p',\,p'-p)+\theta_{\nu\mu}(p,\,p',\,0)$ are those for which ν belongs to the base line.

If now we associate p with the base line for meson self-energy graphs, a differentiation gives precisely all the base-line vertex parts and no photon line is differentiated. This establishes (16).

Similarly on associating p, p' with the base line in vertex parts, the operator $[\partial/\partial p+\partial/\partial p']$ would give all the C parts with ν belonging to the base line and these are the only ones contributing to the right-hand side of (17), as shown. If μ itself does not belong to the base line, but to one of the closed meson loops, some photon line joining this loop to the base line must carry momentum $(p-p'+l_a)$, while a part of the loop itself may have momentum variables $(p-p'+l_b)$. The operator $[\partial/\partial p+\partial/\partial p']$ insures that neither this photon line, nor any part of the closed loop is differentiated. This establishes (17).

The foregoing proofs depend on a very particular choice of momenta; p, p' must be associated with the base line. This choice can sometimes lead to difficulties in isolating divergences. This question will be examined further in Sec. V, when we deal with M parts.

We now show by an inductive application of the identities (16) and (17) that these differential relations give rise to relations between true divergences and also hold for the convergent parts of the functions concerned as well. These convergent parts are the same parts of the divergent integrals as are obtained by our subtraction procedure.

[14] Abdus Salam, Phys. Rev. **79**, 910 (1950). These (or similar) identities were derived independently by F. J. Dyson (private communication), F. Rohrlich (reference 2). Rohrlich's derivation of the relations between divergent constants from them was, however, incomplete because difficulties connected with overlaps were not noticed.

We treat the case of vertex parts in detail. It is obvious that the C parts produced by applying the operator $\partial/\partial p+\partial/\partial p'$ to an irreducible vertex part are themselves irreducible. (An extra external line always improves the chances of irreducibility and reduces overlaps.) Thus, from (2), for irreducible graphs,

$$2L\delta_{\mu\nu}+(\partial/\partial p+\partial/\partial p')_\nu\Lambda_{\mu c}(p,p') =2R\delta_{\mu\nu}+\theta_{\mu\nu c}(p,p',p'-p)+\theta_{\nu\mu c}(p,p',0). \quad (18)$$

Setting $p=p'=p_0$ shows that $L=R$ and also that the differential relation holds for convergent parts as well.

Consider now a reducible vertex part. The integral corresponding to it is $\Lambda_\mu=\Lambda_{\mu c}+$the true divergence constant $L\times(p+p')_\mu+$true divergent constants $D\times$the reduced integrals, where each reduced integral represents a vertex part of a lower order. Therefore $(\partial/\partial p+\partial/\partial p')_\nu\Lambda_\mu=(\partial/\partial p+\partial/\partial p')_\nu\Lambda_{\mu c}+$divergent constants $D\times(\partial/\partial p+\partial/\partial p')_\nu$ applied to the reduced integrals.

Consider now the C parts produced by this operator from the given vertex part. We can show that for such graphs $\theta_{\mu\nu}+\theta_{\nu\mu}=\theta_{\mu\nu c}+\theta_{\nu\mu c}+2\delta_{\mu\nu}\times$the true divergence constant $R+$the same true divergence constants D as above$\times$precisely such C parts as are obtained by

FIG. 4.

applying the differentiation operator to the aforementioned reduced vertex graphs.

A term by term comparison would thus allow us to write an equation of type (18), from which the equality of L and R and a differential relation between $\Lambda_{\mu c}$ and $\theta_{\mu\nu c}$ can be deduced.

The proof of this proceeds inductively. Since the differentiation operator affects only the base line in the given vertex part V, the true divergences for those parts of this graph which do not contain portions of the base line are the same as the true divergences for the relevant C parts obtained by differentiating V, while the reduced integrals in the two cases are themselves connected by the differential relation. Thus it is only for those subintegrations which extend over a part of the graph containing portions of the base line that a proof is needed. If, in the vertex part under consideration, such subintegrations correspond to inserted self-energy, vertex part or C part divergences, the differentiation operator converts them into, respectively, vertex part, or C part divergences, while the last type of divergence becomes superficially convergent. To bring out the points involved we consider, as an example, the case of a vertex part V, with its base line containing as an insertion the irreducible self-energy graph S (subintegration t_r) in Fig. 4.

Disregarding the mass renormalizing constant A from this self-energy graph S, the relevant divergent term is $B'\times V_{\text{Red}}$ where B' is charge-renormalizing constant from S, and V_{Red} is obtained from V by removing this self-energy insertion from the base line altogether.

Let us now suppose that the number of vertices on the base line of V is n, of which k are 3-vertices. The differentiation operator produces from the graph V, precisely $(n-1+2k)$ C parts. Of these 5 are such that they represent the replacing of S in the base line of V, by the 5 (irreducible) vertex parts which a differentiation of S yields, while in the remaining $(n-6+2k)$ C parts, the insertion S remains unchanged in the base line. Therefore the divergence separated corresponding to the subintegration t_r from this class of $(n-1+2k)$ C parts is $=B'\times C_{\text{Red}}'+L'\times C_{\text{Red}}''$. C_{Red}' are the $(n-6+2k)$ reduced C parts obtained by omitting S altogether from the base line, L' is the sum of the true divergent constants from the 5-vertex parts obtained by differentiating S, while C_{Red}'' is the reduced C part (just one graph) obtained by omitting any of the 5-vertex parts, and replacing it by a 3-vertex. Two of the graphs C_{Red}' are identical with the graph C_{Red}'', i.e., the reduced graphs from those two C graphs obtained by inserting the external photon line ν, just "before" and just "after" S, on the base line of V.

Now from Eq. (2) and (16), $B'=-L'$ (all graphs concerned in this relation are irreducible and the factor $1/2\pi i$ is absorbed in the definition of the reduced integral C_{Red}''); consequently, the term separated corresponding to the subintegration t_r is $=B'\times C_{\text{Red}}$ where C_{Red} represents $(n+2k-7)$ (different) C graphs; but these are precisely the graphs which we obtain by applying the differentiation operator $(\partial/\partial p+\partial/\partial p')$ to the graph V_{Red}, as can be checked by noticing that V_{Red} has $n-2$ vertices on the base line, of which $k-2$ are 3-vertices and therefore the number of C parts obtained by differentiating V_{Red} is $n-3+2(k-2)=n+2k-7$.

The proof is thus arranged, by considering each of the true divergence$\times$the reduced integral separated from the vertex part V. It is shown that for the corresponding C parts, the true divergences$\times$reduced integrals can be grouped such that the true divergences are equal by an inductive application of (16) and (17), and, furthermore, that the reduced integrals from C parts are precisely those which can be obtained by applying the differentiation operator to the reduced graphs. Since the argument proceeds by considering all subintegrations, overlaps are automatically taken care of.

The proof, therefore, of the required relations for a vertex part of order e^{2n+2} depends on establishing relations between true divergent constants of corresponding S, V, and C parts up to order e^{2n}. As the induction starts with irreducible graphs for which such relations are obviously true from the very definitions, the foregoing result follows. Thus, finally (putting $p=p'=p_0$),

we have

$$(\partial/\partial p+\partial/\partial p')_\nu\Lambda_{\mu\epsilon}(p,p') = \theta_{\mu\nu\epsilon}(p,p',p'-p)+\theta_{\nu\mu\epsilon}(p,p',0). \quad (19)$$

We shall now show that Z_1 can be chosen such that

$$\Gamma_\mu=(p+p')_\mu+\Lambda_\mu(p,p')=Z_1^{-1}[(p+p')_\mu+\Lambda_{\mu\epsilon}(p,p',e_1)]$$

where by definition $\Lambda_{\mu\epsilon}(p_0,p_0)=0$. Let

$$\theta_{\mu\nu}(p,p',p'-p)+\theta_{\nu\mu}(p,p',0)=2G_{\mu\nu}(p'+p,p'-p).$$

Then defining

$$r^\lambda=(p+p')\lambda+2p_0(1-\lambda), \quad s^\lambda=(p'-p)\lambda$$

we rewrite (17) as

$$(\partial/\partial r_\nu{}^\lambda)\Lambda_\mu(r^\lambda,s^\lambda)=G_{\mu\nu}(r^\lambda,s^\lambda)$$

but

$$(\partial/\partial\lambda)\Lambda_\mu(r^\lambda,s^\lambda)=(p+p'-2p_0)_\nu G_{\mu\nu}(r^\lambda,s^\lambda) +(p'-p)_\nu\partial\Lambda_\mu/\partial s_\nu{}^\lambda;$$

consequently,

$$\Lambda_\mu(p,p')-\Lambda_\mu(p_0,p_0) =\int_0^1 d\lambda(p+p'-2p_0)_\nu G_{\mu\nu}(r^\lambda,s^\lambda) +\int_0^1 d\lambda(p'-p)_\nu\partial\Lambda_\mu/\partial s_\nu{}^\lambda. \quad (20)$$

Also, from (19),

$$\Lambda_{\mu\epsilon}(p,p')=\int_0^1 d\lambda(p+p'-2p_0)_\nu G_{\mu\nu\epsilon}(r^\lambda,s^\lambda) +\int_0^1 d\lambda(p'-p)_\nu\partial\Lambda_{\mu\epsilon}/\partial s_\nu{}^\lambda. \quad (21)$$

We have already shown, however, that Z_4 can be chosen such that

$$\theta_{\mu\nu}(p,p',q)=\delta_{\mu\nu}(Z_4^{-1}-1)+Z_4^{-1}\theta_{\mu\nu\epsilon}(p,p',q,e_1).$$

Therefore, (20) can be rewritten as

$$\left[(p+p')_\mu+\Lambda_\mu(p,p')-\int_0^1 d\lambda(p'-p)_\nu\partial/\partial s_\nu{}^\lambda(r_\mu{}^\lambda+\Lambda_\mu)\right] -[(2p_0)_\mu+\Lambda_\mu(p_0,p_0)]=Z_4^{-1}\left[(p+p')_\mu +\int_0^1 d\lambda(p+p'-2p_0)_\mu G_{\mu\nu\epsilon}\right]-Z_4^{-1}[(2p_0)_\mu]. \quad (22)$$

Since by definition, $\Gamma_{\mu 1}=(p+p')_\mu+\Lambda_{\mu\epsilon}(p,p',e_1)$, we have, from (22) using (21)

$$\Gamma_\mu(p,p')-\int_0^1 d\lambda(p'-p)_\nu\partial\Gamma_\mu/\partial s_\nu{}^\lambda =Z_4^{-1}\left[\Gamma_{\mu 1}(p,p')-\int^1 d\lambda(p'-p)_\nu\partial\Gamma_{\mu 1}/\partial s_\nu{}^\lambda\right]. \quad (23)$$

This leads us to infer the required result, namely, that $\Gamma_\mu=Z_4^{-1}\Gamma_{\mu 1}(e_1)$.

Knowing the value of $G_{\mu\nu\epsilon}$ we cannot obtain that of $\Lambda_{\mu\epsilon}(p,p')$ from Eq. (21), but that of $\Lambda_{\mu\epsilon}(p,p)$ can be readily found by a simple integration. Since

$$\sum_\epsilon{}^*(p)=-2\pi i\int_0^1 d\lambda(p-p_0)_\mu\Lambda_{\mu\epsilon}(p^\lambda,p^\lambda) \quad (24)$$

where $p^\lambda=p\lambda+p_0(1-\lambda)$, it is not needful for the derivation of $\sum_\epsilon{}^*(p)$ to consider the meson self-energy graphs any longer. The proof that $\Delta_F'=Z_4\Delta_{F1}'(e_1)$ follows from Eq. (16) in a similar manner to (23); in this case $\sum_M{}^*(p_0)$ is canceled by combining it with the contribution to the self-energy arising from the mass-renormalization term $-\delta\kappa^2\phi^*\phi$ in the Hamiltonian. We have also incidentally shown that $Z_1=Z_2=Z_4$, which satisfies condition (d) of the introduction.

4. THE FUNCTION D_F'

For photon self-energy graphs, we extend a formal technique introduced by Ward and define the functions, $\Delta_\mu(p)$ and $\Phi_{\mu\nu}(p)$, by equations,

$$-1/2\pi(\partial/\partial p_\mu)\Pi^*=\Delta_\mu(p) \quad (25)$$

$$(\partial/\partial p_\mu)\Delta_\mu(p)=\Phi_{\mu\nu}(p). \quad (26)$$

Also, let

$$W_\mu(p)=2ip_\mu+\Delta_\mu(p) \quad (27)$$

$$X_{\mu\nu}(p)=2i\bar\delta_{\mu\nu}+\Phi_{\mu\nu}(p). \quad (28)$$

The bar in $\bar\delta_{\mu\nu}$ distinguishes it from the $\delta_{\mu\nu}$ for a 4 C-vertex. These functions $W_\mu(p)$, and $X_{\mu\nu}$ stand in analogy to Γ_μ and $C_{\mu\nu}$ while Δ_μ and $\Phi_{\mu\nu}$ are analogous to Λ_μ and $\theta_{\mu\nu}$.

By integration we obtain from the foregoing

$$\Delta_\mu(p)=\int_0^1 d\lambda\Phi_{\mu\nu}(\lambda p)p_\nu \quad (29)$$

and

$$\Pi^*(p)=-2\pi\int_0^1 d\lambda\Delta_\mu(\lambda p)p_\mu. \quad (30)$$

Thus, in order to obtain $\Pi^*(p)$ we only need construct the function $\Phi_{\mu\nu}(p)$ which is logarithmically divergent. Dropping its divergent terms, the integrations in (29) and (30) give the desired convergent part of Π^*. In actual fact Π^* is not a scalar but a tensor[15] and its correct form (for the case of a simple irreducible photon self-energy part) is given by

$$\Pi_{\mu\kappa}{}^*=(\delta_{\mu\kappa}p^2-p_\mu p_\kappa)(C+D_c(p^2)).$$

The terms $-p_\mu p_k$ are omitted on account of charge conservation.[16]

[15] Julian Schwinger, Phys. Rev. **76**, 790 (1949), Appendix.
[16] R. P. Feynman, Phys. Rev. **76**, 781 (1949).

FIG. 5.

Thus, the function $\Phi_{\mu\nu}$ is in fact of the form:

$$\Phi_{\mu\nu,\,\rho\kappa}=[C+D_c(p^2)][2\bar{\delta}_{\mu\nu}\delta_{\rho\kappa}-\delta_{\rho\mu}\delta_{\kappa\nu}-\delta_{\rho\nu}\delta_{\kappa\mu}]+(\delta_{\rho\kappa}p^2-p_\rho p_\kappa)(\partial^2/\partial p_\mu\partial p_\nu)D_c(p^2).$$

However, if the terms $-\delta_{\rho\mu}\delta_{\kappa\nu}-\delta_{\rho\nu}\delta_{\kappa\mu}$ and $-p_\rho p_\kappa$ are dropped after the evaluation of $\Phi_{\mu\nu,\,\rho\kappa}$, we have

$$\Phi_{\mu\nu,\,\rho\kappa}=2\bar{\delta}_{\mu\nu}\delta_{\rho\kappa}(C+D_c(p^2))+\delta_{\rho\kappa}(\partial^2/\partial p_\mu\partial p_\nu)D_c(p^2)=\delta_{\rho\kappa}\Phi_{\mu\nu}.$$

In order to evaluate the function $\Phi_{\mu\nu}$ we must examine the implications of our formal differentiation $\partial/\partial p$. In general a photon self-energy graph may have both its external photon lines, μ and ν, belonging either to the same meson loop or to two distinct interconnected meson loops. In the latter case the momentum p must run along some photon lines joining the two distinct loops. The differentiation $\partial/\partial p$ which applied to a meson line carrying momentum p graphically signifies insertion of an external photon line (with energy-momentum zero), when applied to a photon line gives a new type of "vertex," illustrated in Fig. 5 with the vertex factor $2ip_\mu$ since $[-1/2\pi i(\partial/\partial p_\mu)D_F=D_F\cdot 2ip_\mu\cdot D_F]$. Thus to obtain the graphs corresponding to $\Phi_{\mu\nu}$ we first adopt some convention for the path of the variable p through the photon self-energy graphs. After "differentiating" all the photon self-energy graphs twice, we obtain the graphs corresponding to $\Phi_{\mu\nu}$ which contain vertices of the type in Fig. 5(a) and (b). The number and complexion of these graphs is governed by the convention[17] we adopt for the path of p but as the integrations (29) and (30) show, the choice of a convention does not matter as far as the evaluation of $\Pi^*(p)$ is concerned. After drawing all graphs $\Phi_{\mu\nu}$ we select the irreducible $\Phi_{\mu\nu}$, the criterion for irreducibility being the same as in Sec. 1, with the obvious extension that if a photon self-energy graph inside an internal photon line is differentiated, in order to obtain the irreducible skeleton, this is replaced by either of the vertices in Fig. 5 as the case may be. The advantage, as we shall see, in considering the function $\Phi_{\mu\nu}$ rather than Π^* itself is that the overlaps occurring for $\Phi_{\mu\nu}$ are relatively simple and it is easier to categorize the graphs corresponding to $\Phi_{\mu\nu}$ rather than Π^*. It may be emphasized that Δ_μ and $\Phi_{\mu\nu}$ are "fictitious" primitive divergents, being entirely defined by Eqs. (25) and (26) and have no real place in the theory. The convention for the path of p adopted here is illustrated in Fig. 6. Single arrows give the direction of charge, while double arrows follow p. In Fig. 6(a), p runs along the edge of the diagram; in (b) the path of p is "complementary," in the sense that if in (a), a portion of a closed loop is "differentiated," (b) insures the "differentiation" of the remaining portion of this same closed loop. Thus

$$(-1/2\pi)\partial/\partial p_\mu[(a)+(b)]=2\Delta_\mu(p).$$

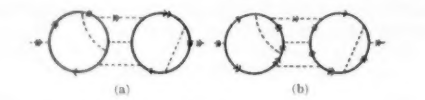

FIG. 6.

To illustrate the possible types of errors, let us notice that the graph in Fig. 7 is not reducible, because what appears as a C part with external photon lines ρ and μ is not in fact a C part comprised in the functions $C_{\mu\rho}$ so that this graph cannot be treated as reducible. When selecting the irreducible graphs for $\Phi_{\mu\nu}$ from the totality of graphs obtained, the following consideration is helpful. We have shown in Sec. 2, that $\theta_{\mu\rho}(p, p', 0)$

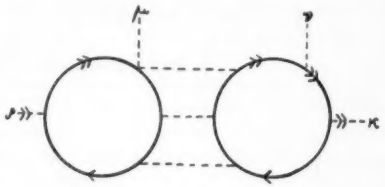

FIG. 7.

$=\theta_{\mu\rho}{}^b(p, p', 0)$, where $\theta_{\mu\rho}{}^b$ denotes the sum of the integrals corresponding to C parts with the photon line μ (with energy-momentum zero) necessarily belonging to the base line. Thus, if in a set of reducible $\Phi_{\mu\nu}$, only base-line C parts $\theta_{\mu\rho}{}^b$ appear, the irreducible skeleton for such $\Phi_{\mu\nu}$ contains the factor $\delta_{\mu\rho}$ and to obtain $\Phi_{\mu\nu}$ this factor can be replaced by $C_{\mu\rho}$ (the function for all and not merely base-line C parts) without incurring any error. The foregoing choice of "complementary" convention for p was designed, such that if a portion of a closed meson loop acts as the base line for graphs $\theta_{\mu\rho}$ (say) contained in a set of graphs $\Phi_{\mu\nu}$, the convention should insure (by differentiating the entire loop) that all relevant base line $\theta_{\mu\rho}{}^b$ do appear. The entire set $\theta_{\mu\rho}{}^b$ can then be replaced by a 4-vertex $\delta_{\mu\rho}$ and a (unique) skeleton thus defined.[18]

By categorizing the relevant graphs and using our inductive procedure, we shall establish the following equations (which are completely analogous to the set

[17] The choice of a convention is arbitrary but it is absolutely essential that once a convention is adopted it must be consistently followed.

[18] In this section (and subsequent sections) the distinction of δ_{ij} and δ_{ji} will be understood and the arguments will proceed in terms of 4-vertices, invoking the "weight factors" if necessary.

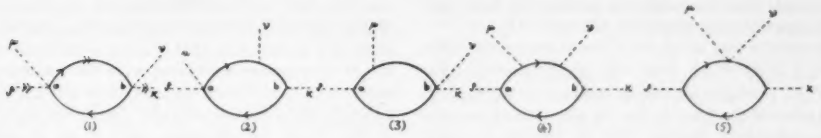

FIG. 8.

of Eqs. (4)):

$$\left.\begin{aligned} X_{\mu\nu} &= Z_3^{-1} X_{\mu\nu 1}(e_1) \\ W_\mu &= Z_3^{-1} W_{\mu 1}(e_1) \\ D_F' &= Z_3 D_{F1}'(e_1). \end{aligned}\right\} \tag{31}$$

Except for the graphs in Fig. 8, it is possible to make unambiguous insertions (4) and (31) in all the lines and vertices of the irreducible $\Phi_{\mu\nu}$ (the vertices now including those in Fig. 5), so as to obtain all derived graphs and their corresponding integrals.

For the graphs in Fig. 8, however, insertion of certain types of C parts causes overlaps. Barring these, and considering all other irreducible graphs for $\Phi_{\mu\nu}$, we can express the sum of their integrals and of the reducible graphs derived from them in the fundamental form.

In Appendix I we will show, by a procedure of categorization, that the sum of the integrals from the graphs in Fig. 8 and all graphs derived from them can also be given in the fundamental form. Adding together the contribution from these and $2i\bar{\delta}_{\mu\nu}$ for the 4-vertex in Fig. 5(b), we obtain

$$X_{\mu\nu} = 2i\bar{\delta}_{\mu\nu} + Z_3^{-1}[2iC(e_1)\bar{\delta}_{\mu\nu} + \Phi_{\mu\nu c}(e_1)].$$

At this stage a choice of $Z_3 = 1 - C(e_1)$ establishes the relation, $X_{\mu\nu} = Z_3^{-1} X_{\mu\nu 1}(e_1)$. From this and (29) and (30) we prove as in Sec. 2 that $D_F' = Z_3 D_{F1}'(e_1)$.

5. M PARTS

In this section the problem of M parts is dealt with. We show that with a correct choice of $\delta\lambda$ in a term $\delta\lambda\phi^{*2}\phi^2$ in the Hamiltonian, we cannot only consistently cancel all M divergences in the theory (whether they arise inside the graphs representing other primitive divergents or from what would otherwise be nondivergent graphs), we can also arrange that the graphs with 4-M vertices introduced into the theory by this term introduce no new infinities. It is easy to verify that if the $\delta\lambda$ term constituted the only interaction term the number of primitive divergents in the theory would be precisely two; namely, the graphs with two external meson lines (meson self-energy graphs) and those with four external meson lines (M parts).

The choice of $\delta\lambda$ is made in three steps.

(1) Consider all irreducible simple M parts. If M_d represents the sum of their true divergences, a choice of $\delta\lambda$ such that $\delta\lambda + M_d = 0$ cancels all divergences arising from these graphs.

(2) For the case of irreducible nonsimple M parts, unlike scalar meson-nucleon theories, joining two simple M parts may lead to an $M-M$ overlap. An example is shown in Fig. 9. However, whether or not these overlaps occur, our subtraction procedure gives the result that the correct choice of $\delta\lambda$ is once again given by $\delta\lambda + M_d = 0$, where $\delta\lambda$ is the sum of true divergences arising from all irreducible M parts, whether simple or otherwise. In spite of the overlap, the manner of proof is exactly similar to that given in detail in I, Sec. A, and is not repeated.

(3) To obtain all the original M parts from irreducible M parts, we make the usual insertions in all the lines and the vertices. Assuming (a) that the relations (3) hold and (b) that an insertion does not cause a further overlap, we immediately see by counting up the number of lines and vertices (including M vertices) that the correct final value for $\delta\lambda$ is given by $Z_2^{-2} M_d(e_1) + \delta\lambda = 0$ where $M_d(e_1)$ is the sum of the true divergences from all M parts. Condition (b) is satisfied for all except the three irreducible graphs in Fig. 10.

In these graphs, insertion of certain types of C parts causes $C-M$ overlaps. By a procedure of categorization it is not difficult to prove that the contribution made by such graphs to $\delta\lambda$ is also found as $-Z_2^{-2} M_d$, where M_d is the sum of their true divergences.

To prove (a) we remark that the foregoing proof for the cancellation of M-divergences extends to the case when M parts are contained inside other graphs. In particular for photon self-energy graphs or C parts there exist other graphs in the theory derived by replacing the contained M parts by M vertices in all possible ways. These graphs combine to cancel the M divergences times the corresponding "reduced integrals" so that neither need be considered at any stage of our inductive procedure for the formation of the functions Π^* or $C_{\mu\nu}$.

Since our procedure for deriving relations for operators Σ^* and Λ_μ is not to follow the relevant graphs but to obtain these analytically from $\theta_{\mu\nu}$ we have to show that the explicit neglect of M divergences and of the corresponding graphs with 4-M vertices in $\theta_{\mu\nu}$ does not affect the proof of the identities (16) and (17); in

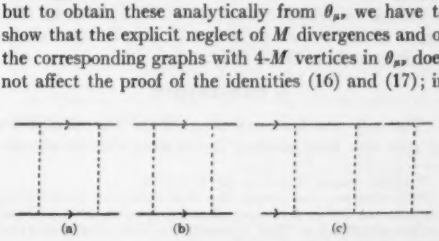

FIG. 9.

other words that this neglect is justified for both sides of the equations represented in (16) and (17).

The proof would be trivial if, for example, the differentiation $\partial/\partial p$ which, from the graphs corresponding to $\sum^*(p)$, produces all graphs relevant to $\Lambda_\mu(p, p)$ (in the manner of the proof in Sec. 3), also took all compensatory self-energy graphs with M vertices to corresponding compensatory vertex graphs. Since the proof of equality of $-(1/2\pi i)(\partial/\partial p)\sum^*$ with $\Lambda_\mu(p, p)$, for example, must depend on letting p run along the base line we have to show that a choice of basic momentum vectors which allows the path of p to lie along the base line also allows us to isolate M divergences.

The entire problem is closely linked with the problem of the general possibility of a "correct" choice of basic variables. This was discussed in detail in a previous paper[19] and only the results will be given here. For vertex parts situations arise when the number of divergences exceeds the number of subintegrations. In such cases, however, the extra divergences are M divergences which prove to be "final," and need not be separated. This happens, however, only on account of the gauge-invariance of the theory.

For meson self-energy graphs there is (as in the meson-nucleon case) another class of M divergences

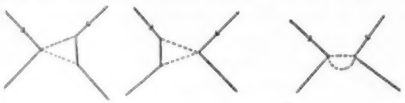

FIG. 10.

which were also called "final"[20] in Sec. B, I. The reduced integral corresponding to such "final" divergences is, by definition, independent of the external momentum p. Their effect is to leave just one type of graph with a 4-M vertex (illustrated in Fig. 6, I) and those derived from it by insertions in the meson line, as "odd" graphs which do not act as compensatory graphs like all other graphs with 4-M vertices, and so have to be considered separately. Here, as in the meson-nucleon case, these graphs only contribute to the mass renormalization constant, making it an explicit function of $\delta\lambda$; a fact finding analytic expression in that a differentiation $\partial/\partial p$ for such graphs gives the result zero.

Similar considerations apply for Π^*, Δ_μ, and $\Phi_{\mu\nu}$. The proof of the finiteness of the S matrix now follows precisely as in D II Sec. VII.

6. CONCLUSION

The only new feature arising for the renormalization of spin zero Bose particles interacting with the electromagnetic field is the introduction into the Hamiltonian of the (infinite) direct interaction term $\delta\lambda\phi^{*2}\phi^2$. In a sense it is satisfactory that this same term can remove the M divergences associated with the scattering of a meson by a meson when these particles interact through an exchange of virtual nucleons. The definition adopted in Sec. V of the divergent part of an M integral, however, makes $M_c(p_0, p_0, p_0)=0$, so that no graph of any order higher than the second in e^2, can contribute to the scattering amplitude of two mesons of equal initial and final momenta. Theoretically it is possible to proceed slightly differently and to introduce into the Hamiltonian, besides the compensatory $\delta\lambda\phi^{*2}\phi^2$, another "real" direct-interaction term $\lambda\phi^{*2}\phi^2$. The graphs involving 4-vertices with $\delta\lambda$ as coefficient are differentiated from those with λ as coefficient, the definition of original graphs being extended to include, besides the graphs involving 3-e- and 4-e^2-vertices, also the graphs containing 4-λ-vertices. The renormalization of the theory (not presented here in detail) proceeds as before, except that the Z factors now appear as functions of both e_1 and λ_1 (the renormalized value of λ) while the graphs with $\delta\lambda$-vertices compensate the additional M divergences introduced by the graphs containing these new λ-vertices as well. Thus $\delta\lambda$ is to be chosen as $\delta\lambda+Z_2^{-2}M_d(e_1, \lambda_1)=0$ while $\lambda_1=Z_2^{-2}\lambda$. The entire theory, after renormalization, appears in terms of two constants λ_1 and e_1. The retention of the condition $M_c(p_0, p_0, p_0)=0$ has the desirable feature, however, that even with this new term, the additional contribution to the Møller scattering amplitude, for mesons of equal initial and final momenta, is not given as a power series in λ_1 but consists merely of λ_1 itself.

The scheme presented here sketches what is theoretically possible. On account of the new feature noted, the physical validity of our renormalization scheme cannot be extrapolated from the fact that a very close agreement with experiment exists for the renormalized theory of spinor electrodynamics. To determine whether a constant λ_1 exists (even if only to find that its value is zero) and whether the answers to any physical problems given by the foregoing scheme approximate to the truth, we must turn again the pages of nature.

ACKNOWLEDGMENTS

The investigation was suggested by Dr. P. T. Matthews to whom the author is indebted for numerous discussions and detailed criticism of the manuscript. It gives the author great pleasure to express his profound indebtedness to Dr. N. Kemmer and Dr. F. J. Dyson for continual encouragement received throughout the progress of the work and to the Education Department of the Government of Punjab, Pakistan, and the Institute for Advanced Study, Princeton, for financial support.

[19] Abdus Salam, Phys. Rev. **83**, 426 (1951).

[20] Opening any one photon line in a meson self-energy graph (or a meson line in a photon self-energy graphs) gives a C part with a corresponding "final" C divergence. Their effect is precisely similar to that of "final" M divergences.

APPENDIX I

Here we consider the graphs in Fig. 8 and all reducible graphs which can be derived from them and prove that their contribution to $\Phi_{\mu\nu}$ can be expressed in the fundamental form.

In the 4-vertices appearing in the graphs in Fig. 8 an insertion of those C parts which have their two external photon lines belonging either to the same 4-vertex (class B) or to two consecutive 3-vertices on the same meson line (class C), causes an overlap. These same C parts inserted at one end 4-vertex of the graphs in Fig. 8, appear simultaneously as an insertion at the other end. The situation is completely analogous to the insertion of vertex parts in end-vertices of photon (or electron) self-energy graphs in spinor electrodynamics (the "b divergences" of D II Sec. VII). Let the class of C parts $B+C$ be called A, while let T denote all C parts other than those in class A. From Sec. 2,

$$T_{\mu\nu}=Z_4^{-1}[T_d\delta_{\mu\nu}+T_{\mu\nu e}(e_1)].$$

We now categorize the graphs derived from those in Fig. 8. The categories obtained are similar to those in Sec. IV, (I). In graphs (1), (2), (3), a and b stand for the end 4-vertices. Graph (1) has both its end-vertices as 4-vertices, (2) and (3) have either the left- or the right-hand vertex (as drawn here) as a 4-vertex while (4) has no 4-vertex at all. Let the graphs (1), (2), (3), and (4) in Fig. 8 belong to category [1]. Insert all *irreducible* A at the 4-vertex $a_{[1]}$ in [1|1] and [1|2], thereby obtaining a set of graphs belonging to category [2]. These graphs can once again be distinguished as [2|1], [2|2], [2|3], and [2|4], according as their end-vertices are 3-vertices or 4-vertices. Insertion of irreducible A at the 4-vertices $a_{[2]}$ in [2|1] and [2|2] then gives all graphs in category [3] and so on. $a_{[n]}$ and $b_{[n]}$ stand for the end 4-vertices appearing in [n|1], [n|2], and [n|3] at every stage.

Given a graph in [n]; let $A_a{}^1$ denote the true divergent constant arising from the irreducible A which was inserted at $a_{[n-1]}$ to obtain this particular graph in [n]; $A_a{}^2$, the constant of true divergence from the reducible graph A which could be inserted at $a_{[n-2]}$ to obtain this graph in [n]. This last graph is reducible because it contains as an insertion the irreducible graph with true divergence $A_a{}^1$. Similar definitions apply for $A_b{}^1$, $A_b{}^2$, $A_b{}^3\cdots$, etc. These definitions are analogous to those of $L_a{}^1$, $L_a{}^2$, $\cdots$, $L_b{}^1$, $L_b{}^2$, $\cdots$ in Sec. IV, I.

With these definitions we have the following lemma.

Lemma 1

$$\begin{aligned}[n]&=[n|1]+[n|2]+[n|3]+[n|4]\\&=A_a{}^1[n-1|1]+A_a{}^2[n-2|1]+A_a{}^3[n-3|1]+\cdots\\&\quad+A_b{}^1[n-1|1]+A_b{}^2[n-2|1]+A_b{}^3[n-3|1]+\cdots\\&\quad-[A_a{}^1A_b{}^1[n-2|1]+A_a{}^1A_b{}^2[n-3|1]+\cdots\\&\quad+A_a{}^2A_b{}^1[n-3|1]+\cdots]+A_a{}^1[n-1|2]+A_a{}^2[n-2|2]\\&\quad+\cdots+A_b{}^1[n-1|3]+A_b{}^2[n-2|3]+\cdots\\&\qquad+2iF_d\bar{\delta}_{\mu\nu}+F_{\mu\nu e}.\end{aligned}\tag{1A}$$

$2i\bar{\delta}_{\mu\nu}F_d$ gives the true divergence of [n], while $F_{\mu\nu e}$ is the convergent part. The proof of the lemma is given exactly on the lines of the proof of Lemma 1 (Sec. IV, I) and is not repeated.

In any graph [n], we can insert self-energy and vertex parts without causing any overlaps, while at all 4-vertices except $a_{[n]}$ and $b_{[n]}$, all C parts can be inserted unambiguously. Correspondingly, we replace Δ_F by $\Delta_F'=Z_2\Delta_{F1}'$, D_F by Z_3D_{F1}', $(p+p')_\mu$ by $Z_1^{-1}\Gamma_{\mu 1}$ in all the lines and 3-vertices of the graphs in these categories; while for all 4-vertices except $a_{[n]}$ and $b_{[n]}$, replace $\delta_{\mu\nu}$ by $Z_4^{-1}C_{\mu\nu 1}$. For $a_{[n]}$ and $b_{[n]}$, however, only the replacement of $\delta_{\mu\nu}$ by $\delta_{\mu\nu}+T_{\mu\nu}=Z_4^{-1}[(Z_4+T_d-1)\delta_{\mu\nu}+(\delta_{\mu\nu}+T_{\mu\nu e})]$ is analytically valid.

In terms of graphs, we obtain unambiguously by the insertions corresponding to these substitutions all graphs derived from the irreducible graphs in Fig. 8, no graph appearing more than once.

Let $\Sigma[n]^*$ represent the totality of graphs after these replacements, $[n]^\times$ represent graphs [n] with $\Delta_{F1}'(e_1)$, $D_{F1}'(e_1)$, $\Gamma_{\mu 1}(e_1)$, and either $C_{\mu\nu 1}(e_1)$ or $\delta_{\mu\nu}+T_{\mu\nu e}(e_1)$ appearing for their lines and vertices, $[n]_a{}^\times$ represent all graphs with the above factors $\Delta_{F1}'(e_1)$, $D_{F1}'(e_1)$, etc., except at the 4-vertex a where factor $\delta_{\mu\nu}$ remains unchanged, and let similar definitions apply for $[n]_b{}^\times$ and $[n]_{ab}{}^\times$. Then precisely as in Lemma 2, the entire class of graphs $\Sigma[n]^*$ can be expressed compactly as

$$\begin{aligned}\Sigma[n]^*=Z_3^{-1}\Sigma\{&[n]^\times+(Z_4+T_d-1)([n]_a{}^\times+[n]_b{}^\times\\&+(Z_4+T_d-1)[n]_{ab}{}^\times)\}.\end{aligned}\tag{2A}$$

From Lemma 1, however, by summing up

$$\begin{aligned}\Sigma[n]^\times=A_d{}^\times\{&\Sigma([n]_a{}^\times+[n]_b{}^\times-A_d[n]_{ab}{}^\times)\}\\&+2iF_d{}^\times(e_1)+F_{\mu\nu e}{}^\times,\end{aligned}\tag{3A}$$

where $A_d{}^\times=A_a{}^{1\times}+A_a{}^{2\times}+A_a{}^{3\times}+\cdots=A_b{}^{1\times}+A_b{}^{2\times}+A_b{}^{3\times}+\cdots$. Here $A_a{}^{1\times}$, etc., denote the true divergences with Δ_{F1}', D_{F1}', etc., replacing Δ_F, D_F, etc. $F_d{}^\times(e_1)$ is the sum of the true divergences of $[n]^\times$.

We have shown in Sec. 2 that $Z_4=1-T_d-A_d{}^\times$. So substituting (3)A in (2)A we obtain

$$\Sigma[n]^*=Z_3^{-1}\{2iF_d{}^\times(e_1)\bar{\delta}_{\mu\nu}+F_{\mu\nu e}{}^\times(e_1)\}.\tag{4A}$$

It still remains to consider the graph (5) in Fig. 8. The set consisting of graphs (1), (2), (3), and (4) was completely symmetrical regarding the classes B and C ($B+C=A$) but the graph (5) contains only one 4-vertex $\delta_{\mu\nu}$. This vertex will be called $e_{[1]}$. Inserting irreducible B at $e_{[1]}$ we obtain graphs belonging to [2|1] while insertion of irreducible C at $e_{[1]}$ gives [2|2]. These (irreducible B and C) can be inserted again at $e_{[2]}$ in [2|1] to obtain [3]=[3|1]+[3|2] and so on. The graph (5) in Fig. 8, itself constitutes the category [1|1], there being no graph in [1|2]. When the divergence in such a graph [n] is being isolated, the "reduced" graph left after the true divergence corresponding to the C part (which C part necessarily belongs to class C) has been removed, will be denoted by [n|3]. A graph [n|3] does not itself belong to the class of graphs [n], because for [n|3], $\rho\epsilon$ must be a 4-vertex. This new 4-vertex will be called f. Similarly let [n|4] denote the graph obtained by a simultaneous reduction of [n] at both ends, so that in the graph [n|4] both e and f appear as 4-vertices. Again a graph [n|4] does not itself belong to the class of graphs [n].

To obtain all graphs that can be derived from the graph (5), we construct the above categories [n] and then in their lines and vertices make the replacements $\Delta_F=Z_2\Delta_{F1}'(e_1)$, etc., except at the 4-vertex e where $\delta_{\mu\nu}$ is replaced by $Z_4^{-1}[(Z_4+T_d-1)\delta_{\mu\nu}+(\delta_{\mu\nu}+T_{\mu\nu e}(e_1)]$. If $[n]^*$, $[n]^\times$ are defined as those [n] in which, instead of Δ_F, for example, appear, respectively, the factors Δ_F' and Δ_{F1}', while $[n]_e{}^\times$ are $[n|1]^\times$ except that at the 4-vertex e, $\delta_{\mu\nu}$ is left completely unchanged, then by counting lines and vertices we obtain, as in (2)A

$$\Sigma[n]^*=Z_3^{-1}\{\Sigma([n]^\times+(Z_4+T_d-1)[n]_e{}^\times)\}.\tag{5A}$$

Now considering the implications of the subtraction procedure the result corresponding to Lemma 1 for [n] is as follows.

Lemma 2

$$\begin{aligned}[n]&=[n|1]+[n|2]=A^1[n-1|1]+A^2[n-2|1]+A^3[n-3|1]\\&\quad+\cdots+C^1[n-1|3]+C^2[n-2|3]+C^3[n-3|3]\\&\quad+\cdots-(A^1C^1[n-2|4]+A^1C^2[n-3|4]+\cdots\\&\qquad+A^1C^1[n-3|4]+\cdots)+2iG_d\bar{\delta}_{\mu\nu}+G_{\mu\nu e}.\end{aligned}\tag{6A}$$

By replacing Δ_F, by Δ_{F1}', etc., in [n] and summing up, we obtain from the foregoing

$$\begin{aligned}\Sigma[n]^\times=\Sigma\{&A_d{}^\times[n]_e{}^\times+C_d{}^\times([n]_f{}^\times-A_d{}^\times[n]_{ef}{}^\times)\}\\&+2iG_d{}^\times(e_1)\bar{\delta}_{\mu\nu}+G_{\mu\nu e}{}^\times(e_1).\end{aligned}\tag{7A}$$

$[n]_f{}^\times$ are [n|3] with Δ_{F1}', etc., replacing Δ_F except that the 4-vertex f is completely unchanged, and $[n]_{ef}{}^\times$ are similarly obtained from [n|4] except that for both e and f, the factors $\delta_{\rho\epsilon}$ and $\delta_{\mu\nu}$ are not changed. Substituting for $\Sigma[n]^\times$ in Eq. (5)A,

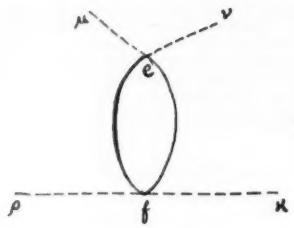

FIG. 11.

and using $Z_4=1-T_d-A_d^{\times}$ we obtain

$$\Sigma[n]^a=Z_3^{-1}(2i\bar{\delta}_{\mu\nu}G_d^{\times}(e_1)+G_{\mu\nu c}^{\times}(e_1)) +Z_3^{-1}(\Sigma C_d^{\times}\{[n]_f^{\times}-A_d^{\times}[n]_{ef}^{\times}\}). \quad (8)\text{A}$$

We now prove the result:

Lemma 3

$$Z_3^{-1}(\Sigma C_d^{\times}\{[n]_f^{\times}-A_d^{\times}[n]_{ef}^{\times}\})=0. \quad (9)\text{A}$$

For the proof consider the graph in Fig. 11. Construct various categories from it, by inserting irreducible A, successively, at the vertex e only. The characteristic of these graphs then is that f is necessarily a 4-vertex for all of them. After these categories are constructed, make substitutions (4) in all lines and vertices, except in vertex e where $\delta_{\mu\nu}$ is replaced by $Z_4^{-1}[(Z_4+T_d-1)\delta_{\mu\nu}+(\delta_{\mu\nu}+T_{\mu\nu c})]$ and the 4-vertex f which is left completely unchanged. The result is that we obtain as the sum of integrals corresponding to all these graphs, precisely the expression,

$$Z_4Z_3^{-1}\Sigma([n]_f^{\times}+(Z_4+T_d-1)[n]_{ef}^{\times})(e_1),$$

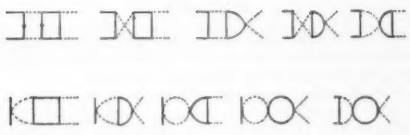

FIG. 12.

but this $=(\partial^2/\partial p_\mu\partial p_\nu)\int F(p+i,l^i,e)dld^i$ which is identically equal to zero, as can be seen by shifting $p+l\to l'$. Since $Z_4=1-T_d-A_d^{\times}\neq 0$ the proof is complete.

On account of Lemma 3, (8)A now gives

$$\Sigma[n]^a=Z_3^{-1}[2i\bar{\delta}_{\mu\nu}G_d^{\times}(e_1)+G_{\mu\nu c}(e_1)], \quad (10)\text{A}$$

which is once again in the fundamental form. The required result is thus established.

APPENDIX II

The graphs R mentioned in Sec. 2 are a set of chain graphs "derived" from the 10 irreducible graphs in Fig. 12. Since C parts have two external photon lines, a chain of meson loops joined to each other by two photon lines can cause $C-C$ and $C-M$ overlaps. The proof that all possible types of $C-C$ overlaps are comprised in the classes P, Q, R is not difficult to give from very simple topological considerations. To show, further, that the sum of integrals from graphs R can be expressed in the fundamental form, a careful scheme of categorization needs to be developed. The general principles on which the proof proceeds is already illustrated in Sec. 2. The details are much more complicated but, as no new principles are involved, we shall not reproduce them here (Fig. 12).

Nuclear Magnetic Resonance of Hydrogen Absorbed into Palladium Wires*†

R. E. NORBERG
Department of Physics, University of Illinois, Urbana, Illinois
(Received January 21, 1952)

Nuclear magnetic resonance signals have been observed for hydrogen which had been absorbed into palladium wires. Steady-state absorption and pulsed "echo" experiments were performed. The wires were connected as circuit elements and the resonance signals observed were caused by protons contained in the skin layer of the wires. Samples were loaded by means of a glow discharge to concentrations from 0.2 to 0.8 (expressed as atom ratios H/Pd). Measurements were made, as a function of temperature and hydrogen concentration, of line width, T_1, T_2, and resonance shifts. The results are interpreted to give information on the diffusion of the protons among the interstices of the palladium lattice and on the interaction of the protons with the conduction electrons. The observation of an asymmetric line shape for the absorption signal has led to a theory of a "lossy" resonance to be expected in metal wires.

I. INTRODUCTION

A. Description of the Experiment

An enormous number of investigations have been carried out on hydrogen-palladium "alloys" by means of the conventional techniques of solid state physics.[1] The present paper describes a new examination of the H-Pd system using nuclear magnetic resonance techniques. The examination consisted of nuclear magnetic resonance experiments performed on hydrogen which had been absorbed into metallic palladium wires. The loaded wires were used as integral parts of the electrical circuit and the signals observed were caused by those protons contained in the surface layers of the wires.

Pulsed and steady-state experiments were performed using the echo technique of Hahn[2] and the bridge and modulation method of Bloembergen, Purcell, and Pound.[3] The measurements made of line widths, shifts in the Larmor frequency caused by magnetic shielding, spin phase memory times (T_2), and spin lattice relaxation times (T_1) will be interpreted to give information about the relative location and state of motion of the protons and on their magnetic interactions with each other and with the conduction electrons.

B. The Hydrogen-Palladium System

It is known from conventional measurements that at least some of the occluded hydrogen atoms are mobile and that most are present as protons.[4] X-ray data[5] have indicated the coexistence of two distinct face-centered cubic phases of the palladium lattice over a range of hydrogen concentration from C near 0.1 to 0.58 (C expressed in atom ratio, H/Pd). The transition from the low concentration α-phase to the high concentration β-phase is marked by a 3.6 percent increase of the lattice parameter. Lacher[6] has been able to predict the H-Pd absorption isotherms and critical temperature from statistical considerations by assuming the existence of the occluded hydrogen as a gas of mutually interacting protons. The coefficient of diffusion has been measured for the hydrogen with widely varying results. Barrer[4] tabulates much of these data and quotes as an average value, $D=1.5\times10^{-3}\exp(-E/RT)$ cm²/sec. (Where $E=6800$ calories/gram atom.)

Palladium metal exhibits a very large paramagnetic susceptibility ($\chi_{\text{atomic}}=6\times10^{-4}$),[7] which decreases linearly as hydrogen is occluded, reaching zero at $C=0.66$[8] and remaining negligible at higher concentrations. Such behavior is explainable in terms of the band theory of metals.[9] Metallic palladium has a residual magnetization corresponding to about 0.6 Bohr magneton per atom, which implies that 0.6 electron per palladium atom are missing from the d band. One may consider each hydrogen as a potential electron donor through which the palladium seeks to remedy the d electron deficiency. Calculations have been reported[10] which indicate that a hydrogen atom dissolved in any known metallic lattice, gives up its electron because of the shielding of the proton charge by the conduction electrons. The concentration dependence described above for the susceptibility of the H-Pd indicates that, at least for $C<0.66$, each occluded hydrogen gives up its electron to the d band.

Hydrogen can be loaded into palladium from solution (by electrolysis) or directly from the ambient gas (cathodically, with a glow discharge or thermally, in an oven). Smith[1] believes that the loading is into a rift

* Taken in part from a thesis submitted in partial fulfillment of the requirements for the degree of Ph.D. in physics at the University of Illinois. A preliminary report of the work was given at the Chicago (Nov. 24–25, 1950) meeting of the American Physical Society [Phys. Rev. **81**, 305 (1950)].

† Supported in part by the ONR.

[1] D. P. Smith, *Hydrogen in Metals* (University of Chicago Press, Chicago, 1948), bibliography and supplementary notes.

[2] E. L. Hahn, Phys. Rev. **80**, 580 (1951).

[3] Bloembergen, Purcell, and Pound, Phys. Rev. **73**, 679 (1948) (hereinafter referred to as BPP).

[4] R. M. Barrer, *Diffusion In and Through Solids* (University Press, Cambridge, England, 1941), p. 220.

[5] See reference 1, Chapter VII.

[6] J. R. Lacher, Proc. Roy. Soc. (London) **A161**, 525 (1937).

[7] See reference 1, Chapter XIII.

[8] The value is for wires. A somewhat lower critical C has been reported for powders (reference 1).

[9] F. Seitz, *The Modern Theory of Solids* (McGraw-Hill Book Company, Inc., New York, 1940).

[10] I. Isenberg, Phys. Rev. **79**, 736 (1950).

network extending through the metal, followed by diffusion from the rifts into the lattice proper. Concentrations slightly in excess of $C=0.8$ can be attained during charging, but after the charging is stopped, the concentration drops rapidly to 0.8. A proton lattice made up of the hexagonal interstitial positions at the centers of the cube edges or one made up of alternate interstices of tetrahedral symmetry would each allow the formation of a one to one alloy with the palladium sites. Either set of interstices forms a fcc lattice with a parameter identical to that of the palladium but with different near neighbor palladium configurations for the two. A rigid lattice of the tetrahedral interstices and the palladium sites would form a structure of the sphalerite type. According to Wyckoff[11] this structure is "favored by (1) compounds with especially small cations (e.g., Be^{2+}) and (2) halides, oxides, etc., of incompleted shell transitional metals." The sphalerite arrangement might then be expected for an H-Pd alloy on both counts.

II. EXPERIMENTAL ARRANGEMENT

The dc magnetic field of about 7000 gauss was provided by an electromagnet which was constructed by Professor R. F. Paton of this department. The main current was provided by storage batteries, and an additional regulating current was controlled by a nuclear resonance detector. In the regulator the proton resonance from a frequency modulated transitron nuclear resonance detector,[12] the probe of which had been placed in the magnet gap, was fed as an error signal to a discriminator and dc amplifier. The error signal was peak-detected, permitting regulation of the central value of the field even with field modulation of amplitude much greater than the transitron signal line width. The field was measured by monitoring the central frequency of the transitron with a BC-221 frequency meter. The beat pattern between the two was fed from a communications receiver to an oscilloscope and visual observation of the zero beat allowed the field to be read and set reproducibly to ± 0.02 gauss in 7000.

The radiofrequency equipment used in many of the steady-state measurements was of conventional design and was used in the general bridge arrangement of BPP.[3] The output of a crystal controlled oscillator, operating near 30 mcps, was transformer-coupled into an electrically symmetrical twin-T rf bridge. One of the two resonant arms of the bridge was a balancing dummy and the other, which was placed in the magnetic field, contained the H-Pd wire sample as a direct part of the electrical circuit. In some cases the sample had the form of a coil resonated at 30 Mc. In other instances the flexible coaxial arm of the bridge was replaced with a rigid brass coaxial line approximately a quarter wavelength long. In the latter arrangement a straight wire H-Pd sample 1.5 cm long was inserted as a terminating stub at the end of the line.

In either case the signal appearing at the bridge output was fed through a narrow band preamplifier to a communications receiver. The detected signal was then viewed on an oscilloscope or observed as the output of a narrow band phase sensitive amplifier.[3] For the measurements of line width and line shape the field was modulated at 30 cps with amplitudes near 0.02 gauss, and the center value of the field slowly varied by varying the transitron frequency.

The shifts in gauss of the center field value of the H-Pd proton resonance were measured with respect to that for water by inserting a vial of water in the coil or by simply brushing some water onto the coil or on the H-Pd stub in the quarter wave line. The apparent width of the water resonance was also used to provide a correction factor for broadenings of the H-Pd lines caused by modulation effects and magnet inhomogeneities. The apparent width of the water resonance was usually about 0.03 gauss. Both shifts and line widths could be measured to ± 0.02 gauss, corresponding to the limit of accuracy of the vernier scale on the frequency meter.

Saturation studies of the spin lattice relaxation time T_1 were made by observing the deflection of the "lock-in" output meter as a function of varying rf power level.[3]

The pulsed experiments were performed with the "echo" techniques of Hahn.[2] For these measurements the rf bridge was driven by a pulsed crystal oscillator. Sequences were available of from one to four rf pulses spaced at arbitrary intervals and of durations from 7 μsec upwards. The signal from the bridge was coupled into a 30-mcps radar I.F. amplifier of MIT Radiation Laboratory design. The output of the amplifier was either detected and placed on an oscilloscope or else fed into a communications receiver which had been broadbanded to provide an attenuation of 3 db at a width of 30 kc. The additional gain and reduced band width provided by the receiver proved necessary for the observation of the very weak signals from some of the lower concentration samples.

Photographs were taken of the oscilloscope face for various pulse arrangements. T_2, the spin phase memory time, is measurable if one applies two pulses, separated by time τ, and observes, for various τ's, the amplitude of the echo signal occurring at 2τ.[2] Similarly, T_1, the spin lattice relaxation time, is measurable if one applies a third pulse at time T and observes, as a function of T, the amplitude of the "stimulated echo" occurring at time $T+\tau$. In order to improve the signal to noise ratio, each photograph represented a multiple exposure made over twenty-five repetitions of the pulse and echo sequence. The signal to noise ratio on the films was such that T_2 could usually only be measured to ± 15 percent and T_1 to ± 20 percent. It became quite difficult to

[11] R. W. G. Wyckoff, *Crystal Structures* (Interscience Publishers, Inc., New York, 1948).
[12] H. W. Knoebel and E. L. Hahn, Rev. Sci. Instr. **22**, 904 (1951).

measure T_1 in those samples having the shortest of the T_2 values observed.

The data were taken between 218°K and 348°K. The magnet gap used was only $\frac{1}{16}$ in., which made the use of a Dewar vessel difficult. The low temperature control apparatus generally used consisted of a copper trough filled with CS_2 in which the samples were immersed. Copper tubing was soldered around the longitudinal edges of the trough and acetone allowed to flow at a controlled rate from an acetone-dry ice reservoir. A copper-constantan thermocouple was placed near the sample in the bath and the temperature measured with a potentiometer. The trough was insulated from the magnet pole faces by asbestos cloth.

For runs above room temperature hot water was maintained in the reservoir in place of the acetone and dry ice. The high temperature range was limited by the fact that above 70°C hydrogen is rapidly driven out of an H-Pd alloy exposed to air.

III. PREPARATION OF SAMPLES

The samples used were prepared from palladium wires of 0.030-in. diameter and >99.5 percent purity. For some of the experiments 30 cm of the wire were wound into an eight turn coil 1 cm long and 0.7 cm in diameter. Such coils were loaded with hydrogen by means of a glow discharge[13] to concentrations, expressed as atom ratios $C=\mathrm{H/Pd}$, from 0.2 to 0.8.

It has been observed[14] that the electrical resistance of a palladium wire increases markedly as hydrogen is absorbed. In the present work the hydrogen concentration in the H-Pd samples was monitored during the loading and subsequent experiments by measuring the resistance of the wire between two standard points. A nearly linear relation exists[14] up to $C=0.76$ between the relative resistivity, $\rho=r/r_0$, and the concentration. At $C=0.76$ the resistance has increased to the point $\rho=1.7$. As will be pointed out in Sec. IV, certain of the shifts measured in the nuclear resonance experiments essentially measured the bulk susceptibility of the alloy and provided a check on the resistance measurements of the hydrogen concentration.

The success of a loading, in terms of the C finally attained and the rate of filling, proved to be a very sensitive function of the treatment of the wire. A typical successful load began with a cleaning of the wire with acetone. The coil was then wound and placed in a vacuum system. The coil was connected as a cathode and surrounded by a cylindrical brass anode. If the wire was next annealed by electrically heating it to an orange glow in a vacuum, the loading rate was much retarded. However, if the wire was heated in about one-third atmosphere of hydrogen, the surface was "opened" [13] and an enhanced loading rate resulted. It was noted, in agreement with the findings of Ulbricht,[13] that after a wire had been heated in hydrogen, the concentration, which had increased during the heating, returned to nearly zero and no subsequent loading occurred even if the sample were allowed to remain for many days in the hydrogen. The behavior is somewhat strange in view of the success of the oven technique of loading palladium powders.[15]

The typical loading continued with a glow discharge in hydrogen at a pressure of a few cm of Hg. Such a discharge started at 300 v and 10 ma and ran for from thirty minutes to one hour, having arrived at 400 v and 4 ma at the end of that period. This electrical behavior has been described by Jacobs and Martin[16] as the result of a rise of cathode temperature. A small increase in concentration is detectable during the discharge. After the discharge hydrogen was admitted to the chamber to a pressure of some 30 cm of Hg. Full loads of $C\simeq 0.7$ were reached in times ranging from a few hours to a month. The exact role of the discharge in the loading is in some doubt. Ulbricht[13] has described the process as an activation of the surface, but it seems to the author to be more likely that the mechanism is a simple cleaning or perhaps rift-opening at the surface. It is interesting to note that successful hydrogen loads have been reported[13] following discharges in argon. Commercial grade hydrogen was generally used in the present experiments. For some loadings the hydrogen was passed through a palladium valve, but this precaution did not materially affect the loading rate or final concentration attained.

The loaded samples were removed from the hydrogen atmosphere, washed with acetone, and the experiments then performed with the wires exposed to air. This nonequilibrium situation resulted in a slow loss of charge, generally of less than 10 percent per month for a carefully handled sample. The retention of the load was perhaps aided by the formation of a surface oxide layer. The stability of the loaded wires on exposure to air in comparison to the combustibility of powder samples[15] can be attributed to the reduced ratio of surface area to volume for the wires. One might fear that the migration of hydrogen to the surface and subsequent oxidation would result in a continually replenished layer of water on the wire which might be responsible for the nuclear resonance signals observed. However, those signals will be shown in the next section to have none of the characteristics of the water resonance.

The H-Pd coils were mounted within a brass shield by crimping copper leads onto the H-Pd. No soldering was done because of the instability of the alloy under the application of heat. In the case of the quarter wavelength line technique, the sample consisted of a 1.5-cm section cut from a loaded wire and mounted in the end of the coaxial line. The line was made of $\frac{3}{8}$-in. rigid

[13] R. Ulbricht, Z. Physik **121**, 351 (1943).
[14] See reference 1, p. 125.
[15] Torrey, Alpert, Ginsburgh, and Kohane (to be published). The existence of this independent parallel research on H–Pd alloys came to the author's attention during the course of his own work. He is much indebted to the Rutgers group for numerous discussions of data prior to its publication.
[16] H. Jacobs and J. Martin, J. Appl. Phys. **21**, 681 (1950).

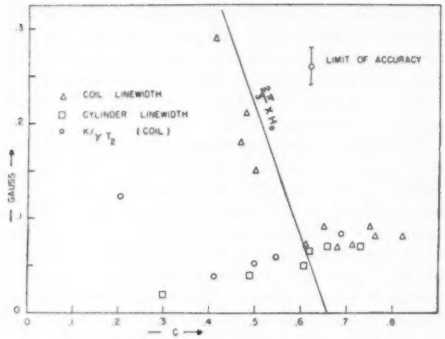

FIG. 1. Proton line width as a function of hydrogen concentration.

brass co-ax and had a 90° bend near the tip. The H-Pd alloy was placed as the center conductor in the bent tip and copper leads crimped on. The whole line could be rotated in such a manner that the H-Pd wire was oriented parallel or transverse to the magnetic field, H_0. Using as a criterion the ratio of the radius of the wire to its length, the deviation of such a sample from a true infinite cylinder can be estimated to be a few percent.

The nuclear resonance signal observed is caused by the protons contained within a surface layer of thickness the order of δ, the skin depth. δ is 1.2 mils in palladium at 30 mcps. Such a layer includes $\frac{1}{8}$ of the volume of a wire with 0.03-in. diameter. For a sample 30 cm long and a uniform proton distribution within the wire, the skin layer includes $2.8\times C\times 10^{21}$ protons. For comparison a 0.4-cc vial of water, which would just fit within the coil, contains some 3×10^{22} protons.

IV. EXPERIMENTAL RESULTS AND THEORY

A. Concentration Dependence of Line Width, T_2 and T_1

Figure 1 shows the proton line widths observed at room temperature plotted as a function of hydrogen concentration. The line widths quoted are the separation in gauss between peak deflections of the output meter of the "lock-in" amplifier, and hence, between inflection points of the resonance absorption curve. These data have been corrected for modulation and magnet broadening by comparison with the water resonance as described in Sec. II. The line widths measured above $C=0.65$ cluster about 0.08 gauss. For lower C the coil data increase with decreasing concentration and are interpreted to reflect a broadening imposed by surface demagnetization effects. A naive consideration of the variation in local field to be expected around the interior of a paramagnetic torus situated with its axis normal to H_0 leads one to expect a maximum local field excursion of $2\pi\chi H_0$, the value for the two orientations of an infinite cylinder. Further considerations, which will not be reproduced here, of the variation of the effective population of nuclear moments around the torus leads to the estimate of $\frac{2}{3}\pi\chi H_0$ for the order of magnitude of the line width observed. The solid line in Fig. 1 corresponds to $\frac{2}{3}\pi\chi H_0$ for the susceptibility data on H-Pd wires referred to in Sec. I.

The data obtained with the straight wire samples in the quarter wavelength line indicate a slowly decreasing line width below $C=0.65$ and reach the limit of accuracy of the measurements at $C=0.3$.

Figure 2 shows the concentration dependence observed for T_2 and T_1 with pulsed experiments at room temperature. A steady increase of T_2 was observed with decreasing concentration from 5.7 milliseconds at $C=0.69$ to 11 milliseconds for a sample at $C=0.41$. However, there is one much lower value of 3.6 milliseconds for the lowest concentration examined, $C=0.2$, which may correspond to an α-phase alloy.

The most striking feature of all of the above data is the narrowness of the lines or long T_2 values. One can obtain an order of magnitude for the rigid lattice line width due to a fixed array of protons which might exist in the palladium lattice. An array of the alternate tetrahedral interstitial positions forms a face-centered cubic lattice with a parameter identical to that of the palladium. Van Vleck[17] has calculated the mean square line width for a powder of randomly oriented fcc crystals to be $\langle\Delta H^2\rangle_{\text{Av}}=7.2n^2\times 2\mu^2$, where n is the number of moments per unit volume. Substitution of the value of n corresponding to the density of palladium yields a value of 3 gauss for the rigid lattice proton linewidth. The much narrower lines observed indicate the existence of rapid proton motions which cause the local fields mutually produced by the proton moments to average out to a great extent.

It is customary to write the applied rf magnetic field as the real part of $\mathbf{H}=H_1e^{i\omega t}$, and the transverse bulk magnetization as the real part of the product of $\mathbf{H}$, and the complex nuclear paramagnetic susceptibility $\chi_{\text{nuc}}=\chi'-i\chi''$; thus, $M=H_1(\chi'\cos\omega t+\chi''\sin\omega t)$. The power absorption in a nuclear resonance experiment may be written

$$P=v\int_{t=0}^{t}\mathbf{H}\cdot d\mathbf{M},$$

and since we are interested only in changes in the amplitude of $\mathbf{M}$, the integral gives $P=\frac{1}{2}\omega H_1^2\chi''$ ergs/mole second. The functional dependence of χ'' on ω thus gives the shape of the absorption mode of the resonance. Pake and Purcell[18] define a shape function by

$$\chi''(\nu)=\pi\chi_0 g(\nu),$$

$$\int_0^\infty g(\nu)d\nu=1, \quad \text{and} \quad T_2=\tfrac{1}{2}g(\nu)_{\max}. \qquad (1)$$

[17] J. H. Van Vleck, Phys. Rev. **74**, 1168 (1948).
[18] G. E. Pake and E. M. Purcell, Phys. Rev. **74**, 1184 (1948).

For a given line shape there exists a unique relation between T_2 and the line width measured between inflection points of the $\chi''(H)$ curve, $\Delta H = K/(\gamma T_2)$, where γ is the gyromagnetic ratio and K has the value $2/(3)^{\frac{1}{2}}$ for a Lorentzian line shape or $(2\pi)^{\frac{1}{2}}$ for a Gaussian.[19]

If one simultaneously considers the line width and T_2 data reported here, a discrepancy is evident. The $K/(\gamma T_2)$ points plotted in Fig. 1 were calculated from the T_2 data of Fig. 2 using the arbitrary value $K=12$. The significance of the result is not clear. It is difficult to accept the large number and the peculiar sharp-shouldered line that it implies, especially since no such line shape was observed. The discrepancy has led the author to examine the data for a few other solids that are suitable for both pulsing and steady-state measurements. Values of K of the order of 10 were obtained from crude preliminary data taken on paraffin, rubber and metallic sodium, and lithium. It must be pointed out that (contrary to the case in liquids[2]) in all of these measurements on solids, the noise present was such as to prevent a definite determination of the exponential character of the echo decay envelope. The time constants were measured by drawing a best straight line through the data plotted on semilogarithmic paper. Bloch's equations,[20] which assume a Lorentzian line shape, have been used in the analysis[2] that gives T_2 as the time constant for the spin echo decay. The more general case of non-Lorentzian lines has not been treated in the literature.

B. Skin Effects

An asymmetric line shape was observed during the line width measurements. If the rf bridge was so balanced with a vial of water in the coil as to present a pure absorptive mode ($d\chi''/dH$) on the output meter and then the water removed and the bridge balanced to the same criterion of detected voltage, then the H-Pd resonance line was observed to be somewhat dispersive in shape. If the bridge was balanced for an absorptive H-Pd signal at a low rf level, then the signal rapidly acquired a dispersive component upon increase of the rf voltage. The bridge was always rebalanced to present a symmetric line shape before a line width measurement was made.

In order to show that the asymmetric shapes observed were not the result of slight shifts of the bridge balance, the experiment was repeated using a transitron detector[12] to drive the coil instead of the bridge and fixed oscillator. Although the transitron device detects only those voltages in phase with the resistive (normally χ'') component, the same asymmetric line was observed for the H-Pd signal. The effect was shown not to be caused by the bulk paramagnetic susceptibility of the palladium, since similar shapes were observed for concentrations above and below 0.66. The effect was also observed for the straight wire samples as well as for the coils.

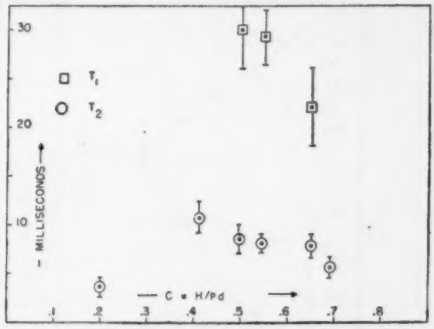

FIG. 2. Room temperature values of T_1 and T_2 as functions of hydrogen concentration.

The reason for the dispersive component of the resistive nuclear signal becomes clear if one considers that the resonance signal was caused by protons contained within a metallic conductor having finite conductivity. There was therefore no unique phase for the rf current within the wire, a phase shift of $\pi/2$ in fact being attained at a depth equal to the skin depth, δ. Physically, the penetration is limited by χ', the real part of the nuclear susceptibility, and the resulting ohmic losses produce a skewed resonance.

Slichter has carried out calculations, which will not be reproduced here, showing the existence of a dispersive component to the resistive signal from a wire, the change in the coil resistance turning out to be proportional to $\chi'+\chi''$. A simple calculation of the saturation behavior was made based upon a step function model for the nuclear susceptibility within the wire with a saturated region, where χ_{nuc} is taken to be zero, existing near the surface. The relative amount of the dispersive component was shown to be a function of the rf voltage. Using a saturation criterion indicated by the theory, a comparison of saturation runs made on H-Pd and on water led at first to erroneous estimates of T_1 of the order of 1 second.[21]

A more nearly exact calculation has since been made based upon the representation of χ_{nuc} by a linear rise from zero in the saturated region near the surface over a distance 2δ to the unsaturated value. At the halfway point of the rise the rf field H_1 has attained the critical value for the onset of saturation; $H_1(\text{crit.}) = (1/\gamma^2 T_1 T_2)^{\frac{1}{2}}$ and χ'' has decreased by one-half. The application of this model results in saturation values for T_1 which are in agreement with the results of the pulsed experiments.

Pake and Schuster of Washington University have kindly provided the author with additional verification

[19] N. Bloembergen, *Nuclear Magnetic Relaxation* (M. Nijhoff, The Hague, 1948).
[20] F. Bloch, Phys. Rev. **70**, 460 (1946).
[21] R. E. Norberg, Phys. Rev. **81**, 305 (1950).

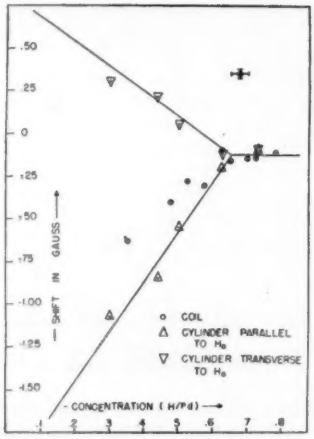

FIG. 3. Shift of H−Pd proton resonance, with respect to that in water, as a function of orientation and of hydrogen concentration.

of the theory. They have a nuclear resonance spectrometer detecting only the resistive mode with which they have obtained a tracing for the quadrupole-split Al^{27} resonance in a crystal. The tracing shows an incidental Cu^{63} resonance, caused by the copper coil, with excellent signal to noise ratio and of clearly asymmetric shape. Similar effects should be observed in metal powders for which the ratio of grain size to skin depth is sufficiently large.

C. Resonance Shifts

Figure 3 shows relative shifts of the H-Pd resonance as a function of C. The shifts were measured with respect to the proton resonance observed in water which had been brushed onto the sample or (for the coil) placed within it. The shifts measured with the quarter wave method were obtained with the sample in two orientations, i.e., with the cylinder axis normal to and parallel to the applied dc magnetic field. The shifts measured for concentrations below 0.65 thus correspond to resonance measurements made within a nearly infinite paramagnetic cylinder which had been oriented in an external magnetic field. The straight lines drawn correspond to $H_0[1+(4\pi\chi/3)]-H'$ and $H_0[1+(4\pi\chi/3)-2\pi\chi]-H'$, respectively, where H' is the small shift observed at high concentrations and the susceptibility data are those referred to in I. The $-2\pi\chi H$ demagnetization term has been added to the Clausius-Mossotti local field relation to take into account the effect of the surface magnetization induced in the transverse orientation. The fact that the data fall so closely along the lines indicates that in H-Pd the local field contribution from the very near-neighbor dipoles included in the Lorentz sphere is negligible.[22] The agreement was sufficiently good to provide a rough check on the resistanec-measured values of hydrogen concentration.

The shifts observed with the coils for C below 0.65 also are of the right sign and order of magnitude to be attributed to surface demagnetization effects rather than to any nuclear interactions. All of the shifts observed below $C=0.65$ exhibited a $1/T$ temperature dependence within experimental error. Since χ for the palladium goes nearly as $1/T$ in the temperature interval in question, the behavior provides further evidence of the bulk character of the effects.

The shift, ΔS, measured for $C>0.65$ appears independent of concentration and agrees for both coil and straight wire samples. This high C shift averages 0.12 ± 0.03 gauss and represents a percentage shift of $\Delta S/H_0=0.0017$ percent. The shift is paramagnetic and appeared independent of temperature within experimental error. The shift is interpreted to be of the type observed by Knight[23] arising from interaction of metallic nuclei with the conduction electrons. The small size of the shift in H-Pd indicates the existence of a small amplitude of the electron wave function at the protons.

D. Temperature Dependence of Line Width, T_2 and T_1

Figures 4 and 5 show the temperature dependence observed for line width, T_2 and T_1 between 218°K and 303°K. Again in Fig. 4 as in Fig. 1, the $K/(\gamma T_2)$ curve gives a reasonable fit to the line width data only with an abnormal value for K. The points plotted are for $K=12$. All of the samples were observed to exhibit a line width which broadened with decreasing temperature. One sample (not shown) with a concentration near 0.8 reached a line width of 0.6 gauss at 230°K. Pulsed data were not taken on any samples with $C>0.69$. Figure 5 is a composite of T_1 and T_2, values

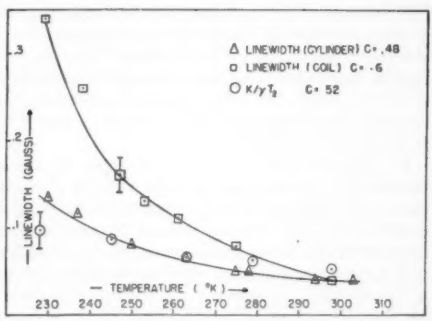

FIG. 4. Temperature dependence of proton line width for several hydrogen concentrations.

[22] W. C. Dickinson, Phys. Rev. **81**, 717 (1951).
[23] W. D. Knight, Phys. Rev. **76**, 1259 (1949); Townes, Herring, and Knight, Phys. Rev. **77**, 852 (1950).

taken for each of two samples with C near 0.52. The data indicate the existence of a T_1 minimum near 250°K.

It has proved possible in other metals, which exhibit a sufficiently narrow line to allow the application of the pulsing technique to interpret[24] the T_2 data in terms of an extension of the theory of relaxation times in liquids developed by BPP.[3] Such an analysis has yielded a reasonable value for the coefficient of self-diffusion for sodium nuclei. The theory predicts the existence of a T_1 minimum in the absence of other relaxation mechanisms when the characteristic frequency associated with the random fluctuations of the relative coordinates of the diffusing nuclei is nearly equal to the Larmor frequency for the nuclei. One may define a correlation time τ_c for a pair of nuclei as the time necessary for the local field of one nucleus at the other to change appreciably. For two diffusing nuclei this time is that required for diffusion over a distance of the order of the initial separation. Such a definition results in an exponential temperature dependence for the correlation time

$$\tau_c = 1/\omega_c = r^2/12D, \tag{2}$$

where, conventionally, $D = D_0 \exp(-E/RT)$.

Bloembergen[19] analyzes the spin-lattice interaction in terms of a Fourier analysis of the spectrum of translational fluctuations of the coordinates and obtains the expression,

$$\frac{1}{T_1} = 1.6\pi n\gamma^4\hbar^2 I(I+1) \times \int_{r_1}^{\infty} \frac{1}{r^4}\left(\frac{\tau_c}{1+\omega_0^2\tau_c^2} + \frac{2\tau_c}{1+4\omega_0^2\tau_c^2}\right)dr, \tag{3}$$

where n is the number of nuclei per unit volume and r_1 the distance of closest approach. For $\omega_0^2\tau_c^2 \ll 1$, which apparently corresponds to our room temperature case, the expression becomes

$$1/T_1 = 0.4\pi n\gamma^4\hbar^2 I(I+1)/Dr_1. \tag{4}$$

For $n = C \times$ atom density of Pd, (4) reduces to

$$1/T_1 = 3.16\times10^{-14} C/Dr_1. \tag{5}$$

Substitution in (5) of the room temperature value $T_1 = 0.03$ sec for $C = 0.53$ and taking as the lower limit of integration the separation of the tetrahedral wells of the Pd lattice, $r_1 = 2.8\times10^{-8}$ cm, yields the result $D = 1.8\times10^{-8}$ cm²/sec. The value is an order of magnitude less than that computed from Barrer's[4] averages, $D = 1.8\times10^{-7}$ cm²/sec.

If one plots the T_1 data of Fig. 5 on a logarithmic scale *versus* the reciprocal of the temperature and draws a best straight line through the data above 250°, the slope of the line corresponds to an activation energy $E = 3.7\pm1$ kcal/gram atom. The value is considerably less than the average quoted by Barrer, $E = 6.8$ kcal/gram atom. The values $D = 1.8\times10^{-8}$ and $E = 3.7\pm1$ yield an order of magnitude for D_0 of $10^{-3\pm1}$ cm²/sec. Such a small D_0 has been interpreted by Zener[25] to indicate that the main mechanism of diffusion is via "short circuit" paths along lattice imperfections.

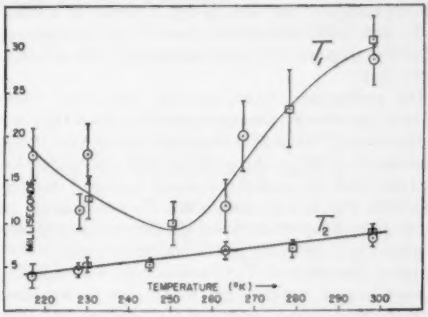

FIG. 5. Temperature dependence of T_1 and T_2. Composite curves for two samples with C near 0.52.

Professor Torrey[15] has performed an analysis of the H-Pd relaxation processes, among which he includes the effect of rift diffusion. It is possible to fit the Rutgers data by the results of his theory. The Rutgers data were taken at 9 mcps with H-Pd powders and indicate a minimum of 13 milliseconds near 240°K for a sample with $C = 0.64$. Their lower Larmor frequency leads one to expect that the temperature of the T_1 minimum should be shifted downward about 20° from the 250° reported here.

The mechanism that usually determines T_1 for metallic nuclei is interaction with the conduction electrons. Korringa[26] has derived a relation between the Heitler and Teller[27] expression for T_1 in a metal and the Townes, Herring, and Knight[23] expression for the metallic shift,

$$1/T_1 = (\Delta S/H_0)^2(\pi kT/\hbar)(\gamma_{nuc}/\gamma_e)^2. \tag{6}$$

Substitution of the shift, $\Delta S/H_0 = 1.7\times10^{-5}$, observed at high concentrations yields a value for the electron-induced T_1 of the order of two seconds. The very large T_1 and the predicted $1/T$ temperature dependence apparently exclude interaction with the conduction electrons as the source of the proton T_1 observed for C near 0.5.

E. Discussion of the Line Widths

Since T_1 is greater than T_2 at room temperature, it appears that there exists a broadening of the line width beyond that determined by spin-lattice interactions. The broadening may be described in terms of a time T_2' so defined that $1/T_2' = 1/T_2 - 1/T_1$. Application of

[24] R. E. Norberg and C. P. Slichter, Phys. Rev. **83**, 1074 (1951).

[25] C. Zener, J. Appl. Phys. **22**, 372 (1951).

[26] J. Korringa, Physica **16**, 601 (1950).

[27] W. Heitler and E. Teller, Proc. Roy. Soc. (London) **A155**, 629 (1936).

this expression to the data of Fig. 5 results in a value of T_2' near 0.012 second over most of the temperature range investigated. The exact source of this broadening is not clear.

The mechanisms which are the most likely competitors for the determination of the observed line widths include: mutual interactions among the proton moments or of the proton moments with the conduction electrons and the palladium nuclei or the d electron vacancies. For $\omega_c > \omega_0$, (which the T_1 data indicate to be our room temperature case) the simple liquid theory of mutually interacting proton moments predicts that T_2 be of the order of T_1.[3] Furthermore, a broadening independent of temperature would not be expected until the rigid lattice line width had been reached. The application of the liquid model to H-Pd may be naive in the use of the separation of lattice interstices as the lower limit of the radial integration or distance of closest mutual approach of the occluded protons. Even if the diffusion is primarily a lattice diffusion, the theory assumes spherical symmetry and neglects the existence of lattice-imposed restrictions on the relative coordinates of near neighbor protons. Also, it may be that T_2 is determined by a combination of spin-spin relaxation associated with a local order-disorder jumping of the protons among nearby wells and an additional static line broadening caused by long range interaction with the more distant proton moments.

The T_2 measurement made at $C=0.2$ may correspond to the α-phase of the alloy. The α-phase diffusion coefficient would be expected to be less than that for the β-phase since the lattice has not yet undergone the 10 percent volume expansion. The fact that the β-phase T_2 is less than that observed for higher concentrations may indicate that the broadening, T_2', is sensitive to the state of diffusion or it may simply reflect a reduction in T_1. The signal to noise ratio attainable with the low concentration sample was so small as to prevent a reliable measurement of T_1.

Among the other possible interactions we may discard any effects caused by nuclear magnetization of the palladium on the following grounds. All the Pd isotopes except Pd^{105}, which occurs in 23 percent abundance and whose moment is not known, are even-even nuclei and cannot on present theory have nonzero moments. In addition to the abundance factor of $\frac{1}{4}$ there is a factor of 5/9 to be considered in the effectiveness of nonidentical nuclei in the interaction theory.[17]

The line broadening arising from the interaction of the protons with the s conduction electrons amounts to a negligible fraction of the line widths observed since the electron-induced $T_1 \simeq T_2$ has been calculated in Sec. IV-D to be of the order of a second. The interaction with the d electron vacancies is similar to that with ordinary conduction electrons rather than to an interaction with paramagnetic ions. Since the mobility of the vacancies is large compared to that of the protons, the interaction may be described as occuring with a small effective electron moment. The interaction may be diminished by the filling of the vacancy nearest to any given proton by the electron originally associated with that proton. T_2' arising from the interaction with the d vacancies should increase with increasing hydrogen concentration.

SUMMARY

The experimental data for T_1, T_2, and line widths indicate that the occluded protons are moving rapidly within the metal. The application of a relaxation theory based on a simple model which represents the motion as self-diffusion in a proton liquid results in good qualitative, but only fair quantitative, agreement with the data. The theory, which has previously been shown to yield good results for self-diffusion in metallic sodium would be defective in the H-Pd case if the proton diffusion occurs primarily via lattice imperfections. The small value of D_0 estimated from the data would support such a 'short circuit" diffusion hypothesis.

Relaxation mechanisms based on phenomena other than the mutual interactions of the proton moments may be excluded on the basis of the above data and the measurements of resonance shifts.

The wire sample technique has certain convenient features for the experiments, notably in the "infinite cylinder" measurements. In these same measurements, however, the primary defect of the technique, a small signal to noise ratio, is at its worst. Work is currently in progress in our laboratory on narrow band equipment for observing the echo phenomena which, it is hoped, will result in a significant increase in the attainable signal to noise ratios. With such equipment the wire sample method might be applicable to nuclear resonance investigations of systems related to H-Pd, such as D^2-Pd, Cu-Ni, and Ag-Pd.

The author is indebted to Professor J. H. Bartlett for advice during the course of the research and to Professor C. P. Slichter for his constant counsel and encouragement. The author has further benefited from discussions and correspondence with H. C. Torrey, N. Alpert, and I. Ginsburgh of the Rutgers group and is especially indebted to Professor Torrey for the opportunity to see, in advance of publication, some of the results of the application of his new treatment of diffusion-induced relaxation to the H-Pd problem.

Much of the electronic equipment was designed and constructed by Mr. L. S. Kypta and Mr. H. W. Knoebel.

Gamma-Ray Spectra of the Los Alamos Reactors*

J. W. Motz
Radiation Physics Laboratory, National Bureau of Standards, Washington, D. C.
(Received January 14, 1952)

The gamma-rays emitted from a U^{235} slug at the center of the Los Alamos water boiler and from the core of the "fast reactor" were analyzed with a magnetic Compton spectrometer during the period that each reactor operated at a constant power level (30 kilowatts for the water boiler and 25 kilowatts for the fast reactor). An absolute gamma-ray spectrum (neglecting line structure) was determined for each reactor in an energy range from about 0.5 Mev to 12 Mev. In both cases, the number of photons emitted per unit energy interval decreased exponentially with photon energies so that the value at 8 Mev was less by a factor of 10^4 than the value at 0.5 Mev. The average quantum energy for this type of spectrum was approximately 1 Mev. The total energy release of gamma-radiation from the U^{235} slug (diameter 2.22 cm, length 0.426 cm, weight 28.5 g, 95 percent purity) occured at a rate of about 2×10^{13} Mev/sec.

THE γ-ray beams emerging from the collimator hole of the Los Alamos water boiler[1] (operating at 30 kilowatts) and of the "fast reactor" (operating at 25 kilowatts) were allowed to impinge on a beryllium foil, and the momentum distribution of the Compton electrons ejected from the foil into a small solid angle in the forward direction of the beam was measured with a magnetic spectrometer.[2] For the water boiler the source of the collimated γ-rays was a U^{235} cylindrical slug (diameter 2.22 cm, length 0.426 cm, weight 28.5 g, 95 percent purity) placed at the center of the sphere, while for the fast reactor the γ-rays originated in the reactor core.

The spectrometer measurements covered a range of electron energies from approximately 0.5 Mev to 12 Mev. "Hot wire" measurements[3] indicated that the focusing properties of the spectrometer did not change over this energy range. The measurements for the water boiler and fast reactor were made with a beryllium foil 11 mils thick and 33 mils thick, respectively. The secondary electron spectra for both reactors are shown in Fig. 1.

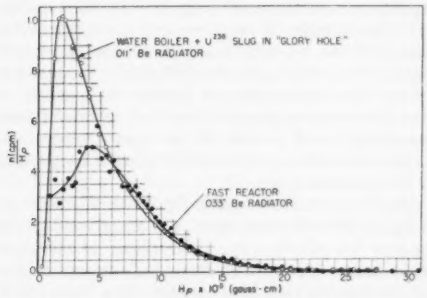

FIG. 1. Secondary electron spectrum produced by gamma-rays from the Los Alamos reactors.

Each momentum distribution in Fig. 1 was converted to a corresponding absolute γ-ray spectrum. The following factors were significant in the analysis:

(1) For the small acceptance angle of the spectrometer the angular dependence of the Compton electron energy could be neglected, so that the latter was related uniquely to the incident photon energy.

(2) The cross section $\sigma(k)$ (shown by the solid line in Fig. 2) for the emission of Compton electrons into the solid angle defined by the spectrometer acceptance angle θ was computed from the expression

$$\sigma(k)=\int_0^{\theta} f(\theta)\sigma(k,\theta)d\theta,$$

where k is the incident photon energy, $f(\theta)$ is a function dependent on the spectrometer geometry and baffle positions, and $\sigma(k,\theta)d\theta$ is the Klein-Nishina differential cross section. The effect of electron scattering in the foil and the geometry effect introduced by the foil

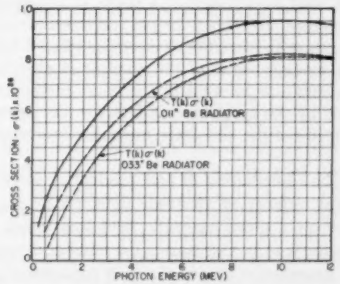

FIG. 2. The solid line represents the cross section for Compton electron emission into the solid angle defined by spectrometer acceptance angle θ as a function of the incident photon energy k. The dashed lines represent the "effective" cross section which includes the effect of electron scattering in the radiator and the effect of the finite extent of the radiator.

* Work done at the Los Alamos Scientific Laboratory under the auspices of the AEC.

[1] Los Alamos Scientific Laboratory of the University of California, Rev. Sci. Instr. **22**, 489 (1951).

[2] Motz, Miller, and Wyckoff, Bull. Am. Phys. Soc. **27**, No. 1, 9 (1952). A description of this spectrometer and the method of data analysis is being prepared for publication. A similar experimental method has been used by G. D. Latyschev *et al.*, J. Phys. (U.S.S.R.) **3**, 251 (1940).

[3] J. Loeb, L'ONDE Electrique **27**, 27 (1947).

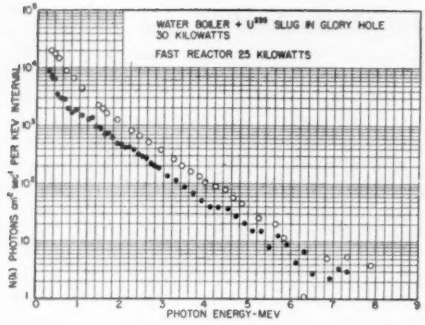
WATER BOILER + U235 SLUG IN GLORY HOLE
30 KILOWATTS
FAST REACTOR 25 KILOWATTS
N(k) PHOTONS cm² sec⁻¹ PER KEV INTERVAL
PHOTON ENERGY-MEV

FIG. 3. Gamma-ray spectra of the Los Alamos reactors.

width and length were evaluated from studies of the line shapes obtained for different foil sizes when monoenergetic photons (0.661 Mev, 1.38 Mev, and 2.76 Mev) were incident on the foil. These effects were expressed as a function $T(k)$, with an energy dependence that was governed by the fact that the electron scattering effect varied with energy in approximately the same way as the Coulomb scattering cross section. The quantity $T(k)\sigma(k)$ shown by the dashed lines in Fig. 2 represents an "effective" cross section that applies to those Compton processes in which an electron is accepted by the spectrometer after emergence from the foil.

(3) The spectrometer was calibrated from the line shapes obtained when the monoenergetic γ-rays from a ten-curie source of Cs^{137} (0.661 Mev)[4] and a one-curie source of Na^{24} (1.38 Mev, 2.76 Mev)[5] were incident on the beryllium foil in the spectrometer. The absolute intensity of the collimated γ-ray beam for each source was measured with an ionization chamber and the measured values agreed within 5 percent with the values computed from the "effective" cross section (Fig. 2) at the three photon energies.

(4) It was assumed that each spectrum was continuous, and no attempt was made to determine the line structure. To correct for the spectrometer response to a continuous spectrum of electrons ejected from the foil, an average value of the number of electrons per unit momentum interval in the total energy interval accepted by the spectrometer detector was determined with the aid of the line shape measurements mentioned in (3).

(5) The contribution of pair production electrons to the total number of electrons detected by the spectrometer at a given magnetic field was found by reversing the field and measuring the number of positrons, on the assumption that in the pair production process the cross section is symmetrical with regard to the positron and electron.[6] The number of pair production electrons relative to the number of Compton electrons, which emerge into the solid angle defined by the spectrometer acceptance angle θ with an energy (including rest energy) between E and $E+dE$, depends on the shape of the γ-ray spectrum in the energy region above $E+mc^2$. For the pile-type spectrum in the present case, the maximum contribution of the pair production electrons to the total number of electrons detected in any energy interval was less than 4 percent.

The absolute γ-ray spectrum (neglecting line structure) for each reactor is shown in Fig. 3. The quantity $N(k)$ is the number of photons per kev interval that are incident on the foil per cm^2 per second for a given photon energy k. The results indicate that for each reactor the number of photons emitted per unit energy interval decreases exponentially with the photon energy in an energy range from 0.5 Mev to 8 Mev. For each spectrum the number of photons per kev interval at 8 Mev was less by a factor of 10^4 than the value at 0.5 Mev. The average quantum energy for this type of spectrum was found to be approximately 1 Mev.

In the case of the water boiler, the results indicated that the total energy release of gamma-radiation from the U^{235} slug occurred at a rate of approximately 2×10^{13} Mev/sec. The fission and capture rates in the slug could not be determined accurately because the thermal neutron flux varied in a complicated way inside the slug. Because the measurements were made with the reactors operating in a steady-state condition, the γ-rays comprising the spectrum consist of (1) prompt γ-rays accompanying the fission process, (2) delayed γ-rays following the β-decay of the fission products, and (3) capture γ-rays primarily from the product nucleus U^{236}. (The intensity of capture γ-rays for isotopes other than U^{235} can be neglected.[7]) From the fission and capture cross section values[7] of U^{235} and the γ-ray energy release[8,9] per fission and per capture, it is estimated that the γ-rays of groups (1) and (2) each contribute approximately 45 percent of the total energy of the gamma-radiation compared to 10 percent contributed by the γ-rays in group (3).

The writer wishes to thank Dr. H. O. Wyckoff, Dr. William Miller, Mr. Fred Kirn, and Mr. Harold Gibson for their contributions to various phases of this work. He is also grateful for the valuable advice and cooperation rendered by Dr. L. M. Langer and Dr. Bob E. Watt of the Los Alamos Scientific Laboratory.

[4] L. M. Langer and R. D. Moffat, Phys. Rev. **78**, 74 (1950).
[5] K. Siegbahn, Phys. Rev. **70**, 127 (1946).
[6] H. Bethe and W. Heitler, Proc. Roy. Soc. (London) **146**, 83 (1934).
[7] "Nuclear Data for Low Power Research Reactors," Atomic Energy Project, Chalk River, Can. J. Phys. **29**, 203 (1951). R. K. Adair, Revs. Modern Phys. **22**, 249 (1950).
[8] M. Deutsch and J. Rotblatt, Los Alamos Declassified Contribution No. 910 (November, 1944).
[9] K. Way and E. P. Wigner, Phys. Rev. **73**, 1318 (1948).

Theory of the Production of Secondary Electrons in Solids*

A. J. DEKKER AND A. VAN DER ZIEL
Department of Electrical Engineering, University of Minnesota, Minneapolis, Minnesota
(Received January 29, 1952)

On the assumption of a simple Coulomb interaction between a primary and a lattice electron, a general formulation of the problem of the production of secondary electrons is given. The basic features of the existing theories of secondary emission are presented and discussed as different approximations of this formulation. Special attention is given to the process of production of secondaries and to the energy losses suffered by the bombarding primaries. Finally, the ratio is estimated of the number of secondary electrons emitted due to processes considered by Wooldridge and those investigated by Baroody.

I. INTRODUCTION

FROM the theoretical point of view the emission of electrons by a substance bombarded by a beam of primary electrons may be divided into two parts: the production of secondaries and the mechanism of their escape. In dealing with the process of production one may, at least for high primary energies, introduce approximations based on the assumption that the wave vector of the primary particle is large compared with the wave vector of a lattice electron. The wave vector of a secondary electron is usually not large enough to deal with the escape mechanism on a similar basis. This is one of the reasons why the quantitative aspect of the theory of secondary emission is rather incomplete. The first author to give a wave mechanical treatment of secondary emission was Fröhlich.[1] More recently his work was improved by Wooldridge.[2] According to these authors the free electron model of metals cannot lead to secondary emission when the primary beam is incident perpendicularly to the surface of the metal. The laws of conservation of momentum and energy would make it impossible for the lattice electrons to gain momentum in the direction towards the surface. Their theories are thus based entirely on the so-called Peierls' "Umklapp-Prozesse."

Rudberg and Slater[3] discussed the discrete energy losses suffered by inelastically reflected primaries on the basis of quantum mechanics. Recently Baroody[4] investigated the possibility of explaining some of the characteristic features of secondary emission on the basis of a free electron model, assuming that the escape of excited lattice electrons is caused by single or multiple scattering.

In all papers just referred to the interaction energy V between a primary electron with radius vector $\mathbf{R}$ and a lattice electron with radius vector $\mathbf{r}$ is assumed to be given by

$$V=e^2/|\mathbf{R}-\mathbf{r}|. \tag{1}$$

The validity of (1) may well be questioned. For metals, for example, a better approach may be to consider the conduction electrons together with the positive ion cores as a "plasma," thus taking into account the rather organized behavior of the system.[5] For insulators one should take into account the polarization of the medium, thus reducing (1) by a factor equal to the effective dielectric constant. In the latter case the essentials of the theory would not be affected. Notwithstanding the possible criticism with regard to the validity of (1), it will be assumed to hold in the present paper. It is our intention to present the theories referred to above as different approximations of a general formulation of the problem, focusing attention mainly on the production of secondaries and the energy losses suffered by the primary beam. Also, a comparison between the different approximations will be given, as well as an estimation of their relative importance to the theory of secondary emission.

II. THE FUNDAMENTAL PROCESS

Consider a primary electron with wave vector $\mathbf{K}$ moving in a crystal of unit volume. The energy of the primary particle is assumed to be large enough to consider it as free, so that its energy is $\hbar^2K^2/2m$ and its wave function $\exp[i(\mathbf{K}\cdot\mathbf{r})]$. The wave function of a lattice electron with wave vector $\mathbf{k}$ is represented by $\psi_\mathbf{k}(\mathbf{r})$ and is assumed to be normalized per unit volume. If there were no interaction between the two particles, the wave function of the system would be

$$u_0=e^{i(\mathbf{K}\cdot\mathbf{R})}\psi_\mathbf{k}(\mathbf{r})\exp(-iEt/\hbar), \tag{2}$$

where the total energy

$$E=E(\mathbf{k})+\hbar^2K^2/2m. \tag{3}$$

Because of the interaction, however, transitions are possible such that the lattice electron goes from state $\mathbf{k}$ to $\mathbf{k}'$ and the primary from $\mathbf{K}$ to $\mathbf{K}'$. The basic problem then consists of calculating the number of transitions per unit time $p(\mathbf{Kk}\rightarrow\mathbf{K}'\mathbf{k}')d\Omega'$ for which the primary electron is scattered into a solid angle $d\Omega'$ around the vector $\mathbf{K}'$ and the lattice electron is excited into $\mathbf{k}'$. Following the usual procedure, the wave

* Work supported by U. S. Signal Corps.
[1] H. Fröhlich, Ann. Phys. **13**, 229 (1932).
[2] D. E. Wooldridge, Phys. Rev. **56**, 562 (1939).
[3] E. Rudberg and J. C. Slater, Phys. Rev. **50**, 150 (1936).
[4] E. M. Baroody, Phys. Rev. **78**, 780 (1950).
[5] D. Bohm and E. P. Gross, Phys. Rev. **75**, 1851 and 1864 (1949); D. Bohm and D. Pines, **80**, 903 (1950); **82**, 625 (1951); D. Pines and D. Bohm, Phys. Rev. **85**, 338 (1952); D. Pines, Phys. Rev. **85**, 931 (1952).

function representing the two electrons under consideration at a time t, may be expanded as follows,

$$u(t)=\sum_{\mathbf{k}'}\sum_{\mathbf{K}'} a_{\mathbf{k}'\mathbf{K}'}(t)e^{i(\mathbf{K}'\cdot\mathbf{R})}\psi_{\mathbf{k}'}(\mathbf{r})\exp(-iE't/\hbar), \quad (4)$$

where

$$E'=E(\mathbf{k}')+\hbar^2K'^2/2m. \quad (5)$$

Assuming the interaction is given by (1) and commences at $t=0$, one finds

$$a_{\mathbf{K}'\mathbf{k}'}(t)=\frac{1}{i\hbar}\int_0^t\int_\tau\int_{\mathbf{R}} e^{i(\mathbf{K}-\mathbf{K}')\cdot\mathbf{R}}\frac{e^2}{|\mathbf{R}-\mathbf{r}|}\psi_{\mathbf{k}}(\mathbf{r})\psi_{\mathbf{k}'}{}^*(\mathbf{r}) \times\exp[-i(E-E')t/\hbar]d\tau d\mathbf{R}dt, \quad (6)$$

where the integrations over $d\mathbf{r}$ and $d\mathbf{R}$ extend over the volume of the crystal. According to Bethe[6]

$$\int\frac{e^2}{|\mathbf{R}-\mathbf{r}|}e^{i(\mathbf{K}-\mathbf{K}')\cdot\mathbf{R}}d\mathbf{R}=\frac{4\pi e^2}{q^2}e^{i(\mathbf{q}\cdot\mathbf{r})}, \quad (7)$$

with $\mathbf{q}\equiv\mathbf{K}-\mathbf{K}'$. Substitution into (6) leads for the transition probability to

$$|a_{\mathbf{K}'\mathbf{k}'}(t)|^2=\frac{16\pi^2e^4}{q^4}\frac{2\{1-\cos(E'-E)t/\hbar\}}{(E'-E)^2}|I|^2, \quad (8)$$

with

$$I\equiv\int e^{i(\mathbf{q}\cdot\mathbf{r})}\psi_{\mathbf{k}}(\mathbf{r})\psi_{\mathbf{k}'}{}^*(\mathbf{r})d\mathbf{r}. \quad (9)$$

For large values of t expression (8) has a strong maximum for $E'-E=0$, i.e., for processes in which energy is conserved. According to standard procedure one has to integrate over a large number of final states for which the primary particle has a value in the neighborhood of $\mathbf{K}'$. Expression (8) should therefore be multiplied by the number of states with a wave vector of magnitude between K' and $K'+dK'$ within a solid angle $d\Omega'$ around $\mathbf{K}'$, i.e., by $K'^2dK'd\Omega'=mK'dE'd\Omega'/\hbar^2$, and integrated over dE'. The time derivative of the resulting expression then gives the rate $p(\mathbf{Kk}\rightarrow\mathbf{K}'\mathbf{k}')d\Omega'$ at which these transitions occur. Thus,

$$p(\mathbf{Kk}\rightarrow\mathbf{K}'\mathbf{k}')d\Omega'=(4me^4K'/\hbar^3q^4)|I|^2d\Omega'. \quad (10)$$

In what follows it is convenient to consider a beam of primary particles of density m/hK, so that one particle crosses unit area per unit time. The rate of the transitions defined above then becomes

$$P(\mathbf{Kk}\rightarrow\mathbf{K}'\mathbf{k}')d\Omega'=(4m^2e^4K'/h^4q^4K)|I|^2d\Omega'. \quad (11)$$

The various theories referred to in the introduction differ essentially only in the manner in which the integral I, given by (9), is evaluated. Assuming the lattice electrons to be free, the theory of production of secondaries should become identical with Baroody's theory. The "nearly free" approximation yields results similar to those obtained by Wooldridge. The "tightly bound" approximation is in accordance with the discussion by Rudberg and Slater and, as far as energy losses are concerned, corresponds to the theory of Bethe. The first two approximations will be discussed in the next section, the third one in Sec. IV.

[6] H. Bethe, Ann. Phys. 5, 325 (1930).

III. WEAKLY BOUND LATTICE ELECTRONS

Describing the lattice electrons by Bloch functions, we may write,

$$\psi_{\mathbf{k}}(\mathbf{r})=e^{i(\mathbf{k}\cdot\mathbf{r})}u_{\mathbf{k}}(\mathbf{r}), \quad (12)$$

where $u_{\mathbf{k}}(\mathbf{r})$, a function with the same periodicity as the lattice, may be expanded in a Fourier series,

$$u_{\mathbf{k}}(\mathbf{r})=\sum_{n_1,n_2,n_3=0}^{\infty} c_{\mathbf{n}}(\mathbf{k})\exp[i(\mathbf{n}\cdot\mathbf{r})],$$

with

$$\textstyle\sum_{\mathbf{n}}|c_{\mathbf{n}}(\mathbf{k})|^2=1. \quad (13)$$

Here, $\mathbf{n}/2\pi$ is a vector denoting one of the points in the reciprocal lattice. For cubic crystals with a lattice constant a, $a\mathbf{n}/2\pi$ represents a vector with integral components. For body-centered cubic crystals those coefficients are zero for which the sum of the components of $a\mathbf{n}/2\pi$ is odd. Because the absolute value of the coefficients c decreases with increasing values of n, the most important terms that do not vanish for a b.c.c. lattice are c_{000}; c_{110}, etc.; c_{200}, etc.$\cdots$. We should note, however, that if $\mathbf{k}$ is equal or nearly equal to $\mathbf{n}$, $c_{\mathbf{n}}$ is not small compared with c_{000}. For a face centered cubic lattice only those coefficients do not vanish for which all components of $a\mathbf{n}/2\pi$ are odd or even. In this case then, the coefficients not equal to zero are, in order of decreasing magnitude, c_{000}; c_{111}, etc.; c_{200}, etc. $\cdots$. For a given $\mathbf{n}$ the coefficients $c_{\mathbf{n}}(\mathbf{k})$ also increase with increasing values of k, though slowly as long as k is appreciably smaller than n. It will be assumed in what follows that the lattice electrons excited by the primary beam into states denoted by $\mathbf{k}'$ may be considered as completely free, i.e., $c_{000}(\mathbf{k}')=1$ and $c_{\mathbf{n}}(\mathbf{k}')=0$ for $\mathbf{n}\neq0$.

On the basis of this assumption, substitution of (12) and (13) into (9) leads for the matrix element to

$$I=\textstyle\sum_{\mathbf{n}} c_{\mathbf{n}}(\mathbf{k})\int\exp[i(\mathbf{q}+\mathbf{k}-\mathbf{k}'+\mathbf{n})\cdot\mathbf{r}]d\mathbf{r}. \quad (14)$$

The integral is unity if

$$\mathbf{q}+\mathbf{k}-\mathbf{k}'+\mathbf{n}=0 \quad \text{or} \quad \mathbf{K}+\mathbf{k}+\mathbf{n}\equiv\mathbf{C}_{\mathbf{n}}=\mathbf{k}'+\mathbf{K}', \quad (15)$$

and has a negligible value otherwise. (15) expresses the law of conservation of momentum of the system. For a particular value of $\mathbf{n}$ the contribution to expression (11) is given by

$$P_{\mathbf{n}}(\mathbf{Kk}\rightarrow\mathbf{K}'\mathbf{k}')d\Omega'=|c_{\mathbf{n}}(\mathbf{k})|^2(4m^2e^4K'/h^4q^4K)d\Omega'. \quad (16)$$

Obviously, large values of $P_{\mathbf{n}}$ only occur for small values of q. According to the energy conservation law,

the minimum value of q is equal to

$$q_{\min}=\frac{2m}{\hbar^2}\frac{E(\mathbf{k}')-E(\mathbf{k})}{K+K'}\simeq\frac{m}{\hbar^2}\frac{E(\mathbf{k}')-E(\mathbf{k})}{K}, \quad (17)$$

which is very small for high primary energies. The approximation holds if $K\gg k$. For transitions defined by $\mathbf{n}\neq 0$, it thus follows from (15) and (16) that only those are allowed for which the excited state of the lattice electrons is determined by

$$\mathbf{k}'\simeq\mathbf{k}+\mathbf{n} \quad \text{for} \quad \mathbf{n}\neq 0, \quad (18)$$

i.e., for which the reduced wave vector does not change. For transitions defined by $\mathbf{n}=0$, (18) does not hold and (15) reduces to the "classical" momentum law

$$\mathbf{K}+\mathbf{k}=\mathbf{K}'+\mathbf{k}' \quad \text{for} \quad \mathbf{n}=0. \quad (18a)$$

Each of these types of transitions will now be discussed separately.

a. Transitions Defined by $n\neq 0$

The number of transitions $P_n(\mathbf{k},\mathbf{k}')$ taking place per unit time from an initial state defined by $\mathbf{K}$, $\mathbf{k}$, and $\mathbf{n}$ may now be calculated from (16). The final state of the lattice electron is given immediately by (18), so that $E(\mathbf{k}')-E(\mathbf{k})$, and hence, also K', is fixed. Introducing in momentum space a polar coordinate system with $\mathbf{K}$ as z-axis and θ and ϕ as polar angles defining the orientation of $\mathbf{K}'$, one may thus write

$$q^2=K^2+K'^2-2KK'\cos\theta, \quad (19)$$

or

$$qdq=-KK'd(\cos\theta). \quad (20)$$

It follows that

$$d\Omega'=(qdq/KK')d\phi. \quad (21)$$

Substituting (21) into (16) and integrating over q from $q_{\min}=K-K'$ to $q_{\max}=K\gg q_{\min}$ one obtains

$$P_n(\mathbf{k},\mathbf{k}')\simeq|c_n(\mathbf{k})|^2 4\pi e^4/E_{k'k}^2,$$

with

$$E_{k'k}\equiv E(\mathbf{k}')-E(\mathbf{k}). \quad (22)$$

It should be observed that the number of these processes is independent of the energy of the primary particle, although it should be kept in mind that the derivation is based on the assumption that $K\gg k$. As a consequence of the occurrence of $E_{k'k}^2$ in the denominator and $|c_n(\mathbf{k})|^2$ in the numerator, the number of processes under consideration decreases with increasing values of n. Except for a factor that is practically equal to unity, (22) is identical with Wooldridge's formula (32) in the paper referred to above.

Each transition of the kind just discussed leads to a secondary electron in a state $\mathbf{k}'=\mathbf{k}+\mathbf{n}$. Therefore, Eq. (22) describes the production of secondaries when multiplied by the number of lattice electrons initially in state $\mathbf{k}$. It may be noted that an electron with a wave vector $2\pi/a$, where $a\simeq 3A$ has an energy of about 20 ev. As k is usually appreciably smaller than n, the secondaries produced have momenta strongly determined by the direction of $\mathbf{n}$.

The influence of the direction of $\mathbf{k}$ relative to $\mathbf{n}$ on the magnitude of expression (22) may be estimated by making use of the approximation

$$E(\mathbf{k})\simeq\hbar^2k^2/2m. \quad (24)$$

In that case

$$E_{kk'}=(\hbar^2/2m)(n^2+2\mathbf{k}\cdot\mathbf{n})=(\hbar^2/2m)(n^2+2k_n n), \quad (25)$$

where k_n is the component of $\mathbf{k}$ along the direction $\mathbf{n}$. For a given vector $\mathbf{n}$ and a given value of k the transition probability is a maximum when $\mathbf{k}$ has the opposite direction of $\mathbf{n}$ and a minimum for $\mathbf{k}$ and $\mathbf{n}$ parallel.

According to (25) the energy lost by the primary particle because of a transition of the lattice electron from $\mathbf{k}$ to $\mathbf{k}+\mathbf{n}$ only depends on n^2 and on k_n. Thus, for a given vector $\mathbf{n}$ all those lattice electrons for which the component of $\mathbf{k}$ along $\mathbf{n}$ has a value between k_n and k_n+dk_n will gain energy between $E_{kk'}$ and $E_{kk'}+dE_{kk'}$ where $E_{kk'}$ is given by (25). Denoting the number in this group by $N(E_{kk'})dE_{kk'}$, the distribution of energy losses is given by

$$P_{n\ \text{total}}(E_{kk'})dE_{kk'}=v_n\langle|c_n(k)|^2\rangle_{k_n}\frac{4\pi e^4}{E_{kk'}^2}N(E_{kk'})dE_{kk'}. \quad (26)$$

In this expression v_n denotes the number of vectors $\mathbf{n}$ that have the same absolute value n. The coefficient $\langle|c_n(k)|^2\rangle_{k_n}$ represents a suitable average to take into account the fact that not all lattice electrons in the group $N(E_{kk'})dE_{kk'}$ have the same coefficient $c_n(\mathbf{k})$. Clearly, $\langle|c_n(k)|^2\rangle_{k_n}$ depends on k_n and therefore on $E_{kk'}$, though not strongly. For a "Fermi sphere" with maximum wave vector k_m, the number of electrons in the group dk_n defined above would be equal to $(k_m^2-k_n^2)dk_n/4\pi^2$. Hence, only for $k_n\ll k_m$ would $N(E_{kk'})$ be nearly constant.

The total energy loss of the primary beam caused by transitions defined by a specific value of n may be roughly estimated by observing that the value of $E_{kk'}$ given by (25) averaged over all electrons with the same initial value of k is equal to $\hbar^2n^2/2m=E_0$, and hence, independent of k. Together with (26) this leads to the following contribution to the energy loss of the primary beam per unit path

$$-\left(\frac{dE_p}{dx}\right)_n=\frac{8\pi e^4Nm}{\hbar^2n^2}v_n\langle|c_n(k)|^2\rangle_{k_n}=\frac{4\pi e^4N}{E_0}v_n\langle|c_n(k)|^2\rangle_{k_n}. \quad (27)$$

This expression is again independent of the energy of the primary particles. It should be noted, however,

that by using the average value E_0, the higher probability of small energy losses has not been taken into account, so that (27) is only a rough approximation. Similarly, the production of secondaries as determined by (22) may be approximated by

$$P_n(k')\simeq(4\pi e^4N/E_0^2)v_n\langle|c_n(\mathbf{k})|^2\rangle_{\mathrm{Av}}. \quad (22a)$$

b. Transitions Defined by $n=0$

This case corresponds to transitions of completely free electrons, i.e., to a Sommerfeld model of a metal. Because of the momentum law (18a) and the energy conservation law, the lattice electrons mainly gain momentum in a direction perpendicular to the wave vector $\mathbf{K}$ of the primary particle. In other words, when $\mathbf{K}$ is directed perpendicularly away from the surface, the lattice electrons mainly gain momentum parallel to the surface. This led Fröhlich and Wooldridge to believe that transitions of this type are unimportant for the process of secondary emission. However, as assumed by Baroody, electrons that have gained momentum parallel to the surface may still be able to escape by scattering processes. The scattering may be caused by impurities or by lattice vibrations. In both cases, the periodicity of the lattice is disturbed, but in the latter case the cross section for scattering is temperature dependent. Besides, of course, the excited lattice electrons will interact with the other free electrons, thus leading to absorption of the secondaries during their escape. Also, the primary electrons, even though they may impinge perpendicularly on the surface, will be subject to Rutherford scattering inside the metal and their path will be curved rather than linear. This is born out by experiments with high primary energies, whereby an appreciable percentage of primaries has been observed to leave the metal again at the surface of incidence after having lost a certain amount of energy. Therefore, even without scattering of the secondaries it should be possible to obtain secondary emission with a free electron model. *A priori* it is not at all obvious that the case $\mathbf{n}=0$ should not enter into a discussion of secondary emission.

To discuss these transitions Eq. (16) will again be used as a starting point, but with a transformation of $d\Omega'$ different from (21) as used for $\mathbf{n}\neq0$. Suppose the wave vectors of the primary electron and a lattice electron are given. Then the momentum law requires $\mathbf{K}+\mathbf{k}\equiv\mathbf{C}_0=\mathbf{K}'+\mathbf{k}'$. Because of the energy law, $(K'^2+k'^2)$ is also determined by the initial state. Introducing a polar coordinate system with $\mathbf{C}_0$ as z-axis and the angles θ and ϕ to define the direction of $\mathbf{K}'$ one may thus write

$$k'^2=K'^2+C_0^2-2C_0K'\cos\theta, \quad (28)$$

and by differentiation of both sides

$$-d(\cos\theta)=\frac{k'dk'}{K'}\left(\frac{2}{C_0}-\frac{\cos\theta}{K'}\right)\simeq\frac{k'dk'}{KK'}, \quad (29)$$

so that $d\Omega'$ may be expressed in the variables k' and ϕ,

$$d\Omega'\simeq(k'dk'/KK')d\phi. \quad (30)$$

The approximation is valid as long as $K\gg k$. Substitution of (30) into (16) thus leads for the number of transitions per unit time whereby the lattice electron, initially in state $\mathbf{k}$, is scattered into a state between k' and $k'+dk'$ to

$$P_0(k')dk'=\frac{4m^2e^4k'dk'}{\hbar^4K^2}\int_0^{2\pi}\frac{d\phi}{|\mathbf{k}'-\mathbf{k}|^4}, \quad (31)$$

(the coefficient $c_0(\mathbf{k})$ has been put equal to unity). In case $k'\gg k$, the integral is simply $2\pi/k'^4$. This condition is equivalent to the assumption $\mathbf{k}=0$, used by Baroody to calculate the momentum transferred from the primary to the lattice electron. For N free electrons per unit volume, this assumption leads for the total number of lattice electrons scattered into states between k' and $k'+dk'$, per unit time, to

$$P_{0\ \mathrm{total}}(k')dk'=(8\pi m^2e^4N/\hbar^4K^2)dk'/k'^3=(\pi e^4N/E_p)dE_{k'}/E_{k'}^2, \quad (31a)$$

there E_p represents the primary energy and $E_{k'}$ the energy loss involved in any one of these transitions.

In general, however, the assumption $k'\gg k$ is not allowed because transitions for which $|\mathbf{k}'-\mathbf{k}|$ is small are more frequent than those for which this quantity is large. More accurate results are therefore obtained as follows: multiply (31) by the number of lattice electrons that may be scattered into states $\mathbf{k}'$ by an increase of momentum $\hbar|\mathbf{k}'-\mathbf{k}|$. If α is the angle between $\mathbf{k}$ and $\mathbf{k}'$, this number is equal to $k^2dk\ \sin\alpha d\alpha/2\pi^2$. Integration of the resulting expression over α and ϕ then yields

$$P_{0\ \mathrm{total}}(k')dk'=\frac{8m^2e^4}{\pi\hbar^4K^2}k'dk'\int_0^{k_m}\frac{k^2dk}{(k'^2-k^2)^2}, \quad (32)$$

where the upper limit k_m corresponds to the wave vector of an electron at the top of the Fermi distribution. Integration over k gives

$$P_{0\ \mathrm{total}}(k')dk'=\frac{2me^4}{\pi\hbar^2E_p}k'dk'\left[\frac{k_m}{k'^2-k_m^2}-\frac{1}{2k'}\log\left(\frac{k'+k_m}{k'-k_m}\right)\right]. \quad (31b)$$

This expression reduces to (31a) by making a series expansion in terms of k_m/k' and retaining only the terms of lowest order in this variable, and finally putting $k_m^3=3\pi^2N$.

The distribution of energy losses may be obtained from (32) by introducing $E_{kk'}=\hbar^2(k'^2-k^2)/2m$ as variable instead of k', and integrating over k. Thus

$$P_{0\ \mathrm{total}}(E_{kk'})dE_{kk'}=\frac{\pi e^4N}{E_p}\frac{dE_{kk'}}{E_{kk'}^2}\quad\text{for}\quad E_{kk'}>E_m, \quad (33a)$$

$$=\frac{\pi e^4N}{E_p}\left[1-\left(1-\frac{E_{kk'}}{E_m}\right)^{\frac{1}{2}}\right]\frac{dE_{kk'}}{E_{kk'}^2}\quad\text{for}\quad E_{kk'}<E_m. \quad (33b)$$

The difference between these two expressions is caused by the fact that in the later case only those lattice electrons can contribute for which

$$k_m(1-E_{kk'}/E_m)^{\frac{1}{2}}<k<k_m,$$

because k' must be larger than k_m in view of the exclusion principle. For $E_{kk'}\ll E_m$ Eq. (33b) varies as $1/E_{kk'}$.

The total energy loss per unit primary path length is obtained by multiplying (33a) and (33b) by $E_{kk'}$ and integrating from zero to E_p. This yields

$$-(dE_p/dx)_{n=0} = (\pi e^4 N/E_p)[8/3-\log 4+\log(E_p/E_m)]. \quad (34)$$

To compare this result with that obtained in the next section for strongly bound electrons, it is convenient to write it as

$$-(dE_p/dx)_{n=0}=(\pi e^4 N/E_p)\log(2E_p/E_i), \quad (34a)$$

with $E_i=8E_m e^{-3/2}=0.55E_m$.

IV. THE APPROXIMATION OF STRONGLY BOUND ELECTRONS

For strongly bound electrons the wave functions are nearly identical with the atomic wave functions. In other words, the wave function of an electron strongly bound to an atom located at a lattice point defined by a vector $\mathbf{r}_i$, has appreciable value only in the vicinity $|\mathbf{r}-\mathbf{r}_i|$ of the order of the atomic radius. Also, according to (11) only transitions for which q is closely equal to $q_{\min}$ have appreciable probability of occurrence. For usual primary energies of some hundreds of volts, $q_{\min}$ is small compared with the reciprocal interatomic distance. Thus, the factor $e^{i(\mathbf{q}\cdot\mathbf{r})}$ appearing in the integral I given by (9) may be written in good approximation as

$$e^{i(\mathbf{q}\cdot\mathbf{r})}=[1+i\mathbf{q}\cdot(\mathbf{r}-\mathbf{r}_i)]e^{i(\mathbf{q}\cdot\mathbf{r}_i)}. \quad (35)$$

Making use of the orthogonality of $\psi_{\mathbf{k}}(\mathbf{r})$ and $\psi_{\mathbf{k}'}(\mathbf{r})$, this leads to

$$|I|^2=\left|\int\{\mathbf{q}\cdot(\mathbf{r}-\mathbf{r}_i)\}\psi_{\mathbf{k}}(\mathbf{r})\psi_{\mathbf{k}'}^*(\mathbf{r})d\mathbf{r}\right|^2=q^2|L_{\mathbf{kk}'}|^2 \quad (36)$$

where $|L_{\mathbf{kk}'}|^2$ is the optical transition probability. It is zero unless the reduced wave vector before and after the transition is the same, i.e., the selection rule is the same here as for the weakly bound approximation in Sec. IIIa.

The number of transitions $P(\mathbf{kk}')$ of a lattice electron from an initial state $\mathbf{k}$ to a final state $\mathbf{k}'$, per unit time, may then be found by substituting (36) into (11); introducing q and ϕ as new variables by means of the transformation (21) and integrating over q and ϕ one obtains

$$P(\mathbf{kk}')=\frac{4\pi me^4}{\hbar^2E_p}|L_{\mathbf{kk}'}|^2\log\frac{q_{\max}}{q_{\min}}.$$

The limits are the same as before, i.e., $q_{\min}=K-K'$ $=mE_{kk'}/\hbar^2K$ and $q_{\max}=K$. Thus,

$$P(\mathbf{kk}')=\frac{4\pi me^4}{\hbar^2E_p}|L_{\mathbf{kk}'}|^2\log\frac{2E_p}{E_{kk'}}=\frac{2\pi e^4}{E_p}\frac{f_{\mathbf{kk}'}}{E_{kk'}}\log\frac{2E_p}{E_{kk'}}, \quad (37)$$

where

$$f_{\mathbf{kk}'}=\frac{2m}{\hbar^2}E_{kk'}|L_{\mathbf{kk}'}|^2. \quad (38)$$

Expression (37) governs the production of secondaries into states with a prescribed wave vector $\mathbf{k}'$. For the distribution of energy losses suffered by the primary particles it follows immediately that

$$P(E_{kk'})dE_{kk'}=\text{const.}f_{\mathbf{kk}'}N(E_{kk'})dE_{kk'}/E_{kk'}, \quad (39)$$

where $N(E_{kk'})dE_{kk'}$ represents the number of transitions that give rise to an energy loss in the defined range.

The energy loss per unit primary path length caused by the interaction with a single lattice electron making transitions from $\mathbf{k}$ to $\mathbf{k}'$ is given by expression (37) multiplied by $E_{kk'}$. The total energy loss per unit path caused by a single atom is thus obtained by summation over all initial states $\mathbf{k}$ and all final states $\mathbf{k}'$. If there are N_a atoms per unit volume the total energy loss of the primary beam per unit path is thus given by

$$-\left(\frac{dE_p}{dx}\right)=\frac{2\pi e^4}{E_p}N_a\sum_{\mathbf{k}'}\sum_{\mathbf{k}}f_{\mathbf{kk}'}\log\frac{2E_p}{E_{kk'}}, \quad (40)$$

an expression identical with Bethe's formula (66) in the paper referred to above. Now, for an atom the oscillator strength summed over all initial and final states is equal to the number of electrons Z. When the primary energy is larger than the binding energy of an electron in the K-shell all electrons take part in the absorption process. For smaller primary energies, less than Z, say Z' electrons contribute to the loss of energy of the primaries. Introducing an average energy E_i' defined by

$$Z'\log E_i'=\sum_{\mathbf{k}'}\sum_{\mathbf{k}}f_{\mathbf{kk}'}\log E_{kk'}, \quad (41)$$

wherein the summation over $\mathbf{k}$ includes all initial states taking part in the absorption process, (40) may be written as,

$$-(dE_p/dx)=(2\pi e^4/E_p)N_aZ'\log(2E_p/E_i'). \quad (40a)$$

From what has been said above it follows that E_i' is a slowly varying function of E_p.

V. CONCLUDING REMARKS

Each particular one of the approximations dealt with above should apply to those energy bands for which the approximation is most fitting. However, a certain amount of overlapping of the cases $\mathbf{n}=0$ and $\mathbf{n}\neq 0$ on the one hand and, of $\mathbf{n}\neq 0$ and the tightly bound electron approximation on the other, can hardly be avoided. The approximation of completely free electrons would be expected to hold reasonably well for the

valence electrons of the alkali metals, whereas for the valence electrons of other metals a combination of $\mathbf{n}=0$ and $\mathbf{n}\neq 0$, i.e., of Baroody's and Wooldridge's theories, is probably more suitable. The contribution of the innermost electronic shells to the production of secondaries and to the energy losses suffered by the primaries is probably best described by the strongly bound approximation.

It is interesting to note that both the free electron model and the strongly bound approximation lead for the energy losses of the primaries per unit path to the same dependence on E_p, *viz.*, $E_p^{-1}\log E_p$. The only difference between (34a) and (40a) is the occurrence of a factor 2 in the latter. That this factor does not occur in (34a) is a consequence of the free electron approximation.[7] Formula (27) for the case $\mathbf{n}\neq 0$, although a rough approximation, shows that the energy loss per unit path is independent of the primary energy, so that the range of the primaries would be proportional to E_p. The only case where this has been observed in the literature, to the knowledge of the authors, is in experiments by Copeland[8] on the maximum depth of origin of the secondaries in platinum films on aluminum. Copeland found the maximum depth to be proportional to E_p below 500 ev and reports this to be in agreement with Wooldridge's theory. Above 500 ev the depth of origin of the secondaries increased more rapidly, indicating a decrease of dE_p/dx with increasing values of E_p.

The distribution of energy losses, expressed by formulas (26), (33a, b), and (39) for the three approximations will be discussed with reference to experimental results in a forthcoming paper by one of us (A.v.d.Z.).

As an application to secondary emission, a rough comparison will now be made between the relative importance of the cases $\mathbf{n}=0$ and $\mathbf{n}\neq 0$ when applied to the valence electrons of copper. As no quantitative theory of the escape mechanism exists as yet, the following simplifying assumptions will be made:

(a) The secondaries are distributed isotropically when leaving the metal. This implies a polycrystalline target or a process of scattering for a single crystal target.

(b) The absorption of secondaries affects both cases in the same manner, so that in a comparison it may be neglected.

(c) Production of tertiaries by secondary electrons is neglected. On the basis of these assumptions, the secondary emission current is

$$\int_{k_1}^{K} P(k')g(k')dk', \tag{42}$$

where $g(k')$ is the probability of escape of a secondary electron with wave vector $\mathbf{k}'$ and $P(k')dk'$ is the number of secondaries produced per unit time per unit volume in a given range. $P(k')dk'$ is different for the two cases, but $g(k')$ is the same. Assuming k_1 is the minimum component of $\mathbf{k}'$ perpendicular to the metal surface required to escape, one may write,

$$g(k')=\tfrac{1}{2}(1-k_1/k') \quad \text{for} \quad k'>k_1, \tag{43}$$

whereas $g(k')=0$ for $k'<k_1$.

For transitions defined by $\mathbf{n}=0$, $P_0(k')dk'$ is given by expression (31b). Upon substitution into (42) and replacement of the upper limit K by ∞, integration leads to

$$I_0=\frac{\pi e^4 N}{6E_1E_p}\left[1+\left(\frac{3}{5}\right)^2\left(\frac{E_m}{E_1}\right)+\left(\frac{3}{7}\right)^2\left(\frac{E_m}{E_1}\right)^2+\left(\frac{3}{9}\right)^2\left(\frac{E_m}{E_1}\right)^3+\cdots\right], \tag{44}$$

where $E_1=\hbar^2k_1^2/2m$. For transitions defined by a given value of n, the production of secondaries is given approximately by (22a). As each of the secondaries has an energy $E_0=\hbar^2n^2/2m$, (42) becomes for $\mathbf{n}\neq 0$

$$I_n=v_n\langle|c_n(k)|^2\rangle_{\text{Av}}(2\pi e^4N/E_0^2)\{1-(E_1/E_0)^{\frac{1}{2}}\}. \tag{45}$$

Inasmuch as the latter expression is independent of the primary energy, the relative importance of the two cases may be estimated by calculating the value of E_p for which (44) and (45) become equal. For energies below this value (44) is predominant, for higher energies (45) is predominant. Taking Cu as an example, with the following values as given by Wooldridge: $v_n=8$ (f.c.c. lattice), $E_m=7$ ev, $E_1=12$ ev, $E_0=35$ ev, $(c_{111})^2\simeq 0.01$, one finds that (44) and (45) become equal for $E_p\simeq 300$ ev.

The energy loss of the primary electrons per unit path may also be compared for the two cases, by making use of (34a) and (27). For Cu these expressions become equal for $E_p\simeq 600$ ev. This is appreciably larger than the primary energy for which the secondary emission currents are equal, as calculated above. The reason for this difference is apparently that the secondaries produced by transitions of the type $\mathbf{n}=0$ have less energy than those produced by transitions $\mathbf{n}\neq 0$. Consequently, the probability of escape of the former is smaller and although the value of dE_p/dx for $E_p=300$ ev is larger for the free electron case, $I_0<I_n$.

From what has been said above it seems justified to conclude that for metals bombarded by primaries of several hundred volts, a combination of the theories of Baroody and Wooldridge is necessary. The range of predominance of each of these approximations will depend on the particular target under consideration. It would be interesting to investigate experimentally the angular distribution of the secondaries emitted by single crystals. In this way, some more pertinent information about the scattering process during the escape might be obtained.

[7] See also N. F. Mott and H. S. W. Massey, *Atomic Collisions* (Oxford University Press, London, England, 1949), second edition, p. 252.

[8] P. L. Copeland, Phys. Rev. **58**, 604 (1940).

Angular Correlation of First and Third Gamma-Rays

G. B. ARFKEN, L. C. BIEDENHARN, AND M. E. ROSE
Oak Ridge National Laboratory, Oak Ridge, Tennessee

(Received February 18, 1952)

In a nuclear cascade involving three or more gamma-rays it is both desirable and feasible to measure the angular correlation of nonconsecutive gammas either to confirm the results of correlating consecutive radiations or to resolve possible ambiguities. The angular correlation functions for the observation of the first and third gammas in a triple cascade have been calculated with the use of Racah functions for cases of physical interest. While the anisotropies tend to be somewhat less than those from the correlation of consecutive gamma-rays, they are easily detectable by present experimental techniques.

IN investigations of nuclear decay schemes one frequently finds three or more gamma-rays in cascade. The angular correlation of any two consecutive gammas has been developed in detail[1-3] and has proven a valuable experimental tool in determining multipolarity of the radiation and angular momenta of the nuclear levels. In the case of three gamma-rays in cascade it is, in general, possible to measure the angular correlation of the first and third as easily as the correlation of the first and second or second and third. If the order of emission of the gamma-rays is not known from other evidence and the radiations can be distinguished by their energies, it is clearly possible to measure three correlations by taking the gamma-rays in pairs. A comparison of the measurement with the calculated results will then serve to establish the order of emission. If evidence whereby the order of emission may be established is available, then the one-three correlation will serve as a useful check on the correlation experiments involving consecutive gamma-rays, and in some instances it will make possible the resolution of ambiguities in the interpretation of the correlation of consecutive gammas. Two such cases are given below. The numerical results for this one-three correlation form the subject of this paper.

The theory of the correlation of three (or more) radiations has been discussed in some detail in a previous paper.[4] It was shown that when the second of three radiations was not observed, all interference terms were removed by taking the z axis along either the first or the third gamma. The angular correlation function for the emission of pure multipoles can then be written in the form

$$w(\vartheta)=\sum_{m_3M_3M_1}(j_3L_3m_3\pm1\,|\,j_2m_2)^2(j_2L_2m_2M_2\,|\,j_1m_1)^2\times(j_1L_1m_1M_1\,|\,j_0m_0)^2F_{L_1}{}^{M_1}(\vartheta). \quad (1)$$

Here and in the remainder of this paper j_0 will be used to denote the ground state (or final state) of the cascade while j_1, j_2, and j_3 denote the excited states in order of increasing energy. The m's and M's give the projection of the j's and L's, respectively, on the quantization axis. As the vector addition coefficients indicate, a 2^{L_i} pole quantum is emitted in the transition $j_i\rightarrow j_{i-1}$. The $F_L{}^M(\vartheta)$ is the relative angular distribution function as defined by Falkoff and Uhlenbeck.[2] The summation over these magnetic quantum numbers may be carried out as in Appendix I of reference 4. Dropping irrelevant scale factors the result is

$$w(\vartheta)=\sum_\nu(L_1L_1{-}1\,|\,\nu0)(L_3L_3{-}1\,|\,\nu0)\times W(j_1j_1L_1L_1;\nu j_0)W(j_1j_1j_2j_2;\nu L_2)\times W(j_2j_2L_3L_3;\nu j_3)P_\nu(\cos\vartheta). \quad (2)$$

The summation index ν is restricted to even non-negative integers and may not exceed the smallest of $2L_1$, $2L_3$, $2j_1$ and $2j_2$. It is not limited by L_2, the angular momentum of the unobserved intermediate gamma-ray. The three W functions are Racah functions; their properties have been given by Racah.[5,6] It will be noted that $w(\vartheta)$ is invariant under the transformation $L_1\leftrightarrow L_3$, $j_0\leftrightarrow j_3$, $j_1\leftrightarrow j_2$ corresponding to the Hermitian character of the matrix elements. This ambiguity, which also characterizes the correlation of the consecutive radiations, could be eliminated if one j_i, the ground-state spin, say, were known.

For conciseness define a set of Δ's by

$$j_i=\Delta_i+j_{i-1}, \quad (3)$$

and let $L_i=1$ when $\Delta_i=0,\pm1$ and $L_i=2$ when $\Delta_i=\pm2$. Higher values of $|\Delta_i|$ are not considered here. This limits consideration to cascades involving no multipoles higher than quadrupoles and assumes that in a given transition the lowest multipole possible participates which latter is the practical case. The restriction to dipoles and quadrupoles may be relaxed as discussed in reference 7, Sec. V-e.[7]

With these restrictions and with the normalization $\langle w(\vartheta)\rangle_{4\pi}=1$ (averaged over all directions), the ratios of Racah functions needed are given in Table I.

* This document is based on work performed for the AEC.

[1] D. R. Hamilton, Phys. Rev. **58**, 122 (1940).
[2] D. L. Falkoff and G. E. Uhlenbeck, Phys. Rev. **79**, 323 (1950).
[3] S. P. Lloyd, Phys. Rev. **83**, 716 (1951).
[4] Biedenharn, Arfken, and Rose, Phys. Rev. **83**, 586 (1951).
[5] G. Racah, Phys. Rev. **62**, 438 (1942).
[6] L. C. Biedenharn, Tables of Racah Functions, Oak Ridge National Laboratory Report No. 1098.
[7] Rose, Biedenharn, and Arfken, Phys. Rev. **85**, 5 (1952).

Some simplification can be obtained by noting that $A_1A_{-1}=1/10$, $A_{\pm 2}=2(5/7)^{\frac{1}{2}}A_{\pm 1}$, and $A_{24}A_{-24}=1/126$. If one wishes to obtain the individual Racah functions,[6] they can be obtained from these ratios by using the result

$$W(jjLL;0K)=(-1)^{L+j-K}(2L+1)^{-\frac{1}{2}}(2j+1)^{-\frac{1}{2}}, \quad (4)$$

TABLE I. Ratios of Racah functions for one-three correlation.

$$A_0\equiv\frac{W(j\,j\,1\,1;2\,j)}{W(j\,j\,1\,1;0\,j)}=-\left[\frac{(2j-1)(2j+3)}{10j(j+1)}\right]^{\frac{1}{2}}$$

$$A_1\equiv\frac{W(j\,j\,1\,1;2\,j-1)}{W(j\,j\,1\,1;0\,j-1)}=\left[\frac{(j+1)(2j+3)}{10j(2j-1)}\right]^{\frac{1}{2}}$$

$$A_{-1}\equiv\frac{W(j\,j\,1\,1;2\,j+1)}{W(j\,j\,1\,1;0\,j+1)}=\left[\frac{j(2j-1)}{10(j+1)(2j+3)}\right]^{\frac{1}{2}}$$

$$A_2\equiv\frac{W(j\,j\,2\,2;2\,j-2)}{W(j\,j\,2\,2;0\,j-2)}=\left[\frac{2(j+1)(2j+3)}{7j(2j-1)}\right]^{\frac{1}{2}}$$

$$A_{-2}\equiv\frac{W(j\,j\,2\,2;2\,j+2)}{W(j\,j\,2\,2;0\,j+2)}=\left[\frac{2j(2j-1)}{7(j+1)(2j+3)}\right]^{\frac{1}{2}}$$

$$B_0\equiv\frac{W(j\,j\,j\,j;2\,1)}{W(j\,j\,j\,j;0\,1)}=\frac{j^2+j-3}{j(j+1)}$$

$$B_1\equiv\frac{W(j\,j\,j+1\,j+1;2\,1)}{W(j\,j\,j+1\,j+1;0\,1)}=\frac{1}{j+1}\left[\frac{j(j+2)(2j+5)(2j-1)}{(2j+1)(2j+3)}\right]^{\frac{1}{2}}$$

$$B_2\equiv\frac{W(j\,j\,j+2\,j+2;2\,2)}{W(j\,j\,j+2\,j+2;0\,2)}=\frac{1}{2j+3}\left[\frac{j(j+3)(2j+7)(2j-1)}{(j+1)(j+2)}\right]^{\frac{1}{2}}$$

$$A_{24}\equiv\frac{W(j\,j\,2\,2;4\,j-2)}{W(j\,j\,2\,2;0\,j-2)}=\frac{1}{3}\left[\frac{(j+1)(2j+3)(j+2)(2j+5)}{14j(2j-1)(j-1)(2j-3)}\right]^{\frac{1}{2}}$$

$$A_{-24}\equiv\frac{W(j\,j\,2\,2;4\,j+2)}{W(j\,j\,2\,2;0\,j+2)}=\frac{1}{3}\left[\frac{j(2j-1)(j-1)(2j-3)}{14(j+1)(2j+3)(j+2)(2j+5)}\right]^{\frac{1}{2}}$$

$$B_{04}\equiv\frac{W(j\,j\,j\,j;4\,1)}{W(j\,j\,j\,j;0\,1)}=\frac{j^2+j-10}{j(j+1)}$$

$$B_{14}\equiv\frac{W(j\,j\,j+1\,j+1;4\,1)}{W(j\,j\,j+1\,j+1;0\,1)}=\frac{1}{j+1}\left[\frac{(j-1)(j+3)(2j-3)(2j+7)}{(2j+1)(2j+3)}\right]^{\frac{1}{2}}$$

$$B_{24}\equiv\frac{W(j\,j\,j+2\,j+2;4\,2)}{W(j\,j\,j+2\,j+2;0\,2)}$$

$$=\frac{[j(j-1)(j+3)(j+4)(2j-3)(2j-1)(2j+7)(2j+9)]^{\frac{1}{2}}}{(j+1)(j+2)(2j+3)[(2j+1)(2j+5)]^{\frac{1}{2}}}$$

provided $|j-L|\leqslant K\leqslant j+L$. The Clebsch-Gordan coefficients that appear in $w(\vartheta)$ are

$$(111-1|20)/(111-1|00)=2^{-\frac{1}{2}},$$

$$(221-1|20)/(221-1|00)=-(5/14)^{\frac{1}{2}}$$

and

$$(221-1|40)/(221-1|00)=-(8/7)^{\frac{1}{2}}.$$

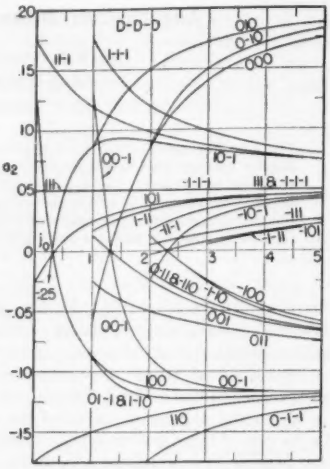

FIG. 1. The coefficient a_2 for dipole-dipole-dipole transitions (D–D–D) as a function of ground-state spin, j_0. The curves are labeled with the values of the Δ's, $w(\vartheta)=1+a_2P_2(\cos\vartheta)$.

From these and Table I the coefficients of $P_2(\cos\vartheta)$ and $P_4(\cos\vartheta)$ in the Legendre polynomial expansion

$$w(\vartheta)=1+a_2P_2(\cos\vartheta)+a_4P_4(\cos\vartheta) \quad (5)$$

have been calculated for the various one-three gamma-cascades subject to the above-mentioned restrictions. Since almost all of the gamma-ray cascades of interest terminate at the ground state and since the spin of the ground state will frequently be known, the angular cor-

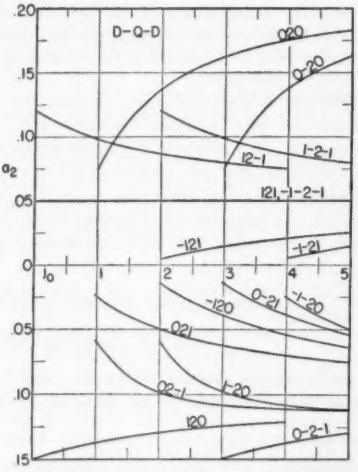

FIG. 2. The coefficient a_2 for dipole-quadrupole-dipole (D–Q–D) transitions.

relation functions are tabulated for the various possible values of the ground-state spin, j_0. The results are exhibited in Figs. 1, 2, 3, and 4. Cascades in which quadrupoles would always be competing with crossover dipole radiation have not been included since the competition is generally so unfavorable to the cascade transition. An example of this is the case $j \to j+2 \to j+1 \to j+3$ or the inverse transition scheme (Δ_1, Δ_2, $\Delta_3 = 2, -1, 2$ or $-2, 1, -2$).

When $L_i = |\Delta_i|$ and the j's are monotonic, the coefficients a_2 and a_4 are independent of j_0. A similar situation exists for two γ-rays in consecutive cascade as has been pointed out by Lloyd.[3] That this holds for the one-three correlation may be verified using Table I.

For convenience the values of a_2 and a_4 have been plotted against j_0 for all the sets of Δ's. These curves

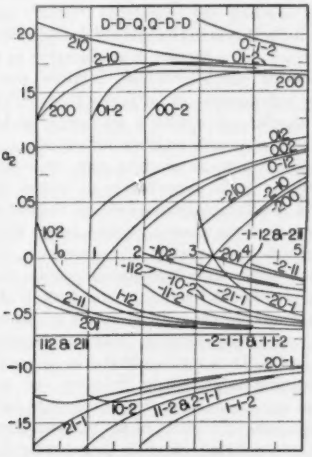

FIG. 3. The coefficient a_2 for dipole-dipole-quadrupole (D–D–Q and Q–D–D) transitions.

show all possibilities subject to the three restrictions (1) $L_i \leqslant 2$, (2) $L_i = 1$ when $\Delta_i = 0, \pm 1$, and (3) no crossover dipole gamma-rays competing with quadrupoles. Of course the curves have physical meaning only for integral and half-integral values of j_0.

It is perhaps of interest to note that in at least two cases the one-three gamma-gamma angular correlation

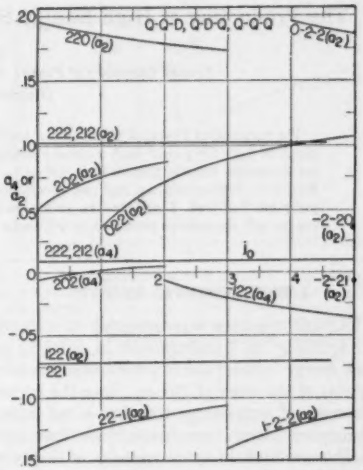

FIG. 4. The coefficient a_2 for quadrupole-quadrupole-dipole (Q–Q–D and D–Q–Q) transitions. The coefficients a_2 and a_4 for quadrupole-dipole-quadrupole (Q–D–Q) and quadrupole-quadrupole-quadrupole (Q–Q–Q) transitions.

can give new information that cannot be obtained from the correlation of consecutive gammas. An example is the pair of level schemes 0–1–1–2 and 0–2–1–1 where the numbers designate j-values. In each case the coefficient of $P_2(\cos\vartheta)$ for the first two gammas is -0.2500. In each case the coefficient a_2 for the last two gammas is -0.0250. It is impossible even with infinite resolution to distinguish the two decay schemes by correlating consecutive gamma-rays. However, if one correlates the first and third gammas the results for a_2 are -0.0250 and 0.1250 for the respective level schemes. The two cases may be easily distinguished. The pair of level schemes $\frac{1}{2}$–$\frac{3}{2}$–$\frac{3}{2}$–$5/2$ and $\frac{1}{2}$–$5/2$–$\frac{3}{2}$–$\frac{3}{2}$ show the same ambiguity under the correlation of consecutive gamma-rays and may also be resolved by the one-three correlations. These cases are, of course, rather exceptional. In general, with the increased number of parameters in the one-three correlation ($3L$'s, $4j$'s) it may be expected to yield more ambiguities than the consecutive gamma-correlation. The extent of the ambiguities may be estimated from the graphs.

The Production of High Energy Secondaries by Cosmic Rays Underground*

W. E. HAZEN
Randall Laboratory of Physics, University of Michigan, Ann Arbor, Michigan
(Received January 16, 1952)

The traversal of a total of 100 meters of lead by penetrating particles has been studied at an underground depth of 8.4×10^4 g cm^{-2} with a cloud chamber containing 2.54-cm lead plates. The observed probability for an energy transfer greater than 10^9 ev to the soft component is $3.0(\pm0.7)\times10^{-4}$ per g cm^{-2} of lead. Knock-on, bremsstrahlung, and pair-production processes are calculated to give a probability of 2.1×10^{-4} per g cm^{-2} of lead. Therefore, the above electromagnetic phenomena account for nearly all of the high energy soft secondaries produced by μ-mesons of energy $\sim10^{11}$ ev.

I. EXPERIMENTAL RESULTS

A CLOUD chamber was operated at a depth of 8.4×10^4 g cm^{-2} underground in order to study the high energy interactions of μ-mesons whose average energy was of the order of 10^{11} ev. Since the frequency of occurrence of high energy transfers is not large, the cloud-chamber plates were made thick (one inch of lead). This resulted in a compromise with the most useful thickness for observation of the details of the events themselves, but since only high energy events were studied the compromise did not seriously reduce the certainty of the observations.

The controlling counters were placed exclusively above the cloud chamber for about one-half of the experiment. With this arrangement there can be no bias in favor of μ-mesons that interact in the plates, but the cloud-chamber volume and operating time cannot be utilized efficiently with simple counter telescopes. During the remainder of the experiment, the counter trays were placed above and below the chamber. The results were indistinguishable from the unbiased detector results, which was to be expected since the dimensions of the lower counter tray were large and most of the showers did not emerge from the bottom lead plate anyway.

The photographs were searched for electron showers produced in the lead plates by the μ-mesons. The results are presented in Table I.

The main uncertainty in the experiment derives from estimating the most probable energy of the ray that initiates a shower of given appearance in the lead plates. The major difficulty occurs in estimating the effect of scattering in reducing the number of observed particles when a shower develops in lead. The experiments at Cornell[1] on showers produced in lead by electrons of known energy indicate that the observed numbers of electrons near the maximum of the shower and beyond are about one-half the calculated "total" numbers.[2] The same reduction is to be expected at higher initiating energies, since the reduction is attributable to the low energy shower particles whose relative number is essentially independent of initiating energy. Thus, we choose a shower curve with a maximum of 10 or 12 electrons as a reasonable estimate for a shower produced by a single electron, an electron pair, or a photon of energy 10^9 ev. It is unprofitable to utilize the data either for a smaller maximum, because the thick plates hide too much of the shower, or for a larger maximum, because of the small number of observations.

TABLE I. Observed probability of production of showers.

Number of μ-meson traversals of lead plates = 4143			
Minimum shower size at observed maximum	5	7	10
Number of showers	60	40	25
Probability per traversal	0.0145	0.0097	0.0060
Probability per g cm^{-2} of lead	5.4×10^{-4}	3.6×10^{-4}	2.2×10^{-4}

Since the plates were four radiation units thick, the maximum of a shower frequently would not be observed. For the average shower with an actual maximum of 10 or 12 particles, the observed maximum could be as small as 7 or 8. Thus we should choose as an observed rate something intermediate between the rates for showers of maximum 10 or 12 and the rate for 7 or 8. Strictly speaking, the effect of fluctuations should also be taken into account. Showers (numbering 4) with a maximum less than the selected size but with an unusually long longitudinal extension were included and showers (numbering 1) with the selected maximum but with an unusually short longitudinal extension were excluded from the count. In this way, fluctuations were taken into account to a sufficient degree of accuracy.

From the above considerations, it seems most reasonable to choose a probability intermediate between the values for showers of size ≥7 and size ≥10, i.e., $3.0\pm0.5\times10^{-4}$ g^{-1} cm^2 (Table I) for the observed probability that an energy transfer greater than 10^9 ev will occur. The uncertainty deriving from the conversion of shower size to initial energy is estimated to be about the same as the statistical uncertainty and therefore we might consider the over-all uncertainty to be $\sim\pm0.7$.

* Supported in part by the joint program of the ONR and AEC.

[1] A. M. Shapiro, Phys. Rev. **82**, 307 (1951).
[2] B. Rossi and K. Greisen, Revs. Modern Phys. **13**, 240 (1941).

II. EXPECTED PROBABILITY

The integrated probabilities for energy transfer $\geq 10^9$ ev by μ-mesons of spin one-half by knock-on, bremsstrahlung, and pair-production processes were calculated. For knock-on and bremsstrahlung production, the expressions for the differential cross sections given by Rossi and Greisen[2] were used. The bremsstrahlung cross section is not valid for μ-meson energies $>5\times10^{11}$ ev, but we shall see later (Fig. 1) that contributions to the burst rate by mesons with energy $>5\times10^{11}$ ev are small. For pair production, the cross sections of Bhabha[3] were used,

$$dQ=(8/\pi)(\alpha Z r_0)^2(\gamma mc^2)^2\ln(183E/\gamma mc^2Z^{\frac{1}{3}})dE/E^3$$

for

$$2/\gamma<E/mc^2<2Z^{\frac{1}{3}}/183\gamma^2,$$

and

$$dQ=(8/\pi)(\alpha Z r_0)^2(\gamma mc^2)^2\ln(2\gamma)dE/E^3$$

for

$$2Z^{\frac{1}{3}}/183\gamma^2<E/mc^2<\gamma\mu c^2/mc^2,$$

where α, Z, r_0, and m have their usual meanings, γ is the Lorentz factor, and μ the mass of the incident meson, and E is the total energy of the pair. The total probability of production of soft secondaries with energies greater than 10^9 ev as found by integrating the differential cross sections and adding is shown as a function of the μ-meson energy in Fig. 1.

The local spectrum of μ-mesons underground can be obtained by using the data of Wilson[4] for absorption in additional thickness of earth. The rates of energy loss by radiation and pair production can be sufficiently well approximated by adding their average values to the rate of energy loss by collision. This technique for including the radiation and pair-production losses gives an excellent approximation for energies up to 10^{11} ev, since the rate of energy loss by collisions constitutes 90 percent of the total, and it gives a good approximation up to 5×10^{11} ev, since the rate of energy loss by collisions is still 70 percent of the total. The approximations are justified by the fact that 90 percent of the secondaries with $E\geq10^9$ ev are contributed by μ-mesons with energies less than 5×10^{11} ev (Fig. 1).

The average probability that a meson will produce a secondary with $E\geq10^9$ ev was obtained by numerical integration of the curves shown in Fig. 1. The result is 2.1×10^{-4} per g cm^{-2} of lead.

III. CONCLUSIONS

As mentioned previously, the main uncertainty in the measured probability arises while establishing the energy of the secondaries. It is believed that the energies have been overestimated rather than underestimated. Since the experimental probability would reduced if correction for an overestimate of energy were necessary, it is believed that there is no evidence for a significant contribution by processes other than those considered (e.g., π^0-meson production by μ-mesons). We might, however, set an upper limit to the cross section for the production of neutral mesons of energies $\geq10^9$ ev by μ-mesons of energy $\sim3\times10^{11}$ ev by assuming that the probability is no greater than 5×10^{-5} per g cm^{-2} of lead. Hence the cross section, $\sigma(\mu,\pi^0)$, is less than 10^{-28} cm^2 per nucleon, which is not surprising. The most likely process is photoproduction by the virtual quanta of the contracted Coulomb field. The average photomeson cross section for neutral mesons $\bar{\sigma}(\nu,\pi^0)$, is related to $\sigma(\mu,\pi^0)$ by

$$\sigma(\mu,\pi^0)=\frac{2\alpha}{\pi}\int_{10^9}^{\bar{E}_\mu}\bar{\sigma}(\nu,\pi^0)\ln(\bar{E}_\mu/h\nu)d\nu/\nu,$$

where $\bar{E}_\mu\simeq3\times10^{11}$ ev, an appropriate mean energy of the mesons. The result is $\bar{\sigma}(\nu,\pi^0)<10^{-27}$ cm^2 per nucleon, which is not unexpected since the measured value at $h\nu\simeq300$ Mev is about 10^{-28} cm^2 per nucleon.[5]

For the case of production of charged π-mesons we can set a somewhat smaller upper limit to the cross sections than for neutral π-mesons. It is believed that few, if any, events were missed in which a charged π-meson with a range of two or three lead plates was produced. This statement is based on the belief that most contributions to the total number of secondary charged mesons would come from low energy nuclear interactions in which π^0-mesons, if produced at all, would have such low energy that their subsequent showers would not conceal charged π-mesons. Since no events were observed, we can set an upper limit of about 1.5×10^{-29} cm^2 per nucleon for the production of charged π-mesons with kinetic energies greater than 10^9 ev by μ-mesons of energy $\sim10^{11}$ ev. George and

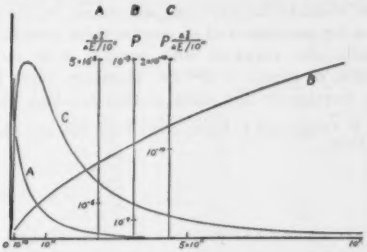

FIG. 1. A—Differential intensity of μ-mesons in units of number per sec cm^2 sterad; B—probability of production of soft secondaries with energy $\geq10^9$ ev per g cm^{-2} of lead by knock-on, bremsstrahlung, and pair-production processes; C—differential probability distribution. The abscissa is the μ-meson energy in units of electron-volts. Curves (A) and (C) are for a depth of 8.5×10^4 g cm^{-2} underground.

[3] H. V. Bhabha, Proc. Roy. Soc. (London) **152**, 559 (1935); S. Hayakawa and S. Tomonaga, Prog. Theoret. Phys. **4**, 287 (1949).

[4] V. C. Wilson, Phys. Rev. **53**, 337 (1938).

[5] Steinberger, Panofsky, and Steller, Phys. Rev. **78**, 802 (1950).

Evans[6] obtained 4×10^{-30} cm² per nucleon for the cross section for production of shower particles (which were probably also π-mesons with energies $>10^8$ ev) by μ-mesons of energy $\sim10^{10}$ ev. Therefore, there is no rapid increase in the cross section for high energy nuclear interactions with increasing energy of μ-mesons. If we again consider the specific process of photomeson production, the cross section $\sigma(\nu, \pi^{+,-})$ is less than 10^{-28} cm² per nucleon, which again is not surprising.

Cooperation by the management and personnel of the International Salt Company Detroit Mine made this work possible.

[6] E. P. George and J. Evans, Proc. Phys. Soc. (London) **63**, 1248 (1950).

PHYSICAL REVIEW VOLUME 86, NUMBER 5 JUNE 1, 1952

Neutron Diffraction Study of the Crystal Structure of Ammonium Chloride*

HENRI A. LEVY AND S. W. PETERSON
Chemistry Division, Oak Ridge National Laboratory, Oak Ridge, Tennessee

(Received February 11, 1952)

The crystal structure of the room-temperature phase of ammonium chloride has been determined by powder and single crystal neutron diffraction methods. The N—H links are directed essentially toward four of the eight surrounding chloride ions, and, contrary to a recent report, the two orientations fulfilling this condition are occupied at random in the crystal. Thermal motion of the hydrogen atoms is nonspherical and suggests a rotatory oscillation of the ammonium ion as a whole with a half-angle of about 10°. The length of the N—H link is 1.03 ± 0.02 *A*. The second-order transition at −30°C is thus shown to be of the order-disorder type.

INTRODUCTION

AMMONIUM chloride undergoes a second-order transition at −30.4°C, and deutero-ammonium chloride undergoes one at −23.7°C, the nature of which has been the subject of much experimental and theoretical study.[1] The most recent of these studies is a neutron diffraction investigation of the crystal structure of this substance at room temperature and at liquid nitrogen temperature, carried out by Goldschmidt and Hurst.[2] These investigators report that at both temperatures the structure consists of an ordered array of ammonium and chloride ions conforming to space group symmetry T_d^1, the room temperature phase differing from the other only in displaying greatly increased motion of the hydrogen atoms of a sort that can be described as a rotatory oscillation of the ammonium ions.

This reported room-temperature structure contrasts sharply with that found by us, also by neutron diffraction for room-temperature ammonium bromide.[3,4] The ammonium bromide structure was found to conform statistically to space group symmetry O_h^1 and to contain ammonium ions oriented at random in two orientations with hydrogen atoms directed essentially toward four of the eight surrounding bromide ions. This significant feature of the ammonium bromide structure confirms the suggestion of Nagamiya[5] concerning the specific nature of the transition and might reasonably be expected to be a characteristic feature of the structures of other ammonium halides which display second-order transitions. Thus it is of some importance to have an independent check on the ammonium chloride result.

The methods used in the present investigation of ammonium chloride consist of both powder and single crystal studies using neutron diffraction techniques. It was considered essential to repeat the work of Goldschmidt and Hurst using a deuterated powder sample. In addition, since single crystal neutron diffraction techniques have been shown to be feasible,[6] they were also employed. Data obtained by the latter method were particularly decisive in establishing the correct structure, which consists of orientationally disordered ammonium ions altogether similar to that found in room-temperature ammonium bromide.

POWDER DATA FROM ND_4Cl

Experimental

The general design of the spectrometer and associated circuits is similar to that of Wollan and Shull[7] and will be described elsewhere. The monochromatic beam was produced by reflection from a (111) face of a copper crystal and yielded a wavelength of 1.16A, which was used in both the powder and single crystal work.

* This work was performed for the AEC.

[1] Previous work is summarized by E. L. Wagner and D. F. Hornig, J. Chem. Phys. **18**, 296 (1950), and in reference 2.

[2] G. H. Goldschmidt and D. G. Hurst, Phys. Rev. **83**, 88 (1951). (This will be referred to as G. and H.)

[3] H. A. Levy and S. W. Peterson, Phys. Rev. **83**, 1270 (1951).

[4] H. A. Levy and S. W. Peterson, "The crystal structures of four phases of deutero-ammonium bromide by neutron diffraction," J. Am. Chem. Soc. (to be published).

[5] T. Nagamiya, Proc. Phys. Math. Soc. Japan **24**, 137 (1942).

[6] S. W. Peterson and H. A. Levy, J. Chem. Phys. **19**, 1416 (1951); G. E. Bacon, Proc. Roy. Soc. (London) **A209**, 397 (1951).

[7] E. O. Wollan and C. G. Shull, Phys. Rev. **73**, 830 (1948).

Deutero-ammonium chloride was prepared by repeated recrystallization of reagent grade ammonium chloride from 99.8 percent D_2O. The resulting product had a deuterium content of 98 mole percent, established as described elsewhere.[4] The sample was handled under dry box conditions and exposed to the neutron beam in tightly sealed cylindrical aluminum cells. A number of runs were made at room temperature on the same deuterated powder sample with varying degrees of collimation in the neutron detector. Runs were also made at dry ice and liquid nitrogen temperatures in order to look for any anomalous behavior; they yielded essentially identical patterns and intensities in good agreement with those of Goldschmidt and Hurst at liquid nitrogen temperature.

X-ray studies of NH_4Cl at room temperature have shown the structure to be of the CsCl type with a unit cell length of 3.866A.[5] The neutron diffraction pattern from deuterated ammonium chloride was consistent with the above structure and spacing and was indexed on this basis. A typical room-temperature pattern is illustrated in Fig. 1. It was evident that the background of diffuse scattering is angle-dependent, its most prominent feature being a hump in the neighborhood of 40° scattering angle. Integrated intensities were obtained directly from chart records of the diffracted counting rate, after fixing the estimated background rate as illustrated in the figure, by application of the trapezoid rule. When necessary, corrections were made for scattering by the empty sample container. Final values were averages of those from several patterns. Values of jF^2 were obtained in the usual way, the instrument-beam parameter being evaluated by comparison with nickel powder ($\sigma_{coh}(Ni) = 13.4$ barns).

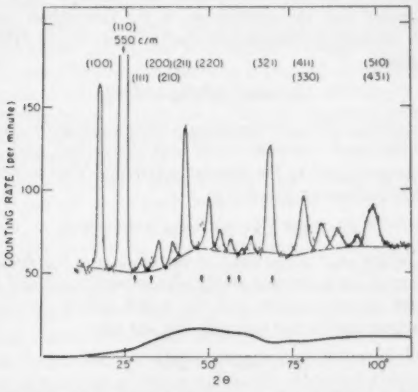

FIG. 1. The neutron diffraction pattern of room-temperature deutero-ammonium chloride. The short vertical lines represent the observed counting rate and the precision of reading from the original strip-chart records. The uppermost curves show the principal Bragg reflections as they would be idealized on the original charts for intensity estimation. The undulating curve through the base of the pattern is the estimated background. The lower curve is the calculated disorder scattering. Arrows indicate angles at which appreciable scattering by aluminum occurs.

[5] R. W. G. Wyckoff, *Crystal Structures* (Interscience Publishers, Inc., New York, 1951), Vol. I, Chapter III, table p. 23.

TABLE I. Comparison of data and calculated structure factors for ND_4Cl.

hkl	Experimental $\|F\|$ G. and H.	Experimental $\|F\|$ This research	Calculated $\|F\|$ Ordered[a]	Calculated $\|F\|$ Disordered[b]
100	1.41±2%	1.33±0.03	1.41	1.31
110	2.47±2%	2.48±0.06	2.48	2.52
111	0.89±5%	0.37±0.07	0.95	0.33
200	1.09±20%	0.96±0.09	1.11	1.02
210	0.68±20%	0.39±0.07	0.56	0.44
211	1.43±20%	1.36±0.06	1.54	1.32
220	1.39±20%	1.40±0.15	1.25	1.56
222	1.08±40%	1.14±0.20	1.54	1.31
321	1.32±5%	1.50±0.08	1.28	1.45

[a] From reference 2.
[b] For the final model described in the text.

Direct comparison of our neutron diffraction pattern and resulting intensities with those of G. and H. (see Table I) makes evident a considerable disagreement in the range of reflections from (111) through (211) and (321). The large discrepancy in the (111) reflection is of especial significance because of the importance placed on this reflection by G. and H. in their structure analysis. We have made repeated measurements of this reflection and have in no case obtained an intensity which was close to their value. It seems likely that a different estimate of the background counting rate on the part of G. and H. is at least partly responsible for the disagreements. It may well be that when intensities of imperfectly resolved reflections are estimated from an integral curve, as was done by G. and H., proper background treatment is difficult and variations in background are obscured.

We have recently been informed that Dr. Hurst has remeasured neutron diffraction intensities from ND_4Cl and now obtains relative values of the structure factors in agreement with ours.†

Structure Determination

In view of the earlier neutron studies of ND_4Cl and ND_4Br the only models considered here are those involving ordered and disordered ammonium ion arrangements, space groups T_d^1 and O_h^1, respectively. Nitrogen is placed at the origin and bromine at the body center in both models. In the ordered model the hydrogens are centered at the fourfold positions $x\,x\,x$, $x\,\bar{x}\,\bar{x}$, $\bar{x}\,\bar{x}\,x$, and $\bar{x}\,x\,\bar{x}$; in the disordered model hydrogens are distributed at random between this set of positions and the remainder of the eightfold set obtained by inversion through the origin. In both models nonspherical distribution of the hydrogen atoms was considered, such as would result from a rotatory oscil-

† Dr. Hurst's new measurements are described elsewhere in this issue.

TABLE II. Powder neutron diffraction data for ND_4Cl.

hkl	$f\|F\|^2$ Obs	$f\|F\|^2$ Calc[a]	hkl	$f\|F\|^2$ Obs	$f\|F\|^2$ Calc[a]
100	10.6±0.3	10.3	400	<3.3	0.5
110	74.0±3.5	75.9	410	7.4±5.4	4.9
111	1.1±0.5	0.85	322		0.0
200	5.5±1.1	6.2	411	71±26	17.4
210	3.6±1.5	4.6	330		45.1
211	43.4±5.0	41.6	331	<10.8	5.5
220	23.6±5.8	29.2	420	45±13	39.5
221	12.0±3.0	0.0	421	<8.6	1.3
300		14.1	332	<25.6	12.8
310	<9.1	7.1	422	<20.1	15.7
311	<5.5	5.4	500	<14.9	0.0
222	10.4±4.0	13.7	430		6.3
320	<3.0	2.7	510	83±21	18.6
321	108±12	100.2	431		56.0

[a] For the final (disordered) model described in the text.

lation of the ammonium ion as a whole. Structure factors were calculated for both models with the ideal position parameter x and the characteristic half-angle of rotatory oscillation α as principal parameters. The effect of rotatory oscillation was approximated in the same way as in our treatment of room-temperature ammonium bromide,[4] in which the expressions used to approximate the structure factors are given. Separate temperature factors for each of the atoms were introduced as additional parameters. Trial and error calculations were continued until it was seen that no fit could be obtained with the ordered model, and a satisfactory best fit was found for the disordered model. The parameter values found to give the best fit are

$$x=0.154\pm0.003, \quad \alpha=10^\circ\pm3^\circ,$$

$$B_D=2.25, \quad B_N=2.0 \text{ and } B_{Cl}=2.0.$$

Table I gives the experimental and calculated structure factors of Goldschmidt and Hurst as compared with similar values obtained for the same reflections in this work. The ($hk0$) reflections are not sensitive to whether the ordered or disordered model is used; variations in these values between columns 4 and 5 of the table arise from different values of atomic scattering factors and temperature factors and slightly different approximations in treating the effects of rotatory oscillation. The remainder of the calculated values reflect also the effect of ordered or disordered structure. The atomic scattering factors used here were in units of 10^{-12} cm, $f_N=0.94$,[9] $f_{Cl}=0.99$,[10] and $f_{D,H}=0.62$[10] (for 98 percent D, 2 percent H). (The calculations were begun with $f_N=0.85$, as measured and used by G. and H.; however, our single crystal data strongly indicated the necessity for a larger value, subsequently confirmed by measurements[9] on VN and KN_3.)

The most significant reflection in deciding between the ordered and disordered arrangements is clearly (111) although (211), (222), and (321) also are of importance. The new data presented here are clearly not compatible with the calculated values presented by G. and H., and no variation of parameters in the ordered model suffices to bring agreement. Further, the G. and H. data are, except for the controversial (111) reflection, in as good agreement, on the whole, with the disordered model as with their ordered model. The somewhat surprising result that the same N−D distance is obtained as by G. and H. is due to the necessity of fitting the strong (100) and (110) reflections which are independent of the model and, in addition, to the accidental compensating effect in their use of scattering amplitudes larger for deuterium and smaller for nitrogen and chlorine than were used in this work. The use of these somewhat different scattering amplitudes of G. and H. would not change our conclusion regarding the correctness of the disordered structure but would slightly change the parameter values giving the best fit. Table II presents experimental and calculated structure factors for the whole range of scattering angle obtainable with our present spectrometer and wavelength. Good agreement is achieved throughout for the disordered model.

Disorder Scattering

The angle dependent diffuse background might be expected to arise from the disorder in the ammonium chloride crystal structure. That this is indeed the case is indicated by an application of the general theory of disorder scattering described by Zachariasen.[11] If it is assumed that the orientations of the ammonium ions are statistically independent, Zachariasen's Eq. (4.216b) applies,

$$J_2=\text{const}[\langle|F|^2\rangle_{hl}-|\bar{F}|^2],$$

in which $\langle|F|^2\rangle_{hl}$ is the mean square structure factor, $\bar{F}$ the mean structure factor over the crystal, and J_2 is proportional to the disorder scattering. This reduces in Zachariasen's notation to

$$J_2=\text{const}\sum_{k,k'}\varphi_{kk'}{}^0\exp[i\delta\cdot(\bar{r}_k-\bar{r}_{k'})],$$

in which $\varphi_{kk'}{}^0$ is the mean of the product of the deviations of the scattering amplitudes at positions k and k' from the mean value, and the double sum is over the various sites in one unit cell. For our case

$$\varphi_{kk'}{}^0=\pm\tfrac{1}{4}f_D{}^2$$

with a positive or negative sign according to whether k and k' designate corners of the same or different tetrahedra. Upon averaging over all orientations of the vector $\bar{r}_k-\bar{r}_{k'}$ we obtain

$$J_2(s)=\text{const}\cdot 2f_D{}^2\{1-3(\sin r_1s)/r_1s+3(\sin r_2s)/r_2s-(\sin r_3s)/r_3s\}, \quad (1)$$

where $s=(4\pi/\lambda)\sin\theta$ and r_1, r_2, and r_3 are the distances

[9] H. A. Levy and S. W. Peterson, "The coherent neutron scattering cross-sections of nitrogen and vanadium" (to be published).
[10] C. G. Shull and E. O. Wollan, Phys. Rev. 81, 527 (1951).
[11] W. H. Zachariasen, *Theory of X-Ray Diffraction in Crystals* (John Wiley and Sons, Inc., New York, 1945), p. 213.

between deuterium sites separated by a cube edge, face diagonal, and body diagonal, respectively. In applying this expression we have included temperature factors in the same way as is usual in the case of gas scattering, namely a factor $\exp(-\frac{1}{2}\langle\delta r_i^2\rangle_{hk}s^2)$ multiplying each angle-dependent term, in which $\langle\delta r_i^2\rangle_{hk}$ is the mean square variation in distance r_i. For the distances r_1 and r_3 values of $\langle\delta r_i^2\rangle_{hk}$ were estimated from the values of B_D and α found from the Bragg scattering, while $\langle\delta r_2^2\rangle_{hk}$ was estimated from vibrational frequencies, namely ~ 2300 cm^{-1} for stretching and ~ 1100 cm^{-1} for bending.[1]

In Fig. 1 there is plotted the function obtained when numerical values are substituted into Eq. (1), namely

$$J_2(s)=11.37\{1-3\exp(-0.04s^2)g(1.190s)$$
$$+3\exp(-0.02s^2)g(1.682s)-\exp(-0.03s^2)g(2.061s)\},$$

where $g(x)$ represents $(\sin x)/x$. The multiplying constant was evaluated from a Bragg peak of the same pattern, so that J_2 is given in counts per minute on an absolute scale. The qualitative similarity to the observed diffuse background is striking. The remainder of the background is expected to arise from thermal scattering, nuclear diffuse scattering, and multiple scattering in the sample.

SINGLE CRYSTAL DATA ON NH_4Cl

In view of the disagreements in data in powder studies it seemed desirable to have a further independent check on the proposed structure by means of the more sensitive single crystal method. The low backgrounds and high intensities obtainable with single crystal methods eliminate large uncertainties in intensities of low angle peaks of such an intensity as (111). In addition, it is possible to work with the hydrogen compound which makes an interesting comparison with the deuterium substituted compound.

Single crystals of ammonium chloride were grown by the method of Holden[12] from a saturated aqueous solution of ammonium chloride containing approximately 10 percent of urea. Specimens of cubic habit with dimensions up to 1 cm or more on edge were easily obtained. The amount of urea incorporated is very small,[13] and the specimens were optically very clear. Small rectangular specimens were first selected for study; however, measurements soon indicated that absorption was an important factor (apparent absorption due to large diffuse scattering). Selected specimens were then ground to cylindrical shape by slow abrasion or etching while they were rotating at a high speed in a drill press. Precise absorption corrections could then be made using the measured linear absorption coefficient, and the intensity data could be placed on an absolute scale.

[12] A. N. Holden, Disc. Faraday Soc. No. 5, 312 (1949).
[13] An x-ray diffraction pattern showed no urea lines.

TABLE III. Neutron diffraction data from NH_4Cl single crystals.

hkl	$\lvert F\rvert_{obs}$	$\lvert F\rvert_{calc}$ Disordered[a]	Ordered[b]
100	0.88±0.03	0.88	
110	1.36±0.04	1.36	
111	0.31±0.05	0.26	0.71
200	2.00±0.06	2.04	
210	0.23±0.07	0.20	
211	1.72±0.05	1.71	1.82
220	1.46±0.05	1.46	
221	<0.10	0.04	0.60
300	0.83±0.04	0.78	
310	1.81±0.06	1.82	
320	0.18±0.06	0.20	
400	1.59±0.06	1.54	
410	0.12±0.10	0.17	
330	0.62±0.04	0.63	
420	0.85±0.04	0.84	
500	<0.10	0.02	
430	0.16±0.10	0.24	
510	0.81±0.05	0.78	
520	<0.10	0.08	

[a] For the final model described in the text.
[b] For an ordered model, symmetry T_d^3, based on the same parameter values as the final model.

Equatorial data were obtained in a manner previously described by Peterson and Levy[6,14] on specimens ground to cylindrical shape with [100] and [110] zone axes vertical. The weights and dimensions of the specimens were 13.0 mg, 5.3-mm high×1.4-mm diameter, and 13.6 mg, 4-mm high×1.6-mm diameter. The observed integrated reflections, corrected for absorption, were converted to absolute structure factors by use of a standard NaCl reflection.[6] The final value used was in most cases an average of two runs. The thin crystal criterion of Bacon and Lowde[15] would permit a maximum thickness with negligible extinction of 0.8 mm on the assumption of a mosaic spread parameter of 5 minutes.[6] The somewhat larger specimens used gave no indication of extinction as shown by the following direct comparison of absolute F values obtained from the strongest reflections of NH_4Cl powder and from a single crystal:

	Structure factor	
hkl	Powder	Single crystal
100	0.90	0.88
110	1.34	1.36

The excellent agreement obtained with the proposed structure is further evidence that extinction was not a problem here.

The data obtained are presented in Table III along with calculated structure factors for the model which gave the best fit. The excellency of the over-all agreement is evidence for the validity of the structure and temperature parameters. The parameters, which were evaluated by trial and error, are $x=0.154\pm0.003$, $\alpha=12°\pm3$, $B_N=2.0$, $B_{Cl}=2.0$, and $B_H=2.5$. The scat-

[14] S. W. Peterson and H. A. Levy, J. Chem. Phys. (to be published).
[15] G. E. Bacon and R. D. Lowde, Acta Cryst. 1, 303 (1948).

tering amplitudes used were

$$f_N=0.94,^9 \quad f_{Cl}=0.99,^{10} \quad \text{and} \quad f_H=0.38.^{16}$$

The three (*hkl*) reflections (111), (211), and (221) are decisive in eliminating the ordered structure, for which calculated F values are presented in column 4, based on the same set of parameters. The disagreements are so great that no reasonable variation of the parameters can resolve them.

A by-product of the work is evidence that the earlier value of f_N, 0.85,[2,10] is incorrect and that a scattering amplitude for hydrogen of 0.38[16] is to be preferred to the earlier value of 0.40.[10] The (100) reflection which is quite sensitive to the hydrogen amplitude and little affected by the temperature and structure parameters is most significant in this respect.

DISCUSSION

The data presented establish clearly that the room temperature structure of NH_4Cl involves a disorder in the orientation of the ammonium ions. This is in agreement with less direct evidence.[1] Since the low temperature structure of ammonium chloride is clearly an ordered one, the lambda-transition is of the order-disorder type. The N−H distance of 1.03±0.02A found for both the hydrogen and deuterium compound is closely equal to that found in ND_4Br,[4,17] 1.03±0.02 A by neutron diffraction, and in good agreement with values obtained by nuclear magnetic resonance[18] 1.025 and 1.039A, respectively. The thermal motion of hydrogen as indicated by both B and α appears to be somewhat greater than that of deuterium, in accord with expectation.

Since ND_4Cl patterns at −180°C and −78°C showed no essential differences, the line width transition at about −140°C in NH_4Cl observed in nuclear magnetic resonance experiments[19] may be reasonably presumed to involve no appreciable change in atomic positions.

[16] Hughes, Burgy, and Ringo, Phys. Rev. **77**, 291 (1950).

[17] The smaller value quoted in reference 3 is revised upward when the new value of f_N is used.

[18] Gutowsky, Kistiakowsky, Pake, and Purcell, J. Chem. Phys. **17**, 972 (1949).

[19] H. S. Gutowsky and G. E. Pake, J. Chem. Phys. **16**, 1164 (1948).

PHYSICAL REVIEW VOLUME 86, NUMBER 5 JUNE 1, 1952

Scattering of Electrons in Metals by Dislocations*

D. L. DEXTER
Department of Physics, University of Illinois, Urbana, Illinois
(Received February 18, 1952)

The problem of the change in electrical conductivity in metals upon cold-working is treated by the method of Koehler in which the scattering of electrons by pairs of parallel edge-type dislocations is assumed to be the major effect. A comparison is made between the electronic shielding assumed in the scattering potential used by Koehler and the shielding assumed by Landauer in a somewhat different treatment. The large effect of the discontinuity in the ionic displacement across the plane connecting the dislocation axes is shown to cancel that of a previously neglected term in the scattering potential. The scattering matrix element is evaluated, and the change in resistivity is computed by the perturbation method of Mackenzie and Sondheimer. Finally, the anisotropy in the resistivity is discussed, and it is shown that the slip direction is the direction of low resistivity.

I. INTRODUCTION

SEVERAL recent publications[1–4] have treated theoretically the problem of the change in electrical conductivity of metals upon cold-working. In all of this work it is assumed that the change is primarily because of the scattering of electrons from edge-type dislocations, and the possible effects of associated clusters of vacancies, or of screw-type dislocations, are ignored. The calculations differ mainly in the type of scattering potential employed, Koehler[1] (K) and Mackenzie and Sondheimer[2] (MS) using in their potentials the ionic displacements around a pair of dislocations, and Landauer[3] (L) and Dexter[4] (D) making use of only the density change. These two potentials take account of the shielding of the positive charge by the electrons in somewhat different ways. In Sec. II a general comparison is made among these methods and Bardeen's self-consistent method[5]; it is shown that all three approaches agree in the limit of slowly varying potentials, i.e., perfect shielding.

One of the characteristic features of an edge-type dislocation is that there is a discontinuity in the ionic displacement across the missing plane of atoms. In the

* Research supported by the ONR.

[1] J. S. Koehler, Phys. Rev. **75**, 106 (1949), to be referred to as K.

[2] J. K. Mackenzie and E. H. Sondheimer, Phys. Rev. **77**, 264 (1950), to be referred to as MS.

[3] Rolf Landauer, Phys. Rev. **82**, 520 (1951), to be referred to as L.

[4] D. L. Dexter, Phys. Rev. **85**, 936 (1952), to be referred to as D.

[5] J. Bardeen, Phys. Rev. **52**, 688 (1937).

treatments of K and MS, in which the scattering potential depended on the displacements, this discontinuity gave rise to a large amount of fictitious scattering; attempts were made to get rid of this effect by changing the expression for the ionic displacements as obtained from elastic theory. Section III contains an alternative procedure for taking account of the discontinuity, and examines the results of the approximations in K and MS, particularly as regards the anisotropy in resistivity.

II. ELECTRONIC SHIELDING

It is well known that the "free" electrons in a metal distribute themselves around any charge in such a way as to shield the potential from that charge; the shielded potential caused by a point charge, Ze, for example, can easily be found[6] by the Thomas-Fermi method to be

$$v(r)=(Ze/r)\exp(-qr), \tag{1}$$

where

$$q^2=(4m^*e^2/\hbar^2)(3n_0/\pi)^{\frac{1}{3}}. \tag{2}$$

Here n_0 is the density of free electrons, and the other symbols have their usual meanings. For most good metals q turns out to be $\gtrsim 10^8$ cm^{-1}.

One possible method[7] for taking account of the shielding of extended charge distributions is by the deformation potential method, sketched below in simplified form. The width of the filled portion of the conduction band can easily be found by free-electron theory to be

$$E(\mathbf{r})=(\hbar^2/2m^*)[3\pi^2 n(\mathbf{r})]^{\frac{2}{3}}, \tag{3}$$

where $n(\mathbf{r})$ is the density of electrons at position $\mathbf{r}$. Since in equilibrium the Fermi level is constant, the bottom of the conduction band varies as $-E$. Assuming that the scattering potential V follows the bottom of the conduction band and that the electron density closely follows the positive charge density, we obtain, for small density changes,

$$V(\mathbf{r})=\tfrac{2}{3}(E_0/e^2n_0)\delta\rho^+(\mathbf{r}), \tag{4}$$

where $\delta\rho^+(\mathbf{r})$ is the change in positive charge density at the position $\mathbf{r}$, and E_0 is the width of the filled part of the conduction band in the perfect crystal. This is the scattering potential used in L and D, where $\delta\rho^+(\mathbf{r})$ was calculated[8] for a single edge-type dislocation from the elastic theory of a continuous, isotropic medium.

Another method[1,2] is to use as a potential the difference between the sums of the shielded ionic potentials [Eq. (1)] for the distorted and perfect lattices,

$$V(\mathbf{r})=\textstyle\sum_j v(|\mathbf{r}-(\mathbf{R}_j+\mathbf{u}_j)|)-\sum_j v(|\mathbf{r}-\mathbf{R}_j|), \tag{5}$$

where the $\mathbf{R}_j$ are ionic positions in the perfect lattice, and the $\mathbf{u}_j$ are the ionic displacements associated with the distorted lattice; this is the procedure followed in K and MS. Landauer[3] has criticized this approach as not properly taking into account the redistribution of electrons around a distortion, and has suggested instead the use of the potential in Eq. (4). It will be seen that Eq. (5) leads to results equivalent to those obtained by use of Eq. (4) in the region where the latter is valid (perfect shielding) and is a better approximation than Eq. (4) in the region of imperfect shielding.

In order to compare Eqs. (4) and (5), it will be convenient to make use of the operator ∇^2-q^2. It can be seen from Eq. (1) that $(\nabla^2-q^2)v(\mathbf{r})=-4\pi Ze\delta(\mathbf{r})$, where $\delta(\mathbf{r})$ is the Dirac delta-function; by use of this operator we obtain from Eq. (5)

$$(\nabla^2-q^2)V(\mathbf{r})=-4\pi Ze\textstyle\sum_j\{\delta(\mathbf{r}-\mathbf{R}_j-\mathbf{u}_j)-\delta(\mathbf{r}-\mathbf{R}_j)\}, \tag{6}$$

or

$$(\nabla^2-q^2)V(\mathbf{r})=-4\pi\delta\rho^+(\mathbf{r}). \tag{7}$$

We shall later make use of the fact that this equation has the solution,

$$V(\mathbf{r})=(1/Ze)\int v(|\mathbf{r}-\mathbf{r}'|)\delta\rho^+(\mathbf{r}')d\tau'. \tag{8}$$

Let us now expand $V(\mathbf{r})$ and $\delta\rho^+(\mathbf{r})$ in Eq. (7) into lattice waves, and obtain

$$V(\mathbf{r})=4\pi\sum_{\mathbf{K}}[\rho_{\mathbf{K}}e^{i\mathbf{K}\cdot\mathbf{r}}/(K^2+q^2)]. \tag{9}$$

Thus when the charge density may be expressed in terms of waves of wavelength large compared with 10^{-8} cm ($q^2\gg K^2$), the potential becomes

$$V(\mathbf{r})=(4\pi/q^2)\delta\rho^+(\mathbf{r}). \tag{10}$$

By using Eqs. (2) and (3) we see that this is equal to the expression in Eq. (4); thus the two methods are equivalent for slowly varying potentials.

Equation (9) can be compared with the results of Bardeen's self-consistent solution[8] for the potential by making use of Eqs. (30) and (32) in reference 5, from which we obtain, changing the notation in reference 5 to agree with ours,

$$V(\mathbf{r})=4\pi\sum_{\mathbf{K}}\frac{\rho_{\mathbf{K}}e^{i\mathbf{K}\cdot\mathbf{r}}}{K^2+q^2(1-\xi^2/3-\xi^4/15-\cdots)}, \tag{11}$$

if $\xi\equiv K/2k_0$ is less than unity, where k_0 is the wave number of an electron at the surface of the Fermi distribution. If $\xi^2\ll 1$, this agrees with Eq. (9), but a more significant comparison can be made in the form

$$V(\mathbf{r})\cong 4\pi\sum_{\mathbf{K}}\frac{\rho_{\mathbf{K}}e^{i\mathbf{K}\cdot\mathbf{r}}}{q^2+K^2(1-q^2/12k_0^2)}. \tag{12}$$

If we take $q\sim 2.2\times 10^8$ cm^{-1} and $k_0\sim 1.4\times 10^8$ cm^{-1} for copper, the denominator becomes $q^2+K^2(1-0.21)$.

[6] N. F. Mott and H. Jones, *The Theory of the Properties of Metals and Alloys* (Oxford University Press, London, England, 1936), pp. 88, 294.

[7] J. Bardeen and W. Shockley, Phys. Rev. **80**, 72 (1950), and references contained therein.

[8] J. S. Koehler, Phys. Rev. **60**, 398 (1941).

Since q^2/k_0^2 varies as $1/n_0^{\frac{1}{3}}$, the correction term in the coefficient of K^2 is larger in absolute magnitude for metals with a lower electron density, as is to be expected; similarly, the shielding of the positive charge is less effective in the poorer metals, and the potential is greater.

III. EVALUATION OF THE SCATTERING MATRIX ELEMENT

The scattering of an electron between two plane wave states $\mathbf{k}$ and $\mathbf{k}'$ is governed by the matrix element

$$\langle \mathbf{k}'|-eV|\mathbf{k}\rangle=\frac{1}{\tau}\int \exp(-i\boldsymbol{\kappa}\cdot\mathbf{r}')V(\mathbf{r}')d\tau', \quad (13)$$

where $\boldsymbol{\kappa}\equiv\mathbf{k}'-\mathbf{k}$, and τ is the volume of the metal; thus it is this matrix element that will be required for the calculation of the change in resistivity associated with the presence of scattering centers. Let us examine in detail the potential in a metal lattice containing one or more edge-type dislocations, i.e., a lattice from which part of the material has been removed. Quite generally, we may write the perturbing potential in the lattice at the point $\mathbf{r}'$ as

$$V(\mathbf{r}')=\sum_j{}' v(\mathbf{r}'-\mathbf{R}_j-\mathbf{u}_j)-\sum_j v(\mathbf{r}'-\mathbf{R}_j)$$
$$\cong\sum_j{}' \mathbf{u}_j\cdot\boldsymbol{\nabla}_j v(\mathbf{r}'-\mathbf{R}_j)-\sum_l{}'' v(\mathbf{r}'-\mathbf{R}_l), \quad (14)$$

where the prime after the summation symbol reminds us that we are not to sum over the missing atoms, and the double prime indicates summation over only the missing material. The subscript j on the nabla operator indicates differentiation with respect to the coordinates of $\mathbf{R}_j$. Replacing the summations by integrations, we obtain

$$V(\mathbf{r}')=\Delta^{-1}\int \mathbf{u}(\mathbf{r})\cdot\boldsymbol{\nabla}v(\mathbf{r}'-\mathbf{r})d\tau-\Delta^{-1}\int v(\mathbf{r}'-\mathbf{r}'')d\tau''$$
$$=V_1(\mathbf{r}')+V_2(\mathbf{r}'), \quad (14')$$

where Δ is the atomic volume. Because the rearranged lattice is approximately in register over the region of the missing material, the first term $V_1(\mathbf{r}')$ is evaluated over the entire volume of the metal; it is this term $V_1(\mathbf{r}')$ that was used as a scattering potential in K and MS. In the second term $V_2(\mathbf{r}')$ the integration extends over just the region of missing atoms; in the same approximation that we have made in connection with V_1, the term V_2 may be replaced by the surface integral $-(\lambda/\Delta)\int v(\mathbf{r}'-\mathbf{s}'')dS''$, where λ is the unit crystallographic slip distance.

Now the displacement $\mathbf{u}$ has a discontinuity across the missing material, corresponding to putting the lattice back in register; this discontinuity makes a large contribution to the term V_1. It will now be shown that $V_2(\mathbf{r}')$ cancels the contribution to V_1 from the discontinuity. By use of the vector identity for the divergence of a product $v\mathbf{u}$, the first term in Eq. (14′) becomes

$$V_1(\mathbf{r}')=(Ze)^{-1}\int \delta\rho^+(r)v(\mathbf{r}'-\mathbf{r})d\tau$$
$$+\Delta^{-1}\int \boldsymbol{\nabla}\cdot(v\mathbf{u})d\tau, \quad (15)$$

where we have made use of the relation

$$\delta\rho^+=-(Ze/\Delta)\boldsymbol{\nabla}\cdot\mathbf{u}.$$

Now let us remove an infinitesimal slice along the plane of missing atoms; with the exception of this deleted volume, the function $v\mathbf{u}$ is continuous, and the divergence theorem may be applied to the second term in Eq. (15). The exponential dependence in v prevents any contribution from the outer surface, and we are left with the result

$$V_1(\mathbf{r}')=(Ze)^{-1}\int v(\mathbf{r}'-\mathbf{r})\delta\rho^+(\mathbf{r})d\tau$$
$$+\Delta^{-1}\int v(\mathbf{r}'-\mathbf{s}'')\mathbf{u}(\mathbf{s}'')\cdot\mathbf{n}dS'', \quad (16)$$

where the second integral is over the surface of the deleted section, and $\mathbf{n}$ is the outward normal to the surface. Since $\mathbf{u}(\mathbf{s}'')\cdot\mathbf{n}$ is equal to $\lambda/2$, the second term on the right of Eq. (16) just cancels $V_2(\mathbf{r}')$, and Eq. (14′) becomes

$$V(\mathbf{r}')=(1/Ze)\int v(\mathbf{r}'-\mathbf{r})\delta\rho^+(\mathbf{r})d\tau,$$

as found [Eq. (8)] and discussed in the last section.

Following K and MS, let us consider the scattering of electrons from a positive-negative dislocation pair, the positive edge-type dislocation at $x=0$, $y=R/2$, and the negative at $x=0$, $y=-R/2$. The corresponding displacements have been evaluated by Koehler,[8]

$$u_x=A\left\{\tan^{-1}\frac{y-R/2}{x}-\tan^{-1}\frac{y+R/2}{x}\right\}$$
$$+2Bx\left\{\frac{y-R/2}{x^2+(y-R/2)^2}-\frac{y+R/2}{x^2+(y+R/2)^2}\right\},$$
$$u_y=-C\log\left\{\frac{x^2+(y-R/2)^2}{x^2+(y+R/2)^2}\right\}^{\frac{1}{2}} \quad (17)$$
$$-2Bx^2\left\{\frac{1}{x^2+(y-R/2)^2}-\frac{1}{x^2+(y+R/2)^2}\right\},$$
$$A=\lambda/2\pi, \quad B=(\lambda/8\pi)/(1-\nu),$$
$$C=(\lambda/4\pi)(1-2\nu)/(1-\nu),$$

where ν is Poisson's ratio. The matrix element Eq. (13)

can be evaluated by elementary methods, and we find

$$\langle \mathbf{k}'|-eV|\mathbf{k}\rangle=-\left[\frac{32\pi^3Ze^2\sin(\kappa_x\tau^1/2)\sin(\kappa_yR/2)}{\tau\Delta(\kappa^2+q^2)\kappa_x\kappa_z^2}\right]$$
$$\times\{A\kappa_z^2/\kappa_y+(2B-C)\kappa_y-A\kappa_x^2/\kappa_y\},\quad(18)$$

where we have made use of Eqs. (14′) and (17). In this expression $\boldsymbol{\kappa}=\mathbf{k}'-\mathbf{k}$, $\kappa_z^2=\kappa_x^2+\kappa_y^2$ and τ^1 is the length of the cubic metal specimen. The last term in the curly brackets is the contribution from $V_2(\mathbf{r}')$. Squaring, and setting the interference factor $\sin^2(\kappa_yR/2)$ equal to $\frac{1}{2}$ for the reasons given in K, we obtain

$$|\langle \mathbf{k}'|-eV|\mathbf{k}\rangle|^2$$
$$=\left[\frac{512\pi^4Z^2e^4\sin^2(\kappa_x\tau^1/2)(2B-C-A)^2\kappa_y^2}{\Delta^2\tau^2q^4(1+\kappa^2/q^2)^2\kappa_x^2\kappa_z^4}\right].\quad(19)$$

Note that except for the factor $(1+\kappa^2/q^2)^{-2}$, which is associated with the difference in electronic shielding in the two potentials, this is just twice the square of the matrix element found in D, as corresponds to the scattering from two dislocations instead of one. Also note that the scattering is small for κ_x primarily along the slip direction. This can best be understood from a consideration of the variation in positive charge (which around a single dislocation goes as $y/[x^2+y^2]$).

This expression differs from the corresponding results in K [Eq. (K26)] and MS [Eq. (MS19)] primarily in the angular dependence. Mackenzie and Sondheimer neglected the potential term V_2 and attempted to take account of the discontinuity in displacement by replacing y by its absolute value in the arctangent terms in the expression for u_x [Eq. (16)] between $y=-R/2$ and $y=R/2$. The resulting displacement is, of course, not in accord with the equations of elasticity, and in fact corresponds to replacing and smearing out the atoms previously removed to create the dislocation. The result is an increase in the resistance in the slip direction and a decrease in the y direction (since the positive charge density, and hence, scattering potential are smoothed out for an electron traveling in the y direction). Similarly omitting the contribution from V_2, Koehler replaced x by its absolute value in the arctangent terms in Eq. (17) for all values of y. This procedure is also not in accord with the elastic equations, and corresponds to the introduction of a discontinuity in charge density along the missing plane of atoms, and thus to a large increase in resistance along the slip direction.

Making use of Eq. (19), we now evaluate the resistivity by the method[9] described in MS, and find for the change in resistivity in the x (slip) direction,

$$\Delta\rho_x=\frac{3\pi^2Z^2e^2m^{*2}N\lambda^2}{\hbar^3k_0^2q^4\Delta^2n_0}\left(\frac{1-2\nu}{1-\nu}\right)^2$$
$$\times\{a\cot^{-1}a+a^2/(a^2+1)\},\quad(20)$$

where $a\equiv q/2k_0$ and N is $\frac{1}{2}$ the number of dislocations per cm^2. $\Delta\rho_z$ is of course zero, and the ratio $\Delta\rho_z/\Delta\rho_y$ is equal to $\frac{1}{4}$. Values for this ratio of about 8 and 2 were obtained in K and MS, respectively. That the slip direction is the direction of low resistance can be seen qualitatively in the following ways. First, the potential changes are less abrupt for an electron traveling in the slip direction, and so the scattering will be less, than for an electron traveling in the y direction. Secondly, although the (approximately) $1/\kappa_x^2$ dependence in the square of the matrix element indicates that small angle scattering is of importance (which would strongly weight the resistance in the x direction), the additional dependence on κ_x in the transport equation overcomes this factor, and in fact it is large angle scattering that contributes most to the resistance, particularly in the y direction. Now for a current traveling in the x direction the possible electronic momentum changes available in phase space are also, on the average, primarily in the x direction. But we have already seen that the matrix element is small for the case in which the momentum change is primarily in the x direction. Hence, the electrical resistance in this direction is relatively small.

This expression for the resistivity change can be obtained from Eq. (MS34) by setting equal to zero in MS in term in A^2, and replacing the quantity $(2B-C)^2$ by $\frac{1}{2}(2B-C-A)^2$ [see Eqs. (19) and (MS19)]. The average value of the resistivity change for a polycrystalline specimen, equal to 4/3 times $\Delta\rho_x$ above, differs by a factor $(2B-C-A)^2/2[A^2+(2B-C)^2]$ from the average change calculated in MS. For copper ($\nu=0.34$) this factor has the value 0.092.

By use of Eqs. (2) and (3), we may write the average change in resistivity in the form

$$\langle\Delta\rho\rangle_{\text{av}}=\frac{m^2\lambda^2k_0E_0^2}{27\pi^2\hbar^3e^2n_0^2(n_0\Delta)^2}\left(\frac{1-2\nu}{1-\nu}\right)^2$$
$$\times\{a\cot^{-1}a+a^2/(a^2+1)\}\times(m^*/m)^2Z^2N.\quad(21)$$

Making use of specific heat data[10] for copper, we set $E_0=4.78$ ev, $m^*/m=1.47$, $k_0=1.37\times10^8$ cm^{-1}, $q=2.19\times10^8$ cm^{-1}, and $a=0.80$; taking $\lambda=2.55\times10^{-8}$ cm, $\nu=0.34$, and assuming one free electron per atom (so that $n_0\Delta=1$ and $n_0=0.85\times10^{23}$ cm^{-3}), we obtain

$$\langle\Delta\rho/\rho\rangle_{\text{av}}=2.46\times10^{-15}Z^2N,$$

[9] Equation (4) for the collision operator in reference 2, and the resulting expressions, should be multiplied by the factor $\frac{1}{2}$.

[10] F. Seitz, *Modern Theory of Solids* (McGraw-Hill Book Company, Inc., New York, 1940), Chapter IV.

where we have used the thermal resistivity at 20°C, $\rho = 1.89 \times 10^{-18}$ Gaussian units, i.e., 1.69×10^{-6} ohm cm. The observed fractional change in heavily cold-worked copper is about 2 percent, which corresponds to $N \sim 8 \times 10^{12}$ pairs of dislocations per cm², if the effective atomic number Z is unity. Koehler[8] has estimated that $N \sim 3 \times 10^{11}$ pairs per cm² on the basis of energy storage measurements. With a different set of values for k_0 and n_0, MS obtained $N \sim 5 \times 10^{12}$ dislocation pairs/cm². Correcting this result by the factor $2[A^2+(2B-C)^2]/(2B-C-A)^2$, we would obtain $N \sim 6 \times 10^{12}$/cm². However, this value is probably too high, since it has assumed the normal electronic mass and a density of 1.4 electrons per atom in the evaluation [see Eq. (MS40)]. Koehler quotes a result $N \sim 7 \times 10^{11}$/cm². (See, however, MS, p. 269.)

We may also compare Eq. (21) with the results obtained by the deformation potential method, Eq. (D3). The resistivity change per dislocation calculated here is equal to that in D times a factor $\frac{1}{2}[a \cot^{-1} a + a^2/(a^2+1)]$. For a large in comparison with unity this factor reduces to 1, but in this case neither approximation is a good one [see Eq. (12)]. For copper $a = 0.80$ and the factor becomes 0.55. Since the deformation potential is somewhat larger than the potential used here [compare Eqs. (4), (9), and (10)], one would indeed expect to calculate a larger resistivity by the use of the deformation potential, and according to Eq. (12), in fact, one would expect to bracket the correct answer by the two methods. The effect of the fictitious singularity in the assumed density change on the dislocation axis was estimated in D to give too large a resistance change by a factor of about 2, and since it is only in the region close to the singularity that the two potentials differ appreciably, this factor is in qualitative agreement with the result obtained just above.

The estimate made here for the number of dislocation pairs, 8×10^{12} per cm², should perhaps be modified in the following way, making use of a calculation similar to Bardeen's[5] for the thermal part of the resistance in monovalent metals. The electrical resistivity ρ arising from collisions of the electrons with lattice vibrations can be calculated by the model used here, i.e., a model which neglects effects associated with the particular ionic potentials near the nuclei and considers just the effects resulting from changes in density; this value for ρ can then be compared with the experimental value, thus giving some idea of the accuracy of the results of this model. From reference 5 we find ρ to be proportional to $(C/\zeta)^2$, which for the present model is given by Eqs. (51), (49), and (47) of reference 5 with $V(r_s)+E_c=0$ and $f(u)=1$. Inserting the experimental values given above for copper (so that Bardeen's parameter β becomes 1.31), we find that numerically $(C/\zeta)^2$ is equal to 0.460. The experimental value is 1.74, so that the resistance calculated according to this model is about $\frac{1}{4}$ that observed. Now the calculation for phonons makes use of the same matrix elements as were used for the dislocation calculation, and both calculations required summations over the distribution of electron propagation vectors and the Fourier expansions of the lattice irregularities. Although these expansions are not the same in the two problems, the error incurred by use of this general approach should be of the same order of magnitude in the two cases; we thus correct N by the above factor, and obtain $N \sim 2 \times 10^{12}$ per cm².

The conclusion of the writer is that the best estimate, based on this simple theory, for the density of dislocations is about an order of magnitude higher than the estimate obtained from the energy storage measurements. If the latter is fairly accurate, closer agreement must be sought in an interpretation of the effects of clustered vacancies, screwtype dislocations, half-dislocations, and anisotropy in the elastic constants.

The writer welcomes this opportunity for expressing his appreciation to Professor J. S. Koehler for his kind and helpful interest, and to Professor J. Bardeen who, both directly and indirectly, has made valuable contributions to this work.

Gamma-Rays Associated with Selected Neutron-Induced Radioactivities

W. C. RUTLEDGE, J. M. CORK, AND S. B. BURSON
Argonne National Laboratory, Chicago, Illinois, and University of Michigan, Ann Arbor, Michigan
(Received February 4, 1952)

By means of photographic magnetic spectrometers located close to the heavy water moderated reactor, the following radioactive nuclei have been examined: Se^{77m} (17.5 sec), Se^{79m} (3.5 min), Se^{81m} (58 min), Se^{81} (17 min), Se^{83} (69 sec), Se^{83} (26 min), Nd^{147} (11.9 days), Nd^{149} (1.8 hr), Nd^{151} (12 min), Pm^{149} (50 hr), Pm^{151} (27.5 hr), Sm^{145} (410 days), Sm^{151} (>20 yr), Sm^{153} (46.5 hr), Sm^{155} (23.5 min), Eu^{156} (1.7 yr), Mo^{101} (14 min), Tc^{101} (15 min), and Th^{233} (23.6 min). The 27.5-hour activity assigned to Pm^{151} was discovered in this work. A new vacuum gate for the camera of the spectrometer permits the study of activities with half-lives as short as ten seconds. Energy level schemes for the product nuclei are proposed on the basis of a spectrographic analysis of the gamma-rays and also of coincidence and absorption measurements. Changes in spin and parity between many of the energy levels are determined from measurements of the K/L ratios of the corresponding gamma-rays.

INTRODUCTION

PHOTOGRAPHIC beta-ray spectrometers (called spectrographs hereafter) in close proximity to the heavy water moderated reactor of the Argonne National Laboratory make it possible to carry out investigations of short-lived radioactive nuclei.[1] The pneumatic tube which passes through the shielding of the reactor permits rapid transport of samples to and from the active region. It has been found possible to conduct spectrographic studies of activities having half-lives as short as ten seconds. The energies of the gamma-rays are principally determined by measuring the energies of internal conversion electrons and photoelectrons from various radiators. Additional information is obtained from absorption and coincidence experiments, and from measurements of the intensity of the internal conversion electron lines. From these results several new energy level schemes are proposed.

APPARATUS AND PROCEDURE

The present investigation makes use of the existing magnetic spectrographs of Keller and Cork.[1,2] To facilitate the study of radioactivities with half-lives shorter than one minute, it was necessary to modify the cameras by constructing a faster vacuum gate. This was accomplished by the use of the multiple *O*-ring vacuum seal shown in Fig. 1. The source is placed in a cavity in the brass cylinder which extends through the camera. By the above simplification it is possible to put the source in position in the main chamber by a single continuous motion of the supporting cylinder through its *O*-ring vacuum seals. As the source cavity moves into the region between the first two *O*-rings, it is sealed off from the atmosphere. As the motion continues, the air trapped in the sample cavity is practically all removed by a forepump connected to the vacuum port between the second and third *O*-rings. Two additional *O*-rings on the other side of the main chamber permit the cylindrical tube to extend through the camera so that there is no net thrust due to atmospheric pressure. With this type of vacuum gate the introduction of a source into position in the camera requires about one second.

The sources that were used in the study of internal conversion electrons were usually mounted on a strip of Scotch-tape. They were approximately 0.35 mm wide, 20 mm long, and from 0.5 to 1 mg/cm² thick. The strip of tape was supported on frames made of either Lucite or pure graphite. No disturbing radiation was emitted by the source holder and mounting after irradiation in the reactor. Short-lived sources for studies of photoelectrons were sealed and irradiated in small Lucite tubes. The charged particles emitted by these sources were absorbed by interchangeable copper or aluminum tubes on the source holder; the radiator was 0.35 mm wide, 20 mm long, and approximately 30 mg/cm² thick.

Because of its sensitivity, no-screen x-ray film was used for a qualitative survey of each radioactive nucleus. For quantitative work Kodak NTB nuclear track plates were used. The fine grain and low background of these plates make them far superior to x-ray film for the comparison of intensities of electron lines with a photodensitometer.

The magnetic fields were calibrated and checked at

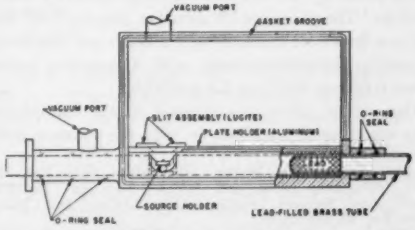

FIG. 1. A fast-entry camera for a magnetic spectrograph.

[1] R. Caldwell, Argonne National Laboratory Report 4408 (1949); Phys. Rev. **78**, 407 (1950); H. Keller and J. Cork, Argonne National Laboratory Report 4595 (1951); Phys. Rev. **84** (1952).
[2] J. Cork, Phys. Rev. **72**, 581 (1947).

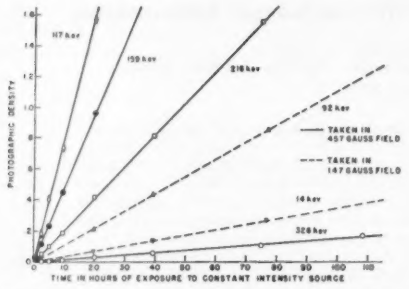

FIG. 2. Variation of density with exposure for NTB plates.

intervals with standard sources of iodine 131, cobalt 60 and radium.[3]

In order to determine the ratio of the electrons that are ejected from the K and L atomic orbits in the process of internal conversion, the relative intensities of the corresponding electron lines on photographic plates are determined by photometric methods. Before these intensities can be obtained, it is necessary to correct the photodensitometer traces of the electron lines for the following factors: background, exposure, attenuation due to the geometry of the camera, and energy sensitivity of the photographic emulsion. It was not feasible to follow the procedure usually used in optical spectroscopy of putting proper calibrating exposures of known relative intensity on every plate. In this work separately exposed plates were used to determine the various corrections in the following manner. For each kind of experiment for the calibration, photographic plates from the same box in the same shipment were used. The plates and developer were stored at a temperature of about 1°C to retard aging processes. Identical conditions of exposure and development of the photographic plates were maintained. Each plate was developed for 2 minutes at 20°C with previously unused D-8 developer from the same batch of stock solution. Instead of varying the intensity of the radioactive source, the time of exposure was varied. That the reciprocity law of equivalence of variation of intensity and time of exposure is valid to better than the accuracy of these measurements for the blackening of the plates by fast electrons has been shown by other workers.[4] The photographic densities ($\log_{10} I_0/I$) of the electron lines were measured with a Leeds and Northrup recording photodensitometer with a scanning beam about 0.02 mm wide and 1.8 mm high.

One set of plates was exposed to the continuous beta-spectrum of scandium 46 with the constant-field spectrograph for times of exposure ranging from 0.5 to 108 hours. The densities at different selected positions, the same position on each plate, were measured to obtain sets of values of density for various times of exposure, each set corresponding to electrons of a particular energy. The results are shown in Fig. 2. It is apparent that for values of density below 1.6 the density is directly proportional to the time of exposure. By the reciprocity law, the density is thus proportional to the intensity of exposure.

The correction for attenuation of the intensities of the electron lines caused by the geometry of the camera was determined by making successive identical exposures of a well-known electron line on different plates at different radii of curvature, ρ. This was accomplished by varying the magnetic field in appropriate steps from 70 to 460 gauss, and by using electron lines at 50, 103, and 139 kev. The variation of the intensity of an electron line with the corresponding radius of curvature is dependent upon a choice of using the density at the peak of the line, or the density integrated over a complete line distribution. The experimentally determined attenuation of the integrated density, or area under the densitometer trace, of a line located on increasing radii of curvature is shown in Fig. 3. The slightly greater attenuation of the intensities of the peaks of the electron lines with radii of curvature is also shown in the same figure. Because of scattering of the electrons from the low energy edge of the metal plate holder, both curves may be relatively inaccurate at values of ρ from 2.75 to 3.25 cm. Additional experiments showed that the intensity of a section of a beta-spectrum was attenuated at various radii of curvature by the same amounts as that of a peak of an electron line.

The sensitivity of various emulsions to electrons of different energy has been considered in detail by several

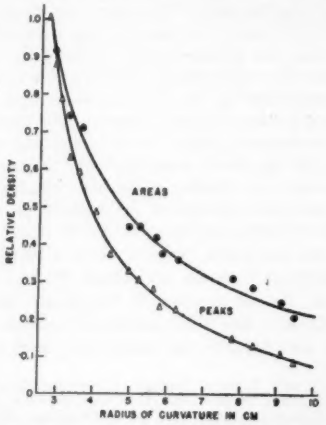

FIG. 3. Variation of photographic density due to geometry.

[3] Lind, Brown, Klein, Muller, and DuMond, Phys. Rev. **75**, 1633 (1949); Lind, Brown, and DuMond, Phys. Rev. **76**, 1838 (1949); Cork, Branyan, Stoddard, Keller, LeBlanc, and Childs, Phys. Rev. **83**, 681 (1951).

[4] W. Bothe, Z. Physik **8**, 243 (1922); C. Ellis and W. Wooster, Proc. Roy. Soc. (London) **A114**, 266 (1927).

authors.[5] In the present investigation the energy sensitivity of the NTB emulsion (25 microns thick) is determined from 14 to 350 kev, as shown in Fig. 4, by comparing the beta-spectrum of scandium 46 obtained[6] by the use of a constant radius beta-spectrometer with that observed in the constant field spectrograph. The photographic data were, of course, corrected for geometrical attenuation before the comparison was made.

Additional experiments were run to check the validity of the correction for attenuation caused by the geometry of the camera when this geometry was varied. Using a range of from 1 mm to 10 mm for the separation of the slits and from 0.20 mm to 1.2 mm for the width of the source, a maximum deviation of ± 10 percent from the average was obtained for the K/L ratio of a prominent gamma-ray. No correlation was observed between the deviations and the parameters that were varied. Taking account of these experiments and the fluctuations of the densitometer traces caused by the size of the grains and defects in the emulsion, it was concluded that it is often possible to obtain K/L ratios within ± 10 percent from the corrected intensities of the electron lines. In a comparison of a K/L ratio determined by the photographic method with that from beta-spectrometer measurements, excellent agreement was obtained.[7] The ratios determined from area measurements and corrected either by the geometrical attenuation curve for areas, or by the one for peaks on a point-to-point basis, are found to agree within experimental error. In this work, however, the K/L ratios are determined from area measurements corrected in the former manner in view of the comparative ease of applying the necessary corrections.

To determine the multipolarity and character (magnetic or electric) of a gamma-ray from its K/L ratio and energy, recently published curves of K/L *versus* Z^2/E were used.[8] In the case of isomeric transitions, the multipolarity and character may also be assigned from lifetime-energy relationships.

In a few cases absorption measurements with GM counters as detectors indicated the presence of weak gamma-rays of over 600 kev that were not observable by the photographic method. More accurate values for these and other unresolved weak gamma-rays were obtained by Dr. B. Hamermesh with a NaI (thallium activated) scintillation spectrometer with a twenty channel pulse-height discriminator.[9]

A standard coincidence circuit with a resolving time of 4.5×10^{-7} second was also used in this research.

[5] C. Ellis and G. Aston, Proc. Roy. Soc. (London) **A119**, 645 (1928); A. Charlesby, Proc. Phys. Soc. (London) **52**, 657 (1940); B. Barries, Physik. Z. **43**, 190 (1942); Baker, Ramberg, and Hillier, J. Appl. Phys. **13**, 450 (1942); L. Cranberg and J. Halpern, Rev. Sci. Instr. **20**, 641 (1949).

[6] E. Salmi, dissertation, University of Michigan (1950); S. Burson and W. Rutledge, unpublished work at Argonne National Laboratory (1951).

[7] S. Burson and W. Rutledge, (Bull. Am. Phys. Soc. **27**, No. 1, 58 (1952)).

[8] M. Goldhaber and A. Sunyar, Phys. Rev. **83**, 906 (1951).

[9] B. Hamermesh and V. Hummel, Phys. Rev. **83**, 663 (1951).

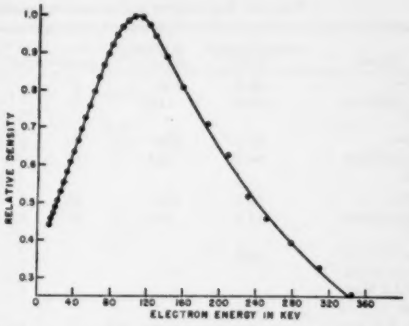

FIG. 4. Sensitivity of Kodak NTB plates to electron energy.

The actual experimental arrangement and techniques have been described previously.[10]

RESULTS

A summary of the significant results is given in Table I, It includes measurements of the half-life, energy of the beta-rays, energy of the electron lines, interpretation of the electron lines, relative intensity of the internal conversion electron lines, energy of the corresponding gamma-rays, and K/L ratio of the prominent gamma-rays. The probable multipolarity and character of these gamma-rays are suggested where data are available. Alternate assignments of the type of the radiation that are less definite are listed in parentheses. Types of radiation classified as mixtures of $M1$ and $E2$ transitions may possibly be either pure $M2$ or $E1$ transitions, depending upon the particular case in question.

A. Selenium

Six stable isotopes of selenium exist in nature with atomic masses and abundances as follows: 74—0.9 percent, 76—9.1 percent, 77—7.5 percent, 78—23.6 percent, 80—49.9 percent, and 82—8.9 percent. For the present study stable isotopes were obtained with the following mass enrichments: 76—57 percent, 78—83 percent, 80—95 percent, and 82—52 percent. Of the eleven radioactivities in selenium that are believed to exist, six short-lived, neutron-induced activities are discussed.

Se^{77m}

The 17.5-second isomer Se^{77m} was first produced[11] by the (n,γ) reaction and later[12] by x-ray excitation. The energy of a single gamma-ray which was reported[13] as

[10] Burson, Blair, Keller, and Wexler, Phys. Rev. **83**, 62 (1951).

[11] J. Arnold and N. Sugarman, J. Chem. Phys. **15**, 703 (1947); M. Goldhaber and C. Muehlhause, Phys. Rev. **74**, 1248 (1948).

[12] Gideon, Miller, and Waldman, Phys. Rev. **75**, 329 (1949).

[13] A. Flammersfeld and C. Ytheir, Z. Naturforsch. **5a**, 401 (1950); E. der Mateosian and M. Goldhaber, Phys. Rev. **82**, 116 (1951); Canada, Cuffey, Lessor, and Mitchell, Phys. Rev. **82**, 750 (1951).

TABLE I. The electron and gamma-ray energies from selected neutron-induced radioactive nuclei.

Nucleus	Electron energy[a] (kev)	Relative intensity	Interpretation	Energy sum (kev)	Gamma energy (kev)	K/L ratio	Type
Se^{77m}	148.9	100	K^1	161.6	161.6	4.6 ±0.3	$E3$
17.5±0.5 sec	160.0	21.6	L^1	161.6			
I.T.				150[d]			
Se^{79m}	83.2	100	K^1	95.9	95.9	2.9 ±0.5	$E3$
3.5±0.2 min	94.2	34.8	L^1	95.8			
I.T.				85[d]			
Se^{81m}	90.5	100	K^1	103.2	103.1	3.0 ±0.3	$E3$
58±1.5 min	101.4	33.1	L^1	103.0			
I.T.				95[d]			
Se^{81}	none				none		
17±1.5 min							
β=1.5 Mev							
Se^{83}	none				none		
69±1.5 sec							
β=3.4 Mev[b]							
Se^{83}	27.8	100[c]	K^1	41.3	41.3		
26±2.5 min	30.2	100[c]	K^2	43.5	43.5		
β=1.5 Mev	47.5	100[c]	K^3	61.0	61.0		
	160.6		$L_{(Pb)}{}^4$	175.9	175.9[e]		
				173[d]	950[e]		
				950[d]			
Nd^{147}	31.4		Auger α_1-L_I				
	36.9		Auger α_1-M				
11.9±0.3 days	46.0	100	K^1	91.2	91.2	4.9 ±0.5	$M1+E2$
	75.3	4[c]	K^3	120.5	120.5		
β=0.825 Mev	83.9	20.6	$L_{I,II}{}^1$	91.2			
0.598 Mev	89.4	4.0	M^1	91.1			
0.384 Mev	90.7	1.0[c]	N^1	91.0			
	112.9	2.4[c]	$L_I{}^2$	120.4			
			(K)	(168.1)	(168.1)		
	151.9	2.2[c]	K^3	197.1	197.1		
	186.0	0.3[c]	K^4	231.2	231.2		
	214.6	0.06[c]	K^5	259.8	259.8		
	228.0	0.5[f]	K^6	273.2	273.3		
	255.6	0.05[c]	K^7	300.8	300.8		
	266.5	0.12[c]	$L_{II}{}^6$	273.5			
	272.9	1.28[f]	K^8	318.1	318.1		
	311.2	0.2[c]	$L_{II}{}^8$	318.2			
	353.2	0.3[c]	K^9	398.4	398.4		
	396.1	0.3[c]	K^{10}	441.3	441.4		
	434.5	0.04[c]	$L_{II}{}^{10}$	441.5			
	487.0	4.54[f]	K^{11}	532.2	532.3	5.7 ±1.4	$E2$
	525.5	0.79[f]	$L_{II}{}^{11}$	532.5			
				95[d]			
				290[d]			
				540[d]			
Nd^{149}	22.5	4[c]	$L_{II}{}^1$	29.5	29.5		
1.8±0.1 hr	28.0	1[c]	M^1	29.6			
	36.2		Auger α_2-M				
β=1.5 Mev	51.3	14	K^2	96.5	96.5	0.87±0.25	$E2$
1.1 Mev							
0.95 Mev	67.1	30	K^3	112.3	112.3		
	68.9	100	K^4	114.1	114.1	4.8 ±1.6	$E2+M1(M2)$
	78.9	15[c]	K^5	124.1	124.1		
	89.2	16	$L_{I,II}{}^2$	96.4			
	106.7	21	$L_I{}^4$	114.2			
	112.3	3.3	M^4	113.9			
	120.8		$K_{(Pb)}{}^6$	209.1			
	142.6	3.2	K^6	187.8	187.8		
	150.6		$K_{(Pb)}{}^{10}$	238.9			
	152.7	1.7	K^7	197.9	197.9		
	165.4	29	K^8	210.6	210.5[e]	6.6 ±1.4	$M1$, $(M2)$
	178.0		$K_{(Pb)}{}^{11}$	266.3			
	180.9	1.7	K^9	226.1	226.1		
			$(L_{II}{}^6)$	(187.9)			
	181.4		$L_{I(Pb)}{}^7$	197.3			
	194.8	14.9	K^{10}	240.0	240.0		
	195.0		$L_{II(Pb)}{}^8$	210.2			
	203.0	4.4	$L_I{}^8$	210.4			
	209.0	0.8	M^8	210.6			
	221.3	4.2	K^{11}	266.5	266.4[e]	(10)	$(M1)$
	250.6		$L_{I(Pb)}{}^{11}$	266.4			

TABLE I.—*Continued.*

Nucleus	Electron energy[a] (kev)	Relative intensity	Interpretation	Energy sum (kev)	Gamma energy (kev)	K/L ratio	Type
	258.9	0.4[e]	L_I[11]	266.3			
	335.3		$K_{(Pb)}$[12]	423.6	423.5[e]		
	407.0		$L_{I(Pb)}$[12]	422.9			
	449.9		$K_{(Pb)}$[12]	538.2	538[e]		
	561.9		$K_{(Pb)}$[14]	650.2	650[e]		
				110[d]			
				266[d]			
				680[d]			
Nd^{151}	40.2	24[e]	K^1	85.4	85.4		
12±1 min	64.8	17[e]	K^2	110.0	110.0		
	71.9	100	K^3	117.1	117.1	4.1 ±1.7	$(M1+E2)$
$\beta=1.93$ Mev	78.1	21[e]	$L_{I,II}$[1]	85.3			
	83.8	5[e]	M^1	85.4			
	110.0	24.5	$L_{I,II}$[2]	117.2			
	115.5	6[e]	M^2	117.1			
	376.1		K^4	421.3	421[e]		
		By scintillation spectrometer		725±50	725±50[e]		
				1140±25	1140±25[e]		
				995[d]			
Pm^{149}	32.5		Auger α_1-L_{III}				
50±1.5 hr	238.0	100	K^1	284.9	284.9	8.0 ±2.5	$M1(M2)$
	277.6	12.5	$L_{I,II}$[1]	284.9			
$\beta=1.05$ Mev				1300[d]	1300(±200)		
Pm^{151}	17.8	28	K^1	64.7	64.7	0.30±0.15	$E2$
27.5±1.5 hr	18.9	18	K^2	65.8	65.8	0.25±0.15	$E2$
	22.8	13	K^3	69.7	69.6	0.25±0.10	$E2$
$\beta=1.1$ Mev	32.6		Auger α_2-L_{III}				
	37.4		Auger $\beta-L_I$				
	53.1	100	K^4	100.0	100.0	5.0 ±1.7	$M1+E2(M2)$
	57.2	93	$L_{I,II}$[1]	64.7			
	58.3	71	$L_{I,II}$[2]	65.8			
			(K)	(105.2)	(105.2)		
	61.9	50	$L_{I,II}$[3]	69.4			
	63.1	8[e]	M^1	64.8			
	64.1	5.5[e]	M^2	65.8			
	69.2	17.8	K^5	116.1	116.2		
	92.3	20.2	L_I[4]	100.1			
	97.1	23.4	K^6	144.0	144.0	(9)	$(M1)(M2)$
			(L_I)	(104.8)			
	109.0	2.2	L_{II}[5]	116.3			
	116.3	14.7	K^7	163.2	163.1	(7)	$(M1+E2)$
	121.1	14.6	K^8	168.0	168.0	3.3 ±2.2	$M1+E2$
	130.2	22.6	K^9	177.1	177.1	8.7 ±3.0	$M1+E2(M2)$
	136.4	2.5[e]	$L_{I,II}$[6]	143.9			
	155.5	2.0[e]	$L_{I,II}$[7]	163.0			
	160.4	4.4	$L_{I,II}$[8]	167.9			
	161.5	4.7	K^{10}	208.4	208.3	3.6 ±2.5	
	169.4	2.6	L_I[9]	177.2			
	174.9	0.6	M^9	176.6			
	185.0	3.7	K^{11}	231.9	231.9		
	186.5	weak	$K_{(Pb)}$[13]	274.8			
	192.8	2.7	K^{12}	239.7	239.9		
	200.7	1.3	$L_{I,II}$[10]	208.2			
	224.4	0.8	$L_{I,II}$[11]	231.9			
	228.3	5.8	K^{13}	275.2	275.2	(>10)	$(M1)$
	232.6	0.7[e]	$L_{I,II}$[12]	240.1			
	251.7	strong	$K_{(Pb)}$[14]	340.0			
	293.2	39.2	K^{14}	340.1	340.2[e]	9.1 ±2.8	$M1(M2)(E1)$
	324.0		$L_{II(Pb)}$[14]	339.8			
	332.9	4.31	$L_{I,II}$[13]	340.4			
	668.5	weak	K^{15}	715.4	715[e]		
	707.4	weak	$L_{I,II}$[15]	714.9			
				170[d]			
				300[d]			
				700[d]			
Sm^{146}	16.1	100	K^1	61.3	61.3	1.0 ±0.3	$E2+M1$
410 days[b]	31.6		Auger α_3-L_{III}				
K-capture	36.3		Auger α_3-M				
	53.9	98	$L_{I,II}$[1]	61.2			
	59.6	5	M^1	61.3			
				65[d]			
Sm^{151}	none				none		
>20 yr							
$\beta=0.076$ Mev[b]							

TABLE I.—*Continued.*

Nucleus	Electron energy[a] (kev)	Relative intensity	Interpretation	Energy sum (kev)	Gamma energy (kev)	K/L ratio	Type
Sm^{153}	14.5		$K_{(Pb)}^{2}$	102.8			
46.5±1 hr	21.2	5.5	K^{1}	69.8	69.8	0.29±0.03	$E2$
	33.5		Auger α_2-L_I				
β=0.820 Mev	39.8		Auger α_2-M				
	54.5		$L_{II(Pb)}^{1}$	69.7			
	54.7	100	K^{2}	103.3	103.4	3.5 ±0.6	$E2+M1$
	61.7	18.5	L_I^{1}	69.8			
	62.9	0.4	L_{III}^{2}	69.9			
	68.1	2.0	M^{1}	69.9			
	69.3	0.2	N^{1}	69.7			
	87.0		$L_{I(Pb)}^{2}$	102.9			
	88.2		$L_{II(Pb)}^{2}$	103.4			
	90.5		$L_{III(Pb)}^{2}$	103.6			
	95.3	28.5	L_I^{2}	103.4			
	101.5	5.8	M^{2}	103.3			
	102.9	0.4	N^{2}	103.3			
	533.7	weak	K^{3}	582.4	582		
				100[d]			
				600[d]			
Sm^{155}	16.1		$K_{(Pb)}^{1}$	104.4			
23.5±0.4 min	56.0	100	K^{1}	104.6	104.6	3.6 ±1.0	$E2+M1(E1)$
	57.3	(4)[e]	$K_{(Sm)}^{1}$	104.2			
β=1.8 Mev	88.6		$L_{I(Pb)}^{1}$	104.5			
	89.7		$L_{II(Pb)}^{1}$	104.9			
	91.9		$L_{III(Pb)}^{1}$	105.0			
	96.6	27.6	L_I^{1}	104.7			
	100.6		$M_{(Pb)}^{1}$	104.4			
	104.4	(3)	M^{1}	104.8			
	156.2		$K_{(Pb)}^{2}$	244.5			
	197.2	(100)	K^{3}	245.8	245.8	(8)	$(M1)(M2)$
	228.6		$L_{I(Pb)}^{2}$	244.5			
	237.4	(12.5)	L_I^{2}	245.5			
				100[d]			
				240[d]			
Eu^{155}	10.0	3	K^{1}	60.4	60.4		
1.7±0.2 yr	36.6	100	K^{2}	87.0	87.0	8.0 ±2.8	$M1(M2)$
	52.1	31	L_I^{1}	60.5			
β=0.15[b] Mev	55.3	75	K^{3}	105.7	105.7	8.3 ±2.8	$M1(M2)$
0.25[b] Mev	58.5	5	M^{1}	60.4			
	71.1		$L_{I,II(Pb)}^{2}$	86.7			
	78.9	12.5	$L_{I,II}^{2}$	87.0			
	82.0	10	K^{4}	132.4	132.4		
	83.0		$M_{(Pb)}^{2}$	86.9			
	85.0	1.5	M^{2}	86.9			
	90.0		$L_{I,II(Pb)}^{3}$	105.6			
	97.9	9	L_{II}^{2}	105.7			
	103.9	1[c]	M^{3}	105.8			
				80[d]			
Mo^{101}	74.6		$K_{(U)}^{1}$	191.0			
~14 min	103.2		$K_{(Pb)}^{1}$	191.5			
β=1.2 Mev	168.6		$L_{III(U)}^{1}$	190.0			
2.1 Mev	170.2	100	K^{1}	191.2	191.2	6.0 ±2.5	$M1(M2)(E2)$
	175.9		$L_{I,II(Pb)}^{1}$	191.4			
	188.0	16.7	L_I^{1}	191.1			
		By scintillation spectrometer		960±50	960±50[e]		
				1100[d]			
				150[d]			
Tc^{101}	190.7		$K_{(U)}^{1}$	307.1			
~15 min	218.5		$K_{(Pb)}^{1}$	306.8			
β=1.3 Mev	284.8	100	K^{1}	306.9	306.9	6.3 ±3.0	$M1(M2)(E2)$
	290.8		$L_{I,II(Pb)}^{1}$	306.3			
	303.8	16	L_I^{1}	307.0			
				310[d]			
Th^{233}	none			none			
23.6±0.6 min							
β=1.23 Mev							

[a] The electron energies are measured with an accuracy of ±0.3 percent of the energy.
[b] These measurements were not made in this investigation.
[c] Visual estimates were made of these intensities.
[d] These energies are obtained from absorption measurements.
[e] These values for the energy of the gamma-rays are either checked or obtained with a scintillation spectrometer by Dr. Hamermesh.
[f] These relative intensities are determined from photodensitometer measurements but are not normalized to the same intensity scale as other measurements for the radio nucleus in question.

150–165 kev from various spectrometric and absorption measurements is now shown to be 161.6±0.5 kev. A series of 315 successive irradiations and cumulative photographic exposures failed to show any additional gamma-rays. The K/L ratio of 4.6±0.3, shown in Table I, compares favorably with the value of 4.5 predicted by Goldhaber and Sunyar[8] whose life-time-energy plots indicate that the radiation is electric octopole ($E3$).The photodensitometer trace of the K and L electron lines is shown in Fig. 5 as an example of the results that may be obtained for short-lived activities.

Se^{79m}

A 3.9-minute metastable state in selenium 79 was found to emit a single gamma-ray of 90±10 kev by Flammersfeld and Herr.[14] The existence of this state is confirmed and its half-life is measured as 3.5±0.2 minutes. The energy of the gamma-ray is found to be 95.9±0.3 kev. The lifetime-energy plot indicates that this transition is also $E3$. The K/L of 2.9±0.5 agrees with the value of 2.8 predicted by Goldhaber and Sunyar.

Se^{81m} and Se^{81}

In early investigations of the radionuclei of selenium, a 56–60 minute activity with a gamma-ray of 98–104 kev was associated with Se^{79m} or Se^{81m}.[15–18] Later this activity was assigned to Se^{81m}. A 14–19 minute daughter was found to decay by the emission of a beta-ray of 1.4–1.5 Mev.[16–21] In the present work the assignment of the 58.0±1.5 minute isomer to Se^{81m} is confirmed. An analysis of the internal conversion electrons shown in Table I indicates that the energy of the gamma-ray is 103.1±0.3 kev. From the lifetime-energy plot this transition is also $E3$. The K/L ratio of 3.0±0.3 is appreciably less than that reported by Bergstrom and Thulin,[18] and by Helmholz,[17] but agrees well with the value of 2.8 predicted by Goldhaber. The 17.0±1.5 isomeric state of selenium 81 is found to decay solely by the emission of a beta-ray of 1.5 Mev to Br^{81}.

Se^{83}

It has been proposed[11,18] that two isomeric states exist in selenium 83, with no gamma-transition between them. A 67-second isomeric state was found[11] to emit only a beta-ray of 3.4 Mev. No internal conversion electron or photoelectron lines are associated with this short-lived isomer in the spectrograms of the present study.

A second isomer with a half-life of 25–30 minutes has been assigned to selenium 83.[18,22] Using absorption techniques, Glendenin[20] found that this state decayed via a beta-ray of 1.5 Mev and gamma-rays of 170, 370, and 1100 kev. In the present investigation, a half-life of 26±2.5 minutes is measured after absorbing the softer radiation emitted by contaminations of other radioisotopes of selenium. Scintillation spectrometer and lead absorption measurements confirm the existence of the first and third gamma-rays that were reported by Glendenin, but no evidence is seen for the 370-kev transition. The energy of the beta-ray is also found to be 1.5 Mev from absorption measurements in aluminum. Only one very weak photoelectron line and three weak conversion lines are associated with the 26-minute activity. These internal conversion lines are weaker than several lines that were the result of small contaminations of Se^{79} and Se^{81}. Thus the interpretation of these lines is less definite than is desirable. By the proper selection of bombardment and exposure times, however, it is established that these weak conversion lines are the result of an activity with a half-life less than one hour, and not to any longer-lived contaminates or daughter products.

B. Neodymium

A section of the Segrè chart pertinent to the study of the radioisotopes of neodymium is shown in Fig. 6. Where enriched isotopes have been obtained, the percentages of the enriched masses are listed in parenthesis

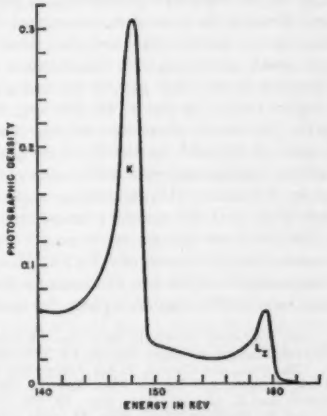

FIG. 5. Photodensitometer trace of K and L electron lines for a gamma-ray of 161.6 kev (17.5 second Se^{77m}).

[14] A. Flammersfeld and W. Herr, Z. Naturforsch. **5a**, 569 (1950).
[15] A. Snell, Phys. Rev. **52**, 1007 (1937).
[16] A. Langsdorf and E. Segrè, Phys. Rev. **57**, 105 (1940).
[17] A. Helmholz, Phys. Rev. **60**, 415 (1941).
[18] I. Bergstrom and S. Thulin, Phys. Rev. **76**, 1718 (1949).
[19] H. Wäffler and O. Hirzel, Helv. Phys. Acta **21**, 200 (1948).
[20] L. Glendenin, *Radiochemical Studies: The Fission Products* (McGraw-Hill Book Company, Inc., New York, 1950), Paper No. 61, National Nuclear Energy Series, Plutonium Project Record, Vol. **9**, Div. IV.
[21] The Plutonium Project, Revs. Modern Phys. **18**, 513 (1946).
[22] Katcoff, Finkle, and Sugarman, *Radiochemical Studies: The Fission Products* (McGraw-Hill Book Company, Inc., New York, 1950), Paper No. 59, National Nuclear Energy Series, Plutonium Project Record, Vol **9**, Div. IV.

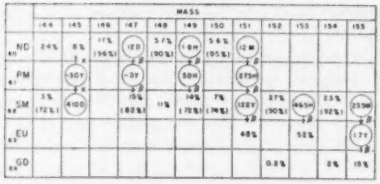

FIG. 6. The radioisotopes from neutron bombardment of neodymium and samarium (enriched by isotope percentages are given in parentheses).

directly under those for the natural abundance. Three neutron-induced neodymium activities are observed.

Nd^{147}

Earlier work on neodymium established[23,24] a 11–12 day activity in neodymium 147 which decayed through three competing beta-branches of 825,600, and 380 kev, each followed by gamma-emission. The energies of the gamma-rays were reported as 91, 309–320, and 520–534 kev; an additional gamma-ray of about 391 kev was also measured, but its association with this activity was not certain. Since the photoelectron spectrum has been thoroughly examined in previous studies, only the internal conversion spectrum is discussed now. In addition to the electron lines for the three strong gamma-rays, many weaker lines shown in Table I are definitely associated with the 11.9-day activity. The accurate spectragraphical determination of the energies of the gamma-rays eliminates the possibility of the sum of the 91.2- and 318.1-kev gamma-rays being equal to the energy of the 398.4-kev gamma-ray, as previously suggested. Besides the coincidences observed between the three strong gamma-rays and the three known beta-rays, weak gamma-gamma coincidences are observed between the 91.2-kev gamma-ray and a gamma-ray of higher energy of about 300–500 kev, which is presumably the newly discovered 441-kev transition. A K/L ratio of 4.9 ± 0.5 for the 91.2-kev gamma-ray agrees within experimental error with a value of 6.5 ± 1.5 reported by Kondaiah. This gamma-ray appears to be a mixture of $E2$ and $M1$ radiation from the measurements. The 532.3-kev gamma-ray is an $E2$ transition on the basis of its K/L ratio of 5.7 ± 1.4. An approximate computation[25] of the log(ft) values for the beta-transitions indicates[26] a change in parity for each of the three known beta-rays. An energy level scheme for prometheum 147 which incorporates all of the observed beta- and gamma-rays, together with the results of coincidence measurements and K/L ratio determinations, is shown in Fig. 7. Two additional unresolved beta-rays are shown in dotted lines to complete the scheme.

Nd^{149}

A 1.7-to 2.0-hour activity was assigned[24] to Nd^{149}. A 1.5-Mev beta-ray and some evidence of low energy gamma-radiation was observed.[27,28] It is now found that at least 14 gamma-rays are associated with this activity. The 114.1- and 240.0-kev gamma-rays are highly converted, whereas the 423.5-, 538-, and 650-kev gamma-rays show little or no internal conversion and are observed only by photoelectron techniques and by scintillation spectrometer studies. Coincidence measurements show that beta-rays of 0.95, 1.1, and 1.5 Mev are followed by gamma-rays of 650, 210–266, and 114 kev, respectively. At least two of the 210-, 240-, and 266-kev gamma-rays are in coincidence with each other, and one gamma-ray from this group is in coincidence with the 114-kev gamma-ray. The energy level scheme shown in Fig. 8 for prometheum 149 presents these results, together with those obtained from determinations of a few K/L ratios.

Nd^{151}

A 12-minute activity produced by neutron bombardment of neodymium was previously associated[28,29] with

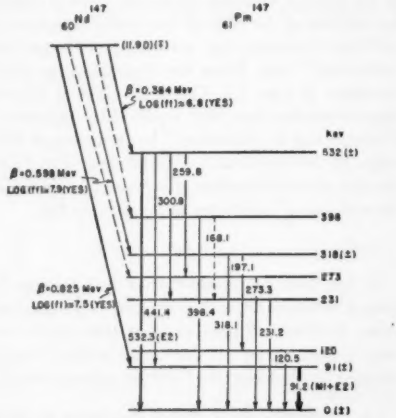

FIG. 7. Proposed energy level scheme for $_{61}Pm^{147}$.

[23] Law, Pool, Kurbatov, and Quill, Phys. Rev. **59**, 936 (1941); C. Muehlhause, Plutonium Project Report, CP-**3750**, 48 (1947); Marinsky, Glendenin, and Coryell, J. Am. Chem. Soc. **69**, 2781 (1947); Cork, Shreffler, and Fowler, Phys. Rev. **74**, 240 (1948); C. Mandeville and E. Shapiro, Phys. Rev. **79**, 391 (1950); E. Kondaiah and K. Siegbahn, Phys. Rev. **81**, 1056 (1951); W. Emmerich and J. Kurbatov, Phys. Rev. **81**, 1062 (1951).

[24] W. Bothe, Z. Naturforsch. **1**, 179 (1946).

[25] S. Moszkowski, Phys. Rev. **82**, 35 (1951).

[26] L. Nordheim, Phys. Rev. **75**, 1894 (1949), **78**, 294 (1950); E. Feenberg and K. Hammach, Phys. Rev. **75**, 1877 (1949); Mayer, Moszkowski, and Nordheim, Argonne National Laboratory Report 4626 (1951).

[27] Marinsky, Glendenin, and Coryell, J. Am. Chem. Soc. **69**, 2781 (1947).

[28] J. A. Marinsky and L. E. Glendenin, *Radiochemical Studies: The Fission Products* (McGraw-Hill Book Company, Inc., New York, 1950), Paper No. 194, National Nuclear Energy Series, Plutonium Project Record, Vol. **9**, Div. IV.

[29] B. Ketelle, Oak Ridge National Laboratory May Quarterly Report (1949).

either Nd^{151} or Pm^{151}. It was known to decay by emitting a beta-ray of 1.9 Mev, followed by a gamma-ray of about 1 Mev. This activity is now assigned[30] to Nd^{151} on the basis of prometheum *K-L-M* work function differences of two low energy gamma-rays, and of prometheum *K*-x-rays. In addition to several low energy gamma-rays which are observed by internal conversion studies, two gamma-rays of higher energy are resolved with a scintillation spectrometer. No energy level scheme is presented, although the beta-ray is in coincidence with one or more gamma-rays having an energy of about 100 kev and the gamma-ray of 1140 kev. This high energy gamma-ray appears to be in coincidence with the low energy group, and it is probably the cross-over transition for gamma-rays of 421.5 and 725 kev.

C. Prometheum

Since no stable forms of prometheum exist in nature, its radioactive nuclei are produced as daughter products. Two of these that are studied in this investigation result from the bombardment of neodymium with thermal neutrons. One activity is observed that was not previously known.

Pm^{149}

A 47–49-hour activity caused by Pm^{149} was reported[24,27,31] to decay via a beta-ray of about 1 Mev and a gamma-ray of about 200–250 kev. The half-life is now measured as 50.0±1.5 hours. The beta-ray has an energy of about 1.05 Mev and a log(*ft*) of 6.95, and it is thus accompanied by a change in parity. This beta-ray is in coincidence with an intense magnetic dipole gamma-ray of 284.9 kev. A second, less intense gamma-ray which is associated with the 50-hour activity is found to have an energy of 1300±200 kev by absorption measurements.

Pm^{151}

A newly discovered daughter product of Nd^{151} is found[30] to have a half-life of 27.5±1.5 hours. The assignment of this activity to Pm^{151} is based upon the facts that it is produced by bombarding enriched Nd^{150} with neutrons, and the internal conversion lines associated with the fifteen observed gamma-rays show work function differences of samarium. This agrees with the usual relationship where the half-lives of members of a radioactive chain with odd mass numbers increase successively down the chain. An average energy of 1.1 Mev is obtained for the beta-ray by absorption measurements; its log(*ft*) value is 6.8, which indicates a change in parity. Coincidence experiments show that both low and high energy gamma-rays are in coincidence with the 1.1-Mev beta-ray, but no other beta-ray is resolved. One experiment to determine the attenuation of beta-electron coincidence rates as a function of absorber thickness is done with aluminum absorbers in front of one counter and nothing in front of the other. This shows that the beta-ray is in coincidence with x-rays and with conversion electrons which correspond to prominent gamma-rays of about 100, 165, 275, 340, and 715 kev. No gamma-gamma coincidences are observed. This probably means that the 715 and 340 kev are not in coincidence. The gamma-rays of lower energy are highly converted, so that it is impossible to conclude anything further about the sequences of the gamma-rays from this type of experiment. However, additional information is obtained from an experimental arrangement of filters and Geiger counters that allows only x-rays and gamma-rays to pass into the gamma-counter, and beta-rays, conversion electrons, and gamma-rays to pass into the beta-counter. The hard components are found to be in coincidence with conversion electron groups corresponding to gamma-rays of about 65, 169, and 340 kev. No coincidences are observed between x-rays or gamma-rays and conversion electrons associated with the 715-kev gamma-ray. An energy level scheme for Sm^{151} based upon these data and results from K/L ratio determinations is shown in Fig. 9. This diagram is in good agreement with energy determinations, coincidence measurements, and changes in spin and parity indicated by the K/L ratios. An alternate scheme based primarily upon identities of mathematical sums that requires two unobserved beta-rays is shown in Fig. 10.

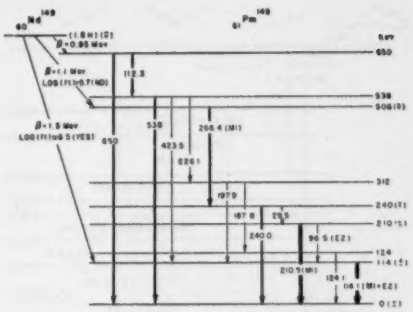

FIG. 8. Proposed energy level scheme for $_{61}Pm^{149}$.

D. Samarium

Because of the high activation cross section and presence of an europium contaminate in amounts from 0.3 to 0.6 percent in all of the enriched isotopes of samarium, the predominate electron lines of the 9-hour and 5-year europium activities are often as intense as

[30] Rutledge, Cork, and Burson, Bull. Am. Phys. Soc. **26**, No. 6, 38 (1951).

[31] B. Ketelle, Oak Ridge National Laboratory Report **229**, 34 (1948); C. Mandeville and M. Scherb, Phys. Rev. **76**, 186 (1949); J. Marinsky and L. Glendenin, *Radiochemical Studies: The Fission Products* (McGraw-Hill Book Company, Inc., New York, 1950), Paper No. 193, National Nuclear Energy Series, Plutonium Project Record, Vol. **9**, Div. IV.

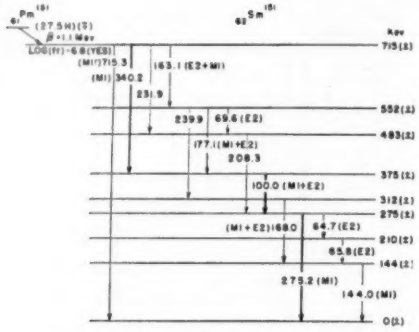

FIG. 9. Proposed energy level scheme for $_{63}Sm^{151}$.

the lines associated with the samarium activities. This contaminate prevented the observation of reliable coincidence measurements on the longer-lived activities of samarium. Four different activities are studied, and several new gamma-rays are observed. The results are summarized in Table I.

Sm^{145}

Values of the half-life of Sm^{145} have been reported[32] ranging from 60 to 410 days, with the latter value currently favored. Neither of the previously reported gamma-rays are found to be associated with this activity; that they are undoubtedly the result of an europium contaminant is known from K-L work function differences and energy values. A single gamma-ray of 61.3 kev is now observed with K-L-M work function differences of prometheum, which implies that it is emitted following K-electron capture. From the K/L *versus* Z^2/E curves, this gamma-ray with a K/L ratio of 1.0 ± 0.3 appears to be either $E1$, $M3$, or a mixture of $E2$ and $M1$. The choice of $E1$ may be ruled out by the observation[33] that in odd nuclei gamma-transitions between low-lying states appear never to be $E1$, although this is sometimes not valid in the rare earth region. Since an $M3$ transition has a measurable lifetime, the 61.3-kev gamma-ray is probably a mixture of $E2$ and $M1$ radiation.

Sm^{151}

An activity in Sm^{151} with a half-life reported[34,35] as 20 to 1000 years, and currently as 122 years, is known[35,36] to emit a soft beta-ray of about 76 kev. A single gamma-ray of 21 kev was detected[37] by a proportional counter. In the present investigation no internal conversion electrons or photoelectrons are associated with this activity. The half-life is found to be greater than 20 years.

Sm^{153}

An excited state of Sm^{153} is known[24,32,38] to decay with a half-life of 47 hours by the emission[39] of beta-rays of 680 and 800 kev followed by gamma-radiation reported[40] as 69.5, 102 to 110, and 570 to 610 kev. It is now observed that the half-life of 46.5 ± 1 hours, and that the energies of the gamma-rays are 69.8, 103.4, and 582 kev. The K/L ratios for the more intense low energy gamma-rays are slightly lower than shown in previous results. The 69.8-kev gamma-ray appears to be an $E2$ transition on the basis of its energy and its K/L ratio of 0.29 ± 0.03. Both the K/L ratio and the conversion coefficient of the 103.4-kev gamma-ray indicate that it is probably a mixture of $M1$ and $E2$ radiation. From coincidence measurements, these two intense gamma-rays appear to be in cascade. Since the less energetic of the two radiations is also much less intense, it is assumed that the 800-kev beta-ray proceeds directly to the ground state of Eu^{153}, that the 680-kev beta-ray precedes the 103.4-kev gamma-ray, and that another unresolved beta-ray is followed by the 69.8-kev gamma-ray. No definite coincidences are established between the very weak high energy gamma-ray and other radiations.

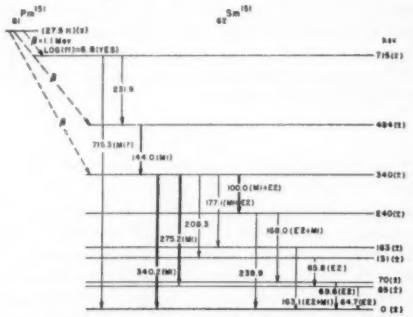

FIG. 10. An alternate level scheme for $_{63}Sm^{151}$.

[32] Kurbatov, MacDonald, Pool, and Quill, Phys. Rev. **61**, 106 (1942); Inghram, Hayden, and Hess, Phys. Rev. **71**, 643 (1947); Cork, Shreffler, and Fowler, Phys. Rev. **74**, 240 (1948); F. Butement, Nature **167**, 400 (1951).

[33] M. Mayer, Phys. Rev. **78**, 16 (1950).

[34] Parker, Lantz, Ruch, and Hebert, Oak Ridge National Laboratory Report 65, 105, and Atomic Energy Commission Declassified Report 2160 (1948).

[35] B. Ketelle and G. Parker, Phys. Rev. **76**, 1416 (1949); J. Marinski, thesis, MIT, and Progress Report Laboratory Nuclear Science Engineering July (1949); M. Inghram, *et al.*, Atomic Energy Commission Declassified Report 2759 (1950).

[36] H. Agnew, Phys. Rev. **77**, 655 (1950).

[37] Scharff-Goldhaber, der Mateosian, McKeown, and Sunyar, Phys. Rev. **78**, 325 (1950).

[38] L. Winsberg, *Radiochemical Studies: The Fission Products* (McGraw-Hill Book Company, Inc., New York, 1950), Paper No. 195, National Nuclear Energy Series, Plutonium Project Record, Vol. **9**, Div. IV.

[39] J. Hill and L. Shepherd, Proc. Phys. Soc. (London) **A63**, 126 (1950).

[40] L. Miller and L. Curtiss, Phys. Rev. **70**, 983 (1946); R. Hill, Phys. Rev. **74**, 78 (1948); S. Burson and C. Muehlhause, Phys. Rev. **74**, 1264 (1948).

Sm^{155}

A short-lived activity in samarium of 21–25 minutes half-life was first assigned[41] to Sm^{155} by Pool. It was found[42] by absorption techniques to decay via a beta-ray of 1.8–1.9 Mev and a gamma-ray of 300 kev. The value of 1.8 Mev for the energy of the beta-ray is confirmed in this study. This determination, together with a measured half-life of 23.5±0.4 minutes, enables one to compute its log(ft), as 6.0, which implies a change in parity. Two gamma-rays of equal intensity of 104.6 and 245.8 kev are measured on the internal conversion electron and photoelectron spectrograms. A K/L ratio of 3.6±1.0 for the 104.7-kev gamma-ray implies that it is probably a mixture of $E2$ and $M1$ radiations. The relatively high beta-background prevents an accurate determination of the K/L ratio for the gamma-ray of higher energy, but it is estimated as 8. Because of the fact that this activity is much shorter-lived than the 9-hour europium contaminate, it is possible to make reliable coincidence measurements. These measurements show that the 1.8-Mev beta-ray is in coincidence with x-rays and each of the gamma-rays, which are in coincidence with each other. These data are used to construct the energy level scheme for Eu^{155}, as shown in Fig. 11.

FIG. 11. Proposed energy level scheme for $_{64}Gd^{155}$ and $_{63}Eu^{155}$.

E. Some Additional Radioactivities

In the study of short-lived activities, four miscellaneous radioactive emitters are also examined. The information that is obtained is summarized in Table I.

Eu^{155}

The daughter product of 23.5-minute Sm^{155} is known[43] to be a long-lived radioactive nucleus, Eu^{155}. Two beta-rays of 0.15 and 0.24 Mev and two gamma-rays of 85 and 100 kev have been associated[35,44] with this activity. It is now found that the half life is 1.7±0.2 years, and that two weak gamma-rays are emitted in addition to the two intense ones. The latter are measured as 87.0 and 105.7 kev and appear to be $M1$ (or $M2$) transitions on the basis of respective K/L ratios of 8.0±2.8 and 8.3±2.8. These results are added to the previously discussed decay scheme of Sm^{155}, shown in Fig. 11.

Mo^{101}

A radioisotope of molybdenum with a half-life of 14 minutes has been ascribed[45] to mass 101. It was reported from absorption studies[46] to decay by the emission of two beta-rays of 1.0 and 1.9 to 2.2 Mev, and two gamma-rays of 900 and 150 to 300 kev. The complex beta-decay is now confirmed, and the corresponding energies are measured as 1.2 and 2.1 Mev. A low energy gamma-ray of 191.2 kev is found in the study of the internal conversion electron and photoelectron spectra emitted by this excited nucleus. Thus the previously reported values of 150 and 300 kev appear to be measurements of the same gamma-ray and not of other unconverted ones. The energy of the other gamma-ray is measured as 960 kev with the scintillation spectrometer. The K/L ratio of 6.0±2.5 indicates that the 191.2-kev gamma-ray may be interpretated as $M1$, $M2$, or $E2$ radiation. According to results reported[46] by Mihelich and Church, $M1$ transitions are converted predominantly in the L_I shell, whereas $E2$ radiation is converted predominantly in the L_{II} shell. This is confirmed in this research in all of the cases where definite assignments can be made. Since the low energy gamma-ray is converted predominantly in the L_I shell, it is assumed that it is a $M1$ transition. Coincidence measurements indicate that the high energy gamma and the low energy beta-rays are in coincidence, and that the two gamma-rays are probably in cascade. A tentative energy level scheme for Tc^{101} is proposed in Fig. 12.

Tc^{101}

This 15-minute daughter product of Mo^{101} is known[45,47] to emit a beta-ray of about 1.3 Mev, and gamma-rays of 260–300 and 560 kev. No evidence for the gamma-ray of higher energy is now found with either the magnetic spectrographs or the scintillation

[41] M. Pool and L. Quill, Phys. Rev. **53**, 437 (1938).

[42] Kurbatov, MacDonald, Pool, and Quill, Phys. Rev. **61**, 106 (1942); L. Winsberg, *Radiochemical Studies: The Fission Products* (McGraw-Hill Book Company, Inc., New York, 1950), Paper No. 196, National Nuclear Energy Series, Plutonium Project Record, Vol. **9**, Div. IV.

[43] Hayden, Reynolds, and Inghram, Phys. Rev. **75**, 1500 (1949); L. Winsberg, *Radiochemical Studies: The Fission Products* (McGraw-Hill Book Company, Inc., New York, 1950), Paper No. 199, National Nuclear Energy Series, Plutonium Project Record, Vol. **9**, Div. IV.

[44] B. Ketelle, Oak Ridge National Laboratory Report 607, 50 (1950).

[45] Sagane, Kojima, Mujamoto, and Ikawa, Phys. Rev. **57**, 1179 (1940); W. Maurer and W. Ramm, Naturwiss. **29**, 368 (1941), Z. Physik **119**, 339 (1942); O. Hahn and F. Strassmann, Naturwiss. **30**, 324 (1942); E. der Mateosian, Phys. Rev. **83**, 223 (1951).

[46] J. Mihelich and E. Church, Phys. Rev. **85**, 733 (1951).

[47] M. Perlman and G. Friedlander, Phys. Rev. **74**, 442 (1948); Mack, Waddel, Fagg, and Tobin, Phys. Rev. **74**, 1536 (1948); G. Boyd and B. Ketelle, Phys. Rev. **83**, 216 (1951).

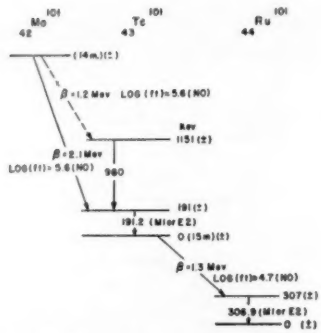

FIG. 12. Proposed energy level scheme for $_{44}Ru^{101}$ and $_{43}Tc^{101}$.

spectrometer. A single gamma-ray of 306.9 kev is found in the study of the internal conversion electron and photoelectron spectra. High coincidence rates are obtained between the beta-ray and this intense gamma-ray. The K/L ratio of 6.3 ± 3.0 implies that the gamma-ray may be interpretated as $M1$, $M2$, or $E2$. Since it is predominantly converted in the L_I shell, it is probably an $M1$ transition on the basis of the argument given for Mo^{101}. The probable energy levels in Ru^{101} are also shown in Fig. 12.

Th^{233}

In a study of Th^{233}, a beta-ray of 1.23 Mev that decays with a 23.6 ± 0.6-minute half-life is measured. These results agree with previously reported data.[48] No gamma-rays are associated with this activity.

CONCLUSIONS

It is possible to obtain the K/L ratios for many prominent gamma-rays to an accuracy of ±10 percent, after correcting the observed electron line intensities for attenuation due to the geometry of the camera and for the energy sensitivity of the photographic emulsion. This method is probably the best means of obtaining K/L ratios of gamma-rays that are associated with short half-lives. Where check points are possible, the experimental results agree closely with the recently published curves of Goldhaber and Sunyar of K/L ratios for gamma-radiation of a specific type. Also, in a comparison of the results of the photographic method with those of a constant radius beta-spectrometer using a G-M counter for the detector, excellent agreement is obtained.

In general, the predominant internal conversion of $M1$ and $E2$ transitions occurs in the L_I and L_{II} subshells, respectively. This is in agreement with the recently proposed rules of Mihelich and Church. Only one exception is noted; a transition associated with the decay of Sm^{153} appears to be converted mostly in the L_I shell and is assumed to be electric quadrupole radiation on the basis of its energy and K/L ratio. It is also observed that all of the $E3$ transitions are predominantly converted in the L_I shell in this work. A further confirmation of the fact that $M1$ transitions are converted predominantly in L_I shell is that the theoretical K/L_I ratios for $M1$ transitions at various values of Z^2/E are nearly identical to the corresponding K/L ratios given by Goldhaber and Sunyar, the theoretical K/L_I ratios being computed from the relativistic K conversion coefficients of Rose, *et al.*[49] and the L_I coefficients of Gellman, *et al.*[50] for $M1$ radiation.

ACKNOWLEDGMENTS

This investigation was carried out by the Argonne National Laboratory in conjunction with the University of Michigan as a part of the university participating program sponsored by the Laboratory. The beta-ray spectrographs which were used were constructed at the University of Michigan with support from the AEC and ONR; they were then brought to the Argonne National Laboratory for the purpose of carrying out the present program. All of the other facilities that were used in this work were made available by the Argonne National Laboratory. The work was done in partial fulfillment of the requirements for a doctor's degree at the University of Michigan by W. C. Rutledge,[51] under the supervision of Professor J. M. Cork, University of Michigan consultant to Argonne National Laboratory, and Dr. S. B. Burson, of the Argonne National Laboratory.

It is a pleasure to express our appreciation of the many courtesies extended by Dr. J. C. Boyce, Dr. H. B. Keller, Dr. W. H. McCorkle, Dr. S. A. Moszkowski, Dr. C. O. Muehlhause, Dr. L. A. Turner, and others of the Argonne staff. We are especially indebted to Dr. B. Hamermesh for his enthusiastic cooperation in searching for and measuring weak gamma-ray transitions with a scintillation spectrometer. We also wish to thank Dr. F. Tomkins and Mr. J. Brody of the Chemistry Division of the Argonne National Laboratory for the use of a recording photodensitometer. All of the enriched isotopes were prepared by the Isotope Division at the Oak Ridge National Laboratory. An especially purified sample of thorium oxide was obtained from Dr. Pappas of the Chemistry Division of the Argonne National Laboratory.

[48] Grosse, Booth, and Dunning, Phys. Rev. **59**, 322 (1941); Seaborg, Gofman, and Stoughton, Plutonium Project Report, CN-126 (1942), Phys. Rev. **71**, 378 (1947); Bunker, Langer, and Moffat, Phys. Rev. **80**, 468 (1950).

[49] Rose, Goertzel, Spinrad, Harr, and Strong, Phys. Rev. **83**, 79 (1951).

[50] Gellman, Griffith, and Stanley, Phys. Rev. **80**, 866 (1950).

[51] Phoenix Project Fellow, University of Michigan (1950–1951), now at Philips Laboratories, Inc., Irvington-on-Hudson, New York.

Critical Shear Stresses in Body-Centered Cubic Lattices*

R. SMOLUCHOWSKI
Carnegie Institute of Technology, Pittsburgh, Pennsylvania
(Received January 14, 1952)

A consideration of the shape and of the atomic configuration of dislocations in a body-centered cubic lattice allows an estimate of the ratio of critical shear stresses on various slip planes as a function of temperature. A comparison with experimental data is satisfactory.

THEORIES of plastic deformation of crystal usually consider idealized simple cubic lattices or close-packed lattices in which dislocations move only on one slip plane. The situation in the body-centered cubic lattices is more involved. There, as has been known for some time[1] slip occurs in the close-packed direction ⟨111⟩ on {110}, {112}, or {123} planes. However, little attempt has been made to elucidate the controlling factors, the influences of temperature, composition,[2] etc. Recently Opinsky and the author[3] have shown that the index of the active slip plane is strongly dependent on the orientation of the crystal and that, if the critical shear stresses on the {112} and {123} planes are, respectively, 16 and 13 percent higher than on the {110} planes, then only the latter will be active in slip. In several instances it has been possible to determine,[4] from the available data, the relative values of the critical shear stresses S_{hkl} as summarized in Table I.

The purpose of this paper is to suggest an explanation of these observations.

Since slip on {110}, {112}, and {123} planes occurs always in the ⟨111⟩ directions, the distance between consecutive equilibrium positions of the moving dislocation is always the same and is equal to the distance between nearest neighbors d. Also the shear modulus G can be considered in one direction only, and thus its anisotropy does not play a role. On the other hand the "front" of the dislocation, that is its projection on the (111) plane, is different in each case as shown in Fig. 1. In this picture the boundary of the incomplete layer of atoms, i.e., the dislocation, consists of a sequence of atoms separated by not more than the lattice constant a. A comparison of these dislocations permits a rough estimate of the relative values of the critical shear stresses if it is assumed that the shear is proportional to the ratio of the length of a dislocation to the length of its projection on the slip plane. Figure 1 gives for the shears necessary on {110}, {112}, and {123} the relative values 1, $2/\sqrt{3}$ and $3/\sqrt{7}$ or 1, 1.16, and 1.13, respectively. This indicates that at absolute zero only the {110} planes would act as slip planes.

The temperature variation of the critical shear stresses has been considered in detail by Kochendörfer[5] and can be expressed by

$$S_T = S_0[1-\{(kT/A)\log\alpha d\}^{\frac{1}{2}}], \quad (1)$$

where α is a constant and A plays the role of an activation energy. From experimental data for several metals, including the body-centered tungsten, Kochendörfer obtained $\log\alpha d$ equal to about 30 and A/k to about 25,000. In order to evaluate A we can use an approximation employed by Nabarro,[6] in which the cohesive energy is expressed as Bz^2 and the repulsive forces have a potential proportional to $\exp(-\beta r^2)$, where z is the distance between slip planes and r is the distance from the center of an atom. For a simple model of close-packed atoms one obtains for the energy per atom,

$$W = B(z^2+1/\beta),$$

where only interactions between nearest neighbors are considered. In this expression z corresponds to equilibrium distance between slip planes of atoms at various stages of slip. In particular, for a normal crystal we have $W_N = B(z_N^2+1/\beta)$ and for a dislocated crystal $W_D = B(z_D^2+1/\beta)$. The difference,

$$W_D - W_N = B(z_D^2 - z_N^2) = Bu, \quad (2)$$

is assumed to be the activation energy A for a body-centered lattice.

The interplanar distance in the normal crystal, z_N, is given by $a/(h^2+k^2+l^2)^{\frac{1}{2}}$. Its increase at a dislocation, i.e., $z_D - z_N$, can be roughly estimated by treating the atoms as hard spheres. For slip on a {110} plane there are three kinds of atoms to consider (Fig. 1),

TABLE I. Relative values of critical shear stresses.

		S_{110}	S_{112}	S_{123}
Cu Zn (β)	293°K	1.00		1.05
Fe	293°K	≥1.00	1.00	0.99
Fe+6.4 atomic % Si	133°K	1.00	≥1.16	≥1.13
	293°K	1.00	1.08	1.07
	463°K	1.00	1.07	1.06

* This research was supported by the AEC.
[1] Barrett, Ansel, and Mehl, Trans. Am. Soc. Metals **25**, 702 (1937).
[2] R. Smoluchowski, Physica **15**, 179 (1949).
[3] A. Opinsky and R. Smoluchowski, J. Appl. Phys. **22**, 1380 (1951).
[4] A. Opinsky and R. Smoluchowski, J. Appl. Phys. **22**, 1488 (1951).
[5] A. Kochendörfer, *Plastische Eigenschaften von Kristallen* (Verlag Julius Springer, Berlin, Germany, 1941).
[6] F. R. N. Nabarro, Proc. Phys. Soc. (London) **59**, 256 (1947).

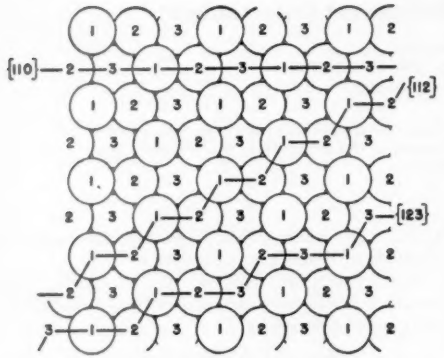

FIG. 1. The (111) plane of a body-centered cubic lattice and the traces of the three types of slip planes.

and their respective displacements from equilibrium positions during motion are $(3-2\sqrt{2})/4$, $(3-2\sqrt{2})/4$ and $(\sqrt{7}-\sqrt{6})\sqrt{3}/6$, giving an average $\Delta=0.047$ in terms of the lattice constant a. For the two kinds of atoms in the {112} plane, one obtains correspondingly $(3-\sqrt{6})/6$ and $(3\sqrt{3}-2\sqrt{6})/6$ with an average $\Delta=0.071$. These lead to $u_{110}=0.068$ and $u_{112}=0.063$, which now have to be inserted into (1) and (2). In order to reproduce the constants obtained by Kochendörfer we put $B/k=400{,}000$, which results in

$$S_T=S_0(1-0.0087T^{\frac{1}{2}}u^{-\frac{1}{4}}). \tag{3}$$

Figure 2 shows the plot of the ratio of the critical shear stresses calculated by means of Eq. (3) assuming that at absolute zero $S_{112}=1.16S_{110}$ as explained previously. A similar calculation for the {123} plane involves displacements of nine kinds of atoms. Some of these cannot be evaluated without ambiguity and so the corresponding ratios have not been computed.

The agreement between theory and the experimental points[3] for iron-silicon alloys, as indicated in Fig. 2, is fair. The experimental points should, in general, lie above the theoretical curve because of the presence of silicon, as explained tentatively below. It should be pointed out that the assumption of a dislocation model is essential in this calculation. Had one used instead the notion of a simultaneous slip of the whole plane, then the atomic configurations and displacements of atoms in the slip plane would be different and the calculated ratios of the shear stresses would be in obvious disagreement with experiment. For instance, a simultaneous slip on the {110} plane leads to a higher u and to a correspondingly more rapid drop of the theoretical curve S_{112}/S_{110}, as indicated in Fig. 2 by the dashed line.

An addition of more than 7.5 atomic percent silicon to iron eliminates slip on {112} and {123} planes. An interpretation of this strong influence of silicon on the ratio of critical stresses in iron, can perhaps be obtained in the following manner: A silicon atom is smaller than an iron atom, and thus its presence at a dislocation decreases locally the displacement Δ by a certain amount. Since Δ_{112} is about 50 percent greater than Δ_{110}, the decrease of Δ is relatively larger for slip on the {110} plane than on the {112} plane. This leads to an increase of u_{112} with respect to u_{110} and thus to an increase of the ratio of S_{112} to S_{110} in accord with experiment. It should be stressed that this argument is not based on the gradual decrease of the lattice constant of iron with increasing silicon concentration. The absolute value of the lattice constant does not affect the calculation of the ratios of critical shear stresses.

Andrade[7] has indicated that for body-centered cubic metals there exists a relationship between the index of the plane active in slip and temperature, measured in terms of the melting point T_m as shown in Table II for Na, W, and K. He did not consider the role of the orientation of the tensile direction. That this simple relationship is not generally obeyed is evident from the behavior of Mo,[8,9] Fe,[1,3] Fe-Si alloys,[1,3] and β-brass.[10] Actually Andrade's results for sodium only are in disagreement with the slip mechanism here discussed. This is not surprising at all since, as is well known, in alkali metals the interaction between cores of the ions is negligible and the hard sphere approximation is not applicable. For the same reason one may expect potassium to show a behavior somewhat similar to sodium, while tungsten should be similar to the other metals.

It has often been suggested that the experimentally observed slip on {112} and {123} planes is actually a slip on alternating segments of two nonparallel {110} planes. For certain orientation of the tensile axis this possibility may be particularly plausible, especially if the lattice is highly imperfect. It may be possible to

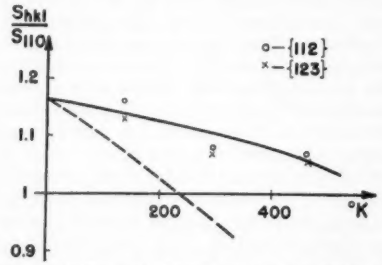

FIG. 2. Calculated and observed ratios of the critical shear stresses on various slip planes as a function of temperature (full line-dislocation model, dotted line-simultaneous slip).

[7] E. N. da C. Andrade, Proc. Phys. Soc. (London) **52**, 1 (1940).
[8] L. C. Tsien and Y. S. Chow, Proc. Roy. Soc. (London) **A163**, 19 (1937).
[9] N. K. Chen and R. Maddin, Trans. Am. Inst. Met. Eng. **191**, 937 (1951).
[10] G. I. Taylor, Proc. Roy. Soc. (London) **A118**, 1 (1928).

distinguish between the two possibilities in the following way: According to the model here used, the temperature dependence of slip is controlled by the activation energy A, which in turn depends on the average displacement Δ_{hkl}. The latter is obtained by averaging the displacements for atoms in various nonequivalent positions along a dislocation. For instance, for slip on the {112} planes there are two kinds of positions to be taken into account. If on the other hand the active "112" plane were composed of segments of {110} planes, several atoms wide, then other kinds of positions would have to be considered and the average displacement would be different. This would lead to a different value of A and a different temperature dependence of the critical shear stress. The available experimental data do not permit drawing definite quantitative conclusions about this aspect of slip in various metals.

Another important factor which may affect the nature of the slip plane has been pointed out by Calnan and Clews.[11] They suggest that in alloys a variation of local concentration may lead to a variation of the ratio of the local critical shear stresses and produce a wavy slip "plane" composed of segments of various active planes. This may occur even in perfectly random alloys[12] near compositions which separate regions of different slip systems.

TABLE II. Slip planes in body-centered cubic metals.

T/T_m	Na	K	W	Mo	Fe[a]	Fe-Si[b]	β-Cu Zn
0.08–0.24	112	?	112	110 112 123	110 112 123	110	?
0.26–0.50	110	?	?	?	110 112 123	110	110 123
0.80	123	123	?	?	?	110	?

[a] At temperatures lower than $0.08T_m$ only the [110] plane is active in iron and in iron-silicon alloys with less than 7.5 atomic percent silicon.
[b] More than 7.5 atomic percent silicon.

[11] E. A. Calnan and C. J. B. Clews, Phil. Mag. **42**, 616 (1951).

[12] R. Smoluchowski, Phys. Rev. **84**, 511 (1951).

Letters to the Editor

PUBLICATION of brief reports of important discoveries in physics may be secured by addressing them to this department. The closing date for this department is five weeks prior to the date of issue. No proof will be sent to the authors. The Board of Editors does not hold itself responsible for the opinions expressed by the correspondents. Communications should not exceed 600 words in length and should be submitted in duplicate.

The Parities of the Ground States of N^{14} and C^{14}†

D. A. BROMLEY AND L. M. GOLDMAN
Physics Department, University of Rochester, Rochester, New York
(Received April 15, 1952)

IN view of the well-known difficulty in reconciling the apparently allowed shape and second forbidden lifetime of the C^{14}, N^{14} beta-decay with theory, we considered that it would be of interest to determine whether or not a parity change exists. We have carried out experiments based on the stripping theory of Butler[1] to determine the relative parities of N^{14} and C^{14}.

Using 4-Mev deuterons from the Rochester 26-inch cyclotron we have examined the angular distribution of the neutrons from the $C^{13}(d, n)N^{14}$ reaction and the distribution of the protons from the $C^{13}(d, p)C^{14}$ reaction. The neutrons were detected by use of a cylindrical ionization chamber filled with helium at 20-atmospheres pressure, and the protons were detected by use of a sodium iodide crystal with a 1P21 photomultiplier. At each angle the amplified detector outputs were analyzed by a 30-channel pulse-height discriminator to give pulse-height spectra.

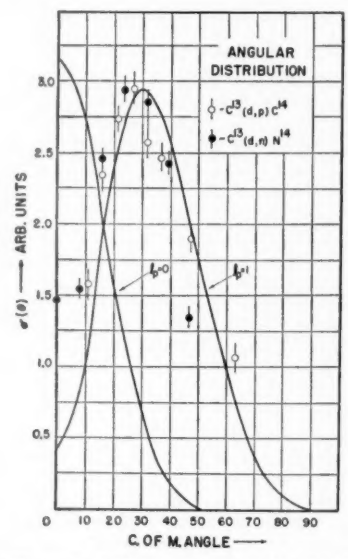

FIG. 1. The angular distribution of the neutrons from the $C^{13}(d, n)N^{14}$ reaction and the angular distribution of the protons from the $C^{13}(d, p)C^{14}$ reaction. The curves are the angular distributions predicted by the Butler theory corresponding to a deuteron energy of 4 Mev. l_p is the angular momentum transferred to the target nucleus by the absorbed nucleon. The angular distribution corresponding to $l_p=2$ has a maximum at about 60°; conservation of spin and parity forbids this value for both of the above reactions.

Figure 1 shows that the angular distributions of the protons and neutrons are almost identical. There are minima at 0° and maxima at about 28° in the center-of-mass system. These are in very good agreement with the curve, corresponding to our energy, calculated from the Butler theory for a transition in which the absorbed nucleon transfers one unit of angular momentum to the target nucleus. This shows conclusively that the parities of the N^{14} and C^{14} ground states are the same. Hence, it is no longer possible to invoke a parity change in the explanation of the C^{14}, N^{14} beta-decay.

We have confirmed the previous measurement[2] of the relative parities of the C^{13} and C^{12} ground states using the $C^{12}(d, p)C^{13}$ reaction. Consequently, we have shown that the parities of the ground states of N^{14} and C^{14} are the same as that of the C^{12} ground state, which we assume to be even.

A detailed description of the work will be submitted for publication at a later date. We are indebted to Professor H. W. Fulbright for suggesting the problem and for his continued interest and suggestions.

† This work assisted by the AEC.
[1] S. T. Butler, Proc. Roy. Soc. (London) **A208**, 559 (1951).
[2] J. Rotblat *et al.* as quoted in reference 1.

Rotational Temperatures of Vegard-Kaplan Auroral Bands*

W. PETRIE
Physics Department, University of Saskatchewan, Saskatoon, Saskatchewan, Canada
(Now at Radio Physics Laboratory, Defense Research Board, Ottawa.)
(Received April 21, 1952)

CONFLICTING data exist regarding one of the more important physical properties of the earth's upper atmosphere, namely, the temperature. The particle density at the 220-km level indicates that the temperature is of the order of 1000°K, whereas the numerous investigations by Vegard of the rotational structure of auroral N_2^+ bands yield temperatures of around 350°K at perhaps the 200-km level. Recent summaries of the temperature problem have been given by Bates[1] and Gerson.[2]

Although the N_2^+ bands arise from permitted transitions, there is no apparent reason why the rotational structure should not yield a true temperature. Nevertheless, bands from forbidden transitions should give a more reliable value for the temperature of the region from which the emissions arise. A number of $^1\Sigma_g^+ - {}^1\Sigma_u^+$ Vegard-Kaplan N_2 bands have been photographed in the spectra of several intense auroral displays. The grating spectrograph was used in the third order, giving a dispersion of 28 A/mm. These bands have considerable widths; for example, the (1, 11) and (2, 12) bands with heads at λλ3683, 3767 are each about 25 angstroms wide. The rotational structure can be seen, and it is possible to estimate the position of the strongest line on the P branch.

The intensity of a rotational line may be written as $I=cv^4S \times\exp[-B_{v'}K'(K'+1)hc/kT]$. Since the P and ^PQ lines overlap, the "line strength" factor S in the above equation must be the sum of the two branches. According to Schlapp[3] the value of S is $(K+3/2)$, K referring to the lower $^1\Sigma$ state. If we form the derivative dI/dK', equate to zero, and solve for the K' value at which I is a maximum, then $T=1.44B_{v'}(2K'+1)(K'+5/2)$. The formula for the lines of the P branch of the (1, 11) band is $\nu-\nu_0 = -3.228K-0.374K^2$. The writer judges that the distance from the zero gap to the maximum of the P branch is 14 angstroms, or 103 cm^{-1}. From the above formula the corresponding K value is 13; hence $K'=12$. Substituting in the temperature formula yields a value of approximately 750°K. The mean temperature derived from five V-K bands in the wavelength range λλ3400–3800 is 850°K.

Several of the V-K bands are bordered to the red by 2P.G. bands. The writer has judged the maximum of the (1, 11) V-K band to be well away from the position of the (2, 4) 2P.G. band in order to avoid overlapping. For this reason, the temperature quoted may well be a minimum value. In view of this result, it is important that the rotational structures of both the V-K and N_2^+N.G. bands be examined with higher dispersion, and spectrographs now under construction should give adequate spectra. A decision regarding the temperature may then be reached.

The writer wishes to thank Dr. A. V. Jones for discussion on rotational temperatures.

* This work has been supported by contract with the Geophysics Research Division, Air Forces Cambridge Research Centre.

[1] D. R. Bates, Monthly Notices, Royal Astron. Soc. **109**, 215 (1949).
[2] N. C. Gerson, Rep. Prog. Phys. **14**, 316 (1951).
[3] R. Schlapp, Phys. Rev. **51**, 342 (1937).

Nuclear Emulsion and Scintillation Crystal Processes

J. B. Birks
Physics Department, Rhodes University, Grahamstown, South Africa
(Received April 17, 1952)

THERE is a close analogy between the observation of an ionizing particle by a nuclear emulsion and by a scintillation crystal. In each case the particle energy is dissipated in molecular excitation and ionization in condensed matter, but the observed effect is a secondary process, not in general proportional to the specific energy loss dE/dr. For a nuclear emulsion the photographic action can be expressed quantitatively in terms of the specific grain density dG/dr, and for a scintillation crystal the light output can be expressed in terms of the specific fluorescence dS/dr.[1]

Fowler[2] and Bradt and Peters[3] have observed that dG/dr is a nonlinear function of dE/dr. Typical experimental results[3] for an *NTB* 3 emulsion are plotted in Fig. 1. The form of this curve is similar to that observed by the author[1] and Taylor *et al.*[4] for the variation of dS/dr with dE/dr for an anthracene crystal. An exciton theory has been formulated[5] to account for this behavior in scintillation crystals, and the following relation has been obtained:

$$dS/dr=(AdE/dr)/(1+kBdE/dr). \quad (1)$$

This same relation, substituting dG/dr for dS/dr, is found with a suitable choice of the parameters A and kB to describe satisfactorily the behavior of nuclear emulsions. The theoretical curve from (1) is plotted in Fig. 1 and is seen to be in excellent agreement with the observations.

The relation (1) can be expressed in more general terms than those used in its original derivation. The term $A\,dE/dr$ describes the primary production by the ionizing particle of the excitons, photons, or electrons responsible for the observed secondary effect. The term $B\,dE/dr$ describes the simultaneous production of damaged molecules, ions, or other agents, which quench the excitons, photons, or electrons with a capture probability k, relative to the center (fluorescent molecule or silver bromide grain) at which the secondary effect is produced. Previous evidence favors excitons, rather than photons or electrons, as the mode of energy transfer in organic scintillation crystals. Recent work[6,7] on thin films irradiated by α-particles suggests, however, that photons of higher energy than those emitted in the fluorescence and which are strongly absorbed in the crystal may be responsible. If this is so, the mean free path of these photons in anthracene is probably that attributed previously[8] to the exciton, i.e., about 5000 molecular lengths, which is the same order of magnitude as that found in thin nylon films.[6] Conclusions about the energy transfer mechanism in photographic emulsions cannot yet be drawn, though it will probably be similar. The production of quenching agents within the emulsion by the ionizing particle is, however, definitely indicated.

This laboratory is not yet equipped for experimental work on nuclear emulsions, and it is hoped that others will follow up this aspect of the photographic mechanism. In particular, it should be of interest to investigate whether the specific grain density dG/dr decreases to one-half of the value given by (1) at the surface of the emulsion in a similar manner to the decrease of the specific fluorescence dS/dr at the surface of an organic crystal.[8] The mean free path of the exciton, photon, or electron could thus be determined.

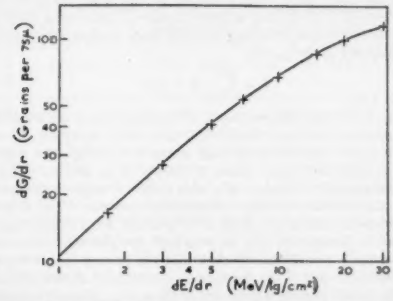

FIG. 1. Specific grain density *versus* specific energy loss. Full curve—theoretical; Crosses—experimental data.

[1] J. B. Birks, Proc. Phys. Soc. (London) **A63**, 1294 (1950).
[2] P. H. Fowler, Phil. Mag. **41**, 169 (1950).
[3] H. L. Bradt and B. Peters, Phys. Rev. **80**, 943 (1950).
[4] Taylor, Jenschke, Remley, Eby, and Kruger, Phys. Rev. **84**, 1034 (1951).
[5] J. B. Birks, Proc. Phys. Soc. (London) **A64**, 874 (1951); Phys. Rev. **84**, 364 (1951).
[6] E. W. T. Richards and J. F. I. Cole, Nature **167**, 286 (1951).
[7] P. I. Dee and E. W. T. Richards, Nature **168**, 736 (1951).
[8] J. B. Birks, Phys. Rev. **86**, 791 (1952).

The Third Forbidden Beta-Spectrum from Rb^{87}

Y. Tomozawa, M. Umezawa, and S. Nakamura
Department of Physics, Faculty of Science, Tokyo University, Tokyo, Japan
(Received December 26, 1951)

RECENTLY, it was pointed out that radiative[1] and mesonic[2] corrections did not affect the consequence of Konopinski's theory of forbidden beta-decay, such as the shape of the spectrum as well as the selection rules. Since this conclusion about the mesonic correction is obtained through consideration of invariance under rotation alone, it can be applied to the case of any

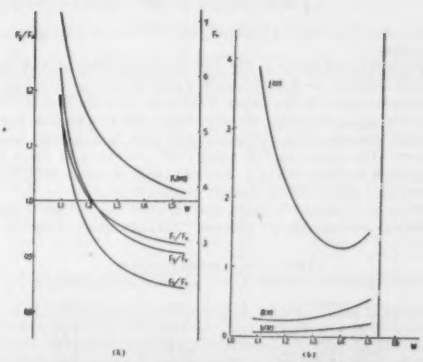

FIG. 1. (a) The functions $F_0(W, Z)$ and F_1/F_0. (b) The functions $f(W)$, $g(W)$, and $h(W)$ in C_{1T}.

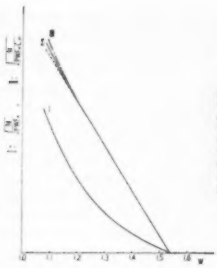

FIG. 2. Curve I is the Fermi plot of the Rb^{87} beta-spectrum. Curve II is the Fermi plot corrected by the third forbidden correction function C_{3T} for the tensor interaction in which the screening effect is taken into account. In Curve III the screening correction is not taken into account.

interaction between nucleons. These facts make us believe firmly the validity of Konopinski's forbidden theory in highly forbidden cases. Recently the Rb^{87} beta-spectrum was measured by Curran, Dixon, and Wilson,[2] and it was found to be quite different from the allowed shape.

Since the known spin and magnetic moment suggest that the configurations of Rb^{87} and Sr^{87} are $(p_{3/2})^{-1}$ and $(g_{9/2})^{-1}$, respectively, the Rb^{87} beta-decay is expected to be third forbidden with a spin change of three and a parity change.

The nT spectrum involves contributions from two matrix elements $Q_n(\beta[\boldsymbol{\sigma}\times\mathbf{r}],\mathbf{r})$ and $Q_n(\beta\boldsymbol{\alpha},\mathbf{r})$, and also from the matrix element $Q_{n+1}(\beta\boldsymbol{\sigma},\mathbf{r})$, but a rough estimate shows that the contribution from the matrix element $Q_{n+1}(\beta\boldsymbol{\sigma},\mathbf{r})$ is comparatively small.

Therefore, we only take into account the contributions from the matrix elements $Q_n(\beta[\boldsymbol{\sigma}\times\mathbf{r}],\mathbf{r})$ and $Q_n(\beta\boldsymbol{\alpha},\mathbf{r})$. They are, in the terminology of Greuling,[4]

$$C_{3T}=\Sigma_{ij}|Q_{ij}(\beta[\boldsymbol{\sigma}\times\mathbf{r}],\mathbf{r})/3!|^2 f(W) -\Sigma_{ij}[|Q_{ij}(\beta[\boldsymbol{\sigma}\times\mathbf{r}],\mathbf{r})/3!|Q_{ij}^*(\beta\boldsymbol{\sigma},\mathbf{r})/3!+\text{c.c.}]g(W) +\Sigma_{ij}|Q_{ij}(\beta\boldsymbol{\alpha},\mathbf{r})/3!|^2 h(W).$$

It was shown by Longmire and Messiah[5] that the ratio

$$\rho=Q_{ij}(\beta\boldsymbol{\alpha},\mathbf{r})/Q_{ij}(\beta[\boldsymbol{\sigma}\times\mathbf{r}],\mathbf{r})$$

is independent of M, M', i, $j\cdots$ and is real. Consequently,

$$C_{3T}=\Sigma_{ij}|Q_{ij}(\beta[\boldsymbol{\sigma}\times\mathbf{r}],\mathbf{r})/3!|^2\{f(W)-2\rho g(W)+\rho^2 h(W)\}.$$

To obtain F_0, F_n in $f(W)$, $g(W)$, and $h(W)$ which are given in Greuling's paper, we must calculate the complex Γ-function, and we calculate the latter according to Martin,[6]

$$\ln R=\ln\Gamma(x+n)-\tfrac{1}{2}y^2\psi'(x+n)+\tfrac{1}{4}!y^4\psi^{(3)}(x+n)-\cdots -\tfrac{1}{2}\ln[x^2+y^2][(x+1)^2+y^2]\cdots[(x+n-1)^2+y^2],$$

where $R=|\Gamma(x+iy)|$, n=integer, and $\psi^{(m)}(x)$ are poly-gamma functions.

The results are shown in Fig. 1. With the following ratio of the matrix elements, $\rho=4.2$, we obtain a good fit for C_{3T} to the experimental spectrum from about 100 kev to the upper limit of 275 kev (Fig. 2). In the region of energy below 100 kev we took into account the screening correction according to Longmire and Brown.[7] The values of $F(W-D_0)/F(W)$ are shown in Table I. The result is shown in Fig. 2. The slight shift in energy of 50 kev seems to be within the uncertainty of experiment.

However, it should be noted that the shift may be due to the "internal bremsstrahlung" electron.[8] The calculation of the "internal bremsstrahlung" electron correction is now in progress. The C_{3V} spectrum is different from the C_{3T} spectrum by only one small term B_n in the terminology of Greuling. As the contribution from B_n is so small, we obtain a good fit for C_{3V} to the experimental spectrum, too. On the other hand, all other matrix elements in the 1st, 2nd, and 3rd forbidden cases fail to explain the Rb^{87} spectrum.

We calculate the ft value and obtain $ft=4.2\times10^{16}$ where $t=6\times10^{10}$ yr, and the f value ($=0.77$) is obtained by graphical integration.

TABLE I. The screening correction.

Wmc^2	1.1	1.2
$F_0(W-D_0)/F_0(W)$	1.04	1.01
$F_1(W-D_0)/F_1(W)$	1.05	1.02
$F_2(W-D_0)/F_2(W)$	~1.06	1.02
$F_3(W-D_0)/F_3(W)$	~1.06	1.02

[1] E. Merzbacher, Phys. Rev. **81**, 942 (1951).
[2] Kotani, Machida, Nakamura, Takebe, Umezawa, and Yoshimura, Prog. Theoret. Phys. (to be published).
[3] Curran, Dixon, and Wilson, Phys. Rev. **84**, 151 (1951).
[4] E. Greuling, Phys. Rev. **61**, 568 (1942).
[5] C. L. Longmire and A. M. L. Messiah, Phys. Rev. **83**, 464 (1951).
[6] D. G. E. Martin, Phys. Rev. **81**, 280 (1951).
[7] C. Longmire and H. Brown, Phys. Rev. **75**, 264 (1949).
[8] J. A. Bruner, Phys. Rev. **84**, 282 (1951).

Possible Influence of κ-Mesons on the Underground Cosmic Radiation

LOUP VERLET
Laboratoire de Physique, Ecole Normale Supérieure, Paris, France

(Received April 21, 1952)

THE existence of many heavy mesons in high energy nuclear events calls for an improvement of the previous theories of the underground μ-mesons, based only on the existence of the π-meson. In fact, μ-mesons may be divided in two categories: Some μ-mesons, which we call μ_κ, come directly from heavy mesons of the κ-type;[1] the others, which we call μ_π, come from π-mesons either directly, or through heavy mesons like V^0 or τ. Since heavy mesons have great masses and short lives relative to the π-meson, these two classes may be discriminated from each other, especially by the study of the thermometric coefficient.

Underground cosmic radiation seemed to have been correctly explained in terms of μ-mesons, on the basis of a 1.7 power law integral source-spectrum for the π-mesons, competition between absorption of the π-mesons in the atmosphere and $\pi-\mu$ decay, and electromagnetic losses for the corresponding μ's.[2] However, the recent discovery of μ-meson energy losses of nuclear origin[3] seems, in spite of the experimental uncertainties, to result in too low a vertical intensity of μ-mesons at great depths.[4] The vertical intensity of μ_π's at a depth d is:

$$I_\pi=\int_{E(d)}^{\infty}E^{-\gamma-1}(I+E/B)dE,$$

with $B=Lm_\mu(\rho\tau_\pi)^{-1}\simeq140$ Bev; L=mean free path of nucleons and π-mesons, taken as 125 g/cm^2; m_μ=mass of the μ-meson $=216\ m_e$; ρ=specific weight of the air at the absorption mean height; τ_π=mean life of π-mesons in their rest system$=2.6\times10^{-8}$ sec; c=velocity of light; γ=spectrum exponent$\simeq1.7$; $E(d)$=minimum energy required from a μ-meson to reach the depth d.

On the other hand, since κ-mesons are not absorbed in the atmosphere up to very great energies, because of their mass, 1200 m_e, their short life-time and their possibly weak nuclear interaction,[5] the intensity of the μ_κ's is:

$$I_\kappa=\int_{E(d)}^{\infty}E^{-\gamma-1}dE.$$

The above relations are true if all nuclear mesons are produced according to the same power law; this power spectrum is conserved under any decay at high energies.[6] Though the experimental uncertainties are great, a mixture of μ_π and μ_κ giving a vertical intensity $I=\alpha I_\pi+\beta I_\kappa$, with $\alpha+\beta=1$, might well explain both the vertical intensity experimental curve and the angular coefficient at 1700 m.w.e., with $\beta\simeq25$ percent. Since a departure of I from I_π is expected only at such high energies where one may hope β to be a constant, we shall take the same β for all depths.

A measurement of the thermometric coefficient at two different depths should provide a good test of the $\mu_\pi-\mu_\kappa$ mixture hypothesis, because the information thus obtained is, up to a certain ex-

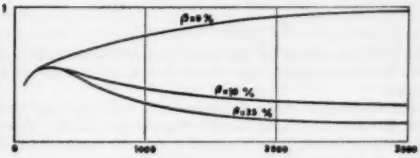

FIG. 1. $(\Delta I/I)\cdot(\Delta B/B)^{-1}$ is plotted against the depth d in m.w.e. for $\beta=0$ percent, 10 percent, 25 percent.

tent, independent of any assumptions about the energy losses of the μ's and the exponent of the power spectrum. A density change in the atmosphere produces a variation ΔB of B. Whereas I_π is not affected, I_π varies, and one has:

$$\frac{\Delta I}{I}=\alpha\frac{\Delta I_\pi}{I}=\frac{\Delta B}{B}\cdot\frac{\alpha B^{-1}\int_{E(d)}^{\infty}E^{-\gamma}(1+E/B)^{-2}dE}{\alpha I_\pi+\beta I_\kappa}$$

$$=\Gamma\frac{\Delta T}{T}\cdot\text{function of } d.$$

T is the temperature recorded at one altitude; if the atmosphere was really isothermal, the correlation coefficient Γ would be unity. If two recordings were made simultaneously at two different depths, (about 250 and 1000 m.w.e.), the term $\gamma\Delta T/T$ would disappear and the ratio $[\Delta I(250)/I(250)]/[\Delta I(1000)/I(1000)]$ would give some indications about the proportion of μ_κ's in the ground, as can be seen from Fig. 1. Since this is known, it is possible to get back to the proportion of κ-mesons *versus* π (and τ, $V^0\cdots$), provided that some assumptions on the decay of these different particles are made. One should notice that the temperature coefficient cannot exceed 0.4 percent/°C, i.e., the value for $\beta=0$, $\Gamma=1$, $d=\infty$.

[1] C. O'Cealleigh, Phil. Mag. **42**, 1032 (1951); Crussard *et al.*, Compt. rend. **234**, 84 (1952). It is not impossible that V^0 and κ-mesons are the same particle: Armenteros *et al.* (private communication).
[2] S. Hayakawa *et al.*, Prog. Theoret. Phys. **4**, 287 (1949); **4**, 447 (1949); **5**, 844 (1950).
[3] E. P. George and J. Evans, Proc. Phys. Soc. (London) **A63**, 1248 (1950); Braddick, Nash, and Wolfendale, Phil. Mag. **42**, 1277 (1951).
[4] G. Wataghin and C. M. Garelli, Phys. Rev. **79**, 718 (1950).
[5] L. Michel and R. Stora, Compt. rend. **234**, 1257 (1952).
[6] A. Daudin, J. Phys. **10**, 65 (1949).

A Ferroelectric Ammonium Metaphosphate*

R. PEPINSKY, C. M. MCCARTY, E. ZEMYAN, AND K. DRENCK
Department of Physics, The Pennsylvania State College, State College, Pennsylvania
(Received April 22, 1952)

AMMONIUM phosphate prepared by the method of Tammann[1] is found to be ferroelectric in the range from −193 to +38°C. Conductivity obscures the ferroelectric hysteresis loop above 38°C, although the dielectric constant appears to climb fairly rapidly in the neighborhood of that temperature. No measurements were made below −193°C. The crystal is unstable in a dry atmosphere at room temperature, and must be stored near 0°C.

X-ray measurements demonstrate that the crystal has a monoclinic cell with $a=19.9$Å, $b=6.91$A, $c=6.28$A, $\beta=98.5°$, space-group C_2 or Cm; and morphology indicates C_2. The density is 1.577 g/cm³. Although Tammann identified the compound as a monometa salt with 3 or 4 H_2O per molecule, a chemical analysis indicates between 5 and 6 H_2O, and x-ray and density measurements show 6 H_2O. The chemistry of the "metaphosphates" is unclear in general, and the precise nature of the compound must apparently await completion of the x-ray structure analysis now in progress. A Patterson projection on (001) indicates the existence of P_2O_6 groups.

* Research supported by OAR.
[1] G. Tammann, J. prak. Chem. **45**, 431 (1892).

Angular Distribution of Pions Scattered by Hydrogen*

H. L. ANDERSON, E. FERMI, D. E. NAGLE, AND G. B. YODH
Institute for Nuclear Studies, University of Chicago, Chicago, Illinois
(Received April 14, 1952)

THE angular distribution of the pions scattered by liquid hydrogen has been studied using the well collimated pion beams of the Chicago synchrocyclotron. A pair of 2-inch diameter scintillation counters define the incident beam which passes through them into a liquid hydrogen cell (Fig. 1). The scattered

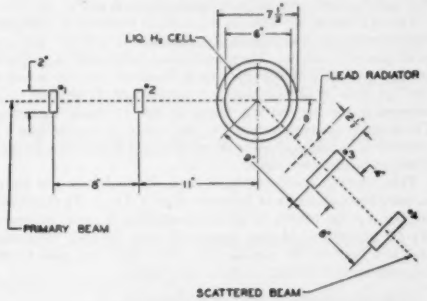

FIG. 1. Experimental arrangement.

particles are detected by two 4-inch diameter scintillation counters at suitable azimuth. A quadruple coincidence of all four counters requires a particle to pass through the first two counters and then to be scattered into the second pair. The quadruple coincidence rate, divided by the double coincidence rate of the first pair, which is recorded at the same time, gives the fraction of the beam which is scattered. The hydrogen cell was designed for rapid insertion and removal of the liquid hydrogen, to distinguish its effect from extraneous scattering. The charge exchange scattering was distinguished from the elastic scattering of negative pions by the insertion of a lead radiator in front of the second pair of counters, in order to enhance their sensitivity to gamma-rays.

The elastic scattering of positive pions at 110 Mev and 135 Mev, and both charge exchange and elastic scattering of negative pions at 135 Mev, were measured. The observations were taken at laboratory angles 45°, 90° and 135°.

The results, in the center-of-mass system, have been expressed in terms of the formula:

$$d\sigma/d\omega=a+b\cos\theta+c\cos^2\theta.$$

This angular distribution is expected when only s- and p-states contribute to the scattering. The values of the coefficients with their statistical errors are presented in Table I.

TABLE I. Coefficients for the differential cross sections.

Primary energy Mev	Process	a 10^{-27} cm²/sterad	b 10^{-27} cm²/sterad	c 10^{-27} cm²/sterad	$\int(d\sigma/d\omega)d\omega$ 10^{-27} cm²
110	$\pi^+\to\pi^+$	3.5 ±0.6	−4.6 ±0.8	7.2 ±1.8	74.5 ±5.4
135	$\pi^+\to\pi^+$	3.8 ±2.2	−6.8 ±2.7	17.5 ±6.6	121 ±19
135	$\pi^-\to\pi^-$	1.2 ±0.2	−0.1 ±0.3	0.3 ±0.7	16.2 ±2.3
135	$\pi^-\to\pi^0$	1.1 ±0.6	−2.5 ±0.5	6.3 ±1.9	40.6 ±2.3

The integrated cross sections listed in Table I are in good agreement with those obtained previously[1] by transmission measurements. For negative pions the contributions of exchange and non-exchange scattering should be added, plus a small contribution of about 0.8×10^{-27} cm² due to the inverse photo effect ($\pi^-\to\gamma$).

The elastic scattering of the positive pions is pronounced in the backward direction, an indication of interference of s- and p-waves. The same is true of the charge exchange scattering of the negative pions. The elastic scattering of the negative pions, on the other hand, is approximately isotropic.

A phase shift analysis has been made on the assumption that the scattering takes place in states characterized by isotopic spin $\frac{1}{2}$ and $\frac{3}{2}$ and by angular momentum $S_{1/2}$, $P_{1/2}$ and $P_{3/2}$. The experimental data are well fitted by the following phase shift angles: At 135 Mev, $\mp 1°$, $\pm 19°$, and $\pm 1°$ for isotopic spin $\frac{1}{2}$; $\pm 25°$, $\mp 10°$, and $\mp 35°$ for isotopic spin $\frac{3}{2}$; at 110 Mev, $\pm 15°$, $0°$, and $\mp 25°$ for isotopic spin $\frac{3}{2}$. The angles are given in order for $S_{1/2}$, $P_{1/2}$ and $P_{3/2}$ and have an uncertainty of about $\pm 3°$.

The fact that at 135 Mev six phase shifts suffice to fit nine data demonstrates the fruitfulness of regarding the isotopic spin as a good quantum number. The pion-nucleon interaction is strongest in the $P_{3/2}$ state with isotopic spin $\frac{3}{2}$. However, the interaction in the $P_{1/2}$ state of isotopic spin $\frac{1}{2}$ is comparable. It appears to be responsible for the isotropy found in the π^- elastic scattering. The sizeable interaction found in the s-state of isotopic spin $\frac{3}{2}$ is believed to be responsible for the pronounced backward scattering observed in the other cases.

This research could not have been done without the active cooperation and advice of Professor Earl A. Long. We thank him and Dr. Lothar Meyer for generous supplies of liquid hydrogen. We are grateful to Messrs. Ronald Martin, Maurice Glicksman and Leo Slattery for contributing their time and skill to the preparation and conduct of these experiments.

* Research sponsored by the ONR and the AEC.

[1] H. L. Anderson, *et al.*, Phys. Rev. **83**, 936 (1952).

Scattering and Capture of Pions by Hydrogen*

H. L. Anderson and E. Fermi
Institute for Nuclear Studies, University of Chicago, Chicago, Illinois
(Received April 14, 1952)

When a negative pion comes to rest in hydrogen, it is promptly captured in a Bohr-like orbit and almost immediately reacts with the proton. As shown by Panofsky and his co-workers,[1] the reaction produces either (a) a neutron and a photon, or (b) a neutron and a neutral pion, with about equal probability. Reaction (b) is closely related to the charge exchange scattering of the negative pion by the proton. The only difference is in the energy which is positive for the scattering, but slightly negative in the Panofsky case. It is the purpose of this note to show how these two phenomena may be correlated.

The experiments, in this laboratory,[2] on the scattering of pions by protons, have been interpreted in terms of the phase shifts of the s and p waves. At low energy, the p phase shifts, which vary as the cube of the momentum, become unimportant compared to the s phase shifts, which are proportional to the momentum. The scattering length a, which is the product of the s phase shift and the de Broglie wavelength, should be constant. From the experiments, $a_{3/2}=(3.8\pm 0.7)\times 10^{-14}$ cm for the state of isotopic spin $\frac{3}{2}$ and $a_{1/2}=(0\pm 1)\times 10^{-14}$ cm for the state of isotopic spin $\frac{1}{2}$.

The cross sections for exchange and nonexchange scattering at low energy can be expressed in terms of $a_{3/2}$ and $a_{1/2}$ by standard procedures of the collision theory. One should take into account the fact that states representing a proton and a negative pion, or a neutron and a neutral pion are linear combinations of pure states of isotopic spin $\frac{3}{2}$ and $\frac{1}{2}$. One finds the two cross sections

$$\sigma_-=4\pi(a_{3/2}+2a_{1/2})^2/9=2\times 10^{-27};$$

$$\sigma_0=8\pi(a_{3/2}-a_{1/2})^2v_0/9v=(4\times 10^{-27})v_0/v,$$

where v and v_0 are the relative velocities of the negative pion with respect to the proton and of the neutral pion with respect to the neutron, respectively.

From this value of σ_0 the rate of capture from the lowest Bohr orbit to give a neutral pion may be as obtained as

$$R_0=\sigma_0 v/\pi b^3=10^{15}\ \text{sec}^{-1},$$

where we have taken for the radius of the mesonic Bohr orbit, $b=2.2\times 10^{-11}$ cm, and for the velocity of the emitted π^0, $v_0=8\times 10^9$ cm/sec.

Unfortunately, a direct measurement of this rate is not available. However, we can use Panofsky's result that the rate of process (a) is equal to the rate of process (b). At low energy, therefore, the cross section σ_π for the process, $P+\pi^-\rightarrow N+\gamma$, must be equal to σ_0. By detailed balancing, the cross section σ_γ for the inverse reaction, which is the photomeson production process, is obtained. The result, near the threshold, is

$$\sigma_\gamma=(p_\pi^2/2p_\gamma^2)\sigma_\pi=\tfrac{1}{3}\times 4\times 10^{-27}\mu_\pi^3 v_0 v/p_\gamma^2\ \text{cm}^2,$$

where μ_π is the reduced mass of pion and proton and p_π and p_γ are the momenta of pion and photon in the center-of-mass system. Near the threshold $p_\gamma\approx\mu c$ and one finds the photo cross section

$$\sigma_\gamma=4.0\times 10^{-28}v/c\ \text{cm}^2.$$

In comparing this formula with the measured values[3,4] of the photomeson production process, there is a certain arbitrariness in the extrapolation to the threshold. Moreover, some discrepancy can be expected because our formula refers to the photoeffect on neutrons, whereas the measurements have been on the photoeffect on protons. The agreement is within a factor of 4 in the worst case, Steinberger's[3] lowest point. It is quite close to the extrapolated curve given in Feld's[4] recent analysis of this and newer data.

It should be stressed that the coefficients in our formulas are affected by large experimental inaccuracies, owing to the combined errors in $a_{3/2}$ and $a_{1/2}$. The over-all uncertainty could well be as large as a factor 2.

* Research sponsored by the ONR and AEC.
[1] Panofsky, Aamodt, and Hadley, Phys. Rev. **81**, 565 (1951).
[2] Anderson, Fermi, Nagle, and Yodh, Phys. Rev., preceding Letter, this issue.
[3] Bishop, Steinberger, and Cook, Phys. Rev. **80**, 291 (1950).
[4] Feld, Frisch, Lebow, Osborne, and Clark, Phys. Rev. **85**, 680 (1952).

The Half-Life of Tantalum-182†

G. G. Eichholz and L. A. Ficko
Radioactivity Division, Mines Branch, Department of Mines and Technical Surveys, Ottawa, Canada
(Received April 9, 1952)

In the course of investigations into radioactivation methods involving Ta^{182} it was found that no precise value of the half-life of this isotope had been published.[1] It was, therefore, decided to carry out an accurate determination of this quantity, supplementing the value since published independently by Sinclair and Holloway.[2] Table I lists the various values of the half-life quoted in the literature.

Measurements were carried out on a small piece of pure tantalum metal which was irradiated with neutrons in the Chalk River pile. After irradiation the sample was sealed into a Lucite mold of cylindrical shape for protection and ease of handling. The

Table I. Data on the half-life of Ta^{182}.

Author	Date	Value, days
Houtermans[a]	1940	99 ± 1
Zumstein *et al.*[b]	1943	117 ± 3
Saxon[c]	1948	113
Cork *et al.*[d]	1949	123.5
Sinclair and Holloway[e]	1951	111 ± 1

[a] F. G. Houtermans, Naturwiss **28**, 578 (1940).
[b] Zumstein, Kurbatov, and Pool, Phys. Rev. **63**, 59 (1943).
[c] D. Saxon, quoted by G. T. Seaborg and I. Perlman, Revs. Modern Phys. **20**, 585 (1948).
[d] Cork, Keller, Sazynski, Rutledge, and Stoddard, Phys. Rev. **75**, 1778 (1949).
[e] See reference 2.

gamma-radiation emitted was measured in a fixed geometry by means of an argon-filled pressure ionization chamber and a vibrating reed electrometer. This equipment possesses excellent stability. Its sensitivity has been monitored by means of a standard uranium source, and it has been found to fluctuate by less than ½ percent over a period of 18 months. The radiation from the tantalum sample was measured once a week for a period of a year (3½ half-lives). Each measurement consisted of twenty separate runs. The decay curve was plotted and the half-life deduced from it by a least squares calculation. The resultant value for the half-life of tantalum-182 was 111.2±0.5 days, in excellent agreement with Sinclair and Holloway.

We are grateful to Mr. C. M. McMahon for assistance with the measurements.

* Published by permission of the Director General of Scientific Services, Department of Mines and Technical Surveys, Ottawa, Canada.
[1] K. Way *et al.*, *Nuclear Data*, Natl. Bur. Standards Circular No. 499, (1950).
[2] W. K. Sinclair and A. F. Holloway, Nature **167**, 365 (1951).

A Collective Description of Electron Interactions

R. KRONIG
Laboratorium voor Technische Physica der Technische Hogeschool, Delft, Nederland
(Received April 14, 1952)

IN two interesting papers under the above title Bohm and Pines[1] have discussed the possibility of replacing the interaction of a given electron with the other electrons in an assembly by the interaction with a plasma. I should like to point out that this viewpoint was first applied to the case of metallic conductors in a publication by Korringa and myself[2] about ten years ago. There, too, some of the results of Pines and Bohm were already derived, in particular the creation of a plasma wave in the wake of a fast charged particle, the analysis of this wave in a Fourier integral, and the retardation of the particle on account of the energy transfer to the plasma. Probably due to the interrupted scientific contact between Europe and the United States, this publication seems to have escaped the attention of the American investigators. In a later note[3] the relation between the treatment based on the notion of a plasma and a purely atomistic calculation of the energy loss by Kramers[4] has been elucidated.

[1] D. Bohm and D. Pines, Phys. Rev. **82**, 625 (1951); D. Pines and D. Bohm, Phys. Rev. **85**, 338 (1952).
[2] R. Kronig and J. Korringa, Physica **10**, 406, 800 (1943).
[3] R. Kronig, Physica **15**, 667 (1949).
[4] H. A. Kramers, Physica **13**, 401 (1947).

Experimental Evidence for Classical Electron Radiation at 300 Mev

JOSEPH W. MATHER
Radiation Laboratory, Department of Physics, University of California, Berkeley, California
(Received April 2, 1952)

IN a recent paper, Parzen[1] has given reasons for expecting quantum deviations from the well-known classical radiation calculations of Schwinger[2] at high electron energies. An experiment, using the 320-Mev Berkeley synchrotron, was proposed by E. M. McMillan to determine whether the quantum mechanical correction, as suggested by Parzen, should be made to the classical radiation formula at electron energies of about 300 Mev. The method involves measuring a particular time on the decreasing portion of the magnetic cycle, after the radio frequency accelerating voltage has been turned off, when the rate of shrinkage of the electron orbit (which is due to electron radiation) is just compensated by an expansion of the electron orbit caused by the negative rate of change of magnetic field.

Normal operation of the synchrotron entails cutting off the rf voltage near the time of peak magnetic field. Here the electron energy and the rate of radiation is a maximum; as a result, the electron loses in radius and spirals toward the internal target. Orbit expansion in this region is negligible because the magnetic field is changing very slowly on its downward cycle. But if the rf is turned off after peak field is reached (Fig. 1), the electron energy

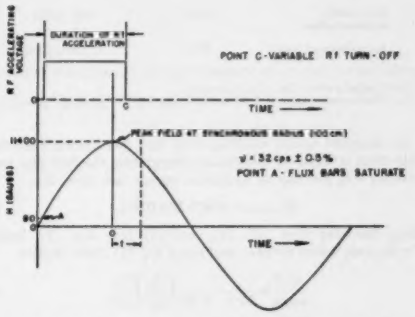
DURATION OF RF ACCELERATION
POINT C-VARIABLE RF TURN-OFF
TIME
PEAK FIELD AT SYNCHRONOUS RADIUS (100 cm)
ν = 32 cps ± 0.5%
POINT A - FLUX BARS SATURATE
TIME

FIG. 1. Magnetic field and rf accelerating voltage waveforms.

and the rate of radiation will be smaller than at peak field, while the increasing rate of fall off of the magnetic field strength will cause the orbit to expand with consequent gain in radius. Thus, by varying the rf turn-off, and therefore the electron energy, it is possible to reach a particular time (in the magnetic cycle) when the gain in radius due to the change of magnetic field just cancels the loss in radius because of radiation. The cancellation of these orbit motions occurs at the internal target radius r_0 at a particular time and can be interpreted as a turning point in the electron trajectory. The time at which the turning point is observed furnishes information from which the rate of radiation can be computed. This time is found in the following manner. A signal from a photomultiplier-crystal detector (located in the x-ray beam) is watched on a cathode-ray screen. A convenient reference time point is obtained by triggering the oscilloscope with a signal from a slab coil which indicates when the magnetic field passes through its maximum value. Thus, as the rf turn-off time is slowly retarded, the x-ray signal on the screen moves to a later time and, at a particular time, simply vanishes. The electron orbit is then starting its inward motion to the target, just grazing it at the turning point, and then going outward. The electrical angle (in the magnetic cycle) describing the lag of this vanishing x-ray signal behind peak magnetic field is θ in Eq. (6).

For a highly relativistic electron the total energy, magnetic field strength and orbit radius are simply related:

$$E=eHr, \quad \text{where} \quad H=H(r,t), \tag{1}$$

and, differentiating, assuming r constant at the turning point, we have

$$\dot{E}=e\dot{H}r. \tag{2}$$

The total rate of energy loss E in Eq. (2) involves:

(a) Radiation loss by a relativistic electron in a circular orbit moving with constant velocity, as given by the classical expression

$$\dot{E}_{\text{radiation}}=(2e^2c/3r^2)(E/mc^2)^4, \tag{3}$$

where E is the total electron energy, m is electron rest mass, and r is orbit radius.

(b) Coherent radiation due to electrons bunching in the orbit. During the observations, the beam intensity was continuously varied from zero to maximum intensity, with no appreciable change in observed time. Hence,

$$\dot{E}_{\text{coherent radiation}}\approx 0. \tag{4}$$

TABLE I. Values of $\sin\theta/\cos^4\theta$ calculated without and with the betatron effect. These are compared with the result obtained from the experimental value of θ.

	$\theta=2\pi\nu t$	$\sin\theta/\cos^4\theta$
Calc. without betatron effect	29.9°	0.88 ±3.3%
Calc. with betatron effect	33.0°	1.10 ±3%
Experimental result	33.4°	1.130±4.3%

r_0 = Target radius (96 cm ±1 percent).
H_0 = Maximum magnetic field at the target (11719 gauss ±1 percent).

(c) Betatron action resulting from field flux linking the orbit. This effect is found by numerically integrating the field plot from $r=0$ to $r=r_0$, yielding an additional energy loss correction

$$\dot{E}_{\text{betatron}}=erH(0.20\pm0.01). \tag{5}$$

Thus, inserting Eqs. (3), (4), and (5) into Eq. (2), letting $H=H_0\cos\theta$, where $\theta=2\pi\nu t$, and using Eq. (1), there results

$$\frac{\sin\theta}{\cos^4\theta}=\frac{1}{3\pi(1-0.20)}\left(\frac{E_0}{mc^2}\right)^3\frac{r_e c}{r_0^2\nu}, \tag{6}$$

where r_e is the classical electron radius (2.82×10^{-13} cm); r_0 is the target radius; E_0 is the maximum electron energy at the target; ν is the magnet excitation frequency; m is the mass of the electron; and c is the velocity of light.

It is interesting to note the large betatron effect present during the entire magnetic cycle, even though the flux bars saturate at approximately 80 gauss. However, the decreasing portion of the magnetic cycle yields the energy loss given by Eq. (5).

The time when the x-ray signal vanishes is experimentally found to be $t=2900\pm50$ microseconds. (See Fig. 1.) The difference between the calculated and experimental value of $\sin\theta/\cos^4\theta$ is 2.7 percent and is seen to be within the assigned experimental error. From the results in Table I, there seems little doubt of the validity of the classical expression, Eq. (3), for electrons in the 300-Mev energy range.

Further theoretical study of the radiation problem has been made by Judd *et al.*[3] and by Olsen and Wergeland,[4] giving additional support to the classical interpretation of radiation by an electron in this energy range moving in a magnetic field.

The author wishes to thank Prof. E. M. McMillan for his suggestions and continued interest, and Drs. D. Judd, J. Lepore, M. Ruderman, and P. Wolff for many helpful discussions. It is also a pleasure to express thanks to Mr. G. McFarland and the crew of the synchrotron for help with this experiment, with particular thanks to Mr. G. Gauer.

[1] G. Parzen, Phys. Rev. **84**, 235 (1951).
[2] J. Schwinger, Phys. Rev. **75**, 1912 (1949).
[3] Judd, Lepore, Ruderman, and Wolff, Phys. Rev. **86**, 123 (1952).
[4] H. Olsen and H. Wergeland, Phys. Rev. **86**, 123 (1952).

Associated Pairs of Particles in Cosmic-Ray Showers in Photographic Emulsions

J. Y. MEI* AND E. PICKUP
Physics Division, National Research Council, Ottawa, Canada
(Received April 18, 1952)

IN an examination of 77 showers associated with stars in Ilford *G* emulsions exposed at 85,000 feet there appear to be more close groupings of tracks ($\lesssim1.5\times$ minimum ionization) than expected statistically. Such possible groupings have been mentioned qualitatively by Hornbostel and Salant.[1] Cosyns[2] has discussed pairs, triplets, etc., although Perkins[3] indicates that they could not confirm Cosyns' results. Recently Danysz, Lock, and Yekutieli[4] investigated a similar phenomenon for stars with two to six

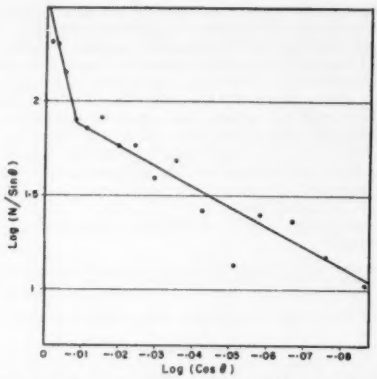

FIG. 1. Average angular distribution of particles in 77 showers. θ = mean angle for 2° interval; N = number of tracks in 2° intervals of polar angle; number of tracks per unit solid angle $= N/(4\pi\sin1°\times\sin\theta)$.

shower particles and suggested as a possible explanation an intermediate, very short-lived, neutral meson, mass $\sim550m_e$ (decaying into two charged pions with a small Q value).

Our stars had an average of 10 shower tracks per star at <90 degrees to the primary direction, and stars with $\lesssim20$ and <6 shower tracks were excluded. Only pairs of tracks with $\gtrsim4$ degrees separation were considered when they were outside any marked forward cone or appreciably off the probable forward direction. Measurements on two of the pairs indicated that the particles were lighter than protons.

TABLE I. Angular details of pairs. p = proton initiated star; n = no visible primary; n_s = number of shower particles; $\theta_{1/2}$ = half angle of shower cone; α = angle between pair and primary direction;[a] δ = half opening angle of pair. The last column gives the calculated statistical chance of the pair occurring in the particular star.

Primary	n_s	$\theta_{1/2}$	α degrees	δ	Estimated chance ($\times10^{-2}$)
p	6	24	7	1.5	16
p	11	5	5	0.8	13
p	8	6	5.5	1.6	20
p	11	29	4.6	1.3	0.36
p	10	14	9	0.8	7.3
p	8	17	36	1.6	1.9
p	16	13	12.5	0.45	2.2
p	11	13	30	1.1	2.5
p	10	30	51.5	1.1	0.07
p	14	26	41	1.6	1.7
n	13	4.5	28	1.6	7.3
n	17	14	37	2.0	5.4
p	14	2.5	21.5	1.5	10.7
n	9	16.3	53	1.75	0.12
p	9	13	10	1.25	17
p	10	5.5	5	1.5	7
			5	1.5	
p	10	11.6	6.75	1.1	3.4
			24	2.5	
p	21	9	40	1.5	0.26
			13.5	0.7	
n	10	5	8.5	0.3	4×10^{-3}
			9.0	1.5	
p	18	8.6	7	0.6	10^{-2}
			7	0.6	
			15	0.6	
p	17[b]	3	4.5	0.5	5.5×10^{-4}
			5.5	0.5	
			8	0.5	
			17	1.1	
			2.5	0.3 (triple)	

[a] Determined by cone symmetry where there is no visible primary.
[b] This may be a case of grouping within the main cone, and the calculated chance is very sensitive to the primary direction.

Table I gives details of the angular measurements,[5] the last column showing the statistical chance for the particular star, calculated using the average distribution curve for all the stars (shown in Fig. 1). If one excludes the last event, which may include forward cone particles, the mean calculated chance from 20 stars with pairs approximates 4×10^{-3}. Assuming these to be representative of all 77 stars, we would, therefore, expect about three chance pairs, whereas 25 pairs were observed. The number of individual cases with two or more pairs is somewhat greater than we would have expected from the total number of pairs, and more data are desirable.

If one assumes the effect to be real, it seems unlikely that it could be explained solely on the basis of secondary collision processes because of the small angles between pairs. It is possible that some are electron pairs from the suggested alternative neutral pion decay, $\pi^0\rightarrow$electron pair$+h\nu$. Dalitz[6] estimates $\sim$1 in 80 for this mode of decay compared with the usual decay into two photons. If 70 percent of the shower particles are pions and there are an approximately equal number of neutral, negative, and positive pions, there will be $\sim$260 neutral pions for the 77 stars and thus about three electron pairs directly from neutral pion decay. Whether such electron pairs do occur in stars is not known at present.[7]

Another possibility is the decay of short-lived neutral mesons of mass $\sim550m_e$.[4] Our results are insufficient to confirm this, and in any case the selection of pairs with small angles means that the Q value obtained, assuming such a decay, would be small and insensitive to the energy of the pions unless this were very unevenly balanced. If the pairs originated in this way, the number of such neutral mesons would be about 10 percent of the number of neutral pions. Wentzel[8] has also discussed a mu-pair theory (e.g., neutral pion may be a bound state of negative and positive muons), but there is no evidence in stars for appreciable numbers of muons, which might then be expected.

Further work is obviously necessary to confirm these results.

* National Research Laboratories Postdoctorate Fellow.
[1] J. Hornbostel and E. O. Salant, Phys. Rev. **76**, 859 (1949).
[2] M. G. E. Cosyns, Nuovo cimento **6**, Supp. 3, 397 (1949); Bull. Center Phys. Nucleaire Bruxelles, No. 18, (1950).
[3] Report of Conference on Heavy Mesons, Bristol, England (December, 1951), p. 32.
[4] Danysz, Lock, and Yekutieli, Nature **169**, 364 (1952).
[5] In estimating angles a shrinkage factor of 2.5 was used for the emulsion.
[6] R. H. Dalitz, Proc. Phys. Soc. (London) **A64**, 667 (1951).
[7] Report of Rochester Conference, January 11, (1952), p. 46.
[8] G. Wentzel, Phys. Rev. **79**, 710 (1950).

The Structure of Ammonium Chloride by Neutron Diffraction

G. H. Goldschmidt* and D. G. Hurst
Atomic Energy Project, National Research Council of Canada, Chalk River, Ontario, Canada
(Received March 7, 1952)

RECENTLY we published neutron diffraction patterns of ND_4Cl at -180°C and room temperature.[1] Subsequent measurements here and at Oak Ridge[2] have failed to confirm our values for the structure factors of the (111) and (210) lines at room temperature. Our deduction that the room temperature phase is ordered depended largely on the strength of the (111) line. The new measurements give much weaker intensity. Consequently, our conclusions concerning the room temperature phase can no longer be sustained. Levy and Peterson[3] have deduced a disordered structure from their results.

The intensity of the (111) line at room temperature was the major error in our measurements. This line was small compared to the background, and it was not well resolved from the strong (111) line because of the aluminum windows of the cassette. The error in the (111) line of ND_4Cl probably arose through a false enhancement owing to the subtraction of a background curve in which the neighboring (111) and (200) aluminum lines were too large. Preferred orientation in the aluminum may have contributed to the effect.

TABLE I. Structure factors of ND_4Cl at 23°C (units of 10^{-12} cm).

hkl	(100)	(110)	(111)	(200)	(210)	(211)
F	1.35	(2.47)	0.35	0.98	0.37	1.34

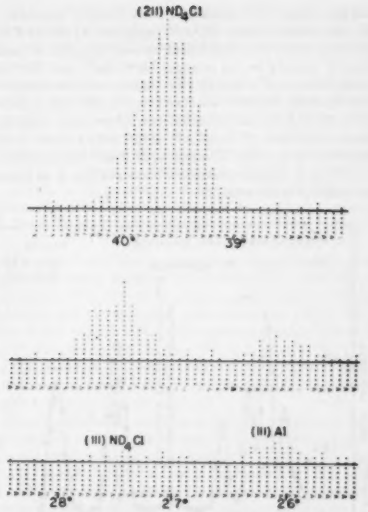

FIG. 1. Records of neutron scattering by ND_4Cl. Each dot represents 20 neutron counts. Each vertical column is recorded at a fixed angle for a predetermined number of neutrons incident on the specimen. The bottom record is the neighborhood of the (111) line at room temperature. Just above it is the same region at -170°C shifted slightly in angle to align the (111) peaks of aluminum. At the top is shown the (211) peak at -170°C. The incoherent background is shown by the horizontal lines.

Since the publication of the earlier results, the instrument has been greatly improved both as to resolution and methods of recording. In a new series of measurements by one of us, the (111) lines of aluminum and ND_4Cl were completely resolved. Only 0.004 inch of aluminum was in the beam, as compared to 0.010 inch previously. Samples of the records are shown in Fig. 1, where it is clear that the change in the (111) line between low and room temperatures is much larger than was found originally.

The structure factors obtained in the new measurements, normalized to 2.47×10^{-12} cm for the (110) line, are given in Table I.

We thank Dr. Levy and Dr. Peterson for bringing the discrepancy in the measurements to our attention.

* Now at the Clarendon Laboratory, Oxford, England.
[1] G. H. Goldschmidt and D. G. Hurst, Phys. Rev. **83**, 88 (1951).
[2] Henri A. Levy and S. W. Peterson, Phys. Rev. **86**, 766 (1952).

Soft Radiations from Am^{241}

J. K. Beling, J. O. Newton, and B. Rose
Atomic Energy Research Establishment, Harwell, Berks, England
(Received April 14, 1952)

THE gamma- and x-radiation produced in the decay of the α-particle emitter Am^{241} have been examined over the energy range 5–120 kev by the proportional counter technique, using counters filled with argon, krypton, and xenon, respectively.

The sources used were extracted from heavily irradiated plutonium, the parent isotope of Am^{241} being the β-emitter Pu^{241}.

The energy scale was established by observing the K radiation following K capture in the isotopes Os^{185}, Sn^{113}, and Zn^{65}, giving lines at 60.8 kev, at 27.3 and 24.1 kev, and at 8.05 kev, respectively. Lines attributable to Am^{241} were observed at 59.7±0.3, 26.3±0.2, 20.9±0.2, 17.3±0.2, and 13.5±0.2 kev. There were indications of the presence of a line at 75±2 kev of intensity roughly ½ percent of that of the 60-kev line. The line at 26.3 kev has not previously been reported. A typical spectrum is shown in Fig. 1, as taken with a thirty-channel pulse analyzer.

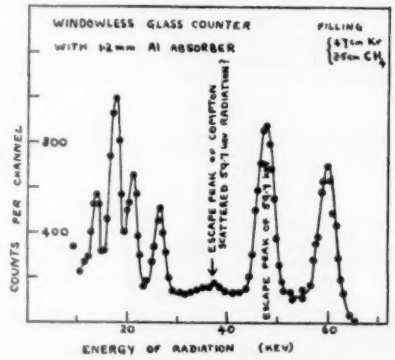

FIG. 1. γ- and L-ray spectrum of Am^{241} observed in a krypton-filled proportional counter.

The relative intensities of the various lines were obtained by collimating the radiation and admitting it to a krypton-filled counter through a thin mica window, the efficiency of the counter being calculated from known mass absorption coefficients. A correction of 14 percent was necessary for the 59.7-kev peak due to wall effect.[1] The intensity of the 13.5-kev peak required correction for two reasons. Firstly, the "escape" peak of the 26.3-kev radiation occurred at 13.6 kev (the difference being the energy of the K radiation of Kr). Secondly, as the 13.5-kev radiation lies below the K absorption edge of Kr and must therefore be detected by absorption in the outer electronic shells of the counter gas, it cannot have a K escape peak, and all absorbed quanta give rise to counts in the "normal" (13.5-kev) peak. The magnitude of these corrections was determined from the observation that the ratio of the counts in the escape peak to counts in the main peak for any energy of radiation was 1.00±0.03. The relative intensities of the principal lines are shown in Table I. Upper limits to the

TABLE I. Relative intensities of γ- and L-rays resulting from the decay of Am^{241}.

Radiation energy (kev)	59.7	26.3	20.9	17.3	13.5
Relative intensity	1	0.075±0.008	0.177±0.018	0.66±0.04	0.42±0.04

relative intensities of lines in the energy ranges 4–10 kev, 29–40 kev, 40–48 kev, 48–56 kev, and 86–120 kev were 2.5 percent, 0.02 percent, 1 percent, 6 percent, and 0.5 percent, respectively, of the 59.7-kev line.

The three lowest energy lines fit well with the energies 13.9, 17.3, and 20.9 kev to be expected for the L_α, L_β, and L_γ x-ray lines of Np^{237}, as determined by extrapolation from the published values for U, Pa, and Th.[2]

To demonstrate that the observed lines were not due to fission product contamination, the spectrum of γ-rays which were in coincidence with α-particles was observed. A coincidence resolving time of 2 μsec was found sufficient to avoid loss of true coincidences, and it was found that the lines appeared in the same relative intensity in the single and coincidence spectra.

The number of 59.7-kev quanta per α-particle was measured by the coincidence method, using a 2-mm thick sodium iodide crystal as the gamma-detector. The discriminator in the gamma-ray channel was set to reject all pulses below the peak due to the 59.7-kev radiation. The results required correction for the fraction of pulses lost into the "escape" peak, which is produced by the escape of iodine K radiation from the crystal. The magnitude of this correction was determined by measuring the relative areas of the main and escape peaks when the source was covered with sufficient platinum to absorb the L rays and the 26.3-kev line. Apart from this correction the net efficiency of the γ-counter was assumed to be equal to the solid angle which it subtended at the source. The absolute intensity of the 59.7 kev γ-ray was found to be 0.40±0.015 per α-particle. This is to be compared with other work,[3] where a value of 0.32 was obtained.

The authors are grateful to Dr. J. Milsted for preparing the sources used and to Mr. D. West for much guidance. One of us (J.K.B.) wishes to express his gratitude to the Director, A.E.R.E., Harwell and to the Officer-in-Charge, ONR Branch Office, London, for permission to work at Harwell and for leave of absence from ONR, London.

[1] D. West (private communication).
[2] A. H. Compton and S. K. Allison, *X-rays in Theory and Experiment* (D. Van Nostrand Company, Inc., New York, 1935).
[3] C. A. Prohaska, University of California Radiation Laboratory Report No. 1395, 1951.

The Microwave Spectrum and Molecular Constants of Hydrogen Cyanide*

A. H. NETHERCOT, JR., J. A. KLEIN, AND C. H. TOWNES
Columbia University, New York, New York
(Received April 7, 1952)

THE microwave spectra of the $J=0\rightarrow1$ transition of three isotopic species of HCN have been re-examined using a harmonic generator driven by a 2K33 klystron with a fundamental wavelength of about 1.3 cm. The third harmonic was used for $DC^{13}N$ and the fourth harmonic for $HC^{13}N$ and $HC^{15}N$, with all frequency measurements being made at the frequency of the fundamental. The observed line frequencies are given in Table I.

TABLE I. Observed line frequencies.

Molecule	Frequency (Mc/sec)
$HC^{13}N$	88,631.4±0.5
$HC^{15}N$	86,340.1±0.5
$DC^{13}N$	72,415.0±0.5

The $HC^{13}N$ and $HC^{15}N$ frequencies differ by approximately 30 Mc from the values previously reported;[1] this difference possibly is due to an error by the earlier workers in the identification of frequency marker pips, which could give an error of exactly 30 Mc.

The errors given are probable errors and are expected to be made smaller by further work.

These measurements form part of a determination of the velocity of light and were undertaken after it was pointed out by Professor D. H. Rank that the previous microwave measurement of the $HC^{13}N$ frequency was inconsistent with his result for the rotational constant. The determination of c is discussed by Rank in his accompanying letter.

The above frequencies lead to slight changes in the previous listed[1] bond distances. The new values for the internuclear distances as determined from the various isotopic combinations are given in Table II. In addition, a computational error seems to have been involved in the bond distances previously derived from

TABLE II. Internuclear distances.

Isotopic pair	d_{CH}	d_{CN}
$DC^{13}N-DC^{14}N$	1.0657A	1.1556A
$HC^{13}N-HC^{13}N$	1.0679A	1.1557A
$HC^{13}N-DC^{13}N$	1.0623A	1.1568A
$HC^{13}N-DC^{13}N$	1.0626A	1.1567A

the $DC^{13}N-DC^{14}N$ pair. Our calculated value for this pair, based on the earlier frequency measurements, is included in Table II. It is seen that the values for the bond distances are now more consistent with each other than formerly. In addition, the D−C distance appears shorter than the H−C distance, rather than longer as previously reported. Variations in the bond distances listed in Table II are primarily due to variation of zero-point vibrations with isotopic substitutions. Since these are particularly large for an H−D substitution, the most accurate distances are probably given by the pairs of isotopes $HC^{13}N-HC^{13}N$ and $DC^{13}N-DC^{13}N$.

The harmonic generator[3] used consists of a pair of crossed guides with a silicon crystal and tungsten cat whisker mounted inside the guide at the junction. One guide is of appropriate size for the fundamental wavelength (1.3 cm), the other guide is of a size suitable for the second harmonic. The use of various sizes of tapered wave guide at the output of the generator allows the separation of the several harmonics produced. The detector used is basically similar to the generator and is described more fully elsewhere.[4] One generator and one detector conveniently operate over a wide range of frequencies and have been used successfully for the second, third, and fourth harmonics. The only changes necessary were adjustments of the tuning plungers in the generator and detector mounts (and replacements of the 2K33 klystron to reach widely different fundamental frequencies).

The authors wish to thank Dr. G. A. Silvey for preparing the chemicals and Mr. George Dousmanis for making the calculations.

* This work was supported jointly by the Signal Corps and the ONR.
[1] Simmons, Anderson, and Gordy, Phys. Rev. **77**, 77 (1950).
[2] The design of the generator is due to Mr. E. Richter, formerly of this laboratory and now with the Sperry Gyroscope Company.
[3] Klein, Loubser, Nethercot, and Townes, Rev. Sci. Instr. **23**, 78 (1952).

The Velocity of Light Determined by the Band Spectrum Method*

D. H. RANK, R. P. RUTH, AND K. L. VANDER SLUIS
Physics Department, The Pennsylvania State College, State College, Pennsylvania
(Received April 11, 1952)

IT is well known that the rotational energy levels of a diatomic or linear polyatomic molecule can be expressed by the relationship $\nu=F(J)=BJ(J+1)-DJ^2(J+1)^2+\cdots$, where J is the rotational quantum number and ν is the frequency; $B=h/8\pi^2I$, where h is Planck's constant and I is the moment of inertia for the particular vibrational state in question; B, D and ν as given above are expressed in pure frequency units. In the microwave absorption spectrum it is possible to measure with high precision in pure frequency units the $0\rightarrow1$ rotational transition for suitable molecules. The frequency of this transition is equal to $2B-4D$ to the approximation given above. B and D for the ground state can be determined from measurement of infrared rotation vibration bands. The values obtained from the optical spectra will be in cm^{-1} units. It follows directly that the ratio of B microwave to B infrared is identically equal to the velocity of light in vacuum.

Dr. A. E. Douglas of Ottawa pointed out to one of us (D. H. R.) that a precision determination of B infrared, preferably by interferometric means, could yield a significant value for the velocity of light. We have completed such a determination making use of two rotation vibration bands of HCN arising from the ground state. The bands used were the 103 and 004 bands, respectively. The absorption tube was an 8-meter multiple reflection tube of the type invented by White[1] and similar to those used extensively by Bernstein and Herzberg.[2]

The spectrograph consisted of a plane grating mounted between collimating and focusing mirrors of 10-meter focal length. The plane grating has 15,000 lines to the inch and 6.5 inches of ruling. This grating, ruled on speculum metal by Anderson, is exceedingly perfect and shows theoretical resolving power in the fifth order as nearly as can be determined. We are indebted to Dr. A. L. Loomis for his generosity in the donation of this grating to The Johns Hopkins University after his many years of ownership, and to Prof. G. H. Dieke of Johns Hopkins for the loan of the grating.

Photographs of the bands were obtained in the first order by using a Fabry-Perot etalon of 21.35-mm spacer external to and in conjunction with the plane grating spectrograph. Calibration of the etalon was by means of neon standards. Plates were also obtained in the second order of the grating without the auxiliary interferometer, using the fourth-order iron standards. The pressure of the gas varied in different experiments from 35 to 70 mm Hg. After measurements of the plates the molecular constants were determined by least squares methods.

Dr. Douglas kindly communicated the preliminary results which he had obtained for the ground state in his extensive unpublished work on the complete near infrared system of HCN. These values of Douglas for B infrared showed that probably the measurements of B microwave by Simmons, Anderson, and Gordy[3] must be in error by some multiple of ten megacycles in spite of their high precision, since no reasonable value of c could be obtained. One of us (D. H. R.) communicated with Professor Gordy concerning this matter and also later with Professor Townes pointing out the importance of obtaining a check determination in the microwave spectrum. The result obtained by Townes and his collaborators, $B=44{,}315.9\pm0.25$ megacycles per second, after correcting for centrifugal distortion, appears in a companion letter in this issue of *The Physical Review*. Our result for B infrared is 1.47830 $cm^{-1}\pm0.000025$. D was found to be 3.1×10^{-6} cm^{-1}. The value obtained for the velocity of light c is $299{,}776\pm7$ km/sec, where the uncertainty stated is the sum of the uncertainties of B microwave and B infrared. From our experience in making these measurements and treating the data we feel that somewhat improved precision of the optical measurements is possible and that systematic error can be discovered if present and materially reduced if found. The precision of measure of this hybrid optical method at present is comparable with previous optical methods and is exceeded only by the very recent pure microwave methods.[4-7] It is certainly too early to say whether any real discrepancy between optical and microwave methods for determining the velocity of light exists. Further, more precise measurements are now in progress. A full account of these experiments will appear elsewhere.

* This research was assisted by support from the ONR.
[1] J. U. White, J. Opt. Soc. Am. **32**, 285 (1942).
[2] H. J. Bernstein and G. Herzberg, J. Chem. Phys. **16**, 30 (1948).
[3] Simmons, Anderson, and Gordy, Phys. Rev. **77**, 77 (1950).
[4] J. A. Bearden and H. M. Watts, Phys. Rev. **81**, 73 (1951).
[5] E. Bergstrand, Ark. fys. **3**, 479 (1951).
[6] K. Bol, Phys. Rev. **80**, 295 (1950).
[7] K. D. Froome, Nature, **169**, 107 (1952).

Photoconductivity of Trapped Electrons in KCl Crystals between 24°C and −190°C

J. J. OBERLY*
Crystal Branch, Metallurgy Division, Naval Research Laboratory, Washington, D. C.
(Received April 22, 1952)

THE photoconductivity of trapped electrons in KCl[1] and KBr[2] crystals at room temperature has been reported previously. The same technique has now been used to study the

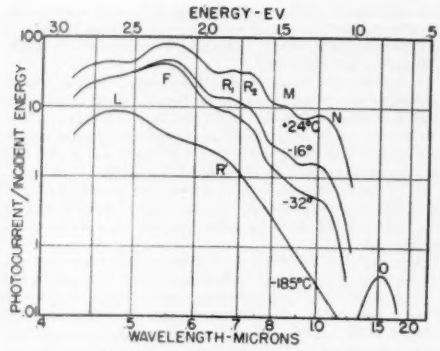

FIG. 1. Spectral response curves (photocurrent/incident energy) of KCl crystal x-rayed 4 hours at room temperature and F bleached at room temperature to form L, R_1, R_2, M, and N absorption bands.

spectral response (photocurrent/incident energy) in KCl at temperatures down to −190°C attained with liquid nitrogen.

Response curves obtained as a crystal of KCl (x-rayed and F bleached at room temperature) was cooled to −185°C are shown in Fig. 1. At 24°C the curve is similar to those reported for KBr[1] except for the R_1 and R_2 peaks which are now clearly separated. Cooling to −16°C and −32°C decreases the F response as shown by Glaser and Lehfeldt[2] and also the response of all the other bands. The amount of the change increases with wavelength above 0.5 micron. At a much lower temperature (−185°C) the F, R, M, and N response vanishes leaving apparently the L response, another broad peak in the region of the R' absorption band reported by Scott and Bupp,[4] and a new peak ("O") at 1.55 microns.

The effect of F bleach at low temperature (−115°) is shown in Fig. 2. At −120°C there are small R_1, R_2, M, and N peaks (indicated by arrows), and the curve is considerably higher than the −32°C curve of Fig. 1 beyond 0.65 micron. The O peak is quite large and another new peak ("P") is present at 1.95 microns. Cooling the crystal to −190°C produces about the same curve as in Fig. 1 with the addition of the P peak and a broad peak presumably resulting from F' centers.

During cooling from 24°C to −32°C (Fig. 1) a constant decrease is expected in all the peaks due to a decrease in the "thermally increased range"[5] of the conducting electron with temperature. The greater decrease for the long wavelength peaks indicates that the quantum yields of the centers are also being reduced and thus that the thermal energy gap from the excited state to the conduction band increases in the order F, R_1, R_2, M, and N. At −185°C the quantum yield of the F to N centers is sufficiently small to remove their response peaks. An additional general decrease is expected from an increased cross section for the capture of an electron by a negative ion vacancy as suggested by Seitz.[5] The two peaks remaining at short wavelengths could possibly be a single, broad maximum split by the nonphotoconductive F band absorbing light around 0.55 micron. Certainly the two peaks are similar in being unaffected by illumination at −185°C with light of their own wavelengths. However, they may also be caused by entirely different mechanisms, the L peak by direct optical ionization of hard F centers[6,5] and the other by R' centers.

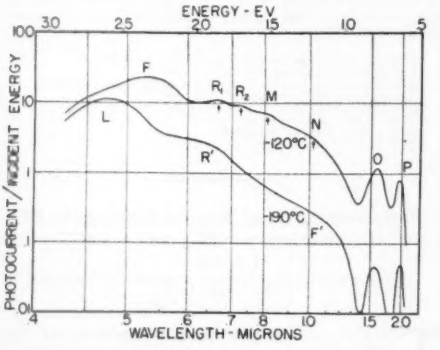

FIG. 2. Spectral response curves (photocurrent/incident energy) of the same KCl crystal after additional F bleach at −115°C.

F bleach at low temperature raises the long wavelength response much more than it would at room temperature. The R, M, and N peaks in the −120°C curve (Fig. 2) may indicate an increased cross section for the formation of these centers at low temperatures. The new O and P peaks are due to centers unstable at 24°C, and their widths, only 0.15 and 0.05 ev, indicate that these centers are excited by the absorbed photon and then ionized thermally. (The presence of the O peak in Fig. 1 was caused by accidental F bleach during the measurements.) The response peak in the −190°C curve which seems to lie above 1.0 micron does not coincide with the reported F' absorption maximum at 0.75 micron when plotted as photocurrent/incident photon and may be due in part to centers similar to the F' formed by the capture of additional electrons at R, M, and N centers.

These measurements and similar work on NaCl and KBr will be discussed at greater length in a forthcoming paper. The writer wishes to acknowledge his helpful discussions with Elias Burstein and the stimulating interest of Dr. E. O. Hulburt during the course of this work.

[a] Now at Freed Radio Corporation, 200 Hudson Street, New York 13, New York.

[1] J. J. Oberly and E. Burstein, Phys. Rev. **79**, 217 (1950).
[2] J. J. Oberly, Phys. Rev. **83**, 228 (1951); **84**, 1257 (1951).
[3] G. Glaser and W. Lehfeldt, Gött. Nachr., Fachgruppe II, **2**, 91 (1936).
[4] A. B. Scott and L. P. Bupp, Phys. Rev. **79**, 341 (1950).
[5] F. Seitz, Revs. Modern Phys. **18**, 384 (1946).
[6] N. F. Mott and R. W. Gurney, *Electronic Processes in Ionic Crystals* (Oxford University Press, London, 1940), first edition, p. 114.

The Spectrum of L X-Rays from RaD and the Possibility of $L_{\mathrm{I}} \rightarrow L_{\mathrm{II}} N$ Auger Transitions

S. G. COHEN AND A. A. JAFFE
Physics Department, Hebrew University, Jerusalem, Israel
(Received April 8, 1952)

IN the course of an investigation of the disintegration of RaD the L x-ray spectrum has been re-examined using a proportional counter in an arrangement similar to that of Curran, Angus, and Cockroft,[1] but paying special attention to low intensity lines. For this purpose it was found convenient to use a proportional counter in conjunction with a triggered single sweep oscillograph, having a camera attachment, the display of a large number of pulses being photographed during a single exposure. It has been found advantageous to modulate the oscillograph beam intensity (with the output of a Schmitt trigger circuit) so that halo from the stationary spot is removed. The amount of modulation is adjusted so that the spot must traverse any path on the screen at least fifty times before any photographic darkening is recorded.

The exposure reproduced in Fig. 1 shows the results obtained. In addition to the three prominent groups at 7.8 (γ-ray), 10.8, and 13.0 kev previously reported,[1,2] the existence of a line at 15.3±0.3 kev is definitely established. K x-rays from Fe^{26} were

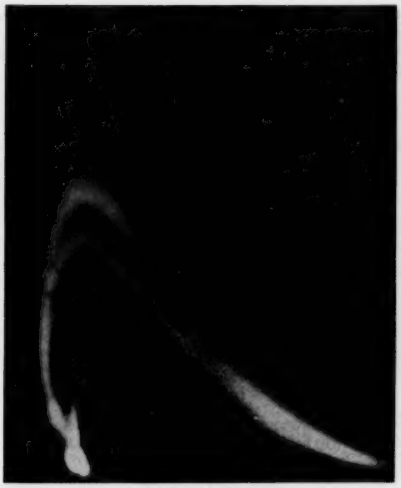

FIG. 1. Exposure showing main lines at 7.8, 10.8, 13.0, and 15.3 kev. (Exposure time 20 sec with an external source of approximately 50 microcuries of RaD, filtered with 4-mm perspex; the proportional counter was 7-cm diameter and filled to a total pressure of 70-cm argon-methane.)

used for calibration of the energy. On the original film the line at 15.3 kev is clearly visible and well resolved. The measured energy of this line coincides with that of the γ_1 x-ray of bismuth ($L_{II} \rightarrow N_V$). Another faint line exists at 17.5 kev which cannot be an x-ray; a discussion of low intensity lines of higher energy will be reported later. The relative intensities of the spectral lines were measured with a single channel pulse analyzer (Fig. 2), and after correction for absorption in the perspex filter and for gas efficiency, a value of 0.10:1 was found for the ratio of intensities of the lines $\gamma_1:\alpha_1$.

Salgueiro and Valadares[2] have measured the relative intensities of the β_4 and α_1 L x-rays (resulting from transitions to the L_I and L_{III} levels, respectively) from RaD using a crystal spectrometer and have compared the intensities with those normally found by

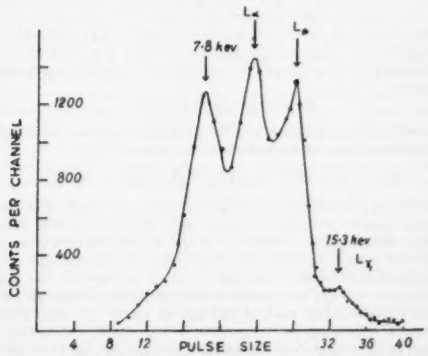

FIG. 2. Pulse size distribution for RaD in the range 0–20 kev, using a single-channel pulse analyzer.

electronic bombardment of bismuth; even after taking into account the difference in the relative numbers of holes in the L_I and L_{III} levels produced in the two cases a large discrepancy is found. This was explained on the hypothesis that $L_I \rightarrow L_{III}M$ Auger transitions occur for 70 percent of the vacancies in the L_I level, leading to doubly ionized atoms (transitions of the type proposed by Coster and Kronig,[3] to account for the existence of x-ray satellite lines). The detection of the γ_1 line from the L_{II} level permits a similar analysis to determine whether $L_I \rightarrow L_{II}$ Auger transitions occur; the Auger transition $L_I \rightarrow L_{II}M$ is energetically impossible ($EL_I - EL_{II} > EM_V$ only if Z is less than 41), but the transitions $L_I \rightarrow L_{II}N$ are possible. The method provides a sensitive test because the ratio of conversion in the L_I and L_{II} levels is large, and the occurrence of such transitions even to a small extent would alter the relative intensities of L_I and L_{II} x-rays considerably.

The relative ionization of the L_I and L_{II} shells produced by electronic bombardment (in bismuth) is approximately 1:1.1 (taking into account that the electron populations are equal and the slightly different binding energies), whereas the relative ionization of the L_I and L_{II} levels following internal conversion in RaD decay are in the ratio 100:9 (Cranberg[4]). Thus we should expect the intensity of the β_4-ray ($L_I \rightarrow M_{II}$) relative to that of the γ_1-ray ($L_{II} \rightarrow N_{IV}$) to be larger in RaD by about 12 times that in the normal bismuth x-ray spectrum, if no $L_I \rightarrow L_{II}N$ transitions occur. In the spectrum produced by electronic bombardment $\beta_4:\gamma_1$ is 1:2.8, and in the case of RaD (taking $\alpha_1:\beta_4 = 100:45$) we find $\beta_4:\gamma_1 = 4.5:1$; thus we have

$$\frac{\beta_4:\gamma_1\ [\text{RaD}]}{\beta_4:\gamma_1\ [\text{electronic bombardment}]} = \frac{12.5}{1},$$

which is close to the ratio 12:1 estimated above, assuming no $L_I \rightarrow L_{II}$ transitions occur.

If only 10 percent of the vacant holes in the L_I level were filled by transitions of electrons from the L_{II} level, instead of the ratio 12:1 we should expect 6:1. Taking into account the limits of accuracy in the above estimates, one may conclude that $L_I \rightarrow L_{II}$ transitions cannot take place in more than 5 percent of the vacancies in the L_I shell.

[1] Curran, Angus, and Cockroft, Phil. Mag. **40**, 36 (1949).
[2] L. Salgueiro and M. Valadares, Portugaliae Physica **3**, 21 (1949).
[3] D. Coster and R. de L. Kronig, Physica **2**, 13 (1935).
[4] L. Cranberg, Phys. Rev. **77**, 135 (1950).

Plastic Flow in Alkali Halide Crystals

W. W. TYLER
Knolls Atomic Power Laboratory, Schenectady, New York*
(Received April 2, 1952)

GYULAI and Hartly[1] have observed that the conductivity of certain single crystals of NaCl can be increased by factors of from 10 to 100 by deformation at room temperature. Stress on the specimen was increased by stepwise loading in a lever press until at stresses of the order of 10^8 dynes/cm^2 and greater, sufficient plastic flow occurred to cause a large discontinuous increase in the conductivity of the specimen. Subsequent to the inception of plastic flow, the specimen was held under constant load and the increased conductivity decayed in times of the order of several minutes.

Seitz[2] has proposed that the Gyulai and Hartly observations may be explained by the assumption that the motion of dislocations during slip processes generates vacancies (or interstitial ions) which then contribute to an enhanced ionic conductivity until they diffuse to the specimen boundaries or combine to form immobile clusters. The decay time of the enhanced conductivity may be associated with the effective life time of the vacancies produced during a slip process.

It is the purpose of this note to call attention to later experiments by Gyulai and Boros[3] which suggest that the enhanced

conductivity observed in alkali halides subsequent to plastic deformation may be partially electronic in origin. Gyulai and Boros studied single crystals of KCl and KBr. The technique was the same as that of Gyulai and Hartley except that use of a vacuum tube electrometer and recording oscillograph in place of a string galvanometer permitted closer observation of times involved in current changes and greater current sensitivity. Stresses of only about 10^7 dynes/cm^2 produced detectable current changes. Half-times for decay of the enhanced conductivity were now observed to be about 0.2 second with no appreciable fraction of the induced current changes persisting for greater than several seconds. The rise time of the current change was observed to be 0.1 second, but it is not clear whether this time is characteristic of the deformation process or represents a limitation of the detection system.

Gyulai and Boros also found that current changes induced by deformation in KCl and KBr crystals colored additively, or by x-rays to about 10^{17} F-centers per cm^3, were approximately twice the magnitude of current changes induced in uncolored crystals under similar conditions of stresses and field strength. However, the times involved in decay of the current changes were the same for colored and uncolored crystals.

Both the short duration of current changes and the sensitivity to coloration suggest that the increased conductivity observed by Gyulai and Boros may be due to electrons liberated in the vicinity of slip planes during plastic flow. The longer times observed by Gyulai and Hartly may be associated with continued plastic flow due to higher stresses rather than the mechanism of conduction. They show evidence (Fig. 4 and Fig. 5, reference 1) that both the work hardening and the dimensional change induced in a specimen subsequent to a suitable increase in stress, continue for a time comparable to the decay time of the current change produced. The authors point out that as plastic flow continues for some time after loading it is not valid to assume that the charge is all liberated at the initial moment of the flow process. Thus the times involved in current decay may represent continued liberation of electrons during a flow process rather than the diffusion of vacancies to clusters or boundaries.

It is reasonable to expect the duration of flow to be much shorter with the considerably lower stresses used by Gyulai and Boros. Independent evidence that stresses of 10^7 dynes/cm^2 are sufficient to produce well-defined slip in alkali halides and in particular in KCl is cited by Schmid and Boas.[4]

Although the work of Gyulai and Boros does not provide evidence that vacancies are not generated during plastic flow, it does suggest that the current changes observed by Gyulai and Hartly do not provide unambiguous evidence for the vacancy generation hypothesis. Experiments at temperatures low enough to completely quench any conductivity due to vacancy diffusion will probably be necessary before current changes observed may be definitely labelled as electronic.

* The Knolls Atomic Power Laboratory is operated by the General Electric Company for the AEC.

[1] Z. Gyulai and D. Hartly, Z. Physik **51**, 378 (1928).
[2] F. Seitz, Phys. Rev. **80**, 239 (1950).
[3] Z. Gyulai and J. Boros, Math. naturw. Anz., ungar Akad. Wiss. **59**, 115 (1940). (Translation from the Hungarian given by the General Electric Company Main Library, Schenectady, New York.)
[4] E. Schmid and W. Boas, *Plasticity of Crystals* (F. H. Hughes Company, London, 1950), p. 234.

Pseudoscalar Coupling in Pseudoscalar Meson Theory

G. WENTZEL
Institute for Nuclear Studies and Department of Physics, University of Chicago, Chicago, Illinois
(Received April 11, 1952)

IT is well known that, in pseudoscalar Yukawa theory, the pseudoscalar and pseudovector coupling types are equivalent within certain limitations.[1] Independent of perturbation expansions, the relationship between the two theories (omitting electromagnetic effects) is most clearly established by Foldy's transformation.[2] Starting out with the Lagrangian of the pseudoscalar coupling, charge-symmetric theory

$$L=L_\varphi-\bar\psi(\gamma_\nu\partial/\partial x_\nu+M)\psi-if M\bar\psi\gamma_5\tau_a\psi\varphi_a,$$
$$L_\varphi=-\tfrac{1}{2}[(\partial\varphi_a/\partial x_\nu)^2+\mu^2\varphi_a^2], \tag{1}$$

and applying the transformation

$$\psi=U\psi', \quad U=\left(\frac{1-if\gamma_5\tau_a\varphi_a}{1+if\gamma_5\tau_a\varphi_a}\right)^{\frac{1}{2}},$$
$$U^{-1}=U^*=\gamma_4U\gamma_4,$$

one finds for L (1) the new form

$$L=L_\varphi-\bar\psi(\gamma_\nu\partial/\partial x_\nu+M[1+f^2\varphi_a^2])\psi'$$
$$-\tfrac{1}{2}if\bar\psi(\gamma_5\gamma_\nu\tau_\beta\psi'\partial\varphi_\beta/\partial x_\nu)[1+f^2\varphi_a^2]^{-1}, \tag{2}$$

which becomes the pseudovector coupling Lagrangian if the terms $f^2\varphi_a^2$ are neglected (in two places). For obtaining approximate equivalence, a first requirement is

$$f^2\varphi_a^2\ll1, \tag{3}$$

effectively. This suggests a power expansion whose leading terms, besides the free field Lagrangians, are

$$L'=-\tfrac{1}{2}if\bar\psi\gamma_5\gamma_\nu\tau_\beta\psi'\partial\varphi_\beta/\partial x_\nu, \tag{4}$$

$$L''=-\tfrac{1}{2}Mf^2\bar\psi\psi'\varphi_a^2. \tag{5}$$

As to L'', it is true that it contains mostly "mass effects" (Dyson[3]), i.e., terms to be subtracted in any renormalization procedure. Nevertheless, L'', even as a first-order perturbation, gives rise to such processes as the scattering of mesons by nucleons, and meson pair creation by nucleons (in the presence of external nuclear fields). In the second order, L'' also contributes to the nuclear forces.[4] Since L'' carries the large factor M, it is clear that the nth-order effects of L'' will outweight the $(2n)$th-order effects of L' unless mesons with momenta $>M$ play a predominant role.

The condition (3) actually characterizes L' as a weak perturbation; not so L''. It is obviously desirable to treat L'' in a more adequate manner, and this is known to be possible because L'' happens to be the interaction of the scalar pair theory. This theory has been worked out[4] in a static approximation ($\bar\psi\psi'\to\Sigma_s\delta(\mathbf{x}-\mathbf{x}_s)$; a charged φ field only was considered, but the inclusion of neutral mesons is trivial). The neglect of nuclear recoils falsifies, of course, the contributions of high energy virtual mesons; but a cutoff, introduced *ad hoc*, eliminates these contributions. In the application to the problem (1) or (2), choosing the cut-off energy in the order of M will ensure qualitatively reliable results.

The rigorous static solutions show, then, that the effects of a large interaction L'' are much alleviated owing to a characteristic dependence on the coupling parameter (Mf^2). For instance, the cross section of meson-nucleon scattering (L'' yields S-scattering only) is

$$d\sigma/d\Omega=[4\pi(Mf^2)^{-1}+A]^{-2} \tag{6}$$

(A = cut-off momentum), and the same factor appears in the expression for the two-nucleon potential (due to L''):

$$V(r)=-\tfrac{1}{2}[4\pi(Mf^2)^{-1}+A]^{-2}\mu e^{-2}|H_1^{(1)}(2i\mu r)| \quad (r\gg A^{-1}). \tag{7}$$

Dropping A in either (6) or (7) would lead to the results of fourth-order (static) perturbation theory. But since A is several times larger than $4\pi(Mf^2)^{-1}$ (taking $f\gtrsim\mu$ and $A=M$), the actual values of both σ and $|V|$ are much smaller than expected from a perturbation treatment.[5] This may mean, of course, that the contribution of L' (4) are possibly of comparable magnitude. Indeed, the spin-dependent part of the nuclear forces[6] can only result from L' [granting (3)]. The same is true for the nonisotropic part of the pion-nucleon scattering (P-scattering). Last not least, it should be observed that the cross section (6) is independent of the mesonic and nucleonic charges, in other words: the scattering

would be the same in S states of isotopic spins $\frac{1}{2}$ and $\frac{3}{2}$, and there would be no charge exchange S-scattering, in disagreement with recent experimental findings.[7] It will, therefore, be a most crucial test for the pseudoscalar coupling theory whether, in a more complete treatment, it can account for the isotopic spin dependence (and the angular distribution) of the pion-nucleon scattering.

An encouraging feature is the saturation character of the nuclear forces arising from L'' (see reference 4), but here, too, the effects of L' will hardly be negligible.

If f turns out too large for treating L' as a perturbation, the transformations of Dyson and Foldy will be practically useless, and the mathematical problem posed by this theory will become very difficult.

[1] E. C. Nelson, Phys. Rev. **60**, 830 (1941); F. J. Dyson, Phys. Rev. **73**, 929 (1948); K. M. Case, Phys. Rev. **76**, 14 (1949).
[2] L. L. Foldy, Phys. Rev. **84**, 168 (1951).
[3] H. A. Bethe, Phys. Rev. **76**, 191 (1949).
[4] G. Wentzel, Helv. Phys. Acta **15**, 111 (1942); Prog. Theoret. Phys. **5**, 584 (1950), Sec. II.
[5] K. M. Watson and J. V. Lepore (Phys. Rev. **76**, 1157 (1949); see Figs. 2, 3 and 5) find that higher corrections to V, up to the eighth order (f^8), tend to increase the two-nucleon interaction. This is hard to reconcile with our qualitative argument.
[6] Unless other (heavier) mesons contribute to the forces.
[7] Fermi, Anderson, and Nagle, Phys. Rev. (to be published).

Low Temperature Thermal Expansion of Uranium*

ADAM F. SCHUCH AND HENRY L. LAQUER
Los Alamos Scientific Laboratory, Los Alamos, New Mexico
(Received April 16, 1952)

IN extending our studies of the elastic constants of uranium[1] a knowledge of the lengths of uranium rods at low temperatures appeared desirable. A dial gauge dilatometer was adapted to low temperature operation by immersing the end of the quartz tube containing the one-inch specimen in various refrigerants. Temperature of the specimen was measured with a copper-constantan thermocouple. Temperature gradients along the inner and outer quartz tubes were kept identical by filling the dilatometer with helium gas at about eight inches of mercury. A check run with a fused quartz rod was satisfactory in that the dial gauge reading remained constant. Another check run with oxygen-free high conductivity copper gave results (Fig. 1) in reasonable agreement with precision literature values,[2] after the necessary corrections had been made for the expansion of the fused quartz.[2,4]

On the other hand, the results obtained with coarse-grained uranium are quite unexpected in that the material expands upon cooling from the temperature of liquid nitrogen to that of liquid hydrogen. This behavior is reversible, and, as far as one can tell, there is no hysteresis. Final length readings are obtained within two or three minutes after changing the refrigerant, which is merely the time required for temperature equilibrium to be established. Similar results were obtained with three different specimens taken from a two-inch diameter casting along the directions shown in the figure. The casting had been annealed for six hours in the β-phase and was then cooled slowly to room temperature. There is a slight orientation effect, but it appears between room temperature and 75°K and is less than the experimental error at lower temperatures. The length changes shown in the figure have been reckoned from the room temperature (298°K) lengths of each specimen. This presentation increases the scatter of the low temperature points over what it would have been if all measurements had been referred to the 20°K lengths. Nevertheless, the increase in length of uranium upon cooling from liquid nitrogen to liquid hydrogen temperature is clearly shown.

One has to conclude that the inversion of thermal expansion corresponds to a density maximum. The present measurements do not give the complete thermal expansion curve below 60°K. However, an abrupt length and, hence, phase change appears unlikely on the basis of the specific heat measurements,[5] which indicate no transitions in this temperature range. Thus, one has to call on the anisotropy of uranium for a possible explanation of this anomalous behavior. X-ray observations indicate that uranium has a negative expansion coefficient for one crystal axis above room

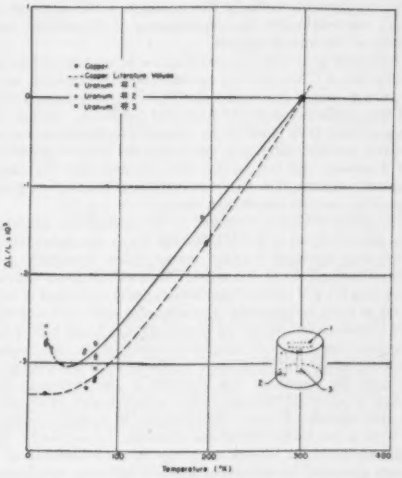

FIG. 1. Low temperature thermal expansion of uranium.

temperature,[6] and it might be that, at low temperatures, the negative expansion along this direction could become dominant in an aggregate of randomly oriented crystals. Further speculation on the nature of the anomaly will have to wait for more complete data on other physical properties.

The writers are indebted to Dr. F. M. Walters, Jr., for the loan of his dilatometer and for stimulating discussions.

* This paper is based on work performed under University of California contract with the AEC.
[1] Laquer, McGee, and Kilpatrick, Trans. Am. Soc. Metals **43**, 771 (1950).
[2] R. E. Gaumer and R. B. Scott, *The Thermal Expansion of Copper, A Literature Survey*, National Bureau of Standards Progress Report No. 2 for ONR Contract NAonr 12-48, pp. 26-29, January 13, 1949.
[3] K. Scheel and W. Heuse, Verhandl. deut. physik. Ges. **16**, 1 (1914).
[4] W. H. Keesom and D. W. Doborzyński, Physica **1**, 1089 (1934).
[5] Long, Jones, and Gordon, **20**, 695 (1952).
[6] J. J. Katz and E. Rabinowitch, *The Chemistry of Uranium* (McGraw Hill Book Company, New York, 1951), Part I, Chap. 5, National Nuclear Energy Series, Plutonium Project Record, Vol. 5, Div. VIII.

Calorimetric Determination of the Relationship between the Half-Life and Average Beta-Energy of C^{14}†

G. H. JENKS AND F. H. SWEETON
Chemistry Division, Oak Ridge National Laboratory, Oak Ridge, Tennessee
(Received April 18, 1952)

CALORIMETRIC determinations have been made of the power generated by the beta-ray emission from samples containing measured amounts of carbon-14. The measured power per atom of C^{14} is equal to the product of the decay constant and the average beta-energy of C^{14}.

The calorimeter used was a modification of a liquid nitrogen calorimeter described by Cannon and Jenks.[1] The modified instrument operated at liquid helium temperatures and was considerably more sensitive than the liquid nitrogen calorimeter.

The amount of C^{14} in the calorimetric samples was estimated from measurements of the density of C^{14}-enriched CO_2 samples relative to that of normal CO_2. The relative density measurements were made by means of a small, extremely sensitive, gas density balance. The volumes of the calorimetric samples were determined by standard methods. The accuracy of the sampling procedure was established by measurements of the relative radioactivity of the various samples.

Chemically pure CO_2 was essential for accurately ascertaining the fraction of $C^{14}O_2$ from the measured relative densities. Active CO_2 was generated from active $BaCO_3$ by thermal decomposition and was purified by repeated fractional distillation. Normal CO_2 was generated from $NaHCO_3$ by thermal decomposition and was similarly purified. After each distillation the relative gas density was measured, and this process was repeated until the density remained constant. The CO_2 was handled in an all-glass system employing mercury cut-off type valves.

The thermal sources employed in the calorimetric determinations were designed to preclude storage of any significant fraction of the total absorbed beta-ray energy. They were made up of approximately 4 ml of the active CO_2 sealed in glass ampoules containing 0.1 g of charcoal and helium gas at a pressure of about 76 cm at room temperature. The ampoules were lined internally with aluminum foil. When the sources were at liquid helium temperatures, the CO_2 was completely adsorbed on the charcoal. Thus, the major portion of the C^{14} beta-rays was absorbed in the charcoal; the remainder was absorbed in the aluminum liner. Storage of absorbed beta-ray energy in metals such as aluminum is highly unlikely. However, the possibility of storage of energy in charcoal at low temperatures was uncertain. Consequently, charcoal was tested for storage of energy by measurements of the powers generated by absorption of Au^{198} beta-rays in aluminum and in charcoal. No storage was detected.

The fraction of $C^{14}O_2$ in the active CO_2 was 0.227, and the active CO_2 generated 3.91×10^{-3} watt per mole. The estimated probable error for each of these experimental values is ±1.0 percent. For pure C^{14}, the power generated per mole is 1.72×10^{-2} watts ±1.4 percent. The product of the decay constant and the average beta-energy of C^{14} is then computed to be 1.79×10^{-10} kev disintegration^{-1} sec^{-1}.

Reported values for the half-life of C^{14} have ranged from less than 5000 to greater than 7000 years. Better agreement exists among recent values, which fall in the approximate range 5400 to 5600 years.[2]

No measurements of the average beta-energy as such have been reported, but the beta-spectrum of the decay has been studied by several investigators.[3] The results are not in agreement as to the exact distribution of the beta-ray energies. Some of these results indicate that the distribution has an allowed shape, but others show deviations from this shape. If the shape of the spectrum is allowed, the average beta-energy can be computed since the maximum energy is known (155 kev). Ketelle[3] has carried out this computation by the method of numerical integration and obtained the value 49.0 kev. Average beta-energy values were also estimated from the published measurements in which an allowed shape was not found. In each case, the estimated value was greater than 49.0 kev.

If the correct value for the average energy is assumed to be 49.0 kev as calculated for a beta-distribution with allowed shape, the results of the present study yield a value of 6030 years for the half-life. Conversely, if the true half-life value is about 5500 years, the average energy calculated from the present results is about 45 kev.

† This work was performed for the AEC.

[1] C. V. Cannon and G. H. Jenks, Rev. Sci. Instr. **21**, 236 (1950).

[2] For references up to 1950, see Hornyak, Lauritsen, Morrison, and Fowler, Revs. Modern Phys. **22**, 333 (1950). Later half-life references are G. G. Manov and L. F. Curtiss, J. Research Natl. Bur. Standards **46**, 328 (1951); A. G. Engelkemeir and W. F. Libby, Rev. Sci. Instr. **21**, 550 (1950); a later reference for the beta-spectrum is S. D. Warshaw, Phys. Rev. **80**, 111 (1950).

[3] B. H. Ketelle, private communication.

Formation and Annulment of Space Charges in Glass and Their Influence on Electric Breakdown

K. J. KELLER
Research Department of the N. V. KEMA, Arnhem, Netherlands
(Received April 7, 1952)

THOUGH it is a well-known fact, the dependence of the electric breakdown field strength of solid dielectrics on the rate of application of stress is often neglected. Previous measurements of the author[1,2] have shown that, in breakdown tests on glass, prebreakdown heating of the test sample is one of the main causes for this dependence, although other effects cannot be excluded. Analogous to the space charges in gases leading to streamer building, it is expected that space charges of ions, left behind by prebreakdown electron avalanches, or of displaced ions in ionic conductors will give rise to field distortion and thus decrease the breakdown voltage with increasing time of application of electric stress.

In recent experiments, it was possible to separate the heat effect from the more permanent space charge effect by (1) prestressing the samples for some seconds with 1.3–1.35 Mv/cm (i.e., for the kind of glass used in these experiments, about 90 percent of breakdown field strength for a time of rise of voltage amounting to 30 seconds), (2) allowing the samples during a few minutes to cool down (if heated) and (3) testing them afterwards with impulse voltage (time of rise 10^{-6} sec, negligible prebreakdown heating). Electrodes consisting of an aqueous solution of $CuSO_4$ were used, as these give the least scattering of breakdown results.

In Fig. 1, N_1 gives the number of impulse breakdown tests with a given breakdown field strength for test specimens, prepared as described in (1), without any pretreatment; N_2 gives the distribution of breakdown field strengths for prestressed samples which show 1 to 3 Mv/cm lower results, owing to field distortion by space charges formed during prestressing. Even after a 20-hour storage at room temperature the effect of prestressing could still be observed. However, prestressed samples that were kept in a furnace at 150°C during 3 hours and cooled slowly showed practically the same distribution (N_3) for impulse tests as the original samples, which proved that prestressing had a reversible effect (space charge) and did not cause permanent damage. N_4 was meant to be a control and showed that the annealing had practically no influence on samples that were not first electrically stressed.

The preceding and other time-dependent effects influencing breakdown field strength measurements should be thoroughly investigated before a theory including these effects can be pro-

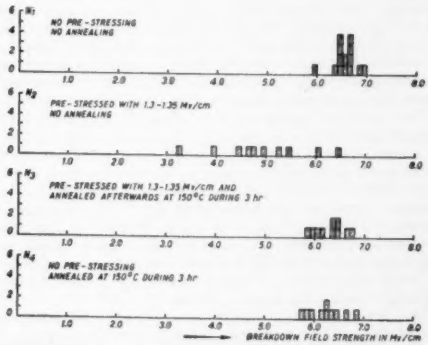

FIG. 1. Histograms showing decrease of breakdown field strength at room temperature of glass caused by space charges generated during prestressing; and removal of the space charges by annealing the test samples after prestressing.

posed, or measurements must be made in which the effects are avoided; to check existing theories with dc experiments is useless.

The author expresses his thanks to Dr. J. J. Went, head of the research department of the N.V. KEMA, for his stimulating interest during the experiments and for valuable discussion of the results and to Mr. Vedder for his assistance in preparing the test samples.

[1] K. J. Keller, Physica **14**, 475 (1948).
[2] K. J. Keller, Physica **17**, 511 (1951).

Recent Studies of the Isotopes of Emanation, Francium, and Radium*

F. F. Momyer, E. K. Hyde, A. Ghiorso, and W. E. Glenn
Ratiation Laboratory and Department of Chemistry, University of California, Berkeley, California

(Received April 18, 1952)

An earlier study[1] of the alpha-decay characteristics of the low mass isotopes of francium and emanation produced by bombardment of thorium with 340-Mev protons for the purpose of correlating these characteristics with the 126-neutron shell has been continued and expanded to include the element radium.

Greatest progress has been made in the case of emanation where the properties listed in Table I have been measured.

Table I. Radioactive properties of low mass emanation isotopes.

Isotope	Observed half-life	Alpha-particle energy ±0.02 Mev	EC/α branching ratio
Em^{209}	31 min	6.0[a]	4–6
Em^{210}	2.7 hr	6.02	~0.1
Em^{211}	16 hr	5.82	2.8
Em^{213}	23 min	6.23[b]	<0.01

[a] This isotope is to be identified with the 2.1-hr activity reported by Ghiorso, Meinke, and Seaborg, Phys. Rev. **76**, 1414 (1949).
[b] This value supersedes that given by Hyde *et al.* (see reference 1); also the Fr^{213} alpha-particle energy should be raised to 6.36 Mev.

This work was greatly facilitated by the development of a method for the preparation of platinum plates with the emanation atoms so firmly affixed that counting techniques typical for nongaseous radioactive samples could be employed. In brief, this method consisted of ionization of the gaseous atoms in a glow discharge and acceleration of these ions into a platinum plate at a potential of a few hundred volts. The method is being applied successfully to krypton and xenon as well as emanation and should be widely applicable in nuclear studies of the nuclides of these elements. This technique resembles that reported by Bergström *et al.*[2] in the study of mass-spectrographically separated radioactive isotopes of rare gas elements.

It is interesting to note that a plot of the alpha-decay energies for the emanation isotopes against neutron number is strikingly similar to the corresponding plot for the isotopes of polonium and astatine as shown in Fig. 1. The alpha-decay energy of At^{211} is given as 5.96 Mev (alpha-particle energy, 5.85 Mev) to correspond with a recent redetermination by us.

Many experiments were performed to obtain information on francium isotopes other than Fr^{212} in this mass region. In this work carrier free fracium fractions were isolated from thorium target solutions by an improved method developed by Hyde.[3] Any isotopes of half-life greater than 5 minutes would have been identified easily. It can be stated that the apparent half-lives of Fr^{213}, Fr^{211}, and isotopes of mass less than 211 are all shorter than 5 minutes. Incomplete results indicate a half-life of 2–5 minutes for Fr^{211} with electron capture (EC) prominent.

Mass assignments in the genetically-linked $Fr^{213}-Em^{213}-At^{209}-Po^{209}$ system were made certain by a mass spectrographic assignment of the key nuclide Fr^{213}. This was done with the time of flight mass spectrometer developed by Glenn.[4]

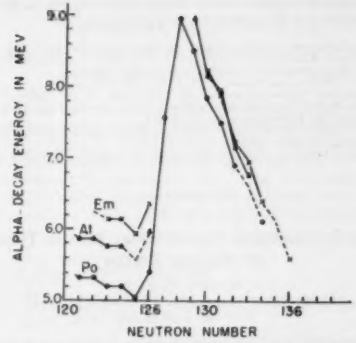

Fig. 1. Similarity of shell effect in elements 84–86 shown by plot of alpha-decay energy *versus* neutron number.

Attempts were made to isolate chemically radium isotopes of mass 214 or less and thus prove that the shell effect extended to this element. However, the stabilization was expected to lengthen the alpha-decay half-lives to the order of only a few minutes. Evidence was found for the following sequence:

$$Ra^{213} \xrightarrow[\sim 2\ \text{min}]{\alpha} Em^{209} \xrightarrow[31\ \text{min}]{EC} At^{209}, \quad Em^{209} \xrightarrow{\alpha} Po^{205}$$

The Ra^{213} was not observed directly because of its short half-life and because of the interference from heavier radium isotopes.

Cross checks are being carried out using a quite distinct method of preparation of the nuclides, namely the bombardment of lead foils with carbon ions. Miller *et al.*[5] have recently reported the attainment of a sizable beam of energetic (>100 Mev) C^{+6} ions in the Crocker Laboratory 60-inch cyclotron and have effected such reactions as $Au^{197}(C^{12}, 4n)At^{205}$. For our purposes bombardment of lead foils produces radium isotopes of mass 216 or less by such reactions as $Pb^{208}(C^{12}, 4n)Ra^{216}$. These directly produced radium isotopes decay quickly by alpha-particle emission or electron capture to the emanation and francium isotopes in which we are interested. An outstanding advantage of this method, particularly for Ra^{213}, is that none of the higher mass isotopes of these elements can possibly be produced, and hence the interference from them is not present.

As a by-product of the studies of the emanation fraction from the thorium plus proton bombardments, some properties of the previously unreported Em^{211} were observed. The gaseous fraction from the dissolution of a thorium foil target bombarded with 100-Mev protons was purified and placed on a platinum plate using the glow discharge collection technique. This plate when examined in the alpha-ray pulse analyzer showed the alpha-particle peaks corresponding to 4.8-minute Fr^{211} and its 0.020 second daughter At^{211}. Later the expected growth and decay of the Po^{211} alpha-peak were observed. The $Fr^{211}-At^{211}$ double peak decayed with a half-life of 24 minutes. These facts can be interpreted only as meaning that Em^{211} is a beta-emitter of 24 minutes half-life. The alpha-branching is appreciable (of the order of 25 percent) and is currently under investigation.

This work is continuing and a complete report will be issued later.

We wish to acknowledge the assistance of J. T. Vale, L. B. Houser, and the 184-inch cyclotron crew in carrying out the high

energy proton bombardments. Thanks also are due G. B. Rossi for assistance in the carbon ion bombardments.

* This work was performed under the auspices of the AEC. Part of this material was presented at the XIIth International Congress of Pure and Applied Chemistry, New York City, September, 1951.

[1] Hyde, Ghiorso, and Seaborg, Phys. Rev. **77**, 765 (1951).

[2] Bergström, Thulis, and Andersson, Phys. Rev. **77**, 851 (1950).

[3] E. K. Hyde, University of California Radiation Laboratory Declassified Report No. 1578 (November 27, 1951).

[4] W. E. Glenn, University of California Radiation Laboratory Declassified Report No. 1628 (1952).

[5] Müller, Hamilton, Putnam, Haymond, and Rossi, Phys. Rev. **80**, 486 (1950).

The Symmetrical Pseudoscalar Meson Theory of Nuclear Forces

MAURICE M. LÉVY
Institute for Advanced Study, Princeton, New Jersey
(Received April 18, 1952)

AN analysis has been made of the neutron-proton interaction yielded by the symmetrical pseudoscalar meson theory, with pseudoscalar coupling, using the Tamm-Dancoff[1] nonadiabatic treatment, which has been extended in order to include pair formation and higher order effects in the exchange of mesons.[2]

By eliminating all the probability amplitudes $a_\lambda^{(m,n)}$ of states where m mesons and n nucleon pairs are present, an equation can be obtained for $a_\lambda^{(0,0)}$, which, in the nonrelativistic region, reduces to the Schrödinger equation.[3] In this region, this amplitude is identical with the "large" Fourier component of the Bethe and Salpeter wave function,[3] for equal times of the interacting nucleons.

In the following treatment, the exact pseudoscalar interaction has been calculated in the nonrelativistic region. For distances of the order of the nucleon Compton wavelength, the interaction has been replaced by an infinitely repulsive potential of radius r_0, since the pseudoscalar meson theory cannot be expected to give reliable results in this region, on account of the existence of heavier mesons than π-mesons, isobaric states of nucleons, etc. Besides, there are some indications that the pseudoscalar interaction becomes indeed repulsive at short distances, the lowest order terms of the potential being dominated by the so-called "contact" terms which actually have a range of order $\hbar/Mc$. For example, the second-order interaction behaves in the relativistic region like a "nonlocal" operator equivalent to a potential $V_0^{(2)}(r)$, defined by

$$V_0^{(2)}(r)\psi^{(0,0)}(\mathbf{r}) = -\frac{1}{3}\frac{f^2}{4\pi}M^2(\boldsymbol{\tau}_1\cdot\boldsymbol{\tau}_2)(\boldsymbol{\sigma}_1\cdot\boldsymbol{\sigma}_2)\frac{K_1(Mr)}{r} \times\int\frac{K_1(Mr')}{r'}\psi^{(0,0)}(\mathbf{r}')d\mathbf{r}', \quad (1)$$

where $\psi^{(0,0)}(\mathbf{r})$ is the Fourier transform of $a^{(0,0)}(\mathbf{p})$, in the center-of-mass system, and $K_n(x)$ the nth order Hankel function of imaginary argument. $V_0^{(2)}$ is repulsive for singlet and triplet even states.

For $r>r_0$, the second-order interaction reduces to the well-known potential (which can also be obtained from the pseudovector coupling)

$$V_2(r) = +\frac{f^2}{4\pi}\left(\frac{\mu}{2M}\right)^2\frac{(\boldsymbol{\tau}_1\cdot\boldsymbol{\tau}_2)}{3}\left\{\boldsymbol{\sigma}_1\cdot\boldsymbol{\sigma}_2+\left[1+\frac{3}{\mu r}+\frac{3}{(\mu r)^2}\right]S_{12}\right\}\frac{e^{-\mu r}}{r}, \quad (2)$$

where $S_{12}=3(\boldsymbol{\sigma}_1\cdot\mathbf{r})(\boldsymbol{\sigma}_2\cdot\mathbf{r})/r^2-\boldsymbol{\sigma}_1\cdot\boldsymbol{\sigma}_2$. In the fourth-order in f, the main contribution to the interaction comes from processes which involve the creation of two pairs of nucleons. It is spin and charge independent and can be written

$$V_4(r) = -3\left(\frac{f^2}{4\pi}\right)^2\left(\frac{\mu}{2M}\right)^3\frac{1}{\mu r^2}\left\{\frac{2}{\pi}K_1(2\mu r)+\left[\frac{2}{\pi}K_0(\mu r)\right]^2\right\}. \quad (3)$$

The first term of (3) comes from virtual processes involving the simultaneous exchange of 2 mesons; the second from effects in which only one meson is present at the same time in the intermediate states.

Higher order terms of the interaction which do not involve radiative effects have been found to be small for $r\geqslant r_0$, for two reasons:

(a) Their strength becomes smaller and smaller even if $f^2/4\pi$ is of the order of 10, because of higher and higher powers of $(Mr)^{-1}$ multiplying the interaction. For example, the sixth-order interaction is of the order of $(f^2/4\pi)(Mr)^{-2}$ times the fourth-order interaction.

(b) Their range also becomes smaller and smaller, since a process involving the exchange of m mesons yields an interaction range of order $(1/m)(\hbar/\mu c)$.

An analysis has also been made of the contribution of the radiative effects to the interaction, starting from the equation of Bethe and Salpeter, and transforming it into a one-time equation, by means of a method which has been given previously.[3] The vertex parts of the irreducible diagrams are taken into account by modifying γ_5, which becomes, to the second order in f, between two states of four-momenta p and p':

$$\Gamma_5(p,p') = \gamma_5[1-(f^2/4\pi^2)U(p'-p)], \quad (4)$$

where

$$U(p) = \int_0^1\frac{x(1-2x)p^2}{x(1-x)p^2+M^2}dx. \quad (5)$$

Similarly, the Δ_F function is replaced by Δ_F', in order to account for closed loops insertion in the meson lines:

$$\Delta_F'(x) = -\frac{2i}{(2\pi)^4}\int e^{ikx}\frac{d^4k}{k^2+\mu^2}\left[1-\frac{f^2}{2\pi^2}U(k)\right]. \quad (6)$$

These radiative terms give contributions to the interaction which are of order $(f^2/4\pi)(Mr)^{-2}$. In Eq. (4), we have omitted terms which arise from the fact that, in the initial and final states, the nucleons are bound. A careful examination of these terms shows that they give corrections of the order of $(f^2/4\pi)(Mr)^{-3}\log Mr$.

A study of the low energy properties of the neutron-proton system has been carried out using, for $r\geqslant r_0$, the potential $V_2(r)+V_4(r)$ defined by (2) and (3), and a repulsive core for $r<r_0$. The range of the forces has been chosen equal to the Compton wavelength of the π-mesons: $\hbar/\mu c=(1.40\pm0.03)10^{-13}$ cm. The two constants $f^2/4\pi$ and r_0 have been determined by fitting exactly the deuteron binding energy, (-2.227 ± 0.003) Mev, and the neutron-proton zero energy scattering length $(-23.68\pm0.06)10^{-13}$ cm. These values are as follows:

$$f^2/4\pi = 9.7\pm1.3, \quad r_0=(0.38\pm0.03)(\hbar/\mu c). \quad (7)$$

This value of r_0 is in agreement with the value of r at which the interaction (1) becomes important.

The following derived quantities have been obtained using these constants:

Singlet effective range: $1.78(\hbar/\mu c)$,
Triplet effective range: $1.185(\hbar/\mu c)$,
Electric quadrupole moment: 2.08×10^{-27} cm^2,
Proportion of D state: 0.051,
Mean value of the momentum: $\langle p^2/(\mu c)^2\rangle=1.76$.

These results are in good agreement with experiment, except the quadrupole moment, which is too small by about 20 percent. This quantity is, however, sensitive to an increase of the tensor force and can probably be improved by including the sixth-order corrections.[4]

The writer is greatly indebted to Professors Oppenheimer, Pais, and Peierls, and to Dr. F. Low, for interesting discussions and helpful suggestions, and to the Institute for Advanced Study for financial support.

[1] I. Tamm, J. Phys. (U. S. S. R.) **9**, 449 (1945); S. M. Dancoff, Phys. Rev. **78**, 382 (1950).

[2] M. Lévy, Bull. Am. Phys. Soc. **27**, No. 1, 51 (1952); M. Lévy (to be published).

[3] E. Salpeter and H. A. Bethe, Phys. Rev. **84**, 1232 (1951); M. Gell-Mann and F. Low, Phys. Rev. **84**, 350 (1951).

[4] After this paper was completed, the writer has seen two abstracts on related work by J. V. Lepore and R. Jastrow, Bull. Am. Phys. Soc. **27**, No. 3, 33 (1952).

Isolated and Adiabatic Susceptibilities*

MARTIN J. KLEIN
Department of Physics, Case Institute of Technology, Cleveland 6, Ohio
(Received April 11, 1952)

IN two recent papers[1,2] there has been a discussion of the difference between the isolated and the adiabatic susceptibilities of a system, a question of interest in connection with the application to experiments of the Casmir-duPré theory of paramagnetic relaxation. It is the purpose of this note to help to clarify the points involved in this discussion.

We consider a system whose energy states W_i depend upon the magnetic field H. The average magnetic moment $\langle M\rangle$ of this system is given by

$$\langle M\rangle=\Sigma_i M_i p_i, \tag{1}$$

where

$$p_i=\exp(-W_i/kT)/\Sigma_j \exp(-W_j/kT), \tag{2}$$

and where

$$M_i=-\partial W_i/\partial H. \tag{3}$$

The adiabatic susceptibility χ_{ad} is defined by the equation

$$\chi_{ad}=(\partial\langle M\rangle/\partial H)_s, \tag{4}$$

where s is the entropy. The isolated susceptibility χ_{iso} is defined by the equation

$$\chi_{iso}=\Sigma_i(\partial M_i/\partial H)p_i. \tag{5}$$

From Eqs. (1) and (5) it is seen that χ_{iso} will be the susceptibility appropriate to a situation in which the p_i are unchanged by a change in magnetic field. Hence, we must have

$$(\partial p_i/\partial H)_{iso}=0 \quad \text{(all } i\text{)}. \tag{6}$$

Our first point is that the system will remain in equilibrium under the conditions imposed by Eq. (6) only if certain rather severe restrictions on the energy states W_i are satisfied. More precisely, if the p_i continue to have the form given by Eq. (2), so that the distribution is characterized solely by its temperature, then the condition expressed by Eq. (8) below must be fulfilled. We can calculate $(\partial p_i/\partial H)_{iso}$ to be given by the expression

$$\left(\frac{\partial p_i}{\partial H}\right)_{iso}=\left(\frac{\partial \exp(-W_i/kT)}{\partial H}\right)_{iso}\Big/\Sigma_j \exp(-W_j/kT) - \exp(-W_i/kT)\Sigma_j\left(\frac{\partial \exp(-W_j/kT)}{\partial H}\right)_{iso}\Big/ (\Sigma_j \exp(-W_j/kT))^2. \tag{7}$$

Setting $(\partial p_i/\partial H)_{iso}$ equal to zero, we readily obtain the condition

$$(\langle\partial W/\partial H\rangle-\partial W_i/\partial H)/(\langle W\rangle-W_i)=(1/T)(\partial T/\partial H)_{iso}, \tag{8}$$

where the symbol $\langle\ \rangle$ stands for an average in the sense of Eq. (1).

Our second point is that when Eq. (8) is satisfied the isolated and adiabatic susceptibilities are identical. The difference between these susceptibilities has been shown by Broer and Van Vleck[3] to be given by the expression

$$\chi_{ad}-\chi_{iso}=(1/kT)[\{\langle W^2\rangle-\langle W\rangle^2\}\{\langle(\partial W/\partial H)^2\rangle-\langle\partial W/\partial H\rangle^2\} - \{\langle W\partial W/\partial H\rangle-\langle W\rangle\langle\partial W/\partial H\rangle\}^2]/[\langle W^2\rangle-\langle W\rangle^2]. \tag{9}$$

Using Eq. (8) we readily obtain

$$\langle\{\langle\partial W/\partial H\rangle-\partial W_i/\partial H\}^2\rangle=\langle(\partial W/\partial H)^2\rangle-\langle\partial W/\partial H\rangle^2 =(1/T^2)(\partial T/\partial H)_{iso}^2(\langle W^2\rangle-\langle W\rangle^2), \tag{10}$$

and

$$\langle\{\langle\partial W/\partial H\rangle-\partial W_i/\partial H\}\{\langle W\rangle-W_i\}\rangle =\langle W\partial W/\partial H\rangle-\langle W\rangle\langle\partial W/\partial H\rangle=(1/T)(\partial T/\partial H)_{iso} \times(\langle W^2\rangle-\langle W\rangle^2). \tag{11}$$

Using Eqs. (10) and (11) in combination with Eq. (9) it follows that

$$\chi_{ad}=\chi_{iso}. \tag{12}$$

One can also show that if the two susceptibilities are equal then a condition of the form of Eq. (8) must be satisfied, namely,

$$\{\langle\partial W/\partial H\rangle-\partial W_i/\partial H\}/\{\langle W\rangle-W_i\}=\alpha, \tag{13}$$

where α is independent of the index i. This result follows by applying the reasoning given above in reverse order, and the details will be omitted.

In conclusion we can say that a necessary and sufficient condition for the equality of the isolated and adiabatic susceptibilities is given by Eq. (13). Further, we have shown that the isolated susceptibility will have meaning, in the sense that the system remains canonically distributed, only if Eq. (8) [equivalent to Eq. (13)] is satisfied, imposing a severe restriction on the nature of the systems to which the concept of isolated susceptibility can be applied.[4]

* Supported in part by ONR.
[1] L. J. F. Broer, Physica **17**, 531 (1951).
[2] A. Wright, Phys. Rev. **76**, 1826 (1949).
[3] Reference 2, footnote on page 1837.
[4] The conditions given by Van Vleck (reference 3) for the equality of χ_{iso} and χ_{ad} are special cases of our result.

Neutron Groups from Protons on Cr^{53}, Co^{59} and Cl^{37}†

P. H. STELSON AND W. M. PRESTON
Laboratory for Nuclear Science and Engineering, Massachusetts Institute of Technology, Cambridge, Massachusetts
(Received April 18, 1952)

IN continuation of our program of investigation of excited states in light-medium weight nuclei ($A\sim40$ to 60) we have measured the neutron groups resulting from proton bombardment of Cr^{53}, Co^{59}, and Cl^{37}. These nuclei have sufficiently low (p, n) thresholds (1.406,[1] 1.889,[2] and 1.640[3] Mev, respectively) to allow the study, with our available proton energies, of the region up to ~1.5 Mev above the ground state in the residual nuclei Mn^{53}, Ni^{59}, and A^{37}.

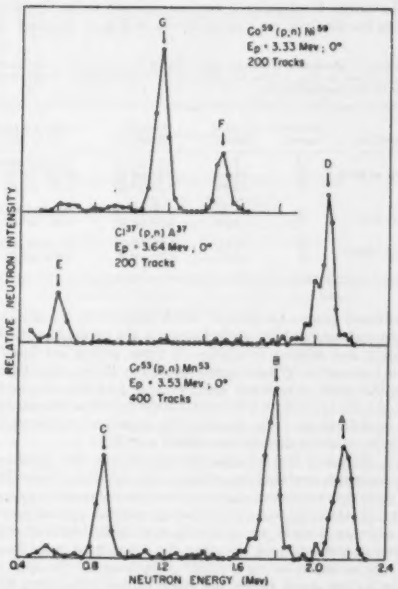

FIG. 1. Energy distributions of neutrons emitted in the forward direction for protons on Cr^{53}, Co^{59} and Cl^{37}.

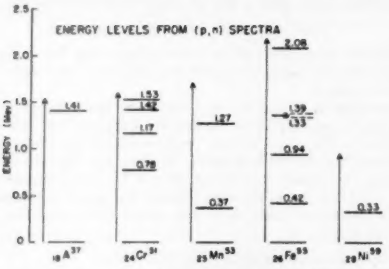

FIG. 2. Energy levels obtained from five (p, n) investigations. The vertical arrows indicate the excitation region studied.

The (p, n) reactions were produced by allowing monoenergetic protons from the Rockefeller electrostatic generator to strike thin targets (25 to 50 kev) prepared by evaporation onto backings of 10-mil tantalum. Target materials of pure cobalt metal, enriched Cr^{53} metal,[1] and NaCl of high purity were used. The (p, n) thresholds of Cl^{35} and Na^{23} are estimated from disintegration data to be above 4 Mev.

The neutron energies were measured by means of proton-recoil tracks in Eastman NTB emulsions of 200 microns thickness. Plates were placed a mean distance of 18 cm from the target at both 0 and 90 degrees with respect to the incident proton beam. Recoil tracks within 10 degrees of the neutron direction were accepted for measurement. The range-energy relation for the emulsion was determined by measuring neutrons of known energies from the $Li(p, n)$ reaction. Standard corrections were applied to convert the track length distributions to relative neutron intensities.[4]

The energy distribution of neutrons emitted in the forward direction for the three reactions is shown in Fig. 1. It is seen that well-defined groups are present which result from transitions to the ground state and low excited states of the residual nuclei. The Q-values and relative intensities of these groups are listed in Table I. Levels in A^{37} have been observed by Zucker and Watson[5] using the $A^{36}(d, p)$ reaction. Their value of 1.44 Mev for the first excited state agrees with our result. Grosskreutz[6] has also observed this level from the (p, n) reaction. No additional information is available on the excited states of Mn^{53} and Ni^{59}.

TABLE I. Measured Q-values and relative intensities for the neutron groups shown in Fig. 1. The last column lists the positions of the excited states in the residual nuclei.

Reaction	Neutron group	Q-value (Mev)	Relative intensities	Excitation energy (ΔQ in Mev)
$Cr^{53}(p, n)Mn^{53}$	A	-1.37	0.35 ± 0.04	Ground state
	B	-1.74	0.43 ± 0.04	0.370 ± 0.05
	C	-2.64	0.22 ± 0.03	1.27 ± 0.05
$Cl^{37}(p, n)A^{37}$	D	-1.58	0.78 ± 0.08	Ground state
	E	-2.99	0.22 ± 0.03	1.41 ± 0.05
$Co^{59}(p, n)Ni^{59}$	F	-1.84	0.28 ± 0.04	Ground state
	G	-2.17	0.72 ± 0.07	0.330 ± 0.05

It is recognized that the selection rules of beta- and gamma-ray emission which result in large differences in transition probabilities will mask the existence of excited states with unfavorable spin and parity. On the other hand, it is relatively easy for the fast protons and neutrons of the (p, n) reaction to carry several units of orbital angular momentum[4] and, therefore, the intensity of transitions to the residual states is not strongly influenced by the spin and parity of these states. Hence, one might expect to find more levels from the (p, n) investigation. This is the case for Fe^{55} where a direct comparison is possible.[4] It should be borne in mind, however, that the limited resolution of our (p, n) measurements prevents recognition as individual levels when the separation is ~ 50 kev or less. In Fig. 2 we have plotted the levels obtained for the five nuclei we have studied.[7]

† This work was jointly supported by the ONR and the Bureau of Ships.

[1] Lovington, McCue, and Preston, Phys. Rev. **85**, 585 (1952).
[2] J. J. G. McCue and W. M. Preston, Phys. Rev. **84**, 384 (1951).
[3] Richards, Smith, and Brown, Phys. Rev. **80**, 524 (1950).
[4] P. H. Stelson and W. M. Preston, Phys. Rev. **82**, 655 (1951).
[5] A. Zucker and W. W. Watson, Phys. Rev. **80**, 966 (1950).
[6] J. C. Grosskreutz and K. B. Mather, Phys. Rev. **77**, 580 (1950).
[7] Stelson, Preston, and Goodman, Phys. Rev. **80**, 287 (1950).

Numerical Work on the Fluctuation Problem in Cascade Shower Theory

J. W. GARDNER*
Atomic Energy of Canada Limited, Chalk River, Ontario, Canada
AND
H. MESSEL
Department of Mathematical Physics, University of Adelaide, Adelaide, South Australia
(Received April 14, 1952)

THE analytical development of the theory of fluctuations in the cascade showers of cosmic radiation has been presented in a series of recent publications. These cover the nucleon cascade in homogeneous nuclear matter,[1,2] the nucleon cascade in a finite absorber,[3] and the electron-photon cascade neglecting ionization loss (approximation A).[4] In each case the diffusion equations for the distribution function have been solved formally, and also general formulas have been obtained for its kth moment (the (k, l)th moment in the electron-photon cascade). The problem of obtaining explicit exact expressions for the distribution function by carrying out the integrations in the formal solutions looks so forbidding as to make one consider alternative, approximate methods, and such a method has been developed by Green and Messel,[5] who expand the distribution function in terms of its moments and the moments of some "trial" function. If the trial function is a reasonable approximation to the actual distribution function the expansion converges rapidly so that only the first few moments are required. (In the present case it turns out that the Pólya distribution is an excellent trial function.) Apart from the problem of finding the distribution functions themselves, a quantitative knowledge of their first few moments would be of great value in interpreting the experimentally observed fluctuations in cosmic-ray cascade showers, their behavior with height, latitude, etc.

The purpose of this note is therefore to announce that we are planning a program of numerical work on the Ferranti electronic computer at the University of Toronto Computation Center. It is proposed first to concentrate on the simplest case, namely the nucleon cascade in homogeneous nuclear matter. Such cascades occur, for example, in the nuclei of photographic emulsions, giving rise to the familiar "stars," so this work should make possible quantitative predictions about the numbers of particles occurring in the stars from various different kinds of nuclei. Moreover, experience gained in this work should pave the way to more difficult calculations of the nucleon cascade in a finite absorber, and the electron-photon cascade. We shall compute the first three moments of $\Phi(\epsilon, n_1, n_2; x)$, which expresses the probability of finding n_1 nucleons with energies $>\epsilon E_0$ and n_2 nucleons with energies $<\epsilon E_0$ at depth x in homogeneous nuclear matter as a result of a single primary nucleon of energy E_0; $\log_{10}\epsilon$ will be taken from -1.0 to -4.0 and x from 0 to 35 collision units, in appropriate intervals. With the Ferranti computer it will be possible to integrate the expressions for the moments directly, thus avoiding the somewhat dubious saddle point integrations of earlier, approximate evaluations of the first two moments, which were carried out on desk machines.[6]

This work will be carried out with the collaboration of Dr. C. C. Gotlieb and his staff at the Computation Center; we are greatly indebted to Dr. Gotlieb for according these facilities and for a discussion of the detailed programming.

* NRL Postdoctoral Fellow.
[1] H. Messel and J. W. Gardner, Phys. Rev. **84**, 1256 (1951).
[2] H. Messel, Proc. Phys. Soc. (London) (to be published).
[3] H. Messel and R. B. Potts, Proc. Phys. Soc. (London), (to be published).
[4] H. Messel and R. B. Potts, Phys. Rev. (to be published).
[5] H. S. Green and H. Messel, Proc. Cambridge Phil. Soc. (to be published).
[6] H. Messel, Comm. Dublin Inst. for Adv. Studies, Series A. No. 7 (1951).

A Method of Synthesis of the Statistical and Impact Theories of Pressure Broadening

P. W. Anderson
Bell Telephone Laboratories, Murray Hill, New Jersey
(Received April 17, 1952)

TWO types of theories of pressure broadening have been current in the literature: the "statistical" theory of Kuhn[1] and Margenau,[2] and the "impact" theory of Weisskopf,[3] Lenz,[4] and others. Spitzer[5] and Holstein[6] have indicated the limits of validity of the two types of theory: At low pressures the statistical theory is certainly valid on the wings of the line, the impact theory in the center, while at high pressures the statistical theory is valid if its fundamental assumption that the frequency perturbation for a given atom is the sum of that due to all others in the gas,

$$\nu = \sum_{i=1}^{N} \nu(R_i), \tag{1}$$

is not too seriously incorrect. Most of these discussions and this note are confined to the "adiabatic" or nondegenerate case in which the perturbations due to the atoms in the gas may be expressed simply as frequency perturbations.

Lindholm[7] carried out a complete study of the transition between the two theories for a frequency perturbation proportional to $1/R^4$. Unfortunately, he used a simplified model of the collision in which the frequency was constant during the collision and thus the perturbation started and stopped abruptly; some of his results seem to be in error because of this fact.

This note presents a more general and more workable technique for synthesizing the two theories and studying the transition between them. The spectral intensity which is desired is given by the Fourier integral

$$I(\omega) = \left| \int_{-\infty}^{\infty} \exp\left[i\left(\omega t - \int_{-\infty}^{t} \nu(t')dt' \right) \right] dt \right|^2, \tag{2}$$

where $\nu(t')$ is the frequency at the time t', given by (1) with the R_i assuming the correct values for this time. Now we transform (2) by the standard correlation-function transformation[8] and obtain

$$I(\omega) = \int_{-\infty}^{\infty} e^{i\omega\tau}\varphi(\tau)\,; \tag{3a}$$

$$\varphi(\tau) = \int_{-\infty}^{\infty} dt \exp\left[i \int_{t}^{t+\tau} \nu(t')dt' \right] = \left\langle \exp\left[i \int_{0}^{\tau} \nu(t')dt' \right] \right\rangle_{Av}. \tag{3b}$$

We now use (1) and obtain

$$\varphi(\tau) = \left\langle \prod_i \exp\left[i \int_0^\tau \nu(R_i)dt \right] \right\rangle_{Av}.$$

To an approximation more than adequate for our purposes the motions of the molecules in the gas are independent, so that

$$\varphi(\tau) = \left\{ \left\langle \exp\left[i \int_0^\tau \nu(R)dt \right] \right\rangle_{Av} \right\}^N. \tag{4}$$

More general methods of averaging are possible than the following, in case the situation is more complicated, but this should suffice to show the method: Suppose that the paths of atoms are straight relative to each other; then the parameters to be averaged over are b, the impact parameter, and x_0, the position of the atom at the start of the time-interval 0 to τ along the straight line of impact parameter b. Now

$$2\pi \int bdb \int dx_0 = V, \tag{5}$$

where V is the volume available to the N atoms of the gas. Then

$$\varphi(\tau) = \left(1 - \frac{2\pi}{V} \int_0^\infty bdb \int_{-\infty}^{\infty} dx_0 \times \left\{ 1 - \exp\left[i \int_0^\tau \nu([(x_0+vt)^2+b^2]^{\frac{1}{2}})dt \right] \right\} \right)^N = \exp[-nV'(\tau)]. \tag{6}$$

Here $n = N/V$ = density of atoms per cc, and

$$V'(\tau) = 2\pi \int_0^\infty bdb \int_{-\infty}^{\infty} dx_0 \times \left\{ 1 - \exp\left[i \int_0^\tau \nu([(x_0+vt)^2+b^2]^{\frac{1}{2}})dt \right] \right\}. \tag{7}$$

It is an easy matter, for which we have no space here, to show that (6) and (7), with (3a), lead to the impact and statistical theories in the proper limits. The criteria for validity of the two theories are easily derived, being the same as those given in references 5 and 6; in particular, these hold even for $\nu \sim 1/R^3$, a case in which there had been some question as to the validity of the impact theory in the low-pressure limit. Analytical methods can be applied to give first corrections to the two types of theories, while V', which is a function only of one variable for a given form of $\nu(R)$, can be approximated numerically for any given $\nu(R)$ without much difficulty. The numerical calculation of the line shape for various densities, from (3a), should then be fairly easy.

Further details, and some computations using the above method, will be given in a later publication.

[1] H. Kuhn and F. London, Phil. Mag. **18**, 983 (1934).
[2] H. Margenau, Phys. Rev. **48**, 755 (1935).
[3] V. Weisskopf, Physik. Z. **34**, 1 (1933).
[4] W. Lenz, Z. Physik **80**, 423 (1933).
[5] L. Spitzer, Phys. Rev. **58**, 348 (1940).
[6] T. Holstein, Phys. Rev. **79**, 744 (1950).
[7] E. Lindholm, Arkiv. Mat. Astr. Fys. **32**, No. 17 (1945).
[8] See, for instance, H. M. Foley, Phys. Rev. **69**, 616 (1946).

Quadrupole Coupling Ratio of the Chlorine Isotopes*

T. C. Wang and C. H. Townes
Columbia University, New York, New York
and
A. L. Schawlow and A. N. Holden
Bell Telephone Laboratories, Murray Hill, New Jersey
(Received April 7, 1952)

THE ratio of the nuclear quadrupole coupling constants, eqQ, for the chlorine isotopes has been found to depend to about 0.02 percent on the molecular environment. Radio frequency transitions were measured for several chlorine compounds in the solid state.

A variation in the ratio $(eqQ)_{35}/(eqQ)_{37}$ with molecular species is to be expected because of nuclear polarization and certain kinds of molecular vibrations.[1] A change as large as 0.1 percent has previously been reported in microwave spectra[2], but measurements of direct quadrupole transitions[3] with an accuracy of the order of 0.01 percent had failed to show conclusively any such variation.

The lines are narrow enough to permit considerably better accuracy, and were hence measured to an accuracy of about 0.001 percent. At Columbia University this degree of precision was obtained by using a Signal Corps type BC221 frequency meter to measure differences between the line frequency and a nearby harmonic of a standard crystal oscillator. At Bell Telephone

TABLE I. Measurements of chlorine nuclear quadrupole couplings (Observers: C—Columbia University; B—Bell Telephone Laboratories). Resonance frequencies are quoted only to the nearest kilocycle because of uncertainties in temperature measurement.

Substance	Temp. °C	Resonance frequency Mc(Cl^{35})	$(eqQ)_{35}/(eqQ)_{37}$	Obs.
p-$C_6H_4Cl_2$	26	34.262	1.268860 ±0.00001	B
	20.6	34.282	1.268861 ±0.00001	C
	0.2	34.349	1.268859 ±0.00001	C
	−195	34.780	1.268800 ±0.00001	C
	−195	34.780	1.268806 ±0.00001	B
(high temp. phase)[a]	27	34.235	1.268856 ±0.00001	B
$SbCl_3$ Strong lines	25.5	19.175	1.268920 ±0.00002	C
Strong lines	0.6	19.199	1.268898 ±0.00002	C
Strong lines	−195	19.305	1.268774 ±0.00002	C
Weak lines	25.5	20.407	1.269001 ±0.00002	C
Weak lines	0.6	20.474	1.268973 ±0.00002	C
Weak lines	−195	20.908	1.268831 ±0.00002	C
$NaClO_3$	26	29.920	1.268754 ±0.00001	B
	0.4	30.025	1.268739 ±0.00002	C
	−195	30.632	1.268736 ±0.00001	B
$KClO_3$	25.2	28.086	1.268758 ±0.00001	B
	−195	28.953	1.268734 ±0.00001	B
CH_2Cl_2	−195	35.993	1.268790 ±0.00001	B

[a] C. Dean and R. V. Pound, J. Chem. Phys. **20**, 195 (1952).

Laboratories harmonics of a General Radio Type 1110A Interpolating Frequency Standard were used. At both laboratories the nuclear quadrupole resonances were observed with frequency modulated oscillating detectors using triodes but differing in circuit details.

The results listed in Table I show that the ratio of $(eqQ)_{35}/(eqQ)_{37}$ depends on the compound and also on the temperature (see p-$C_6H_4Cl_2$ and $SbCl_3$). In $SbCl_3$ there are two nonequivalent sites for Cl in the crystal lattice giving different resonant frequencies, different variations with temperature, and different ratios $(eqQ)_{35}/(eqQ)_{37}$. The variations are within the reasonable upper limit of one part in 2500 for the effect of nuclear mass on zero-point vibrations.[1] Moreover, the dependence on temperature of the ratio confirms the effect of molecular vibrations on this ratio. It is very probably the higher frequency vibrations of the crystal lattice which are most important in changing the coupling ratio.

Some of the variation may be the result of nonisotropic polarization of the nucleus by the valence electrons. However, Table I shows that this effect does not produce variations much larger than 0.02 percent in these cases and is difficult to distinguish from the effects of lattice vibrations.

* Work supported jointly by the Signal Corps and the ONR.
[1] Gunther-Mohr, Geschwind, and Townes, Phys. Rev. **81**, 289 (1951).
[2] Geschwind, Gunther-Mohr, and Townes, Phys. Rev. **81**, 288 (1951).
[3] R. Livingston, Phys. Rev. **82**, 289 (1951).

Hyperfine Structure of $p_{\frac{1}{2}}$ States*

W. W. CLENDENIN
Yale University, New Haven, Connecticut
(Received April 9, 1952)

FOLEY[1] has considered the discrepancies between values of the nuclear moments of gallium and indium measured by atomic beam methods and the values obtained from magnetic resonance experiments. By using a nonrelativistic wave function he finds that a second-order perturbation term resulting from the atomic $p_{1/2}$ state modifies the apparent value of the nuclear moment factor g_I in the $p_{1/2}$ state by the factor

$$1/R=1-(\Delta\nu)/[6(2I+1)g_I\delta].$$

Here $\Delta\nu$ is the zero field hyperfine splitting and δ is the fine structure interval between $p_{1/2}$ and $p_{3/2}$ states.

It seemed desirable to see how this expression might be modified by the use of relativistic wave functions. For this purpose Dirac central field functions were employed for the electron in the $p_{1/2}$ and $p_{3/2}$ states. The terms arising from Dirac's equation resulting from the vector potentials $[\mathfrak{H}\times\mathbf{r}_e]/2$ of the applied field $\mathfrak{H}$ and $[\boldsymbol{\mu}_I\times\mathbf{r}_e]/r_e^3$ of the nuclear moment $\boldsymbol{\mu}_I$, together with the energy $-(\boldsymbol{\mu}_I\cdot\mathfrak{H})$ of the nucleus in an external field, were treated as perturbations. Matrix elements were computed between states of definite F, M_F and the secular determinant was solved to order $1/\delta$. The displacement of $p_{1/2}$ energy levels due to the perturbations was found to be

$$\epsilon=-\frac{\Delta\nu}{2(2I+1)}-g_I'\mu_0\mathfrak{H}M\pm\frac{\Delta\nu}{2}\left(1+\frac{4Mx}{2I+1}+x^2\right)^{\frac{1}{2}}-\frac{2(a''')^2}{\delta}I(I+1)-\frac{2\mu_0^2\mathfrak{H}^2N^2}{9\delta}. \quad (1)$$

Here $x=(g_J'+g_I')\mu_0\mathfrak{H}/\Delta\nu$, where g_J' is the Landé g-factor multiplied by the relativistic correction $(1-\alpha^2\bar{T}/\mathrm{Ry})$.[2] The zero separation $\Delta\nu$ and apparent nuclear moment factor g_I' are given by

$$\Delta\nu=\tfrac{1}{2}(2I+1)[a''-2(a''')^2/\delta],$$
$$g_I'=g_I(1+4Na'''/3g_I\delta),$$

where

$$a''=-\frac{8}{3}\epsilon g_I\mu_0\int_0^\infty F_{1/2}G_{1/2}dr_e,$$

$$a'''=\tfrac{1}{6}\epsilon g_I\mu_0\int_0^\infty(F_{1/2}G_{3/2}+F_{3/2}G_{1/2})dr_e,$$

$$N=\int^\infty G_{1/2}G_{3/2}r_e^3dr_e.$$

Here F_J and G_J are solutions for particular J of Dirac's radial equations in the form used by Darwin[3] with the normalization condition

$$\int_0^\infty(F_J^2+G_J^2)r_e^2dr_e=1.$$

Equation (1) is seen to have the same form as the Breit-Rabi equation except for the addition of terms in $(a''')^2/\delta$ and $\mathfrak{H}^2/\delta$ which are the same for all sublevels of the $p_{1/2}$ state and cancel out in transitions within this state as in the experiments of Becker and Kusch.[4] Thus the only apparent effect of perturbation by the $p_{3/2}$ state is in the substitution of g_I' for g_I.

Expressions for a'' and a''' employing approximations to the radial functions valid near the nucleus, where the integrands are large, have been obtained by Breit and Wills.[5] Using these, one finds that the ratio a'''/a'' is $-(1/16)\lambda$, where λ is the ratio G/F of the relativistic correction factors G and F of Eq. (29) of their paper and is given by

$$\lambda=1-1.396Z^2\alpha^2-0.121Z^4\alpha^4+\cdots.$$

To a good approximation $\Delta\nu\cong(2I+1)a''/2$, since the correction term in $(a''')^2/\delta$ is small, of the order of 10^{-6} a'' for gallium. With this value of $\Delta\nu$ and assuming N to be approximately unity one obtains

$$g_I'\cong g_I\{1-(\Delta\nu)\lambda/[6(2I+1)\delta]\}.$$

Thus Foley's correction to g_I is multiplied by λ. For gallium this makes the fractional change in apparent g_I -0.0058 and for indium one has -0.0035. The gallium value is somewhat lower than that found experimentally (see reference 1) which may, as Foley suggests, be indicative of configuration interaction in the $p_{3/2}$ state. It should be pointed out that the calculated value of the ratio a'/a'' of the hyperfine coupling constant a' for the $p_{3/2}$ state to that for the $p_{1/2}$ state differs from the value found experimentally for gallium by about 30 percent. A different and lower value of the correction to g_I is obtained by using a'''/a' instead of a'''/a'' as above.

The author would like to express his gratitude to Professor G. Breit for suggesting the problem and for several very helpful discussions in the course of it.

* Assisted by the joint program of the AEC and the ONR.
[1] H. M. Foley, Phys. Rev. **80**, 288 (1950).
[2] See, e.g., G. Breit, Nature **122**, 649 (1948); H. Margenau, Phys. Rev. **57**, 383 (1940).
[3] C. G. Darwin, Proc. Roy. Soc. (London) **A118**, 654 (1928). The notation is the same as that used in reference 5.
[4] G. E. Becker and P. Kusch, Phys. Rev. **73**, 584 (1948).
[5] G. Breit and L. A. Wills, Phys. Rev. **44**, 470 (1933).

Half-Life and Mass Assignment of Argon 39†

H. ZELDES, B. H. KETELLE, AND A. R. BROSI
Chemistry Division, Oak Ridge National Laboratory,
AND
C. R. FULTZ AND R. F. HIBBS
Assay Laboratory, Y-12 Plant, Carbide and Carbon Chemicals Corporation, Oak Ridge, Tennessee
(Received April 11, 1952)

AN argon isotope which decays with an "α" type forbidden beta-spectrum and a half-life greater than 15 yr was tentatively assigned to mass number 39 in an earlier report.[1] This tentative mass assignment has been confirmed, and a definite half-life has been established for A^{39} in the work presented here.

The argon produced in four samples of KCl by bombardment in a nuclear reactor for about one year was released by dissolving the KCl in water. After purification with hot calcium vapor the volume of inert gas in three of the samples was measured. The bremsstrahlung radiation of these three samples was compared to that of the fourth sample in a high pressure ionization chamber. The isotopic abundance ratios in the three samples with known volumes, measured in a 60° sector type mass spectrometer, are given in Table I.

TABLE I. Isotopic abundance ratios of argon from bombarded KCl

Mass No.	Percent abundance Sample 1	Sample 2	Sample 3
36	0.24	0.16	0.092
38	85.96	85.76	84.65
39	5.35	5.43	5.32
40	8.38	8.57	9.84
(41)	0.077	0.066	0.10

The disintegration rate of the fourth sample was determined by mounting it, in a thin-walled bulb, as a source in a magnetic lens beta-ray spectrometer. The transmission of the spectrometer was determined by measuring the beta spectra of Na^{24}, P^{32}, Co^{60} and Au^{198} sources with known disintegration rates. From the spectrometer transmission and the integral of the "α"-type beta-energy distribution, the fourth sample was found to have 6.8×10^6 disintegrations per second.

Since the disintegration rate and the number of atoms with masses 36, 38, 39, 40, and 41 are known for each of the three samples, a decay constant can be computed provided that the activity can be assigned to a definite mass number. The argon isotopes with mass numbers 36, 38, and 40 are known to be stable with respect to beta-decay and therefore can be excluded from consideration. From a study of Cl^{39} Haslam and co-workers[2] have concluded that A^{39} has a long half-life. However, Zucker and Watson[3] have produced a 2-min activity by a deuteron bombardment of enriched A^{38} which they assign to A^{39}.

In the present experiments the amount of radioactivity correlates within 10 percent with the number of mass 39 atoms but only within a factor of two with the number of mass 41 atoms. In addition, if the observed activity is attributed to mass 41 instead of mass 39, the data yield a half-life of about 4 yr, whereas direct decay measurements now show that the half-life is greater than 50 yr. It is concluded, therefore, that the long-lived beta-emitter observed in this work is associated with mass number 39, and the computations summarized in Table II have been made on this basis.

The data in Table II have been corrected for two sources of error. When air containing approximately the same volume of argon as the A^{39} samples was treated with hot calcium vapor, the volume percent of inert gas was reproducible, but it averaged 5 percent higher than the accepted value for the abundance of argon in air. Therefore, the volumes recorded in Table II are 5 percent less than the measured volumes. It seems probable that hydrogen was not completely removed by the hot calcium treatment. The disintegration rate of the beta-ray spectrometer source was corrected for absorption losses in the source container. This correction, which amounted to 6.5 percent, was determined by measuring a Au^{198} source with and without absorbers.

TABLE II. A^{39} decay constant data.

Sample	1	2	3
Vol in mm³ at 0°C and 760 mm	32.6	62.3	57.5
Percent abundance of mass 39	5.35	5.43	5.32
Atoms of mass 39	4.7×10^{18}	9.1×10^{18}	8.2×10^{18}
Activity relative to sample 4	0.628	1.11	0.903
Disintegrations per second	4.3×10^6	7.6×10^6	6.2×10^6
Decay constant sec⁻¹	9.2×10^{-11}	8.3×10^{-11}	7.5×10^{-11}
Half-life (years)	240	265	290

On the basis of the measurements reported here it is concluded that A^{39} has a half-life of 265 ± 30 yr. The $\log(ft)$ value is 9.9, and the $\log[(W_0^2-1)/t]$ value is 10.4. The latter falls within the range of values given by Mayer, Moszkowski, and Nordheim[4] for beta-transitions where $\Delta l=1$ and $\Delta I=2$.

We want to thank A. F. Rupp for the samples of bombarded KCl used in making these measurements.

† This work was performed for the AEC.
[1] Brosi, Zeldes, and Ketelle, Phys. Rev. **79**, 902 (1950).
[2] Haslam, Katz, Moody, and Skarsgard, Phys. Rev. **80**, 318 (1950).
[3] A. Zucker and W. W. Watson, Phys. Rev. **80**, 966 (1950).
[4] Mayer, Moszkowski, and Nordheim, Revs. Modern Phys. **23**, 315 (1951).

Broadening of Microwave Absorption Lines by Collisions with the Cell Walls*

R. H. JOHNSON AND M. W. P. STRANDBERG
Research Laboratory of Electronics, Massachusetts Institute of Technology, Cambridge, Massachusetts
(Received December 17, 1951)

THE literature regarding line broadening by collisions with the walls of the absorbing cell presents various formulas. They all assume a Lorentz line shape in which the line breadth parameter is of the form

$$\Delta\nu=(A/\Lambda)(2kT/m)^{\frac{1}{2}}. \tag{1}$$

Here $\Delta\nu$ is half the width of the line between points of half-intensity; Λ is a length characteristic of the cell, or the volume to surface ratio of the cell; $(2kT/m)^{\frac{1}{2}}$ is the mean molecular speed; A is a numerical factor. We consider only the case of a cell consisting of the space between parallel infinite planes separated by a distance a. Taking $\Lambda=a$,

$$\Delta\nu=(A/a)(2kT/m)^{\frac{1}{2}}. \tag{2}$$

Gordy's formulas[1] specialized to the parallel plane case have $A=1/3\pi$ and $A=1/3\pi^{\frac{1}{2}}$; these were later corrected in a mimeographed errata sheet of limited circulation to $A=1/2\pi\sqrt{6}$ and $A=1/\pi\sqrt{6}$. No explanation precedes the statement of the formulas except "It is easy to show that . . ." Bleaney and Penrose[2] give $A=1/4\pi$.

We have experimental and theoretical reason to indicate that these values for A are too small. Suppose that a molecule with an electric dipole moment is exposed to a pulse of electric field

$$E_z=E_0\cos\omega t', \quad 0<t'<t. \tag{3}$$

Proceeding in a way similar to that of Rabi[3] we can show that

$$|a_i|^2-|a_i^0|^2=\frac{\Omega^2(|a_j^0|^2-|a_i^0|^2)}{(\delta\omega)^2+\Omega^2}\sin^2\left\{\frac{t}{2}[(\delta\omega)^2+\Omega^2]^{\frac{1}{2}}\right\}, \tag{4}$$

where $|a_i^0|^2$, $|a_j^0|^2$ are the initial probabilities that a molecule be in molecular state i and j, respectively; $|a_j|^2$ is the final probability that the molecule be in state j; $\Omega=E_0\mu_{ij}/\hbar$; μ_{ij} is the matrix element of the Z-component of electric dipole moment between states i and j; $\delta\omega=\omega_{ij}-\omega$; $\hbar\omega_{ij}=E_i-E_j$; E_i and E_j are the energies of states i and j, respectively. It was assumed that $\omega_{ij}\gg1/t$,

and (4) was averaged over initial phase angles of a_i^0/a_j^0 since this phase is initially unknown.

In collision broadening, each molecule is exposed to pulses of radiation of different lengths t. We suppose that if there are n molecules, the number dn having their last collision between times t and $t+dt$ in the past is

$$dn = nf(t)dt. \tag{5}$$

We also assume that the collision returns the molecule to a random Boltzmann distribution. The time derivative of (4) is the instantaneous rate at which a molecule which had its last collision a time t in the past is making a transition. Now multiply by the number of such molecules, given in (5), and integrate over all molecules. This gives for the net number of absorbing transitions per second,

$$\frac{n\hbar^2(|a_i^0|^2-|a_j^0|^2)}{2(\delta\omega)}\int_0^\infty f(t)\sin t(\delta\omega)dt, \tag{6}$$

in the limit of small electric fields (no saturation). Thus, the power attenuation constant per centimeter is

$$\alpha_{ij}(\delta\omega)=\frac{D_{ij}}{\pi(\delta\omega)}\int_0^\infty f(t)\sin t(\delta\omega)dt, \tag{7}$$

where

$$D_{ij}=\frac{4\pi^2N}{3hc}\frac{e^{-E_i/kT}}{\Sigma_n e^{-E_n/kT}}\frac{\nu_{ij}^2|\mu_{ij}|^2}{kT}, \tag{8}$$

and N is the number of molecules per cm^3; h is Planck's constant; c is the velocity of light; $\Sigma_n \exp(-E_n/kT)$ is the partition sum; $\nu_{ij}=\omega_{ij}/2\pi$; k is Boltzmann's constant; T is the absolute temperature; $|\mu_{ij}|^2=(\mu_Z^{ij})^2+(\mu_Y^{ij})^2+(\mu_X^{ij})^2$. Equations (7) and (8) reduce to the Van Vleck-Weisskopf[4] formula for $f(t)=\exp(-t/\tau)/\tau$.

For the case of broadening solely by collisions with the walls of the parallel-plane cell,

$$f(t)=\frac{2}{a^2}\left(\frac{m}{2\pi kT}\right)^{\frac{1}{2}}\int_{z=0}^{a} z\exp(-mz^2/2kTt^2)dz. \tag{9}$$

Substitution of (9) in (7) results in a difficult integral, but one which can be evaluated approximately for small $(\delta\omega)$. The result is

$$\alpha_{ij}{}^N=\frac{D_{ij}a}{\pi^{\frac{1}{2}}}\left(\frac{m}{2kT}\right)^{\frac{1}{2}}\left\{\log_e\left[\frac{1}{a(m/2kT)^{\frac{1}{2}}|\delta\omega|}\right]-0.4\right\}. \tag{10}$$

There is less than 30 percent error for

$$\delta\omega \lesssim (0.1/a)(2kT/m)^{\frac{1}{2}}, \tag{11}$$

and the percent error approaches zero as $\delta\omega\to 0$. Figure 1 shows the results of the present work and a Lorentz shape using $A=1/2\pi\sqrt{6}$ (Gordy's third value). The very considerable discrepancy is evident. Our work shows a logarithmic singularity at $\delta\omega=0$ which is of little experimental significance; for example, any finite Doppler broadening would eliminate it. Since

$$\int_{-\infty}^{\infty}\alpha_{ij}d(\delta\omega)=D_{ij}, \tag{12}$$

so that the total area under both curves is the same, an estimated effective $\Delta\nu$ for experimental purposes is about six times Gordy's third value and corresponds to $A\cong 0.4$. An exact solution for this parallel-plane case would require a numerical integration, but appears feasible. More complicated cases require more difficult integrations.

The value $A\cong 0.4$ substituted in Eq. (2) gives

$$\Delta\nu\cong 0.4(1/a)(2kT/m)^{\frac{1}{2}}. \tag{13}$$

Although Eq. (13) was derived for the parallel-plane case, it represents a lower limit for $\Delta\nu$ if a is the shortest dimension of the cell.

Unpublished experimental results (at room temperature) obtained by J. R. Eshbach of this laboratory a year ago showed that the limiting line half-width for OCS, as pressure and microwave power level are reduced, was $\Delta\nu\cong 50$ kc/sec in X-band Stark guide ($a=0.48$ cm) and $\Delta\nu\cong 100$ kc/sec in K-band Stark guide ($a=0.19$ cm). For these cells the shortest dimension is several times less than the other dimensions, so the wall-collision half-width is expected to be only slightly greater than that given by Eq. (13). That half-width is combined with the Doppler half-width to get the observed half-width. As Table I indicates, Eshbach's experiments agree quite well with the present theory.

TABLE I. OCS half-width at half-intensity.

Cell	Calculated Doppler half-width	Calculated lower limit for wall-collision half-width (from Eq. (13))	Observed minimum half-width
X-band Stark	19 kc/sec	26 kc/sec	50 kc/sec
K-band Stark	19 kc/sec	65 kc/sec	100 kc/sec

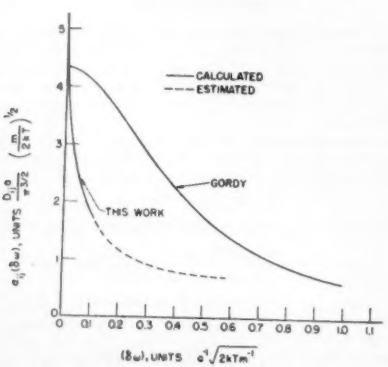

FIG. 1. Line shapes in wall broadening; infinite planes separated by distance a; area under both curves is same.

* This work has been supported in part by the Signal Corps, the Air Materiel Command, and the ONR.

[1] W. Gordy, Revs. Modern Phys. **20**, 668 (1948).
[3] B. Bleaney and R. P. Penrose, Proc. Phys. Soc. (London) **60**, 83 (1948).
[2] I. I. Rabi, Phys. Rev. **51**, 652 (1937).
[4] J. H. Van Vleck and V. F. Weisskopf, Revs. Modern Phys. **17**, 227 (1945).

The Stability of Plane Poiseuille Flow

L. H. THOMAS
Watson Scientific Computing Laboratory, Columbia University, New York, New York

(Received April 17, 1952)

FOR small disturbances to the plane parallel steady flow of incompressible fluid between parallel planes at $y=\pm 1$, the change in the stream function may be analyzed into components of the form

$$e^{i\alpha x}e^{ict}\varphi(y),$$

where $\varphi(y)$ must satisfy the Orr-Sommerfeld equation

$$\varphi''''-2\alpha^2\varphi''+\alpha^4\varphi+i\alpha R[(1-c-y^2)(\varphi''-\alpha^2\varphi)+2\varphi]=0,$$

with boundary conditions

$$\varphi=0,\quad \varphi'=0,\quad \text{for}\quad y=\pm 1,$$

where R is the Reynolds number of the flow. For given α and R this has solutions only for characteristic values of c.

Work by many authors on this equation, culminating in that of Lin,[1] using asymptotic formulas, leads to the conclusion that for a certain region in the $\alpha-R$ plane, c has a negative imaginary part, corresponding to a disturbance increasing in amplitude exponentially with the time, so that for $R>5300$ (about), the steady flow should be unstable. This conclusion has been criticized, particularly by Pekeris,[2] who made computations indicating stability for

values of α and R for which, according to Lin, the flow should be unstable.

It was suggested three or four years ago by J. von Neumann, C. C. Lin, and C. L. Pekeris, that this question could be settled by numerical work and an attempt was then made which was successful in finding c only up to $R=1600$. We have now found it possible to integrate the equation successfully for larger values of R and have obtained the results for c given in Table I, which

TABLE I. Characteristic values of c.

α \ R	1600	2500	6400	10,000	25,000
0.9		0.2857+0.0211i	0.2444+0.0012i	0.2261−0.0040i	
1.0	0.3231+0.0262i	0.3011+0.0142i	0.2569−0.0009i	0.2375−0.0037i	0.1886+0.0009i
1.1	0.3384+0.0306i	0.3148+0.0108i	0.2677+0.0007i	0.2470+0.0003i	0.1911+0.0116i
1.2		0.3267+0.0107i	0.2763+0.0056i	0.2535+0.0075i	

For $\alpha=1.05$, $R=8000$, $c=0.2524-0.0017i$

are believed accurate to 0.5 in the last place. Interpolation gives a critical Reynolds number $R=5780$ for $\alpha=1.02$, which has been checked by integrations. These numbers confirm Lin's results closely, and it may now be regarded as proved that plane Poiseuille flow becomes unstable at about $R=5800$. It may be noted that for a given value of α the flow is unstable only for a finite range of Reynolds numbers as was also found by Lin.

This latest work was done on International Business Machines Corporation's Selective Sequence Electronic Calculator by Donald A. Quarles, Jr. and Phyllis K. Brown. The numerical work was done to 13 digits using a step of 0.01 in y with an integration formula having an error per step proportional to the 8th derivative. The problem took about 150 hours of operating time, equivalent to about 100 years of hand computing.

[1] C. C. Lin, Quart. Appl. Math. **3**, 288 (1946).
[2] C. L. Pekeris, Phys. Rev. **74**, 191 (1948).

Radiations from Nb^{97}†

C. E. MANDEVILLE, E. SHAPIRO, R. I. MENDENHALL, E. R. ZUCKER,* AND G. L. CONKLIN
Bartol Research Foundation of the Franklin Institute, Swarthmore, Pennsylvania
(Received January 14, 1952)

THE properties of the 17-hr Zr^{97} and of its daughter element, the 70-minute Nb^{97}, have been the subject of considerable investigation.[1–5] Spectrometric measurements[5] have yielded beta-ray energies of 1.91±0.02 Mev and 1.267±0.02 Mev, and gamma-ray energies of 0.747±0.005 Mev for Zr^{97} and 0.665±0.005 Mev for Nb^{97}. The gamma-ray at 0.747±0.005 Mev was shown to be emitted from an isomeric level in Nb^{97} of half-period 60 sec.

In the present investigation $Zr^{96}O_2$ (isotopic concentration 90 percent in Zr^{96}), obtained from the Y-12 plant, Carbide and Carbon Chemicals Division, Union Carbide and Carbon Corporation, Oak Ridge, Tennessee, was irradiated by slow neutrons in the Oak Ridge pile. The radioactive materials were received within twenty-four hours after cessation of irradiation and chemical separations were immediately commenced. The slow neutron irradiated zirconium dioxide was dissolved by potassium pyrosulfate fusion, and the separation of the niobium daughter activity from zirconium was effected by the use of Steinberg's "oxalate" procedure.[6]

The decay of Nb^{97}, freshly separated from its parent element, was followed for ten half-periods, and the half-period, taken from the slope of the decay curve was found to be 72.1±0.7 minutes. This value is to be compared with previously reported values of 68 minutes[7] and 75 minutes.[3] The decay of Zr^{97} was followed for 200 hours, and the resulting half-period was calculated to be 17.0±0.2 hours, in agreement with the earlier measurements.

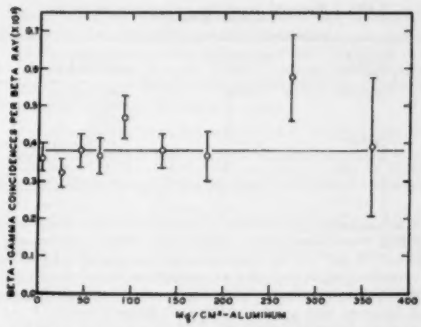

FIG. 1. Beta-gamma coincidence rate of Nb^{97} as a function of the surface density of aluminum placed before the beta-ray counter.

The beta-rays of Nb^{97}, freshly separated from its parent element, were absorbed in aluminum, and a Feather[8] plot of the data gave a maximum beta-ray energy of 1.40 Mev.

The beta-gamma coincidence rate of the 72-minute Nb^{97} is shown as a function of absorber thickness before the beta-ray counter in Fig. 1. It is seen to be constant, independent of the beta-ray energy, suggesting that the beta-ray spectrum of Nb^{97} is simple. Calibration of the beta-gamma coincidence counting arrangement by the beta-gamma coincidence rate of Sc^{46} showed that each beta-ray of Nb^{97} is followed, on the average, by 0.7 Mev of gamma-ray energy. Each point of Fig. 1 was, of course, properly corrected for decay of the source.

† Assisted by the joint program of the ONR and AEC.
* Frankford Arsenal, Philadelphia, Pennsylvania.
[1] Sagane, Kojima, Mijamoto, and Ikawa, Phys. Rev. **57**, 1179 (1940).
[2] A. V. Grosse and E. T. Booth, Phys. Rev. **57**, 664 (1940).
[3] S. Katcoff and B. Finkle, *Radiochemical Studies: The Fission Products* (McGraw-Hill Book Company, Inc., New York, 1951), Paper No. 83, National Nuclear Energy Series, Plutonium Project Record, Vol. 9, Div. IV.
[4] O. Hahn and F. Strassman, Naturwiss. **29**, 285 (1941).
[5] Burgus, Knight, and Prestwood, Phys. Rev. **79**, 104 (1950).
[6] E. P. Steinberg, *Radiochemical Studies: The Fission Products* (McGraw-Hill Book Company, Inc., New York, 1951), Paper No. 243, National Nuclear Energy Series, Plutonium Project Record, Vol. 9, Div. IV.
[7] G. E. Boyd, communication to G. T. Seaborg and I. Perlman, Revs. Modern Phys. **20**, 585 (1948).
[8] N. Feather, Proc. Cambridge Phil. Soc. **30**, 599 (1938).

Microwave Spectroscopy at High Temperature-Spectra of CsCl and NaCl*

M. L. STITCH, A. HONIG, AND C. H. TOWNES
Columbia University, New York, New York
(Received April 21, 1952)

A SPECTROMETER for measurement of microwave absorption by gases at high temperature has been constructed,[1,2] and with it spectra of gaseous NaCl, KCl, CsCl, and TlCl have been obtained. Microwaves pass through a 5-foot absorption cell which can be held at temperatures at least as high as 875°C. Absorption lines are modulated by Stark effect to give sensitive detection.

At approximately 775°C the pure rotational transition $J=1\rightarrow2$ of NaCl was observed. Frequencies for the two Cl isotopes and various vibrational states are listed in Table I. These give $B_v(Cl^{35})=6536.9\pm0.3$ Mc, $\alpha_v(Cl^{35})=48.1\pm0.1$ Mc, and the internuclear distance $r_0=2.3606\pm0.0003$A. Frequency measurements of the absorption lines were made with a frequency standard. However, experimental conditions gave lines several megacycles broad, which limited the precision of measurements which could be easily obtained to that indicated in Table I.

TABLE I. Measured lines of the $J=1\rightarrow 2$ pure rotational transition of NaCl.

Isotopic species	Vibrational state	Frequency in megacycles/sec
$NaCl^{35}$	$v=0$	26051.1 ±0.75
	1	25857.6
	2	25666.5
	3	25473.9
$NaCl^{37}$	$v=0$	25493.9
	1	25307.5
	2	25120.3

A measurement of the ratio of intensities of the $NaCl^{37}$ $v=0$ and $NaCl^{35}$ $v=3$ lines gives a value for the vibrational frequency $\omega_e(35)=378$ cm^{-1}, if the dipole moment is assumed independent of vibrational state. Including a reasonable variation of the dipole moment, this measurement may be in error ±15 percent. It agrees well, however, with a value of 380 cm^{-1} obtained by Levi.[3]

At approximately 715°C, the $J=5\rightarrow 6$ transition of CsCl was observed, and lines listed in Table II were measured. These give

TABLE II. Measured lines of the $J=5\rightarrow 6$ pure rotational transition of CsCl.

Isotopic species	Vibrational state	Frequency in megacycles/sec
$CsCl^{35}$	$v=5$	25300.0 ±1.5
	6	25180.1
	7	25061.0
	8	24941.2
$CsCl^{37}$	$v=0$	24798.2
	1	24685.7
	2	24571.4
	4	24337.9

values $B_e(Cl^{35})=2163.8\pm0.2$ Mc, $\alpha_e(Cl^{35})=10.06\pm0.06$ Mc, and the internuclear distance $r_e=2.9041\pm0.0003$A.

The observed spectrum of KCl gave molecular constants in agreement with those found by measurement of rotational transitions in molecular beams.[4] A rich spectrum of lines between 25,000 Mc and 23,500 Mc was observed[3] in TlCl vapor at approximately 305°C. This spectrum showed no obvious regularities, and cannot be produced by a diatomic molecule, so that the vapor of TlCl must contain a considerable amount of dimers or some other combination of Tl and Cl.

It may be noted that the r_e value of CsCl is 4 percent less than the value of 3.02±0.03A obtained from electron diffraction measurements of the average over-all vibrational states at 1200°C, but falls within the experimental error of molecular beam measurements,[5] which is 2.88±0.03A. Likewise, the r_e value for NaCl is 5 percent less than the value of 2.48±0.03A given by electron diffraction measurements.[6] This discrepancy is unexplained.

The value of α for $CsCl^{35}$ obtained from molecular beam measurements of the product of the dipole moment and the moment of inertia[5] is 15.6±1.5. The large discrepancy between this result and the directly measured value given here may be due to an incorrect assumption about the variation of the dipole moment with vibration state.

We are very grateful to Mr. C. O. Dechert, foreman of the Columbia Radiation Laboratory machine shop, for considerable aid in the design and construction of the apparatus, as well as to Mr. A. P. Marshall and others of the machine shop staff. We also appreciate the help of Mr. A. Javan and Mr. W. A. Hardy with several of the experimental measurements.

* Work supported jointly by the Signal Corps and ONR.
[1] M. L. Stitch and C. H. Townes, Quarterly Report, Columbia Radiation Laboratory, December 31, 1950 and subsequent CRL reports.
[2] Stitch, Honig, and Townes, Bull. Am. Phys. Soc. **27**, No. 1, 32 (1952).
[3] H. Levi, dissertation, Berlin, (1934).
[4] Fabricand, Carlson, Lee, and Rabi, Bull. Am. Phys. Soc. **27**, No. 1, 32 (1952).
[5] R. G. Luce and J. W. Trischka, Phys. Rev. **83**, 851 (1951).
[6] Maxwell, Henderson, and Mosely, Phys. Rev. **52**, 968 (1937).

μ-Meson Decay and β-Radioactivity*

LOUIS MICHEL†
Institute for Theoretical Physics, University of Copenhagen, Copenhagen, Denmark
(Received April 14, 1952)

THE decay $\mu^{\pm}\rightarrow e^{\pm}+2\nu$ cannot be consistently explained by indirect interaction through any known virtual particles. Thus we are led to suppose a direct interaction between the four fermions μ, e, ν, ν.

If we restrict ourselves to the kind of interaction terms used in β-radioactivity [no derivatives of the wave functions; however, the use of imaginary and/or pseudoscalar coupling constants would not modify formula (1)], the theoretically predicted possible energy spectra[1] for the secondary electrons are (with the normalization $\tau\int_1^W P(E)dE=1$, where τ is the μ-meson mean life and E is the electron energy):

$$\tau P(E)=(4E^2/W^4)[3(W-E)+\tfrac{2}{3}\rho(4E-3W)], \qquad (1)$$

where ρ is a parameter satisfying $0\leq\rho\leq 1$. The agreement with experimental results is very satisfactory and ρ may be obtained from experiments.[2]

Direct interaction[3].—With four Dirac wave functions ψ or ψ^* (I shall write ψ^K for both types of functions), we can form only five linearly independent scalars J_i, and the most general interaction Hamiltonian density is

$$H=\Sigma g_i J_i+\text{Hermitian conjugate}. \qquad (2)$$

A set of five linearly independent J_i is usually constructed as follows: with two ψ^K in a given order one can form five Lorentz covariants S, V, T, A, P; each J_i is then a scalar product of one of these covariants by corresponding covariant made with the two other ψ^K (also in a given order).

If the order of the ψ^K in J_i is changed, the new J_i is a linear combination of the old ones. This corresponds in H to a change of reference system for the five-dimensional vector space of the g_i. The only vector g invariant for all permutations corresponds to the Critichfield and Wigner interaction.[4]

If two ψ^K are identical (this occurs for instance when there are two indistinguishable particles), there are only three linearly independent J_i and this corresponds to a projection on three dimensions of the five-dimensional g space. Therefore we have to consider two cases:

(1) The two emitted neutrinos are experimentally distinguishable (for example, by the sign of their magnetic moment). This case can occur if the neutrinos are described by Dirac's hole theory and the two emitted neutrinos are particle and antiparticle, respectively. Then $0\leq\rho\leq 1$.

(2) The two emitted neutrinos are identical particles. This may occur if the emitted neutrinos are both particles or both antiparticles in Dirac's hole theory, or if they are described by Majorana's theory[5] according to which all neutrinos are identical. Then $0\leq\rho\leq 3/4$.

The triangle of interactions.—Several authors[6] have shown that direct interactions with the same magnitude for coupling constants can explain β-radioactivity, μ-meson decay and μ-meson capture by heavy nuclei. It is then natural to test first the simplest hypothesis that the "same" interaction is responsible for these three phenomena.

But it is clear that the direct interaction of one set of four fermions can be compared to the direct interaction of another set of four fermions only if a one-to-one correspondence between the particles of the two sets is agreed on. It can be shown that except for minor questions of signs (immaterial for β-radioactivity) it is sufficient to have a correspondence between pairs of particles. The "triangle" suggests such a correspondence

$$(n,\ p)\leftrightarrow(e,\ \nu)\leftrightarrow(\mu,\ \nu).$$

If one refers to the usual notations of β-radioactivity, calling f_1 the five coupling constants (f_1 for the "scalar" interaction, f_2 for the "vector" interaction, and so on $\cdots$), ρ is given by

(1) different neutrinos:

$$0\leq\rho=\frac{3}{4}\frac{(f_1-f_3)^2+(f_2+f_4)^2+2(f_3+f_4)^2}{f_1^2+4f_2^2+6f_3^2+4f_4^2+f_5^2}\leq 1;$$

(2) identical neutrinos:

$$0\leq\rho=\frac{3}{2}\frac{[f_1+f_5-2(f_3+f_4)]^2}{(f_1+6f_2-f_5)^2+16(f_3-f_4)^2+2[f_1+f_5-2(f_2+f_4)]^2}\leq\frac{3}{4}.$$

Another quadratic relation [different for (1) and (2)] between f_i is given[7] by the ratio

(neutron mean life)/(μ-meson mean life).

A better knowledge of the nature of the direct interaction responsible for β-radioactivity, of the neutron mean life and of the energy spectrum of the secondary electrons from μ-meson decay will allow one to answer the following questions:

(a) Can a "same" direct interaction explain β-radioactivity and μ-meson decay?

(b) Are the two neutrinos emitted in μ-meson decay identical or not?

From the present experimental data it can already be concluded that question (a) cannot be answered separately.

I wish to express my sincere appreciation to Professor N. Bohr for the opportunity to work at the Institute for Theoretical Physics. I am also grateful to the French Service des Poudres for its understanding and its financial support.

* The content of this letter was communicated at the Copenhagen Conference, July 1951.

† Now at Laboratoire de Physique, Ecole Polytechnique, Paris 5, France.

[1] Calculations have been made for some particular couplings by Tiomno, Wheeler, and Rau, Revs. Modern Phys. **21**, 144 (1949) and for the general coupling by L. Michel, Nature **163**, 959 (1949).

[2] A. Lagarrigue and C. Peyrou, [Compt. rend. **233**, 478 (1951), and J. phys. et radium, **12**, 848 (1951)] have given a statistical method for the determination of the most probable value of ρ from a set of measurements of the energies of the secondary electrons from μ-meson decay. Their experimental results and those of Leighton, Anderson, and Seriff, [Phys. Rev. **75**, 1432 (1949)] give $\rho=0.19\pm0.15$.

[3] L. Michel, Proc. Phys. Soc. (London) **A63**, 514 and 1371 (1950).

[4] C. L. Critchfield and E. P. Wigner, Phys. Rev. **60**, 412 (1941); see also C. L. Critchfield, Phys. Rev. **63**, 417 (1943).

[5] O. Majorana, Nuovo cimento **14**, 171 (1937).

[6] G. Puppi, Nuovo cimento **5**, 587 (1948) and **6**, 194 (1949); J. Tiomno and J. A. Wheeler, Revs. Modern Phys. **21**, 153 (1949); Lee, Rosenbluth, and Yang, Phys. Rev. **75**, 905 (1949).

[7] L. Michel, *Progress in Cosmic Rays Physics* (North Holland Publishing Company, Amsterdam, 1951), Vol. I, Chap. III.

Proceedings of the American Physical Society

Minutes of the 1952 Spring Meeting of the New York State Section in Corning

THE twenty-seventh meeting of the New York State Section of the American Physical Society was held at the Corning Glass Center, Corning, New York, on Friday and Saturday, April 18 and 19, 1952. About 100 registrants took advantage of the opportunity to inspect the exhibits in the Center's Museum of Glass, and to watch the blowing and forming of Steuben glass. On Friday evening, a social hour and dinner in the Glass Center Clubrooms preceded the address, "The Nature of Research in Physics," by W. F. G. Swann.

Two sessions on Saturday were devoted to the contributed papers, abstracts of which appear below.

L. W. PHILLIPS, *Secretary*
New York State Section
American Physical Society
The University of Buffalo
Buffalo 14, New York

Contributed Papers

Multiple Scattering of Protons in Gases. EUGENE H. GERBER, *University of Buffalo.*—The low energy protons resulting from the reaction $_{13}Al^{27}(\alpha,p)_{14}Si^{30}$ were observed in a cloud chamber filled with air, argon, or helium. The curvatures due to multiple scattering in the absence of a magnetic field were observed and the radii of curvature over the last 5 cm of the tracks were measured. The mean square curvature $\langle C^2\rangle_{Av}$ calculated from the experimental data is, for air, $\langle C^2\rangle_{Av}=0.323\times10^{-3}$ cm^{-2}, and for argon, $\langle C^2\rangle_{Av}=0.935\times10^{-3}$ cm^{-2}. The experimental histograms of the radii of curvature agree with theoretical distributions obtained by assuming a Gaussian distribution for the curvatures. The experimental results agree with the theories of H. A. Bethe[1] and W. T. Scott.[2]

[1] H. A. Bethe, Phys. Rev. **70**, 821 (1946).
[2] W. T. Scott, Phys. Rev. **76**, 212 (1949).

Absorption Bands in the Electrical Spectrum of a Glass and Quartz. FRANCES BRITT, *Corning Glass Works.*—A study has been made of the dielectric properties of the B_2O_3-SiO_2 glass system in which Li_2O was added in amounts varying from 0–3.72 percent by weight. A plot of loss tangent *vs* temperature showed an absorption band which is not characteristic of glasses in general. The dielectric constant increased rapidly in the temperature region of maximum absorption. A similar behavior was observed in samples of quartz crystals cut parallel to the principal axis. The glass formed quartz crystals when heat-treated so as to produce devitrification. Temperature runs were made at frequencies of 60 and 10^6 cycles per second. The absorption band shifted to a higher temperature at the higher frequency. In the glass containing 2.48 percent Li_2O the temperature shift was from 160°C at 60 cycles to 400°C at 10^6 cycles. Apparently the incipient quartz crystallization in the glass enables a sufficient number of the Li ions to have the same activation energy rather than the broad distribution of energies normally associated with the random network of the glassy state. Alkali ions are usually found as an impurity in natural quartz crystals, and it is known that Li^+ can migrate along the principal axis. Apparently at a certain temperature the ions have the activation energy to move in a direction perpendicular to the principal axis.

Application of Fluorescence X-Rays to Metallurgical Microradiography. H. R. SPLETTSTOSSER AND H. E. SEEMANN, *Kodak Research Laboratories.*—Several experimenters have used more or less homogeneous x-rays in the radiography of thin specimens. So far as we are aware, all of the metallurgical investigations have been done with radiation from x-ray tube targets chosen for a particular line emission, the continuous background being a necessary but undesired accompaniment. Fluorescence x-rays, excited in a target external to the x-ray tube, have been used by other workers in the radiography of biological specimens. In the present experiments, fluorescence radiation has been applied to the radiography of several metallurgical specimens in which segregation of elements or phases has been brought out by proper choice of K fluorescence with respect to the K absorption edges of the constituents. The advantages of fluorescence x-rays are that they are more homogeneous than radiation from a tube target and a large number of fluorescence targets are easily made up from the elements, or from their oxides or carbonates, thus requiring the use of but one x-ray tube. The disadvantage of the use of fluorescence radiation is its low intensity, so that fairly long exposures are necessary in some instances. The technique will be discussed and a bibliography given.

Pure Fused Silica—A New Material. CLAYTON H. ALLEN, *Corning Glass Works.*—Corning fused silica is similar to fused quartz but contains fewer impurities and has a more homogeneous structure. Fused quartz necessarily contains the impurities included in the natural quartz crystals from which it was made and frequently shows some remanent crystal structure and variations in density across former grain boundaries. A pure fused silica is described which is devoid of any crystalline structure and is free from foreign elements because it is made by a chemical process from noncrystalline materials of controlled purity. These differences in chemical purity and physical structure result in such great improvement in several physical characteristics that it may be considered as a basic new material with low ultrasonic attenuation, low dielectric loss, high ultraviolet transmission, and good optical quality.

Measuring Small Strains with Polarized Light (A Lecture Demonstration of the Principles of the Friedel Eyepiece). H. P. GAGE, *Corning Glass Works.*—Goranson and Adams[1] in 1933 described a practical method of measuring the birefringence of strained transparent specimens based on the techniques of H. de Senarmont[2] (1840 and 1847) for a compensator for elliptically polarized light according to a plan ascribed to Friedel[3] (1893). Goranson and Adams made elaborate calculations of the errors resulting if the quarterwave plate is not aligned with its axis exactly parallel to the plane of polarization, if it is not of exactly one-quarter wavelength retardation, and if the specimen is not aligned with its axis at 45° to the plane of polarization. The phenomenon of apparent rotation of the plane of polarization in proportion to the amount of birefringence in the specimen is easily demonstrated by the use of 1¼-inch glass laminated disks made by the Polaroid Corporation. Aside from being a convincing lecture demonstration the same apparatus can serve for serious measure-

ments of the amount and direction of strain in transparent specimens if provided with accurate angular scales.

[1] Goranson and Adams, Journal Franklin Inst. **216**, 471 (1933).
[2] H. de Senarmont, Ann. chim. et phys. **73**, 337 (1840); **20**, 397 (1847).
[3] G. Friedel, Bull. Soc. Min., France **16**, 19 (1893).

Fluorescence and Absorption Spectral Data and Other Physical Characteristics of Xanthopterin-like Pigment Synthesized by the Human Tubercle Bacillus and Isolated by Chromatographic and Fluorescence Analyses. M. O'L. CROWE AND A. WALKER, *New York State Department of Health.*—The pterins are pigments having a pteridine ring system. They were isolated from the wings of butterflies and from the integument of other insects. They were first studied by Hopkins[1] and later by Wieland, by Schöpf and Becker,[2] and by others. Evidence already has been presented that an erythropterin-like pigment is derived from the tubercle bacillus.[3] Another one of this group, an xanthopterin-like pigment, has been obtained from an acetone extract of human tubercle bacilli grown in Long's synthetic medium. It was isolated and purified by fractionation with immiscible solvents, by precipitation and centrifugation experiments, and by repeatedly passing the fractions through chromatographs of aluminum oxide. Its fluorescence and absorption spectral characteristics, its behavior on the chromatographs, and the crystal forms of its sodium and barium salts closely parallel these characteristics reported for xanthopterin.

[1] F. G. Hopkins, Trans. Roy. Soc. (London) **B186** Pt II, 661 (1895); Proc. Roy. Soc. (London) **B130**, 359 (1941–42).
[2] C. Schöpf and E. Becker, Ann. Chem. **507**, 266 (1933); Ann. Chem. **524**, 49 (1936); **524**, 124 (1926). C. Schöpf and A. Kottler, Ann. Chem. **539**, 128 (1939).
[3] M. O'L. Crowe and A. Walker, Science **110**, 166 (1949).

The Effect of Ball Milling on the Surface Area and Porosity of Silica Soot. B. J. TODD, *Corning Glass Works.*—The physical adsorption of nitrogen on a sample of silica soot has been measured before and after ball milling the soot. The surface areas and pore radii of the smallest pores have been deduced from the adsorption isotherms, using the methods of Brunauer, Emmett, and Teller. Additional information on the pore structure has been obtained by using helium and mercury as the displacing fluids in density determinations.

X-Ray Studies of the Graphitization Process. H. T. PINNICK, *University of Buffalo.*—X-ray diffraction studies were made on a series of carbon blacks with particle sizes ranging from 50A to 3000A, all graphitized to 3000°C. The crystallite diameters were calculated from the half-width of the asymmetric 10 line and it was found that the average crystallite diameter is about one-third of the particle size. This line is the result of two-dimensional diffraction from a single graphitic layer, and thus is present whether the layers are ordered as in graphite or in randomly rotated positions which is the case in very small crystallites. As an indication of the degree of orientation, the appearance of the cross lattice 101 line on the large angle side of the two-dimensional 10 line was observed. A similar study was made on a soft coke heat-treated to various temperatures to give comparable crystallite sizes. In both the coke and the carbon black series, the 101 line appeared when the crystallite diameter reached 150A. It is suggested that the alignment is the result of two opposing forces, valence bonds between neighboring crystallites tending to stabilize the layers in rotated positions, and the attractive forces between the layers tending to align them.

Size Effect in the Strength of NaCl Crystals. JOHN C. FISHER, *General Electric Company.*—The idea that fracture cracks originate at defects suggests that larger specimens, having greater probability of containing severe defects, will have smaller fracture stresses.[1] The influence of specimen size on the fracture of glass, cotton fiber, cement, and many other materials can be interpreted satisfactorily in this manner.[2] NaCl crystals have been studied by several investigators[3–7] with conflicting results. When specimens were dissolved to size in water or molten NaCl, smaller specimens were stronger. When they were cleaved to size, there was no size effect. The conflict is resolved by noting that specimens dissolved to size fail at surfaces, which decrease in area as the specimen diameter decreases, whereas cleaved specimens fail at edges, which do not change in length as the specimen cross section decreases.

[1] A. Griffith, Phil. Trans. Roy. Soc. **A221**, 163 (1921).
[2] W. Weibull, Ing. Ventenskaps Akad., Handl. No. 151 (1939).
[3] H. Müller, Physik. Z. **25**, 223 (1924).
[4] A. Joffe and M. Levitsky, Z. Physik **31**, 576 (1925).
[5] E. Rexer, Z. Physik **75**, 777 (1932).
[6] E. Jenckel, Z. Elektrochem. **38**, 569 (1932).
[7] K. Wendenburg, Z. Physik **88**, 727 (1934).

Proceedings of the American Physical Society

Minutes of the 1952 Spring Meeting of the Ohio Section at Kent State University, Kent, Ohio, April 18 and 19, 1952

THE regular spring meeting of the Ohio Section of The American Physical Society convened at Kent State University, Kent, Ohio, on April 18–19, 1952. As is the usual custom, this was a joint meeting with Section F of the Ohio Academy of Science. Thirty-eight members were present at the beginning and forty-nine were in the room at the time of adjournment. In addition to the ten papers, abstracts of which follow, three others were read, namely: The Mass of Pluto, by Lloyd R. Wylie, Wittenberg College; Infrared Spectra of Tetraphenylporphine and Tetraphenylisophorphine, by H. V. Knorr of the C. F. Kettering Foundation, Yellow Springs, Ohio; and The Meteorological Program at The Ohio State University, by A. N. Dingle. Friday afternoon was used for a Symposium on *The Promotion of Science in the Secondary Schools;* the speakers were Harley Ellinger, Logan High School, Logan, Ohio; Frederick H. Krecker, Ohio University, Athens, Ohio; and Robert E. McKay, Bowling Green State University, Bowling Green, Ohio. The final item on the programme on Saturday consisted of a panel discussion, *Careers in Physics.* The speakers on this panel were W. E. Forsythe, Smithsonian Institution; Leonard O. Olsen, Case Institute of Technology; Fred F. Householder, University of Akron; and Paul B. Taylor, Wright-Patterson Air Force Base.

Officers for the year 1952–53 were selected as follows: Dr. John E. Edwards, Chairman, of Ohio University, Athens, Ohio; Vice-Chairman, Dr. William L. Davidson, Jr., of The B. F. Goodrich Company Research Center, Brecksville, Ohio, Secretary-Treasurer; Leon E. Smith, Denison University, Granville, Ohio.

Abstracts of the remaining contributed papers follow.

Leon E. Smith, *Secretary*
Ohio Section
Denison University
Granville, Ohio

The Specific Heat of Lead in the Temperature Range 1.0°K to 75°K.* M. Horowitz, A. A. Silvidi, S. F. Malaker, and J. G. Daunt, *The Ohio State University.*—The specific heat of a high purity lead sample has been measured in the temperature range 1.0°K to 75°K using an adiabatic calorimeter. The temperatures were measured using both lead and phosphor-bronze resistance thermometers, which gave high sensitivity, and the heating cycles were recorded, a procedure which enabled high accuracy to be obtained. Details of the recording arrangements are reported. The results in the temperature range above 4.0°K are in agreement with previous workers, giving Debye characteristic temperature of between 85°K and 90°K. The results for the specific heat in the superconducting state below 4.0°K differ from the measurements reported by Keesom and van den Ende,[1] in that they do not reproduce the anomaly at the lowest temperature. It appears that at the lowest temperatures our results indicate that the specific heat of the superconductive state falls below a T^3 function. Some possible interpretations of this result are given.

* Assisted in part by contracts between the AEC and ONR and The Ohio State University Research Foundation.

[1] Keesom and van den Ende, Leiden Comm. 203d and 213c.

On the Influence of Physical Strain on the Physical Properties of Superconductors.* T. S. Smith and J. G. Daunt, *The Ohio State University.*—Measurements have been made of the magnetic threshold curves below 1.0°K of zirconium (kindly loaned to us by the Oak Ridge National Laboratory). It was found that when measurements were made on the metal as supplied (the metal was formed by deposition from the iodide), the transition temperature T_c was 0.6°K and the slope of the magnetic threshold curve at T_c was 390 gauss per degree; whereas after annealing T_c was reduced to 0.546°K and the slope of the threshold curve was 138 gauss per degree. The higher values are in agreement with previous measurements made elsewhere, whereas the lower values are indicative of an approach to a reversible thermodynamic transition. Using these new results, we estimate that the specific heat of the electrons in the normal state is $2.57\times10^{-4}T$ calories per degree per mole, a value well below that given by recent calorimetric measurements. A detailed discussion of the significance of the results is given.

* Assisted in part by a contract between the AEC and The Ohio State Research Foundation.

Some Demonstrations of High Frequency Phenomena. Richard H. Howe, *Denison University.*—A simple, easily constructed high frequency oscillator capable of delivering approximately 30-watts radiofrequency power is described. The oscillator is built of surplus material commonly available. It is used to demonstrate several of the fundamental characteristics of electromagnetic waves and their application in some of the more common high frequency antennae arrays.

A Unique Form of the Ellicott Compensated Pendulum. E. H. Johnson, *Kenyon College.*—The pendulum of a large jeweler's regulator clock is exhibited in which constancy of the effective length is secured by an unusual arrangement of the Ellicott temperature compensating mechanism. The pendulum rod consists essentially of brass and steel bars which support a heavy bob by means of a horizontal lever arrangement wherein the arms are proportioned to counteract the thermal expansions of the supporting bars, and thus maintain an invariable distance between the point of support and the center of oscillation. Means are provided for close manual adjustment.

Experiments on Multiple-Beam Interferometry. Thurston E. Manning, *Oberlin College.*—The experimental techniques of applying multiple-beam interferometry to the classic experiments of Newton's rings and the air wedge in a form suitable to the undergraduate laboratory will be described. Differences between the present techniques and those of Tolansky[1] include the use of aluminum as the partially reflect-

ing coating and the use of a sodium light source. Extension of the method to the examination of surfaces will be discussed.

[1] S. Tolansky, *Multiple Beam Interferometry of Surfaces and Films* (Oxford University Press, New York, 1948).

Applications of a Small Radium-Beryllium Neutron Source in the Undergraduate Laboratory. I. Source Characteristics. DAVID L. ANDERSON, *Oberlin College.*—Characteristics of neutron sources suitable for use in undergraduate teaching are discussed, with particular emphasis on a radium-beryllium source containing 25 mg of radium now in use at Oberlin. This source is ordinarily used in conjunction with a moderating sphere of paraffin two feet in diameter, arranged so that a variety of experiments may be performed. Requisite safety precautions will be discussed.

Applications of a Small Radium-Beryllium Neutron Source in the Undergraduate Laboratory. II. Typical Experiments. THURSTON E. MANNING AND DAVID L. ANDERSON, *Oberlin College.*—The use of the neutron source described by Anderson[1] in teaching experiments and demonstrations will be discussed, with experiments on half-life determination, neutron flux distribution in a moderator, secular equilibrium under neutron bombardment, and relative cross sections for neutron bombardment being emphasized. Application of the source to research problems (such as the Szilard-Chalmers reaction) will be treated.

[1] See David L. Anderson, preceding abstract.

Measurements in the Far Infrared Spectrum.* E. E. BELL, R. L. HANSLER, R. A. OETJEN, AND H. E. SCHAUWECKER, *The Ohio State University.*—Development of techniques for determining spectral absorption at wavelengths greater than twenty-five microns is worthwhile since such data can provide information about molecular structure not otherwise available. A grating spectrograph for use in the far infrared spectral region has been constructed. The problems which are most difficult to solve in a long wave investigation result from the smallness of the amount of energy available and the necessity for eliminating the large amount of short wave radiation that is present. Atmospheric water vapor spectra in the spectral region between forty and one hundred forty microns show that the problems have been solved satisfactorily.

* The work described in this paper was sponsored by the Air Research and Development Command (Wright Air Development Center) through a contract with The Ohio State University Research Foundation.

Some Properties of Multi-Layer Optical Reflection Interference Filters.* W. H. SHAFFER AND R. A. OETJEN, *The Ohio State University.*—Further investigation[1] of the theory and development of techniques of fabrication have been carried out for simple multi-layer optical interference filters of the reflection type. A one-layer reflection interference filter is constructed by depositing on a good reflecting plane surface a dielectric layer followed by a metallic film; a multilayer filter is constructed by continuing the alternate deposition of dielectric layers and metallic films. General theoretical expressions have been derived giving the reflection properties of simple two- and three-layer filters in terms of the optical constants and thicknesses of the constituent materials. Appropriate approximations have been made to yield suitable criteria for controlling the properties of filters. Good agreement has been obtained between predicted and observed reflection characteristics of fabricated filters.

* The work described in this paper was sponsored by the Air Research and Development Command (Wright Air Development Center) through a contract with The Ohio State University Research Foundation.

[1] W. H. Shaffer and R. A. Oetjen, Phys. Rev. **78**, 187 (1950).

The Gamma-Rays from Excited States of Al^{27}.* LEONARD N. RUSSELL, WARREN E. TAYLOR, AND JOHN N. COOPER, *The Ohio State University.*—The energies of the gamma-rays emitted from five excitation levels in Al^{27} have been measured by coincidence and absorption methods. These levels were excited by bombardment of the separated isotope[1] Mg^{25} with protons from a Van de Graaff generator. The reaction induced, $Mg^{25}(p,\gamma)Al^{27}$, has a Q-value of 7.5 Mev. Measurements by Tangen[2] of the gamma-ray energies excited by 336- and 450-kev protons yielded values of 4.9 and 6.2 Mev, which suggested that the compound nucleus did not decay directly to the ground state in either case. Additional data with 450-kev protons confirm Tangen's results. Measurements of gamma-ray energies from levels excited by capture of 813-, 840-, 954-, and 1015-kev protons yielded values of 7.2, 5.3, 7.3, and 5.5 Mev, respectively. This suggests that transitions from these levels are not ordinarily to the ground state. An internally consistent energy level diagram can be proposed if one postulates transitions to known[3] low-lying levels in Al^{27}.

* Assisted by a contract between the AEC and The Ohio State Research Foundation.

[1] Supplied by the Carbide and Carbon Chemicals Division, Oak Ridge National Laboratory.

[2] R. Tangen, Kgl. Norske. Videnskab. Selskabs. Forh. Skrifter No. 1 (1946).

[3] Swann, Mandeville, and Whitehead, Phys. Rev. **79**, 598 (1950).

THE AMERICAN INSTITUTE OF PHYSICS

INCORPORATED

57 East 55 Street, New York 22, N.Y.

MEMBER SOCIETIES:

American Physical Society
Karl K. Darrow, *Secretary*, Columbia University, New York 27, New York

Optical Society of America
Arthur C. Hardy, *Secretary*, Massachusetts Institute of Technology, Cambridge 39, Massachusetts

Acoustical Society of America
Wallace Waterfall, *Secretary*, 57 East 55th Street, New York 22, New York

Society of Rheology
G. J. Dienes, *Secretary*, Brookhaven National Laboratory, Upton, Long Island, New York

American Association of Physics Teachers
R. F. Paton, *Secretary*, University of Illinois, Urbana, Illinois

AFFILIATED SOCIETIES:

American Crystallographic Association
Electron Microscopy Society of America
Physical Society of Pittsburgh
Physics Club of Chicago
Physics Club of Philadelphia
Cleveland Physics Society
Physics Club of the Lehigh Valley
Sigma Pi Sigma

ASSOCIATES:

Over seventy-five leading industrial enterprises and other institutions which contribute to the support of the Institute

JOURNALS:

The Physical Review
S. A. Goudsmit, *Editor*, Brookhaven National Laboratory, Upton, Long Island, New York

Reviews of Modern Physics
J. W. Buchta, *Editor*, University of Minnesota, Minneapolis, Minnesota

Journal of Chemical Physics
Wallace R. Brode, *Editor*, National Bureau of Standards, Washington 25, D.C.

The Journal of the Acoustical Society of America
Floyd A. Firestone, *Editor*, 57 East 55th Street, New York 22, New York

American Journal of Physics
Thomas H. Osgood, *Editor*, Michigan State College, East Lansing, Michigan

The Review of Scientific Instruments
Gaylord P. Harnwell, *Editor*, Randal Morgan Laboratory of Physics, University of Pennsylvania, Philadelphia 4, Pennsylvania

The Journal of Chemical Physics
Joseph E. Mayer, *Editor*, Institute for Nuclear Studies, University of Chicago, Chicago 37, Illinois

Journal of Applied Physics
Elmer Hutchisson, *Editor*, Case Institute of Technology, Cleveland 6, Ohio

Physics Today
Gaylord P. Harnwell, *Editorial Director*; Ralph E. Sharp, *Managing Editor*, American Institute of Physics, 57 East 55th Street, New York 22, New York

OFFICERS:

Gordon K. Harrison, *Chairman*
Massachusetts Institute of Technology

George B. Pegram, *President*
Columbia University

GOVERNING BOARD:

Karl K. Darrow
G. J. Dienes
S. A. Goudsmit
G. P. Harnwell
Gordon K. Harrison
F. V. Hunt
Rudolph Kingslake
Hugh S. Knowles
C. C. Lauritsen
F. W. Loomis
William F. Meggers
George B. Pegram
I. I. Rabi
Duane Roller
Frederick Seitz
Francis G. Slack
John C. Slater
Richard M. Sutton
Marc W. Zemansky

Consultant on Publications:
Melvin Lord

ADMINISTRATIVE STAFF:

Harry A. Barker, *Director*
Wallace Waterfall, *Executive Secretary*
Theodore Vermilye, *Advertising Manager*
Ruth F. Sheets, *Publications Manager*
Betty H. Gardner, *Assistant Secretary*
Eileen B. Nielsen, *Circulation Manager*
Katherine Smith, *Assistant Treasurer*

THE American Institute of Physics was founded in 1931 as a federation of leading societies in the field of Physics. It combines into one operating agency those functions in behalf of physics which can best be done by the Societies jointly. Its purpose is the advancement and diffusion of physics and its applications to human welfare. To this end it operates for itself or the Societies the journals listed on this page; promotes unity and economy of effort among all who are interested in physics; provides numerous direct services to physicists and to the public; and cooperates with government agencies, research associations, educational institutions, technical industries, and others in such manner as to realize the opportunities and fulfill the responsibilities of physics as an important and constructive force in science